U.S. DEPARTMENT OF ENERGY

Office of ENERGY EFFICIENCY & RENEWABLE ENERGY

# Electrification

## 2017 Annual Progress Report

Vehicle Technologies Office

(This page intentionally left blank)

# Disclaimer

# Acronyms and Abbreviations

## A

| | |
|---|---|
| AC | Alternating Current |
| ACC | Adaptive Cruise Control |
| accel | Acceleration |
| ACS | Advanced Combustion Systems |
| ACSforEVER | Advanced Climate Systems for EV Extended Range |
| AER | All-electric range |
| AFV | Alternative Fuel Vehicle |
| AMI | Advanced Metering Infrastructure |
| AMT | Automated Mechanical Transmission |
| ANL | Argonne National Laboratory |
| ANN | Artificial Neural Network |
| AOI | Areas of Interest |
| APEC | Asia Pacific Economic Council |
| APRF | Advanced Powertrain Research Facility |
| APT | Pressure Sensor |
| ASD | Aftermarket Safety Device |
| AVTA | Advanced Vehicle Testing Activity |
| AVTE | Advanced Vehicle Testing and Evaluation |

## B

| | |
|---|---|
| BaSce | Baseline and Scenario |
| Batt | Battery |
| BEB | Battery Next-Generation Electric Transit Bus |
| BEC | Bussed Electrical Center |

| | |
|---|---|
| BEMS | Building Energy Management System |
| BET | Battery Electric Truck |
| BEV | Battery Electric Vehicle |
| BMW | Bayerische Motoren Werke AG |
| BSFC | Brake Specific Fuel Consumption |
| BTE | Brake Thermal Efficiency |

## C

| | |
|---|---|
| CAC | Charge Air Cooler |
| CACC | Cooperative Adaptive Cruise Control |
| CAE | Computer-Aided Engineering |
| CAFE | Corporate Average Fuel Economy |
| CAN | Controller Area Network |
| CAV | Connected and automated vehicles |
| CARB | California Air Resources Board |
| CBD | Central Business District |
| CCS | Combined Charging System |
| CW, CCW | Clockwise, Counter Clockwise |
| CD | Charge-Depleting |
| CERV | Conference on Electric Roads and Vehicles |
| CFD | Computational Fluid Dynamics |
| CFDC | Commercial Fleet Data Center |
| CFL | Combined Fluid Loop |
| CH4 | Methane |
| CHTS | California Household Travel Survey |
| CIP | Common Integration Platform |
| Cm3 | Cubic |
| CNG | Compressed Natural Gas |
| CO | Carbon monoxide |
| CO2 | Carbon Dioxide |

| | |
|---|---|
| COMM | Commuter |
| Conv | Conventional Vehicle |
| COP | Coefficient of Performance |
| CRADA | Cooperative Research and Development Agreement |
| CS | Charge Sustaining |
| Cs | Cold start |
| CV | Conventional vehicle |

## D

| | |
|---|---|
| D3 | Downloadable Dynamometer Database |
| DC | Direct current |
| DCFC | Direct Current Fast Charge |
| DCT | Dual-clutch transmission |
| decel | Deceleration |
| DER | Distributed energy resource |
| DFGM | Digital Flux Gate Magnetometer |
| DFMEA | Design of Failure Modes Analysis |
| DOE | U.S. Department of Energy |
| DOHC | Dual overhead cam |
| DS | Down speeding |
| DSM | Distributed Security Module |
| DSM | Diagnostic Security Module |
| DSP | Digital Signal Processor |
| DSRC | Dedicated Short Range Communications |
| dt | Change in time |
| dv | Change in velocity |
| Dyno | Dynamometer |

## E

| | |
|---|---|
| EAVS | Electrically Assisted Variable Speed Supercharger |
| EC | European Commission |

| | |
|---|---|
| EDV | Electric Drive Vehicle |
| EDT | Electric Drive Technologies |
| EDX | Energy dispersive x-ray spectroscopy |
| EERE | Energy Efficiency and Renewable Energy |
| EGR | Exhaust Gas Recirculation |
| EG/W | Ethylene glycol/water |
| EOL | End of life |
| EPA | Environmental Protection Agency |
| ePATHS | Electrical PCM Assisted Thermal Heating System |
| EREV | Extended-Range Electric Vehicles |
| ESIF | Energy Systems Integration Facility |
| ESS | Energy Storage System |
| ETT | Electric Transportation Technologies |
| E-TREE | Electric Truck with Range Extending Engine |
| EUMD | End-Use Measurement Device |
| EV | Electric Vehicle |
| EV2G | Electric Vehicle-to-Grid |
| EVSE | Electric Vehicle Service Equipment |
| EXV | Electronic Expansion Valve |

## F

| | |
|---|---|
| F | Force |
| FASTSim | Future Automotive Systems Technology Simulator |
| FC | Fuel cell |
| FC | Fast charge |
| FCons | Fuel consumption |
| FCTO | Fuel Cell Technologies Office |
| FE | Fuel Economy |
| FEA | Finite Element Analysis |
| FEX | Front-end Heat Exchanger |

| | |
|---|---|
| FHWA | Federal Highway Administration |
| FLNA | Frito-Lay North America |
| FM | Friction Modifier |
| FMEP | Friction Mean Effective Pressure |
| FOA | Funding Opportunity Announcement |
| FTIR | Fourier transform infrared spectroscopy |
| FTP | Federal Test Procedure |
| FWD | Four wheel drive |
| FY | Fiscal year |

## G

| | |
|---|---|
| g | gram |
| GB | Gigabyte |
| GCEDV | Grid Connected Electrical Drive Vehicles |
| GEM | Gas Emissions Model |
| GHG | Greenhouse Gas |
| GITT | Grid Interaction Tech Team |
| GMLC | Grid Modernization Lab Consortium |
| GnPs | graphene nanoplatelets |
| GO | Graphene Oxide |
| GPRA | Government Performance and Results Act |
| GPS | Global Positioning System |
| GREET | Greenhouse gases, Regulated Emissions, and Energy use in Transportation |
| GSF1 | Generic Speed Form 1 |
| GSU | Grid side unit |
| GUI | Graphic User Interface |
| GVW | Gross Vehicle Weight |

## H

| | |
|---|---|
| h-APU | hybrid Auxiliary Power Unit |
| HATCI | Hyundai America Technical Center, Inc. |
| HC | Unburned hydrocarbons |
| HD | Heavy Duty |
| HEV | Hybrid-Electric Vehicle |
| H-GAC | Houston-Galveston Area Council |
| HHDDT | Heavy Heavy-Duty Diesel Truck |
| HHV | Hydraulic Hybrid Vehicle |
| HIL | Hardware-In-the-Loop |
| HP | Heat Pump |
| Hp | Horsepower |
| HTML | HyperText Markup Language |
| HV | High Voltage |
| HVAC | Heating Ventilating and Air Conditioning |
| HWFET | Highway Fuel Economy Test |
| HPMS | Highway Performance Monitoring System |
| HVTB | High Voltage Traction Battery |
| HWY | Highway Program or Highway Fuel Economy Test Cycle |
| HPC | High Performance Computing |
| HTR | Heater |
| Hz | Hertz |

## I

| | |
|---|---|
| I | Inertia |
| IC | Internal Combustion |
| ICD | Interim Component Durability |
| ICDV | Internal Combustion Drive Vehicles |
| ICE | Internal Combustion Engine |
| ICTF | Intermodal Container Transfer Facility |

| | |
|---|---|
| ICU | Inverter-Charger Unit |
| IEB | Information Exchange Bus |
| IEC | International Electrotechnical Commission |
| IGBT | Insulated Gate Bipolar Transistors |
| IHX | Internal Heat Exchanger |
| INL | Idaho National Laboratory |
| INTEGRATE | Integrated Network Testbed for Energy Grid Research and Technology |
| IOT | Internet of Things |
| IR | Infrared Radiation |
| ISO | International Organization for Standardization |
| ITS | Intelligent Transportation Systems |

## J

| | |
|---|---|
| JIT | Just-in-Time |

## K

| | |
|---|---|
| kg | Kilogram |
| km | Kilometer |
| kW | Kilowatt |
| kWh | Kilowatt hour |

## L

| | |
|---|---|
| L | litre |
| L1 | Level 1 benchmark |
| L2 | Level 2 benchmark |
| Lbf | Pounds force |
| LCC | Liquid-Cooled Condenser |
| LD | Light-duty |
| LH | line haul |
| Li | Lithium |
| LIB | Lithium ion battery |

| | |
|---|---|
| LLNL | Lawrence Livermore National Laboratory |
| LTC | Lockport Technical Center |
| LV | Leading Vehicle |

## M

| | |
|---|---|
| M | Mass |
| MBSE | Model Based System Engineering |
| MD | Medium Duty |
| mpg | Miles per gallon |
| MMTCE | Million Metric Tons of Carbon Equivalent |
| MIIT | Ministry of Industry and Information Technology |
| mi | Mile |
| MJ | Megajoules |
| MOSFET | Metal-Oxide Semiconductor Field-Effect Transistor |
| mph | Miles per hour |
| MPGe, MPGGe | Miles per gallon equivalent, Miles per gallon gasoline equivalent |
| MTDC | Medium Truck Duty Cycle |
| MOVES | Motor Vehicle Emission Simulator |
| MRF | Moving Reference Frame |
| MURECP | Medium-Duty Urban Range Extended Connected Powertrain |
| MY | Model year |
| M2 | Meters squared |

## N

| | |
|---|---|
| NACFE | North American Council for Freight Efficiency |
| NDA | Non-Disclosure Agreement |
| NETL | National Energy Technology Laboratory |
| NHTS | National Household Travel Survey |
| NHTSA | National Highway Transportation Safety Administration |
| NM | Newton meters |
| NOx | Nitrogen oxides |

| | |
|---|---|
| NR | Natural Rubber |
| NRE | Non Recurring Engineering |
| NREL | National Renewable Energy Laboratory |
| NRT | National Retail Trucking |
| NVH | Noise, vibration, and harshness |
| NVUSD | Napa Valley Unified School District |
| NYSERDA | New York State Energy Research Development Authority |

## O

| | |
|---|---|
| OBC | On-board charger |
| OCBC | Orange County Bus Cycle |
| OEM | Original Equipment Manufacturer |
| OneSAF | One Semi-Automated Forces |
| ORNL | Oak Ridge National Laboratories |

## P

| | |
|---|---|
| P | Active Power |
| PC | Polycarbonate |
| PCM | Phase-Change Material |
| PCU | Power Control Unit |
| PCU | Powertrain Control Unit |
| PEEM | Power Electronics and Electric Motor |
| PFC | Power factor correction |
| PFI | Port fuel injection |
| PGW | Pittsburgh Glass Works |
| PHEV | Plug-in Hybrid Electric Vehicle |
| PHEV## | Plug-in hybrid electric vehicle with ## miles of all-electric range |
| PI | Principal Investigator |
| PM | Permanent Magnet |
| PM | Particulate Matter |
| ppm | Parts per Million |

| | |
|---|---|
| PTC | Positive Temperature Coefficient (Electric Heater) |
| PTO | Power Take-Off |
| PVP | Polyvinylpyrrolidone |
| PWWMD | Public Works and Waste Management Department |
| λ | Power Factor |
| φ | Power Angle |

## Q

| | |
|---|---|
| Q | Reactive power |
| QA | Quality assurance |
| QC | Quality control |

## R

| | |
|---|---|
| R2 | Coefficient of Determination |
| R/D | Receiver / Dryer |
| REV | New York State's Reforming the Energy Vision Initiative |
| REx | Range Extending Engine |
| rGO | reduced graphene oxide |
| RH | Relative Humidity |
| RMS | Root Mean Square |
| ROL | Ring-On-Liner |
| rpm | Revolutions Per Minute |
| RSU | Road Side Unit |
| RWDC | Real-World Drive-Cycle |

## S

| | |
|---|---|
| S | Apparent power |
| SAE | Society of Automotive Engineers |
| SBR | Styrene-Butadiene Rubber |
| SC03 | SC03 Supplemental Federal Test Procedure |
| SCAG | Southern California Association of Governments |

| | |
|---|---|
| SCAQMD | South Coast Air Quality Management District |
| SCIG | Southern California International Gateway |
| SCR | Silicon Controlled Rectifier |
| SCR | Selective Catalytic Reduction |
| SDO | Standards Definition Organizations |
| SI | Système International d'Unités |
| SI | Gasoline Spark Ignition |
| SNR | Sensor |
| SOC | State of Charge |
| SPL | Sound Pressure Level |
| SR | Speed Ratio |
| SS | Steady State |
| S/S | Start/Stop |
| SPaT | Signal Phase and Timing |
| StAR | Storage-Assisted Recharging |

## T

| | |
|---|---|
| T | Torque |
| TA | Technical Area |
| TA | Torque Assist |
| TC | Thermocouple |
| TE | Thermoelectric |
| TE | Transmission Error |
| TES | Thermal Energy Storage |
| TGA | thermogravimetric analysis |
| THC | Total hydrocarbon emissions |
| TIM | Thermal Interface Materials |
| TLRP | Thermal Load Reduction Package |
| TN | Testing Network |
| TOU | Time-Of-Use |

| | |
|---|---|
| TSDC | Transportation Secure Data Center |
| TSI | Turbocharged stratified injection |
| TUSD | Torrance Unified School District |
| TV | Trailing Vehicle |
| TXVs | Thermal Expansion Valves |

## U

| | |
|---|---|
| U.S. DRIVE | U.S. Driving Research and Innovation for Vehicle Efficiency and Energy Sustainability |
| UA | Transfer Coefficient |
| UC | Ultra-capacitor |
| UCR | University of California, Riverside |
| UDDS | Urban Dynamometer Driving Schedule |
| UM | University of Michigan |
| UN ECE | United Nations Economic Council for Europe |
| UPS | United Parcel Service |
| URL | Uniform Resource Locator |
| US06 | Environmental Protection Agency US06 or Supplemental Federal Test Procedure |
| USABC | United States Advanced Battery Consortium |
| USCAR | U.S. Council for Automotive Research |
| Util | Battery capacity utilization |

## V

| | |
|---|---|
| V | Voltage |
| V2G | Vehicle-to-Grid |
| VAr | Volt-Amp-reactive |
| VGI | Vehicle-Grid Integration |
| VGT | Variable Geometry Turbocharger |
| VIP | Vacuum Insulated Panels |
| VMT | Vehicle Miles Traveled |
| VS | Vehicle Systems |

| | |
|---|---|
| VSATT | Vehicle Systems Analysis Technical Team |
| VSI | Vehicle Systems Integration |
| VSST | Vehicle Systems Simulation and Testing |
| VTCab | Vehicle Thermal Cab Simulator |
| VTIF | Vehicle Testing and Integration Facility |
| VTO | Vehicle Technologies Office |

## W

| | |
|---|---|
| dw | Change in Angle W |
| WCC | Water Cooled Condenser |
| WEC | World Endurance Championship |
| WEG | Water/Ethylene Glycol |
| Wh | Watt hour |
| WHR | Waste Heat Recovery |
| WPT | Wireless Power Transfer |
| WTW | Well-to-Wheels |

## X

| | |
|---|---|
| XPS | x-ray photoelectron spectroscopy |

## Y

## Z

| | |
|---|---|
| ZECT | Zero-emissions cargo transport |

# Executive Summary

During fiscal year 2017 (FY 2017), the U.S. Department of Energy (DOE) Vehicle Technologies Office (VTO) funded early stage research & development (R&D) projects that address Batteries and Electrification of the U.S. transportation sector. The VTO Electrification Sub-Program is composed of Electric Drive Technologies, and Grid Integration activities. The Electric Drive Technologies group conducts R&D projects that advance Electric Motors and Power Electronics technologies. The Grid and Charging Infrastructure group conducts R&D projects that advance Grid Modernization and Electric Vehicle Charging technologies. This document presents a brief overview of the Electrification Sub-Program and progress reports for its R&D projects. Each of the progress reports provide a project overview and highlights of the technical results that were accomplished in FY 2017.

(This page intentionally left blank)

# Table of Contents

# List of Figures

# List of Tables

# Vehicle Technologies Office Overview

Vehicles move our nation. Vehicles transport more than $36 billion worth of goods each day[1] and move people more than 3 trillion vehicle-miles each year[2]. Growing our national economy requires transportation and transportation requires energy. The average U.S. household spends nearly one-fifth of its total family expenditures on transportation[3], making transportation the most expensive spending category after housing. The transportation sector accounts for 70% of U.S. petroleum use. The United States imports 25% of the petroleum consumed – sending more than $10 billon per month[4] overseas for crude oil.

To strengthen national security, enable future economic growth, and increase transportation energy efficiency, the Vehicle Technologies Office (VTO) funds early-stage, high-risk research on innovative vehicle and transportation technologies. VTO leverages the unique capabilities and world-class expertise of the national laboratory system to develop innovations in electrification, advanced combustion engines and fuels, advanced materials, and energy efficient mobility systems.

VTO is uniquely positioned to address early-stage challenges due to strategic public-private research partnerships with industry (e.g., U.S. DRIVE, 21st Century Truck Partnership). These partnerships leverage relevant expertise to prevent duplication of effort, focus DOE research on critical R&D barriers, and accelerate progress. VTO focuses on research that industry does not have the technical capability to undertake on its own, usually due to a high degree of scientific or technical uncertainty, or it is too far from market realization to merit industry resources. VTO's research generates knowledge that industry can advance to deploy innovative energy technologies to support affordable, secure, and efficient transportation systems across America.

## VTO Organization Chart

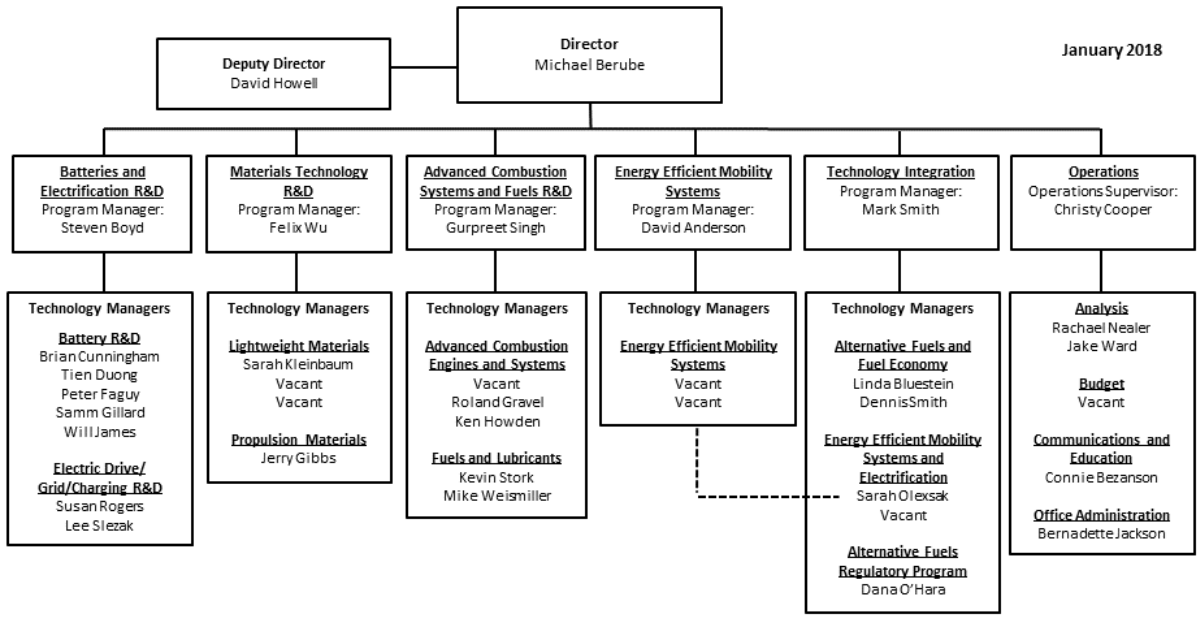


[1] https://ops.fhwa.dot.gov/publications/fhwahop16083/ch1.htm#t1
[2] https://www.fhwa.dot.gov/policyinformation/statistics/2015/vm1.cfm
[3] https://www.bls.gov/cex/2015/standard/multiyr.pdf
[4] Transportation Energy Data Book Edition 34, ORNL, Table 1.7 and Table 10.3; Overseas includes countries and territories outside the 50 States and the District of Columbia.

# Electric Drive Technologies Program Overview

## Introduction

The Electric Drive Technologies (EDT) program's mission is to conduct early stage research and development on transportation electrification technologies that accelerate the development of cost-effective and compact electric traction drive systems that meet or exceed performance and reliability requirements of internal combustion engine (ICE)-based vehicles, thereby enabling electrification across all light-duty vehicle types.

## Goals and Objectives

The goal of the EDT program is to develop an electric traction drive system at a cost of $6/kW for a 100 kW peak system by 2025. In addition, the program has a 2025 power density target of 33 kW/L for a 100 kW peak system. While achieving these targets will require transformational technology changes to current materials and processes, it is essential for enabling widespread electrification across all light-duty vehicle platforms.

## Program Design and Execution

The EDT program provides support and guidance for many cutting-edge automotive technologies now under development. Researchers focus on developing revolutionary new power electronics (PE), electric motor (EM), and traction drive system (TDS) technologies that will leapfrog current on-the-road technologies. This will lead to lower cost and better efficiency in transforming battery energy to useful work. Research and development (R&D) is also aimed at achieving greater understanding of, and improvements in how the various components of tomorrow's automobiles will function as a unified system.

In supporting the development of advanced vehicle propulsion systems, the EDT program fosters the development of technologies that will significantly improve efficiency, costs, and fuel economy.

The EDT program directs early-stage research through a three-phase approach intended to

- Identify overall propulsion- and vehicle-related needs by analyzing programmatic goals and reviewing industry recommendations and requirements, and then develop and deliver the appropriate technical targets for systems, subsystems, and component R&D activities
- Develop, test, and validate individual subsystems and components, including EMs and PE
- Estimate how well the components and subsystems work together in a vehicle environment or as a complete propulsion system and whether the efficiency and performance targets at the vehicle level have been achieved.

The research performed under this program addresses the technical and cost barriers that currently inhibit the introduction of advanced propulsion technologies into hybrid electric vehicles (HEVs), plug-in HEVs, battery electric vehicles (BEVs), and fuel cell powered automobiles that meet the DOE goals.

A key element in making these advanced vehicles practical is providing an affordable electric TDS. This will require attaining weight, volume, efficiency, and cost targets for the PE and EM subsystems of the TDS. Areas of development include:

- Novel traction motor designs that result in increased power density and lower cost
- Inverter technologies that incorporate advanced wide bandgap (WBG) semiconductor devices to achieve higher efficiency while accommodating higher-temperature environments and delivering higher reliability

- Converter concepts that leverage higher-switching-frequency semiconductors, nanocomposite magnetics, higher-temperature capacitors, and novel packaging techniques that integrate more functionality into applications offering reduced size, weight, and cost
- New onboard battery charging electronics that build from advances in converter architectures for decreased cost and size
- More compact and higher-performing thermal controls achieved through novel thermal materials and innovative packaging technologies
- Integrated motor-inverter TDS architectures that optimize the technical strengths of the underlying PE and electric machine subsystems.

VTO competitively awards funding through funding opportunity announcement (FOA) selections, and projects are fully funded through the duration of the project in the year that the funding is awarded. The future direction for direct-funded work at the national laboratories is subject to change based on annual appropriations.

# Grid and Infrastructure Program Overview

## Introduction

The Grid and Charging Infrastructure (G&I) program's mission is to conduct early stage research and development on transportation electrification technologies that enable reduced petroleum consumption by light, medium, and heavy duty vehicles. The program identifies and enables the role of vehicles in the future electrical grid.

## Goals and Objectives

**Program Goal**: The G&I Program identifies systems pathways and conducts research to facilitate the development and harmonization of a robust, interoperable, and cyber secure, electric vehicle charging and grid infrastructure which incorporates advanced charging technologies, distributed energy resources, grid, and grid services.

The program achieves it goal by accomplishing the following objectives:

- **EV Grid Integration and Services:** Identify system requirements and research Grid to Vehicle power transfer and storage (V1G) and Vehicle to Grid power transfer (V2G) technologies that optimize vehicle charging efficiency, minimize systems disruptions, and facilitate integration of distributed energy resources

- **High Power Static / Dynamic Wireless Charging:** Conduct feasibility studies and technology research and development of high power static and dynamic wireless charging to enable additional consumer charging options and greater vehicle autonomy

- **EV / EVSE / Grid Interoperability & Control:** Research and develop technologies and tools to enable seamless interoperability (connectivity and communications) and control that maximize charging convenience and minimize impacts to the grid

- **Extreme Fast Charging (XFC):** Identify and assess system requirements and conduct research to enable extreme fast charging while minimizing impacts to the grid. (During the FY 2017 period, these activities were limited to preliminary requirements analysis and planning for FY 2018 projects)

- **Cyber Security:** Address on-road vehicle and charging infrastructure related cyber security gaps.

## Program Design and Execution

The G&I Program carries out its mission by focusing its R&D investments on early stage, medium and long-term technology projects that are unlikely to be pursued by industry alone, but have significant potential public benefit.

### G&I R&D Functions:

- Perform R&D that focuses on defining requirements, designing, prototyping, and validating the enabling technologies that are needed. Document and share the results in public and industry forums where appropriate and feasible.

- Perform modeling and evaluation activities that provide objective, publicly-available data to identify the most appropriate Federal investments and pathways for technology improvements and lessons learned for cost-effective future activities.

- Initiate outreach that provides technical assistance, tools, and resources to help stakeholders understand the technologies.

- Engage in research partnerships with industry to leverage technical expertise, prevent duplication, ensure public funding remains focused on the most critical barriers to technology commercialization, and

accelerate progress. G&I will work collaboratively with its industry partners in the U.S. DRIVE Partnership (Grid Interaction Tech Team (GITT)) to analyze and identify technical R&D opportunities for passenger vehicles.

- Coordinate with other programs in EERE and across the DOE complex – National Laboratories, DOE's Office of Science, Office of Electricity Delivery and Energy Reliability (OE), and the Advanced Research Projects Agency-Energy (ARPA-E) to ensure the effective use of resources while avoiding duplication and facilitates the transfer of successful technologies across the research and development continuum. (i.e., Grid Modernization Initiative)

- Collaborate via strategic partnerships with end-users and other key stakeholders

The G&I program was established in January 2017. The program inherited many of its FY 2017 projects from VTO's Vehicle Systems program. As a result the G&I projects have been assigned to Grid Modernization, Industry, or Vehicle Systems sections of this Electrification Annual Progress Report (APR). The Grid Modernization section contains project reports that were awarded to members of the Grid Modernization Laboratory Consortium (GMLC). The Industry section describes projects that were awarded to commercial industry performers via DOE's Funding Opportunities Announcement (FOA) solicitation process. The Vehicle Systems projects were awarded to National Laboratories via direct funding agreements.

## Research Highlights

| Accomplishments | Organization | Focus Area | Project Title |
|---|---|---|---|
| The Eaton project developed a multi-speed gearbox for Medium Duty electric vehicles. Engineers selected a 4-speed Automated Mechanical Transmission as the winning concept. The vehicle model was developed and validated with on-route data of Proterra BE35 electric transit bus. Simulations predicted up to 20% increase in system energy efficiency depending on drive cycles, a top speed of greater than70 mph on flat road, 40% faster acceleration and a doubled gradeability with 4-speed transmission as compared to the baseline EVs. Prototyping of 6 fully functional and one display units of 4-speed transmission were completed. Prototype units were integrated on dynos and tested at Eaton and ORNL .Powertrain in the loop tests at ORNL validated all the performance gains predicted by the simulations. One unit was integrated on Proterra BE35 Electric Bus and tested at Eaton and NREL. Chassis Dyno Tests at NREL verified the simulation results and also the Hardware in the Loop (HIL) test results at ORNL | Eaton Corporation | Industry Award | Multi-Speed Transmission for Commercial Delivery Medium Duty PEDVs |
| The Bosch project developed an innovative PHEV powertrain which can reduce fuel consumption by over 50% in charge sustaining mode when utilizing a multi-mode powersplit transmission with integrated electric motors. Over 18 million designs were evaluated against given collocation, | Robert Bosch LLC | Industry Awards | Medium-Duty Urban Range Extended Connected Powertrain (MURECP) |

| Accomplishments | Organization | Focus Area | Project Title |
|---|---|---|---|
| functional, and performance attributes, yielding 83 feasible designs. Of those 83 configurations, 14 were estimated to meet or exceed the program objective in charge sustaining mode. Design label 698b has been selected as the target architecture for the integration and demonstration phases of the project. Greater than 56% fuel consumption reduction has been achieved in simulation when operating in charge sustaining mode (~19 MPG). The flexible multi-mode/ powersplit transmission also enables an estimated all-electric range of greater than 60 miles, at an energy efficiency of 1.51 miles/kW-hr (56 MPGe) on the target drive cycle (CSHVC). | | | |
| The Electric Truck with Range Extending Engine (ETREE) project has selected and obtained the relevant powertrain components in order to meet the target objective of providing at least a 50% fuel consumption reduction across a wide range of class 6 pickup and delivery duty cycles. Test cell testing has increased the confidence in the simulation methods employed and, therefore, simulation can be used to continually optimize the system control algorithms. These accomplishments are significant steps in achieving the ETREE project goal to develop a class 6 (GVW 26k lb.) box truck, with equivalent performance to conventional diesel powered trucks, that reduces fuel consumption by at least 50% over a wide range of urban/suburban pickup and delivery applications. | Cummins | Industry Awards | Cummins Electric Truck with Range-Extending Engine (ETREE) |
| The CALSTART project determined grid-interface power electronic components for a Medium Duty grid connected ellectric vehicle. Researchers also designed and integrated a phase-locked-loop system with the three-phase rectifier/inverter model developed for this project. The simulation results demonstrated that the system can be operated in full active power, inductive reactive, and capacitive reactive modes of operation | CALSTART | Industry Awards | Bidirectional Wireless Power Flow for Medium Duty Vehicle Grid Connectivity |
| The EPRI project developed V2G control algorithms and performed simulation test verification using an EV emulator representing multiple V2G capable PEVs associated to a Transformer Management and Monitoring System within a residential application. Residential load and solar generation profile data used for the simulation testing was extrapolated from US Energy Information | EPRI | Industry Award Grid Moderni zation | Comprehensive Assessment of On-and Off-Board Vehicle-to-Grid Technology Performance and Impacts On Battery |

| Accomplishments | Organization | Focus Area | Project Title |
|---|---|---|---|
| Administration data sources. The ISO and DSO signal simulators were implemented into the simulation testing model for Demand Response (DR) and Distributed Energy Resource (DER) functions and parameters. Project staff developed the Smart Power Integrated Node (SPIN) system design architecture and Component Technical Specification. Developed the SPIN master controller which integrates power electronics mode control functions for bi directional power flow management between DER assets (including PEV), the grid, and facility loads. | | | and the Grid [DE-EE0007792] |
| The AVTE project provided data, reports, and lessons-learned from vehicle testing that are available for further study by DOE national laboratories and dissemination to the public. | Intertek Testing Services NA | Industry Awards | Advanced Vehicle Testing & Evaluation (AVTE) [DE-EE0005501] |
| The ZECT 1 project completed seven plug-in electric trucks. Collectively, these electric trucks have logged over 41,000 miles in real world drayage service. The truck tests provided valuable data on performance and operational characteristics to help evaluate technical feasibility and viability of advanced technologies for drayage applications. These trucks have also generated significant interest from trucking companies, which will certainly help to promote and accelerate market adoption of electric truck technologies in cargo transport operations. | South Coast Air Quality Management District | Industry Awards | Zero Emission Drayage Trucks Demonstration (ZECT I) |
| The McLaren project specified a system using advanced modeling and simulation tools that will show the design parameters for an electrified vehicle powertrain system that will achieve the overall program objectives of 50% decrease in fossil fuel consumption on real world drive cycles.The project designed and began building a prototype eAxle system. | McLaren Engineering division of Linamar | Industry Awards | Medium Duty Vehicle Powertrain Electrification and Demonstration |

Questions regarding the Grid and Infrastructure Program can be directed to the Program Manager, Lee Slezak via email: Lee.Slezak@ee.doe.gov or telephone: (202) 586-2335.

# I. Electric Drive Technologies Research

## I.1 Advanced Electric Motor Materials Research

**Tim Burress, Principal Investigator**
Oak Ridge National Laboratory
1 Bethel Valley Road
Oak Ridge, TN 37831
Phone: (865) 576-3654
E-mail: burressta@ornl.gov

**Susan A. Rogers, Technology Manager**
U.S. Department of Energy
Phone: (202) 586-8997
E-mail: Susan.Rogers@ee.doe.gov

Start Date: October 1, 2016 End Date: September 30, 2017
Total Project Cost: $184,344 DOE share: $184,344 Non-DOE share: $0

### Project Introduction

The electric motor is one of the main components of HEV and EV drivetrains and improving efficiency, performance, and cost-effectiveness is crucial to the hybridization and electrification of vehicles. The Advanced Electric Motor Materials Research project provides information to researchers on other ORNL motor projects to help in the development of high accuracy modeling tools. This involves the study of magnetic materials on atomistic and microstructural scales to study formation of magnetic domains and domain wall propagation while observing the impact of various microstructural properties and impacts of other phenomena such as residual stress-strain that may occur as a result of manufacturing, mounting methods, and operating conditions.

### Objectives

In FY17, the three electric motor projects were performed in unison to target the DOE objectives of developing low-cost non–RE motor solutions with high power density, specific power, and efficiency. This project helps by providing information useful for the development of novel high-accuracy motor modeling tools, and ultimately motor design optimization.

### Approach

Motor design optimization in FY 2017 was conducted with commercial FEA packages as well as in-house custom-designed tools in combination with other software packages for parametric optimization algorithms and state space simulations. The progress and results in the area of motor design are discussed after the following sections describing the parallel efforts in materials R&D. These parallel efforts are ultimately in support of improving motor designs by developing or facilitating the use of more efficient materials and by conducting fundamental research to improve the modeling accuracy of electrical steel characteristics.

### Results

In soft magnetic materials such as Fe and Fe-Si alloys used in motor laminations, the magnetic behavior during operation is linked to the evolution of the magnetic domain structure during external magnetization and demagnetization cycles. The effects of elastic strains and pinning due to non-magnetic defects in the steel microstructure significantly influence the temporal evolution of the domain structure and hence the magnetic response. A simulation effort at the mesoscale was undertaken in order to quantify the magnetic behavior under such conditions and to provide realistic magnetic constitutive behavior to continuum-level simulations of motor performance. The simulations of magnetic domain evolution are based on a Monte Carlo (MC) technique [1]. The

MC technique uses atomic magnetic moments distributed in a body centered cubic (BCC) structure of iron. The four magnetic energy contributions are expressed in terms of the atomic quantities as shown below:

$$E_{ext} = -H.M \quad [1]$$

$$E_{exch} = -\sum J_{ij}\hat{m}_i.\hat{m}_j. \quad [2]$$

$$E_{dip} = M^2 \sum_{j=1}^{n} \sum_{k\neq j}^{n} \frac{\hat{m}_j.\hat{m}_k - 3(\hat{m}_j.e_{jk})(\hat{m}_k.e_{jk})}{4\pi\mu_0 r^3}. \quad [3]$$

$$E_{an} = K_1(\alpha_1^2\alpha_2^2 + \alpha_2^2\alpha_3^2 + \alpha_1^2\alpha_3^2) + K_2\alpha_1^2\alpha_2^2\alpha_3^2. \quad [4]$$

In Eqn. 1, *H* is the external magnetic field strength and *M* is the atomic magnetic moment vector. In Eqn. 2, $E_{exch}$ is for each atom *i* where the $\hat{m}_i$ and $\hat{m}_j$ are the unit magnetic moment vectors of the *i* and *j* atoms where the *j* atoms included are up to the fourth nearest-neighbors and $J_{ij}$ is the exchange interaction parameter between *i* and *j* atoms. In Eqn. 3, $e_{jk}$ is the unit vector of the displacement that connects an atom *j* with atom *k*, and $\mu_0$ is the permeability of space. In Eqn. 4, $K_1$ and $K_2$ are the magneto-crystalline anisotropy constants for iron, and $\alpha_1$, $\alpha_2$ and $\alpha_3$ are the direction cosines of the total atomic magnetic moment vector with respect to the coordinate axes. Residual tension has a significant effect on the domain structure of the Goss-oriented crystal. In order to include the effect of the tensile strain, the following two energy terms are included in the energy Hamiltonian.

$$E_{El_1} = 0.5C_{11}(\varepsilon_{11}^2 + \varepsilon_{22}^2 + \varepsilon_{33}^2) + C_{12}(\varepsilon_{11}\varepsilon_{22} + \varepsilon_{22}\varepsilon_{33} + \varepsilon_{33}\varepsilon_{11}) + 2C_{44}(\varepsilon_{12}^2 + \varepsilon_{23}^2 + \varepsilon_{31}^2). \quad [5]$$

$E_{El_1}$ is the elastic strain energy arising from the application of the strain components $\varepsilon_{ij}$ and the elastic constants $C_{mn}$ for the steel. The coupling of the elastic strain with the magnetization in the steel leads to another elastic energy term, $E_{El_2}$, given by

$$\mathrm{E_{El_2}} = 1.5\lambda_{100}(\mathrm{C_{11}} - \mathrm{C_{12}})(\varepsilon_{11}\mathrm{m_1^2} + \varepsilon_{22}\mathrm{m_2^2} + \varepsilon_{33}\mathrm{m_3^2}) -$$

$$6\lambda_{111}\mathrm{C_{44}}(\varepsilon_{12}\mathrm{m_1m_2} + \varepsilon_{23}\mathrm{m_2m_3} + \varepsilon_{31}\mathrm{m_3m_1}). \quad [6]$$

In the current MC simulation approach, the total magnetic energy of the system is represented as the sum of the energy contributions arising from Eqns. 1 through 4. The external field H was set to zero in the simulations. The Metropolis algorithm was used for the acceptance probability, *p*, defined as

$$p = 1.0 \quad \Delta E \leq 0.0\,, \qquad p = e^{\frac{-\Delta E}{kT}} \quad \Delta E > 0.0\,, \quad [7]$$

where $\Delta E$ is the change in the energy due to an attempted MC move. The two MC moves considered are as follows: (1) a random rotation of the magnetic moment of a single atom and (2) a cluster move that involves the rotation of all atoms in the simulation domain by a specified angle. The MC simulations were carried out in a parallel computing environment using Message Passing Interface (MPI) for inter-process communications. Although parallel computing allows simulations to be carried out in large volumes, it would still be prohibitive to extend the atomic-level simulations to micrometer length scale, especially because of the $O(N^2)$ nature of the $E_{dip}$ calculations. Therefore, a scaling law was used for $E_{dip}$ and $E_{ex}$ so that the scaled values could be used in coarse-grained simulations. The scaling procedures are described in [1].

Recent experiments to characterize the effect of applied tensile stress on domain refinement used tensile stresses up to roughly 60 MPa that correspond to elastic strains of the order of 0.03. In the current simulations, a uniaxial strain of 0 and 0.05 was used to distinguish the effect of strain on domain wall morphology. In all the simulations, the initial orientations of the magnetic moments were randomly assigned and the evolution of the moments was followed as a function of the simulation time. The lattice temperature in the simulations was scaled by the scaling factor corresponding to the exchange energy. In the simulations, a scaling factor of $n$ corresponds to a real size of $n \times l_s \times lp$, where $l_s$ is the number of lattice points in the simulation domain along a coordinate axis, and $lp$ is the lattice parameter of Fe.

The formation of the domain structure in a simulation volume of 64 × 16 ×16 lattice points with $n$ = 501 in the absence of external strain is shown in Figure I.1.1. The simulations were carried out for a BCC crystal in the [100]<001> orientation. The domain structure is characterized by the presence of two parallel domains in the x-direction along with closure domains where the magnetic domains are turned through 90 degrees. However, when an external strain of 0.05 is applied, the closure domains disappear and the parallel domains become more stable. This is in agreement with results from previous studies. Simulations were then extended to larger domains and with different levels of scaling in order to follow the evolution of the domain structure with simulation volume. Figure I.1.2 shows the extension of the simulations to a 64 × 64 × 16 simulation volume with $n$ ranging from 501 to 3001. The domain structure for $n$ = 1001 is marked by three parallel domains aligned along the x-direction, along which the external strain is applied. When $n$ is increased to 2001, a domain structure of four stripes is obtained. When $n$ is increased to 3001, a domain structure of three striped domains is obtained, with an increase in the domain width. The simulations indicate that the domain width is a function of the thickness of the simulation domain. In order to obtain the domain in a sheet of 0.3 mm in thickness, the corresponding $n$ value of approximately 66,000 should be used as the scaling factor. The estimated domain width based on a linear interpolation of the results to $n$ = 66000 yields a value of 0.435 mm. The simulation results have been successfully compared against measurement of magnetic domains in grain-oriented Fe-3%Si-steel using neutron diffraction and submitted for a journal publication [1].

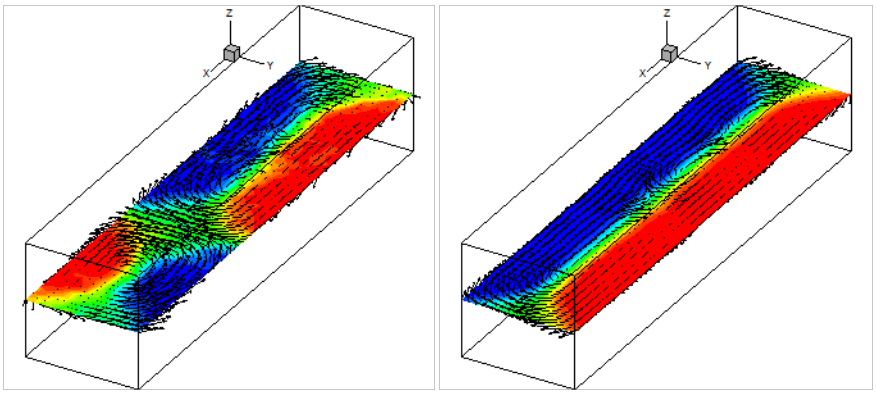

Figure I.1.1 - Domain structure in 64 × 16 × 16 simulation volume with n = 1001 in the absence of external stress (left) and in the presence of strain $\varepsilon_{xx}$ = 0.05 (right)

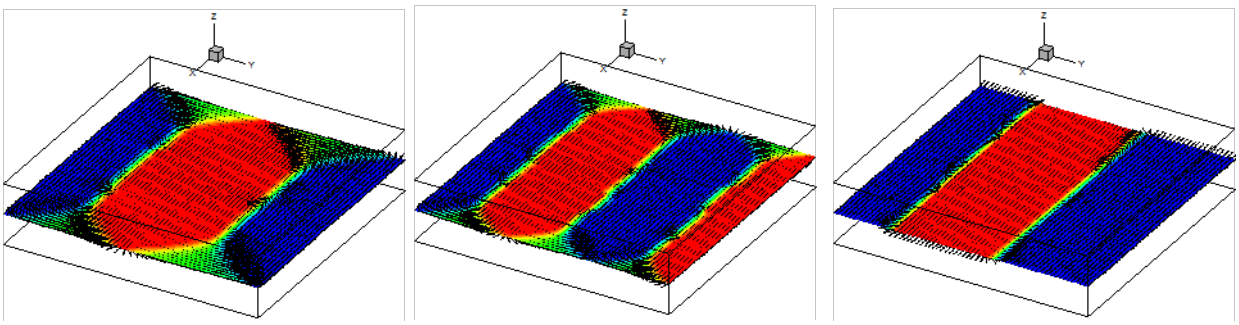

Figure I.1.2 - Domain structure in 64 × 64 × 16 simulation volume with elastic strain εxx = 0.05 and with (left) n = 501, (middle) n = 1001, and (right) n = 3001. The domain width is seen to increase with the thickness of the Fe in the z-direction.

## Conclusions

Scaling laws have been developed to enable large scale simulations of magnetic domains and their behavior. This work correlates with the development of a Fast Multipole Approach to speed up the dipole-dipole interaction calculations. As part of this effort, we have completed partitioning of the input data (which are the dipoles) across participating processors on a distributed memory machine, and implementing a global data indexing mechanism. These steps are undergoing benchmarking based on synthetic data. The global data indexing mechanism has been implemented using Morton ordering (or z-space filling curve) to map the three-dimensional data into a one-dimensional linear array using bit-interleaving of the bit representations of their coordinates. Furthermore, a parallel tree construction algorithm has been implemented. It has multiple components including writing parallel sorting algorithms and routines that can carry out bit-level algebra to maintain and query parent-child information in the hierarchical tree data structure. These routines have been implemented as part of developing the overall parallel tree construction algorithm. The next step is to integrate the governing equations of dipole-dipole interaction into this parallel architecture. While expansion and improvement of magnetic domain simulation code continues, results have already provided useful feedback regarding the behavior of magnetic domains and domain wall propagation resulting from external fields, various microstructural properties, and residual stress/strain in soft magnetic materials.

## Key Publications

1. “A new scaling approach for the mesoscale simulation of magnetic domain structures using Monte Carlo simulations,” *Journal of Magnetism and Magnetic Materials*, 432: 42–48 (2017).

## I.2 Non-Rare Earth Electric Motor R&D

**Tim Burress, Principal Investigator**
Oak Ridge National Laboratory
1 Bethel Valley Road
Oak Ridge, TN 37831
Phone: (865) 576-3654
E-mail: burressta@ornl.gov

**Susan A. Rogers, Technology Manager**
U.S. Department of Energy
Phone: (202) 586-8997
E-mail: Susan.Rogers@ee.doe.gov

Start Date: October 1, 2016 End Date: September 30, 2017
Total Project Cost: $673,000 DOE share: $673,000 Non-DOE share: $0

### Project Introduction

Motor design optimization in FY 2017 was conducted with commercial FEA packages as well as in-house custom-designed tools in combination with other software packages for parametric optimization algorithms and state space simulations. The progress and results in the area of motor design are discussed after the following sections describing the parallel efforts in materials R&D. These parallel efforts are ultimately in support of improving motor designs by developing or facilitating the use of more efficient materials and by conducting fundamental research to improve the modeling accuracy of electrical steel characteristics.

Automotive manufacturers most commonly use interior permanent magnet synchronous motors (IPMSMs) for electric vehicles (EVs) (including HEVs, battery EVs, and range-extended EVs) because of their high efficiency and high power density despite the high costs associated with rare earth (RE) PM material. Motors with low-cost magnets or no magnets (such as synchronous reluctance or induction motors) struggle to match torque and power performance when compared to an RE PM motor of similar size and mass. Efforts on the Non-Rare Earth Motor R&D project directly correlated with Electric Motor Performance Improvement Techniques project, with the former involving the development of fundamental modeling tools and fundamental analysis of alternative motor solutions and the latter project directly apply these modeling tools and findings to perform detailed motor design optimization.

### Objectives

The objective of this project is to improve electric machine modeling techniques at various stages of the design process. More accurate state-space models help improve the development of optimal control strategies as well as machine analysis during the design phase. Improving machine losses models helps increase design efficiency and power density, and brings simulation predictions closer to experimental characterizations of prototypes.

### Approach

Two methods of modeling improvements for electric machine modeling were developed. A general nonlinear direct quadrature (DQ) modeling method was developed for fast and accurate evaluation of simulated motor characteristics under voltage and current constraints. Advancements were made toward our goal of including hysteresis characteristics in finite-element simulation of motors as a proof-of-concept technique was used to simulate toroid inductors in resonant circuits. Development of our HPC code focused on advancing to a state where basic results and parallelism can be demonstrated.

## Results

*High Fidelity DQ Modeling of Synchronous Machines*

The standard direct-quadrature-zero model describes the fundamental behavior of synchronous machines combining saliency and permanent magnets under the assumptions of linear magnetics and sinusoidal airgap flux density. These assumptions lead to some well-known shortcomings. The linearity assumption causes the model to break down at high flux levels. The assumption of sinusoidal variation of the magnetomotive force and rotor saliency excludes torque-ripple and flux-linkage harmonics. This omission affects modeling of the interactions between the machine, current regulators, and voltage source inverter. Coupling between the d- and q-axis flux-linkages is similarly absent, altering the optimal maximum torque-per-amp and maximum torque-per-volt operating regions.

We have developed a method that uses a three-dimensional expansion of the d- and q-axis flux-linkages and torque waveforms to accurately include all these phenomena in a general-purpose model. The waveform values are interpolated using the current vector magnitude, current vector angle, and rotor position as independent variables. A tensor product basis is formed using trigonometric functions for the angular dimensions and Chebyshev polynomials in the current magnitude dimension. A correspondence between Chebyshev polynomials and the discrete-cosine transformation guides the choice of a nonuniform grid of collocation points in the current magnitude dimension. A filtering operation based on a user-supplied error tolerance was also developed to reduce the cardinality of the basis set. This allows the dynamic equations to be solved more quickly without sacrificing much accuracy.

*Continuum Modeling of Hysteresis and Eddy Current Losses*

Finite-element analysis models of electric machines rely on lossless relationships between magnetic flux density (B) and magnetic field intensity (H) in ferromagnetic material. These relationships are described by a single B-H curve, which possibly depends on "external" factors such as temperature or stress. Real ferromagnetic materials are lossy, with hysteretic B-H relationships. This characteristic is more accurately described by a set of loops parameterized by the peak B-field experienced over one cycle. Furthermore, ferromagnetic materials are conductive, resulting in eddy currents at appreciably high frequencies. Therefore, eddy currents introduce frequency dependence into the B-H loops.

We have been pursuing the development of simulation techniques to integrate hysteresis characteristics directly within finite-element simulations to improve the accuracy of motor models. As a first step, we successfully demonstrated high-accuracy magnetic simulations of ferromagnetic toroid inductors. Our approach utilizes the Preisach model of hysteresis to capture low-frequency B-H loop behavior. Figure I.2.1 depicts the Everett function identified from an M19 ring core sample which is used to evaluate the B-H relationship. The Preisach model is quite general purpose and can be applied to a range of materials including electrical steel, ferrites, and permanent magnets. Extensions of the standard scalar model exist to capture rotational hysteresis and more accurately model minor loops.

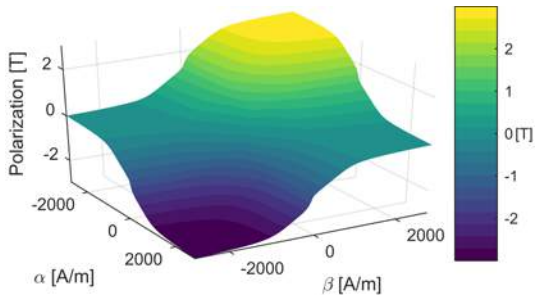


Figure I.2.1 - Everett function identified from an M19 electrical steel ring core sample used to evaluate the hysteresis characteristic during finite-element simulations.

The loop-widening phenomenon associated with eddy currents is captured through dynamic (transient) simulation of the core cross section with a non-zero electrical conductivity. In this approach, eddy currents develop naturally based on the geometry of the core and require no special treatment with respect to waveform shape or frequency. Only one set of measurements (represented by the Everett function) per material is required for analysis. The paper on our initial efforts demonstrates less than 5% error between simulated and measured resonant circuit behavior with no model tuning requirements.

*HPC Code Development for Electric Machine Optimization*

The minimum required features of geometry description, meshing, materials, physics, and post-processing for 2D simulations have been implemented to demonstrate a working motor simulation. Parallelism of the code has been demonstrated to scale on a single-node, multicore CPU system using OpenMP, and work has begun on conceptual models for scaling to multi-node systems using MPI. Over 2 million core-hours were acquired to perform electric machine simulation and optimization on ORNL's supercomputers.

Electric machines have complex geometric configurations describing material interfaces, even in two-dimensional cross sections. Further, equivalent geometries can be described by nonidentical constraint conditions. For example, a circle can be described by any three points on the circumference or equivalently by any three unique lines tangent to the circle. Model geometry description is one of the most time-consuming tasks that an engineer must actively perform in the design of a motor. Therefore, an easy-to-use tool must be intuitive and handle any possible combination of constraints which results in a valid geometric entity.

Conversely, given a set of geometric constraints, more than one entity may exist that satisfies all the constraints, even if the geometric entity under consideration is fully defined. When viewed as a purely mathematical entity, the equations describing constrained geometry are nonlinear and have multiple solutions. As with all multiple solution problems, two factors will determine the ultimate solution: (1) the initial condition and (2) the solution algorithm. The software relies on the engineer to describe an initial geometric configuration that is topologically representative of the desired solution. (This is true of all CAD programs.)

The software, in turn, must be developed to find a geometric entity that is "close" to the initial description in an intuitive way. That is, the algorithm should not do anything surprising. The internal geometry software does this through a robust description of the individual geometric constraints, which gives rise to naturally well-conditioned problems that can be solved reliably using Newton's method for nonlinear equations. Basic line and circular arc segments have been implemented along with length, angle, and tangency constraints and other minor constraints that are required for various technical reasons.

Meshing is a well-studied subject, and the literature on various techniques is extensive. Electric machine simulations impose unique requirements on meshing software that must be handled gracefully and without undue computational burden. First, disjoint boundaries are often mapped onto one another for the purposes of reducing the size of the computation domain using various boundary conditions. Those mapped boundaries are most easily implemented when the mesh on those boundaries is similarly mapped. Finite-element analysis of motors also requires simulation of rotor motion, which requires modification of the mesh in some way during the solution process. Our meshing software has adapted well-known algorithms for fast refinement and implementation of boundary conditions and rotational motion with ease.

Several other libraries implement various important functions related to the electric machine finite-element simulation process. A "materials" library is responsible for describing the nonlinear B-H curve and evaluating the characteristic during the solution phase. An "element" library is responsible for describing the solution basis functions and their derivatives. A "physics" library is responsible for translating element basis functions and derivatives into a suitable representation of phenomenon under study (e.g., magnetics). A "post-processing" library translates the simulation results into scalar quantities of interesting (e.g., flux-linkage, torque).

Figure I.2.2 shows a flux density simulation of a synchronous reluctance machine performed with one version of the code under development. The simulation itself demonstrates (1) magnetic saturation, (2) antiperiodic boundary conditions, (3) magnetic insulation boundary conditions, (4) rotational motion, and (5) post-processing. While the bulk of our code is in C++, we have developed our own file formats and post-processing tools using Python and Matplotlib, which are both free and ubiquitous tools available for most Unix platforms.

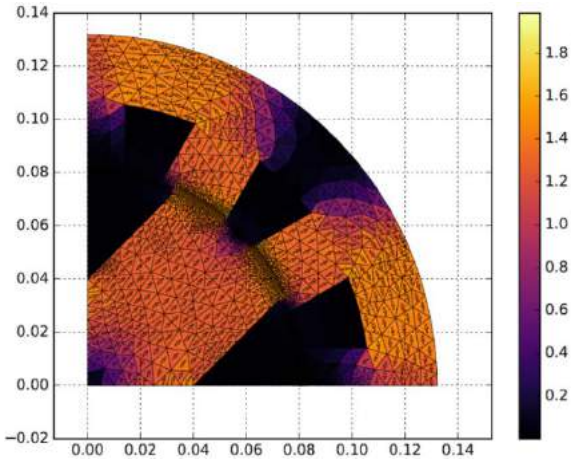


Figure I.2.2 - Simple synchronous reluctance machine flux-density simulation using the software under development. The plot was generated using Python/Matplotlib.

The most efficient use of computational resources on large systems can be achieved by viewing them hierarchically. On the lowest level, each node is composed of (typically) one or two processing units (e.g., CPU, GPU) and a chunk of local memory (e.g., DRAM) that can be accessed by the processing units over a high-speed bus (e.g., PCIe). The next highest level is composed of blocks of nodes which may communicate over an external bus (e.g., Infiniband).

A characteristic of electric machine simulations is that, for a given geometric configuration, many different excitation levels must be simulated to gain a complete understanding of the performance. This is a type of one-to-many relationship where the representation of the physical object can be read from to produce multiple outputs. Because the description of the physical object in terms of geometric constraints, meshes, and matrices tends to be somewhat complex, they are best contained to a single node until computational bottlenecks dominate the internode communication overhead. We have demonstrated that typical 2D electric machine finite-element problems focusing on a single geometry with multiple excitations will scale almost linearly on single processor nodes containing 16 physical cores per CPU.

Our future work will focus on using MPI to simulate different machine designs on different nodes, with each node then exploiting its own internal parallelism. In this strategy, MPI will be used in the context of an optimization algorithm. Each node will receive a small set of parameters that act like instructions to construct the geometry of a machine model. The geometric parameterization of the machine acts as a sort of decompression algorithm for the parameter packet, which reduces communication overhead. All analysis of that machine will occur on the node on which it is constructed. Once complete, only the performance parameters must be communicated back to the head node controlling the optimization process.

## Conclusions

Improving the design, modeling, optimization, and control processes for electric motors requires more accurate tools at all stages of development. This project advanced two such techniques. The first was a high-fidelity state-space modeling technique which can be used for accurate prediction of machine behavior under real

controller behavior, including the effects of finite-switching frequency. The second was a proof of concept implementation of a high fidelity scalar hysteresis model. This was used to predict the behavior of toroid inductors in resonant circuits which is highly sensitive to accurate loss models. Accuracy greater than 95% was achieved for inductors of two different materials operating over a wide range of frequencies. Our ultimate goal is to integrate this and similar models into our HPC motor optimization framework. The development of the HPC code progressed significantly over the year and is nearing the point where it can be used for initial motor design and optimization.

## Key Publications


1. J. Pries and T. Burress, “High fidelity D-Q modeling of synchronous machines using spectral interpolation,” *2017 IEEE Transportation Electrification Conference and Expo (ITEC)*, Chicago, IL, 2017, pp. 779–785. doi: 10.1109/ITEC.2017.7993368
2. J. Pries, L. Tang and T. Burress, "Continuum modeling of inductor hysteresis and eddy current loss effects in resonant circuits," *2017 IEEE Energy Conversion Congress and Exposition (ECCE)*, Cincinnati, OH, 2017, pp. 425-432. doi: 10.1109/ECCE.2017.8095814

## I.3 Electric Motor Performance Improvement Techniques

**Tim Burress, Principal Investigator**
Oak Ridge National Laboratory
1 Bethel Valley Road
Oak Ridge, TN 37831
Phone: (865) 576-3654
E-mail: burressta@ornl.gov

**Susan A. Rogers, Technology Manager**
U.S. Department of Energy
Phone: (202) 586-8997
E-mail: Susan.Rogers@ee.doe.gov

Start Date: October 1, 2016 End Date: September 30, 2017
Total Project Cost: $360,000 DOE share: $360,000 Non-DOE share: $0

### Project Introduction

Since hybrid electric vehicles (HEVs) were introduced to the market in the late 1990s, high power electric machines for automotive applications have been heavily researched. Automotive manufacturers most commonly use interior permanent magnet synchronous motors (IPMSMs) for electric vehicles (EVs) (including HEVs, battery EVs, and range-extended EVs) because of their high efficiency and high power density despite the high costs associated with rare earth (RE) PM material. Motors with low-cost magnets or no magnets (such as synchronous reluctance or induction motors) struggle to match torque and power performance when compared to an RE PM motor of similar size and mass. The first of two main efforts on this project was the research and development of methods and switching arrangements to expand the operation range and efficiency of motors for operation throughout various drive cycles. This includes considerations of cost, complexity, and manufacturability as a part of the system optimization. The second primary effort on the project involves the development of design strategies for reducing PM volume using reconfigurable windings. While reconfigurable winding approaches with IPMSMs were researched on this project, these approaches are applicable to almost all types of electric machines for both motoring and generating applications.

### Objectives

The primary objective of this project is to develop an electric motor without PMs that has a high power density, specific power, and operational efficiency. Key efforts to achieve this objective include advanced motor design, utilization of new motor modeling tools, and empirical verification.

### Approach

Synchronous reluctance motors without PMs were investigated to meet the DOE Electric Drive Technology (EDT) Program's performance targets for hybrid and electric vehicle electric motors. The difficulties associated with high-torque, low-power factor synchronous reluctance motors were overcome using a multispeed design to extend motor power delivery capabilities at high speeds. Initial simulation and optimization results indicate that the motor topology and winding switching strategy can meet the DOE EDT targets on a prototype basis. With further packaging and design optimization using technologies suitable for mass production, multispeed synchronous reluctance motors should be able to exceed those targets.
Motors free of permanent magnets typically have difficulty simultaneously achieving high-torque, wide constant power speed range (CPSR) operation, and low torque ripple. Switched reluctance motors can perform relatively well on the first two metrics, but torque ripple and noise are perceived to be a fatal flaw of these motors for automotive applications. Synchronous reluctance motors, which operate like interior permanent magnet (IPM) motors with the magnets removed, achieve inherently low torque ripple through a combination of rotor topology optimization and step-skewing.

However, it is difficult to match IPMs in both torque and power density due to the comparatively poor (highly inductive) power factor. One typically must choose either (1) high torque over a limited speed range, (2) constant power operation over a wide speed range with much lower peak torque capability, or (3) a larger motor that meets both requirements. The reason larger motors can achieve both high torque and good CPSR operation is due to magnetic saturation. The effectiveness of advanced current angle operation to maintain power as speed increases is related to the saliency ratio of the motor. As the rotor laminations become more saturated, the saliency ratio of the motor decreases. High torque density motors of any type operate with the magnetic circuit in saturation. Therefore, high torque density synchronous reluctance motors will necessarily have poor CPSR operation.

Despite these difficulties, synchronous reluctance motors have many attractive properties that make them worth pursuing. Inherently low torque ripple and noise have already been mentioned. They are also significantly cheaper due to the absence of expensive RE magnets. IPM motors are notorious for their "sweet-spot" efficiency characteristics due to trade-offs between high winding currents and high core losses because of the "always on" permanent magnets. Synchronous reluctance motors have lower core losses at high speeds and at low power at all speeds, resulting in good efficiency where IPMs may fall short.

The absence of permanent magnets also makes synchronous reluctance motors mechanically and thermally robust. The former is due to the simple rotor construction, and the latter is related to the sensitivity of permanent magnet material properties to temperature. Permanent magnet motors must be carefully designed to resist accidental demagnetization, the risk of which increases significantly with temperature. Minimizing permanent magnet mass in IPM motors can, in some instances, involve using supervisory controllers to de-rate motor performance specifications as a function of temperature to avoid magnet thermal failures. Synchronous reluctance motors have none of these issues.

Winding switching schemes have been investigated in the past to solve various issues related to both induction and surface mount permanent magnet (SMPM) motors. For induction motors, the issues typically revolved around line start scenarios in industrial settings where different motor characteristics are desirable during start-up and steady-state operation. Winding switching has been investigated for SMPM motors for extended CPSR operation. In a way, SMPM motors suffer the same drawback as synchronous reluctance motors: Achieving high torque density requires increasing the amount of permanent magnet flux coupling the windings, leading motors having large characteristics currents. This limits the effectiveness of current angle advance to achieve good CPSR operation due to poor (highly capacitive) power factor.

The synchronous reluctance design was optimized to operate in two modes: A low-speed, high-torque mode, and high-speed, high-power mode. The different operating modes are achieving by reconfiguring the number of turns: The high-speed mode has half the number of turns as the low-speed mode. Different methods can be used to achieve the turn doubling/halving. The method we chose fully utilizes all the copper in both high- and low-speed operation by changing the winding connections from series to parallel. This results in a doubling of the winding cross-sectional area in the high-speed mode and an improvement in high-speed efficiency.

Figure I.3.1 shows stator and rotor topology used for design optimization. The number of rotor flux paths and barriers was chosen based on design guidelines found during a literature review, recommending rotor paths equal the number of stator teeth ± 2 for optimal saliency and minimum torque ripple. Little benefit was found moving to more complex rotor geometries. We also decided on a step skewing strategy to eliminate stator slotting torque (12n) harmonics while minimizing the overall torque reduction associated with skewing. This leaves only the sixth torque harmonic (due to non-sinusoidal winding magnetomotive force) to minimize during the optimization process. Overall, there were 16 geometry optimization parameters: stator and rotor outer diameter, stator tooth width and length, and 12 other rotor topology parameters.

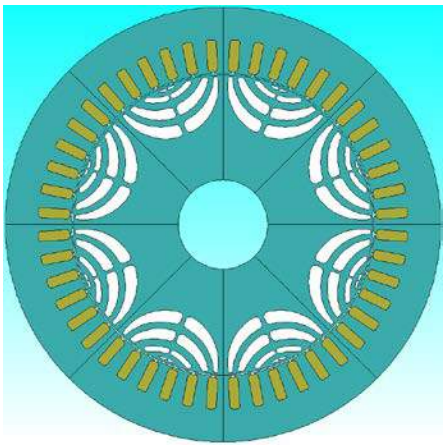

Figure I.3.1 - Synchronous reluctance motor stator and rotor lamination topology for design optimization.

An important consideration during the optimization process is the limits imposed by mechanical stress in the rotor. The widths of the bridges connecting the rotor flux paths determine the maximum operating speed of the motor. Wider bridges also reduce the saliency ratio of the motor, which reduces the overall torque and power output. Our design process included an analytical model of rotor stress in these key areas to optimally choose the bridge widths for each combination of topology parameters. As a result, each analyzed design is feasible with a mechanical safety margin of 2.

Figure I.3.2 shows the optimized design torque-speed and power-speed curves based on 2D analysis. The plots include data for both series and parallel mode operation, and the targeted design of 55 kW and 5:1 CPSR. The peak torque in series mode was overdesigned based on the 2D simulations with the expectation that 3D leakage and end-effects and manufacturing imperfections will reduce this value by around 10%. The power-speed curve on the right clearly shows the optimal series-parallel crossover point at around 6,000 rpm and 60 kW. This illustrates the benefit of the multispeed motor design for extending the peak power operation of synchronous reluctance motors to higher speeds.

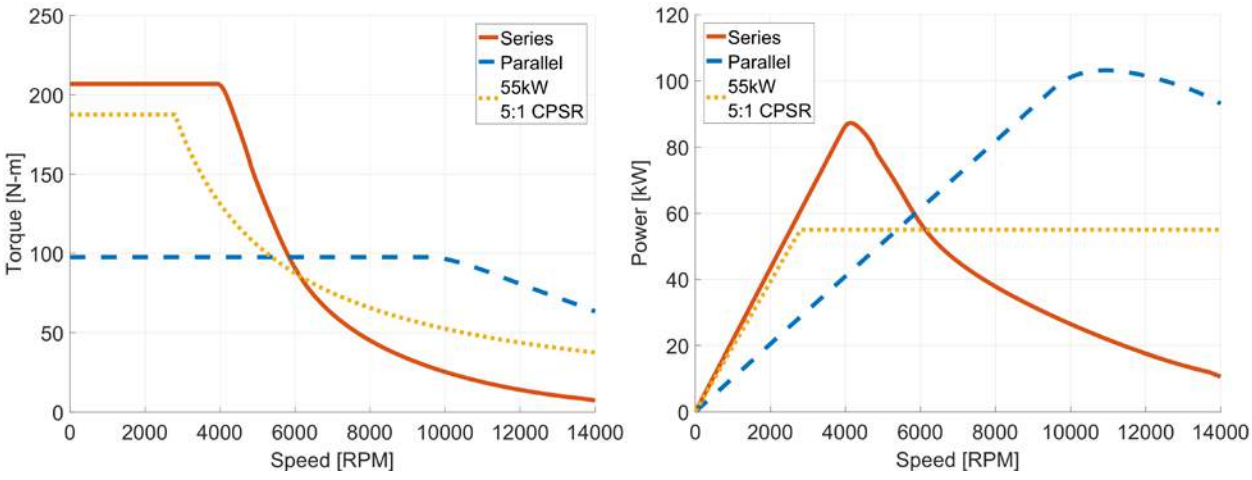


Figure I.3.2 - Simulated low-speed (series) and high-speed (parallel) torque-speed (left) and power-speed (right) curves.

Key metrics of the optimized design include a simulated peak power of 87 kW and 103 kW in series and parallel mode, respectively, and the total system volume of 13.3 L, which includes the total housing and estimated switchbox volume. This gives a peak power density of 6.54 kW/L in series mode and 7.74 kW/L in parallel mode. A key constraint on the operation was the inverter rating of 600 Vdc and 220 Arms phase current, which gives a similar apparent power rating as the US Drive specifications of 325 Vdc (nominal) and

400 Arms phase current (peak). Increasing the current rating would allow modification of our design to reach higher power in series mode.

A switchbox design using commercial anti-parallel thyristor modules was developed. To save time and effort, a previous switchbox printed circuit board (PCB) design was used. In this design, five anti-parallel thyristor modules are populated on a PCB to change the motor winding configuration to achieve high drive system efficiency. To meet the project requirements, two PCBs were needed, as indicated in Figure I.3.3. In PCB A, all five modules are needed; in PCB B, however, only three modules are needed. In serial mode, $K_{S1} \sim K_{S3}$ are on, and $K_{P1} \sim K_{P5}$ are off; in parallel mode, $K_{S1} \sim K_{S3}$ are off, and $K_{P1} \sim K_{P5}$ are on. In either mode, the conduction losses on one module can be calculated by

$$P_{CLR} = I_{PEAK} * \left(\frac{2}{\pi} V_{CERO} + I_{PEAK} * \frac{r_R}{2}\right) \qquad [1]$$

where $I_{PEAK}$ is the max device current (it is 130 Arms in serial mode and 100 Arms in parallel mode, respectively), and $V_{CERO}$ and $r_R$ are the equivalent voltage and resistance of the thyristor. The conduction losses of the switching devices in serial and parallel modes can be calculated as 400 W and 488 W, respectively. The junction temperature can be calculated in Eqn. 9, where P is the power loss, $R_{thm}$ is the module's junction to case thermal resistance, $R_{th}$ is the heatsink's thermal resistance, n is the number of the modules in each mode, and $T_C$ is the coolant's temperature. A two-pass liquid cooled heatsink with thermal resistance of $R_{th}$ = 0.04 °/W was selected.

$$T_j = \mathrm{P} * \left(R_{th} + \frac{R_{thm}}{n}\right) + Tc \qquad [2]$$

If 25°C coolant is selected, the maximum junction temperature in serial and parallel modes can be calculated as 72.3°C and 64.7°C, respectively. Both are well below the maximum allowable junction temperature of 125°C for the thyristor module. Two PCBs were populated and installed on the selected heatsink. A gate drive PCB is being designed and will be used in the dynamic switching test.

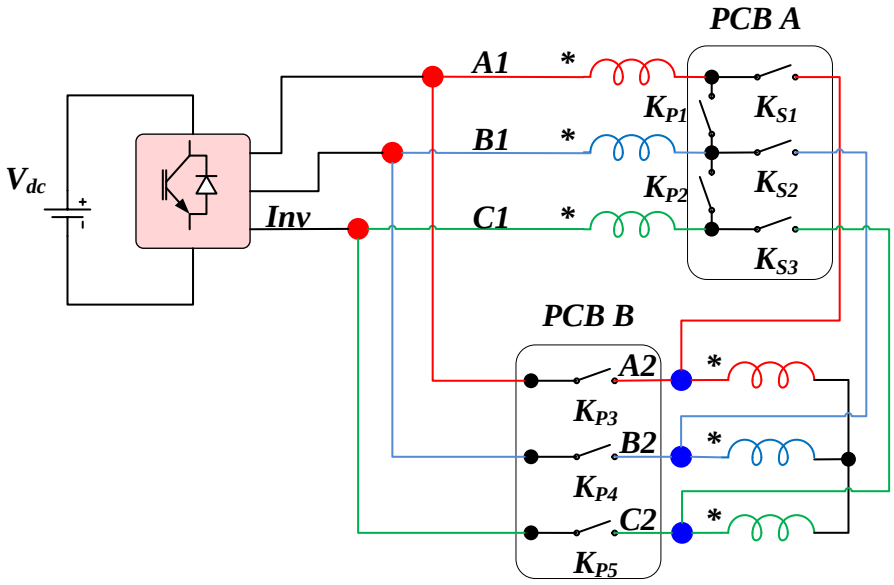


Figure I.3.3 - FY17 Switchbox design based a previous PCB design.

Stator and rotor laminations, shown on the left in Figure I.3.4, were fabricated using 0.35mm JFE 35JN210 electrical steel and a laser cutting process without post-annealing. Although performance degradations are incurred as annealing is avoided, residual stresses from laser cutting can be somewhat representative of residual stresses incurred during low-cost high-volume production. As previously discussed, to reduce torque ripple, several sets of rotor laminations were fabricated such that the lamination pattern is skewed with respect

to the locating key that interlocks with the shaft. The stator was inserted into a custom-made housing with a loose slip fit, and a thermal compound with a thermal conductivity of 3 W/mK was used to fill the void. While a loose slip fit yields lower overall thermal conductivity compared with what is achieved with a typical shrink-fit that is used in mass production, potential assembly issues were avoided, as trial and error may needed in shrink-fit situations where concentricity and airgap tolerances must be maintained. Plastic inserts were installed into the outer periphery of the housing to guide liquid coolant along a serpentine path, and while the inserts are plastic, coolant directly contacts the aluminum housing on both inner and outer sides of the inserts.

Figure I.3.4 - ORNL synchronous reluctance motor prototype stator/rotor (left), stator/rotor assembled and installed in housing (middle), and cooling insert (right).

The measured locked rotor torque versus electrical position for various currents is shown on the left in + Figure I.3.5. A torque of 155 N-m was observed with a current level of 270 Adc (~190 Arms equivalent). The ratio of peak measured locked rotor torque divided by DC current is plotted versus DC current on the right in Figure I.3.5. This plot indicates that no magnetic saturation occurs, as a negative slope indicates magnetic saturation as incremental increases in current result in less torque per current value. Plots in Figure I.3.6 show the maximum measured torque and power, respectively, for series and parallel operation. For series mode, the maximum torque of about 155 N-m was measured up to 4,000 rpm, resulting in a maximum series power level of about 65 kW. In parallel mode, a torque of 80 N-m was achieved up to a speed of 10,000 rpm, resulting in a power level of about 85 kW.

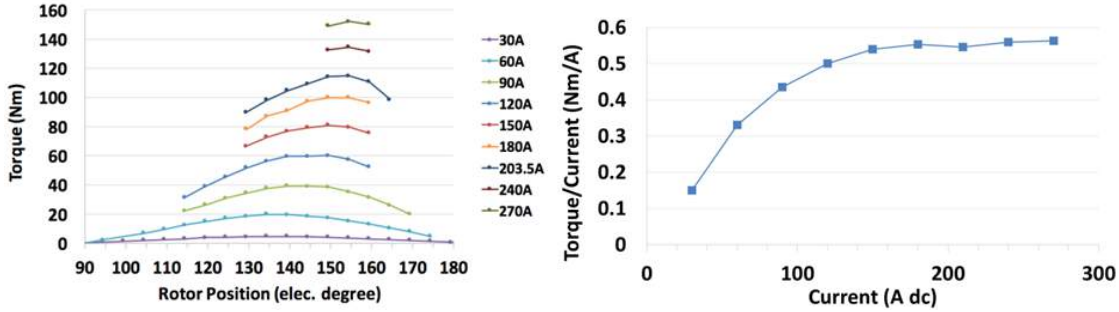


Figure I.3.5 - Measured locked rotor torque (left) and torque/current (right) with series winding configuration.

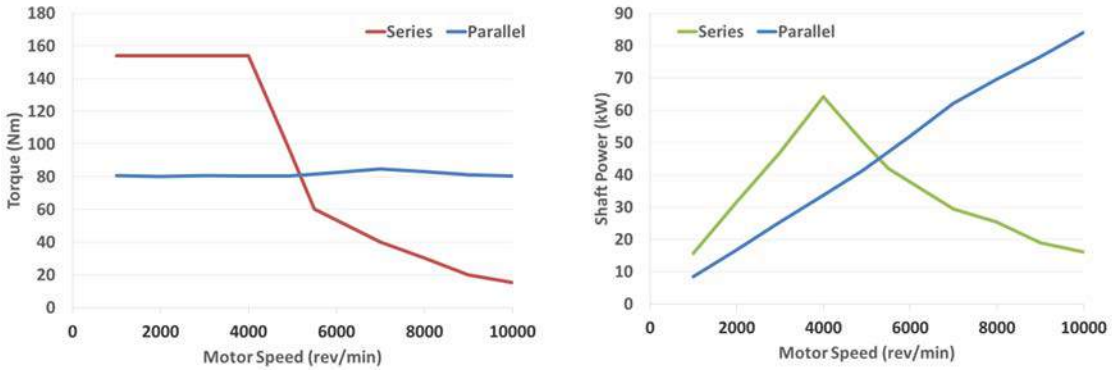


Figure I.3.6 - Measured torque (left) and power (right) for series and parallel winding configurations.

Efficiency measurements were logged for series and parallel operation throughout the torque-speed range, and the optimal efficiency for each point was chosen. The corresponding efficiency contours are shown in the plot in Figure I.3.7. It can be seen that almost all of the operation points above 3,000 rpm correlate with efficiencies greater than 90%, with maximum efficiency reaching above 93%. A blue line is superimposed over the graph, indicating that the motor reached above 50 kW for all speeds above 3,000 rpm. A series of continuous tests were conducted at various speeds and power levels. Prior to testing, six thermocouples were installed in the winding on each end of the stator. Test results from continuous tests at 10,000 rpm are shown in Figure I.3.7. During these tests, power was increased from 20 kW to 40 kW in 5 kW increments, and each power level was maintained for roughly 30 minutes. Operation at 35 kW for 30 minutes resulted in a steady state temperature of about 140°C, and operation at 40 kW resulted in temperatures rising above 150°C. Tests were concluded upon reaching 150°C even though the temperature rating of the insulation is 220°C to ensure further testing is possible. The temperature in the plot below corresponds with hottest of all 12 thermocouples in the winding.

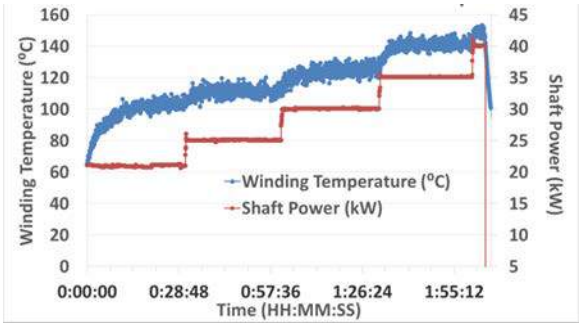


Figure I.3.7 - Optimal series/parallel efficiency contours (left) and continuous parallel mode tests and 10,000 rpm.

## Results

Our optimization study also revealed that longer stack lengths tend to lead to better torque and power density. We artificially decreased our stack length away from the initial (true) optimum design based on previous years' feedback requesting analysis focusing on shorter stack length designs. Increasing the slot copper fill using bar wound conductors would also allow a significant performance increase for our design, but this was beyond the scope of our analysis and prototype efforts for FY 2017.

## Conclusions

The simulated peak power of the synchronous reluctance motor was 87 kW at 3,900 rpm in series mode and over 100 kW at 9,500 rpm in parallel mode. A summary of key simulated performance metrics is given in Table I.3-1. Results for ORNL's ferrite prototype from FY 2016 are also included in the table. Additionally, metrics associated with the measured power of 64 and 84 kW are also included in the table. DOE 2020 targets for power density, specific power, and cost are 5.7 kW/L, 1.6 kW/kg, and $4.7/kW, respectively. It can be seen

that the DOE cost and power targets are met by the synchronous reluctance motor, although the motor has limited torque production capability. Overall, the ferrite motor yields slightly higher specific power, but the synchronous reluctance motor yields the most cost-effective solution.

This work has demonstrated that it is possible to design a synchronous reluctance motor that achieves peak power density and specific power targets without using expensive magnets or exotic lamination materials. However, challenges still remain as the performance notch between series and parallel modes may not be acceptable in some platforms, and switch-box costs per kW will be higher if the required peak power level is considerably lower (e.g., 30 kW). Furthermore, operational efficiencies were reasonable for a first prototype, but higher efficiencies are desirable.

Table I.3-1 - Measured performance data comparison

| | Speed (RPM) | Peak Power [kW] | Power Density [kW/L] | Specific Power [kW/kg] |
|---|---|---|---|---|
| | **DOE Target** | **55** | **5.7** | **1.6** |
| **ORNL Ferrite Prototype** | 10,000 | 103 | 10.3 | 3.1 |
| **ORNL Synchronous Reluctance Prototype** | 10,000 | 84 | 6.3 | 2.3 |

## Key Publications

1. L. Tang, T. Burress, and J. Pries, “A Reconfigurable-Winding System for Electric Vehicle Drive Applications,” presented in June 2017 at the IEEE Transportation Electrification Conference (ITEC), Chicago, IL.

## I.4 Integrated Wired Charger with High Frequency Boost Converter

**Zhiqiang (Jack) Wang, Principal Investigator**
Oak Ridge National Laboratory
National Transportation Research Center
2360 Cherahala Boulevard
Knoxville, TN 37932
Phone: (865) 946-1581
E-mail: wangz@ornl.gov

**Susan A. Rogers, Technology Manager**
U.S. Department of Energy
Phone: (202) 586-8997
E-mail: Susan.Rogers@ee.doe.gov

Start Date: October 1, 2016 End Date: September 30, 2017
Total Project Cost: $600,000 DOE share: $600,000 Non-DOE share: $0

### Project Introduction

Efficiency improvement, volume and weight reduction of passive components, high power density, and overall cost reduction of the power converters are expected features for electric vehicles to meet the DOE EDT targets. An integrated converter, combining and re-using some charging components and powertrain components can reduce converter volume and weight with higher power density. Others have also worked on similar research topics. The focus here is on an integrated converter that contains both a drivetrain boost converter and an isolated dual-active-bridge (DAB) onboard charger. In the integrated converter, the boost inductor is realized by the magnetizing inductance of the DAB transformer. The DAB secondary side transistors are shared with the boost converter, reducing the total number and semiconductor area of power devices. The existing battery management system contactors are used for reconfiguration. No additional mechanical or solid-state switches are required for the converter operation in different modes, saving power dissipation, cost, and size.

For powertrain operation, the interleaved boost converter has been widely used for high power operation. It helps to reduce electromagnetic interference and lower current ripple at the powertrain high-voltage (HV) bus and also helps to increase the power density of the converter. For isolated battery chargers, DAB double-sided inductor-capacitor-capacitor resonant converters and phase shift full bridge converters are commonly used. Due to fixed frequency operation, lower stress on the switches, zero voltage switching (ZVS) operation and bidirectional power flow capability, DAB is gaining attention as an isolated DC-DC converter for onboard chargers.

### Objectives

The overall objective of this project is to design and develop an HV, wide-bandgap (WBG) device based on a 30 kW wired integrated charger with embedded high frequency DC-DC boost converter. This project is targeted toward the application of WBG technology and novel circuit topologies with advanced packaging to address inverter cost, weight, volume, and efficiency goals. Specific research and development efforts in FY 2017 include new circuit topology development for the wired integrated charger and high-frequency, high-density boost converter design with advanced substrate layout and packaging techniques. The new concepts developed under this project will increase the power density and decrease the volume and weight for electric vehicle traction-drive systems and will achieve the DOE 2020 weight, volume, and efficiency targets.

### Approach

The goal of this research is to reduce the size and weight of battery chargers for electric vehicles to meet 2020 DOE power density and cost targets. In this project, a thorough literature review was conducted to identify the

technology gaps in development of commercial high power density battery chargers. Based on the literature review, a novel wired charger circuit topology is proposed to integrate more functionality with a lower component count, thus reducing the volume and cost of the active and passive components. The operating principle of the proposed topology is validated through circuit simulation.

In addition, WBG devices, specifically silicon carbide (SiC) and gallium nitride (GaN) semiconductors, are emerging technologies that enable operation at higher temperatures and frequencies with efficiency and reliability improvements. The development of WBG technology promises to help achieve cost, weight, and volume goals, as well as DOE Vehicle Technologies Office targets. WBG technology assessment performed under this project will help determine when a viable market introduction of these devices for automotive use could occur. By using WBG power modules based on advanced packaging technology, the overall volume and weight of the proposed wired charger topology are expected to be further reduced.

## Results

### *Integrated Wired Charger Topology*

The proposed integrated converter architecture, derived from the conventional architecture, is shown in Figure I.4.1. In conventional electric vehicle (EV) power conversion architectures with an onboard charger (OBC), the charging and powertrain circuits are separate. During the charging operation, the battery contactors (S11–S12) are connected, and the EV is charged from the AC grid through the power factor correction circuit (PFC) and isolation transformer. The integrated converter combines the interleaved boost converter and isolated DC-DC converter. Because the PFC and the inverter of the proposed architecture are connected to the same DC bus, the HV DC bus capacitor can be shared. The same magnetic core is also used for the boost converter and the isolation transformer.

A circuit schematic of the proposed topology is shown in Figure I.4.1, where the charging and powertrain circuits are integrated into a single converter. The advantage of this integration is the reduction in weight and volume of magnetics, lower number of switches, and higher efficiency. The integrated converter can be reconfigured as a two-phase boost converter or DAB converter. To minimize loss and arcing possibility and maximize the lifetime of the mechanical contactors, the transitions must achieve zero current switching when the contactor is opened and ZVS when the contactor is closed. Additionally, to prevent interruption of power flow to the electric drive, transitions must be designed to allow the converter to immediately enter steady-state operation in the new mode without requiring settling time or a lengthy switching transient.

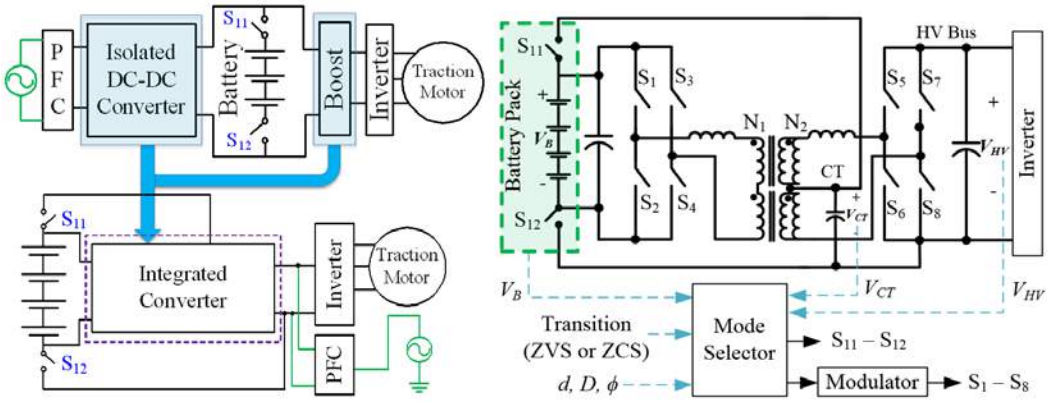


Figure I.4.1 - Proposed powertrain-charger architecture (left) and schematics of the integrated wired converter (right).

### *Integrated Wired Charger—Operating Principle*

The boost configuration of the proposed integrated converter is shown in Figure I.4.2. In the topology, eight active switches (S1–S8) and the two battery contactors (S11–S12) are used. The converter can work as an interleaved boost converter or DAB converter based on the connection of the contactors. During EV high-power powertrain operation, the converter works as an interleaved boost converter by connecting the S11 and

S12 switches. During light-load powertrain operation, the converter works as a conventional phase-shift modulated DAB as shown in Figure I.4.3. As the boost converter suffers from low efficiency at low-power operation and high conversion ratio, the DAB can additionally be used during drivetrain operation to increase the efficiency of conversion. The expected efficiency of the combined converter is shown in Figure I.4.4, using analytical loss modeling of the converter and the magnetics. The model shows that the DAB converter can significantly improve the efficiency in the high-output voltage, low power operating region, where the vehicle frequently operates in normal on-road operation. During EV charging, the converter transfers power from the HV bus to the battery by disconnecting the S11 and S12 contactors. In this way the converter provides galvanic isolation in the EV charging mode.

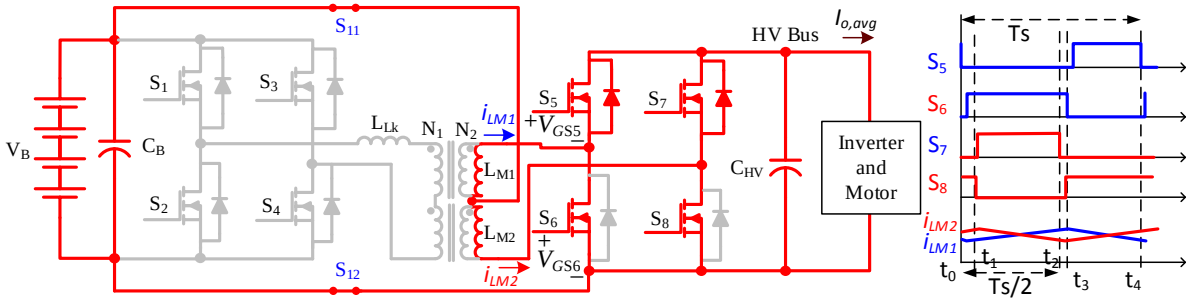


Figure I.4.2 - Proposed integrated EV DC-DC converter working as boost configuration.

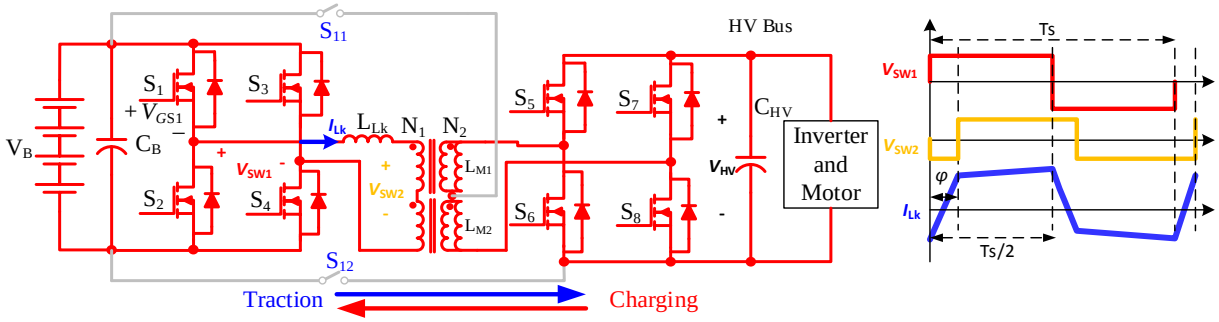


Figure I.4.3 - Proposed integrated EV DC-DC converter working as DAB converter.

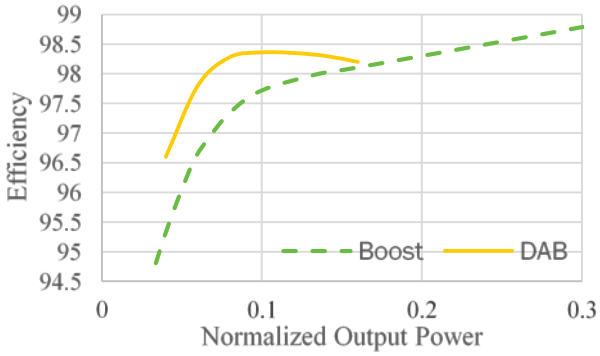


Figure I.4.4 - Analytical loss model for integrated converter during traction operation.

*Integrated Wired Charger—High-Frequency Boost Converter*

Based on the substrate designed in FY 2016, a SiC trench metal-oxide semiconductor field-effect transistor (MOSFET) power module based on the P-cell/N-cell concept was fabricated. In the power module, a dedicated Kelvin drain and source pins are designed to accurately measure the real voltage across the devices during switching transients. Figure I.4.5 shows the physical location of those sensing pins along with the location of gate signal pins in the overall module layout. A 3D-printed house is designed to press the direct-bonded copper (DBC) substrates in close contact with the baseplate. Thermal grease is used in between the bottom of the DBC and the top of the baseplate. All the gate signals and voltage sensing signals are connected to the gate drive board, which is mounted right on top of the module. The fabrication procedures include several steps: (1) die-attach and pin-attach (gate, source, and voltage sensing pins), (2) die interconnection using 5-mil wire bonds, (3) power terminal attach and house attach, and (4) encapsulation to protect the die and wire bonds from mechanical and chemical damage. The fabricated power module is shown in Figure I.4.5.

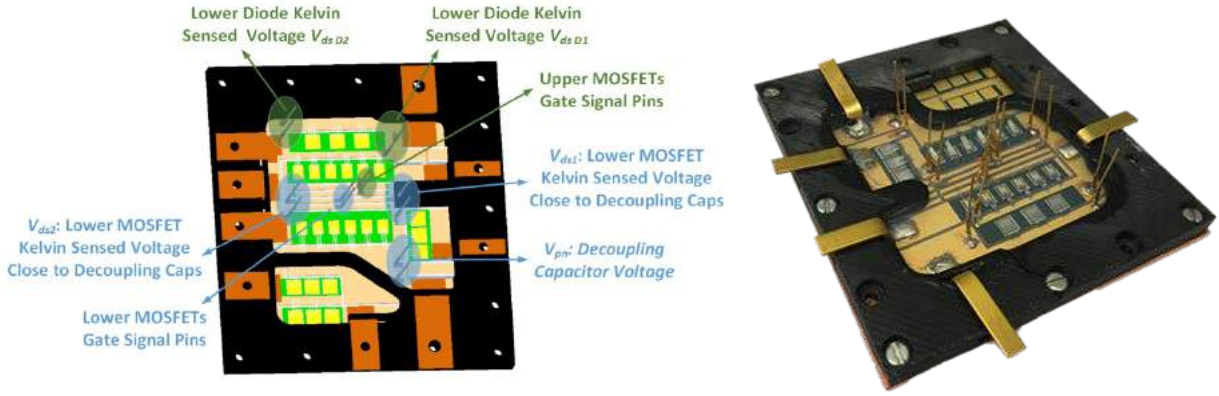


Figure I.4.5 - Power module based on P-cell/N-cell concept: mechanical layout (left) and fabricated phase-leg module (right).

In the fabricated power module, six 1200 V SiC trench MOSFETs and three 1200 V SiC diodes are paralleled as one switch. The output characteristics of a phase-leg module with one high-side switch and one low-side switch was evaluated. Figure I.4.6 illustrates the output characteristics of the power MOSFETs at various gate voltages and temperatures. It can be seen that the positive temperature coefficient of on-state resistance $R_{ds,on}$ (@ $V_{gs}$ = 20 V) is beneficial for current sharing under multichip parallel operation. Moreover, low $R_{ds,on}$ (@ $V_{gs}$ = 20 V) within a wide temperature and current range ensures low conduction loss and high power density operation.

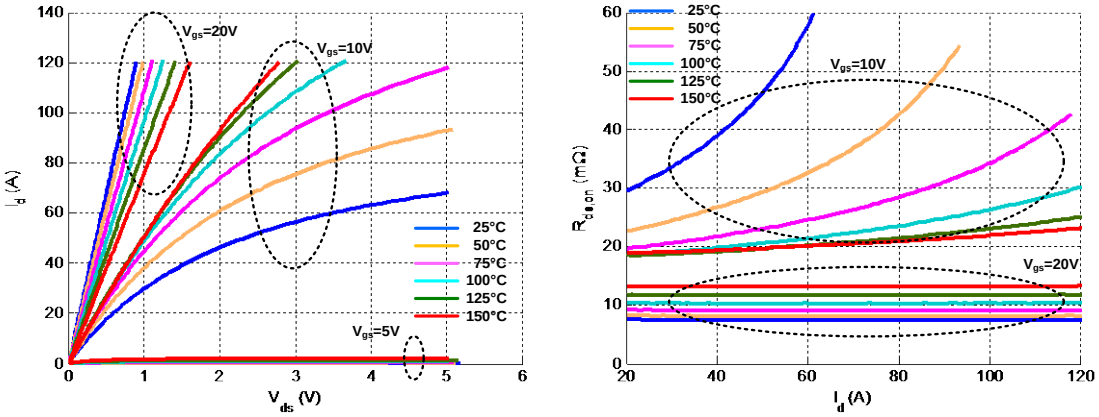


Figure I.4.6 - Low-side MOSFET output characteristic (left) and on-state resistance (right) under different case temperatures.

The parasitic inductance of the power module was extracted experimentally. Figure I.4.7 shows the extraction circuit diagram with N-cell connected to the double pulse test. The voltage across the decoupling capacitance $V_{PN}$ is compared with the real drain-to-source voltage $V_{ds}$ across devices, and the parasitic inductance values are derived from the voltage difference and drain current slew rate measured from the coaxial shunt.

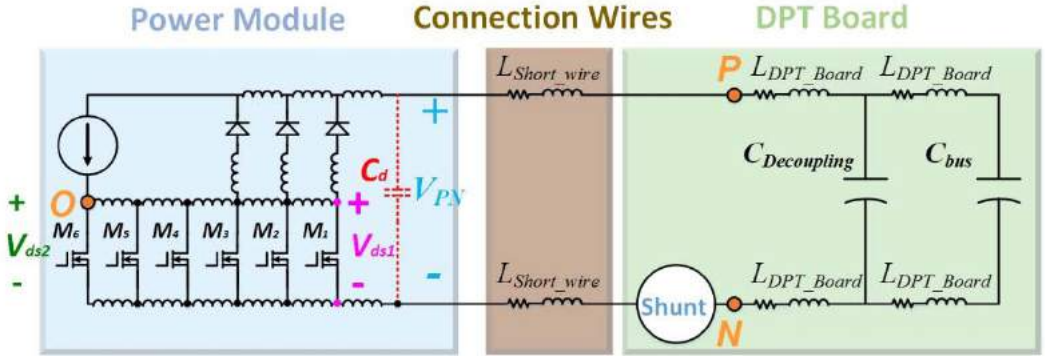


Figure I.4.7 - Circuit diagram for parasitic inductance extraction.

Figure I.4.8 illustrates the turn-off waveforms of terminal voltage $V_{PN}$, Kelvin-sensed voltage $V_{ds1}$, and load current $I_{ds}$. The current slew rate is calculated to be 3.18 A/ns, and the voltage difference is 19.09 V. The power loop parasitic inductance obtained from $V_{ds1}$ is calculated to be $L_{ds1} = 19.09\text{V}/(3.18\text{A/ns}) = 5.15$ nH. Compared with the simulation value listed in Table I.4-1, the value is between the parasitic inductance value of $M_1$ and that of $M_6$ but is closer to the value of $M_1$.

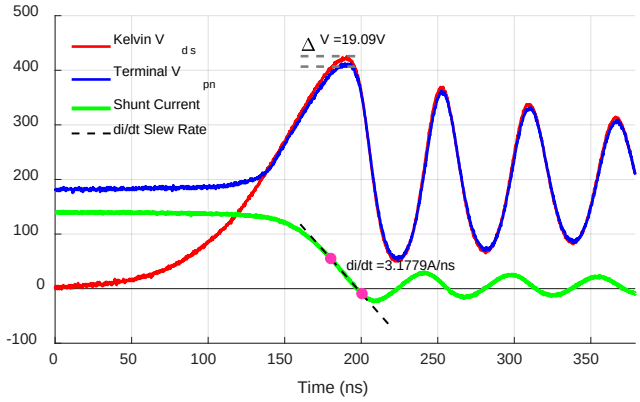


Figure I.4.8 - Turn-off waveforms for inductance extraction from $M_1$ drain-source voltage.

**Table I.4-1 - Comparison of power loop inductance for paralleled devices**

| Condition (@100 MHz) | $M_1$ | $M_2$ | $M_3$ | $M_4$ | $M_5$ | $M_6$ |
|---|---|---|---|---|---|---|
| Turn-Off Power Loop Inductance | 4.58 nH | 4.87 nH | 5.09 nH | 5.78 nH | 6.32 nH | 6.71 nH |

Similar extraction is implemented for the $M_6$, and the waveforms are shown in Figure I.4.9. Under the same switching condition (200 V, 138 A with $R_{g,ext} = 10\Omega$), a larger voltage spike is observed at $V_{ds2}$, and the parasitic inductance is extracted to be

$$L_{ds2} = \frac{20.97\text{V}}{\frac{3.19\text{A}}{\text{ns}}} = 6.62\ \text{nH}\,.$$

The experimental value is closer to the simulated value of $M_6$ because the sensing pins are physically adjacent to $M_6$. As a summary, power loop inductances extracted experimentally for the N-cell of the boost module range from 5.15 nH to 6.62 nH. This value can potentially enable the power module to operate at high-speed, high-frequency applications.

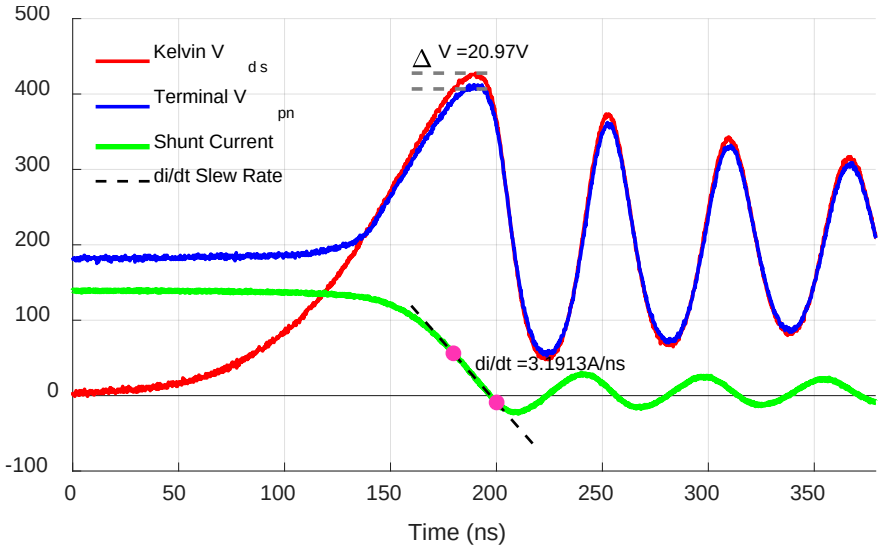


Figure I.4.9 - Turn-off waveforms for inductance extraction from $M_6$ drain-source voltage.

## Conclusions

In this report, an integrated bidirectional converter topology is proposed to save volume and weight for the conventional EV powertrain. The number of components is reduced through sharing of power semiconductor devices, gate drives, sensors, and control circuitry and through the sharing of magnetic components between the OBC and drivetrain DC-DC converter. In addition, a low-inductance multichip power module based on the P-cell/N-cell concept and integrated decoupling capacitance is developed for the boost converter of the proposed integrated charger. Simulation and experimental results show that the power loop inductances are around 5 nH. A comprehensive module evaluation shows that trench devices present lower conduction loss, faster switching speed, and more stable temperature behavior compared to a double-diffused metal-oxide semiconductor.

## Key Publications

1. Zhiqiang (Jack) Wang, Madhu Chinthavali, and Steven Campbell, “Characterization and comparison of planar and trench silicon carbide (SiC) power MOSFETs,” ECS Transactions, vol. 75, no. 12, October 2016, pp. 145–152.
2. Fei Yang, Zhenxian Liang, Zhiqiang (Jack) Wang, and Fred Wang, “Design of a low parasitic inductance SiC power module with double-sided cooling,” in Proc. IEEE Applied Power Electronics Conference and Exposition (APEC), March 2017, pp. 3057–3062.
3. Madhu Chinthavali and Zhiqiang (Jack) Wang, “30-kW all-SiC inverter with 3D-printed air cooled heatsinks for plug-in and full electric vehicle applications,” in Proc. 2017 International Conference on Silicon Carbide and Related Materials (ICSCRM), September 17–22, 2017, in Washington, DC, USA.

## I.5 Wireless Power Transfer Integrated Chargers

**Veda Prakash Galigekere, Principal Investigator**
Oak Ridge National Laboratory (ORNL)
National Transportation Research Center
2360 Cherahala Boulevard
Knoxville, TN 37932
Phone: (865) 946-1291
E-mail: galigekerevn@ornl.gov

**Susan A. Rogers, Technology Manager**
U.S. Department of Energy
Phone: (202) 586-8997
E-mail: Susan.Rogers@ee.doe.gov

Start Date: October 1, 2016 End Date: September 30, 2018
Total Project Cost: $600,00 DOE share: $600,000 Non-DOE share: $0

### Project Introduction

Weight, volume, and cost of the power electronic subsystems of the electric drivetrain continue to be a challenge to cost and performance of electric vehicles (EVs). The electric motor, inverter, charger, and converter are the components of the electric drivetrain of EVs. The charger performs the important function of safely transferring power from the grid to the EV battery, where it is used for driving the motor. Wireless charging provides a convenient and safe way to charge the EV battery and has the following advantages compared to wired charging:

- More suitable for automated charging without the active intervention of the user.
- Safer during inclement weather conditions.

Typically, wireless EV charging systems have power transferred to the EV battery controlled from the primary side power electronics (inverter and power factor corrector); however, having the ability to regulate power transferred to the battery from the secondary side has the following advantages:

- Increased interoperability as the power transferred can be controlled by the vehicle side electronics as well.
- The DC-DC converter acts as a buffer between the wireless power transfer (WPT) receiver and the EV battery; therefore, it can be used for fast protection of the EV battery in case of a fault.

The addition of a secondary side DC-DC converter adds to the mass and volume of the onboard components and increases the cost. The proposed architecture uses the DC-DC converter of the electric drive train, thus integrating the functionality and leading to effective reduction of weight, volume, and cost.
Previous wireless charging work has focused mostly on adding a wireless charger to the existing system. In this project, the focus is on integrating wireless charging into the electric drive system using some of the already existing common components and eliminating the duplicate ones.

### Objectives

The overall objectives of this project are

- To develop an optimized integrated wireless EV charging system that uses the boost converter of the electric drivetrain to meet the DOE Electric Drive Technologies (EDT) 2020 power density and cost targets.

- To have secondary side power transfer control to increase the interoperability of the wireless EV charging system.

## Approach

The important areas which were considered to envisage the wireless integrated charger architecture and achieve optimal power density of the onboard components are as follows.

- **Topology**—Based on the type of primary resonant network used, the primary side behaves as a current source or a voltage source. To achieve secondary side regulation, a primary side that is independent of the load or coupling coefficient variation is preferred as it simplifies the control strategy. An inductor-capacitor-inductor (LCL) or inductor-capacitor-capacitor-inductor (LCCL) compensation network has the feature of behaving as a load independent constant current source, thereby decoupling the secondary side from the primary side. An LCL resonant network requires a step-up transformer between the high-frequency inverter and the resonant network as the input impedance is high and is a function of the coil impedance. The input impedance of an LCCL resonant network can be adjusted by selecting the appropriate tuning capacitor, thus not requiring the use of a step-up transformer. An LCCL network is selected as the primary resonant network as it enables secondary side control and does not require a step-up transformer. A series resonant network is selected as the secondary network as it is simple, with a reduced onboard part count. Figure I.5.1 shows the onboard components of the proposed integrated wireless EV charger, and Figure I.5.2 shows the overall architecture of the integrated wireless EV charger.

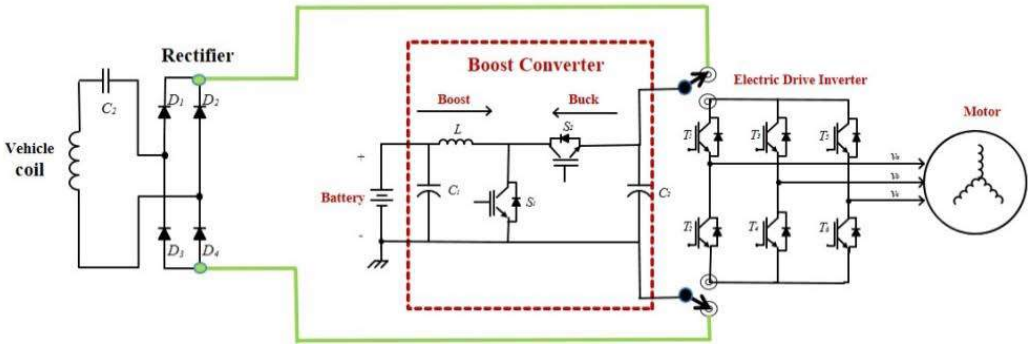


Figure I.5.1 - Onboard components of the proposed integrated wireless EV charger.

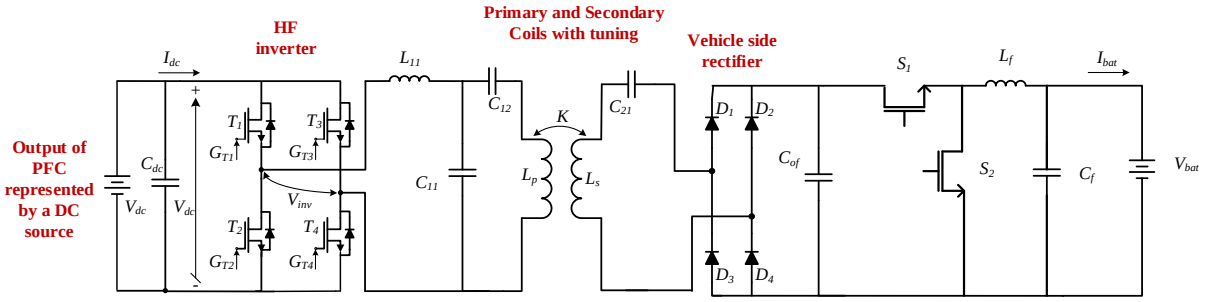


Figure I.5.2 - Integrated wireless charger with secondary side DC-DC regulator.

- **Coil development**—Circular and DD coils are two of the prominent coil designs used for wireless charging of EVs. DD coils have the advantage of a higher power transfer height capability of about half the diameter of the primary coil as compared to one-fourth the diameter of the primary coil for circular coils. Additionally, a DD vehicle coil can be made considerably smaller than the primary coil. This is

advantageous as it reduces the weight and volume of the onboard components of the integrated wireless charger.

- **Stability**—A stable WPT system must be able to tolerate changes in load and variation in coupling coefficient k. Changes in load or coupling coefficient k are reflected to the primary side as an impedance. The stability of the primary side can be evaluated by circuit simulations.
- **System Packaging**—Wide-bandgap–(WBG)-based DC-DC converters offer the advantage of high-frequency and high-temperature operation, leading to reduced heat sink and filter sizes. The proposed integrated wireless charger is designed to work with a WBG-based DC-DC converter in the electric drive train.

The specifications for the 11 kW integrated wireless EV charger are given in Table I.5-1. An LCC resonant network and series resonant network are selected as the primary and secondary tuning networks, respectively. The smallest possible vehicle coil that satisfactorily meets the output power and voltage requirements with minimal component stresses on the primary side is designed iteratively using finite element analysis (FEA) and circuit simulations. The primary coil consists of six turns of bifilar equivalent AWG 6 Litz wire, and the secondary coil is made up of eight turns of monofilar equivalent AWG 6 Litz wire. The dimensions of the primary coil are 770 mm × 750 mm × 28 mm and the dimensions of the vehicle coil without the power electronics are 480 mm × 368 mm × 32 mm.

Table I.5-1 - Specifications for 11 kW integrated wireless charger

| Parameter | Value |
|---|---|
| DC link or input voltage $V_{dc}$ (V) | 450 |
| Rated output power $P_o$ (W) | 11,000 |
| Output voltage range for rated 11 kW (V) | 300–400 |
| Resonant frequency (kHz) | 85 |
| Coil to coil power transfer distance range (inches) | 4–8 |

The maximum primary coil current is fixed to 80 A and is selected to have the capability to deliver 11 kW at the coupling coefficient corresponding to the highest power transfer height of 8 in. Table I.5-2 gives the primary and secondary resonant inductor and capacitor values.

Table I.5-2 - Primary and secondary resonant network component values

| Component | Value |
|---|---|
| $L_{11}$ (μH) | 10 |
| $C_{11}$ (μF) | 0.350 |
| $C_{12}$ (μF) | 0.005 |
| $C_{21}$ (μF) | 0.044 |

Figure I.5.3 shows the variation of predicted input current $I_{in}$, primary coil current $I_{pri}$, and output power $P_o$ as a function of normalized switching frequency $f/f_o$ for k corresponding to highest Z height of 8 in. From Figure I.5.3 it can be inferred that the resonant frequency $I_{pri}$~ 75 A and the output power $P_o$~ 12 kW. Figure I.5.4 shows the CAD model of the 11 kW optimized coils.

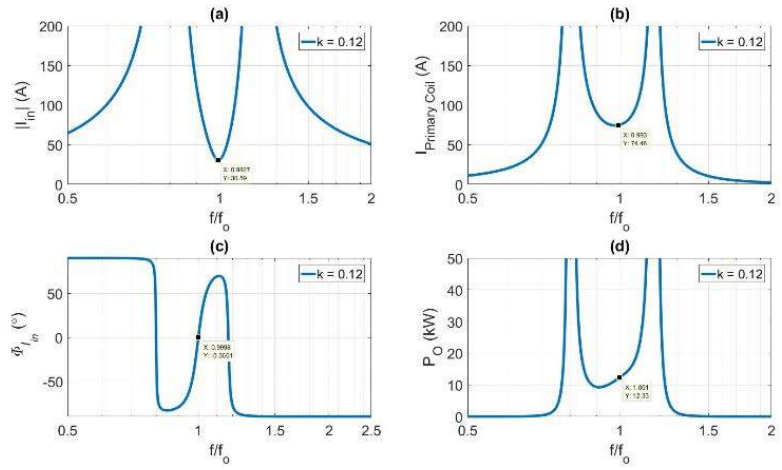


Figure I.5.3 - Predicted input current $\boldsymbol{I_{in}}$, primary coil current $\boldsymbol{I_{pri}}$, and output power $\boldsymbol{P_o}$ as a function of normalized switching frequency.

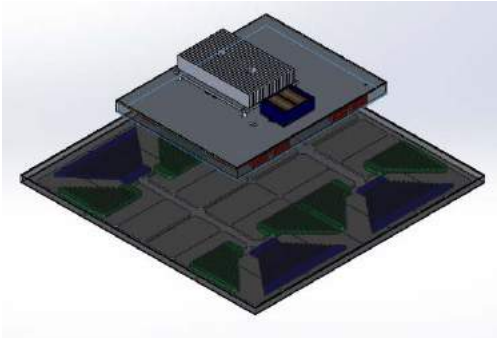

Figure I.5.4 - CAD model of the primary and optimized secondary DD coils designed for 11 kW operation.

High-voltage WBG devices can operate at higher temperature and frequency than conventional silicon devices. This leads to reduced heat sink size and filter components. This work proposes to use the WBG-based DC-DC converter present in a WBG electric drive train as the secondary side regulator. The WBG DC-DC converter is envisaged to operate at a switching frequency $F_s$ of 50 kHz. A filter inductance of $L_f = 200$ µH and $C_f = 250$ µF is selected. This falls within the range of values used for several commercially available EVs.

## Results

The optimized coil designed for 11 kW operation was simulated in JMAG, a commercially available FEA simulation tool. The optimized coils were also prototyped using 3D-printed coil holders and AWG 6 round Litz wires. Figure I.5.5 shows the CAD model of the designed optimized coils for 11 kW operation. Table I.5-3 gives the FEA and measured simulation results for the optimized DD coils.

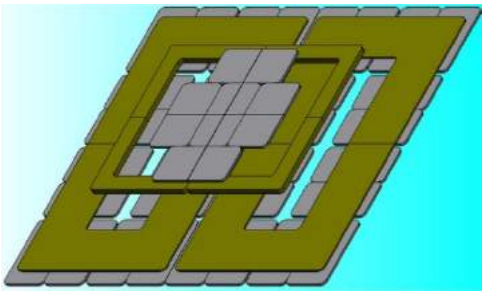

Figure I.5.5 - Model of the 11 kW optimized coil simulated in JMAG.

Table I.5-3 - FEA simulation results of the optimized 11 kW coils

| | Simulated Values | | | Measured Values |
|---|---|---|---|---|
| Z Distance (in.) | Primary coil inductance (μH) | Secondary coil inductance (μH) | Coupling coefficient k | Coupling coefficient k |
| 4 | 82.86 | 84.21 | 0.302 | 0.251 |
| 5 | 81.20 | 81.62 | 0.239 | 0.210 |
| 6 | 80.14 | 79.88 | 0.190 | 0.170 |
| 7 | 79.56 | 78.88 | 0.151 | 0.138 |
| 8 | 79.35 | 79.22 | 0.121 | 0.107 |

Detailed simulations were carried out on the Saber circuit simulation platform using the coil parameters obtained from FEA simulation for coil-to-coil distances of 4 in. and 8 in. The primary and secondary resonant component values used are in Table I.5-2. The simulations were carried out for operating conditions corresponding to those in Table I.5-1.

Figure I.5.6 shows the simulation results corresponding to 11 kW operation at an output voltage of 300 V for a power transfer height of 8 in. Table I.5-4 shows the estimated volume and weight of the major onboard components of the 11 kW wireless charger with DC-DC regulator components and with shared/integrated components (proposed architecture). Table I.5-4 also shows the comparison of the estimated weight and volume of the 11 kW wireless charger with a separate DC-DC regulator and 11 kW integrated wireless EV charger. The filter capacitor, inductor, and smoothing capacitor weight and volume are based on 2010 Prius benchmarking.

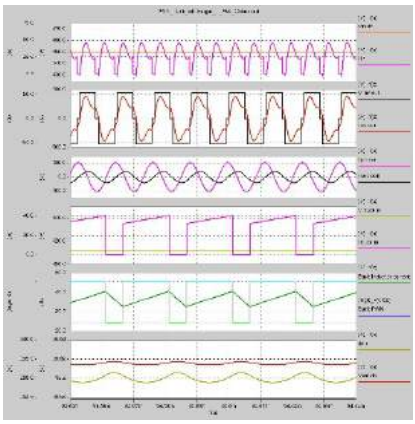

Figure I.5.6 - Saber circuit simulation results corresponding to an 8 in. power transfer height. From the top: input voltage and current, inverter output voltage and current, primary and secondary coil currents, secondary DC-DC regulator input voltage and current, and DC-DC regulator output voltage and current.

Table I.5-4 - Estimated weight and volume of 11 kW wireless charger with and without integration with the DC-DC converter of the electric drive

| Component | 11 kW Wireless Charger + DC–DC Converter | | 11 kW Integrated Wireless EV Charger | |
|---|---|---|---|---|
| | Weight (kg) | Volume (L) | Weight (kg) | (L) |
| Coil (Litz wire + ferrites + Al shield) | 8.23 | 5.65 | 8.23 | 5.65 |
| Capacitor | 0.599 | 0.25 | 0.599 | 0.25 |
| Heat sink | 2.00 | 2.23 | 2.0 | 2.23 |
| Filter capacitor | 0.68 | x | - | - |
| Inductor | 3.67 | 2.59 | - | - |
| Smoothing capacitor | 2.22 | 2.65 | - | - |
| Total | 17.39 | 13.37 | 10.82 | 8.13 |
| Power density/ specific power | 0.632 | 0.822 | 1.015 | 1.353 |

## Conclusions

An 11 kW integrated wireless charger has been designed and the feasibility verified by simulation results. The 11 kW integrated charger implements secondary side control and has optimized coils designed to operate for up to 11 in. of coil-to-coil separation. The primary side tuning has been selected as LCCL as opposed to initially proposed LCL to get rid of the high-frequency transformer. The optimized coil pair was simulated using an FEA simulation tool, then prototyped, and the simulation and experimental results are within agreeable limits. The difference in simulation and experimental results of the characterization of the coils can be attributed to not using aluminum plate and modeling the Litz wire as a uniform copper slab in simulation. The coil characterization results were used to perform detailed circuit simulations, thereby validating the feasibility of the designed integrated charger and optimized coils. The estimated power density increases from 0.632 kW/kg to 1.015 kW/kg, and the specific power increases from 0.822 kW/kg to 1.353 kW/L as a result of integrating the wireless EV charger and the DC-DC converter of the electric drivetrain.

## Key Publications

1. Veda P. Galigekere, Omer C. Onar, Madhu Chinthavali, Zhiqiang (Jack) Wang, “Load Power Agnostic 6.6 kW Wireless EV Charger with LCL Tuned primary and Secondary Side Regulation,” in Proc, IEEE Energy Conversion Congress and Exposition (ECCE’17), October 2017, Cincinnati, OH.

## I.6 Power Train Performance Improvement Techniques

**Zhiqiang (Jack) Wang, Principal Investigator**
Oak Ridge National Laboratory (ORNL)
National Transportation Research Center
2360 Cherahala Boulevard
Knoxville, TN 37932
Phone: (865) 946-1581
E-mail: wangz@ornl.gov

**Susan A. Rogers, Technology Manager**
U.S. Department of Energy
Phone: (202) 586-8997
E-mail: Susan.Rogers@ee.doe.gov

Start Date: October 1, 2016 End Date: September 30, 2017
Total Project Cost: $650,000 DOE share: $650,000 Non-DOE share: $0

### Project Introduction

The need for high-efficiency and high-power-density operation of power electronics in automotive applications is increasing. Generally, the efficiency of the traction-drive inverter at heavy loads is determined by the conduction and switching losses of power semiconductors, whereas their light-load efficiency is primarily determined by switching losses of semiconductors. As the switching losses are almost independent of the load, a typical efficiency curve as a function of the load power shows a fast decrease as the load decreases from the rated condition. To decrease the overall power consumption, improvement of the efficiency at light loads is very important because it can make up a large portion of the overall power consumption depending on the specific drive cycle. Although most passenger-size vehicle inverters are designed for the maximum power of 80–100 kW, the average power consumption usually remains less than 5–15 kW for common drive cycles.

Wide-bandgap (WBG) devices, specifically silicon carbide (SiC) and gallium nitride semiconductors, are emerging technologies that enable operation at higher temperatures and frequencies with efficiency and reliability improvements. The development of WBG devices promises to help achieve the cost, weight, and volume goals, as well as DOE Vehicle Technologies Office targets. The WBG inverter evaluated under this project will provide a comprehensive study of state-of-the-art WBG inverter behavior under various operating conditions, especially light-load conditions. The performance evaluation results will help determine when a viable market introduction of these WBG devices for automotive use could occur.

### Objectives

The overall objective of this project is to improve traction-drive inverter performance under various operation conditions, especially light-load conditions. This project is targeted toward the application of WBG technology and novel circuit topologies and control strategies to address inverter cost, weight, volume, and efficiency goals. Specific research and development efforts in FY 2017 include the construction of a traction-drive system simulation platform with a real WBG semiconductor device model and motor model, as well as a hardware test bed with a motor emulator. The developed simulation platform and test bed under this project will provide guidance for inverter electrical and thermal design, thus increasing the power density and decreasing the volume and weight for electric vehicle traction-drive systems that can achieve the DOE 2020 weight, volume, and efficiency targets.

### Approach

The goal of this research is to improve the overall traction-drive inverter performance for electric vehicles to meet 2020 DOE efficiency, power density, specific power, and cost targets. The technical approach involves

the evaluation of a WBG inverter with commercially available devices using a dedicated simulation platform and hardware test bed, and FY 2017 research efforts were focused on the development of the simulation platform and hardware test bed. Specifically, a WBG inverter with commercial devices and electric vehicle motor need to be selected as the study targets, and then a simulation platform incorporating a real semiconductor device model and a motor model needs to be built to conduct a comprehensive performance evaluation and define the appropriate testing metrics in experiments. With the validation of the whole system in simulation, a hardware test bed can be developed by leveraging past R&D achievements. The inverter drive performance under different operating conditions can be evaluated based on the hardware test bed.

## Results

Following the technical approach, a simulation platform and a hardware test bed incorporating a commercial traction-drive inverter and a motor load need to be developed in the project. To fully leverage previous R&D achievements, the 3D-printed 100 kW all-SiC inverter developed in FY 2015 was adopted as the traction-drive inverter for this project. In addition, based on past ORNL electric vehicle benchmarking research efforts, the 2015 BMW i3 three-phase permanent magnet synchronous motor (PMSM) was identified as the target motor model for the project, and its key parameters are summarized in Table I.6-1. These parameters are implemented into the motor emulator which serves as the load of the three-phase SiC inverter using commercial 1200 V SiC metal-oxide semiconductor field-effect transistor (MOSFET) power modules.

Table I.6-1 - Parameters for motor emulator

| Parameter | Description | Value |
|---|---|---|
| $R_s$ | Stator resistance | 5.2 mΩ |
| $L_d$ | Stator d-axis inductance | 50 μH |
| $L_q$ | Stator q-axis inductance | 250 μH |
| $\Psi_m$ | PM flux linkage | 0.03754 Wb |
| $V_n$ | Nominal phase peak voltage | 112.62 V |
| $P_n$ | Nominal power | 75 kW |
| $\omega_e$ | Nominal electrical frequency | 3000 rad/s |
| $\omega_m$ | Nominal mechanical frequency | 500 rad/s (or 4775 RPM) |
| $T_e$ | Nominal torque | 150 N·m |
| P | Number of pole pairs | 6 |
| $J_m$ | Total mechanical inertia | $6.44 \cdot 10^{-3}$ kg·m$^2$ |
| $B_m$ | Frictional coefficient | 0.01 N·m/(rad/s) |

*Simulation Platform Development*

A PMSM control simulation platform was developed in Saber for inverter drive performance evaluation of electric vehicles under various operating conditions, especially light-load conditions such as high-speed, low-torque and low-speed, high-torque operation. The key features of the developed PMSM control simulation

platform include (1) double closed-loop control (i.e., external rotor speed loop and internal current loop), (2) constant torque angle and constant torque per ampere control strategies implemented, (3) BMW i3 PMSM with electrical and mechanical model, (4) three-phase inverter with SiC MOSFET behavior model and transient thermal model, and (5) real gate driver model for semiconductor devices.
Compared to the traction-drive inverter with a resistive-inductive passive load, the developed simulation system is able to more accurately represent real inverter application scenarios and provide guidance for inverter electrical and thermal design while providing methods for improving the light-load efficiency. The simulation result of the PMSM control system under rated operating condition is shown in Figure I.6.1. In addition, based on the developed PMSM Saber simulation platform, the inverter drive performance testing metrics (including various speed and load torque operating conditions), together with the inverter key operating parameters such as DC bus voltage, switching frequency, and output power, can be defined.

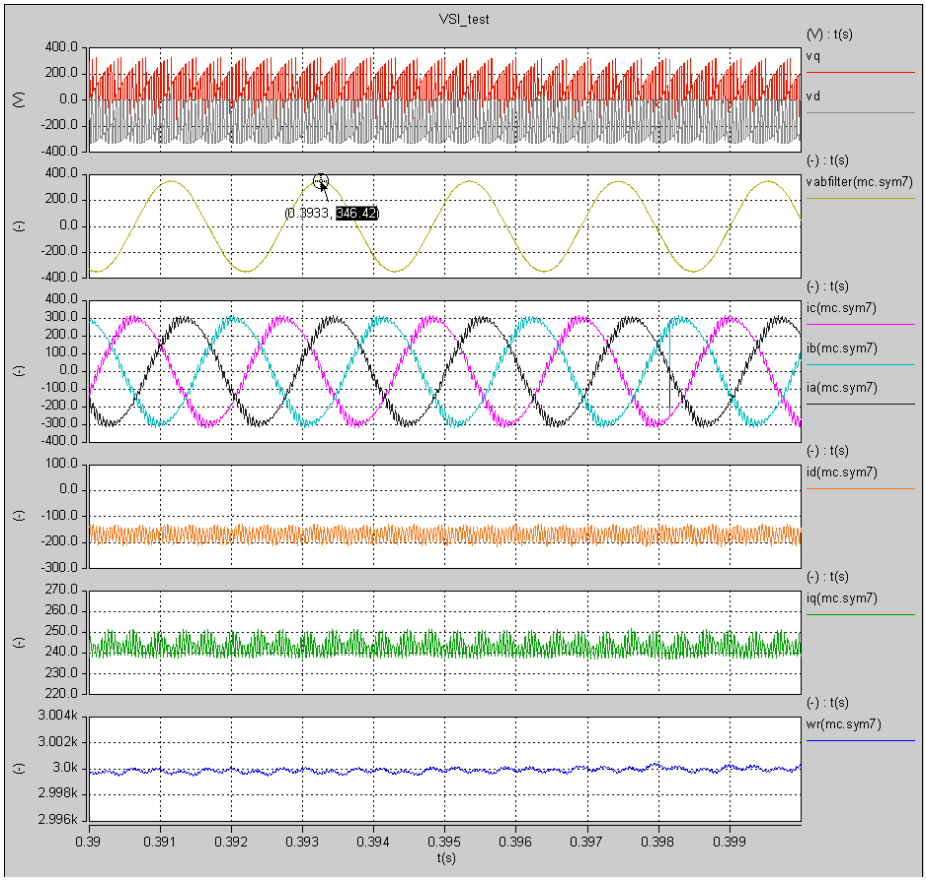


Figure I.6.1 - Simulation results of the developed PMSM system at nominal operating point. Waveforms from top to bottom: inverter d-axis and q-axis output voltage, filtered line-to-line voltage, three-phase current, d-axis current, q-axis current, and electrical angular frequency.

One key research effort in the PMSM simulation platform development is to build a behavior model and transient thermal model for the commercial SiC MOSFET power module. In this project, a temperature-dependent dynamic device behavior model for a commercial 1200 V, 300 A SiC MOSFET power module was created based on the device data sheet, and the model simulation results at 25°C and 125°C are shown in Figure I.6.2. In the Saber double-pulse-test simulation setup, the Cauer thermal model for MOSFET and diode is integrated with the junction temperature terminal of the temperature-dependent dynamic device behavior

model. The parameters used for the MOSFET and diode Cauer thermal network are also extracted and confirmed with data sheet values.

The turn-on and turn-off switching transient of the SiC MOSFET is shown in Figure I.6.3. As seen from the comparison, the switching speed shows the opposite trend with temperature. With the rise of temperature, the turn-on energy loss decreases as a result of a faster switching speed, whereas the turn-off energy loss increases as a result of a slower switching speed. The net result is that the total switching energy loss becomes somewhat higher at higher temperatures. This temperature-dependent feature would be beneficial for thermal stability under high-temperature operation.

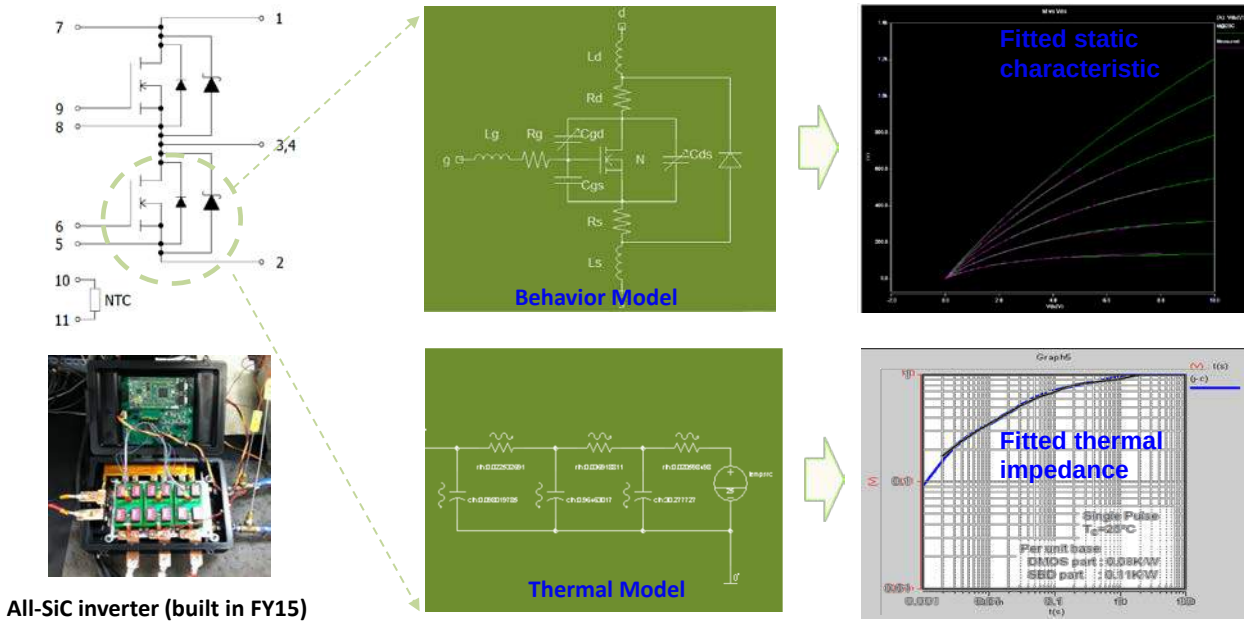


Figure I.6.2 - SiC MOSFET behavior model and transient thermal model.

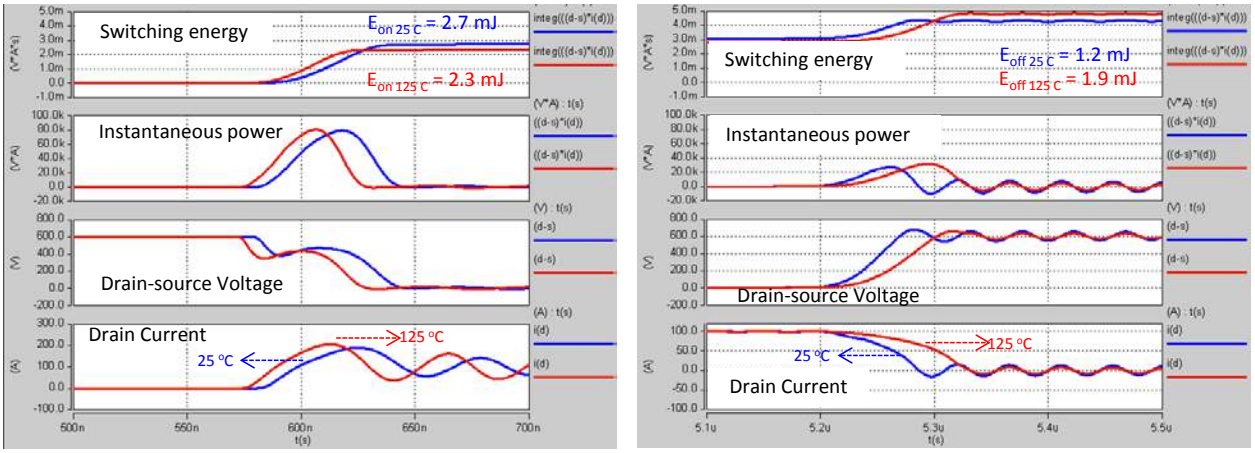


Figure I.6.3 - Simulated switching transient of SiC MOSFET: turn-on transient (left) and turn-off transient (right).

*Hardware Test Bed Development*

The system configuration of the inverter performance evaluation platform with the motor emulator is designed as shown in Figure I.6.4. The proposed configuration here is essentially a power recirculation test bed, which is mainly composed of the SiC inverter, motor emulator, bidirectional DC emulator, and their control interfaces. The bidirectional DC emulator, absorbing AC power from the grid, provides regulated DC voltage and active power to the inverter to drive the motor emulator. The motor emulator converts the AC power from the inverter to DC power, and then the DC power is provided back to the DC emulator to be injected into the grid for energy recycling. The developed platform can be used as a general inverter performance evaluation tool with motor load instead of conventional resistive-inductive load. By using the motor load, the realistic performance of a traction-drive inverter in an electric vehicle can be obtained, which in turn contributes to the future high-efficiency and high-power density inverter design. To represent the BMW i3 motor, the motor parameters shown in Table I.6-1 are first uploaded to the motor emulator. The motor emulator also requires generating the d-axis and q-axis flux tables calculated based on the dime domain PMSM model. The optimal torque angle is also calculated for the operating conditions and used within the inverter controls. The test metrics created for the experimental setup involve running the motor at various torque and speed pairs with different operating conditions. Torque variations include testing at 10, 20, 40, 60, 80, and 100 Nm, while the speed varies at 500; 1,000; 3,000; 5,000; 7,000; and 9,000 rpm set points. This test matrix of 6 × 6 = 36 elements will be obtained at different inverter operating conditions. Inverter operating parameters include DC-link voltage (350, 400, and 450 V), switching frequency (5, 10, and 15 kHz), and inverter coolant temperatures (20, 40, and 60°C). Therefore, the matrix results will be obtained for $3^3 = 27$ times. The inverter performance while meeting the same speed and torque pairs will be evaluated at these different conditions, which in turn will provide insights on how the inverter efficiency could be improved at higher temperature values and at light-load conditions by adjusting the DC-link voltage or the switching frequency.

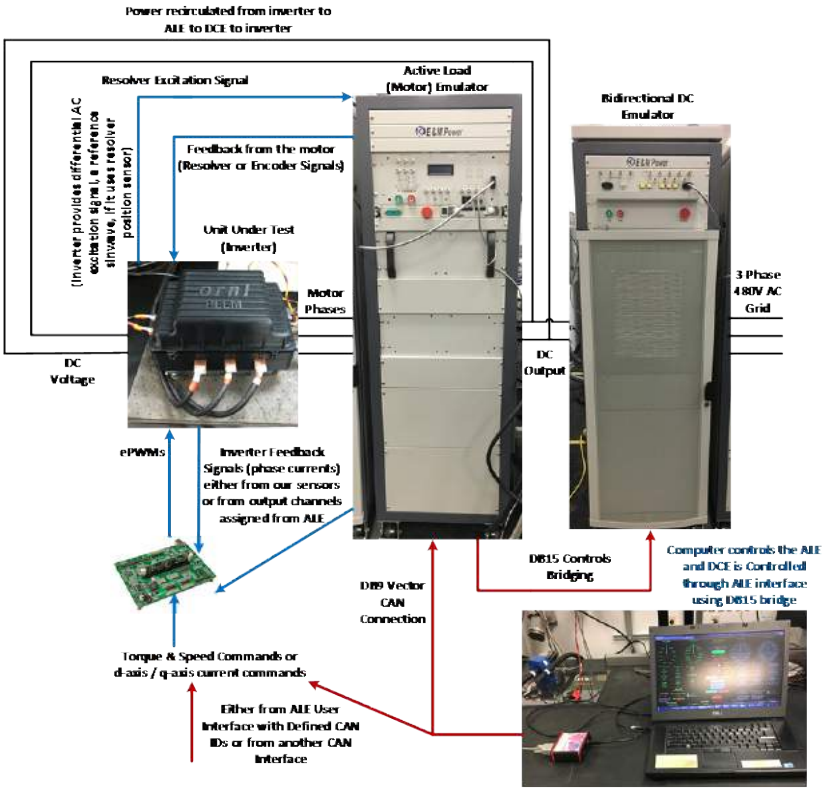


Figure I.6.4 - System configuration for inverter drive performance evaluation.

Some of the example test results are given in Figure I.6.5, which shows results for inverter testing with 350 V input voltage, 5 kHz switching frequency, and 20ºC coolant temperature. The motor emulator speed was set to

1,000 rpm, and the inverter was controlled in closed loop to have the motor provide 10, 20, 40, and 60 Nm mechanical torque to the drive load. For comparisons and for the validation of the model and the maximum torque per ampere model calculations, the calculated and experimental values of the inverter output power, inverter phase-to-neutral output voltage, and the inverter output phase current are provided in Table I.6-2. The power analyzer experimental waveforms as well as the data screenshot for 1,000 rpm, 60 Nm load torque with 6,625 kW inverter output power, are given in Figure I.6.6.

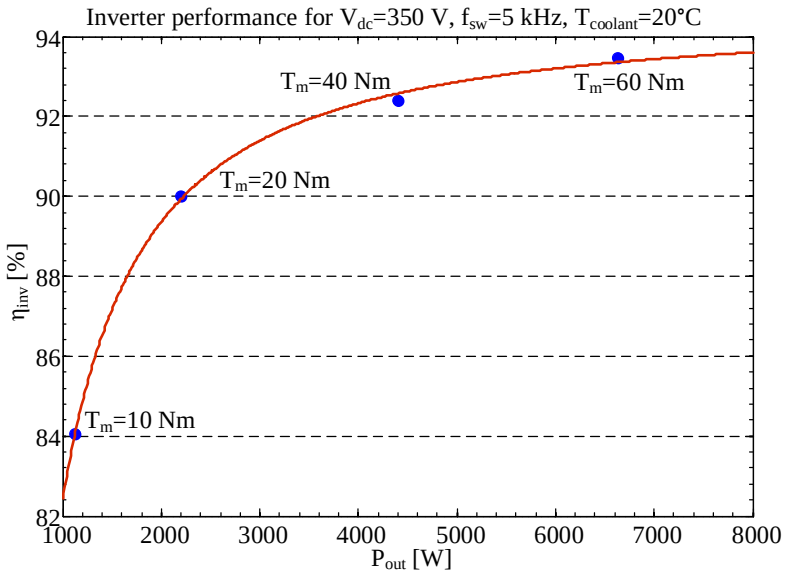


Figure I.6.5 - Inverter performance at 1,000 rpm speed and various load torque levels.

### Table I.6-2 - Maximum torque per ampere calculations and experimental results

| Rotor Speed = 1,000 rpm | | | | | | | | |
|---|---|---|---|---|---|---|---|---|
| **Torque** | **10 Nm** | | **20 Nm** | | **40 Nm** | | **60 Nm** | |
| **Parameter** | **Calc.** | **Exper.** | **Calc.** | **Exper.** | **Calc.** | **Exper.** | **Calc.** | **Exper.** |
| **$P_{inv\_out}$ [W]** | 1167 | 1127.24 | 2228 | 2199.84 | 4389 | 4401.46 | 6563 | 6624.93 |
| **$V_{out\_inv\_pp}$ [V]** | 17.05 | 19.78 | 17.74 | 20.34 | 19.58 | 22.91 | 21.64 | 23.87 |
| **$I_{inv\_out\_line}$ [A]** | 22.69 | 22.92 | 42.07 | 41.86 | 76.23 | 76.12 | 105.36 | 105.69 |
| **λ ($PF_{inv\_out}$)** | 0.998 | 0.983 | 0.995 | 0.985 | 0.980 | 0.986 | 0.959 | 0.985 |
| **Calc. = calculation; Exper. = experimental.** | | | | | | | | |

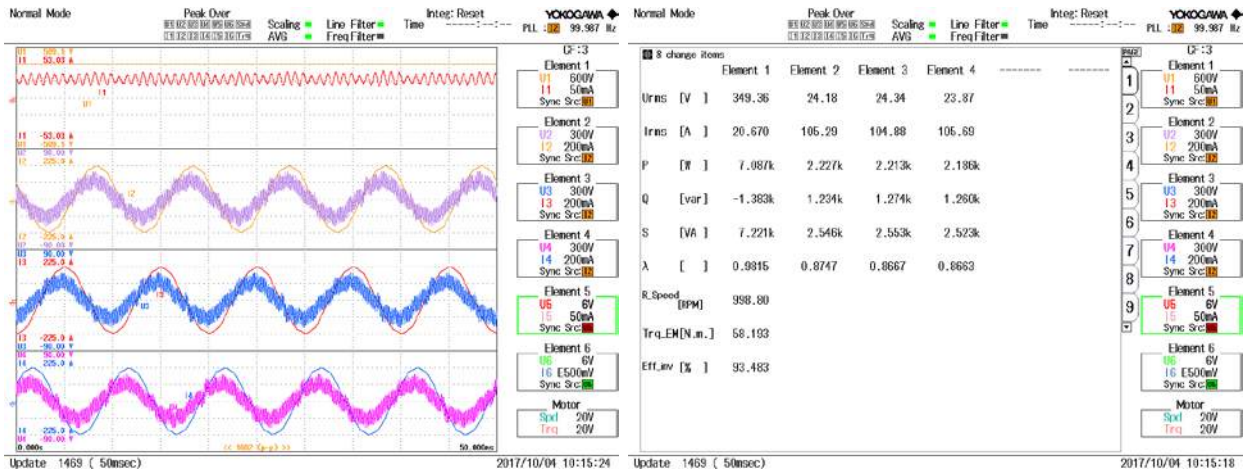


Figure I.6.6 - Experimental inverter waveforms and power analyzer screenshots for 1,000 rpm motor speed and 60 Nm load torque.

## Conclusions

This study aims at developing a traction-drive system model and an experimental test bed to operate the inverter at various torque and speed pairs and other inverter operational parameters to address light-load, low-efficiency issues. The model and the experimental test results are in good agreement, which validates the model developed. Future work involves completing the tests at other operating points to have a complete data set for the full analysis.

## Key Publications

1. Madhu Chinthavali, “Electric drive inverter,” presented at the 2017 DOE Vehicle Technologies Office Annual Merit Review, June 2017, Washington, DC.

## I.7 Electrical Performance, Reliability Analysis, and Characterization

**Tim Burress, Principal Investigator**
Oak Ridge National Laboratory
1 Bethel Valley Road
Oak Ridge, TN 37831
Phone: (865) 576-3654
E-mail: burressta@ornl.gov

**Susan A. Rogers, Technology Manager**
U.S. Department of Energy
Phone: (202) 586-8997
E-mail: Susan.Rogers@ee.doe.gov

Start Date: October 1, 2016 End Date: September 30, 2017
Total Project Cost: $204,427 DOE share: $204,427 Non-DOE share: $0

### Project Introduction

This project provides vital information about the status and developmental trends of electric vehicle/hybrid electric vehicle (EV/HEV) components to the DOE Vehicle Technologies Office (VTO) for strategic planning of technology development projects. ORNL's detailed reports have received tremendous positive feedback from researchers in academia and industry, as well as other individuals with an interest in EV/HEV technologies. This information serves as a valuable educational resource on EV/HEV architectures, yields a track of lessons learned, prevents reinventing/duplication of advancements, and promotes competitive development.

### Objectives

FY 2017 objectives include design assessments and analysis of the drive inverter assembly, electric machines, and transaxle of the 2017 Toyota Prius hybrid. Observations from the analysis were documented in reports and presentations presented to DOE, the Electrical and Electronics Technical Team, and the public.

### Approach

Automotive manufacturers do not typically publish details about the design, functionality, and operation of EV/HEV technologies, and even published details and specifications must be verified and clarified. Therefore, ORNL performs teardown assessments to obtain comprehensive information on design, functionality, and subcomponent characteristics. These activities provide the information needed for DOE to warrant a robust program and provide DOE partners and other researchers with valuable information on state-of-the-art EV/HEV technologies.

### Results

*2017 Toyota Prius Power Control Unit Design and Functionality Assessments*

The 2017 Prius power control unit (PCU), shown in Figure I.7.1, contains a 3-phase motor inverter, 3-phase generator inverter, bi-directional boosting DC-DC converter, and a DC-DC converter for the 12 V accessory supply. The mass of the PCU as received is 10.8 kg, with a volume of about 8.4 L, and the motor has a published peak power of 53 kW. The boost converter boosts from a nominal hybrid battery voltage level of about 200 V to a maximum of about 600 VDC, as the boosted voltage is varied according to driving requirements. Similar to previous Toyota PCU architectures, the boosted voltage supplies a dc link that is shared by both motor and generator inverter, facilitating power flow through a power split planetary gear in the transmission/transaxle, and ultimately electronically controlling the power flow through the continuously variable transmission.

The vehicle has no alternator and a DC-DC converter, shown in Figure I.7.2, connects to the high-voltage hybrid battery and supplies power to accessory loads at about 12 V. In the bottom compartment, key components of the 12 V DC-DC converter are combined into one circuit board, which includes a substantial copper mask with traces for two inductors and a 5-turn transformer such that the inductors and transformer are not wound before manufacturing and split magnetic cores are simply installed around the circuit board. The circuit board attaches to a cast aluminum plate that is cooled by a water–ethylene glycol mixture. A 1.4 kg boost inductor is mounted on the other side of the cooling plate in the middle compartment. The middle compartment also contains a 471 μF high-voltage capacitor that attaches to the boosted dc link. This is the lowest dc-link capacitance observed in a Toyota PCU to date, as the 2010 Prius PCU contains an 888 μF capacitor. Copper bus bars, inverter power connection terminals, and current transducers are located near the capacitor. The bottom edge of individually packaged power modules extend into the middle compartment. The top compartment includes a circuit board that, unlike previous designs, combines communication circuitry, signal level voltage regulators, driver circuitry for power electronics, and many other functions into one compact circuit board. As this circuit board is removed, drive and sense pins for the insulated-gate bipolar transistor (IGBT) modules, shown in Figure I.7.3, are visible.

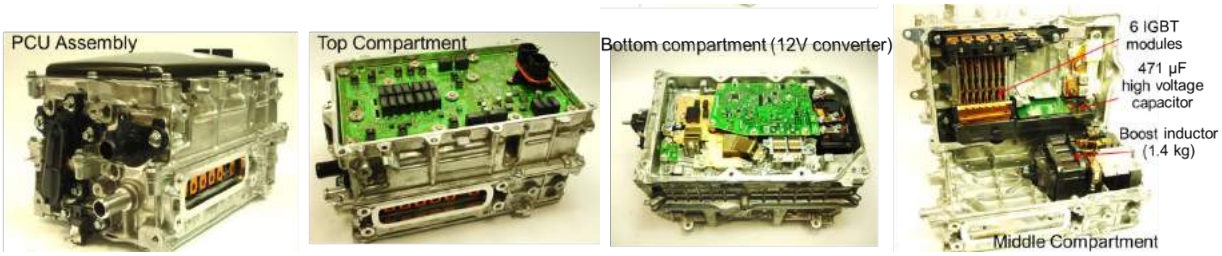


Figure I.7.1 - 2017 Prius PCU assembly and compartments.

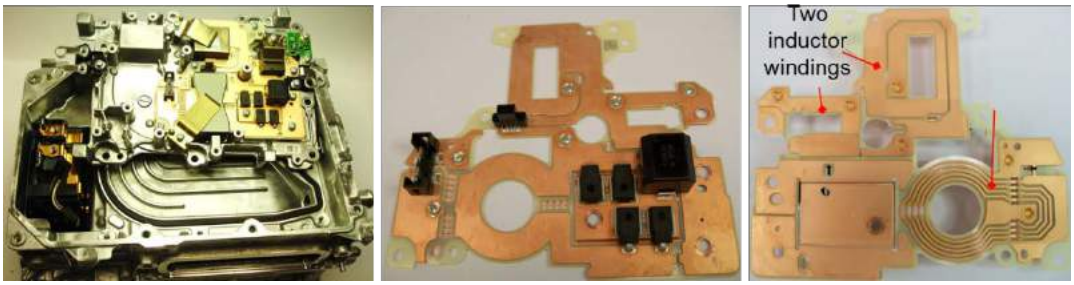


Figure I.7.2 - 2017 Prius DC converter for 12 V supply conversion from high-voltage battery.

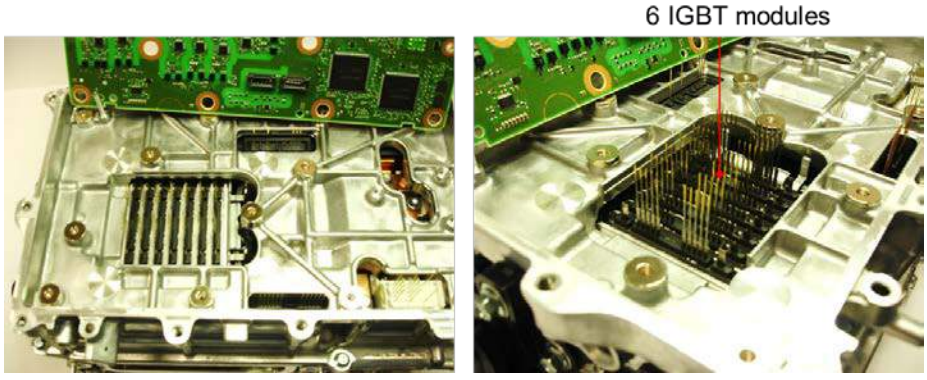


Figure I.7.3 - 2017 Prius PCU top compartment with lid and control/driver board removed.

The general assembly and cooling infrastructure for the two-sided cooling modules, shown in Figure I.7.4, is similar to what is used in Toyota Camry hybrid PCUs beginning with model year 2013, as well as Lexus LS600h PCUs beginning in model year 2008. However, while previous designs had a separate module for each IGBT, the 2017 Prius PCU power modules combine upper and lower switches into one module such that each

module contains two IGBTs and two diodes. An exploded view of the Prius power module is shown on the right in Figure I.7.4. Each module has three leads: two that connect to the positive and negative dc link and one for the switched terminal. IGBTs and diodes are soldered to isolated collector plates, copper-molybdenum spacers (used to match thermal expansion of the devices to the emitter plates) are soldered to the top of the devices, and emitter plates are soldered to the spacers. Dimensions are shown for the motor IGBT and diode, which are 12.18 mm by 13.11 mm and 12.16 mm by 8.98 mm, respectively. Generator IGBT and diode dimensions are 8.77 mm by 8.98 mm and 8.11 mm by 6.91 mm, respectively. Boost IGBT and diodes are much larger with dimensions of 14.22 mm by 14.16 mm and 8.88 mm by 14.18 mm, respectively. The cross-sectional area of the motor IGBTs is about 159.7 $mm^2$, and with six devices, the total motor inverter IGBT cross-sectional area is ~958.1 $mm^2$.

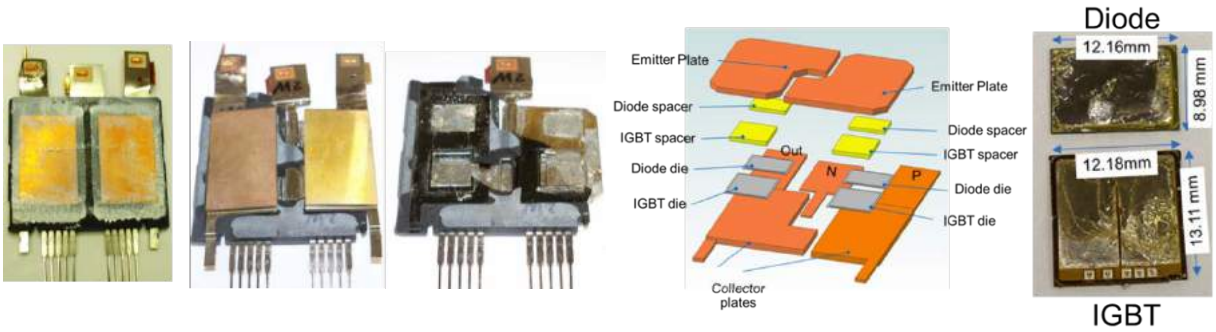


Figure I.7.4 - 2017 Prius power module assembly and components.

The bar chart in Figure I.7.5 compares the ratio of published peak power (in watts) over the total inverter IGBT cross-sectional area. This comparison provides a gauge of device utilization, cost, and thermal management effectiveness for these systems. When making comparisons, it should be noted that some systems have very different roles in the power train. For example, Toyota power trains have a fairly large gap between peak and continuous power ratings, whereas inverters for fully electric vehicles such as the Nissan LEAF must provide all of the traction power. Comparisons amongst Toyota products, and especially across Prius generation products, are more straightforward. It can be seen that the three highest values are associated with PCUs that have power modules cooled on both sides. Values shown on the left for the second-, third-, and fourth-generation Prius indicate clear increases for each generation.

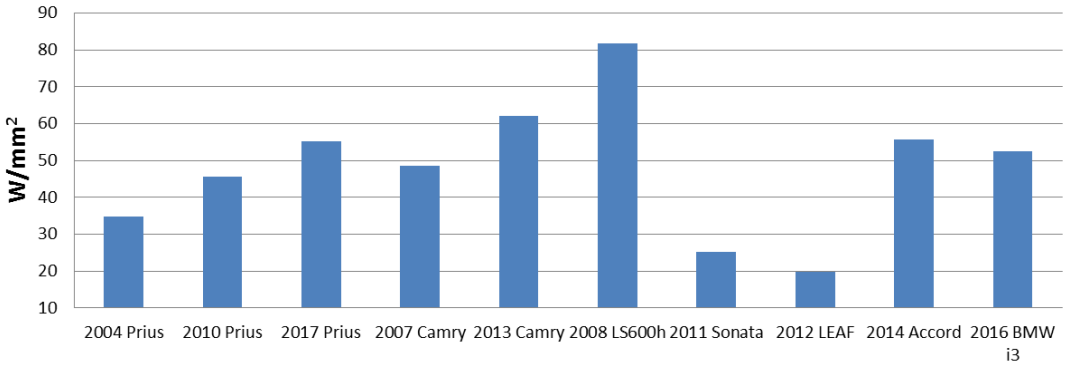


Figure I.7.5 - Comparison of ratios of published motor power rating vs. total IGBT silicon area.

### *2017 Toyota Prius Transmission/Transaxle and Electric Machine Assessments*

The 2017 Toyota Prius transmission/transaxle, shown in Figure I.7.6, includes many significant design improvements compared with its predecessors. Toyota claims that these design changes yield a 20% reduction in mechanical losses and a reduction of the overall transaxle length by 47 mm. As received, the measured transaxle mass was 78.4 kg. Most of the significant improvements center on relocation of the electric machine

that serves as the primary traction motor (and traction generator when braking). Previous generations have the combustion engine, generator, and motor collocated on the same axis. The combustion engine still connects to the planet carrier and the generator still connects to the sun gear of the power-split planetary gear (labeled "Axis 3." The traction motor mates to the ring gear of the power-split planetary gear in previous designs, but the 2017 Prius traction motor is relocated to another location (labeled "Axis 4") and provides and absorbs power through the "final/driven" gear located on "Axis 2." The number of teeth observed on each gear is indicated in Figure I.7.6. Since the engine and transaxle are transverse mounted (as they are in most front wheel drive vehicles), previous designs imposed length restrictions to the motor and generator because the power train must fit between the two drive wheels. In moving the electric motor to another axis, the outer diameters have been reduced and the stack length has been increased for both the motor and generator when compared with previous designs. This change in form factor allows for higher efficiency since the amount of active winding vs. extra end-turn length increases. Furthermore, the motor can be operated at high speeds (it has a published maximum speed of 17,000 rpm) without several stages of gear reductions. Previous designs include an extra planetary gear for speed reduction that shares the ring of the power-split planetary and therefore involves one additional gear mesh between the traction motor and the drive wheels. This is a key contributor to Toyota's claimed mechanical loss reduction.

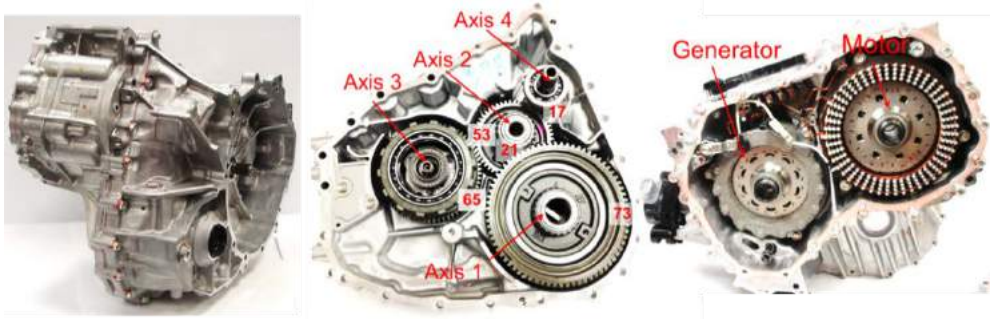


Figure I.7.6 - 2017 Prius transmission/transaxle.

In addition to a small outer diameter and longer length, the 2017 Prius motor stator, shown in Figure I.7.7, far left, includes four 0.150 in. by 0.088 in. bar conductors per slot and form what are often referred to as "hairpin" windings. With a mass of 11.4 kg, the stator has 48 slots, a lamination stack length of 2.35 in., and a total length (including end-turns) of 4.69 in. The stator has an outer diameter of 8.47 in. and an inner diameter of 5.580 in. The 2017 Prius motor rotor and shaft mass is 6.8 kg (5.4 kg without shaft); and, as shown in Figure I.7.7, it has eight poles with three magnets groups per pole. The rotor includes 0.25 mm thick laminations, and each magnet group includes two side-by-side magnets that extend the entire length of the lamination stack. The magnets measure roughly 0.275 in. by 0.144 in. by 2.33 in. and have an individual mass of 11.34 grams. With 48 magnets, the total magnet mass is about 544.3 grams. The 2017 Prius generator stator, shown in Figure I.7.7, has a mass of 6.4 kg, and has 15 slots with windings potted with an aluminum-oxide filled resin. The generator stator has an outer diameter of about 7.486 in., an inner diameter of 5.002 in., a lamination stack length of 1.624 in., and a total length of 3.493 in.

The generator rotor, shown in Figure I.7.7, far right, has a mass of 4.2 kg (3.0 kg without shaft) and laminations that are 0.25 mm thick. The rotor has 10 magnetic poles with the "V" arrangement commonly found in previous Prius rotor designs. Each side of the V includes two side-by-side magnets, with each measuring 0.282 in. by 0.187 in. by 1.623 in. and with a mass of about 10.5 g. With 40 magnets, the total mass is about 420.6 g. A unique cooling method is used to remove heat from the generator stator using oil supplied from the inside of the rotor shaft. Several stages of lamination designs, shown in Figure I.7.8, guide the oil from the axial center of the rotor out radially and axially in both directions and ultimately out axially through the holes shown in the last image of Figure I.7.8.

Figure I.7.7 - 2017 Prius motor stator, motor rotor, generator stator, and generator rotor.


Figure I.7.8 - Oil passageways through several sets of 2017 Prius generator rotor lamination designs.

In looking at the progression of Prius traction motor designs, it has been observed that power density increases with each successive design. Improvements were achieved in earlier designs by moving to increased operational voltages, and the last three designs have had significantly higher maximum speed ratings. The bar chart in Figure I.7.9 shows a comparison of the ratio of copper mass and magnet mass to the published power rating of each system. Since these are the most expensive materials used in the motor, this is an indirect way to make motor cost comparisons. Comparisons should be made carefully among systems that do not perform the same role in the power train (e.g., hybrid vs. fully electric). Similarly, comparison among motors with significantly different power ratings should be made carefully as magnet and copper material can be used more effectively in motors with higher power ratings. For example, the 2008 LS 600h has the lowest material usage per rated power, but it also has the highest rated power (160 kW). Although only an incremental decrease in magnet material mass is observed, a significant reduction in copper usage is observed between the third- and-fourth generation Prius (2010 vs. 2017).

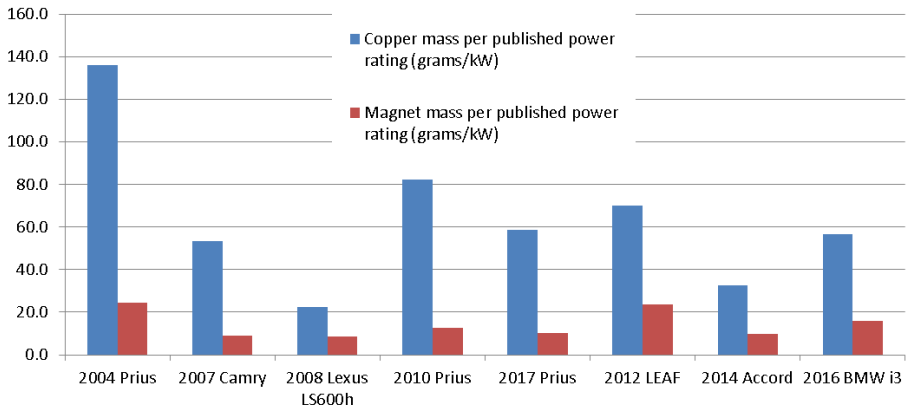


Figure I.7.9 - Comparison of various EV/HEV motor copper and magnet mass versus published peak power.

## Conclusions

A summary of motor and inverter power density and specific power for various Toyota/Lexus power trains is provided in Table I.7-1. Information for the inverters includes two numbers: one that includes the boost converter mass and volume and one that does not. When excluding the boost converter mass and volume, the 2017 Prius PCU has the highest power density and specific power observed thus far and comes only second behind the 2013 Camry when considering boost converter mass and volume. This is particularly notable considering that systems with higher power ratings (such as the 2013 Camry and 2008 LS 600h) typically achieve higher power density and specific power more easily as the mass/volume of peripheral components approaches negligibility. These accomplishments are primarily a result of moving to a compact power module arrangement, enabling efficient packaging with passive components and condensed circuitry. Similar improvements are observed in the electric machine designs, as significant changes and optimization in form factor were facilitated by placing the motor on a separate axis in the transaxle/transmission. Along with yielding a reduction in mechanical losses, the power density of the motor increased considerably, which is largely facilitated by an increase in maximum operating speed, more effective material usage associated with a squarer form factor, and the use of "hairpin windings" to achieve a high slot fill factor and reduce end-turn losses.

Table I.7-1 - Comparison of DOE targets and peak power/specific power

| | 2017 Prius (53 kW) | 2010 Prius (60 kW) | 2008 LS600h Lexus (110 kW) | 2007 Camry (70 kW) | 2013 Camry (105 kW) | 2004 Prius (50 kW) |
|---|---|---|---|---|---|---|
| **Motor** | | | | | | |
| **Peak power density, kW/L** | 5.7 | 4.8 | 6.6 | 5.9 | | 3.3 |
| **Peak specific power, kW/kg** | 1.7 | 1.6 | 2.5 | 1.7 | | 1.1 |
| **Inverter—Excludes generator inverter(parenthetical values exclude boost converter mass/volume)** | | | | | | |
| **Peak power density, kW/L** | 11.5 (21.7) | 5.9 (11.1) | 10.6 (17.2) | 7.4 (11.7) | 12.7 (19.0) | 4.5 (7.4) |
| **Peak specific power, kW/kg** | 8.6 (19.0) | 6.9 (16.7) | 7.7 (14.9) | 5.0 (9.3) | 11.5 (17.2) | 3.8 (6.2) |

## I.8 Materials for Advanced Packaging

**Andrew Wereszczak, Principal Investigator**
Oak Ridge National Laboratory (ORNL)
National Transportation Research Center
2360 Cherahala Boulevard
Knoxville, TN 37932
Phone: (865) 946-1543
E-mail: wereszczakaa@ornl.gov

**Susan A. Rogers, Technology Manager**
U.S. Department of Energy
Phone: (202) 586-8997
E-mail: Susan.Rogers@ee.doe.gov

Start Date: October 1, 2016 End Date: September 30, 2017
Total Project Cost: $400,000 DOE share: $400,000 Non-DOE share: $0

### Project Introduction

For power electronic (PE) devices, the potential use of sintered-silver (Ag) interconnect technology has several advantages over conventionally used solder-based interconnection technology [e.g., better electrical and thermal conductivities, higher temperature capability, microstructural equilibrium, better reliability, and Restriction of Hazardous Substances (EU Directive 2002/95/EC) compliance]. Examples of interconnect locations for sintered-Ag consideration are shown in Figure I.8.1. But its adoption has been sluggish because it is a relatively new technology, its processing is sufficiently different than conventional solder processing (e.g., no melting or reflowing occurs, pressure may be needed, etc.), and the PE community is relatively conservative when it comes to using new processing technologies. This effort seeks to hasten the more confident adoption of sintered Ag by developing more economical ways to process it without compromise to overall mechanical reliability.

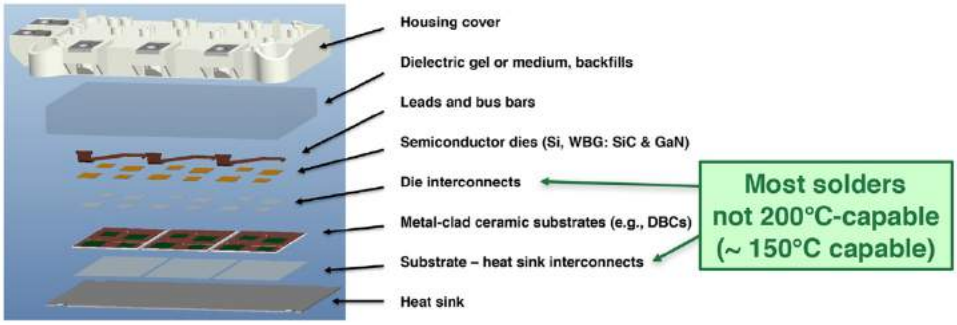


Figure I.8.1 - Example of a single-sided PE device.

### Objective

Advance sintered-Ag interconnect technology to enable a 200°C-capable, low-cost, and reliable electronic package with at least a 15-year life. This is relevant because contemporary PE devices cannot operate at 200°C because most conventional interconnect materials (solders) are not in equilibrium above 150°C.

### Approach

- Advance the processing and mechanical reliability of sintered Ag for PE devices.

- Promote using common reflow oven technology for pressurelessly sintering Ag interconnects.
- Ultimately promote 200°C PE device operation.
- Interact with academia (Alfred University and Mount Union University) and material suppliers (General Metal Finishing, Henkel, Heraeus, Rogers Corporation, and UHV Sputtering) for project support.
- Disseminate results and interpretations in the open literature.

## Results

There were three primary accomplishments in FY 2017: development of contact-drying processing, demonstration of pressureless sintering of Ag interconnects using a reflow oven, and development of two new test methods to quantify the mechanical response of sintered-Ag interconnects.

### *Contact-Drying*

Drying of printed sinterable-Ag paste is a crucial, yet taken-for-granted and overlooked, presintering step. Vendor-advocated and conventionally used convective-drying methods are limiting. But contact-drying, a method not previously advocated with sinterable Ag and contrasted with convective-drying in Figure I.8.2, has been found to be a viable method to improve the versatility and attractiveness-for-use of sinterable Ag.

Contact-drying with pressurelessly sintered Ag can produce good shear strengths and microstructures equivalent to those of pressure-assisted sintering. These are illustrated in Figure I.8.3.

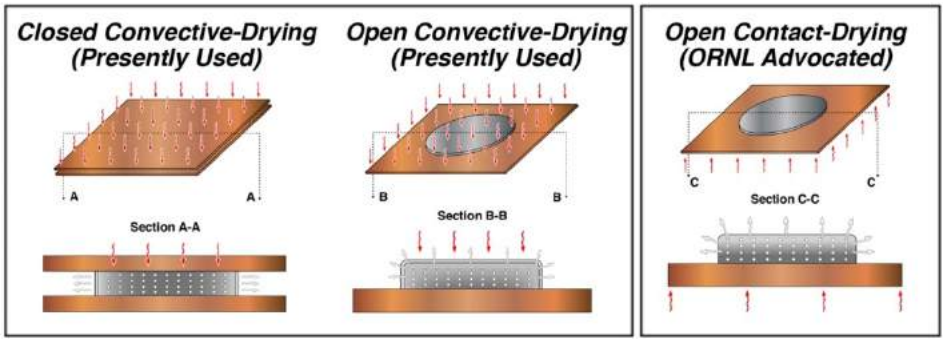


Figure I.8.2 - Convective-drying (left and middle) is different than contact-drying (right).

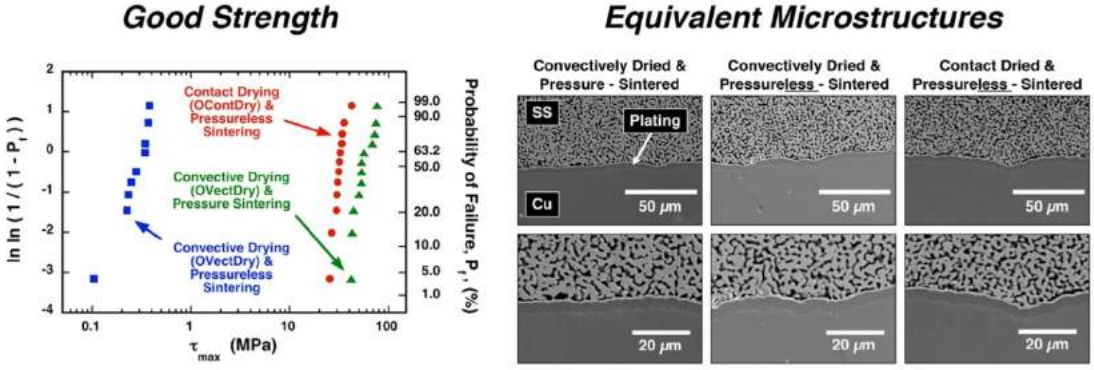


Figure I.8.3 - Use of contact-drying before sintering produces good shear strength (left) and sintered-Ag microstructures equivalent to those when convective-drying is used before sintering (right).

### *Reflow Oven Processing*

This processing method (illustrated in Figure I.8.4) has been commonly used in continuous mass production for decades to process solder interconnects in electronic devices. As a result, there was interest in using the

above-described contact-drying method in an attempt to pressurelessly sinter Ag interconnects using reflow-oven processing. High shear strengths (greater than 40 MPa) were indeed produced as illustrated in Figure I.8.5.


Figure I.8.4 - Reflow-oven processing is being used to sinter 200°C-capable Ag interconnects for PE devices.

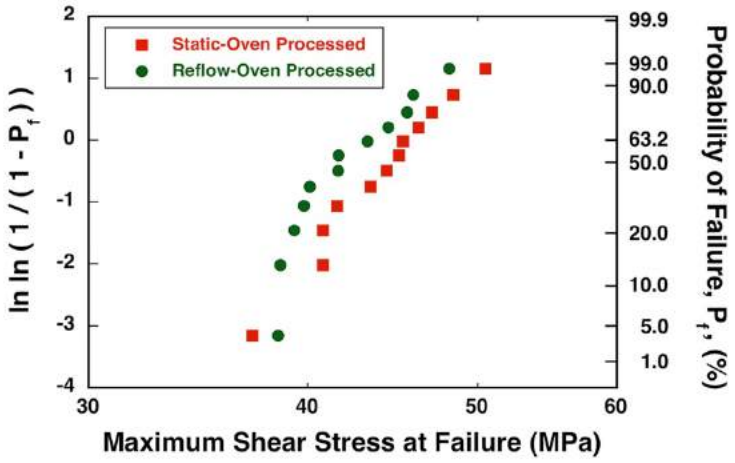


Figure I.8.5 - Example of strength distributions illustrating that pressurelessly sintered Ag interconnects can be fabricated with desirably high strengths.

*Mechanical Evaluations*

**Cantilever Testing**

Cantilever testing advances the understanding of how interconnects (e.g., sintered Ag) mechanically respond. This testing superimposes tension (primarily) and shear, but deep beam theory is needed for making its analysis more accurate. The manner of cantilever testing and examples of test specimens are shown in Figure I.8.6. Two interconnect systems, sintered-Ag interconnects bonded to titanium/nickel (Ti/Ni)/Ag-plated silicon and sintered-Ag interconnects bonded to Ag-plated copper, were mechanically evaluated as part of this test method development.

Cantilever testing was found to be an effective new method to evaluate the mechanical integrity of interconnects. The strength of sintered Ag bonded to Ti/Ni/Ag-plated silicon was found to be quite strong and deep beam theory was found to correctly calculate slight failure stresses (illustrated in Figure I.8.7).

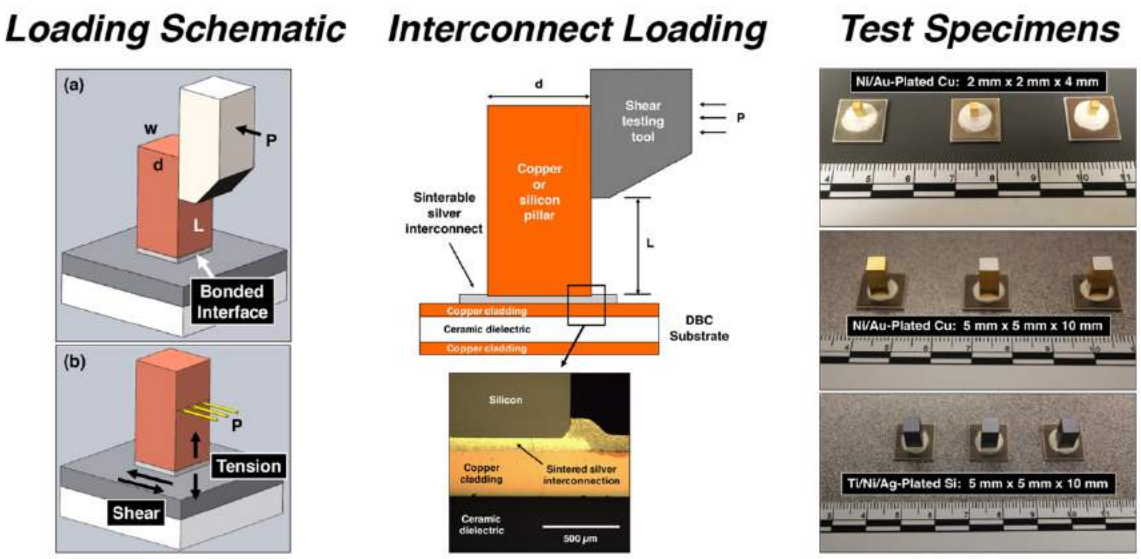


Figure I.8.6 - Cantilever testing desirably subjects interfaces to both tension and shear; such a superimposition exists in power electronic interconnects so this mechanical test is relevant.

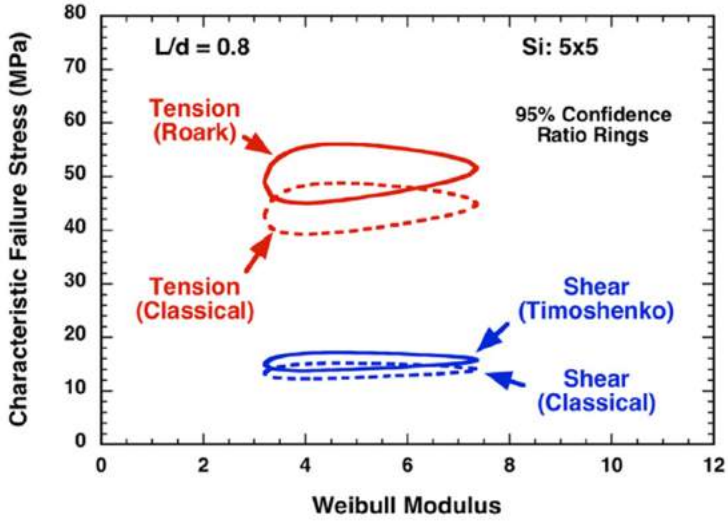


Figure I.8.7 - Accounting for deep beam theory (represented here by Roark and Timoshenko for tension and shear, respectively) more accurately portrays failure stresses of interconnects.

### Apparent Fracture Toughness Testing

An interconnect's susceptibility to crack initiation and crack propagation (fatigue) is related to the interconnect system's apparent fracture toughness ($K_{Ic}$). This parameter is a useful complement to an interconnect's shear strength and tensile strength. In this examination, a test method was adapted from existing ASTM $K_{Ic}$ test methods and developed to measure apparent $K_{Ic}$ of an interconnect test system. Figure I.8.8 illustrates specimen fabrication (based on using a chevron-shaped interconnect), testing, and an example of resulting test output for apparent $K_{Ic}$ of an interconnect system. For the analysis, an example of the output graph shown in Figure I.8.7 is used with classical fracture mechanics principles to estimate $K_{Ic}$.

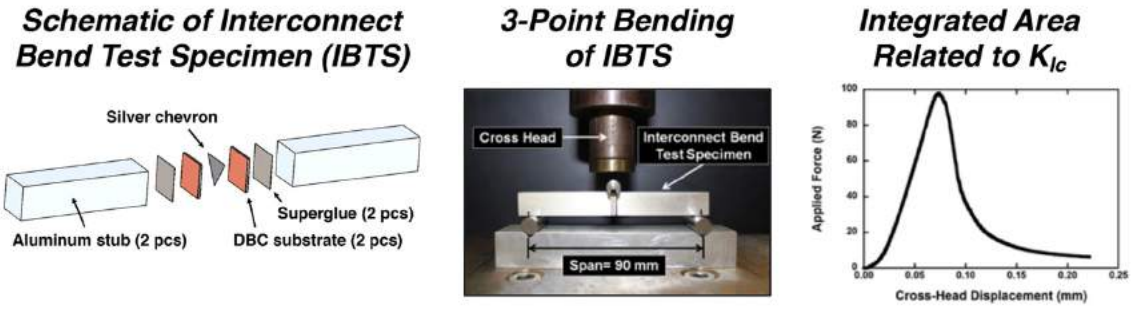


Figure I.8.8 - Specimen configuration (left), testing (center), and an example of a resulting measured response (right).

The developed test method, documented here for the first time, showed that apparent $K_{Ic}$ of the interconnect test system is less than that of bulk sintered Ag. This is illustrated in Table I.8-1. These results mean that if delamination or crack propagation occurs in these sintered-Ag interconnect systems, the cracking is likely to occur between the sintered Ag and the plating and not within the sintered-Ag interconnect.

**Table I.8-1 - Apparent fracture toughness comparisons**

| Interconnect Material | Apparent Fracture Toughness (MPa√m) |
|---|---|
| Bulk sintered Ag | 2.3–2.4 |
| Sintered-Ag interconnect with electroless Ag plating | 1.5 ± 0.2 |
| Various solders | 1–11 |

## Conclusions

- Contact drying enables the use of pressureless sintering, large area bonding, and reflow-oven processing.
- Reflow-oven technology can be used to fabricate strong, pressurelessly sintered Ag interconnects.
- Ti/Ni/Ag plating on silicon, bonded to sintered Ag, resulted in very strong interconnects.
- Susceptibility to crack growth or delamination in interconnects is related to $K_{Ic}$, and the Ag-plating–sintered-Ag combo needs improvement.

## Key Publications

1. A. A. Wereszczak, B. R. Chen, and B. A. Oistad, "Reflow-oven-processing of pressureless sintered-silver interconnects," in review, *Journal of Materials Processing Technology* (2017).
2. A. A. Wereszczak, B. R. Chen, O. M. Jadaan, B. A. Oistad, M. C. Modugno, J. W. Sharp, and J. R. Salvador, "Cantilever testing of sintered-silver interconnects," in review, *Journal of Materials Science: Materials in Electronics* (2017).
3. A. A. Wereszczak, M. C. Modugno, and B. R. Chen, "Apparent mode i fracture toughness of pressureless sintered silver interconnects," in review, *IEEE Transactions on Components, Packaging, and Manufacturing Technology* (2017).

4. A. A. Wereszczak, M. C. Modugno, B. R. Chen, and W. M. Carty, “Contact drying of printed sinterable-silver paste,” in press, *IEEE Transactions on Components, Packaging, and Manufacturing Technology*, (2017).
5. A. A. Wereszczak, J. E. Cousineau, K. Bennion, H. Wang, R. H. Wiles, T. B. Burress, and T. Wu, “Anisotropic thermal response of packed copper wire,” *Journal of Thermal Science and Engineering Applications*, 9(4): 410061-410069 (2017); doi: 10.1115/1.4035972.
6. Z. Liang and A. A. Wereszczak, “Planar interconnection technologies and reliability in 3-D packaged SiC power electronic modules,” *Proceedings of the ASME 2016 International Mechanical Engineering Congress and Exposition, IMECE2016*, November 11–17, 2016, Phoenix, AZ.

## I.9 Carbon Nanomaterial Enabled Novel Ultra Conductive Copper Composites

**Tolga Aytug, Principal Investigator**
Oak Ridge National Laboratory (ORNL)
National Transportation Research Center
2360 Cherahala Boulevard
Knoxville, TN 37932
Phone: (865) 574-6271
E-mail: aytugt@ornl.gov

**Susan A. Rogers, Technology Manager**
U.S. Department of Energy
Phone: (202) 586-8997
E-mail: Susan.Rogers@ee.doe.gov

Start Date: October 1, 2016 End Date: September 30, 2017
Total Project Cost: $475,000 DOE share: $475,000 Non-DOE share: $0

### Project Introduction

This project focuses on the development of a new class of high-performance copper (Cu) tapes (i.e., ultra-conductive copper, UCC, composites) that are higher in electrical (and possibly thermal) conductivity than pure Cu to reduce volume/weight and improve higher temperature operation reliability of electric motors while improving their overall efficiency and power density. The new concepts and methods developed under this project are expected to help meet the DOE 2020 cost and performance targets for electric motors. After more than 10 years of global research and development efforts, the most promising UCC composites are composed of 1D carbon nanotubes (CNTs) and Cu, but the room temperature performance of these composites is inconsistent and the synthetic methods are not scalable and reproducible. Based on a theory-aided experimental approach, this project addresses these fundamental challenges to successful development of UCCs with electrical conductivities exceeding that of pure Cu.

The power losses associated with the electrical resistance of Cu adversely impact the efficiency and performance of all electric devices. Ballistic electrical transport in CNTs (the charge carriers can travel over approximately 500 nm in nanotubes without scattering) is expected to improve the conductivity of the Cu matrix with additional CNT-enabled benefits, including low-weight, flexibility, and better thermal management. A few promising Cu-CNT composites with conductivities increased by 30% compared to the International Annealed Cu Standard have been demonstrated, but only on micrometer-long sample pieces [1,5]. And further improvements on these UCCs have been hampered by poor fundamental understanding of Cu-CNT interactions affecting bulk electrical and thermal transport properties. Besides, most of the present UCC processing strategies are unstable (leading to inconsistent results) and are limited to laboratory-scale operations, rendering them unsuitable for large-scale commercial development and production. The current approaches to make Cu-CNT composites include electrolytic codeposition of Cu ions and CNTs on Cu cathodes, electrolytic coprecipitation of Cu nanoparticles and CNTs followed by consolidation into wire form, die casting of liquid Cu and CNTs, acoustically assisted Cu wire coating with CNTs, high pressure laser chemical deposition with simultaneous laser-induced cladding with Cu, and powder metallurgical approaches using spark plasma sintering to form a Cu composite. The main problems associated with these methods are (1) the lack of controlled alignment of CNTs along the direction of the current flow, (2) the phase segregation of CNTs from the Cu during wire processing, and (3) the lack of fundamental understanding of how nanotube properties and CNT-Cu interfaces/interactions affect macroscale properties. Using scalable, cost-effective, and commercially viable processing methods, this project aims to demonstrate a novel technological platform to

produce UCC conductors not only for components in electric vehicles but also for a broad range of electrical systems.

## Objectives

Electric motor volume reduction and improvements in efficiency are limited in part by the electrical conductivity limitations of copper windings. The overall objective of this project is to design, develop, and implement scalable fabrication approaches and material technologies for the production of an advanced conductor with reduced electrical loss—carbon nanomaterial–enabled UCC conductors. Specific research and development efforts in FY 2016 included (1) establishment of necessary infrastructure, (2) identification of candidate nanocarbon materials, (3) establishment of controllable processing techniques to enable scalable assembly of Cu-CNT multilayer composites, (4) establishment of prototype UCC materials demonstrating improved electrical conductivity, and (5) theoretical modeling to understand metal-nanocarbon interface properties for optimized electronic and thermal transport characteristics.

## Approach

Our overall approach is to couple theoretical and experimental efforts to enable the design and scalable, reproducible fabrication of advanced composites that have electrical and thermal conductivity exceeding that of pure Cu and current Cu-CNT composites. To achieve this, two interrelated and equally important tasks are being pursued: (1) development of controllable processing techniques to enable scalable assembly of Cu-CNT multilayer composites (Figure I.9.1) and (Figure I.9.2) theory-guided optimization for high-performance Cu-CNT multilayer composites. Figure I.9.1 schematically describes the process flow for producing UCC tapes, starting with formulating stable CNT dispersions, deposition of uniform CNT coatings using commercially viable practices, homogeneous deposition of thin films of metals (Cu, Ag) onto CNT-coated tapes, and post-thermal treatment procedures to produce multilayer Cu-CNT-Cu composite architectures.

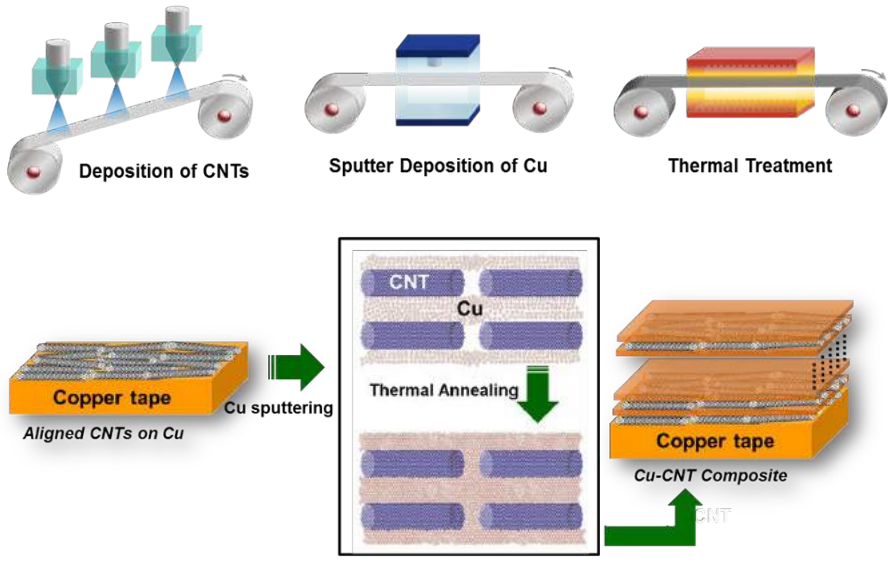


Figure I.9.1 - Top panel: schematic illustration of the process flow for producing UCC tapes. Bottom panel: schematic illustration of the formation of Cu-CNT-Cu multilayer composite architecture.

The degree of nanotube alignment was analyzed by both scanning electron microscopy (SEM) and polarized confocal Raman spectroscopy, where the changes in the intensity of G- and D-bands are highest when nanotubes are parallel to the laser polarization direction. Electrical conductivity of the new composites was characterized in the temperature range from 4 K to 400 K using a physical property measurement system (PPMS) and at room temperature using a four-probe transport setup capable of measuring 7 cm long tapes.

## Results

*Production of stable CNT dispersions and selection of CNT types*

Understanding the dispersion behavior of CNTs in solvents is critical not only for the creation of stable dispersions, but also for the achievement of uniform CNT coatings well-adhered to Cu tapes. A critical part of creating stable dispersions of CNTs in solvents is selection of appropriate surfactants. We have formed more than 100 CNT dispersion formulations in various aqueous and organic surfactant-solvent systems using both single-wall and multiwall nanotubes. So far, the best stable dispersion formulations for effective sonospraying and electrospinning are identified as mixtures of N,N-dimethylformamide and a specially formulated commercial surfactant (AC); and N-Methyl-2-pyrrolidone and AC, respectively. After the deposition of CNTs, the coated Cu tapes were annealed in a vacuum or reducing atmosphere (a mixture of argon and hydrogen) to remove (evaporate) the organic solvent and the surfactant from the CNT matrix. Initial dispersion experiments revealed that the multiwall CNTs (MWCNTs) disperse in aqueous solutions very readily; however, for single-wall CNTs producing stable dispersions proved to be very challenging. We believe that the reason for this behavior is highly dependent on the surface functionality and purity of the CNT materials. That is, the surfaces of MWCNTs are most likely oxidized and possibly have a significant number of defective sites, leading to their easy dispersion in various solutions. To verify this, Raman and SEM analyses were done on MWCNT-coated Cu tapes. Raman analysis showed that there was a high intensity D-band along with the G-band. This band is often referred to as the disorder band or the defect band, and its intensity relative to that of the G-band is often used as a measure of the quality with nanotubes. Based on these results, our efforts were concentrated on optimization of single-wall CNT (SWCNT) dispersions for the fabrication of UCC composites.

*CNT deposition onto flexible Cu tapes*

Currently there are no scalable techniques for deposition of aligned CNTs from a solution. Here, we have identified and explored three new industrially scalable techniques for deposition of aligned CNTs onto metal tapes—an ultrasonic liquid-shear approach (sonospray), electrospinning, and an air-blade technique (Figure I.9.2). These techniques are expected to align nanotubes with their axes parallel to the shear or flow-field direction induced between the droplets and the Cu substrate.

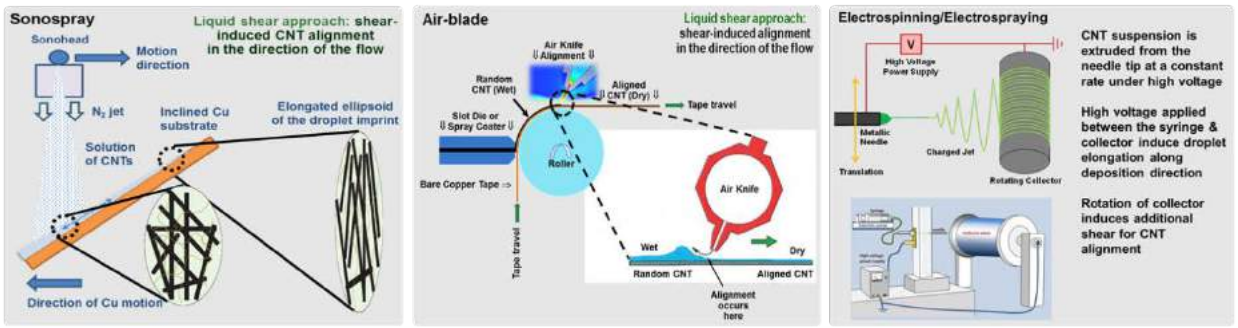


Figure I.9.2 - Left to right: Schematic illustrations of the sonospray, air-blade (and its envisioned reel-to-reel operation), and electrospinning approaches.

In the case of the sonospray approach, two independently controlled syringe pumps deliver the suspension to an ultrasonically activated sonohead (controlled by a piezoelectric crystal oscillating at 120 kHz) that generates a mist of CNT solution in micrometer-size droplets. The $N_2$ jet flowing around the sonohead shapes the mist into round or line contours defined by the design of the sonohead (0.3–10 cm). A continuously aligned CNT layer is deposited as the sonohead moves across the substrate. When a droplet impinges on the inclined surface, it will shear against it to form an elongated ellipsoid-shape droplet imprint, simultaneously aligning nanotubes in the direction of the longest axes. Results from sonospray-processed samples demonstrated that the deposition direction and rastering speed of the spraying nozzle seemed to have the greatest effect on the alignment of the CNTs on the Cu surface. Note that verification of carbon nanotube alignment on Cu tapes is

critical for understanding and optimizing sample performance. Figure I.9.3 compares and correlates the surface morphologies and changes in the G-band intensity (using Raman spectroscopy) of two sonospray samples, processed under different conditions, where one exhibits CNT alignment along the current flow direction and the other shows random surface coverage with no obvious alignment. The Raman data clearly corroborate this observation, demonstrating variations in the intensity of the G-band with respect to sample orientation, where on one sample the polarized beam intensity peaks at roughly 180° intervals, indicating alignment of CNTs along the coating direction, while on the other, G-band intensity stays relatively uniform, implying no prominent alignment of CNTs with respect to sample orientation.

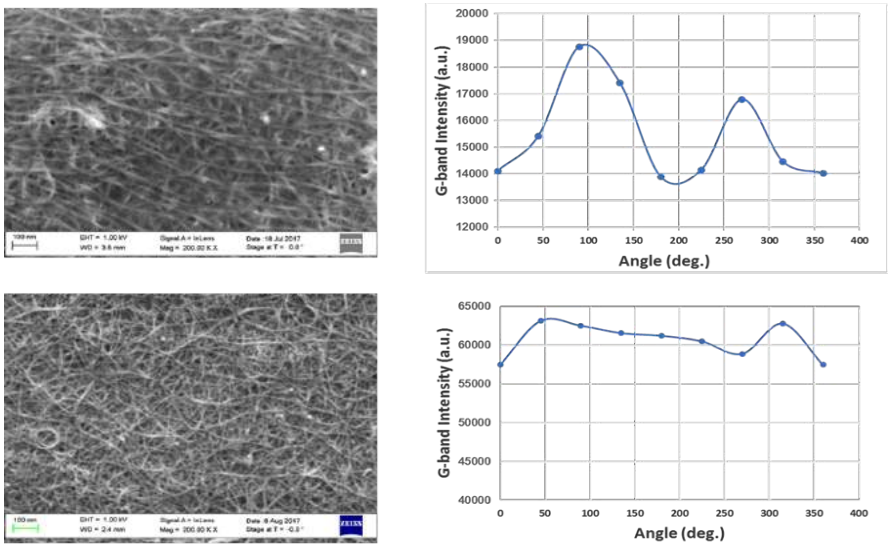


Figure I.9.3 - SEM images and G-band intensity variations on SWCNT-coated copper tapes using an ultrasonic spray coating approach. G-band intensities were determined by Raman spectroscopy as a function of sample orientation angle.

Like the sonospray approach, the air-blade method is expected to provide the maximum shear force to coat and align the CNTs on Cu tapes. In this case, the shear-induced alignment originates from the compressed air flow/jet from a beveled air knife that uniformly spreads the CNTs along the horizontally positioned Cu tape. Except for some preliminary coating studies, FY 2017 efforts were mainly concentrated on sonospray and electrospinning (discussed below), due to achievement of promising results with these two techniques.
As for the electrospinning approach, a CNT suspension is loaded into a syringe and extruded from the needle tip at a constant rate by a syringe pump onto a Cu sheet that is mounted on a rotating drum collector. High voltage applied between the syringe and collector induces droplet elongation along the deposition direction. That is, at a high voltage (typically ranging from 5 to 20 kV), liquid droplets containing CNTs become charged and fly to the collector (i.e., the Cu sheet). Due to the electrostatic force, the charged droplets also split and homogeneously “electrospray” onto the rotating drum covered by the Cu sheet. Accordingly, a rapidly rotating collector results in aligned CNTs. Results showed that the suspension concentration and CNT feeding rate are the two most critical parameters affecting the uniformity and alignment of the coatings. Lower CNT concentration (0.5 mg/mL) combined with feeding rates ranging from 0.1 to 0.3 mL/h, yielded Cu tapes that were homogenously coated and demonstrated orientational harmony, as shown in Figure I.9.4.

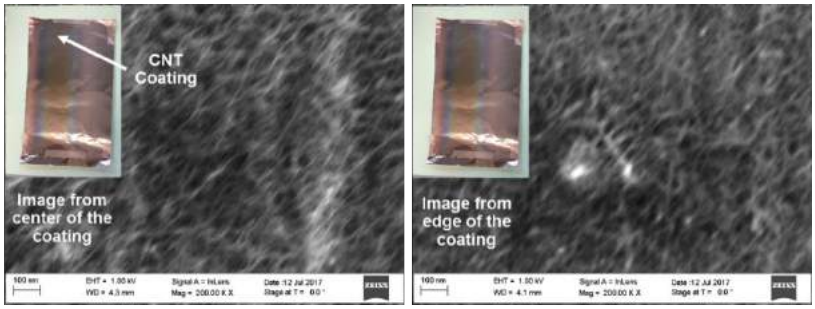


Figure I.9.4 - SEM images of SWCNT-coated Cu sheet using electrospinning approach. Images are taken from the center (left panel) and edge (right panel) of the coated area. Processing parameters: concentration 0.5 mg/mL; feeding rate 0.3 mL/h.

*Assembly and processing of Cu-CNT multilayer architectures*

To establish a highly conductive network, the CNT-coated Cu tapes are covered with a thin layer of Cu film using the magnetron-sputtering technique. To eliminate defects (e.g., porosity), the Cu-CNT composites were post-annealed at temperatures (≤ 500°C) to eliminate any voids/gaps through diffusion of Cu between CNTs and the Cu matrix. The sputtering and annealing steps were conducted in a vacuum and/or a mixture of argon and hydrogen to prevent oxidation of Cu and CNTs. Microstructural characterizations of Cu-CNT-Cu samples revealed the importance of both the metal overlayer thickness and the post-annealing temperature on the quality of the composite architecture. That is, if the metal overlayer is too thin (~50 nm) (Figure I.9.5, left panel), it coalesces and forms a nonuniform discontinuous coverage on the CNT surface after the post-heat treatment step. On the other hand, a thicker metal coating (~500 nm) yields more uniform and dense surface coverage (Figure I.9.5, right panel). These defects are detrimental to the current-carrying capacity of composites.

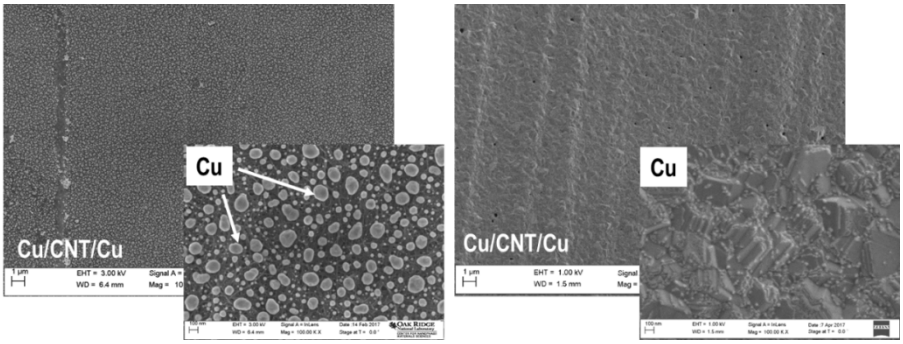


Figure I.9.5 - SEM images displaying the evolution of the surface microstructure of Cu-CNT-Cu tapes. Left panel: Surface morphology of a 50 nm thick Cu-coated CNT/Cu tape after the heat treatment. Right panel: Surface microstructure of a Cu-CNT-Cu sample having thicker Cu overlayer (500 nm).

Understanding the electrical properties of the composite at high temperatures (close to 150°C) is particularly important for reliable and efficient operation of the electric motors. Therefore, using PPMS [top left inset of Figure I.9.6(a)], the resistive behavior of the CNT-Cu samples [inset of Figure I.9.6(a)] was measured at various temperatures ranging from 250 K to 400 K. Results shown in Figure I.9.6a verified reduction of electrical resistivity ~5%–7% over the entire temperature range compared to that of the reference pure Cu samples. The data establish the first quantitative justification of the proposed concept's ability to produce higher conductivity Cu wires. It should be noted that the reproducibility of these initial results needs to be confirmed with additional samples. In efforts to optimize performance, the influence of post-annealing temperature on electrical properties of samples was analyzed. After the CNT depositions, samples were

annealed in a vacuum furnace at two different temperatures and durations (300°C for 4 h, and 500°C for 2 h) followed by sputter deposition of a 1 μm thick Cu overlayer and further annealing at 500°C for 2 h to produce Cu-CNT-Cu tapes.

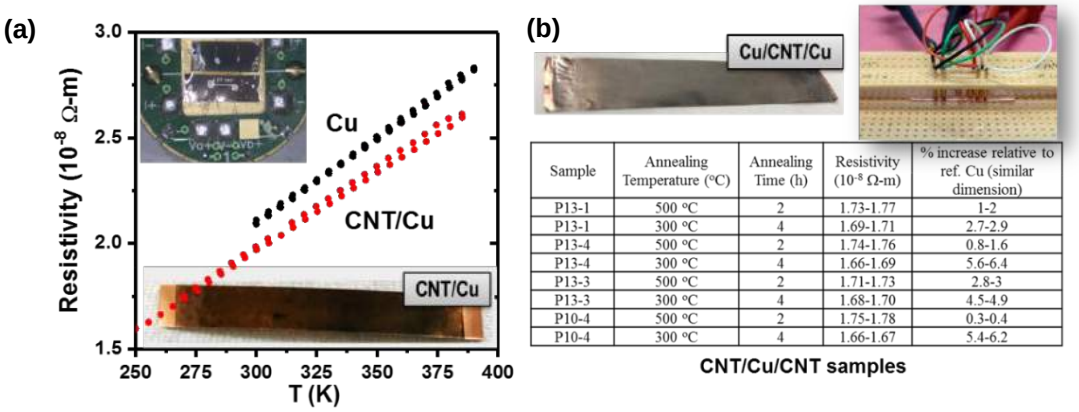


| Sample | Annealing Temperature (°C) | Annealing Time (h) | Resistivity ($10^{-8}$ Ω-m) | % increase relative to ref. Cu (similar dimension) |
|---|---|---|---|---|
| P13-1 | 500 °C | 2 | 1.73-1.77 | 1-2 |
| P13-1 | 300 °C | 4 | 1.69-1.71 | 2.7-2.9 |
| P13-4 | 500 °C | 2 | 1.74-1.76 | 0.8-1.6 |
| P13-4 | 300 °C | 4 | 1.66-1.69 | 5.6-6.4 |
| P13-3 | 500 °C | 2 | 1.71-1.73 | 2.8-3 |
| P13-3 | 300 °C | 4 | 1.68-1.70 | 4.5-4.9 |
| P10-4 | 500 °C | 2 | 1.75-1.78 | 0.3-0.4 |
| P10-4 | 300 °C | 4 | 1.66-1.67 | 5.4-6.2 |

CNT/Cu/CNT samples

Figure I.9.6 - (a) Electrical performance of a SWCNT-coated Cu tape using sonospray (see inset), displaying reduced resistivity as compared to uncoated Cu substrate. Top left inset: Photograph of the PPMS measurement stage. (b) Influence of post-annealing conditions on electrical properties of Cu-CNT-Cu tapes. Insets show photographs of a Cu-CNT-Cu multilayer composite and the four-probe electrical transport setup.

The table in Figure I.9.6(b) summarizes the electrical performance of these samples. Clearly, samples annealed for longer duration, in spite of the temperature being lower, have better electrical properties than their shorter time–processed counterparts. The reason for this could be explained either by incomplete removal of solvent/surfactant from the CNTs or possible damage to the CNTs at high temperatures. In addition to experimental efforts, the project also involves theory-guided optimization of Cu-CNT multilayer composites. The objective of theoretical modeling is to identify key structural parameters of Cu-CNT composites that govern their properties and further optimize those factors to enable high electronic and thermal conductivity. Our hypothesis is that in low-dimensional systems it is the interfaces that define the electric and thermal properties of materials. Therefore, in cases of structural heterogeneity involving interfaces, including Cu layers, the CNT network, individual CNTs interacting with Cu, and the CNT network interacting with Cu, the various components need to be decoupled to understand the individual contributions to the macroscale electrical and thermal properties of UCC. Modeling efforts have been based on first-principles density functional theory to accurately describe the atomistic and electronic structures at the quantum level.

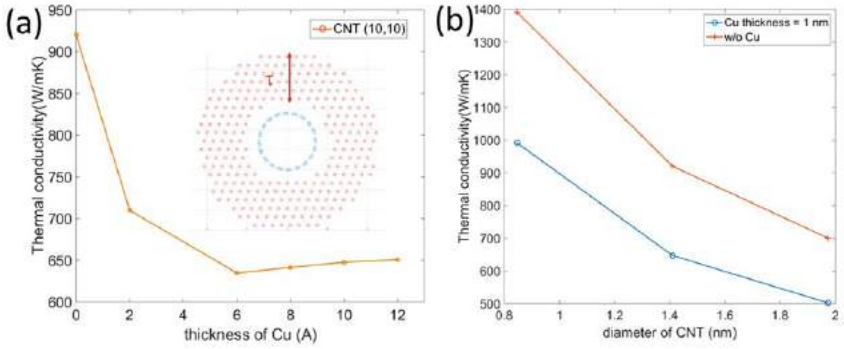


Figure I.9.7 - Thermal conductivity of carbon nanotube (a) depending on the thickness (τ) of the Cu overlayer and (b) depending on the nanotube diameter compared to without Cu coating.

The expectation is that theoretical findings can guide experimental efforts in optimizing materials parameters and ultimately help to develop an advanced low-electrical-loss conductor suitable for integration in electric motors to realize size and volume reductions, power density and efficiency improvements, and DOE cost target requirements. For instance, as shown in Figure I.9.7, investigation of the influence of Cu overlayer thickness and the CNT diameter on the Cu-CNT interfacial thermal transport properties revealed (1) increase in thermal conductivity as the Cu layer thickness decreases [Figure I.9.7(a)], saturating around 6 Å, indicating the optimum thickness for optimum device performance and (2) monotonic decrease in the thermal conductivity as the diameter of the CNT increases [Figure I.9.7(b)], suggesting the need for narrow CNTs for thermal management.

## Conclusions

Under this multiyear project, using scalable, cost-effective, and commercially viable processing methods, we have demonstrated the feasibility of a novel materials/computational modeling platform that can facilitate the design and fabrication of advanced UCC materials for a broad range of industrial applications. The benefits that will be gained from this research can lead to high efficiency, high-density, reduced volume/weight electric motors beyond the limits of what is achievable today. Preliminary results showed reduction of electrical resistivity of around 4%–7% compared to that of the reference pure Cu samples. Due to multistep processing and the associated parameter space for producing UCC tapes, future work will involve optimization of processing protocols and provisions to attain reproducible results along with the highest possible performance characteristics. Future efforts will also include cost analysis and computational feasibility studies to support integration of UCCs in electric drive components.

## Key Publications/Invention Disclosures

1. Tolga Aytug, Ilia Ivanov, and Mina Yoon, “Carbon Nanomaterial Enabled Novel Ultraconductive Copper Composites,” ORNL No. 3766; Sept. 15, 2016.
2. Tolga Aytug, Xiangtao Meng, and Soydan Ozcan, “Carbon Nanomaterial Copper Composites,” ORNL No. 3946; July 25, 2017.

## I.10 High Silicon Laminates for Electric Motors

**Balasubramaniam Radhakrishnan, Principal Investigator**
Oak Ridge National Laboratory (ORNL)
National Transportation Research Center
2360 Cherahala Boulevard
Knoxville, TN 37932
Phone: (865) 241-3861
E-mail: radhakrishnb@ornl.gov

**Susan A. Rogers, Technology Manager**
U.S. Department of Energy
Phone: (202) 586-8997
E-mail: Susan.Rogers@ee.doe.gov

Start Date: October 1, 2016 End Date: September 30, 2017
Total Project Cost: $235,000 DOE share: $235,000 Non-DOE share: $0

### Project Introduction

Iron-silicon (Fe-Si) steels containing up to 6 wt % Si are very attractive soft magnetic materials for motor applications. For high-frequency applications such as in the traction motor, the eddy current loss is significantly reduced because of the high resistivity of the steel. However, steels containing more than 3 wt % Si are very brittle and cannot be thermomechanically processed to thin sheet like conventional Fe-Si steels that are 3 wt % Si. The only commercial process for making Fe-6Si steels is by Si vapor deposition on low-Si Fe-Si steel sheet followed by diffusion annealing, which results in an expensive steel that is not affordable for motor applications. Previous experimental work on Fe-6Si steel focused on the effect of warm working on eliminating the atomic ordering responsible for brittleness in the alloy. Although atomic ordering was destroyed by warm working, the material did not possess sufficient ductility for subsequent cold rolling, making it clear that new processing strategies are required to achieve the aforementioned objective.

### Objectives

- Identify critical material and process variables that influence room-temperature formability of high Si, Fe-Si steel.
- Identify potential alloying additions to Fe-Si to promote bulk thermomechanical processing without significant loss of magnetic properties.

### Approach

One of the methods used in the literature to improve the ductility of the alloy is to subject it to extremely high cooling during solidification from the melt (planar flow casting). Although characterization of the as-cast material shows that the ordering persists in the alloy, an interesting observation is the extent of microstructural refinement that occurs during rapid solidification. Therefore, it is not clear whether the ductility in this case is the result of the extreme microstructural refinement or the lack of atomic order.

One strategy we pursued was to devise a novel thermomechanical processing route to achieve microstructural refinement similar to what is seen during rapid solidification. The thermomechanical processing parameters were systematically varied to optimize the output microstructure. Previous warm-working experiments indicated that the addition of parts-per-million (ppm) levels of boron might be beneficial for promoting room-temperature ductility by strengthening the ferrite grain boundaries. Therefore, as part of the current investigation, eight different Fe-Si-B alloys with varying levels of B from 0 to 500 ppm were processed and their room temperature ductility evaluated.

Another strategy to enable room-temperature formability is to introduce ternary and higher order alloying additions to the steel to delay or eliminate the atomic ordering of Fe and Si that causes brittleness. Since it becomes very expensive to examine a number of alloys with different compositions, we decided to perform high-throughput, first-principles simulations and screen a number of Fe-Si-X-Y alloys to investigate the stability of the ordered phase in the presence of the alloying addition.

All alloys were melted using vacuum arc and were cast into metal molds. They were first homogenized at high temperatures to eliminate any potential microsegregation, followed by hot working, warm rolling, and specially designed annealing heat treatments followed by room-temperature rolling to assess the ductility.

## Results

The results indicated that (1) significant structural refinement could be achieved by optimizing the process parameters and (2) boron had a beneficial effect up to a certain level, beyond which room-temperature rolling suffered. By optimizing the alloy chemistry and the processing parameters, a maximum room-temperature rolling reduction of 77% could be obtained in a Fe-6.5Si-xB alloy. It was also found that such an amount of reduction could be sustained reproducibly under optimized alloy and processing conditions. However, cold rolling introduced significant edge cracking in the steel although a significant width of the steel sheet showed mechanical integrity. Further optimization is necessary to eliminate the edge-cracking issue. The steel sheet after 77% reduction at room temperature is shown in Figure I.10.1.

Figure I.10.1 - Fe-6.5Si-xB steel thermomechanically processed and rolled at room temperature to a reduction of roughly 77% reduction in thickness.

Initial first-principles studies were focused on the ability of the B2 structure in the presence of a transition-metal ternary alloying addition. The focus was to identify those alloying additions that would cause a significant change in the volume of the B2 unit cell, thereby indicating an effect on the stability of the B2 structure. Figure I.10.2 shows the stable volume of the B2 unit cell when half the Si in the B2 structure is substituted by the alloying element. Each row represents a specific transition element. It is clear that of all the elements considered, the element corresponding to row 2 has the largest change in the volume of the unit cell. This finding provided the clue that element #2 will have a significant effect on the stability of B2. However, it is not sufficient to just destabilize B2. We should also make sure that the addition of B2 does not significantly lower the magnetic properties of the Fe-Si alloy. Figure I.10.3 shows the change in the magnetic moment of B2 with ternary alloying. It is clear that alloying addition #2 has a favorable effect on the net magnetic moment of B2; therefore, it is expected that the addition of this element will not decrease the magnetic properties of the Fe-Si steel.

| A | B | C | Alpha | Beta | Gamma | Volume |
|---|---|---|---|---|---|---|
| 4.44657 | 4.44657 | 4.44657 | 90.0000 | 90.0000 | 90.0000 | 87.917566 |
| 3.86893 | 4.93500 | 6.40939 | 90.0000 | 90.0000 | 113.0750 | 112.584798 |
| 4.53791 | 4.54592 | 4.67733 | 90.0000 | 90.0000 | 92.0154 | 96.428947 |
| 4.45849 | 4.46405 | 4.63390 | 90.0000 | 90.0000 | 91.8568 | 92.179687 |
| 4.37296 | 4.39929 | 4.60278 | 90.0000 | 90.0000 | 91.9111 | 88.498713 |
| 4.39202 | 4.41174 | 4.58006 | 90.0000 | 90.0000 | 91.6404 | 88.709018 |
| 4.38328 | 4.50580 | 4.60229 | 90.0000 | 90.0000 | 91.2789 | 90.873575 |
| 4.00552 | 4.97202 | 4.49362 | 90.0000 | 90.0000 | 91.4891 | 89.462566 |
| 4.06040 | 4.98971 | 4.55847 | 90.0000 | 90.0000 | 92.6741 | 92.254939 |
| 4.31676 | 4.93861 | 4.56918 | 90.0000 | 90.0000 | 98.6384 | 96.304447 |

Figure I.10.2 - Change in volume of B2 unit cell in the presence of a ternary alloying addition.

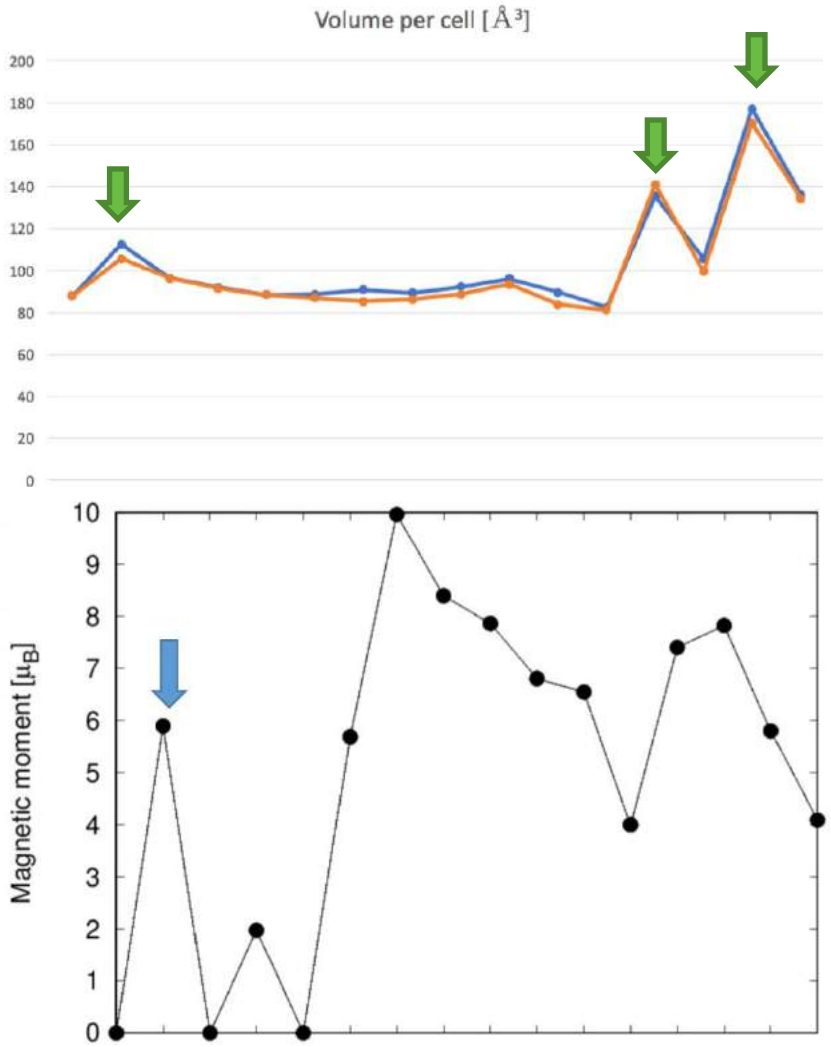


Figure I.10.3 - Change in the unit cell volume of B2 structure (Fe-Si) with ternary alloying addition. Two additional elements (#13 and #15, indicated by arrows) were identified that had higher volume change compared with previously identified element #2.

First principles modeling has identified two different potential ternary alloying elements that have a much more significant effect in destabilizing the B2 order in Fe-Si alloys compared with element #2 discussed

previously in addition to increasing the magnetic moment relative to Fe-Si, shown in Figure I.10.3. However, the two newly identified elements have a significantly lower melting point than Fe. We are in the process of identifying a process by which these alloying elements can be effectively added into an Fe-6Si binary. However, element #2 has a melting point comparable to iron. Ternary Fe-Si-Y alloys (Y = element #2) with varying concentrations of Y have already been cast and are being processed for evaluating room-temperature ductility.

## Conclusions

The design of the novel thermomechanical processing to achieve microstructural refinement and enable room-temperature forming of Fe-6.5Si steel appears to be working, although continued optimization in combination with the proposed ternary alloying additions based on first-principles predictions have to be performed to eliminate edge-cracking issues.

## Key Publications

None. A patent application will be filed before any open publication.

## I.11 Cost Modeling

**Gregory Smith, Principal Investigator**
Oak Ridge National Laboratory (ORNL)
National Transportation Research Center
2360 Cherahala Boulevard
Knoxville, TN 37932
Phone: (818) 522-7067
E-mail: Gregory.Smith@flxpwr.com

**Susan A. Rogers, Technology Manager**
U.S. Department of Energy
Phone: (202) 586-8997
E-mail: Susan.Rogers@ee.doe.gov

Start Date: October 1, 2016 End Date: September 30, 2017
Total Project Cost: $234,108 DOE share: $234,108 Non-DOE share: $0

### Project Introduction

The purpose of this project at a high level is to perform cost modeling of electric traction drive systems (ETDSs) by determining the baseline (As-Is) and new technology (To-Be) volume production cost. The cost is determined with a complete engineering assessment, which helps projects meet program objectives, along with a clear understanding of the commercial implications of insertion of that new technology, and which is critical for vehicle electrification success. Cost and production constraints continue to be the most significant barriers to market adoption of electric propulsion, even with the progress that the DOE Vehicle Technologies Office (VTO) has achieved. A method of quantifying market implications of program initiatives must be done consistently and continuously, and the comprehensive understanding of cost developed in FY 2015 and FY 2016 has been continued. The cost model was used to assess the impact of new technologies towards achieving DOE targets. The existing cost model tool provided a means to make assessments between product requirements, component properties, and technology approaches for motors and power electronics. This information can be used to evaluate the project during all stages of development to determine its value, as well as the project's potential for achieving long-term programmatic objectives.

### Objectives

Use the cost model along with production constraints to make project assessments. These assessments will be used to determine project direction in meeting DOE program objectives. Having a consistent and accepted evaluation of projects provides the necessary tool to determine a viable R&D roadmap. A method of evaluating the implications of inserting new technologies will be developed and implemented in FY 2017. This will require engagement of both original equipment manufacturers (OEMs) and the supply base to understand and document both recurring and nonrecurring costs along with any production constraints. The cost model will be updated, as appropriate, based on these inputs and any new rate and factor information. Understanding the complexity of the production cycle, tools, and waste can aid in establishing fruitful areas for future R&D while also allowing secondary effects to be identified.

### Approach

High-quality engineering assessments need to be credible, well-documented, accurate, and comprehensive. A knowledge base of the industry was built through OEMs and supplier engagement. This project identified and documented basic knowledge of all elements required to produce an electric drive. This included equipment, materials, and manufacturing processes. A cost evaluation of existing technology (As-Is) and new technology (To-Be) including recurring and nonrecurring was performed. Trade-studies were also performed to determine the appropriate direction for ETDS.

Documentation includes an estimated bill of material (BOM) and a bill of process (BOP) to define labor and equipment content. Cost estimates were generated based on the BOM and BOP. Iterations were then performed based on variations of materials, processes, equipment, and development to assess R&D pathways. These iterations provided both recurring and nonrecurring costs used in development of the power electronics and electric machines "cost walk" for achieving ETDS goals.

A review processes was conducted to verify and ensure consistency with auto industry goals and trends. Tracking and verification was performed with the Electronics and Electrical Tech Team (EETT). Engagement with the industry supply base was performed at various public events throughout the year. Auto industry trends were also reviewed to ensure alignment of R&D activity with long-term changes in the market.

### Results

Cost modeling resulted in significant changes in the R&D plan for ETDS. These changes have been driven with a new overall ETDS cost of $6/kW and an increase in power density to 33 kW/L by 2025. Other factors driving charge are continued progress of wide bandgap (WBG) switches and new industry trends in electrified skateboard architectures. These factors have resulted in development of a cost walk driven by high-density packaging and cost that dictates a fundamental rethinking of power electronics and electric machines. Figure I.11.1 shows cost reduction driven by normal production improvements and by R&D.

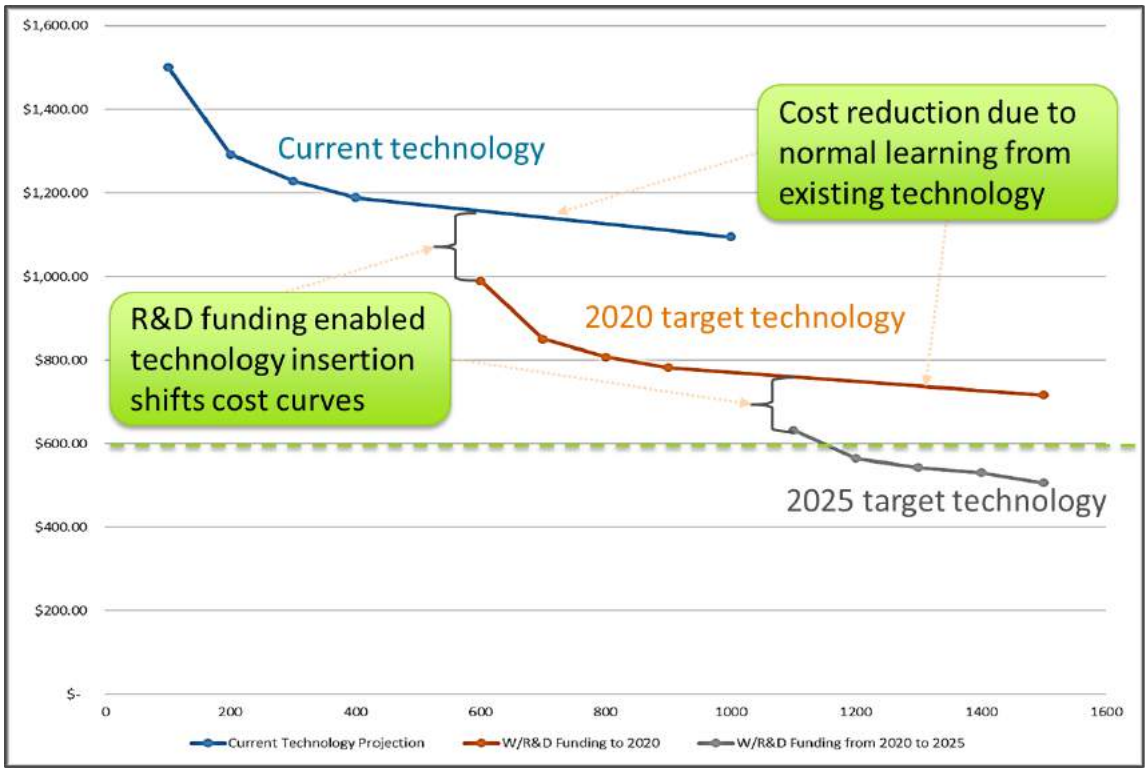


Figure I.11.1 - ETDS cost reduction driven by R&D.

An assessment of industry/market developments was performed to understand how they might impact technology and cost. Vehicle and transportation trends were defined based on literature reviews and OEM inputs. The assessment revealed four significant trends that are occurring in the vehicle and transportation space:

1. Electrified skateboard chassis are being adopted. The skateboard design provides greater vehicle design freedom, more usable passenger space, and a modular platform to increase production scale.

2. Mobility as a service changes vehicle assessment from a traditional ownership model into a fleet ownership model that is driven by life cycle cost. Additionally, this is driving onboard power and electromagnetic interference requirements, autonomous charging, and the need to maximize usable space on the vehicle.
3. The production scale needed for mass market viability has moved from 100K to 500K units per platform. This has been driven by the intense competition in the auto industry.
4. Vehicle performance requirements are driving higher power systems. Customers demand significantly faster acceleration along with larger, more versatile vehicles.

These trends are driving the need for radical changes in the electric drive to be commercially successful. The electric drive system now needs to (1) be packaged within a skateboard chassis; (2) have durability increased from 150,000 to 300,000 miles; (3) have an 8x increase in power density; and (4) be modular and scalable for vehicle platform variants. Achieving this requires heterogeneous or multiphysics integration of materials, carbon fiber–infused metals, a new class of isolation materials, high-temperature materials, and new thermal management techniques.

Technical targets were developed with the EETT early in FY17. The Automotive Integrated Power Module (AIPM) and the Advanced Electric Motor Drive (AEMD) documents were created to set the overall needs of the program and to provide the needed technical metrics. The AIPM and AEMD target development also included supplier feedback. Suppliers verified that the technical targets were appropriate and in line with requests they see globally. Power levels typically are in the 100 to 200 kW range. Operating voltages are trending upward to the 600 to 800 V range.

A cost walk was then developed based on industry trends and technical targets. The development of the cost walk defined how cost targets would be met. Technologies were evaluated for their potential cost and size reduction to determine appropriate areas of work. Figure I.11.2 represents the inverter and motor R&D areas necessary for accomplishing the DOE targets. Subcomponent cost targets were then set (see Table I.11-1). The power electronics strategy is to significantly increase power density through multiphysics integration, which involves the development of interconnect technology, materials, and thermal management techniques. Additionally, component chip set improvements, along with better WBG utilization, will be needed. The electric motor strategy is to develop new materials/processes for steel, copper, and magnets.

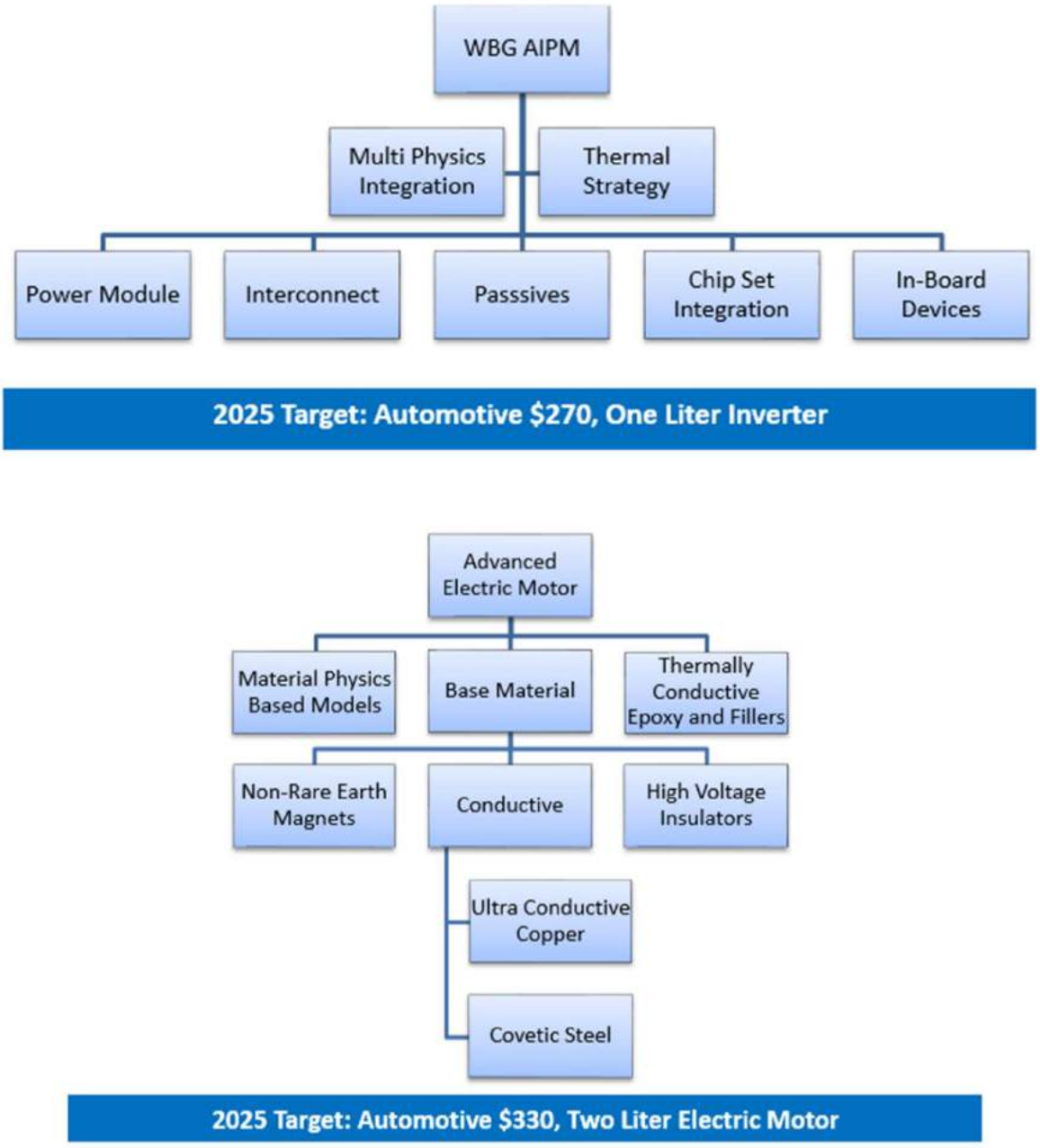


Figure I.11.2 - ETDS inverter and motor R&D areas.

Table I.11-1 - 2025 cost targets for 100 kW ETDS

| Inverter Component | Cost ($) |
|---|---|
| Power Module | 59 |
| DC Bus Capacitor | 38 |
| Control Board | 37 |
| Gate Drive | 60 |
| Bus Bars/Terminal Block | 26 |
| Current Sensors | 11 |
| Miscellaneous | 39 |
| Total Unit Cost | 270 |
| **Motor Component** | **Savings ($)** |
| Stator | 154 |
| Rotor | 78 |
| Magnet | 13 |
| Miscellaneous | 85 |
| Total Unit Cost | 330 |

## Conclusions

An assessment of industry trends and requirements were completed. Both recurring and nonrecurring costs for the As-Is and To-Be configurations were estimated. This lead to a technology development strategy that identified key R&D activities necessary for achieving DOE cost reduction targets. Projects are now being driven by the newly completed cost walk and supporting EETT roadmap. Cost modeling has led to well-defined cost metrics that are reassessed quarterly to ensure program targets will be met. This effort has been accomplished with significant involvement from OEMs, suppliers, national labs, and DOE.

## Key Publications


1. G. Smith, “Electric Drive Technology Research & Development 2025; and the Sub Component 2025 Cost Targets,” presented at EETT, October 2016.
2. G. Smith, “Electric Drive Technology Research and Development 2025,” presented at EETT, November 2016.
3. G. Smith, “Electric Drive Technology Overview,” presented at EETT, January 2017.
4. G. Smith, “Electric Drive Technology Cost Walk Review,” presented at EETT, August 2017.

## I.12 Cost-Effective Fabrication of High-Temperature Ceramic Capacitors for Power Inverters

**U. (Balu) Balachandranm Principal Investigator**
Argonne National Laboratory
9700 S. Cass Avenue
Argonne, IL 60439
Phone: (630) 252-4250
E-mail: balu@anl.gov

**Steven Boyd, Program Manager**
U.S. Department of Energy
Phone: (202) 586-8967
E-mail: Steven.Boyd@ee.doe.gov

Start Date: January 1, 2014 End Date: January 30, 2017
Total Project Cost: $4,524,000 DOE share: $3,714,000 Non-DOE share: $810,000

### Project Introduction

Capacitors are essential components of power electronics for carrying out a host of functions in pulse power and power electronics applications such as pulse discharge, filtering, voltage smoothing, coupling, de-coupling, DC blocking, power conditioning, snubbing, electromagnetic interference suppression, and commutation in power electronics. They are a critical to the performance of power inverter modules within electric drive vehicles (EDVs) which directly affects fuel efficiency and battery life. Capacitors occupy ≈35% of the inverter volume and account for ≈25% of the weight in current designs. Thus, even if all other components in an inverter are reduced significantly, the capacitor requirement is a serious impediment to achieving the required volume and weight reduction. In addition, the use of high-temperature coolants further exacerbates the situation because existing film capacitors lose their capability to absorb ripple currents at elevated temperatures, necessitating the addition of extra capacitors. Increasing the volumetric performance (capacitance per unit volume) of DC bus capacitors is required, and their maximum operating temperature must be increased to assure reliability requirements. Ceramic capacitors have the greatest potential for volume reduction; they could be as small as 30% of the volume of a polymer-based capacitor currently used in EDVs. Ceramics offer high dielectric constants and breakdown fields and, therefore, high energy densities. They also can tolerate high temperatures with a low equivalent series resistance (ESR), enabling them to carry high ripple currents even at elevated temperatures.

Driven by the increasing demand for power electronics with improved performance, high reliability, and reduced size and weight, we developed fabrication technology to make high-temperature, high-dielectric constant ceramic capacitors. Our research [U. Balachandran, D. K. Kwon, M. Narayanan, B. Ma, "Development of PLZT Dielectrics on Base Metal Foils for Embedded Capacitors," J. European Cer. Soc., **30**, 365, 2010; U. Balachandran, M. Narayanan, S. Liu, B. Ma, "Development of Film-on-Foil Ceramic Dielectrics for Embedded Capacitors for Power Inverters in Electric Drive Vehicles," Jpn. J. Appl. Phys. **52**, 05DA10, 2013; B. Ma, M. Narayanan, U. Balachandran, "Dielectric Strength and Reliability of Ferroelectric PLZT Films Deposited on Nickel Substrates," Materials Letters, **63**, 1353, 2009] had shown that the lead lanthanum zirconate titanate ($Pb_{0.92}La_{0.08}Zr_{0.52}Ti_{0.48}O_3$, PLZT) films deposited on base metal foils possess excellent dielectric properties, which are promising for high power applications such as plug-in hybrid electric vehicles. Use of base-metal foils reduces the cost of the capacitor. The stacked and embedded capacitors approaches significantly reduce component footprint, improves device performance, provides greater design flexibility, and offers an economic advantage for commercialization. This technology will achieve the high degree of packaging volumetric efficiency with less weight. Device reliability is improved because the number and size

of interconnections are reduced. The vision of DC bus capacitors by film-on-foil processing of PLZT-based capacitors is compelling and offers U.S. automotive companies a substantial technological advantage over their foreign counterparts.

In power electronics, capacitors with high capacitance are required to work under high voltages. This requirement imposes the additional challenge of fabricating thicker (>5 μm) films. However, due to the well-known critical thickness effect, per-layer thickness that can be achieved by conventional sol-gel method is generally limited to ≈0.1 μm, thus making the conventional spin coating method less attractive to industry when thicker films are needed to meet the operation voltage requirement. A high-rate aerosol deposition (AD) process being developed at Argonne can produce thick PLZT films with desirable high voltage properties at significantly shorter time. AD process can produce dense ceramic films at room temperature without the needs for high temperature sintering; thus making the process amenable for depositing the PLZT films on variety of substrates such as polymer, glass, and metal foils. Therefore, it is a cost-effective method for manufacturing ceramic film capacitors for power inverters in EDVs.

In this project, the team (Argonne, Delphi Electronics & Safety Systems, Sigma Technologies, LLC., and Pennsylvania State University) will collaborate to develop a high-rate, economically attractive AD manufacturing process to produce PLZT-based DC-link capacitors with dielectric properties suitable for advanced power inverter applications. Our R&D efforts focus on developing a lab-scale AD process that is amenable to large-scale manufacturing of PLZT films for EDV inverters, evaluating the underpinning issues of ceramic film capacitor performance and reliability, scaling-up and transferring the AD process technology to industry for manufacturing, and fabricating high-voltage-capable PLZT capacitors defined by the inverter application requirements. Overall project goal is to transfer basic AD process on to a high-throughput rotating-wheel coating system, fabricate and characterize proto-type capacitor, and verifying its performance satisfies the requirements for power invertors.

## Objectives

Overall objective of this project is to develop an efficient, cost-effective process for fabricating PLZT-based capacitors for advanced power inverters in electric drive vehicles. PLZT films satisfy high-temperature and volumetric requirements for advanced capacitors. This project addresses key barriers (capacitor volume, high-temperature operation, as well as fail-safe operation and manufacturability). The proposed aerosol deposition technology will substantially reduce the size, weight, and cost of DC-link capacitors, which will enable the fabrication of smaller, lighter, and less costly EDV power inverters.

## Approach

In our earlier work we have demonstrated that PLZT film capacitors meet EDT performance objectives. However, the spin coating process used to demonstrate PLZT's attractive properties involved several time consuming steps and it is not practical to make large quantities of films needed for practical applications. Therefore, our approach in this project is focused on developing high-rate deposition process to economically make high-dielectric constant, high-temperature, low-cost ferroelectric PLZT dielectric films on thin metal and polymer substrates. Ferroelectrics possess high dielectric constants, breakdown fields, and insulation resistance. With their ability to withstand high temperatures, they can tolerate high ripple currents at under-the-hood conditions. High-dielectric constant materials significantly reduce component footprint, improve device performance, provide greater design and packaging flexibility, achieve high degree of volumetric efficiency with lightened weight, and offer an economic advantage. A high-rate, room-temperature, AD deposition process has been identified as an economically attractive process to make PLZT-based capacitors. PLZT film capacitors made by AD process were evaluated to provide feed-back for process optimization. In collaboration with our industry partners, substantial amount of effort is focused on transferring the AD process to Sigma's rotating-wheel deposition system to make long length PLZT film on moving metalized thin polymer substrate, and fabrication and characterization of prototype capacitors. The longer-length PLZT films deposited on metalized polymer films will be characterized and characterization results are analyzed for improving the process parameters for the rotating-wheel deposition system. The PLZT films produced by the rotating-wheel

deposition system at Sigma will be evaluated at multiple laboratories in order to validate the results and improve the AD process.

The team of Argonne, Delphi, Sigma Technologies, and Pennsylvania State University contains the critical components for bringing to fruition the AD process to manufacture (PLZT)-based DC-link capacitors for advanced power inverters in EDVs. This team continues the fruitful collaboration between Argonne, PSU, and Delphi in developing PLZT-based capacitors, measuring and evaluating the properties of PLZT films, and demonstrating the important advantages of PLZT-based capacitors for automotive power electronics. Sigma Technologies augments the ongoing collaboration between Argonne, PSU, and Delphi by supplying expertise in continuous fabrication of polymer-based capacitors with electrodes designed for benign failure. In this project, Argonne will utilize its experience in processing ceramics to develop first, the combustion synthesis process for producing sub-micron PLZT powder and second, the AD process for fabricating dense PLZT films from the sub-micron PLZT powders. Delphi will verify the properties of PLZT-based DC-link capacitors that are produced and supply critical knowledge of automotive power electronics to engineer the final capacitor to meet the APEEM's specifications. PSU will perform dielectric characterization, reliability testing, electrode design, and testing/validating results. With its expertise in continuous fabrication of polymer-based capacitors, Sigma Technologies provides the background to convert Argonne's laboratory-scale process into an industrial-scale process for fabricating PLZT-based DC-link capacitors with electrodes designed for benign failure.

## Results

In our earlier work, we demonstrated the suitability of using the PLZT film capacitors prepared by sol-gel spin coating fabrication process [B. Ma, D.-K. Kwon, M. Narayanan, U. Balachandran, "Chemical Solution Deposition of Ferroelectric Lead Lanthanum Zirconate Titanate Films on Base-Metal Foils," J. Electroceram. **22**, 383-389, 2009] for power inverter applications. We fabricated high-temperature PLZT film capacitors with high dielectric constant, low dielectric loss, and high dielectric strength by solution deposition techniques [B. Ma, S. Tong, M. Narayanan, S. Liu, S. Chao, U. Balachandran "Fabrication and Dielectric Property of Ferroelectric PLZT Films Grown on Metal Foils," Materials Research Bulletin **46**, 1124-1129, 2011; S. Chao, B. Ma, S. Liu, M. Narayanan, U. Balachandran, "Effects of Pyrolysis Conditions on Dielectric Properties of PLZT Films Derived from a Polyvinylpyrrolidone-Modified Sol–Gel Process," Materials Research Bulletin **47**, 907-911, 2012]. Prototype stacked PLZT film capacitors with capacitance ≈10 μF was fabricated, tested, and verified by Delphi Electronics & Safety Systems and PSU. Despite all the success and positive outcomes with chemical solution process for fabricating PLZT film capacitors, the process itself is slow and requires multiple layers of coatings and intricate heating/annealing schemes to produce capacitors with thickness that can withstand the high voltage (≈450 V) required for DC-link capacitor application. The time consuming sol-gel spin coating process is not practical to make large quantities of PLZT films for practical applications. To overcome this drawback, we developed a high-rate, room temperature aerosol deposition (AD) process that can produce large area dense PLZT films at speeds that are hundreds of time faster than the sol-gel spin coating process. During AD process, PLZT particles are accelerated toward the substrate and, if their speed exceeds a critical value, the particles consolidate upon impact without additional heating of the substrate. Because AD is done without heating the substrate, flexible materials such as polymers, plastics, thin metal foils, glass, etc. can be used as the substrate. By using flexible substrates, PLZT-based capacitors can be produced in a wound configuration, similar to the currently used polymer-based capacitors with benign failure features. The schematic of the AD process is shown in Figure I.12.1.

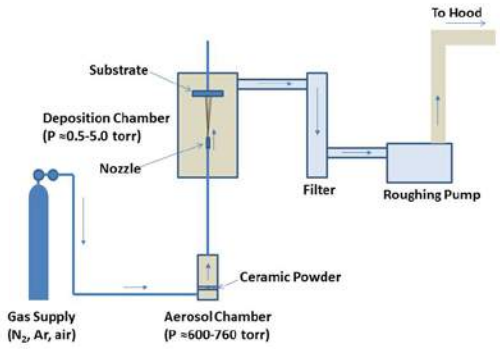


Figure I.12.1 - Schematic of Aerosol Deposition (AD) Process.

Figure I.12.2 shows dielectric properties of a ≈8-µm-thick PLZT film deposited on aluminum metallized polyimide film by AD process at Argonne National Laboratory. The dielectric constant of AD PLZT deposited on aluminum metallized polyimide films exhibits good linear dependence on logarithm of frequency, as shown in Figure I.12.2a. At room temperature and 10 kHz, we measured dielectric constant of ≈100 and dielectric loss of ≈0.015.

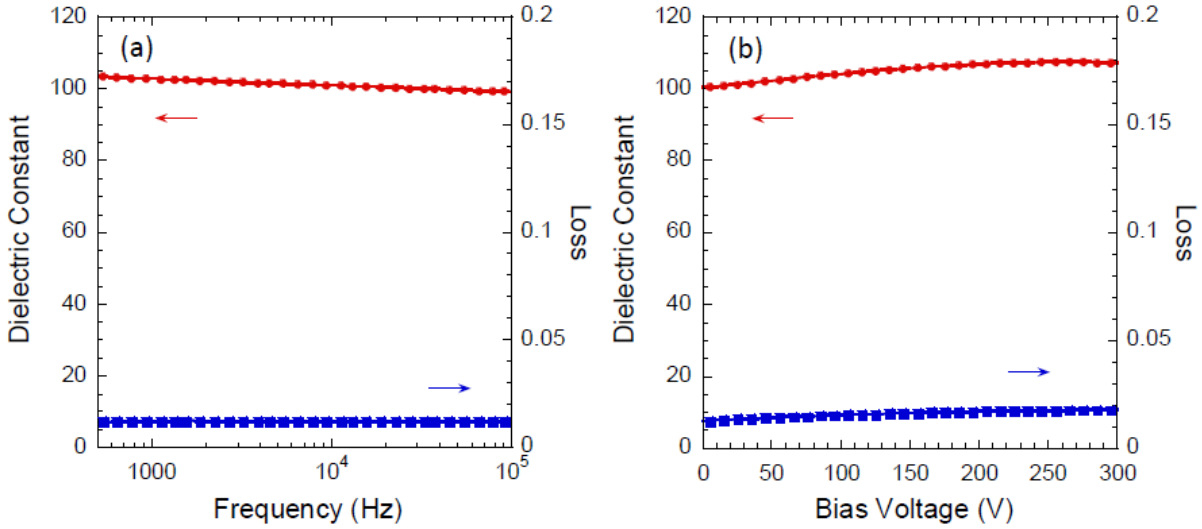


Figure I.12.2 - Dielectric properties of ≈8-µm-thick AD PLZT films deposited on aluminum metallized polyimide substrates as a function of (a) frequency and (b) applied bias voltage.

We transferred the Argonne National Laboratory developed AD process into a rotating-wheel deposition system at Sigma Technologies. We increased the deposition chamber size from <2 $ft^3$ to ≈27 $ft^3$; pumping capacity from ≈150 $m^3/h$ (oil-based pump) to ≈650 $m^3/h$ (dry pump); improved the motion system from experimental X-Y table system (typical film of 7-mm x 15-mm) to rotating wheel system (≈35-mm width x 60-cm diameter); changed the commercial fluidized bed aerosol generator to a proprietary design generator; and moved from offline electrode deposition to inline sputtering process. Figure I.12.3 shows the photos of the rotating-wheel deposition system and the aerosol generator.

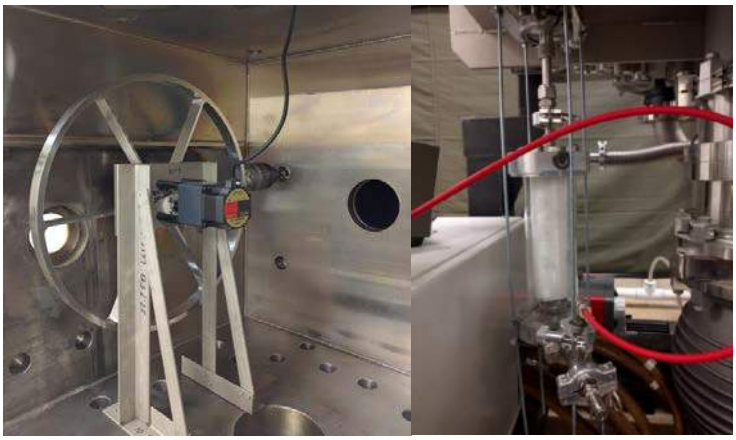

Figure I.12.3 - Rotating-wheel deposition system and the aerosol generator used to make long-length PLZT tapes.

Using the rotating-wheel deposition system at sigma technologies, we fabricated up to ~12" long PLZT tapes on metallized polyimide films. The measured capacitance as function of frequency for long-length PLZT tapes of three different thicknesses before winding are shown in Figure I.12.4. These long-length PLZT tapes were wound around a 0.5" diameter wooden core, arc-sprayed termination metal, and measured the capacitance of the wound capacitor (Figure I.12.5). As seen in Figure I.12.5, there is no significant degradation in the dielectric properties of the wound capacitor. This demonstrates the potential to make wound high-temperature ceramic capacitors with benign failure feature using metallization similar to wound polymer capacitors.

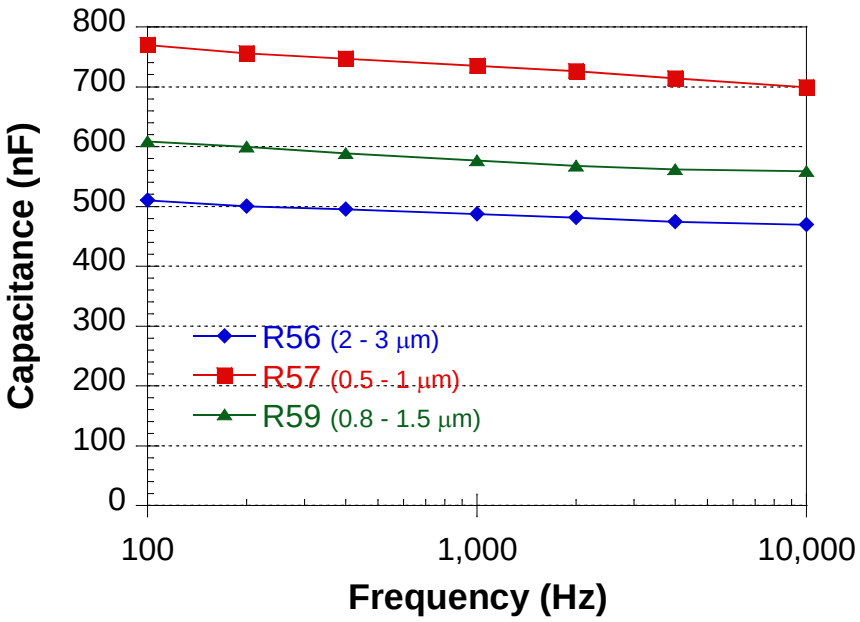


Figure I.12.4 - The measured capacitance as function of frequency for long-length PLZT tapes of three different thicknesses before winding.

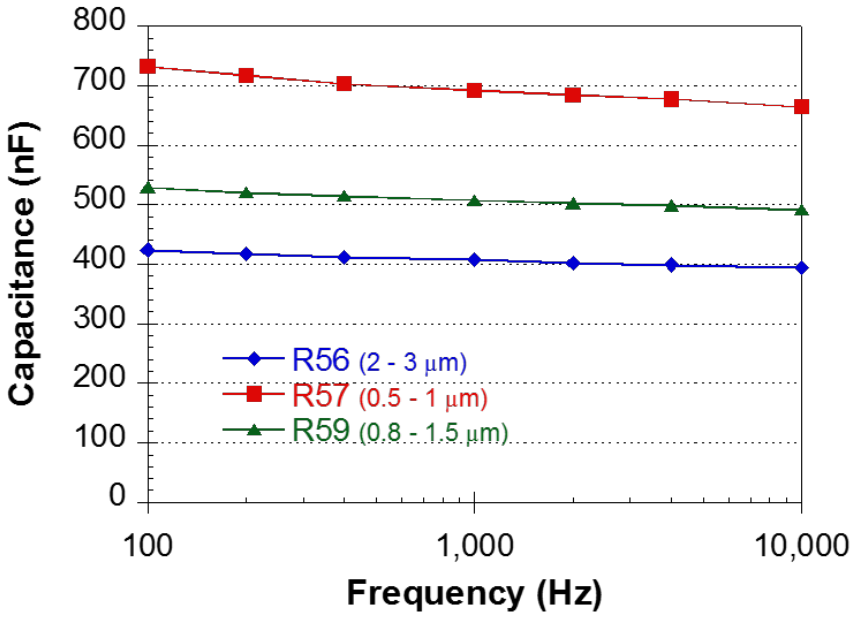


Figure I.12.5 - The measured capacitance as function of frequency for wound capacitors made using the long-length PLZT tapes of three different thicknesses.

## Conclusions

During the past two years, our effort was focused on two important tasks: (1) optimize process parameters of a lab-scale high-rate aerosol deposition process to cost-effectively fabricate PLZT films on thin polyimide substrates, and (2) successfully transfer the AD process to industry for producing long length PLZT tapes. We have succeeded in both tasks. The AD process allows deposition of dense PLZT films at room temperature on variety of substrates. AD PLZT films exhibit superior volumetric and gravimetric specific capacitance. The measured properties show that the PLZT-based ceramic film capacitors meet the EDT requirements for advanced high-temperature capacitors. We successfully optimized fabrication conditions to produce PLZT films by AD process on aluminum metallized polyimide films. PLZT films fabricated by the AD process exhibited a high dielectric constant of ~100, low dielectric loss of <0.02, weak-dependence on applied field, and suitable for high field and high temperature operation. The AD process offers the greatest potential for producing low-cost, reliable, high temperature, compact and light-weight ceramic film capacitors for power inverters. The Lab. Developed AD process was successfully transferred to a rotating-wheel deposition system at Sigma Technologies where up to 12” long x 1” wide PLZT tapes were fabricated. The long-length PLZT tapes made at Sigma technologies were wound around a 0.5” diameter wooden core and metallized for end termination. The wound capacitors were tested for its capacitance as a function of frequency and temperature. We have also demonstrated the benign failure feature of the wound PZT film capacitors. If funds become available, we will make process improvements in the rotating-wheel deposition system to obtain thickness uniformity over longer lengths (~6’ long PLZT tapes), transfer the AD process to a roll-to-roll manufacturing system, demonstrate the high-temperature DC-link capacitor in an inverter, and update detailed cost and commercialization plan.

## Key Publications

1. B. Ma, M. Narayanan, S.E. Dorris, U. Balachandran, “Method for fabrication of ceramic dielectric films on copper foils,” US Patent 9,679,705 B2, awarded 6/13/2017.
2. B. Ma, M. Narayanan, U. Balachandran, S. Chao, S. Liu, “Method for fabrication of crack-free ceramic dielectric films,” US Patent 9,355,761 B2, awarded 05/31/2016.

3. B. Ma, U. Balachandran, S. Liu, "Method of making dielectric capacitors with increased dielectric breakdown strength," US Patent 9,646,766 B2, awarded 5/9/2017.
4. Z. Hu, B. Ma, M. Li, R. E. Koritala, and U. Balachandran, "Ferroelectric PLZT thick films grown by PVA/VA-modified sol-gel process," Mater. Res. Bull., **75**, 167, 2016.
5. M. Narayanan, B. Ma, U. Balachandran, S. E. Dorris, "Method for producing thin film electrodes," US Patent 9,359,223, awarded 06/07/2016.
6. M. R. Fairchild, R. S. Taylor, C. W. Berlin, W. K. Wong, B. Ma, U. Balachandran, "PLZT capacitor on glass substrates," US Patent 9,299,496 B2, awarded 03/29/2016.
7. M. R. Fairchild, R. S. Taylor, C. W. Berlin, W. K. Wong, B. Ma, U. Balachandran, "PLZT capacitor on glass substrates," US Patent 9,230,739 B2, awarded 01/05/2016.
8. B. Ma, Z. Hu, R. E. Koritala, T. H. Lee, S. E. Dorris, U. Balachandran, "PLZT film capacitors for power electronics and energy storage applications," J. Mater. Sci: Mater. Electron, **26**, 9279, 2015.
9. B. Ma, M. Narayanan, S.E. Dorris, U. Balachandran, "Method for fabrication of ceramic dielectric films on copper foils," US Patent 8,974,856 B2, awarded 03/10/2015.
10. B. Ma, S. Liu, Z. Hu, M. Narayanan, and U. Balachandran, "Effect of manganese oxide insertion layer on the dielectric and ferroelectric properties of PLZT films grown by a sol-gel process," Mater. Res. Bull., **67**, 134, 2015.
11. B. Ma, U. Balachandran, S. Chao, S. Liu, M. Narayanan, "Method for Fabrication of Crack-Free Ceramic Dielectric Films," US Patent 8,647,737 B2, awarded 02/11/2014.
12. Z. Hu, B. Ma, S. Liu, M. Narayanan, U. Balachandran, "Ceramic dielectric film capacitors fabricated on aluminum foils by chemical solution deposition," Mater. Res. Bull. **52**, 189, 2014.
13. R.S. Taylor, J.D. Myers, W.J. Baney, "Method of Manufacturing a Shapeable Short-Resistant Capacitor," US Patent 8,407,871 B2, awarded 04/02/2013.

## I.13 Development of Radically Enhanced alnico Magnets (DREaM) for Traction Drive Motors

**Iver Anderson, Principal Investigator**
Ames Laboratory (USDOE), Iowa State University
222 Metals Development
Iowa State University
Ames, IA 50011
Phone: (515) 294-9791
E-mail: andersoni@ameslab.gov

**Susan A. Rogers, Technology Manager**
U.S. Department of Energy
Phone: (202) 586-8997
E-mail: Susan.Rogers@ee.doe.gov

Start Date: October 1, 2014 End Date: September 30, 2018
Total Project Cost: $6,600,000 DOE share: $6,600,000 Non-DOE share: $0

### Project Introduction

This project utilizes a DOE National Lab-lead effort and a demonstrated science-based process to design and synthesize a high-energy-product permanent magnet of the alnico type in bulk final shapes without rare earth (RE) elements, will be competitive with existing commercial RE-based magnets on a cost per MGOe per kg basis, and will have a more sustainable long-term supply and cost outlook. This work utilizes a combination of capabilities centered in Ames Lab, and partnerships with Univ. of Nebraska-Lincoln, NREL (collaboration), ORNL, and with a commercial magnet manufacturer, Arnold Magnetic Technologies, to leverage critical capabilities for permanent magnet development. Through a separate project to extend these results toward commercialization, we are also working in concert with a motor design team at Unique Mobility. The project harnesses the power of fundamental science, modern instrumentation for detailed characterization, and the most advanced processing methods that respond to concerns expressed by industry partners for scale up to full-scale manufacturing capability. New alnico magnets are being developed that do not contain RE elements; instead the main alloy components are Al, Ni, Co, and Fe, which are all abundant and readily available around the world from multiple sources (including recycling) and can be obtained in a sustainable manner. The alnico magnets have superior temperature dependence of their magnetic flux compared to RE-based magnet alloys, without any significant loss through the planned operating range of -55˚C to 180-200˚C. Of key importance for PM drive motors, the new magnets should have superior coercivity (up to 2X) compared to current alnico magnets and retain high levels of magnetization and remanence to enable high-performance operation of advanced PM motors. The magnets also must meet expectations for magnetic anisotropy to satisfy motor load line designs that make full use of their enhanced coercivity and increased mechanical strength and toughness that permits simplified motor design and assembly. Improved alnico magnet alloys and innovative processing methods should enable production of bulk magnets with reduced cost, compared to current RE-based magnets. More specifically, the powder processing method that is being developed will permit mass production of final-shaped magnets in quantities of millions with far less machining and scrap material in a cost-efficient manner.

### Objectives

**Co-lean alnico:** Co facilitates better coercivity and thermal stability in many permanent magnets. In commercial alnico alloys, the total Co content can be as high as ~34-35 at.% in high coercivity grades such as alnico 8 and 9. However, Co is also a strategic element that is subject to price and supply instabilities. Reduction of Co without degrading magnetic and thermodynamic properties of alnico systems is a significant

challenge in the development of new advanced alnico magnets. Our previous work on the chemical ordering of the alnico during spinodal formation has enabled precise guidelines to devise substitution of the Co content by Fe and Ni in a systematic way. This was accomplished by the application of the Rigid Band Approximation approach that assumes the structure of electron bands of the alloy remain rigid even after specific chemical modifications. This is most effective if the applied chemical adjustments do not significantly change the total electron concentration of that alloy, i.e., still abide by the *Hume-Rothery Rule*. New knowledge of the chemistry and phase relationships enables design of several experimental alnico alloys with lower Co content (as much as 40 at.% less) and with gains in coercivity (of 50-60%) as compared to their commercial counterparts.

**Optimized processing and chemistry to enhance coercivity:** Essentially, all of the past studies (and nearly all commercial alnico magnets) and the exploratory portion of our work on improved alnico magnet alloys and properties utilized cast samples. However, we are working to fully develop pre-alloyed gas atomized powder processing to permit rapid adaptation to mass production of final-shape full-scale magnets with an optimum grain-aligned microstructure by a solid state approach. Over the decades, the various classes of alnico underwent extensive optimization of the critical magnetic nano-structure features by magnetic annealing and subsequent heat treatments. Very careful control of times and temperatures were found to be necessary to achieve the best magnetic performance. Quantifying this very sensitive relationship of processing to performance will enable a direct connection of the modelling efforts to the chemical and nano-structural evolution. Using a prototypical alnico 8 alloy, we quenched samples at various points along the rather complex optimized annealing schedule. Extensive characterization of the microstructures, their chemistries and magnetic properties reveal very enlightening insight into the enhancement of coercivity.

**Theory-guided optimization:** The phase evolution and the chemistry of the alnico is quite complex, affecting both the intrinsic and extrinsic properties. Even small changes in the alloy chemistry affect the Curie temperature, which in turn alters the optimal temperature for the magnetic annealing. How the various spinodal phases evolve is dependent, also, on the details of the time and temperature for the subsequent draw cycles. The objective of the multi-scale modeling is to short-circuit the “Edisonian” trial-and-error approach typically used in optimization of alloy design and magneto-thermal processing.

## Approach

The team’s efforts are broken down into three highly synergistic efforts; synthesis of samples, their characterization (which includes chemistry, microstructure, nano-structure and magnetic properties) and theory-guided optimization. Each of these major tasks is comprised of subtasks.

**Synthesis:** This work included: 1)Preparing well-controlled bulk samples to achieve designed levels of nano-structure variation that use current understanding from theoretical analysis to pursue promising modifications of alnico spinodal transformation processing, using: modified alnico 8 and alnico Co-lean (AlNiCo-$8_{AMES}$) with substitutions to modify matrix phase in cast samples, solutionized and quenched, gas atomized pre-alloyed powder, and melt spun pre-alloyed ribbon flake particulate, 2)Examining the effects of ***magnetic annealing*** by studying external “field-on” relationship to spinodal transformation temperature and time at magnetic annealing temperature with effects on spinodal scale and anisotropy, 3)Modifications of alnico annealing (***draw annealing cycles***) for comparison of diffusion kinetics with predictions and use to quantify composition gradients at Fe-Co/matrix interface, 4) Powder processing research to explore the effect of external field applied during compression molding of final-shape magnet bulk samples, along with uni-axial stress effects on stimulating controlled grain growth during secondary sintering in single-phase region. This level of microstructure control is critical to achieving the maximum extent of magnetic property improvements during magnetic annealing and drawing cycles, 5) ***Scale-up*** modified alnico 8 powder processing experiments to fabricate bulk magnets to produce full-size magnet test samples that demonstrate improved magnetic and mechanical properties over similar commercial magnets.

**Characterization:** This work included: 1) Magnetic measurements on bulk samples with hysteresigraph and VSM on micron-scale (powder, ribbon and flake particulate) and other methods as required, 2) Microstructural analysis on all types of samples with FE-SEM, EBSD, STEM with Lorentz imaging, aberration-corrected TEM with atomic resolution, 3) Structural characterization on all types of samples with XRD methods. We used high-energy XRD to characterize the effects of chemical modifications on the relative phase changes in the BCC, $L2_1$ and other low volume phases in the magnetic annealing and draw processes at the Advanced Photon Source at ANL. The characterization of the thermal and mechanical properties provided useful data for magnet synthesis studies providing the motor designers with data to compare to requirements for new motor designs. These measurements will be performed on larger specimens (full-size bulk magnet suitable for electric motor) to characterize the relevant thermal and mechanical properties of the magnet materials, starting with baseline measurements on industry standard magnets. Ames provided samples for specialized testing in NREL test systems who measured the thermal conductivity, compression strength, and transverse rupture strength that spans expected operating temperature ranges from -40 to 150°C.

**Theory:** This work included: 1) Providing accurate atomistic-scale understanding of intrinsic chemical, structural and magnetic properties for comparisons to experiment. This now includes a march up in length scales to simulate the actual microstructure of the alloy and to determine their corresponding magnetic properties, 2) Extending the previous cluster expansion and equilibrium Monte-Carlo modeling developed for Al-Ni-Fe-Co-Ti we include Cu for a more realistic model of alnico 8 and 9. Wang-Landau modeling was used to calculate free energy as a function of temperature and composition while the nano-scale Monte Carlo simulations determined: A) Site occupancies (substitutional alloy concentration effects), B) Interfacial chemical gradients (spinodal decomposition and drawing anneal effects), and C) Elastic properties, 3) Using intrinsic magnetic property calculations (Curie temperature, magnetization, exchange and anisotropy energy profiles and concentration dependencies) to obtain parameters for magnetic nano- and meso-scale simulations. Using input from nanoscale simulations and phase field microstructural calculations, finite element magnetic simulations were performed.

## Results

*Alloy Design and Magnetic Property Development*

**Effects of Ti, Cu and Nb** on microstructure and magnetic properties were systematically studied. Compositions ranging from $Co_{34}Al_{14.25}Ni_{12.5}Cu_yFe_{36.75-x-y-z}Ti_x\ Nb_z$ (x=0~10, y=0-4.2, and z=0- 1.8 in at.%) were obtained by arc-melting in Ar atmosphere.

Since the alloy's ultimate magnetic properties are a fine balance between chemistry and heat treatments, we investigated a range of processes including: solutionized at 1220-1250°C for 30 min. and then quenched in oil; magnetic annealing at 820-850°C for 5-10 min.; drawing at 650°C for 5 hrs+580°C for 15 hrs. An additional drawing step was also applied to some compositions with higher Ti, Cu and Nb contents. The step was: 670°C for 1.5 hrs+650°C for 3 hrs+620°C for 5 hrs+550°C for 10 hrs+520°C for 15 hrs (Figure I.13.1).

The studies of magnetic properties of these samples shows that with increasing Ti, Cu and Nb contents, $H_{cj}$ first increases and reaches a peak value, and then decreases, while $M_s$ and $B_r$ decrease. These behaviors were attributed to the volume changes of $L2_1$ phase, which was verified by TEM microstructure and XRD analysis. A peak value of $H_{cj}$ is obtained when the volume fraction of $L2_1$ phase approaches to ~50%. On the other hand, $M_s$ and Br decreases due to the reduction of FeCo phase. A recorded $H_{cj}$ of 2715 Oe was achieved (Figure I.13.1). In addition, a Br of 7.1 kG and a $H_{cj}$ of 2530 Oe were obtained by appropriately adjusting the contents of Ti, Cu and Nb. These values have met the project milestones for FY 2017.

New knowledge of the chemistry and phase relationships enabled design of several experimental alnico alloys with lower Co content (as much as 40 at.% less) and with gains in coercivity as compared to their commercial counterpart. For example, the total Co content of Co-rich alnico 8 alloys has been reduced by about 15 at.% with a 60% gain in coercivity, up to 2500 Oe. We have filed a patent on this result.

Effect of Cu continues to be puzzling. Aberration-corrected STEM and atom probe tomography is providing keys to its effect. After our full heat treatment Cu clusters coalesce with slightly distorted structure along the Fe-Co rods and matrix (Figure I.13.2). Understanding of this strain effect is being pursued by the theory group.

**Grain Alignment:** Obtaining highly-aligned grains is necessary for high remanence. We are taking a number of approaches. One aspect is to provide a strong magnetic field either to powder particles prior to solutionizing, or during solidification. Another approach is to use the anisotropic growth of the alnico alloy itself.

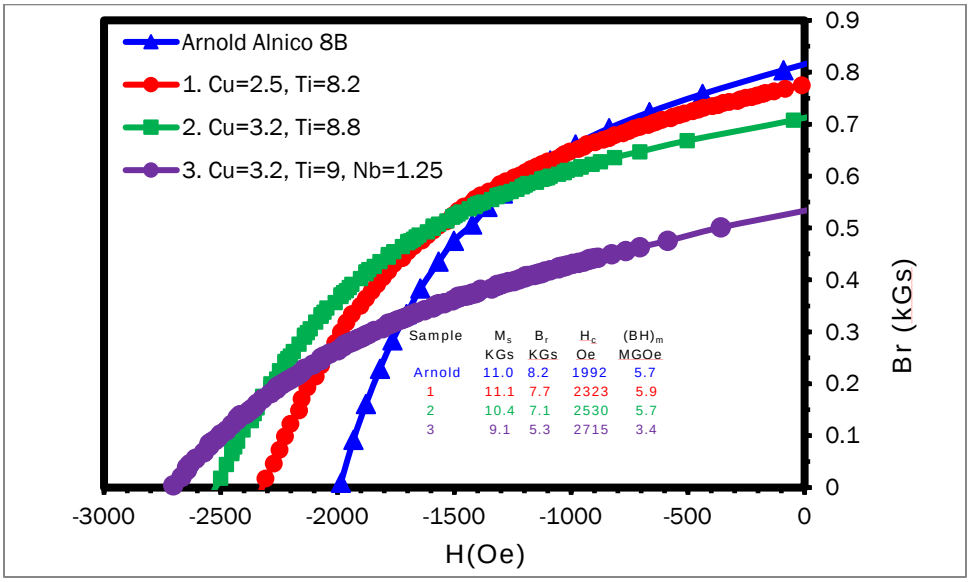


Figure I.13.1 - Demagnetization curves with peak value of Hcj is obtained when the volume fraction of $L2_1$ phase approaches to ~50%. A recorded Hcj of 2715 Oe is achieved. On the other hand, Ms and Br decreases due to the reduction of FeCo phase.

Small additions of Y (1.5 wt.%) develop a (200) texture for the arc-melted alnico 9 magnet. To achieve this goal, we set up a high-field annealing system with a maximum operation temperature of 1250 °C. This system enabled annealing in a field of 45 kOe with subsequent draw annealing for the solutionized buttons; we have been able to substantially increase remanence ratio and coercivity, from 0.70 and 1200 Oe for the Y-free alnico 9 to 0.90 and 1400 Oe for the Y-doped alnico 9, respectively. A high energy product of 7.3 MGOe has been achieved for the fully heat-treated Y-doped alnico 9. The enhancement of coercivity is believed to arise from the introduction of magnetocrystalline anisotropy from 80 nm $Y_2Co_{17}$-type grains, which are exchange-coupled to the main-phase alnico rods.

Another approach is to use a Halbach array to create a highly uniform, precise magnetic field which could be used to orient the magnetic field to specific geometric angles. Specifically, 54° was chosen as the distance between [111] and [001] angles. It is theorized that by controlling the [111] orientation, we can control the final orientation of the [001] direction. EBSD was performed on powder particle cross-sections to establish the number of grains in each particle for a given size. It was quickly apparent that by 17µm powders were bi-crystal, and by 10µm powder was single crystal, this contrasted with the highly poly-crystalline nature of the initial size fraction used which contained 10's of grains (Figure I.13.3). We have filed a patent disclosure on these results.

*Theory and Characterization Correlation*

We have developed accurate and transferable cluster expansion energy models for quinary (Al-Ni-Co-Fe-Ti) and senary (Al-Ni-Co-Fe-Ti-Cu) which enable Monte Carlo simulations to investigate the phase separation and selection as well as the morphology of magnetic phases within the matrix phase of alnico. The simulations

show that phase decomposition into magnetic and matrix phases in alnico are more complete at lower annealing temperature. The concentrations of magnetic elements (Fe and Co) in the magnetic phase are increasing while those in the matrix phase are decreasing as the annealing temperature decreases. The magnetic phase has a B2 ordering with Fe, Al and Ti occupying α-site and Ni and Co occupying β-site. The matrix phase is in a $L2_1$ ordering with Al occupying 4*a*-site, Fe and Ti occupying 4*b*-site and Ni and Co occupying 8*c*-site. We also find that for low annealing temperature a third alloy phase ($\alpha_3$), which is very rich in Ni and in $D0_3$ ordering, will emerge in alnico (see Figure I.13.4. Magnetism, in this third phase, is very weak. Therefore, manipulating the size and position of this phase via controlling the processing condition can provide a possible route to enhance magnetic properties of alnico by increasing isolation of the magnetic phase.

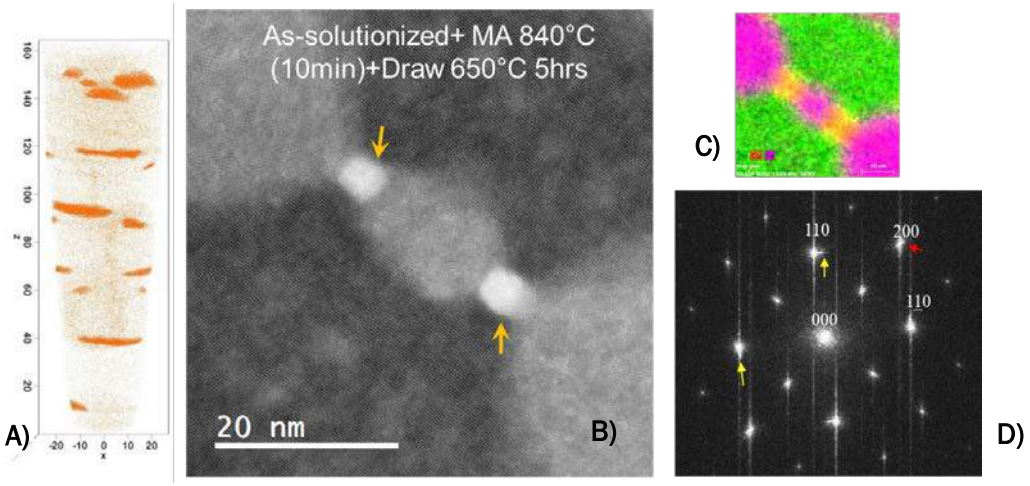


Figure I.13.2 - The final nano-structuring of the alnico showing A) distribution of Cu-rich rods (3D atom probe), B) atomic resolution STEM showing where these Cu-rich rods form (yellow arrows) in-between the Fe-Co phase and the $L2_1$ phases. See chemical map C). The diffraction pattern shows the strain between these Cu-rich rods (yellow arrows) and the matrix.

Monte Carlo simulations for alnico with Cu included suggests that Cu precipitation mainly stems from the elastic interaction in the system. Our first-principles calculations show that the lattice parameter of body-centered cubic Cu is between those of the magnetic and matrix phases of alnico 8 so that the precipitation of Cu to the interface would release the elastic energy. In addition, for a mosaic morphology, corners are the high-strain areas so that excess Cu at the interface boundary could diffuse to the mosaic corners. Previous works also showed that by taking elastic effects into account, phase field simulation will be able to correctly describe the faceting of the magnetic phase. Therefore, expanding the simulation to 2D and including elastic effects within the Monte Carlo simulation and/or phase-field simulation are new issues for sharply focused developments and have been undertaken.

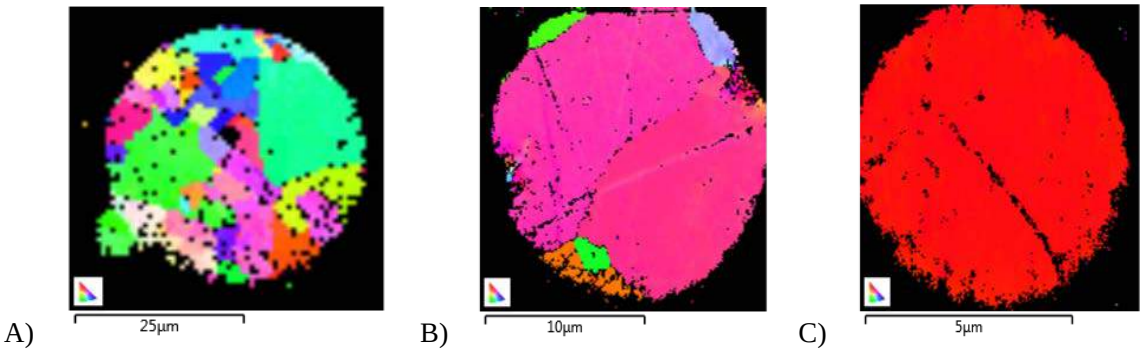


Figure I.13.3 - Grain size and number as determined by EBSD OIM micrograph cross sections of A) 38µm Powder Particle B) 17µm powder particle C) 8µm powder particle

Using both analytic methods and numerical simulation, we investigated how magnetostatic interactions affect the coercivity of alnico-type magnets. Starting from exact micromagnetic relations, we analyzed two limits, namely cooperative reversal processes operative on short lengths scales and non-cooperative reversal processes on long-length scales. Results show substantial deviations from Stoner-Wohlfarth behavior due to the unique size and spatial distribution of the rod-like Fe-Co phase formed during spinodal decomposition in an external magnetic field. The maximum coercivity is limited by single-rod effects, especially deviations from ellipsoidal shape, and by interactions between the rods. Unlike systems dominated by magnetocrystalline anisotropy, coercivity in alnico is highly dependent on size, shape, and geometric distribution of the Fe-Co phase, all factors that can be tuned with appropriate chemistry and thermal-magnetic annealing. We predict that sharp ellipsoidal tips and a staggered arrangement of the rods should promote substantial coercivity improvements, but this morphology may also be the most difficult one to realize experimentally.

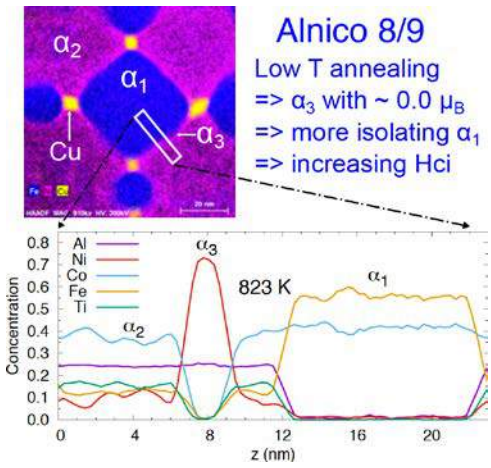


Figure I.13.4 - Monte Carlo simulation of alnico 8 and 9 in quasi 1D model. Top image is an actual high resolution TEM image and the lower plot shows the calculated composition in line with the elemental mapping.

## Conclusions

The project has met all of our milestones. We have produced a bulk anisotropic alnico magnet with $B_r$ in excess of 0.7 T and $H_{ci}$ in excess of 2500 Oe. Properties of these magnets were provided to UQM and ORNL for evaluation in their initial motor designs. In addition, these magnets have superior thermophysical properties over commercial alnico. Well-controlled bulk magnet samples were fabricated with enhanced grain alignment and energy product (MGOe) and superior $H_{ci}$ compared to commercial alnico 8HE. A bulk (full-sized) alnico

magnet sample with improved magnetic properties over similar commercial magnets was produced and delivered to ORNL and NREL and industrial partner (e.g., UQM) for evaluation.

## Key Publications


1. M. C. Nguyen, L. Zhou, W. Tang, M. J. Kramer, I. E. Anderson, C.-Z. Wang, and K.-M. Ho, Cluster-expansion model for complex quinary alloys: Application to alnico permanent magnets, Phys Rev Applied (accepted).

2. L. Ke1, R. Skomski, T. D. Hoffmann, L. Zhou, W. Tang, D. D. Johnson, M. J. Kramer1, I. E. Anderson, and C.-Z. Wang, Simulation of alnico coercivity, Appl. Phys. Lett. 111, 022403 (2017).

3. L. Zhou, W. Tang, L. Ke, W. Guob, J. D. Poplawsky, I. E. Anderson, M. J. Kramer, Microstructural and magnetic property evolution with different heat-treatment conditions in an alnico alloy, Acta Materialia, 133, (2017).

4. Anderson, I.E., A.G. Kassen, E.M.H. White, A. Palasyuk, L. Zhou, W. Tang, and M.J. Kramer, Development of controlled solid-state alignment for alnico permanent magnets in near-final shape. Aip Advances, 7, (2017).

5. R. Skomski, L. Ke, M. J. Kramer, I. Anderson, C.-Z. Wang, W.-Y. Zhang, J. E. Shield, and D. J. Sellmyer, "Cooperative and Noncooperative Magnetization Reversal in Alnicos," AIP Adv. **7**, 056222-1-5 (2017).

6. W. Guo, B. T. Sneed, L. Zhou, W. Tang, M. J. Kramer, D. A. Cullen and J. D. Poplawsky, Correlative Energy-Dispersive X-Ray Spectroscopic Tomography and Atom Probe Tomography of the Phase Separation in an Alnico 8 Alloy, Microscopy and Microanalysis, 22, (2016).

7. R. Skomski, "Permanent Magnets: History, Current Research, and Outlook," in: *Novel Functional Magnetic Materials*, Editor: A. Zhukov, Springer, Berlin 2016, p. 359-395.


*Patent:*


1. Aaron G. Kassen, Iver E. Anderson, Emma M.H. White, Liangfa Hu, Matthew J. Kramer, David J. Byrd, Alignment Promoted in Heat Treatable Magnets Through Application of External Applied Magnetic Field at the Start of Binder-Assisted Molding

# I.14 Performance and Reliability of Bonded Interfaces for High-Temperature Packaging

**Paul Paret, Principal Investigator**
National Renewable Energy Laboratory
15013 Denver West Parkway
Golden, CO 80401
Phone: (303) 275-4376
E-mail: paul.paret@nrel.gov

**Susan A. Rogers, Technology Manager**
U.S. Department of Energy
Phone: (202) 586-8997
E-mail: Susan.Rogers@ee.doe.gov

Start Date: October 1, 2017 End Date: September 30, 2019
Total FY17 Funding: $403,000 DOE share: $403,000 Non-DOE share: $0

## Project Introduction

A power electronics package in an automotive inverter, as shown in Figure I.14.1, will need to be redesigned with novel materials if it is to withstand the thermal and mechanical challenges brought about by the usage of high-temperature, compact, wide-bandgap-device-based components. Materials that can reliably operate at higher temperatures (>200°C) for the life of the component (15 years) need to be used. Sintered silver is one such material that has proven to be a promising candidate for use as a bonded attach material between layers in a package. As opposed to certain solders, it can reliably operate at higher temperatures without creep issues while still efficiently conducting heat away from the devices. Although the choice of sintered silver in electronics packages was not fully without any drawbacks due to the requirement of higher application pressures (~40 MPa) for bonding, research over time has led to several manufacturers developing sintered silver materials that require lower (3–5 MPa) or no bonding pressures. High-pressure sintered silver interfaces have been deployed as a die-attach material in commercially available power modules and inverters, but large-area applications of pressure-less sintered silver material and its reliability evaluation are still in the research and development phase.

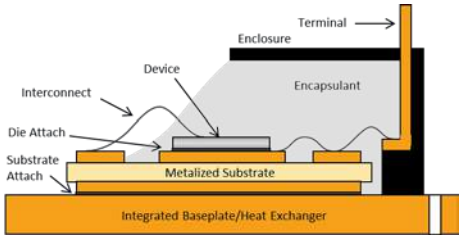


Figure I.14.1 - Schematic of a representative power electronics package

With the current market trend towards high-temperature packaging applications, there is a significant focus on developing sintered silver formulations that require simpler and less severe synthesis procedures that can still meet the desired reliability targets. An important area of research is the development and reliability analysis of nanoparticle-based sintered silver. It has been observed that switching to nanoscale formulations of sintered silver can increase the inter-particle bonding force due to larger surface area and enable sintering at lower temperatures. Furthermore, only lower pressures (< 3 MPa) may be required to obtain a uniform, defect-free bond. A detailed summary of the status of sintered silver as a bonded material in the microelectronics packaging industry is provided by Siow [1], who discusses different types of sintered silver formulations,

methods of application, and also comments on its long-term reliability prospects based on elevated temperature storage tests.

From a modeling perspective, an aspect of sintered silver that requires further research is the identification or development of a suitable constitutive model for use in finite element method (FEM) simulations. Chen et al. [2] studied the ratcheting behavior of a sintered nanosilver-based sample assembly in the context of power electronics packaging. In this study, two viscoplastic constitutive models—one based on the Ohno-Wang and Armstrong-Frederick (OW-AF) non-linear kinematic hardening rule, and the other one based on the Anand model—were investigated for their accuracy and effectiveness in predicting the cyclic ratcheting effects of nanosilver joints. The OW-AF model results were found to be in better agreement with experimental results than results from the Anand model. In yet another study on high-temperature applications of sintered silver, Croteau et al. [3] conducted uniaxial tensile tests on film-like specimens at different stress rates, strain rates, and temperatures to obtain the required stress-strain curves from which the desired constitutive model parameters can be extracted. In addition, they conducted die shear tests and thermal cycling tests and reported on the dependence of shear strength results on temperature and bond line thickness.

In this project, we attempt to evaluate the reliability of pressure-less and low-pressure sintered silver as a high-temperature bonded interface material through accelerated thermal tests and also identify the optimal synthesis conditions with feedback from mechanical characterization. Stress-strain curves obtained from mechanical characterization will be used to generate constitutive model parameters. Also, we performed FEM simulations, the output of which will be correlated with experimental reliability results to formulate a predictive lifetime model. This report is mainly focused on the mechanical characterization aspects and also outlines the remaining characterization experiments to be conducted.

## Objectives

The three major objectives in this project are:

1. Conduct mechanical characterization on sintered silver under multiple strain rates and different temperatures. The output of this characterization will be an array of stress-strain curves from which constitutive model parameters can be obtained through curve fitting. These constitutive model parameters will be used as an input in FEM simulations.

2. Evaluate the reliability of sintered silver by subjecting coefficient of thermal expansion-mismatched coupons - with sintered silver as the bonded interface material - to accelerated thermal cycling tests. Crack propagation or any other failure mechanisms that originate and evolve under thermal cycling will be periodically monitored through scanning acoustic microscopy images. Thermal cycling will be continued until the samples completely delaminate or the cracks grow to a certain pre-defined percentage area.

3. Investigate the suitability of different theoretical parameters such as strain energy density and J-integral in accurately predicting the lifetime of sintered silver under accelerated thermal cycling conditions. FEM simulations will be conducted to obtain these theoretical parameters, and then correlated with experimentally obtained cycles-to-failure results to form the predictive lifetime model.

## Approach

### *Mechanical characterization*

In this project, we collaborated with Virginia Polytechnic Institute and State University (VT) in consideration of their established expertise and significant research on sintered silver material. A large batch of copper (Cu) coupons was sent to VT, which were used to make double-lap samples through different synthesis techniques. Both pressure-less and pressure-assisted sintering techniques were employed at VT to investigate the impact of pressure application during sintering on the shear strength of the samples. In parallel, we purchased sintered silver material from Kyocera International, a leading industry supplier of this material, and synthesized double-lap samples using a pressure-less technique at NREL. The goal behind including two different types of sintered

silver material in this study is to obtain more data and valuable insights, both in terms of synthesis and testing, in qualifying its reliability for use as a high-temperature bonded interface material.

The mechanical characterization involves subjecting the sintered silver bond to shear tests and obtain shear stress-shear strain graphs as the output. The shear stress-shear strain information is important as constitutive model parameters that define the nature of deformation within the material in a simulation model can be obtained from the data. We selected a modified double-lap sample configuration for testing in this study, as shown in Figure I.14.2. As compared to the traditionally used lap-shear joints, the modified double-lap sample geometry minimizes the occurrence of peel stresses and reduces the influence of sample geometry on the shear strength results to a considerable extent. Compressive load was applied onto the middle coupon to induce shear stress on the adjacent sintered silver joints and the failure load was divided by twice the joint area to obtain an averaged shear stress value as the output. The double-lap test sample in the fixture and the Instron 5966 dual column testing system that was used for the characterization are shown in Figure I.14.3.

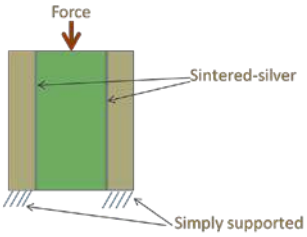


Figure I.14.2 - Modified double-lap sample

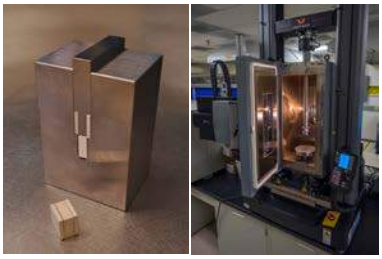

Figure I.14.3 - Double-lap sample and test fixture (left), Instron test machine (right). Photo credits: Douglas DeVoto

*Reliability Evaluation*

Prior accelerated testing of coefficient of thermal expansion-mismatched bonded samples resulted in their complete delamination even before reaching 500 thermal cycles. As a result, increased attention was dedicated this year to synthesis of samples with reasonable bond strength. The anticipated failure mechanism under accelerated testing (thermal cycling) of samples is crack initiation and propagation due to fatigue. Round samples using Cu and Invar coupons will be made using optimal synthesis techniques to obtain samples with good bond quality, and they will be subjected to accelerated thermal cycling tests. In a similar fashion to that of the double-lap samples, round samples will be synthesized at VT as well as at NREL using different types of sintered silver material. Figure I.14.4 shows the Cu and Invar coupons that will be used to make round samples.

Figure I.14.4 - Cu and invar coupons of 25.4-mm diameter. Photo credits: Douglas DeVoto

## Results

As mentioned in the Approach section, double-lap samples were synthesized at VT using both pressure-less and pressure-assisted sintering techniques that were iteratively optimized based on the shear stress results obtained from characterization performed at NREL on these samples. With the pressure-assisted sintering technique, pressure values of 3 MPa and 10 MPa were investigated.

### *Pressure-less samples (VT)*

We conducted a few preliminary experiments to optimize the characteristics of the sintering profile such as sintering temperature and heating rate, and to determine the bond line thickness. Based on the shear stress results from these experiments, we selected a bond line thickness of 100 µm and a sintering profile as shown in Figure I.14.5 for all the remaining samples.

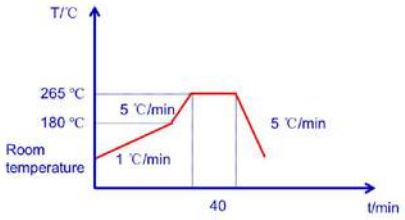


Figure I.14.5 - Synthesis profile for pressure-less samples at VT

With the synthesis profile and the bond line thickness optimized, we then proceeded to conduct shear testing on double-lap samples at different temperatures and strain rates. We scanned all samples before testing using C-mode scanning acoustic microscopy to detect the presence of any voids within the bond material. An image analysis software known as SPIP was used to calculate the actual bond area (excluding voids), which was incorporated in calculating the stress values of all the samples.

Figure I.14.6 shows the effect of ambient temperature on the shear stress values of the double-lap samples for a given strain rate. The output of a shear test conducted using the Instron test equipment is a load-displacement graph, which is then converted to shear stress–shear strain data. The load at which the failure of a sample occurs is noted and is divided by the actual bond area calculated using SPIP to obtain the peak shear stress value. As evident in Figure I.14.6, shear stress values remain more or less the same between samples tested at -40°C and room temperature (RT), and only when the temperature is increased to 200°C does a noticeable drop in the shear stress value occur. The drop in shear stress value at an elevated temperature is possibly due to the weakening of the inter-particle bond strength due to creep deformations in sintered silver at a microstructural level.

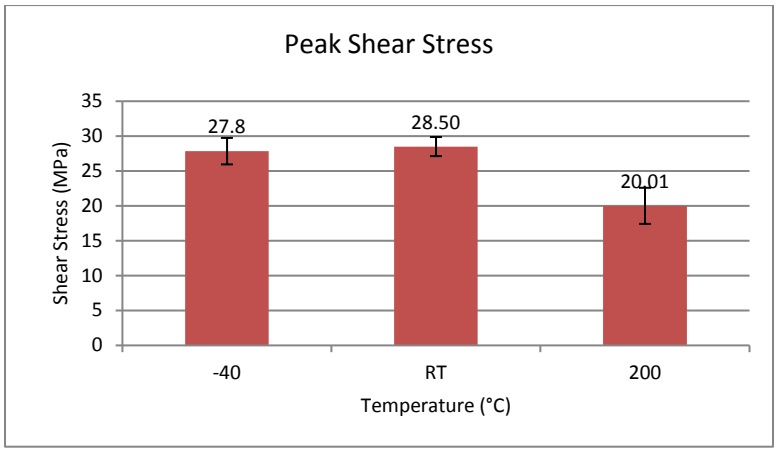


Figure I.14.6 - Shear stress versus temperature at a displacement rate of 0.01 mm/s

Figure I.14.7 shows the shear stress values of samples tested at two different displacement rates and at different ambient temperatures. A decrease in the applied displacement rate from 0.1 $s^{-1}$ to 0.001 $s^{-1}$ resulted in a slight drop in the shear stress values, which is likely due to slower rates allowing more time for deformation mechanisms to take place, thereby weakening its shear strength. The shear stress values listed over the bars denote the average value of sample measurements and the error bars represent the measurement standard error.

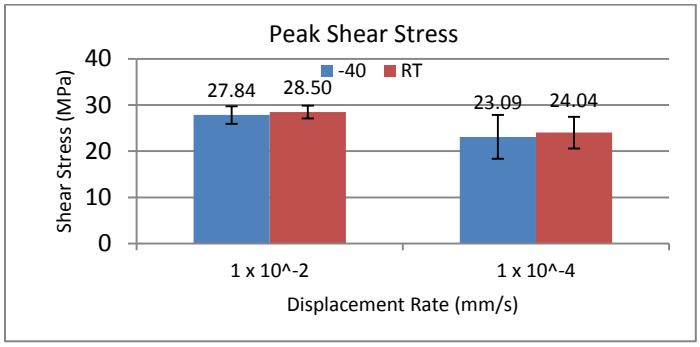


Figure I.14.7 - Impact of displacement rate on shear stress

*Pressure-assisted samples (VT)*

The work on pressure-assisted samples started with preliminary testing, similar to the pressure-less samples, to identify the most optimal sintering profile and synthesis process. In comparison to the pressure-less samples, pressure-assisted samples, in general, yielded higher values of shear strength likely due to the formation of a denser bond with the pressure being applied. A plot of the shear stress values of pressure-less and pressure-assisted samples obtained from preliminary tests is shown in Figure I.14.8. A wider spread in the shear stress values of pressure-assisted samples could possibly be due to the lack of uniformity in bond patterns in the initial stage of sample synthesis, as synthesis techniques were still being optimized. Additional characterization will be conducted on pressure-assisted samples at different strain rates and temperatures.

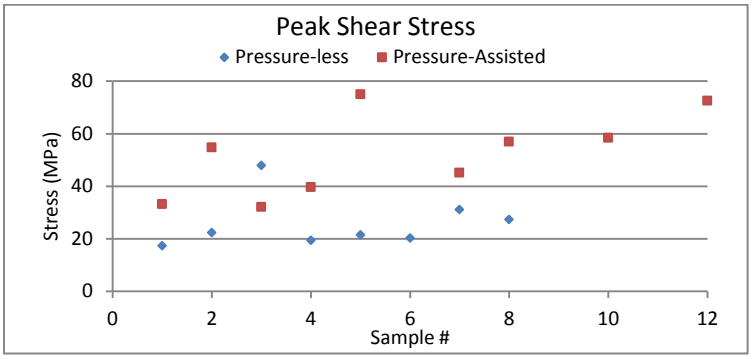


Figure I.14.8 - A comparison of shear stress values between pressure-less and pressure-assisted samples

*Pressure-less samples (NREL)*

This section discusses the pressure-less samples synthesized at NREL using the sintered silver material purchased from Kyocera. Testing was conducted at multiple strain rates and at room temperature. Figure I.14.9 shows the average values of the peak shear stress that we obtained for these pressure-less samples. A drop in the shear stress values was observed with a decrease in the applied displacement rate. A slight increase in the shear stress value between 1 x $10^{-4}$ mm/s and 1 x $10^{-5}$ mm/s could possibly be due to the better initial quality of the bonds and additional tests would prove if this trend holds for similar tests at different temperatures.

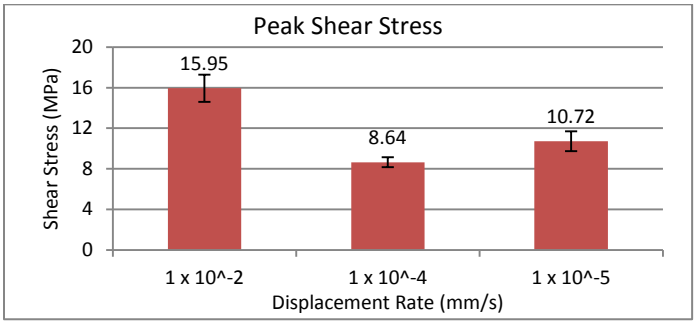


Figure I.14.9 - Impact of displacement rate on shear stress

## Conclusions

This year, significant effort went into optimizing the synthesis profiles of the double-lap samples and conducting mechanical characterization on them. The three major goals in this project are mechanical characterization of sintered silver, evaluation of its reliability, and thermomechanical modeling. Major updates on the thermomechanical modeling were provided in the previous year's report. We initiated preparation of samples for reliability evaluation, and accelerated testing (thermal cycling) will be conducted soon. The main conclusions from the mechanical characterization are provided below.

1. Double-lap samples with sintered silver as the bond line were synthesized using pressure-less and pressure-assisted sintering techniques.

2. Shear testing was conducted on double-lap samples at multiple strain rates and at different temperatures.

3. In general, pressure-assisted samples exhibited higher shear stress as compared to pressure-less samples by more than 20 MPa. The shear stress results indicate that sintered silver - both pressure-assisted and pressure-less, provides sufficient bonding strength for automotive power electronic applications.

4. Once the mechanical characterization - at different strain rates and temperatures – is complete for both pressure-less and pressure-assisted samples, the resultant stress-strain curves will be analyzed to generate appropriate constitutive model parameters, which will be used as an input in the thermomechanical modeling simulations.

5. Cycles-to-failure results obtained from accelerated testing will be correlated with modeling outputs to formulate a predictive lifetime model for sintered silver.

## Key Publications and Presentations

1. P. Paret, D. DeVoto, and S. Narumanchi, “Thermomechanical Modeling of Sintered Silver – A Fracture Mechanics Based Approach,” IMAPS Device Packaging Conference, Fountain Hills, AZ, March 2017.

2. P. Paret, “Performance and Reliability of Bonded Interfaces for High Temperature Packaging.” 2017 DOE VTO Annual Merit Review, Washington, DC, June 2017.

## References

1. K. S. Siow, “Are Sintered Silver Joints Ready for Use as Interconnect Material in Microelectronic Packaging?” *J. of Electron Mater.*, vol. 43, No. 4, pp. 947–961, Jan. 2014.

2. G. Chen, Z. Zhang, Y. Mei, X. Li, G. Lu, and X. Chen, “Ratcheting Behavior of Sandwiched Assembly Joined by Sintered Nanosilver for Power Electronics Packaging,” *Microelectronics Reliability*, vol. 53, pp. 645–651, 2013.

3. P. Croteau, S. Seal, R. Witherell, M. Glover, S. Krishnamurthy, and A. Mantooth, "Test Results of Sintered Nanosilver Paste Die Attach for High-Temperature Applications," *J. Microelec. Electron. Packag.*, vol. 13, pp. 6–16, 2016.

## I.15 Electric Motor Thermal Management

**Kevin Bennion, Principal Investigator**
National Renewable Energy Laboratory
15013 Denver West Parkway
Golden, CO 80401
Phone: (303) 275-4447
E-mail: kevin.bennion@nrel.gov

**Susan A. Rogers, Technology Manager**
U.S. Department of Energy
Phone: (202) 586-8997
E-mail: susan.rogers@ee.doe.gov

Start Date: October 1, 2017 End Date: September 30, 2019
Total FY17 Funding: $600,000 DOE share: $600,000 Non-DOE share: $0

### Project Introduction

Motor thermal management involves a complex interaction of motor-operating conditions, heat-load distribution, material-temperature limitations, passive thermal-heat spreading, and active-convective cooling to achieve performance requirements necessary to accelerate commercialization of motor innovations for vehicle electrification. It is important to reduce the thermal resistance of the motor system to increase power density, reduce footprint and cost of the motor while increasing component lifetimes. Improvements to the motor thermal system will have significant impacts across a wide range of high-performance motor types and impact the operating space of the motor (Figure I.15.1). The optimum cooling solution, from the standpoint of thermal performance, size, cost, and reliability, depends on the motor configuration and component thermal limitations. This requires an understanding of the potential heat-transfer paths of the passive thermal stack and the interactions with potential active-cooling technologies. Motor thermal management impacts the motor power density, maximum current density, magnet cost, material cost, reliability, efficiency, and internal motor temperature distributions. This project's emphasis is to research heat transfer of motor materials, interfaces, and convective cooling technologies to support motor designers in the modeling, analysis, design, and construction of non-rare-earth and reduced-rare-earth electric motors using advanced materials.

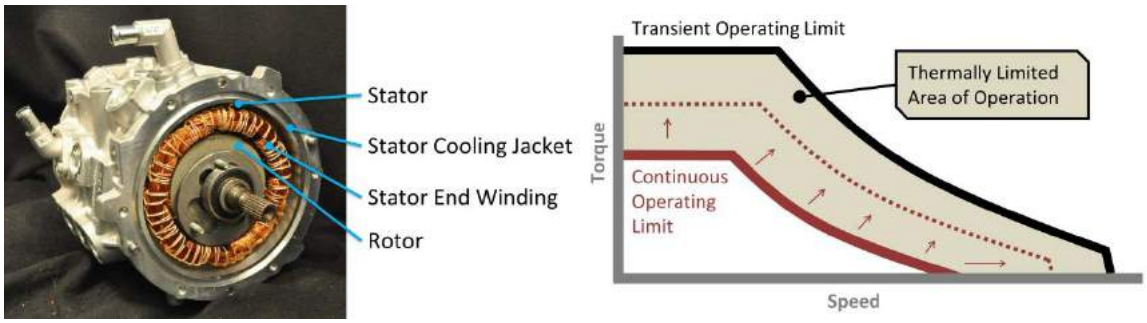


Figure I.15.1 - Example electric drive motor (left) and illustration of thermal management impact on motor operation to increase continuous power operating limits (right).
Photo Credit: Kevin Bennion, NREL

## Objectives

The overall project objective is to provide motor researchers, developers, and suppliers with the data and analysis of motor heat transfer technologies to enable motor innovations and accelerate the use of novel materials and designs for the adoption of vehicle electrification technologies. The work combines unique capabilities, facilities, and expertise in addition to the data, analysis methods, and experimental techniques to improve and better understand heat transfer within rare-earth and reduced rare-earth motors to meet the demands of electric drive vehicles. The National Renewable Energy Laboratory's (NREL's) capabilities enable development, demonstration, and confirmation of active and passive heat transfer technologies and innovations.

## Approach

The approach for the project first focuses on thermal and mechanical characterization of motor materials and material interfaces representative of motor assemblies. Second, detailed physical understanding of the interactions of materials and active cooling are quantified. The work is performed primarily at NREL, utilizing experimental equipment and computational tools focused on the study of advanced materials, thermal interfaces, thermomechanical behavior of materials, heat transfer, and computational fluid dynamics. Project partners include Ames laboratory’s magnet development efforts, and collaboration with motor design and materials experts at the Oak Ridge National Laboratory (ORNL).

Specific actions aligned with the project approach and objectives are summarized in this report and cover the following areas.

- Perform motor thermal material and interface characterization research in collaboration with project partners.
- Research fluid-based cooling technologies supporting reductions in thermal resistance of the motor packaging stack-up and material innovations.
- Collaborate with ORNL to support thermal-management research applied to motor and material research by ORNL.
- Collaborate with Ames Laboratory to support measurement of thermal and mechanical properties of magnet materials.

## Results

### *Material and Interface Thermal Stack-up*

The thermal and mechanical characterization of motor materials and material interfaces representative of motor assemblies focused on motor winding materials, lamination materials, and stator-to-cooling jacket thermal interface resistance modeling. As part of the work with ORNL, NREL and ORNL published a research paper [1] describing methods to measure motor winding thermal conductivity along (or axially or parallel) to the winding wire axis and across (or transverse or perpendicular) to the winding wire axis. The techniques compared included laser flash, transient plane source, and transmittance (Figure I.15.2) approaches for thermal resistance measurement. The experiments demonstrated that the anisotropic thermal conductivity of packed copper wire can be estimated with appropriate specimen preparation using laser flash and transmittance evaluation methods. The results show that thermal conductivity perpendicular to the wire axis is approximately 1/200 to 1/400 of the thermal conductivity in the parallel direction for the configurations investigated. The work also compared methods to model and calculate the direction-dependent winding thermal conductivity when experimental data is not available. The results provide a baseline to motor manufacturers and researchers developing motor thermal models and in motor design against which the performance of new materials can be compared. The work also highlights methods for examining the thermal impact of new materials or winding structures relevant to motor windings.

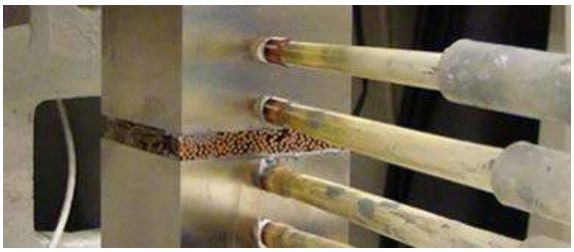

Figure I.15.2 - Sample winding thermal transmission testing
Photo Credit: Emily Cousineau, NREL

In the area of silicon steel lamination materials for motor assemblies, there is a lack of information in the open literature on thermal properties of electric machine lamination stacks such as contact resistance and through-stack thermal conductivity. This information is critical for researchers and engineers in electric machine design and development of new alternative machine designs. Using data measured at NREL for electromagnetic steel laminations and thermal contact resistance [2], NREL developed a thermal contact residence model that enables researchers and designers to estimate the through-stack thermal conductivity for materials beyond those that were directly tested. The model incorporates effects related to steel lamination thickness, thermal conductivity, surface finish (as shown in Figure I.15.3) and contact pressure. An example of the thermal contact resistance model results compared to the experimental data for one of the samples is also shown in Figure I.15.3. The error bars for the data represent 95% confidence limits based on systematic and random experimental uncertainty. As expected, both the data and the model show the thermal contact resistance decreasing with higher contact pressure. Although this work focuses on electric machines for automotive applications, the information is potentially applicable to any component using electromagnetic steel laminations. A journal manuscript is being prepared that describes the experiments, results, and thermal model. The development of the model enables researchers and designers to estimate the impacts of alternative motor lamination materials.

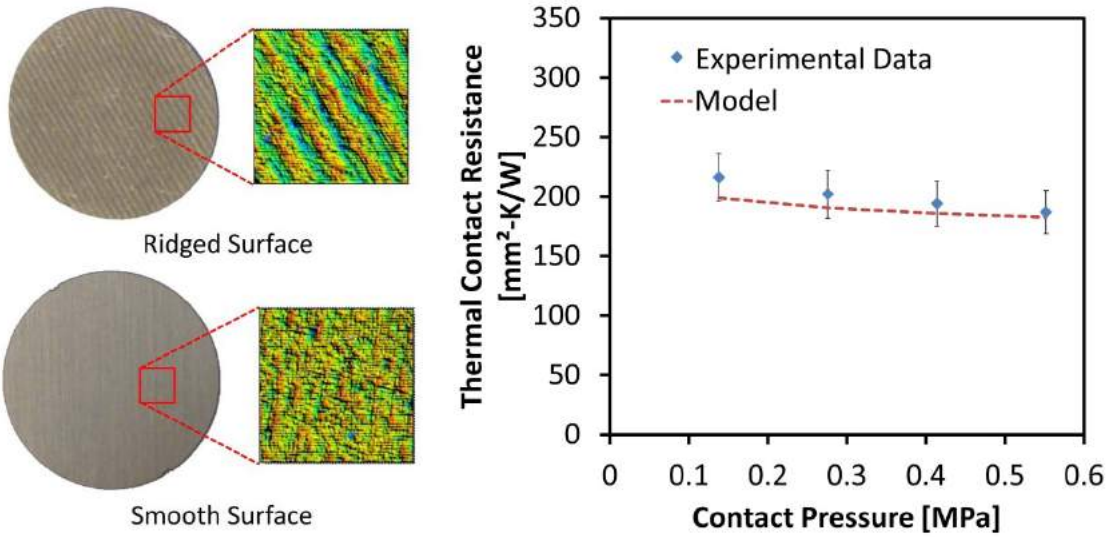


Figure I.15.3 - Sample images of two lamination materials with different surface finish (smooth and ridged) that were captured with the model (left), and data comparing experimental data with model predictions for one lamination material (right).
Photo Credit: Emily Cousineau, NREL

In addition to the winding and steel lamination material efforts, NREL also worked with UQM Technologies to develop a model to predict the thermal contact resistance between the motor stator steel laminations and the

aluminum motor housing. The thermal contact resistance between the electric machine stator and cooling jacket is a significant factor in overall performance and is also not well characterized in the open literature. This interface is typically an interference fit subject to compressive pressure exceeding 5 MPa. Using a unique test fixture at NREL for measuring thermal contact resistance under high pressure, NREL and UQM characterized the interface thermal resistance using pressures between 5.5 and 9.6 MPa. Using the generated data, the results were compared to the results predicted by currently available models for contact resistance, and significant variation was found between the experimental data and predictions from models. Existing models predicted thermal contact resistances ranging from 148 $mm^2$-K/W to 1,400 $mm^2$-K/W, leading to significant variability in the temperature gradient across the contact interface. For this reason, a model was developed that includes both solid and fluid (air) interface components to calculate thermal contact conductance or the inverse of thermal contact resistance. The solid-contact conductance model accounts for the surface roughness of the two contacting surfaces (Figure I.15.4), the applied pressure, and the material hardness. The fluid conductance model incorporates the thermal conductivity of the interstitial gas, the contact pressure, and the material hardness. An example for one material comparing the model results to the experimental data is shown in Figure I.15.4. The error bars for the data represent the 95% confidence interval incorporating random and systematic experimental uncertainties. This work helps electric machine designers accurately estimate the stator to case thermal contact resistance for a range of electric machines without having to resort to overly conservative estimates. A manuscript was prepared, in collaboration with UQM Technologies, and submitted to a journal for consideration of publication.

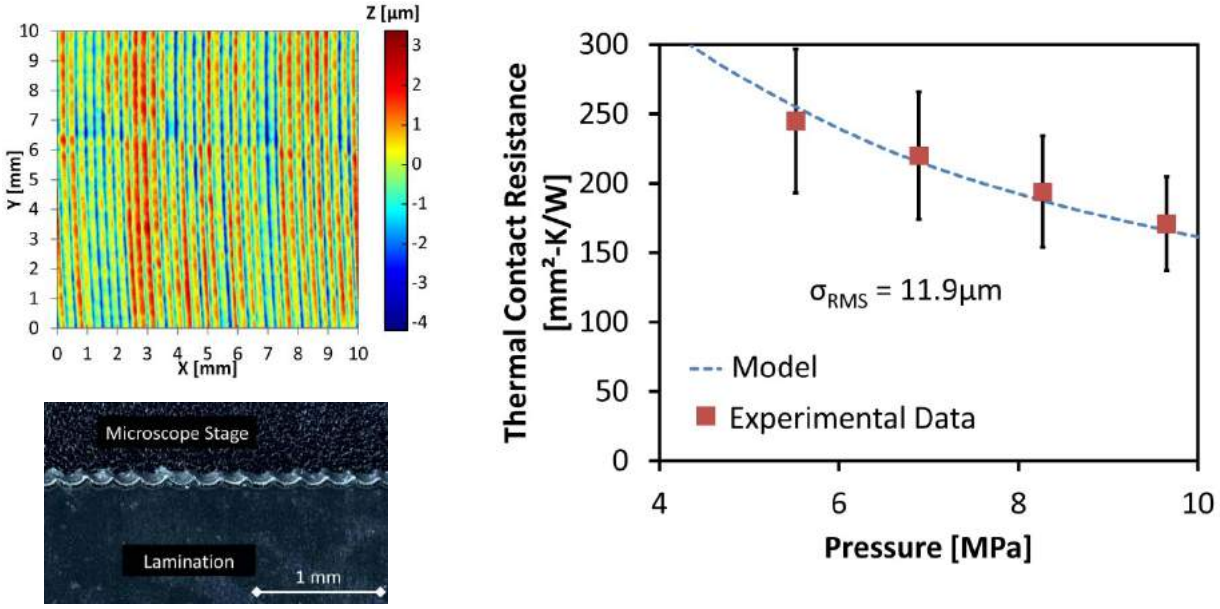


Figure I.15.4 - Detailed profile of the aluminum surface in contact with laminations showing tooling marks (top left). Microscope mage of lamination cut edge pattern (bottom left), and graph comparing experimental data with model predictions for one lamination material (right).

Photo Credit: Emily Cousineau, NREL

*Fluid Based Convective Heat Transfer*

Past work on automatic transmission fluid focused on measuring the average convective heat transfer coefficient directly impinging on the center of a stationary target representative of a motor end winding. The emphasis during FY 2017 was to quantify the impact on the heat transfer coefficient when the orifice jet is not aligned with the target surface. This is shown in Figure I.15.5. The impact of the difference in the measured heat transfer coefficient is also shown in Figure I.15.5 (graph on the right), which shows a 21%–37% reduction in the average heat transfer coefficient when the impingement occurs on the edge as opposed to the center of the target surface. The results highlight that there is significant variation in the heat transfer coefficient along

the motor end winding from the impinging automatic transmission fluid which needs to be accounted for in machine/motor design.

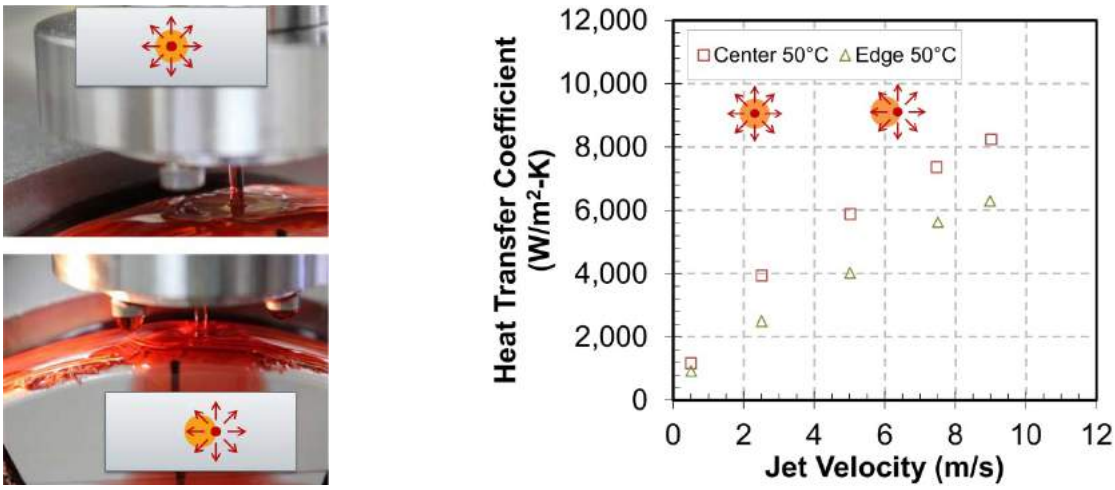


Figure I.15.5 - Picture of orifice jet aligned with target surface for measuring heat transfer coefficient (top left); picture of orifice jet impinging on the edge of the target surface (bottom left). Comparison of orifice nozzle automatic transmission fluid average heat transfer coefficients for impingement on the center and the edge of the target surface (right).

Image Credits: Bidzina Kekelia and Kevin Bennion, NREL

*DOE Laboratory Collaborations*

NREL continued to support collaboration with project partners at ORNL and Ames Laboratory in support of motor research activities. In support of ORNL, NREL focused on thermal management research supporting motor research and testing efforts at ORNL. For example, NREL developed a preliminary computational fluid dynamics model for simulation of the heat transfer and fluid flow for a prototype electric motor designed by ORNL with a cooling jacket surrounding the motor stator. An image of the cooling jacket surrounding the motor stator is shown in Figure I.15.6 (left image). Work will continue with ORNL on the cooling analysis based on motor test results and future project needs.

With Ames Laboratory, NREL continued supporting measurement of mechanical properties of magnet materials. Measurements of transverse rupture strength (TRS) were made, in collaboration with researchers at Ames Laboratory, on new AlNiCo magnets developed at Ames. The transverse rupture strength measurements were performed at NREL. Characterization of prior magnets developed at Ames in FY 2016 showed improved TRS as compared against commercially available materials. New magnets developed during FY 2017 were characterized and showed even greater improvements in TRS as compared to commercial materials and prior generation Ames magnets. The results of the transverse rupture strength are shown in the right image of Figure I.15.6. The new Ames material (2017) demonstrated higher TRS. The significance is a mechanically stronger magnet that is easier for manufacturers to implement into motor designs.

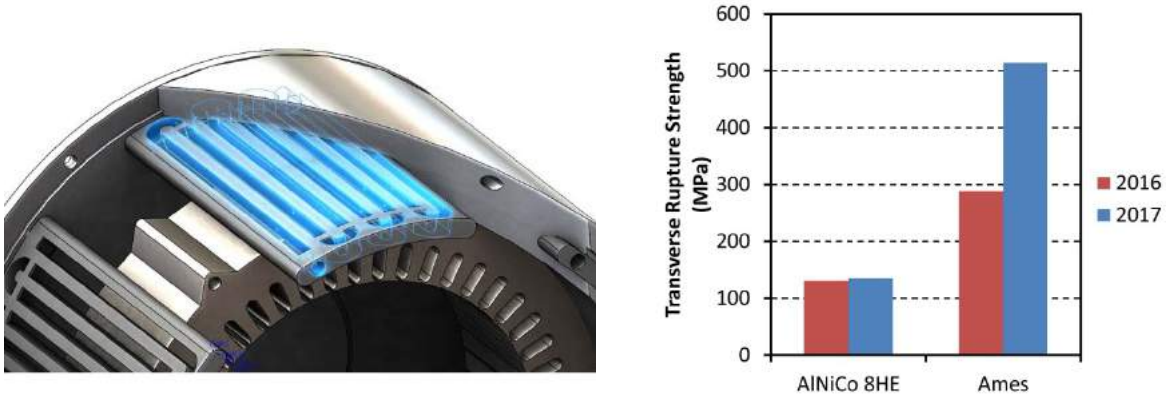


Figure I.15.6 - Cross section view of ORNL stator cooling jacket for computational fluid dynamics thermal and fluid analysis at NREL (left), transverse rupture test results comparing new and prior generation Ames magnets (right).

Image Credits: Emily Cousineau and Kevin Bennion, NREL

## Conclusions

During FY 2017, research was performed to improve the physical understanding of motor materials, material interfaces, heat transfer, and fluid dynamics through experiments and simulation. To aid motor developers and researchers in the analysis of new motor materials, models were developed to provide estimates for material and interface properties applied to motor assemblies. This included the characterization of motor winding materials, lamination stack thermal properties, and stator-to-cooling jacket thermal contact resistances. In addition, research was performed on automatic transmission fluid orifice jets illustrating the variation in heat transfer coefficient of automatic transmission fluid jets impinging on motor end windings. Finally, support was provided to project partners ORNL and Ames Laboratory for projects led by the respective groups emphasizing motor research and magnet material research.

## Key Publications

1. Wereszczak, A. A., Cousineau, J. E., Bennion, K., Wang, H., Wiles, R. H., Burress, T. B., and Wu, T., "Anisotropic Thermal Response of Packed Copper Wire," *J. Thermal Sci. Eng. Appl.*, 9(4), pp. 041006 (9 pages), 2017.
2. Bennion, K. "Electric Motor Thermal Management." 2017 DOE VTO Annual Merit Review, Washington D.C., June 2017.

## References

1. Wereszczak, A. A., Emily Cousineau, J., Bennion, K., Wang, H., Wiles, R. H., Burress, T. B., and Wu, T., 2017, "Anisotropic Thermal Response of Packed Copper Wire," *J. Therm. Sci. Eng. Appl.*, **9**(4), pp. 041006-041006-9.

2. Cousineau, E., Bennion, K., DeVoto, D., Mihalic, M., and Narumanchi, S., 2015, "Characterization of Contact and Bulk Thermal Resistance of Laminations for Electric Machines." NREL Technical Report NREL/TP-5400-63887.

## I.16 Power Electronics Thermal Management

**Gilbert Moreno, Principal Investigator**
National Renewable Energy Laboratory
15013 Denver West Parkway
Golden, CO 80401
Phone: (303) 275-4450
E-mail: gilbert.moreno@nrel.gov

**Susan A. Rogers, Technology Manager**
U.S. Department of Energy
Phone: (202) 586-8997
E-mail: susan.rogers@ee.doe.gov

Start Date: October 1, 2017 End Date: September 30, 2019
Total FY17 Funding: $403,000 DOE share: $403,000 Non-DOE share: $0

### Project Introduction

This project consists of two tasks—the wide-bandgap (WBG) power electronics thermal management task and a collaborative research effort between NREL and John Deere to research and develop advanced cooling technologies for heavy-duty vehicle power electronics applications. The work with John Deere is part of a collaborative research and development agreement (CRADA) and, due to the proprietary nature of the work, the results of this task are not provided in this report.

Work was conducted under the power electronics thermal management task to analyze and develop thermal management strategies for high-temperature silicon and WBG-based automotive power electronics systems. A challenge with WBG devices is that although their losses in the form of heat are lower, the area of the devices is also reduced, which results in higher device heat flux. Additionally, a WBG device's high junction temperatures will result in larger temperature gradients through the power module layers that will present reliability challenges and require high-temperature bonding materials. Another challenge with WBG's higher junction temperatures is that they will expose other system components (e.g., capacitors and electrical boards) to higher temperatures that may exceed their allowable temperature limits.

### Objectives

The overall project goal is to develop thermal management strategies to enable efficient and high-temperature WBG and silicon-based power electronic systems. More specific project objectives are listed below.

1. Develop thermal strategies to enable the use of low-temperature, low-cost capacitors in power electronic systems with devices temperatures up to 250°C
2. Develop thermal management system that allow modular and power dense power electronics systems
3. Collaborate with John Deere to develop a power-dense two-phase-cooled inverter

### Approach

*WBG Power Electronics Thermal Management Task*

System-level (e.g., inverter scale) thermal modeling results from past work [1] revealed that the use of high-temperature (e.g., WBG) devices in power electronics components can result in capacitors and gate driver boards significantly exceeding their temperature limitations. The focus this year was to develop cooling strategies that allow for the use of low-temperature, low-cost capacitors in power electronics systems with device temperatures up to 250°C. The approach was to conduct system-level thermal simulations to determine the most effective capacitor cooling strategy.

*John Deere CRADA Task*

The approach for this task was to collaborate with John Deere to develop a two-phase-cooled inverter. John Deere designed the electrical aspects and selected components and NREL provided thermal management support via modeling and experimental work.

## Results

Thermal modeling studies were conducted to determine the most effective capacitor cooling strategy for elevated-device temperature operation (up to 250°C). Three capacitor cooling strategies were considered, including improving the power module cold plate cooling performance, directly cooling the capacitors, and cooling the bus bars (electrical connections between the power module and capacitors). The effect of each cooling strategy on the capacitor temperatures was modeled for four different inverter configurations.

Two of the inverter configurations used a power module, capacitor, and bus bar design that resembled the 2012 Nissan Leaf design (Figure I.16.1). One configuration used a flexible pad located between the power module and the cold plate as the electrical insulation. This configuration is shown in the middle schematic in Figure I.16.1 and termed the "Leaf" design since its design resembles that of the Leaf. The second design uses a direct-bond copper (DBC) substrate directly below the devices as the electrical insulation. This configuration is termed the "Leaf (DBC)" and is more representative of typical automotive power module configurations. A couple of reports [1, 2] provide more information on the Leaf design and material properties. Both configurations were cooled by means of an aluminum cold plate with thermal grease ($R''_{th}$ = 55 mm$^2$-K/W) at the interface.

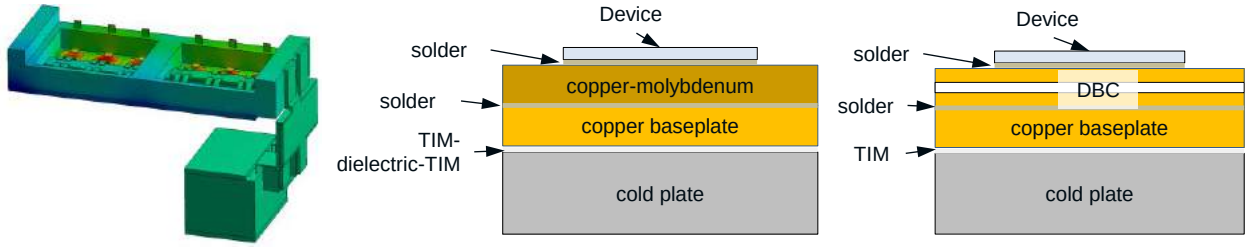


Figure I.16.1 - Model used for the finite element study (left) and the module schematics showing the two material stack-ups considered: copper-molybdenum-flexible dielectric (middle) and conventional DBC (right).

The remaining two inverter configurations modeled used a Cree power module design and included one polypropylene metalized film-type capacitor and the electrical connections (Figure I.16.2). The Cree module uses relatively small silicon carbide (SiC) metal–oxide–semiconductor field-effect transistors (MOSFETs) (3.1 mm × 3.4 mm) and diodes (2.3 mm × 2.3 mm). This configuration was modeled for two cooling strategies—cold-plate cooled and baseplate cooled. The cold plate-cooled configuration cooled the power module using an aluminum cold plate with thermal grease at the interface. The baseplate-cooled configuration applied cooling directly to the base of the power module baseplate and did not use thermal grease.

Thermal modeling was conducted using a finite element (FE) method. For all cases, only the MOSFET and diode heat were imposed since prior modeling results indicate that this heat source is the largest contributor to component overheating. Device heat generation using a 3-to-1 MOSFET-to-diode heat loss ratio was adjusted to achieve the desired maximum junction temperature (175°C, 200°C, and 250°C). Due to symmetry, only one module (half-bridge) and its nearest capacitor winding were modeled. Only one capacitor was modeled (the one closest to the power module) since it is this capacitor that will experience the highest temperatures. SiC properties were used for the semiconductor devices to simulate WBG devices.
First, the effect of improving the power module cooling performance on capacitor temperatures was modeled. This cooling strategy was an attempt to lower capacitor temperatures by decreasing device temperatures. The cooling was modeled by imposing a convective heat transfer coefficient boundary condition on the cooled

surface. Figure I.16.3 plots the maximum capacitor temperature versus the cooled surface convective thermal resistance (inverse of the overall heat transfer coefficient that includes any surface area enhancement effects). Three convective thermal resistance values were imposed and used to represent the cooling provided by cold plates of varying thermal performance. The highest convective value (133 $mm^2$-K/W) represented the cooling performance provided by a typical automotive liquid-cooled cold plate. The lower convective resistance values of 50 $mm^2$-K/W and 20 $mm^2$-K/W represent the cooling performance of a high-end commercially available cold plate and a jet impingement-microchannel cold plate, respectively. A 65°C reference temperature was used for the convective boundary conditions to represent the coolant temperature for automotive power electronics systems. In this analysis, the device heat for all four configurations was adjusted to achieve a maximum junction temperature of 250°C at the highest convective resistance. The device heat was then held constant as the cold plate performance was improved (i.e., convective resistance was decreased).

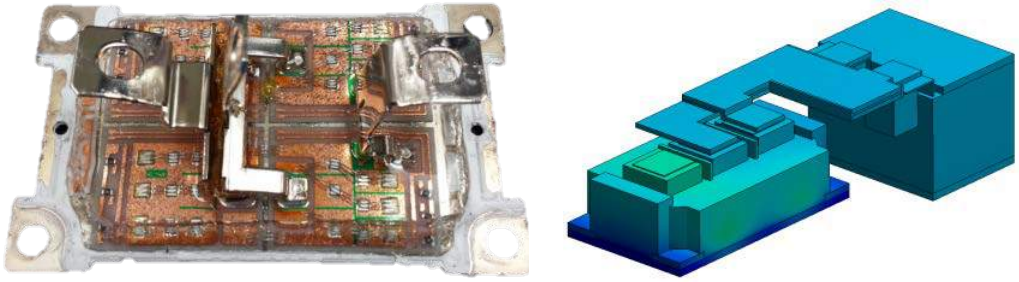

Figure I.16.2 - Picture of the Cree module used for the modeling work (left) and the FE model of the module, capacitor, and bus bars (right).

Image credit: Gilbert Moreno, NREL

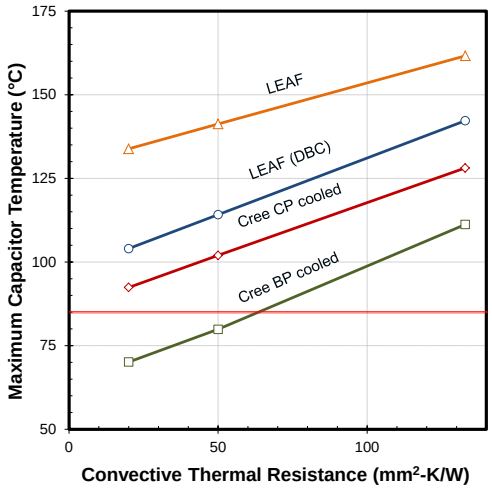


Figure I.16.3 - Plot showing the effect of increasing the power module cooling performance on the capacitor temperatures for four different inverter configurations. The highest convective resistance corresponds to the performance of a typical liquid cooled cold plate and the lowest convective resistance corresponds to a high-performance microchannel cold plate.

As shown in Figure I.16.3, improving the power module cooling can reduce capacitor temperatures by as much as 40°C. It is also clear that power modules with lower overall junction-to-coolant thermal resistance (including conduction and convection resistances) produce lower capacitor temperatures. For example, the Cree baseplate-cooled configuration with the lowest junction-to-coolant resistance produced the lowest capacitor temperatures while the Leaf configuration with the highest junction-to-coolant resistance provided

the highest capacitor temperatures. Lowering the junction-to-coolant resistance decreases heat spreading around the devices, which in turn lowers capacitor (as well as surrounding component) temperatures.

The effect of directly cooling the capacitors and bus bars (using cold plates) on capacitor temperatures was also studied via FE modeling. For these cases, cooling was provided by an aluminum cold plate (65°C coolant) mounted to the capacitors or bus bars. For the capacitor-cooled case, a thermal contact resistance ($R''_{th}$ = 55 $mm^2$-K/W, typical grease thermal resistance) was imposed to simulate thermal grease between the cold plate and the capacitor surface. For the bus bar-cooled case, a thermal resistance of $R''_{th}$ = 323 $mm^2$-K/W (value taken from vendor specification sheet) was imposed between the cold plate and bus bar-cooled surface to simulate the thermal effects of a dielectric thermal pad (i.e., conduction and two contact resistances).

Figure I.16.4 compares the results for the capacitor and bus bar cooling strategies for three inverter configurations. This figure plots the maximum capacitor temperature at 175°C, 200°C and 250°C junction temperatures. The left plot in Figure I.16.4 shows the case when only one side of either the capacitor or bus bars is cooled, and the right plot shows the case when two sides are cooled (double-side cooled). The total cooled surface area for the capacitors was 2,883 $mm^2$ for the case when only one side was cooled. The bus bar-cooled area for the single-side cooled condition was 2,250 $mm^2$ and 1,853 $mm^2$ for the Leaf and Cree configurations, respectively. FE simulations were conducted at various convective resistance values to encompass a wide range of cooling technologies (e.g., liquid and air cooling). The results shown in Figure I.16.4 are for the case where a relatively low convective resistance ($R''_{th}$ = 222 $mm^2$-K/W) was used.

As shown in Figure I.16.4, cooling the bus bars is a more effective method for cooling the capacitors as compared with directly cooling the capacitors. Cooling the bus bars using a relatively low-performance ($R''_{th}$ = 222 $mm^2$-K/W) cold plate can maintain capacitor temperatures below 85°C at junction temperatures up to 250°C. The bus bar cooling approach is more effective since it removes the heat from the power module before it reaches the capacitors. Moreover, the low thermal conductivity of the capacitor materials (i.e., plastics and potting epoxy) limits the benefits of placing a cold plate directly on the capacitors. Using a double-side cooling approach (Figure I.16.4, right plot) enhances performance for both the capacitor and bus bar cooling strategies and enables the cold plate-on-capacitor cooling strategy to maintain capacitor temperatures below 85°C for most of the cases considered.

The effects of reducing the area of the cooled surface and using different dielectric materials were also modeled for the bus bar cooling approach. Results indicated that bus bar cooling can maintain capacitor temperatures below 85°C at junction temperatures up to 250°C even when only a small bus bar surface area (375 $mm^2$) is available for cooling and when a low thermally conductive dielectric material (plastic between cold plate and bus bar) is used.

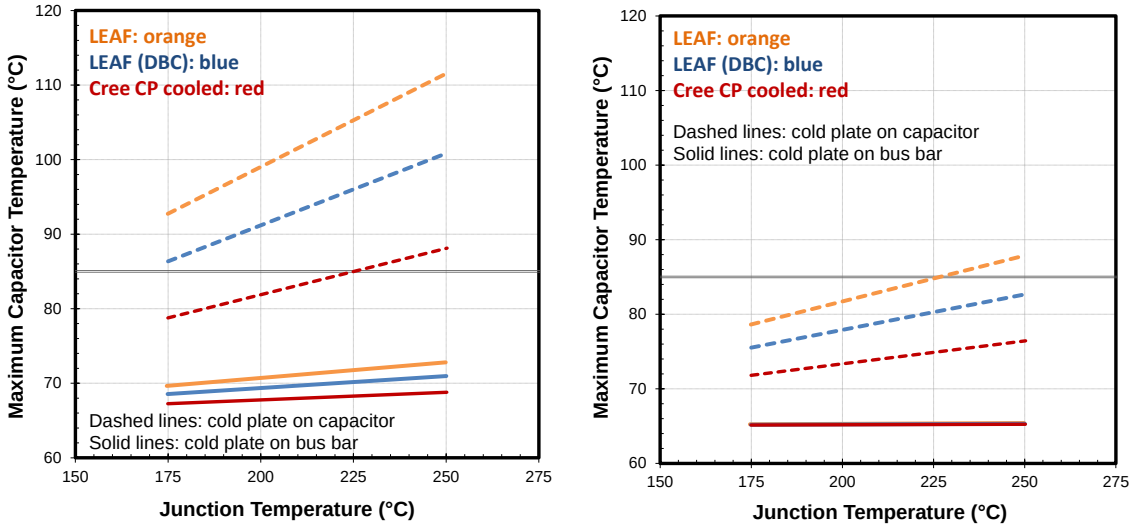


Figure I.16.4 - Plots comparing two capacitor cooling strategies: directly cooling the bus bars or the capacitors. Single-side (left) and double-side (right) cooling results for three inverter configurations are shown.

The need to decrease cost drives the need to develop scalable power electronic systems (same design used for multiple vehicle platforms). System scalability can be enabled using modular and compact, power dense power electronic designs. However, higher WBG device temperatures present a challenge when packaged in very compact assemblies because the higher junction temperatures may expose other components to temperatures that may be beyond their operating limits. As part of this project, we are evaluating thermal management solutions to enable compact power electronics packaging solutions for high-temperature WBG conditions.

The schematics in Figure I.16.5 show two compact power electronics packaging concepts. The concept on the left uses a very thin cold plate placed between the power modules and the capacitors. The concept on the right uses a dielectric fluid to directly cool the devices and electrical connections. This year, modeling work was conducted to design a very thin cold plate for high junction temperatures (250°C) conditions and for the compact packaging concept shown in Figure I.16.5 (left).

Initial work was conducted to design a liquid-cooled (single-phase) channel-flow-type cold plate. First, we computed the target convective thermal resistance value required to dissipate 2 kW of heat (assuming an 80-kW system and 98% WBG inverter and 95% motor efficiencies) and maintain junction temperatures below 250°C. Various inverter sizes and footprints were modeled, but the convective resistance pertaining to the smallest inverter size (65 mm × 63 mm) was used in an effort to reduce size. In addition to the thermal target, a maximum cold plate pressure drop constraint of 13.8 KPa (2 pounds per square inch) was also used in the cold plate design. The cold plate design approach used was as follows:

- Compute the cold plate target convective thermal resistance using the smallest inverter footprint
- Use analytical techniques to compute convective resistance and pressure drop values for different fin geometries (height and thickness) at various WEG flow rates (65°C WEG temperature)
- Select the smallest fin height design that meets the thermal and pressure drop requirements and conduct detailed computational fluid dynamics (CFD) modeling on that design.

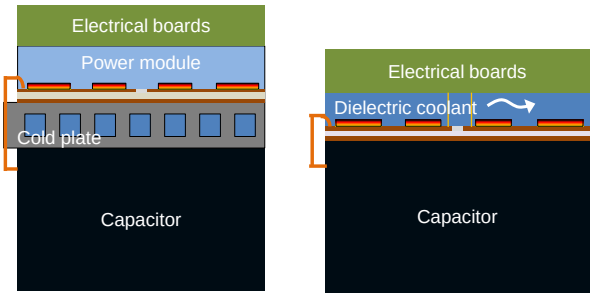


Figure I.16.5 - Schematics of two compact-packaging inverter concepts. The concept on the left uses a thin cold plate between the modules and capacitors. The concept on the right directly cools the devices and electrical interconnections using a dielectric fluid.

The smallest channel width and height used was 0.5 mm in an effort to minimize the potential for clogging. For automotive applications, a minimum channel size of 1-mm-diameter is typically used; however, 0.5 mm was used here to minimize the cold plate size.

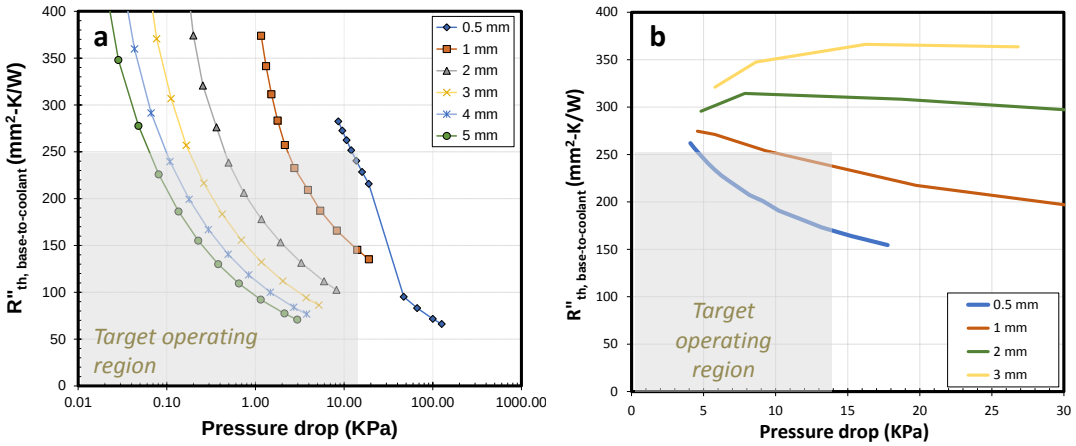


Figure I.16.6 - a) Convective resistance values versus the pressure drop for a cold plate with different fin heights (provided in figure legend). WEG flow rate of 167 $cm^3/s$ and 1-mm-thick fins were used for the results shown. b) Plot showing the CFD-computed convective thermal resistance versus the pressure drop for a cold plate with 0.5-mm-tall fins at a total flow rate of 33 $cm^3/s$. The figure legend provides the fin thickness values.

Modeling results indicate that the thinnest cold plate design (0.5-mm-fin height) can meet the thermal requirements but exceeds the 13.8 KPa pressure-drop constraint at the automotive industry-standard flow rate of 167 $cm^3/s$ (10 LPM) (Figure I.16.6a). Using a lower flow rate of 33 $cm^3/s$ (2 Lpm) for the smallest fin height enabled meeting both the thermal and pressure drop targets. Sensible heat gain calculations show that at 33 $cm^3/s$ and 2kW of heat dissipation, the WEG outlet temperatures are approximately 83°C which is just below the 85°C polypropylene film capacitor limitation. Detailed CFD modeling confirmed that a 0.5 mm × 0.5 mm fin design can meet both thermal and pressure drop requirements (Figure I.16.6b). CFD modeling was then conducted using compact cold plate design and a power module populated with SiC MOSFET and diode devices (commercially-available devices). As show in Figure I.16.7, the thin cold plate design is predicted to keep junction temperatures just below 200°C at 2 kW of heat generation. These results indicate that the increased efficiency (lower heat) and higher operating temperatures of WBG devices can enable very compact inverter designs (65 mm × 63 mm footprint for an entire inverter module). The modeling results show that although the WEG outlet temperatures are below 85°C, the cold plate temperatures can approach 100°C, which may be an issue if low-temperature polypropylene capacitors are in contact with the cold plate's lower surface.

The use of insulating material between the cold plate and low-temperature-rated capacitors or the use of higher-temperature capacitors (i.e., more expensive) may be required.

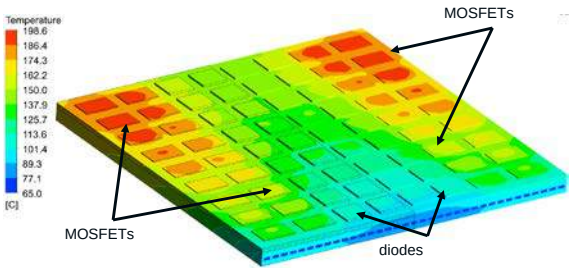


Figure I.16.7 - CFD-generated temperature contours for a compact inverter design (65 mm × 63 mm) concept.

## Conclusions

The major conclusions are listed below.

- Conducted over 2,000 simulations to evaluate various capacitor cooling strategies for high-device-junction temperature (up to 250°C) conditions. The effect of the various cooling strategies on four different inverter configurations was simulated to determine the most effective capacitor cooling solution.
- Identified cooling of the electrical interconnections between the capacitors and the power module as the most effective capacitor cooling strategy—more effective than directly cooling the capacitors. This cooling approach enables the use of low-cost, low-temperature capacitors within a WBG-based inverter with junction temperatures up to 250°C. Additionally, the cold plate thermal performance required to maintain capacitor temperatures below 85°C is relatively low (e.g., air-cooled heat sink).
- Designed a thin cold plate for a power-dense, high-temperature (250°C) junction and WBG-based power electronics packaging concept. We estimate that the use of efficient and high-temperature WBG devices can allow for extremely power-dense power electronics systems (only thermal issues considered).
- Collaborating with John Deere to develop a two-phase cooling strategy for its inverter. Conducted extensive modeling work to simulate various two-phase cooling scenarios.

## Key Publications and Presentations

1. Moreno, G. “Power Electronics Thermal Management Research.” 2017 DOE VTO Annual Merit Review, Washington, DC, June 2017.
2. Moreno, G. “Power Electronics Thermal Management Research.” 2017 presentation to the DOE VTO Electrical and Electronics Technical Team, July 2017.

## References

1. Moreno, G. “Power Electronics Thermal Management Research” 2016 DOE VTO Annual Report, available at https://energy.gov/sites/prod/files/2017/08/f36/FY16%20EDT%20Annual%20Report_FINAL.pdf
2. Moreno, G. “Thermal Performance Benchmarking” 2015 DOE VTO Annual Report, available at https://energy.gov/sites/prod/files/2016/03/f30/FY%202015%20Electric%20Drive%20Technologies%20Annual%20Report.pdf

# I.17 Thermal Performance Characterization and Analysis

**Xuhui Feng, Principal Investigator**
National Renewable Energy Laboratory
15013 Denver West Parkway
Golden, CO 80401
Phone: (303) 275-4439
E-mail: xuhui.feng@nrel.gov

**Susan A. Rogers, Technology Manager**
U. S. Department of Energy
Phone: (202) 586-8997
E-mail: susan.rogers@ee.doe.gov

Start Date: October 1, 2016 End Date: September 30, 2018
Total FY17 Funding: $135,000 DOE share: $135,000 Non-DOE share: $0

## Project Introduction

This project is to thoroughly characterize the performance of state-of-the-art (SOA) in-production automotive power electronics and electric motor thermal management systems. Oak Ridge National Laboratory's (ORNL) reports of electric and hybrid electric vehicle technology provide detailed descriptions of the electrical and packaging aspects of these automotive systems [1, 2]. Information obtained from these studies will be used to:

- Evaluate advantages and disadvantages of different thermal management strategies
- Establish baseline metrics for the thermal management systems
- Identify methods of improvement to advance the SOA
- Increase the publicly available information of automotive traction-drive thermal management systems
- Help guide future electric-drive technologies (EDT) research and development efforts.

The performance results combined with component efficiency and heat generation information obtained by ORNL may then be used to determine the operating temperatures for the EDT components under drive-cycle conditions. In FY17, the 2015 BMW i3 power electronics and electric motors thermal management systems were characterized. Experiments to characterize the performance of the fourth generation of Toyota Prius power electronics thermal management systems started in FY17 and the results will be reported in FY18.

## Objectives

This project is seeking out SOA power electronics and electric motor technologies to characterize their thermal performance. The characterization will focus on the thermal aspects of the system. System metrics, such as thermal resistance of different parts will be measured. The type of heat exchanger (i.e., channel flow, brazed, folded-fin) and any enhancement features will be identified and evaluated to understand their effect on performance. Additionally, the thermal resistance/conductivity of select power module and motor components will also be measured. The research conducted will allow insight into the various cooling strategies to understand which heat exchangers are most effective in terms of thermal performance and efficiency. Modeling analysis will also be carried out to better understand the heat transfer and fluid dynamics of the systems. The research conducted will allow insight into the various cooling strategies to understand the current SOA in thermal management for automotive power electronics and electric motors, and also identify research pathways for improving the SOA.

## Approach

Hardware testing and modeling analyses were conducted to characterize the performance of the SOA power electronics and electric motor thermal management systems. The project approach is outlined below.

- Collaborate with industry and ORNL to identify the vehicle system to benchmark
    - The 2015 BMW i3 power electronics and electric motor thermal management system was benchmarked in FY17. Experiments were initiated to measure the thermal performance of the fourth generation Toyota Prius power electronics thermal management system.
- Experimentally measure the performance of the thermal management systems
    - Measure the power electronics junction-to-liquid thermal resistances
    - Measure the electric motor end-winding-to-liquid and stator-to-liquid thermal resistances
    - Measure the thermal properties of the system components (e.g., thermal pads, stator laminations, motor windings).
- Create thermal models of the thermal management systems
    - Validate the models using experimental results
    - Compute thermal resistances that cannot be experimentally measured
    - Create transient thermal models to estimate component temperatures under various drive cycles.
- Analyze and report data
    - Identify thermal bottlenecks in the system and provide solutions to improve the SOA
    - Establish baseline metrics for the thermal management systems
    - Share results with industry and research institutions
    - Support other EDT projects (power electronics thermal management research, electric motor thermal management research, characterization of electric vehicle and hybrid electric vehicle technologies [ORNL]).

## Results

In FY17, the 2015 BMW i3 power electronics and electric motor thermal management systems were characterized. Experimental characterization of the i3 inverter system was completed in FY16, and the characterization of the i3 electric motor was conducted in FY17 to measure thermal resistance values of the systems. The laboratory characterization was intended to provide an accurate method of measuring thermal performance of the systems and not intended to simulate actual automotive operating conditions. Numerical models were then created and validated against the experimental data. The validated thermal models were used to further understand the heat transfer mechanisms within the systems. Efforts to characterize the Fourth Generation Toyota Prius power electronics thermal management system also started in FY17.

*2015 BMW i3 Power Electronics (Inverter) Thermal Management System*

The experimental results from the i3 power electronics were used to validate the thermal models. Both computational fluid dynamics (CFD) and finite element analysis (FEA) models were applied to simulate the i3 power electronics thermal management systems to better understand the heat transfer within the inverter. In the CFD simulation, only the water–ethylene glycol (WEG) liquid part was simulated with a simplified cold plate that has a heat source to represent the heat loss from devices. With the CFD results, the average temperature on the cold plate surface and the average temperature of the WEG coolant were obtained. Then the wetted-surface average heat transfer coefficients (*h*) at various flow rates were calculated, as listed in Table I.17-1.

**Table I.17-1 - CFD-computed average temperatures of cold plate and WEG coolant, and the heat transfer coefficient values for the BMW i3 inverter**

| Flow rate ($m^3/s$) | $T_{coldplate}$ (°C) | $T_{WEG}$ (°C) | $h$ ($W/m^2 \cdot K$) |
|---|---|---|---|
| $3.3 \times 10^{-5}$ | 77.5 | 70.0 | 638 |
| $8.3 \times 10^{-5}$ | 71.3 | 67.0 | 1,122 |
| $11.8 \times 10^{-5}$ | 69.9 | 66.4 | 1,383 |
| $19.6 \times 10^{-5}$ | 68.8 | 65.9 | 1,693 |

The heat transfer coefficient values were applied as boundary conditions in the FEA model. The FEA model replicated the experimental conditions (dissipate approximately 41 W through one insulated gate bipolar transistor (IGBT)). Material properties and geometry of the layers within the power module were studied using the scanning electron microscope (SEM) analysis. The die is attached to an alumina-based direct-bonded copper (DBC) using tin-based solder, and then the DBC with the devices is attached to the copper cold plate by another layer of tin-based solder. The thickness and physical property of each layer are summarized in Table I.17-2. The material thermal properties were obtained from the ANSYS Engineering database. These values were utilized in the FEA simulation to predict the steady-state and transient thermal resistance values under various conditions.

**Table I.17-2 - Thermal conductivity and thickness, for the various layers, used in the Leaf inverter thermal models**

| Material | k ($W/m \cdot K$) | Thickness (mm) |
|---|---|---|
| Silicon | 148 | 50 |
| Solder | 55 | 50 |
| Copper | 400 | 300 |
| Alumina | 26 | 300 |
| Silicone gel | 0.26 | |

Figure I.17.1 provides the model-estimated maximum (computed using the maximum junction temperature) and average (computed using the average junction temperature) thermal resistance values. As shown, the model-predicted results provide a good match with the experimental data (maximum ~6% difference). The FEA model was then used to generate a temperature profile from the IGBT to the liquid to identify the largest thermal bottlenecks in the system. The graph to the right in Figure I.17.1 shows the temperature profile, clearly indicating that the passive stack (DBC and solder) provides the largest thermal bottleneck within the system.

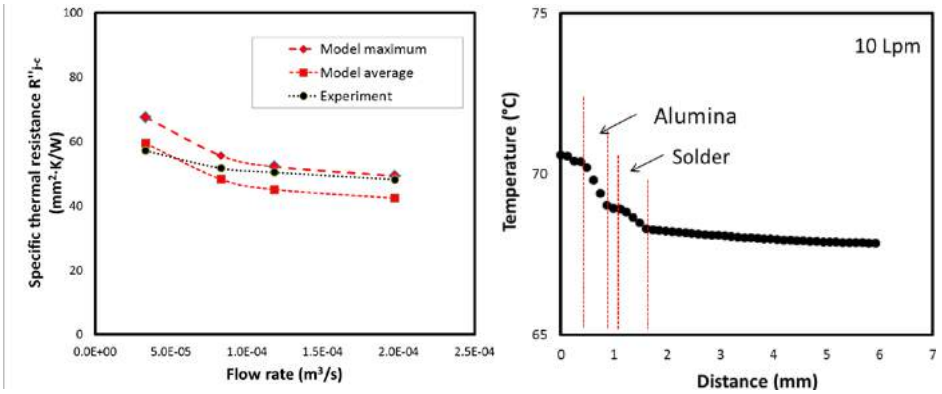


Figure I.17.1 - Experimentally measured and model-computed thermal resistances for the i3 inverter (left) and temperature profile through the i3 power module depicting the thermal path from the IGBT to the liquid (right).

With the validated FEA model, simulations were conducted to analyze the steady-state thermal resistance of the power modules for a wide range of convective thermal resistance values. In this model, all devices were powered up and modeled. A three-to-one (IGBT-to-diode) heat loss ratio was assigned in the simulations. The total power dissipated through the modules was adjusted so that the maximum junction temperatures reached 200°C, which is high for typical silicon-based devices and is intended to simulate the high-temperature wide-bandgap devices. The liquid temperature was set to be 70°C. The graph to the left in Figure I.17.2 provides the specific thermal resistance versus the convective thermal resistance for the i3 inverter system. The thermal resistance was calculated using the maximum junction temperature. When the convective thermal resistance is lower than 100 $mm^2 \cdot K/W$, which provides a convective heat transfer coefficient close to $10^4$ $W/m^2 \cdot K$, the specific thermal resistance shows a relatively smaller slope. This indicated that convective heat transfer is less dominant than the thermal resistance from the passive stack-up at higher convective heat transfer coefficient. FEA simulations were also conducted to study the transient thermal performance of various power modules, including the BMW i3, the Honda Accord and the Leaf, as shown in the right graph in Figure I.17.2. One full half-bridge with multiple IGBTs and diodes was modeled for all modules. The maximum device temperature was controlled to be 200ºC. At a small time scale (less than one second), the BMW i3 power module presents thermal impedance slightly lower than the 2014 Accord, which is attributed to the usage of alumina as the ceramic plate. When the time scale is greater than one second, the i3 inverter presents the lowest thermal impedance, which is about 40% lower than that of the accord at 100 second. The utilization of thermally-conductive alumina and also reduced layer thickness in the power modules has significantly improved the thermal performance if compared to other power modules.

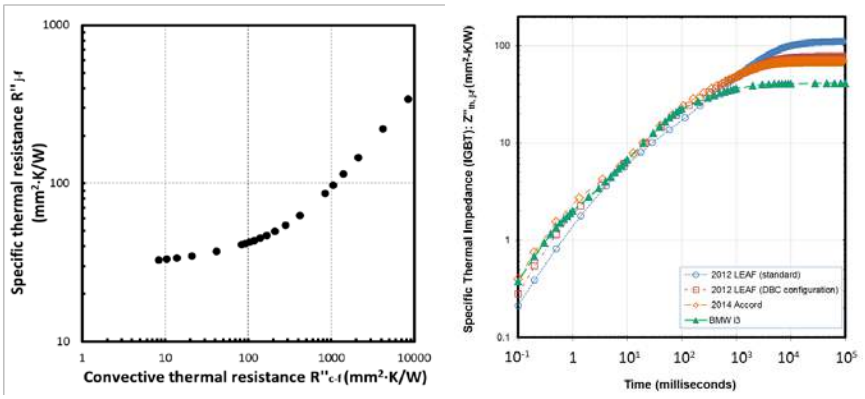


Figure I.17.2 - Specific thermal resistance (junction-to-liquid) versus the convective thermal resistance for the i3 power module (left), and transient junction-to-liquid thermal impedance versus time for four power module systems (right).

### *2015 BMW i3 electric motors thermal management system*

Figure I.17.3 shows a picture of the 2015 BMW i3 electric motor. The motor is an interior permanent magnet synchronous machine that outputs a maximum of 125 kW. The motor uses a distributed winding stator configuration and has a thermal management system that consists of a cooling jacket pressed around the stator. The cooling jacket is fabricated out of aluminum and has a spiral cooling channel that has approximate dimensions of 25 mm in width and 11.5 mm in height. The motor was thermally insulated within thick layers of insulation and WEG with 65°C inlet temperature was circulated through the cooling jacket. Five flow rates were characterized: $3.5 \times 10^{-5}$, $6.7 \times 10^{-5}$, $13.1 \times 10^{-5}$, $16.7 \times 10^{-5}$, and $20.2 \times 10^{-5} m^3/s$, which equal to 2, 4, 8, 10, and 12 liter per minute(Lpm), respectively. Unlike the Leaf motor, only two direct-current (DC), high-current, and low-voltage power supplies were used to provide heating to the motor's windings because the neutral point of the three phases was not accessible. Approximately 120 amps were conducted through the three phases to provide approximately 520 W of total heat. A total of twenty-eight thermocouples were installed on the end-windings, the stator surface and the slot-liner surface to measure the temperatures. Calculations revealed that the maximum heat loss to the surrounding conditions was less than 10% for all five flow rates. The measured thermal resistances versus the WEG flow rate for both the end winding and stator are also provided in Figure I.17.3. The specific thermal resistance between the stator and coolant is significantly lower than that from the end-windings to the coolant. At WEG flow rates $\geq 6.7 \times 10^{-5}$ $m^3/s$, the winding and stator thermal resistances decrease minimally as flow rates increase, indicating that the thermal resistance of the passive stack is significantly greater than the convective resistance at higher flow rates ($\geq 6 \times 10^{-5}$ $m^3/s$).

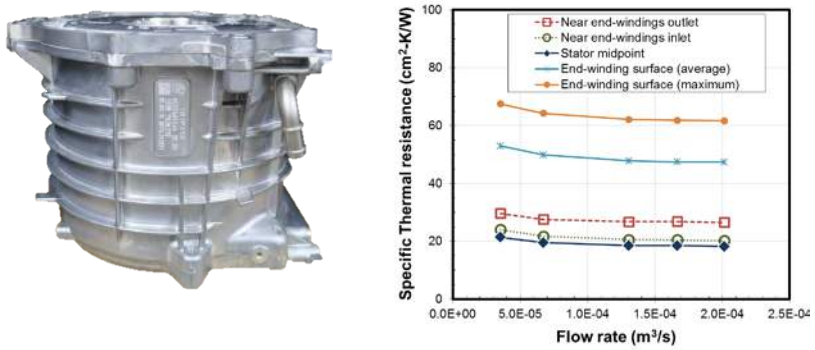


Figure I.17.3 - Picture of the 2015 BMW i3 electric motor (left), and experimentally measured thermal resistance values for different parts of the 2015 BMW i3 motor stator (right).

Photo Credit: Xuhui Feng, NREL

CFD analysis and FEA were also conducted to model the thermal performance of the system. CFD simulations were conducted to model the WEG flow within the cooling channels. Average heat transfer coefficients were obtained from the CFD analyses at various flow rates and over the wetted area, as listed in Table I.17-2. The values were then used as boundary conditions in the FEA model. Because the work to measure component properties (excluding aluminum) and interface contact resistance is still underway, the thermal conductivity of various materials in the motor and the contact resistances at different interfaces are only preliminary estimates.

**Table I.17-3 - Average heat transfer coefficient values for the BMW i3 motor cooling jacket**

| Flow rate ($m^3/s$) | *H* ($W/m^2 \cdot K$) |
|---|---|
| $3.5 \times 10^{-5}$ | 1,009 |
| $6.7 \times 10^{-5}$ | 1,450 |
| $13.1 \times 10^{-5}$ | 2,381 |
| $16.7 \times 10^{-5}$ | 2,898 |
| $20.2 \times 10^{-5}$ | 3,376 |

The FEA-predicted end-winding values are shown as symbols in Figure I.17.4. As shown, the model-predicted thermal resistance results provide an identical trend to the experimentally obtained results. However, as stated above, the thermal properties and contact resistances in the FEA simulation were only estimations. The discrepancy between the modeling and experimental results may be reduced if more accurate parameters are applied in the FEA simulation. It is also worth noting that the models capture the increase in the thermal resistance values at the lowest flow rate, which is associated with the transition from turbulent to laminar flow. The model was then used to compute a temperature profile from the inner slot liner surface to the cooling jacket. The temperature profile shown in Figure I.17.4 was used to identify the major thermal bottlenecks within the stator. It can be inferred that the passive stack-up structure contributes the dominant thermal resistance within the stator. Therefore in order to improve the thermal performance of the motor, both material properties and contact resistance need to be considered. Increasing the thermal conductivity of the resin and improving the resin's ability to bond the slot liner to the stator surface should reduce this thermal resistance.

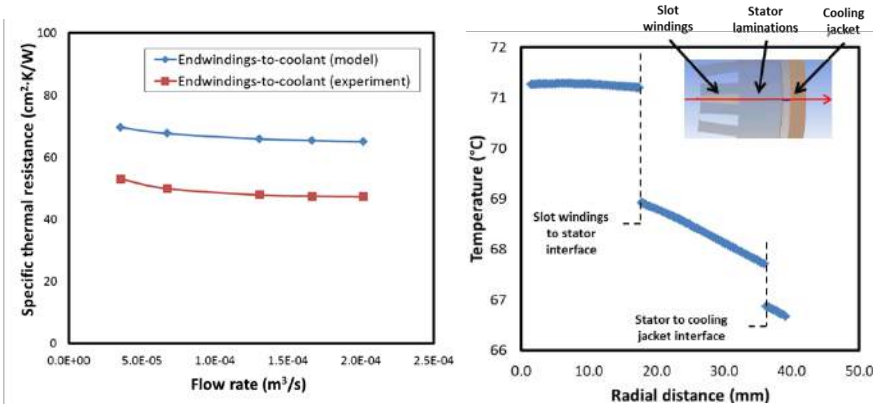


Figure I.17.4 - Comparison of the model-predicted specific thermal resistance and the experiment-based thermal resistance (left), and FEA-generated temperature contours within the partial i3 motor stator (right).

*The fourth generation Toyota Prius power electronics thermal management system*

Characterization of the fourth generation Toyota Prius power electronics thermal management system started in FY 2017. Figure I.17.5 shows the images of the fourth generation Toyota Prius inverter, which utilizes a power stack structure. In this structure, there are eight cooling plates and seven half-bridge power modules: six for the two electric motors and one for the DC/DC boost converter. One unique characteristic of the Prius inverter is that it features two separate cooling compartments. The upper compartment cools the inverter and capacitors, and the lower compartment cools the DC/DC converter. Characterization of the Prius inverter is underway.

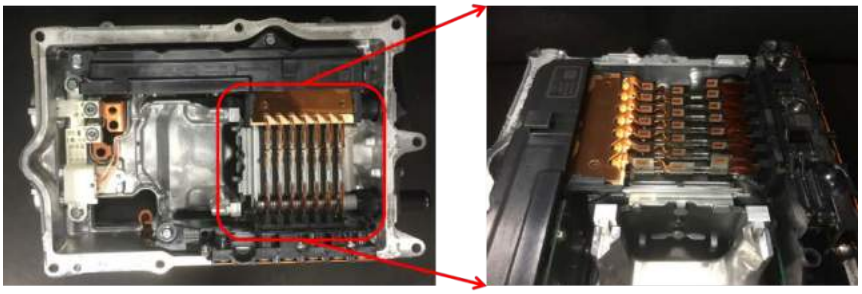


Figure I.17.5 - Fourth generation Prius power electronics: Top view of the Prius inverter section (left), and more details of the power stack structure including the cold plates and half-bridge modules (right).

Photo Credit: Xuhui Feng, NREL

## Conclusions

In FY17, we benchmarked the thermal performance of the 2015 BMW i3 power electronics and electric motor thermal management systems. Both experiments and numerical simulation were utilized to thoroughly study the thermal resistances and temperature distribution in the systems.

- Numerical simulation results provided steady-state and transient performance of the BMW i3 inverter. The steady-state specific thermal resistance decreases with decreasing convective thermal resistance.
- The transient performance of 2015 BMW i3 power module was compared to other three characterized power modules. The simulation results indicate that the i3 power module has the highest thermal impedance at a time scale of less than one second.
- Experimental results – obtained by utilizing WEG coolant – were obtained for the stator-to-liquid and end-windings-to-liquid thermal resistances. Both experimental and modeling results demonstrate that the passive stack is the dominant thermal resistance for the motor systems at the flow rates that were characterized.

## Key Publications

1. Feng, X., Moreno, G., Bennion, K., Cousineau, E. “Thermal Performance Characterization and Analysis.” 2017 Presentation to the US DRIVE Electrical and Electronics Technical Team, Southfield, MI, September 2017.

## References

1. Burress, T. “Benchmarking of Competitive Technologies.” DOE VTO Annual Merit Review, Washington, DC, May 2012.
2. Burress, T. “Benchmarking EV and HEV Technologies.” DOE VTO Annual Merit Review, Crystal City, VA, June 2015.

3. Moreno, G., Bennion, K., King, C., Narumanchi, S. “Evaluation of Performance and Opportunities of Improvements in Automotive Power Electronics Systems.” Presented at the 15th IEEE Intersociety Conference on Thermal and Thermomechanical Phenomena in Electronic Systems, Las Vegas, NV, May 2016.

# II. Electric Drive Technologies Development

## II.1 High-Efficiency High-Density GaN-Based 6.6 kW Bidirectional On-board Charger for PEVs

**Charles Zhu, Principal Investigator**
Delta Products Corporation
39209 Six Mile Road., Suite 105
Livonia, MI 48152
Phone: (734) 469-5716
E-mail: Charles.zhu@deltaww.com

**Steven Boyd, Program Manager**
U.S. Department of Energy
Phone: (202) 586-8967
E-mail: Steven.Boyd@ee.doe.gov

Start Date: October 1, 2014 End Date: December 31, 2017
Total Project Cost: $2,999,158 DOE share: $1,551,564 Non-DOE share: $1,487,594

### Project Introduction

On-board charger (OBC) is a key power electronic component in plug-in hybrid electric vehicles (PHEV) and battery electric vehicles (BEV). It receives power from grid and charges vehicle batteries. Market research done by Fiat Chrysler Automobiles (FCA) shows broad customer interest on using PHEV and EV as an emergency power source at homes or remote sites. This requires an inverter to reverse the power flow from the on-board batteries to the electric loads. With Si devices, the charger function and the inverter function are conducted by two separate modules. The body diode in Si MOSFET is too slow, thus requiring additional fast switching diode and a second MOSFET to make one effective switch. The result will be unsatisfactorily large, with losses and difficult to control.

GaN (Gallium Nitride) power switches have much lower switching losses and reverse recovery charge. This enables operation at much higher switching frequencies (0.3-1MHz) using GaN power switches. With higher switching frequency, reductions can be achieved in the volume and weight of passive components such as inductors and capacitors. The extremely low reverse recovery charge of the GaN power switch also eliminates the need for the series low-voltage MOSFET and parallel fast-recovery diode.

The goal of this project is to accelerate market introduction of OBCs for PEVs utilizing GaN power switches. This project will demonstrate the benefits of GaN power switches in automotive applications through the development of a lightweight, compact and efficient 6.6 kW isolated bidirectional OBC for PEVs.

### Objectives

- The objective of this project is to design, develop, and demonstrate a 6.6kw isolated bi-directional On-33Board Charger (OBC) using Gallium Nitride (GaN) power switches in a vehicle capable of achieving the specifications identified in Table II.1-1, below.
- The developed OBC will reduce size and weight when compared to commercially existing Silicon (Si) based OBC products in automobiles by 30%-50%.

Table II.1-1 - 6.6kw isolated bi-directional On-33Board Charger (OBC) Specifications

| Parameter | Requirement |
|---|---|
| **Switching Frequency** | 0.3 - 1 Mega-Hertz (MHz) |
| **Power Efficiency** | 95% |
| **Power Rating** | 3.3 kilo-Watt (kW) at 120 Volts Alternating Current (VAC), 6.6 kW at 240 VAC (Auto sensing depending on AC input voltage) |
| **Plug-In VAC** | 120/240 VAC |
| **High Voltage (HV) Battery Voltage Range** | 250 - 450 Voltage Direct Current (VDC) |
| **Nominal Battery Voltage** | 350 VDC |
| **AC Line Frequency** | 50 - 60 Hz |
| **Maximum Coolant Temperature** | 70°Celcius (C) |
| **Ambient Temp Range** | -40 to 70°C |
| **Controller Area Network (CAN) Communication** | Yes |

## Approach

This project brings together four organizations that are recognized leaders in their fields including:

- Delta Products Corporation, a Tier-1 automotive supplier and the U.S. subsidiary of Delta Electronics – the world's largest provider of switching power supplies;
- Transphorm, Inc., a technology development company that pioneered the development and manufacture of GaN power devices;
- The Center for Power Electronics Systems (CPES) at Virginia Tech, a world-renowned power electronics research center;
- Fiat Chrysler Automobiles, the global manufacturer of Chrysler, Jeep, Dodge, Ram, SRT, FIAT and Mopar vehicles and products.

The main task in Period III, which is in calendar year 2017, is to test the bi-directional charger at the component level and at the vehicle level. Delta completed C sample design to further enhance the power conversion reliability. Prototypes were built and tested at component level. Delta and FCA worked together and laid out the vehicle integration plan and test plan. The charge and discharge functions will be tested in FCA's 2018 Pacifica PHEV in the fourth quarter of 2017.

## Results

The C-Sample prototypes were built in the second calendar quarter of 2017 and tested in the third quarter of 2017. The volume of the module is

This unit achieved full charge mode and discharge mode functions and reliable operation.

Both Level 1 and Level 2 charge functions can operate in the full voltage range between 250Vdc and 450Vdc. The Level 2 charging operates up to full output power of 6.6 kW. The Level 1 charging operates in the full

Level 1 power range. The efficiency varies with battery voltage. The peak efficiency reached 95.1%. The power factor is better than 0.99%. Figure II.1.1 to Figure II.1.3 shows the key efficiency curve and input output waveforms.

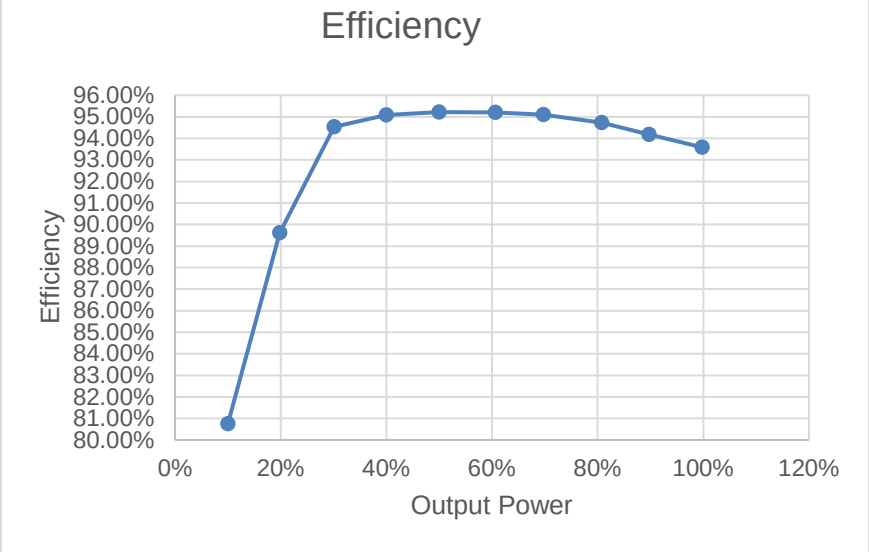


Figure II.1.1 - Level 2 charge efficiency, peak at 95.1% (30 ℃ Water Temp. 240Vac input and 350Vdc output. 100% load is 6.6kw)

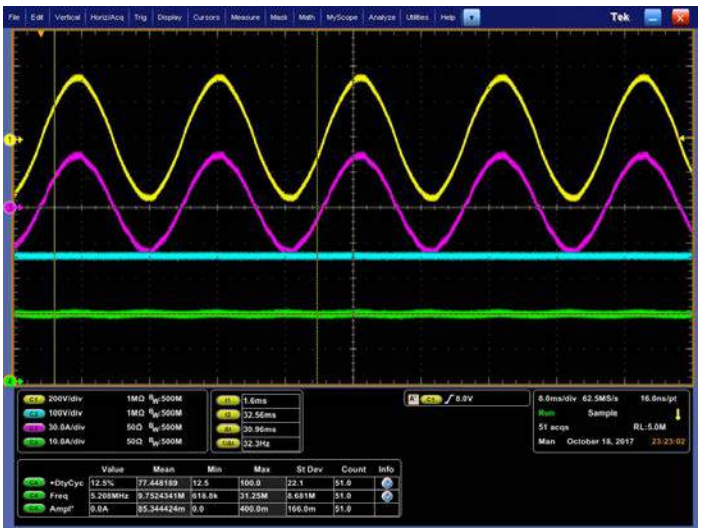

(CH1: Vac, CH2:Vdc, CH3:Iac, CH4:Idc)

Figure II.1.2 - Level 2 charge waveform, Vout=350Vdc (CH1: Vac, CH2:Vdc, CH3:Iac, CH4:Idc)

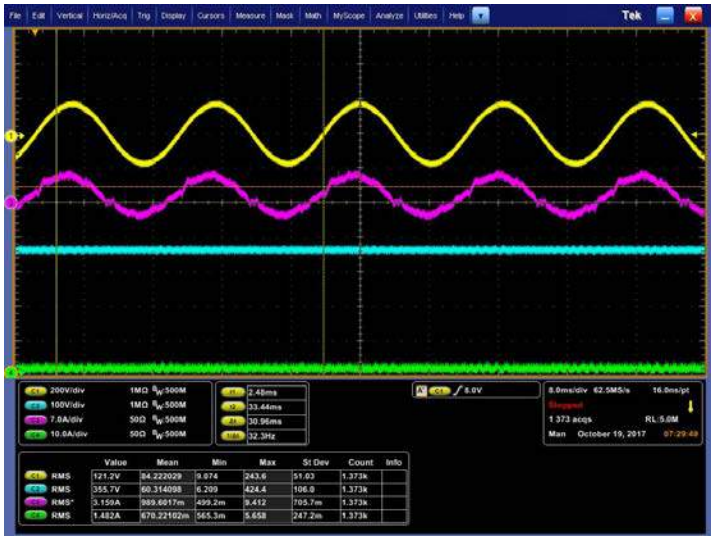

(CH1: Vac, CH2:Vdc, CH3:Iac, CH4:Idc)

Figure II.1.3 - Level 1 charge waveform, Vout=350Vdc (CH1: Vac, CH2:Vdc, CH3:Iac, CH4:Idc)

Both 240Vac and 120Vac discharge starts from 275Vdc and functions up to 450Vdc. The battery power shall be reserved for vehicle operation when the battery low. The Level 2 discharge operates up to output power of 6 kW. The Level 1 discharge operates up to output power of 3 kW. The efficiency varies with output power. The peak efficiency reached 95.1%. The output AC voltage THD is less than 5%. It is capable to power up surge loads, motor loads and capacitive loads. Figure II.1.4 to Figure II.1.7 shows the key efficiency curve and input output waveforms.

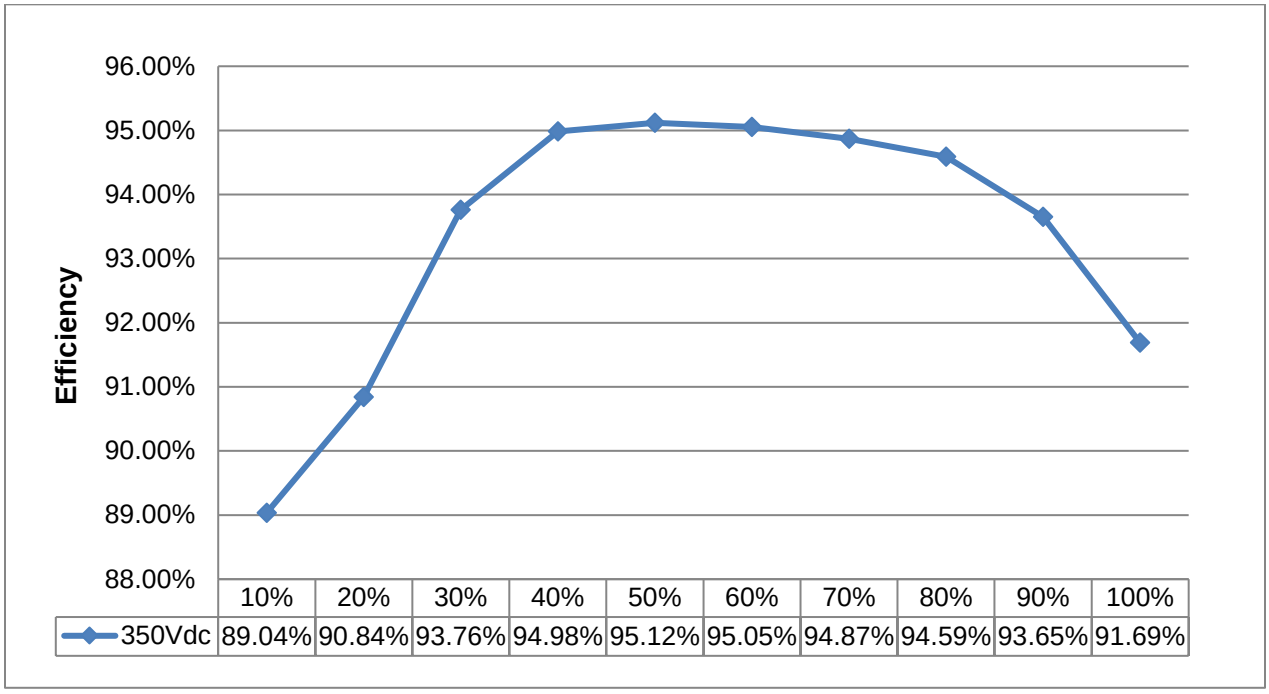


| | 10% | 20% | 30% | 40% | 50% | 60% | 70% | 80% | 90% | 100% |
|---|---|---|---|---|---|---|---|---|---|---|
| 350Vdc | 89.04% | 90.84% | 93.76% | 94.98% | 95.12% | 95.05% | 94.87% | 94.59% | 93.65% | 91.69% |

Figure II.1.4 - 240Vac discharge efficiency, peak at 95.1% (30 ℃ Water Temp. 350Vdc. 100% load is 6.6kw)

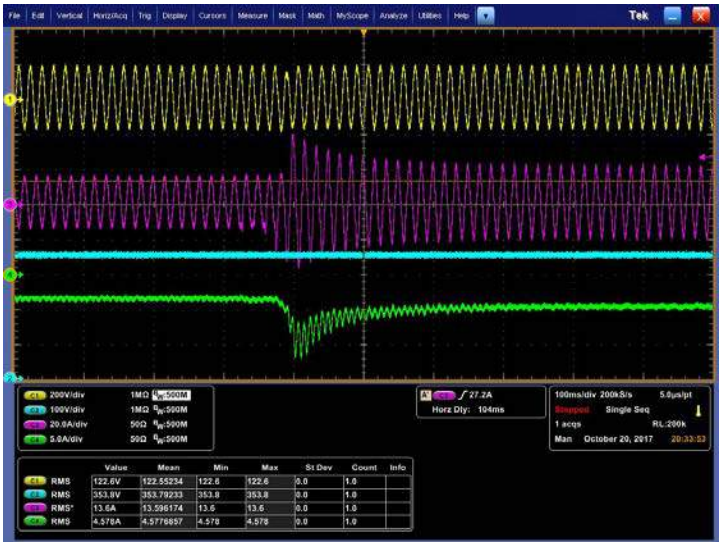

(CH1: Vac, CH2:Vdc, CH3:Iac, CH4:Idc)

Figure II.1.5 - 120Vac charge waveform, Vdc=350V (CH1: Vac, CH2:Vdc, CH3:Iac, CH4:Idc). Load is 400W incandescent light bulbs + 1266W resistor + 5A drill drilling wood

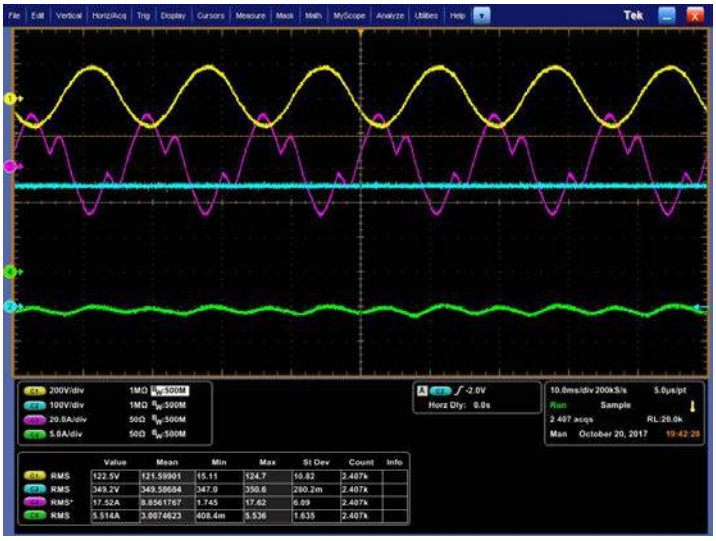

(CH1: Vac, CH2:Vdc, CH3:Iac, CH4:Idc)

Figure II.1.6 - 120Vac charge waveform, Vdc=350V (CH1: Vac, CH2:Vdc, CH3:Iac, CH4:Idc). Load is 400W incandescent light bulbs + 1400W microwave oven

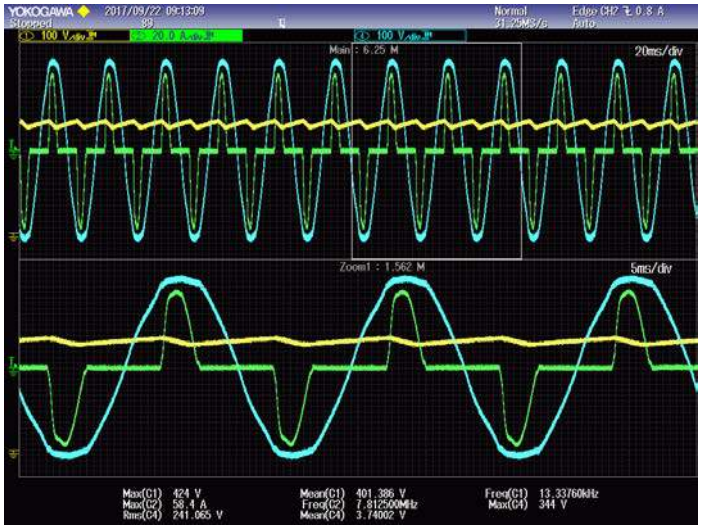


(CH1: Vdc, CH2:Iac, CH4:Vac)

Figure II.1.7 - 120Vac charge waveform, Vdc=350V (CH1: Vdc, CH2:Iac, CH4:Vac). 6 kW rectified capacitive load.

## Conclusions

The C-Sample component test result shows that the bi-directional OBC can operate to its design target. The volume and weight are both reduced by 50% or more of current automotive products. We expect to complete the vehicle integration test in November. There are multiple WBG devices are to be automotive qualified in the year 2018. The bi-directional OCB will be ready for RFQ, targeting model year 2021/2022 PHEV/BEV programs. This DOE funded program plays an important role to bring the WBG device based OBC to the commercial level.

## Key Publications

1. Weijing Du, Xiucheng Huang, Fred C. Lee, and Qiang Li, "Avoiding divergent oscillation of cascode GaN device under high current turn-off condition," in 2016 IEEE Applied Power Electronics Conference and Exposition (APEC). pp. 1002-1009.

2. Zhengyang Liu, Fred C. Lee, Qiang Li, and Bin Li, "Design of SiC-Based High-Frequency CRM AC/DC Converter for 6.6 kW Bidirectional On-Board Charger", in IEEE Energy Conversion Congress and Exposition (ECCE), Milwaukee, WI, 2016.

## II.2 Multilayered Film Capacitors for Advanced Power Electronics and Electric Motors for Electric Traction Drives

**Deepak Langhe, Principal Investigator**
PolymerPlus LLC
7700 Hub Parkway
Valley View, OH 44125
Phone: (216) 264-4818
E-mail: dlanghe@polymerplus.net

**Steven Boyd, Program Manager**
U.S. Department of Energy
Phone: (202) 586-8967
E-mail: Steven.Boyd@ee.doe.gov

### Project Introduction

Biaxially oriented polypropylene (BOPP) film capacitors are the most suitable technology for high voltage, high temperature, and high ripple current power electronic systems in high performance electric vehicles (EVs). These capacitors, however, occupy 1/4th to 1/3rd of the power electronic unit and have a 50% voltage derating above 85 °C due to their drastically deteriorated breakdown strength and lifetime at high temperature. Development of a new dielectric material system for capacitors to increase temperature use and reduce size is critical in many EV related applications. Multilayer dielectric film developed by PolymerPlus and team has demonstrated improved dielectric constant and breakdown strength as compared to BOPP films. In this program, several film formulations were developed and investigated for dielectric performance and further down-selected for production scale up. Because this technology uses commercial polymers, fabrication of film rolls to demonstrate scalability for initial capacitor fabrication trials was successfully achieved. The film production feasibility, metallization and capacitor prototype fabrication was successfully demonstrated in Year 1 of the program. In Year 2 of the program, film production scale-up leading to significantly large film quantities for metallization and capacitor fabrication led to 600 µF size capacitors. Capacitor characterization was also completed during this year.

### Accomplishments

- Multilayer dielectric film processing and production scale-up
  - Identified and processed new resins to add to resin catalog for high temperature dielectric films
  - Investigated various processing conditions to improve the film quality
  - Completed dielectric characterization of newly processed films.
- Multilayer film production scale-up
  - Processed 6,000 sq. dielectric film with 4.3 µm thickness for capacitor fabrication trials
  - Processed 28,000 sq.ft. of high temperature dielectric film (8 µm thickness) for capacitor fabrication trials.
- Capacitor designing and 500 µF capacitor fabrication
  - Multiple metallization trials of 4.3 µm and 8 µm dielectric films completed.
  - 40 µF windings fabricated and characterized to evaluate materials.
  - 600 µF capacitor prototypes fabricated and characterization completed as final part deliverables.

- Material understanding and new material development
    - A detailed understanding of materials is currently being developed in current material systems

      This knowledge will be used to develop new multilayer films for dielectric applications.

## Introduction

For high performance electric vehicles (EVs), film capacitors are the most suitable technology for high voltage, high temperature, and high ripple current power electronic systems. Current state-of-the-art technology uses biaxially oriented polypropylene (BOPP) capacitors usually occupy 1/4 to 1/3 of the power electronic unit and have a 50% voltage derating above 85 °C due to their drastically deteriorated breakdown strength and lifetime. Also, compared to ceramic (e.g., multilayer ceramic or glass capacitors) and electrolytic (e.g., Al) capacitors, polymer film capacitors have advantages in terms of graceful failure, very-stable capacitance, and capability of handling large ripple currents, and are proved to be most suitable for advanced power electronics in EVs. It is also interesting to note that BOPP has reached its development threshold and industry still requires a significant improvement in energy density and temperature use. Many attempts to develop new material systems in last decade are limited to laboratories or very small quantities. One of the key criteria for new material development is demonstrating scale-up capability in addition to improved properties.

**Table II.2-1 - Advanced PEEM Program DC-link Capacitor Targets**

| | |
|---|---|
| **Capacitance ($\mu$F)** | >1000 |
| **Voltage rating ($V_{DC}$)** | 650-900 |
| **Tan$\sigma$ at 10 kHz** | < 0.02 |
| **ESR (m$\Omega$)** | < 2 |
| **ESL (nH)** | $\leq$ 5 |
| **Temperature (°C)** | 140 |
| **Ripple current (A rms)** | 100 |
| **Failure mode** | benign |
| **Lifetime (hrs)** | >20,000 |
| **Volume (L)** | $\leq$ 0.6 |
| **Cost ($)** | $\leq$ 30 |

ESR: equivalent series resistance; ESL: equivalent series inductance

To overcome these challenges, PolymerPlus and team proposed multilayer film based technology, which has demonstrated improved energy density films in its earlier development work. [1-9] In this program, PolymerPlus, SBE Inc., Oak Ridge National Laboratory (ORNL) and Case Western Reserve University (CWRU) are jointly working on multilayer polymer film systems to increase the high temperature performance and stability of the film, and miniaturize film capacitors to reduce cost for advanced power electronic systems in EVs. This unique multilayer film (MLF) coextrusion technology has capability to achieve high temperature capability and high energy density at the same time. The overall goal of the project is to achieve all the requirements for DC-link capacitors listed in Table II.2-1. Development of a multilayered film combining a

high energy density polymer with a high breakdown/low loss polymer, high energy density and low dielectric/hysteresis losses temperature, it is possible to achieve increased temperature performance.

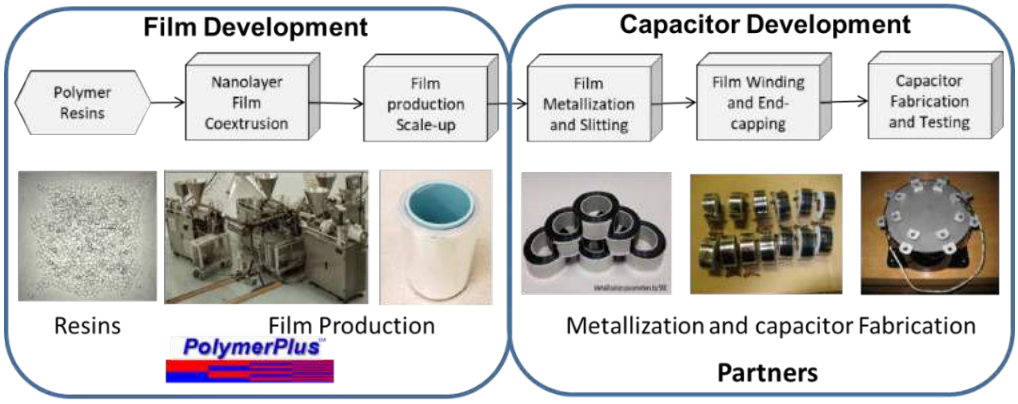


Figure II.2.1 - Technology development approach schematic showing film processing activities are led by PolymerPlus. It works with partners for metallization and capacitor development activities.

In year 1 of the program, PolymerPlus demonstrated fabrication of the high temperature films by systematically investigating various material formulations. Film thickness reduction down to 4 µm, film metallization and 100 µF capacitor part fabrication were some of the key achievements during Year 1 of the program. In Year 2, new resins were identified and added to the catalog as new dielectric materials alternatives. Film production trials to process more than 34,000 sq.ft. of dielectric film for continued metallization and capacitor development activities. Detailed characterization of the capacitors was also completed during this year. Our detailed approach is summarized in Figure II.2.1.

## Approach

*Multilayer Film Processing:*

Using a film coextrusion process, schematically shown in Figure II.2.2, multilayered films with different polymers and formulations were processed in year 1 of the program. The schematic of the coextrusion processing line with layer mutiplying elements and the layered structure consisting of two polymers feeding through two different extruders is shown in Figure II.2.2. An image of PolymerPlus coextrusion line is also shown. The coextrusion process consists of a multi-channel feedblock where two polymers, represented by Resin A and Resin B, meet to form a melt stream with two layers. As the polymer melt fed through a series of multiplier die elements, each of which doubles the number of layers through melt cutting, spreading and stacking process to create a layered structure ranging from few layers to few hundreds of layers. The number of layers is determined by the number of layer multiplier dies used in the coextrusion process. Multilayer dielectric films can contain different number of layers and the relative composition of the two polymers to achieve the optimum performance. The approach involved using commercial polymers, coextrusion processing of down-selected polymers, and processing optimization for film processing activities. Resin selection criteria, preliminary resin characterization, film production scale-up details are discussed in previous annual report. Film production trials are followed by metallization, capacitor fabrication and characterization trials as reported previously.

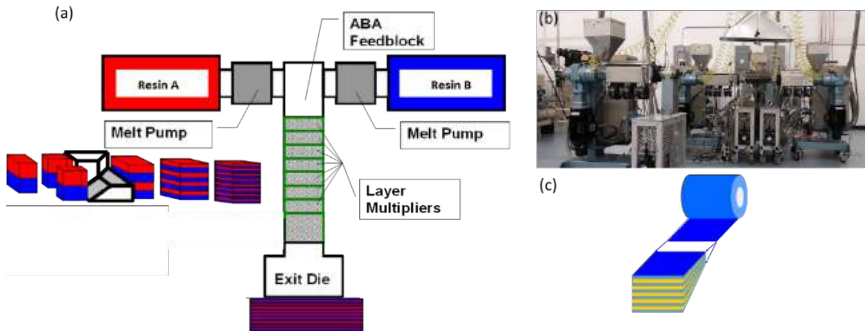


Figure II.2.2 - (a) Coextrusion process schematic showing a two polymer system, with alternating layers of Resin A and Resin B in a film structure. Example of layer multiplying die and layering process is also shown (b) PolymerPlus coextrusion line (c) a schematic representation of dielectric film structure consisting of alternating layers of two polymers

## Results and Discussion

*Multilayer Film Processing:*

A multilayer film system, with a down-selected composition ratio of Resin A and Resin B was processed with number of layers varied from X to Y to Z, where X, Y and Z = 2^n+1 and n is the number of multipliers. As the ratio of the two materials was kept constant, increasing the number of layers changed the thickness significantly. The number of layers were changed approximately by a factor of 4 in these three systems i.e., for a given film thickness, the individual layer thickness of Resin A and Resin B varied by a factor 4 in these systems. It is interesting to note that film thicknesses down to 4 µm are comparable with current commercial BOPP film thickness of 3-4 µm. The individual layer thicknesses can vary from few tens of nanometers to few hundreds of nanometers in these films. Analysis of MLFs with X, Y and Z number of layers and thicknesses ranging from 12 to 4 µm was completed for thickness and breakdown strength uniformity. High sampling frequency testing was completed on rolls at regular intervals across the film width and down the film length to understand the spatial property variation over known areas for the samples. For all the film samples the thickness variation of less than ± 1.0 was measured, with an exception of a couple of samples. For a commercial BOPP films this variation is typically within 5% of the average film thickness. As the multilayer film technology matures with process modifications, PolymerPlus will be working on improving the film thickness uniformity similar to BOPP films. In addition to 5 types of formulations processed in Year 1, two additional formulations were investigated in Year 2 of the program. Detailed dielectric film properties are summarized in Table II.2-2.

**Table II.2-2 - Film system details**

| Film System | No. of Layers | Film Thickness |
|---|---|---|
| 1-Resin a/Resin B | X | 11, 8, 6 |
| 2-Resin A/Resin B | Y | 12, 8, 6, 4 |

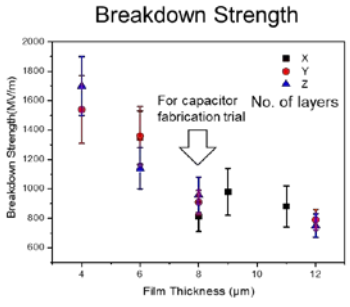


| Properties | Multilayer Film | Commercial BOPP |
|---|---|---|
| Layers | 10s | 1 |
| Composition | X/Y | 100 |
| Thickness, µm | 12-4 | 3-4 |
| Dielectric constant | 4.0 (1 kHz) | 2.25 |
| Breakdown Strength (MV/m) | >1100 | 800 |
| Temperature, °C | 150 | < 105 |
| Tan δ | 0.005 | 0.0003 |

Figure II.2.3 - (left) Breakdown strength of multilayer film with varying number of layers and film thicknesses, (right) Dielectric performance summary of multilayer dielectric film

*Multilayer Film Production Scale-up and Metallization:*

In Year 1, two rolls of 3000 sq.ft. film, with 8 µm thickness were fabricated and metallization for capacitor fabrication trials. The down-selected system was further processed in Year to achieve production of 4.3 µm thickness film as well as 8 µm thickness film. In year 2, 6000 sq.ft. film roll of 4.3. µm thickness film was processed. Several wrinkles were observed in the final roll as well as the metallized reels, which led to poor capacitor winding. Therefore, for the subsequent trials, 8 µm thickness was selected for production trials, which allowed better metallization as well as capacitor winding. Modified film take-off units are necessary for winding of thinner films. Through its internal development, PolymerPlus has acquired a custom-designed film take-off unit to handle thinner films, which can be used for further development activities. In the film processing trials, three films rolls, with a total length of 28,000 sq.ft, were processed and delivered for metallization, Figure II.2.4.

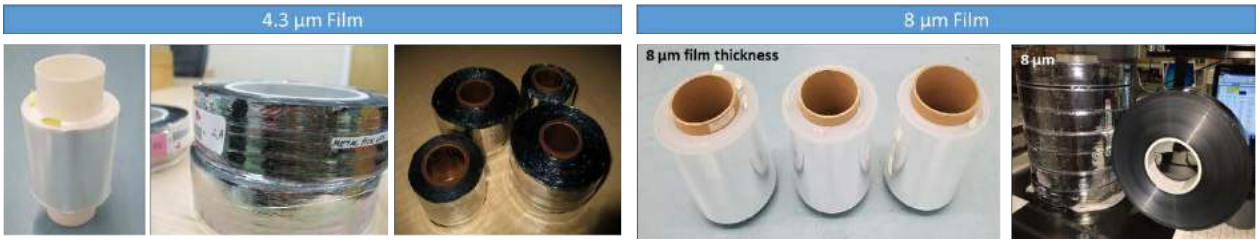


Figure II.2.4 - (top row) Film roll with 6000 ft. length and average thickness of 4.3 µm. Metallized film reels and initial capacitor winding attempts showed significant wrinkles (bottom row) three film rolls with total length of 28,000 ft. and average thickness of 8 µm. Corresponding metallized reels are shown.

The completed film metallization trials provided sufficient film qualities for fabricate 30 µF for initial evaluation, followed by fabrication of > 500 µF capacitor parts, discussed in next section.

*Capacitor Fabrication and Characterization:*

SBE and Oak Ridge National Laboratory investigated baselining BOPP material based capacitors for comparison with new MLF film capacitors using an industry relevant inverter. The capacitors fabricated during Year 1 were characterized and summary of data is shown in Figure II.2.5. As compared to first production trial, high breakdown strength, improved clearing and lower leakage currents were observed in second trial. It should be noted the starting film thickness was 12 µm, as compared to 8 µm as used in next trials. This significant difference in the dielectric performance with improved film quality is indicative of the multilayer film dielectric technology promise. It is important to achieve high performance, high quality dielectric film that will translate into capacitor prototypes with improved performance.

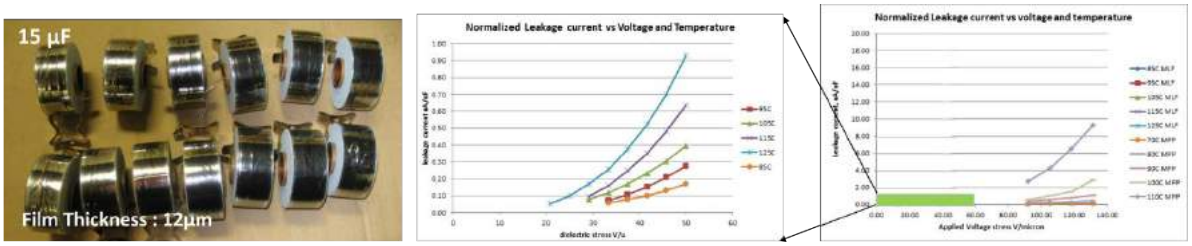


Figure II.2.5 - 15 µF capacitor parts and leakage current measurement

In the capacitor fabrication trials with the new materials, 40 parts with a target capacitance of 30 µF were fabricated. Examples for final capacitor parts are shown in Figure II.2.6. Capacitor fabrication process followed typical winding, and end-spraying activities. The capacitors characterized for capacitance pre- and post-curing showed no significant change in the capacitance. Capacitors were further characterized for voltage withstanding as a function of temperature. Capacitors were tested in 65 to 105°C temperature range. In a typical BOPP capacitor, a breakdown event results into a small drop and fast voltage recovery, while

multilayer films showed slightly higher discharge and recharge. The voltage drop represents the energy used to vaporize the metallization surrounding the dielectric puncture at the fault site. Although the BOPP capacitor functionally "self-heals" at most dielectric fault locations, there is a very slight [difficult to measure] increase in leakage current that flows at each fault site. BOPP capacitors are usually able to successfully self-heal even when placed across very low impedance DC sources. For MLF film windings, the large voltage reduction observed when a dielectric puncture occurs implies that far more energy [than for BOPP] is dumped into a dielectric fault location prior to the removal of the fault [which then allows the capacitor to begin a recharge]. After several clearing attempts, the charge rate would decrease for a given power supply setting. This implies that the leakage current that occurs at each fault site is somewhat higher than is the case for MPP capacitors. For MLF capacitors tested at higher temperatures, the temperature defined leakage current appears to dominate the leakage current created by fault sites. Further development and data analysis is required to understand behavior of multilayer films in the capacitor parts. New capacitor parts with sizes > 600 µF were fabricated in most recent fabrication trials, as shown in Figure II.2.6(b). These were the largest capacitors fabricated in this program as final deliverables.

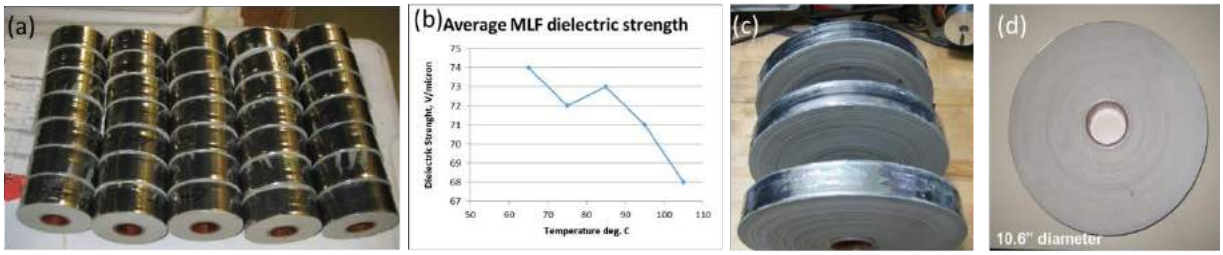


Figure II.2.6 - (a,b) 30 µF capacitor parts and dielectric strength characterization as a function of temperature, (c,d) 600 µF capacitor prototypes using multilayered dielectric film

*Multilayer Film Mechanisms and New Material Development:*

Understanding the multilayer film dielectric materials is critical for success in various applications. Some of the issues investigated in this program are as follows. A significant difference between multilayer and blend films was demonstrated in the ultimate dielectric properties such as breakdown strength and lifetime. For multilayered films higher breakdown strength than the linear average of the two components was attributed to interfacial polarization in multilayer films, which reduced electronic conduction in the sample. In contrast, blend films demonstrated various morphologies like island-in-sea and co-continuous phase, depending upon the relative ratio of the materials. Based on the observations and the data, a unique working mechanism for multilayer films was proposed as shown in Figure II.2.7. In this mechanism, we propose interfacial polarization from space charges. These interfacial charges serve as effective traps for hot electrons injected from the metal electrodes. Further investigation of this multilayer system was conducted to identify routes to reduced dielectric losses. The optimal unipolar poling conditions identified were: 80 MV/m (peak field), 10 Hz, 165°C, and 1 h poling. It was established that the impurity ions can be "locked" in alternating layers of multilayer film system to reduce ionic conduction loss in multilayer films.

This process can be used for packaged multilayer film capacitors in order to reduce conduction losses from impurity ions for electric vehicle applications at high temperatures.

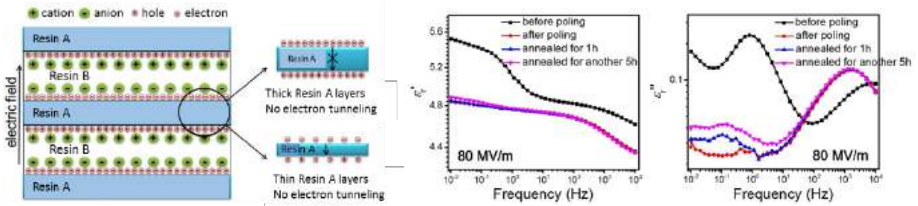


Figure II.2.7 - (left) Proposed interfacial polarization from both electrons/holes and anions/cations, (right) Frequency-scan BDS results for multilayer films showing thermal annealing and poling effects on multilayered films.

## Conclusions

PolymerPlus demonstrated development of multilayer films for capacitor applications using commercial resins. Improved dielectric constant and increased breakdown strength values of multilayer films were higher than current state-of-the-art BOPP dielectric film used for capacitor applications. Several film formulations were investigated in the first year of the program to down-select for capacitors prototypes for advanced power electronics and electric motors for electric traction drives. In year 2, film production scale-up up to several tens of thousands of square feet film was demonstrated for metallization and capacitor fabrication trials. Fabrication of small capacitor parts and winding parameters were investigated for subsequent large capacitor part fabrication. A pre-selected metal alloy recipe was used for metallization trials, followed by fabrication of 600 µF capacitor parts. The completed functional capacitor is presently being evaluated for DC leakage subject to temperature and voltage conditions.

## FY 2017 Presentations/Publications/Patents

1. D. Langhe, L. Zhu, M. Brubaker, L. Marlino, Web meeting, November 2016
2. D. Langhe, L. Zhu, M. Brubaker, L. Marlino, Web meeting, March 2017
3. D. Langhe, L. Zhu, M. Brubaker, L. Marlino, Annual Review Meeting, Washington DC, June 2017.
4. D. Langhe, L. Zhu, M. Brubaker, L. Marlino, Web meeting, July 2017

## References

1. Baer, E.; Hiltner, A.; Shirk, J. S.; Wolak, M. A. US 20100172066, 20100708, 2010.
2. Mackey, M.; et al., J. Phys. D: Appl. Phys. 2009, 42, 175304.
3. Mackey, M.; et al. Macromolecules 2012, 45, 1954-1962
4. Mackey, M.; Schuele, D. E.; Zhu, L.; Baer, E., J. Appl. Phys. 2012, 111, 113702.
5. Zhou Z, Mackey M, Carr, Zhu L, Flandin L, Baer E, J. Polym. Sci. Part B Polym. Phys, 50 (14), 993-1003 (2012)
6. Tseng J K, et al. Polymer 55, 8-14 (2014)
7. Langhe, D.; Ponting, M.; Coextrusion Processing of Multilayered Dielectric Polymeric Films, SPE ANTEC 2015, Orlando, FL, 2015.
8. Langhe, D.S.; Ponting, M.; High Temperature Multilayered Polymeric Films for Capacitor Applications, SPE ANTEC 2014, Las Vegas, NV, 2014.
9. Langhe D., Ponting M., Manufacturing and Novel Applications of Multilayer Polymer Films, Plastics Design Library, ISBN 978-0-323-37125-4 (2016)

## II.3 High Speed Hybrid Reluctance Motor Utilizing Anisotropic Materials

**Edwin Chang, Principal Investigator**
General Motors Global Propulsion Systems
777 Joslyn Avenue
Pontiac, MI 48340
Phone: (248) 310-7056
E-mail: edwin.chang@gm.com

**Steven Boyd, Program Manager**
U.S. Department of Energy
Phone: (202) 586-8967
E-mail: Steven.Boyd@ee.doe.gov

Start Date: October 1, 2016 End Date: September 30, 2019
Total Project Cost: $7,081,060 DOE share: $4,637,060 Non-DOE share: $2,444,000

### Project Introduction

The objective of this project is to design and verify motor designs with reduced heavy rare earth (HRE) content capable of achieving DoE Motor Year 2020 performance and cost targets. Initial work focused on a hybrid motor containing HRE-free magnets and grain oriented electrical steels. Motor designs with grain oriented steel were strongly pursued with many different orientations of the material, however, the grain oriented electrical steels were found to be largely ineffective in improving performance, and the project was re-scoped to focus on three motor variants. These focused three variants are 1) HRE-free PM machine, 2) Synchronous Reluctance Motor with Small HRE-free Magnet Assist, and 3) Hybrid Induction Motor with Insert Copper Bars and Cast Aluminum End-rings.

### Objectives

The objective of the project is to research, develop, and demonstrate 3 new motor types for traction applications. Each design should be capable of achieving or exceeding the following technical targets, set by the DoE to be achieved by 2020:

- Cost ($/kW) less than $4.7
- Specific Power (kW/kg) greater than 1.6
- Power density (kW/L) greater than 5.7

These motors are enabled by the following technologies, which are evaluated through the course of this project:

- HRE-free magnets must be developed to meet stringent coercivity and remanence performance criteria
- Copper – aluminum interfaces must be developed to be robust in a traction motor environment
- Motor electromagnetic and mechanical design techniques must be developed to ensure that these enabling technologies can be incorporated to meet motor performance requirements.

Each design should demonstrate advantages over conventional baseline designs in one or more of the following categories: cost, efficiency, and power density. Each design is also expected to have proven manufacturability and to undergo typical durability and performance testing by GM, to ensure they meet market requirements.

## Approach

Three motor design types will be studied to determine the feasibility of each approach. These three motor variants will be selected based on their expected ability to meet the technical targets. These design approaches will take advantages of material advancements which will allow these motors to meet the performance requirements without heavy rare earth elements or rare earth elements altogether.

The project will concentrate on four major tasks:

Task 1: Material Evaluation and Selection
Task 2: Electromagnetic and Mechanical Machine Design
Task 3: Electric Motor Prototype Manufacturing
Task 4: Verification Testing and Performance Evaluation

*Task 1: Material Evaluation and Selection*

- Development of the requirements for Grain Oriented Electrical Steel (GOES)
- Survey of available grades of GOES
- Industry survey of GOES available grades and Selection for Electromagnetic Design Studies
- Execution of FEA-based design studies for Synchronous Reluctance Motor using GOES, and Hybrid Synchronous Reluctance Motor using Anisotropic HRE-free magnets and GOES
- Development of, working with suppliers, HRE-free anisotropic magnet material
- Evaluation of the developed anisotropic HRE-free magnets and Non-Oriented Electrical Steel (NOES) for use in the motor laminations.

*Task 2: Electromagnetic and Mechanical Design of 3 Machines*

- Detailed structural, thermal, and electromagnetic analysis of the machine concepts to ensure that the motors meet both the performance and reliability objectives required for use in General Motor's electrified vehicle portfolio
- Generation of an Indentured Bill of Materials (BoM)

*Task 3: Electric Motor Prototype Manufacturing*

- Prototype motors will be built to ensure that those meet all GM Production Bill of Process (BoP) requirements
- Production Manufacturing Equipment will be identified and its associated costs will be documented
- Comprehensive test plan for machine verification will be defined and durability test plan for demonstration will be developed

*Task 4: Verification Testing and Performance Evaluation*

- All three motor designs will be calibrated for peak torque and efficiency
- Machines will be tested for performance and efficiency verification
- Torque and power vs. speed curves will be generated
- Complete efficiency maps for both motoring and generating will be generated for operations at different voltage levels

- Measured performance maps will be compared to the predicted results for data correlation purposes
- Rotor durability testing will be executed on two variants (Synchronous Reluctance motor with HRE-free Magnet Assist and High Performance Hybrid Induction Motor using Inserted Copper Bars and Aluminum Die Cast End-rings) and will include rotor speed cycling at various RPM to induce fatigue failures in the rotor laminations
- HRE-free PM motor variant will be excluded from rotor durability testing due to its similarity to other production designs that have previously demonstrated superior reliability

Oak Ridge National Laboratory, ORNL, a co-recipient of this project, is responsible for aspects of materials testing. The objectives are to coordinate materials testing and research, and the results of that research may be included in the motor assemblies built and tested in Budget Period 2 and 3. However, due to the results of the initial GOES study, the CRADA is pending, having been re-scoped to further studies of NOES and Cu-Cast Al interfaces.

## Results

*Materials Testing and Evaluation*

**GOES Industry Survey: Preliminary Selection and Initial Motor Design Studies**

An industry survey was conducted with, but not limited to, electrical steel suppliers with whom GM has extensive experience of working with on production and development projects for non-grain oriented steels. The best available steels were compared across suppliers, based on their provided data. In addition, calculations were carried out based on available academic knowledge to understand theoretical limits of saturation flux density and performance of grain oriented steels. Targets were set for material improvement based on that.

Detailed design studies were carried out using grain oriented steel in the rotor as well as in the stator. The goals of these design studies were to increase motor torque density and subsequent increase in efficiency. Several rotor geometries were fully optimized using GOES in different orientations. Some of these studied also included GOES in the stator. Motor manufacturability and cost were specifically studied.

These extensive design studies with the introduction of GOES in the rotor only resulted in a modest (<3%) increase in motor torque. In addition, designs optimized for best electromagnetic performance were largely not manufacturable. Improvement in torque was best realized through the substitution of grain oriented steel in the stator. However, this was not only difficult to manufacture but also deemed to be cost-prohibitive.

Due to the limited success with the increase of motor performance with GOES it was decided to discontinue any additional design efforts using GOES. The project goal was re-scoped with more promising technologies.

*HRE-Free Magnet Testing*

HRE thrifting and eventual total elimination is a major goal toward which GM is working in conjunction with several major magnet suppliers. Significant advancements are made with HRE-free magnet development. Several anisotropic magnet technologies show promise in increasing magnet coercivity without HRE material, which is critical for surviving demagnetization at elevated temperature. This has enabled the investigation of HRE-free magnets in traction motor applications. A few properties of promising HRE-free magnets are compared in Figure II.3.1 with a more conventional baseline magnet with HRE additives. Magnet coercivity of some of the HRE-free magnets is comparable or even higher than a more conventional HRE magnet. The increase in coercivity of HRE-free magnet is achieved at the expense of residual flux density as shown in Figure II.3.1. This is one area the magnet manufacturers are working to overcome. Lower remanence basically means more magnet to compensate for lower energy, thus increasing magnet cost. Nevertheless, the HRE-free

magnets are crucial to overcome the supply and price volatility of HRE magnet materials which is a major concern for automotive industry.

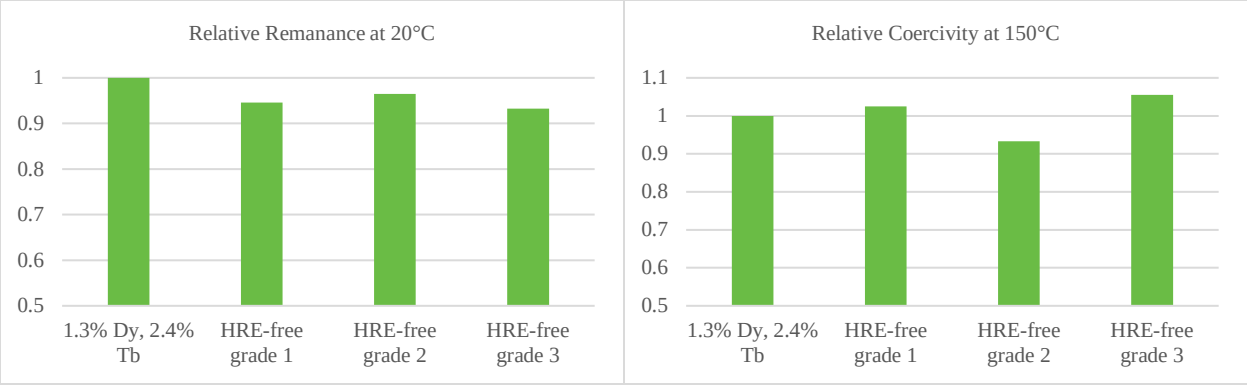


Figure II.3.1 - Magnetic Properties (GM testing)

*Non-Oriented Electrical Steel (NOES) Selection*

General Motors have been working with major steel suppliers towards the development of non-oriented electrical steel (NOES) with high permeability, low iron loss, and high mechanical strength. GM has set a target for electrical steel for EV and plug-in hybrid applications based on the motor operation's standard drive cycles. Non-oriented electrical steels used in the Synchronous Reluctance Motor (SRM) and HRE-free interior PM (IPM) Motor were selected based on these magnetic and mechanical properties. Table II.3-1 compares the magnetic and material properties of a few 0.27 mm thick steels from major steel suppliers developed towards GM set targets. GM conducted standard Epstein and tensile tests internally to estimate magnetic and mechanical properties respectively as listed in Table II.3-1. Final sourcing for prototype builds will depend on the optimized electric motor performance of these steels for standard vehicle drive cycles and also on material availability.

Induction motors require high permeability electrical steel to minimize excitation energy while building the rotor magnetic field. GM has been working with electrical steel supplier to develop steels specifically for induction motors. NOES used in induction motor was selected for high permeability and reasonably low iron losses and good mechanical strength. A survey of 0.3mm thick NOES with the best permeability properties across leading steel mills was conducted and results were compared based on supplier provided data. Two high performing steels were identified based on this criteria, and will be selected based on material availability during sourcing for prototype builds.

Table II.3-1 - Steel Evaluation Data of 0.27mm Steel

| Supplier | Supplier A | Supplier B | Supplier C | Supplier D |
|---|---|---|---|---|
| Grade | Grade A | Grade B | Grade C | Grade D |
| Thickness | 0.27 mm | | | |
| Iron loss, W10/400 (W/kg) | 11.7 | 12.2 | 11.4 | 12.0 |
| Flux density, B50 (T) | 1.67 | 1.67 | 1.68 | 1.67 |
| Yield strength, YS (MPa) | 417 | 420 | 431 | 413 |

*Copper-Aluminum Bar Interface Testing*

The predominant method of induction rotor construction is die cast with aluminum. Copper rotors are built, to improve efficiency and rotor thermal performance, by fabricating copper bars and welding copper end-rings after bar insertion. GM is pursuing a new rotor manufacturing method where aluminum end-rings are die cast to make electrical connections with the inserted copper bars resulting in a hybrid aluminum-copper rotor. In order to confirm the robustness of the Cu-Al interface, thermal shock and fatigue testing were performed. The thermal shock testing demonstrated no difference between the coated copper bars and bare copper bars. However, the coated copper bars performed significantly better in fatigue cycling, demonstrating improvements in robustness to mechanical stress. The objective is to replicate these characteristics for all bars in a die cast aluminum ring rotor. Table II.3-2 shows the Cu-Al bar test results.

Table II.3-2 - Cu-Al Bar Test Results

| | Stress (MPa) | Average Cycles to Failure | Failure Location |
|---|---|---|---|
| Coated Cu-Al bar | 161 | 360000 | Copper Broke at aluminum |
| Coated Cu-Al bar | 175 | 235000 | Copper Broke at aluminum |
| Coated Cu-Al bar | 189 | 87000 | Copper Broke at aluminum |
| Bare Cu-Al bar | 175 | 16000 | Copper pulled out at aluminum |

*Electromagnetic and Mechanical Motor Design of 3 Machines*

The electromagnetic design has shown that the motor variants are capable of exceeding the DoE 2020 goals for performance. The evaluation of cost is still ongoing. Table II.3-3 shows a summary of the motor performances of the three machine variants. DoE target and status of GM designed motors is listed in Table II.3-4.

Table II.3-3 - Motor Design Targets

| Criteria | HRE-free PM Motor | Synchronous Relucance Motor with HRE-free PM Assist | Hybrid Induction Motor with Insert Cu Bars and Cast Al End-rings |
|---|---|---|---|
| Stator Outer Diameter (mm) | 208 | 190 | 190 |
| Stator Core Length (mm) | 200 | 100 | 100 |
| Power (kW) | 150 | 86 | 86 |
| Torque (N-m) | 360 | 255 | 328 |
| Max RPM | 12000 | 18000 | 14000 |

Table II.3-4 - DoE Motor Year 2020 Power Density Targets

| Criteria | HRE-free PM Motor | Synchronous Relucance Motor with HRE-free PM Assist | Hybrid Induction Motor with Insert Cu Bars and Cast Al End-rings |
|---|---|---|---|
| Specific Power ≥1.6 (kW/kg) | Exceeds | Exceeds | Exceeds |
| Power Density ≥5.7 (kW/L) | Exceeds | Exceeds | Exceeds |

Table II.3-5 shows electromagnetic and mechanical design status (to date) of the three motor variants.

Table II.3-5 - Motor Variant Design Status

| Criteria | HRE-free PM Motor | Synchronous Relucance Motor with HRE-free PM Assist | Hybrid Induction Motor with Insert Cu Bars and Cast Al End-rings |
|---|---|---|---|
| EM design | Complete | In Progress | Complete |
| Mechanical analysis | In Progress | In Progress | Complete |
| Thermal analysis | Not Started | Not Started | Not Started |

## Conclusions

Motor designs with grain oriented electrical steel did not demonstrate performance improvement in any significant way. GM recommended to discontinue all the design efforts with grain oriented steel. GM proposed two alternate designs, a HRE-Free PM assist synchronous reluctance rotor and an Al-Cu hybrid induction rotor, in addition to the HRE-Free PM rotor. Early design works show promise with these design variants. All three designs appear capable of meeting DoE set 2020 targets for power densities. GM plans to build

prototypes with these design variants for performance evaluation and validation. The HRE-free magnet and non-oriented electrical steel grades were selected based on the GM internal testing.

The prototypes will be built at the GM Advanced Propulsion Motor Center in Pontiac, MI. They will undergo calibration and validation testing in GM's Global Propulsion Systems facility, in Pontiac. Motor calibration will be carried out using GM proprietary control and calibration methods. Motor performance and efficiency testing will be carried out based on the GM control methods. Additionally, durability testing will be carried out to validate the life of the design variants for possible GM production applications.

### Key Publications

None

## II.4 Dual Phase Soft Magnetic Laminates for Low-cost, Non/Reduced-Rare-Earth Containing Electrical Machines

**Frank Johnson, Ph.D., Principal Investigator**
GE Global Research
One Research Circle
Niskayuna, NY 12309
Phone: (518) 387-5087
E-mail: johnsonf@ge.com

**Steven Boyd, Program Manager**
U.S. Department of Energy
Phone: (202) 586-8967
E-mail: Steven.Boyd@ee.doe.gov

Start Date: October 1, 2016 End Date: September 30, 2019
Total Project Cost: $6,148,335 DOE share: $4,299,285 Non-DOE share: $1,849,050

### Project Introduction

In this project, GE is scaling-up the processing of an innovative dual phase soft magnetic material which will enable electric traction drive manufacturers to achieve the cost target of $4.7/kW peak power. Cost reduction is driven by enabling non-rare earth materials containing machine designs with over 40% reduction in active material cost due to the elimination of rare earth magnets. A full-scale prototype motor with 55 kW peak power, 30 kW continuous power capability will be manufactured with the dual phase material to prove both performance and manufacturability.

The dual phase magnetic material is a uniquely programmable material with the capability of having its magnetic permeability being locally controlled at the millimeter scale. The magnetization can be programmed to have values between zero and full saturation to meet the machine design requirements without having to remove the material in these regions to reduce the flux leakage. This capability enables rotor and/or stator poles to be magnetically decoupled, while maintaining mechanical integrity of the laminations. As shown in Figure II.4.1, bridges and centerposts used to define flux barriers in SynRel and IPM machines may be made non-magnetic, improving the effectiveness of the barrier. The magnetic decoupling of the poles reduces the flux leakage from pole to pole on the rotor, and improve the flux linkage between the rotor and stator. Maintaining the mechanical integrity enhances the mechanical strength for high speed operation, thus enhancing the machine power capacity, power factor, power density, and efficiency. The ability of the non-magnetic regions to act as retaining elements shows the greatest advantage in machines with high tip speeds. Thus dual phase materials are particularly well suited to the high power density, high efficiency designs used in the transportation market sector.

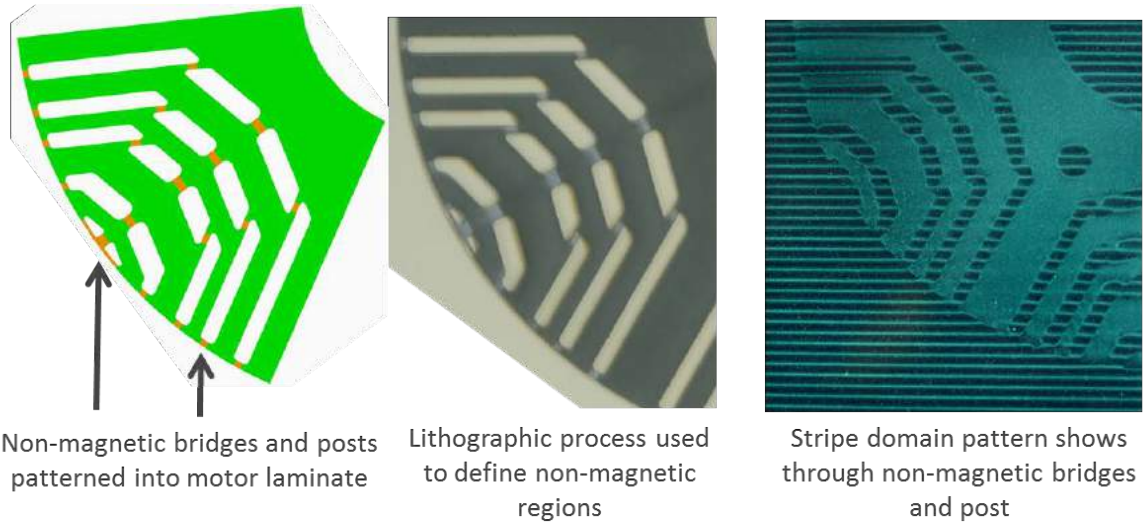


Figure II.4.1 - Illustration of the dual phase structure in a laminate used to manufacture a SynRel machine. The left image shows where the non-magnetic (orange) regions are patterned into the magnetic (green) laminate. The middle image shows an actual laminate in which a ceramic mask has been applied. The exposed regions will become non-magnetic after nitrogenation. The right image shows a laminate after nitrogenation, placed underneath a magnetic indicator film. The stripe domains shine through the regions which have been made non-magnetic.

## Objectives

GE Global Research leads a team comprised of Carpenter Technology Corp., UQM Technologies, Inc., and Oak Ridge National Lab to advance unique and innovative dual phase soft magnetic material technology to Technology Readiness Level (TRL) 7 and demonstrate the material in a 30 kW electric motor for electric vehicles. Dual phase laminate materials will revolutionize the design of electric machines by opening the design space for new cost-effective and sustainable topologies. Dual phase laminates have the potential to be the first, completely new class of soft magnetic materials to be introduced in over a quarter of a century. Their introduction will lead to a step change in system performance and could dramatically accelerate the penetration of electric vehicles into the global automotive market. Dual phase magnetic materials offer the electric motor designer the ability to locally control the magnetic saturation level in a motor laminate at the millimeter scale, while at the same time enhancing the mechanical strength of the laminate material, resulting in an enhancement in motor performance and efficiency.

The project goal is to demonstrate scaled-up manufacturing of the dual phase magnetic materials, and demonstrate a full-scale traction motor manufactured with this material. Two motor proto-types will be fabricated using the dual phase material: 1) A subscale prototype with a continuous power rating of ≈3.7 kW (5 hp) will be fabricated in the second year of the effort to demonstrate dual phase alloy process improvement; and 2) a full-scale prototype with a continuous power rating of ≈30 kW (40 hp) will be fabricated in the third year of the effort to demonstrate a manufacturable machine that can be tested in an operational environment, thus achieving TRL 7.

## Approach

The team is comprised of GE Global Research, Carpenter Technology Corporation, UQM Technologies, and Oak Ridge National Lab. GE will have responsibility for selecting the motor topology, writing performance specifications, and performing detailed design activities for each of the two prototypes. GE will transmit the detailed design to UQM. UQM will have responsibility for generating design manufacturing drawings and procuring all motor components except the dual phase soft magnetic laminate stack, which will be supplied by GE. UQM will perform limited testing of each prototype to verify electromagnetic functionality and fit and finish of the integrated components. GE will perform in depth testing of each prototype on test facilities

located in the Electric Machines Laboratory. Existing motor drive electronics will be used to validate performance over the envelope of speed, power and torque conditions defined for electric vehicle motors.

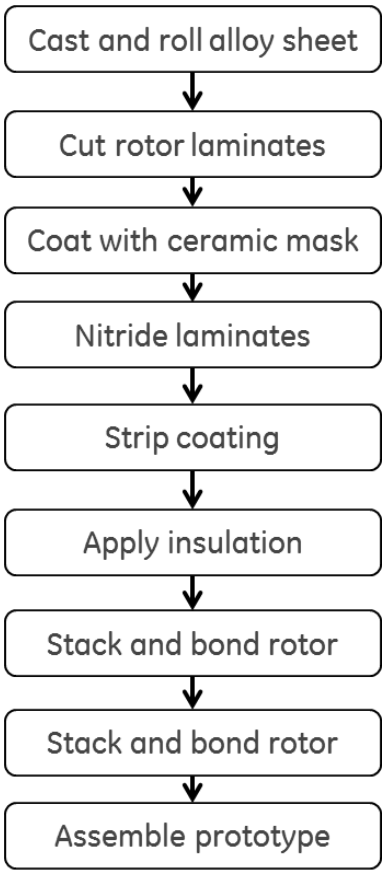


Figure II.4.2 - Manufacturing sequence for prototypes containing dual phase magnetic laminates.

Figure II.4.2 shows the manufacturing method for the prototypes with dual phase magnetic laminate rotors. Carpenter will have responsibility for producing the 0.010" rolled sheet of the dual phase magnetic material needed for the prototypes. This will require developing the melt practice, heat treatment sequences, and rolling schedules customized for this alloy. This amount of material is sufficient for producing both prototypes. The rotor design for each prototype will be lasercut from the rolled sheet. GE will apply the ceramic mask needed to modulate the uptake of nitrogen into the laminates and create the specified pattern of magnetic and non-magnetic regions. The coated laminates will be gas nitrogenated at high temperature, which will austenitize the regions to be made non-magnetic. GE will then remove the ceramic mask prior to assembly of the rotor stack. UQM will shrink fit the rotor stack onto a shaft prior to integration into the prototypes.

In parallel, GE and ORNL are performing an in-depth study of the nitrogenation kinetics of the dual phase alloy material. The initial studies will be performed on coated coupons prepared by GE. ORNL will explore the effect of nitriding conditions on the austenitization of the alloy. Residual stress analysis will be performed to verify finite element calculations of the stress states caused by differential thermal expansion between the magnetic and non-magnetic regions. The results of the coupon tests will be used to optimize gas nitrogenation furnace parameters to minimize total cycle time and cost. Further, the residual stress analysis will be used to set design rules that will avoid warpage and minimize distortion in the nitride processing of the rotor

laminates. ORNL will continue this analysis as the detailed design of the subscale and full-scale rotor laminates becomes available.

The first annual performance period will focus on 1) scale-up of alloy production at Carpenter, 2) optimization of nitriding furnace parameters at ORNL, and 3) detailed subscale prototype design at GE. The first annual Go/NoGo condition is the creation of a subscale motor design that shows a calculated level of performance in excess of a best in class design using conventional materials. The second annual performance periods will focus on 1) scaled-up processing of the subscale dual phase rotor laminates, 2) assembly and test of the subscale prototype, and 3) detailed design of the full-scale prototype. The second annual Go/NoGo condition is a demonstration of the subscale prototype and measured power output of 3.7 kW. The third annual performance period will focus on 1) scaled processing of the full-scale dual phase rotor laminates for the full-scale prototype, 2) and assembly and test of the full-scale prototype.

## Results

Figure II.4.3 presents electromagnetic calculations performed for the sub-scale (3.7 kW) prototype motor design. These calculations show that a prototype with a rotor manufactured from 0.010" thick dual phase alloy sheet will have higher torque output than a similarly sized prototype with a rotor manufactured from 0.010" thick Silicon Steel (the HF10 grade). These performance gains persist over a wide speed range. At low speed, the dual phase machine will have 50% greater torque output than a silicon steel machine. This leaves substantial margin to achieve the 20% performance increase targeted for the completed prototype. With these results we have passed the Go/NoGo decision point at the end of Budget Period 1 and have proceeded into Budget Period 2.

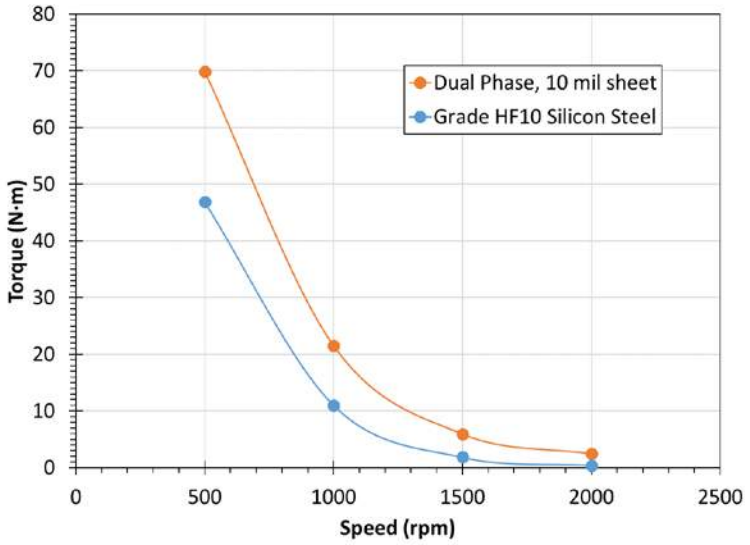


Figure II.4.3 - Electromagnetic calculations of the performance of the sub-scale motor prototype. A prototype with a rotor manufactured from 0.010" thick Dual Phase sheet is calculated to have higher torque output than a prototype manufactured with grade HF10 Silicon Steel.

Carpenter Technology Corporation has produced and shipped the coil of dual phase alloy sheet needed to fabricate the prototype motors. The thickness specification was 0.010" ± 0.0005". A measurement of the thickness at GE Global Research was 0.0098" ± 0.0001" which satisfies the thickness specification. The composition, magnetic properties, and mechanical properties of the sheet were also within specification.

Significant development work has been completed on the masking, heat treating, and demasking of the dual phase motor components. These activities have led to improved control of the saturation magnetization within

the two phases, reduction of AC core loss, and refinement of the heat treatment cycle. Preparations are being made for the batch processing of the several hundred laminates needed to produce one rotor stack.

The analysis work that had been conducted at Oak Ridge National Laboratory has provided valuable data on the processing conditions needed to properly nitrogenate the dual phase alloy. Nitrogen penetration depths have been measured on coupons heat treated under controlled conditions at Oak Ridge. Continuous cooling curves were measured using a calorimeter available at Oak Ridge. This data provided valuable guidance in selecting the proper furnace for scaled-up production of the dual phase motor components. Residual stress measurements were conducted on nitrogenated coupons with a Synchrotron X-Ray beam available at the Advanced Light Source at Argonne National Laboratory. The stress data verifies assumptions used in the calculation of the stress state in the rotor laminates which can influence performance. This analysis work will be continued with samples of the sub-scale and full-scale rotor laminate as they are produced.

## Conclusions

The first Go/NoGo decision point has been passed with the development of a sub-scale SynRel motor design made from dual phase material with increased performance relative to a similar design made with conventional silicon steel. Carpenter Technology Corporation has produced the 0.010” dual phase alloy sheet needed to fabricate both the sub-scale and full-scale prototype designs. The processing steps needed to form the dual phase structure has been refined to improve control of the magnetization within the two phases. Preparations are being made to fabricate the several hundred dual phase laminates needed for the sub-scale prototype. Work performed at Oak Ridge National Laboratory has resulted in valuable data on the nitrogenation kinetics and residual stress in coupons of the dual phase material.

## II.5 Vehicle-to-Grid Electric School Bus Commercialization Project

**Dennis Whitaker, Principal Investigator**
Blue Bird Corporation
402 Blue Bird Boulevard
P.O. Box 937
Fort Valley, GA 31030
Phone: (478) 822-2089
E-mail: dennis.whitaker@blue-bird.com

**Steven Boyd, Program Manager**
U.S. Department of Energy
Phone: (202) 586-8967
E-mail: Steven.Boyd@ee.doe.gov

Start Date: August 1, 2017 End Date: July 31, 2020
Total Project Cost: $9,804,529 DOE share: $4,902,238 Non-DOE share: $4,902,291

### Project Introduction

Battery-electric school buses have the potential to be one of the first electric vehicle types to compete and succeed commercially without any form of subsidy. Reaching this point will involve a synergistic combination of three elements: operational savings on fuel and maintenance; volume-driven manufacturing cost reduction; and the generation of revenues from participation in ancillary grid service markets. The overall goal of the Vehicle-to-Grid Electric School Bus Commercialization Project is to realize the potential of electric school buses by developing a vehicle that delivers exceptional results in each of these areas.

### Objectives

The proximate objectives of the project are oriented around operational savings and grid-service revenues. Two technology advancement modules will help Blue Bird's type C electric school bus set a new standard for energy efficiency and thereby maximize savings on fuel. The project's target of equal to or less than 1.1 kWh per mile will be a 20-25% improvement over the current state of the art. A third technology advancement module will involve developing and certifying an on-board bidirectional inverter with a power capacity of 200 kW. This inverter and its associated hardware and software will allow the Blue Bird buses to participate robustly in regional markets for ancillary grid services such as frequency regulation. Finally, the project team will work on commercialization methods that will mobilize near-term sales volumes sufficient to realize the potential for manufacturing cost reductions.

### Approach

*Drivetrain Architecture*

The drivetrain architecture module will involve collaboration in vehicle performance modeling by team members Adomani, Efficient Drivetrains, Inc. (EDI), and National Renewable Energy Laboratory (NREL). The partners will start by profiling prevalent school bus drive cycles using data from the school bus file within NREL's Fleet DNA Database. EDI will use this data to create a simulation environment on its proprietary performance modeling platform. Simulations will be run for the range of potential drivetrain architectures (direct drive, two-speed gearbox, etc.), with the goal of identifying the architecture that delivers the best energy efficiency while meeting drivetrain power specifications. The results will be cross-checked using NREL's FASTSim (Future Automotive Systems Technology) simulator. In the module's final step, drivetrain components will be selected and optimized based on interpretation of the simulated performance.

The project's first prototype bus (P1) will be used as a baseline for performance comparisons. It will have EDI's PD7000 EV drive system which utilizes direct-drive architecture. The 3000NM high-torque motor

(Figure II.5.1 below) is directly connected via a drive shaft to the differential. This provides very smooth operation with no shifting required.

Figure II.5.1 - 3000NM Electric Motor Installed in Bus P1

*Enhancing Battery Efficiency*

Temperature is universally acknowledged as a key determinant of lithium ion battery performance. Not least among the parameters affected by temperature is coulometric efficiency, more familiarly known as "round-trip" efficiency, i.e., the ratio between the amount of energy spent in charging and the amount of energy a battery can produce to do useful work. Deviations from a battery's optimal temperature range, in either direction, can significantly decrease coulometric efficiency, with an ultimate increase in the number of kWh consumed per mile of travel.

The project's battery efficiency module will focus on thermal management of the on-board battery packs. The animating principle is thermal integration of the battery packs with other on-board subsystems. The targeted advance will involve both enhanced temperature sensing in the battery packs and other temperature-variable components such as air compressors and hydraulic motors (and possibly climate control devices); and an enhanced ability to direct coolant flow from one subsystem to another. The air compressor installation in P1 is shown in Figure II.5.2 below. The relevant functionality will be enabled by extending the scope and capability of EDI's vehicle control software. The result will be more reliable maintenance of each subsystem's temperature within in its optimal range, and also a reduction in the amount of energy drawn from the batteries to accomplish thermal management tasks.

Figure II.5.2 - Air Compressor Installation in Bus P1

*200 kW Bidirectional Inverter*

The inverter module will build on previous collaborations between EDI and inverter vendor and project partner EPC. These joint efforts resulted in utility trucks that could export power at the rate of 160 kW to support grid repair and maintenance operations. Several improvements will be made in the current work. First, the power capacity will be increased to 200 kW. Second, the inverter will be given grid-forming capability so that the power it exports can meet all specifications that apply to conventionally generated grid electricity. This will enable the buses to be used as disaster-resilience resources. Third, the inverter will be put through Underwriters Laboratory and other relevant certification protocols so that the buses can be readily interconnected with the grid in any utility's service territory. Finally, a low-power charging capability will be added so that the buses can be charged with conventional level 2 electrical vehicle supply equipment.

*Vehicle-to-Grid Integration*

The eight electric school buses produced by the project will be conveyed to Rialto Unified School District in Southern California. Once in place, the buses will demonstrate vehicle-to-grid operation via participation in the wholesale ancillary grid service markets managed by the California Independent System Operator (CAISO). This will entail installation of appropriately rated charging infrastructure and charging system control functionality. It will also entail steps for interconnection with Southern California Edison's distribution system and enrollment as a CAISO market participant. Once all arrangements are in place, the team will set up a protocol wherein the buses are managed first to achieve their pupil transportation mission and second to maximize revenues from grid services.

*Commercialization*

The commercialization challenge will be addressed through close attention to customer needs and preferences. One set of needs relates to the physical characteristics and capabilities of the bus itself. In the fundamental design decisions, the project team has emphasized comparability with conventional school buses while minimizing cost differentials. The amount of on-board energy storage is one especially critical variable. On the one hand, it determines the daily range of the bus and ultimately whether customers will have confidence in the buses' ability to service their routes. On the other hand, the cost of batteries is still high enough that any non-essential energy storage will undermine the economic competitiveness of the buses. The team's focus on energy efficiency is based on the fact that it is the single expedient that avoids sub-optimizing either end of this tradeoff.

Another set of customer needs relates to the structure of the purchase transaction. School districts typically do not have flexibility in how they make capital acquisitions, and pupil transportation functions have limited capacity for pursuits beyond transporting pupils. This means that successful commercialization will require a comprehensive strategy to reduce the acquisition cost and total cost of ownership. This could include the use of the V2G inverter as a means to allow a fleet of buses to function as a grid resource and generate revenue for the school districts. Blue Bird will also explore the option of selling buses without batteries, with the latter leased in a separate transaction.

## Results

The Blue Bird team started work on the project in August 2017. The first step involves installation of a basic version of the EDI electric drivetrain on a Blue Bird type C glider. Prototype bus P1, shown in Figure II.5.3 below, will allow the team's engineers to establish the fit and function of the drivetrain's key components as well as integrate the drivetrain with auxiliary systems such as brakes and climate control. The assembly of EDI's PD7000 EV drive system into the Blue Bird type C glider is nearly complete as of mid-October 2017. All components are installed and a first drive of the vehicle achieved. Drive and subsystem testing of the various systems are underway. Final inspection and delivery are scheduled for October 30, 2017.


Figure II.5.3 - Prototype Bus P1 Assembly Near Completion

## Conclusions

The project team has gained enough perspective on the larger technology currents of vehicle-grid integration, distributed energy storage, and campus-based microgrids to clearly define the potential of V2G school buses as both pupil transportation and grid-stabilizing energy storage resources. Over the next three years, the team will be devoted to establishing electric school buses as value-adding, dual-purpose assets.

## II.6 650V SiC Integrated Power Module for Automotive Inverters

**Monty B. Hayes, Principal Investigator**
Delphi Automotive Systems, LLC
2151 East Lincoln Road
Kokomo, IN 46902
Phone: (765) 438-6419

**Steven Boyd, Program Manager**
U.S. Department of Energy
Phone: (202) 586-8967
E-mail: Steven.Boyd@ee.doe.gov

Start Date: January 1, 2016 End Date: February 28, 2018
Total Project Cost: $2,161,561 DOE share: $1,488,303 Non-DOE share: $673,258

### Project Introduction

Delphi has been developing power electronics and related energy system technologies for over 25 years. Since 2000, Delphi has been granted more than 100 patents in these key enabling technologies. Responsibility for Power Electronics development in Delphi Automotive Systems resides in the Electronic Controls organization located in Kokomo, Indiana. Along with conventional powertrain controls, this development group also addresses electronic controls for vehicle electrification, which enables Delphi to be a complete systems supplier for power electronics design and manufacture for hybrid or fully electric drive vehicles (EDVs). Delphi's Advanced Electronic Controls department is co-located in Kokomo with the product and manufacturing engineering, as well as production, so R&D in power electronics is focused on vehicle OEM requirements, particularly for reducing the weight, size and cost of power electronics and their associated vehicle systems. By considering both component and vehicle manufacturing requirements early in the R&D stages, Delphi is able to both reduce the size/weight and lower the cost of powertrain electrification through component design, system design, controls and algorithm development, and design for manufacturability.

Inverters and converters are high cost power electronic components utilized in all electrified vehicle propulsion systems. The cost, as well as the size and weight, of these key components are constrained by the need to transfer heat away from their solid-state devices used for electrical power control. This results in the designer of the power electronics to use larger die or multiple die in parallel for a particular application, increasing the cost and size of the power electronics used in EDVs. Wide bandgap (WBG) power semiconductors have the potential to reduce the amount of thermal waste-heat that must be transferred away from the device, due to their greater energy efficiency than today's Silicon-based power semiconductor devices. Additionally, such WBG power devices have the potential to operate at significantly higher junction temperatures and higher frequencies, further increasing the space and material effectiveness for removing the waste-heat that is generated. Therefore, a high efficiency WBG device has great potential for reducing the cost of the power semiconductor devices required by today's inverters and converters, as well as device size, packaging and cooling requirements, thereby reducing the cost, size and weight of the inverters and converters, as well as their associated cooling system. To summarize, WBG devices, with packaging and cooling optimized for these device should lower the system cost and size/weight by utilizing smaller or fewer power devices and simplifying the power electronics cooling systems. Additionally, by operating with an increased margin between the operating temperature and the maximum device junction temperature, this technology also has the potential to enhance overall reliability and durability for higher powered inverters and converters such as those required by EDVs.

## Objectives

The overall goal of the project is to develop and demonstrate an integrated WBG power module that will enable Delphi to meet DOE's 2020 EDV inverter targets for size, weight, cost and efficiency, and to meet OEM-customer requirements for future vehicle platforms in the 2020 timeframe. Critical to the successful application of WBG modules is a well-engineered power conversion subsystem that fully exploits the beneficial aspects of these semiconductor materials in a cost-effective way while eliminating the potential negative impacts on associated components or subsystems. To facilitate good understanding of the performance and to minimize design turns, modelling and simulation will be performed by the Oak Ridge National Laboratory (ORNL). This project is starting at TRL 4 and expected to achieve TRL 7 upon its completion.

To accomplish the goal, Delphi Automotive Systems, LLC (Delphi) and Cree, Inc. (Cree) will team with Oak Ridge National Laboratory (ORNL) and Volvo Car Corporation (Volvo) to advance the performance and cost curve of WBG power modules to meet mainstream automotive non voltage boosted electrified drivetrain requirements. For drivetrains with 400-500V bus voltages, a 650V SiC MOSFET combined with packaging optimized to reduce parasitics is a strong candidate for the inverter power switches; the developed package will also be capable of handling lower and higher voltage rated components for both boosted and non-boosted systems.

## Approach

SiC MOSFETs have recently garnered significant attention with regard to Electric-drive Vehicles (EVs) as the conduction losses can be lowered up to 70% [1-2] relative to Si IGBT devices. This advantage traces back to the 10X higher electric field strength of SiC, which allows SiC MOSFETs to be used in voltage ranges where Si IGBTs are often used, and the MOSFET naturally has no "knee voltage" in the on-state. Therefore the MOSFET has a lower on-state voltage drop as compared to equivalent rated devices operating at light loads of the vehicle operational profile. Although SiC MOSFETs and diodes are used in some DC/DC Converter and Charger applications for the most part MOSFETs are not widely used in Traction Drive Inverter applications for electrified drivetrains due to current rating limitations and undefined reliability metrics.

The approach was to develop a new 650V SiC MOSFET with a top-side solderable and sinterable metal stack. For the package, two packages a single switch and a SiC based half-bridge module were developed to utilize parallel multiple ~25 mm2 SiC MOSFETs (to allow for high yield and lower cost) in a ceramic based package compatible with solder or sinterable interconnections. Both concepts allow for direct cooling on both sides and the second approach allows for a lower inductance package to take advantage of the SiC performance. Also investigated was the use of overmolding on the device leaving the DBM of the ceramics utilized exposed to be in intimate contact with the heatsink through a thermal interface material or direct connection to the heatsink or cooling medium (direct coolant).

## Results

The work here is the first result of a new 650V SiC MOSFET with a top-side Ni:Au plated metal stack designed for top-side soldering or sintering, which eliminates top-side wirebonds, which are often a point of failure in power cycling and will also allow for dual side cooling of the device in the package. Due to SiC's relatively small die size compared with Si, the thermal excursions could be wider, amplifying the advantage of wirebond-free modules.

The 7mΩ measured on-state of the 650V SiC MOSFET is the lowest $R_{DSON}$ we are aware of for a single die at 650V in any technology (Si or SiC), which enables simpler module assembly using fewer die in high amperage (300-900Arms) power modules. Additionally, the chip was designed with an optimized on-chip $R_G$ to:

a) Reduce switching oscillations

b) Potentially eliminate the external gate resistor in the module

c) Optimize device performance over the vehicle drive cycle and reduce yield loss by the reduction of additional components inside the power module.

Further benefits to reducing inverter losses this significantly would be in the regeneration drive, reducing weight, reducing thermal management, and battery cost for a given range. To achieve these savings, high-performance SiC power MOSFET chips and modules need to be developed which enable very low conduction losses over vehicle drivetrain normal operation at light-load. What is presented here, to the best of our knowledge, is a record low 1.25mΩ on-resistance (low conduction losses) for a 900V 62mm ½ bridge power module. The switching energy and $R_{DS(ON)}$ is characterized up to 175°C, and initial High Temperature Reverse Bias (HTRB) testing is shown up to 175˚C.

The SiC MOSFET chip used here is a newly developed 650V, 7mΩ SiC MOSFET using a planar DMOS design recently described elsewhere [**3**]. While retaining the reliable DMOS structure (see Figure II.6.1), specific $R_{DS(ON)}$ is 1.8mΩ•cm$^2$, significantly less than competing Si and SiC MOSFET products in this voltage range. The total chip area of the 650V MOSFET is 8.6mm by 4.3mm, or ~37mm$^2$, with top-level over-layer Al:Cu metal alloy, 4µm thick, with a thicker layer of Ni added, followed by a thin Au over layer. The gate pad is at upper left corner, and two source pads lie adjacent to each other over the majority of the chip area. The top-layer metal Au is clearly seen in Figure II.6.1.

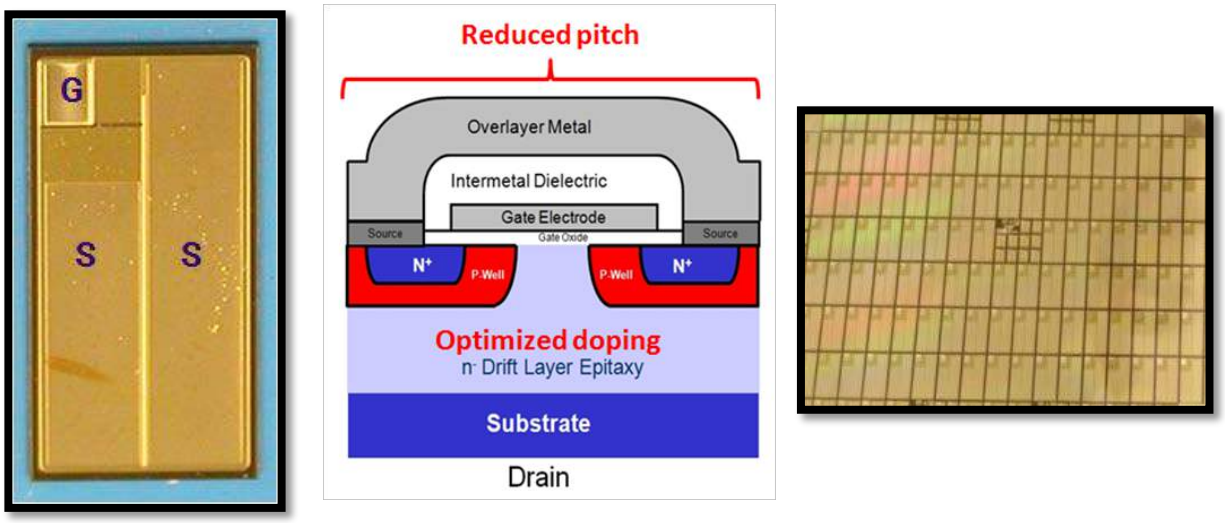


Figure II.6.1 - 650V, 7mΩ, 37mm² SiC MOSFET die shown singular (left image), cross-section (center image), and on-wafer (right image)
Delphi Technologies/Cree

The SiC MOSFETs were measured and the results are shown table 2 below. The on-state measurements at room temperature resulted in ~7.7 to 8.0mΩ of $R_{DSON}$ from 50A to 150A, corresponding to a specific $R_{DSON}$ of 1.8mΩ•cm$^2$ at 25˚C. The on-state measurements of RDSON were repeated at 175˚C, also shown in Figure VI.22, with a 35% increase in $R_{DSON}$ to 10.5-10.8mΩ.

The blocking voltage was measured to be a mean of 964V for approximately 400 MOSFETs measured, with a standard deviation of 31V. For a 650V rating the margin is quite sufficient.

Table II.6-1 summarizes the electrical characteristics of the 650V SiC MOSFET chip with top-side and back-side Ni:Au metal. While dependent upon the thermal environment, the nominal current rating of this chip at temperature (100˚C) is 150A, allowing designers of drivetrain power modules to create a 600A or 750A nominal rated power module with either four or five MOSFETs in parallel, respectively.

Table II.6-1 - Electrical summary characteristic data for 650V, 7mΩ SiC MOSFET chip

| Symbol | Parameter | Value | Unit | Test Conditions |
|---|---|---|---|---|
| $V_{GSmax}$ | Gate-Source Voltage | -8/+19V | V | Absolute Maximum values |
| $V_{GSop}$ | Gate – Source Voltage | -4/+15V | V | Recommended operational values |
| $I_D$ | Continuous Drain<br><br>Current (Depends on thermals) | 200<br><br>150 | A | $V_{GS}$ = 15 V, $T_C$ = 25 °C<br><br>$V_{GS}$ = 15 V, $T_C$ = 100 °C |
| $I_{D(pulse)}$ | Pulsed Drain Current | 520 | A | Pulse width $t_P$ limited by $T_{jmax}$ |
| $R_{DS(on)}$ | Drain-Source On-State Resistance | 7.7<br>10.7 | mΩ | VGS = 15 V, $I_D$ = 75 A $T_J$ = 25 °C<br>VGS = 15 V, $I_D$ = 75 A $T_J$ = 125 °C |
| $E_{ON}$ | Turn-On Switching Energy | 3.3 | mJ | $V_{DS}$ = 360 V, $V_{GS}$ = -4/+15V,<br>$I_D$ = 100A, $R_G$(ext) = 20.0Ω |
| $E_{off}$ | Turn-Off Switching Energy | 3.6 | mJ | $V_{DS}$ = 360 V, $V_{GS}$ = -4/+15V,<br>$I_D$ = 100A, $R_G$(ext) = 20.0Ω |

Shown below in Figure II.6.2 is a 650V, 1.7mΩ, SiC MOSFET Power Module

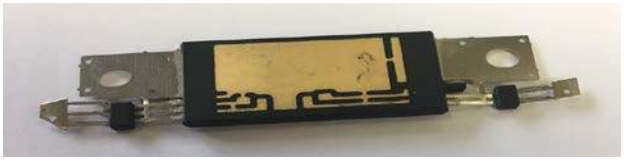

Figure II.6.2 - 650V, 1.7mΩ, SiC MOSFET Power Module
Delphi Technologies

The power modules were built into an inverter systems and characterized for loss performance as compared to a best-in-class Silicon semiconductor shown below in Figure II.6.3. As can be seen from the results the SiC device has up to 70% lower losses at a low current operating point and 40% lower losses at the maximum operating current.

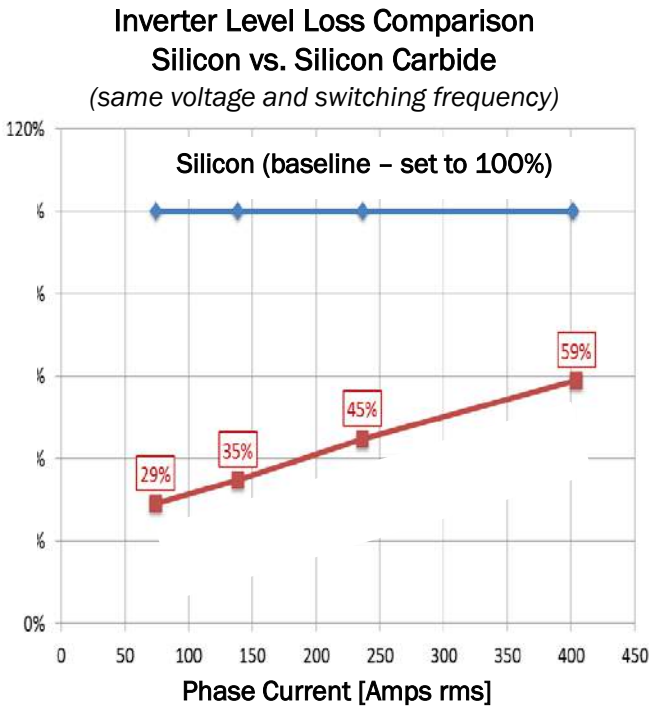


Figure II.6.3 - Inverter Loss Comparison of Silicon Carbide versus Silicon Semiconductor Based System
Delphi Technologies

For the power modules characterized in Figure II.6.2, using the wirebond-free assembly, it is important to ascertain the mechanical stability of the attached MOSFETs. A power cycle was set up with the following parameters as highlighted below to check from 50˚C to 150˚C cycling (ΔT = 100˚C). The resulting data is shown below in Figure II.6.4. The on-state (y-axis) shift allowed was up to 20%, and no shifts over 5% were noted while operating under DC setup current of 520A, up to 36,000 cycles. This number of cycles is indicative of a rugged operation under normally accepted JEDEC based industry standards.

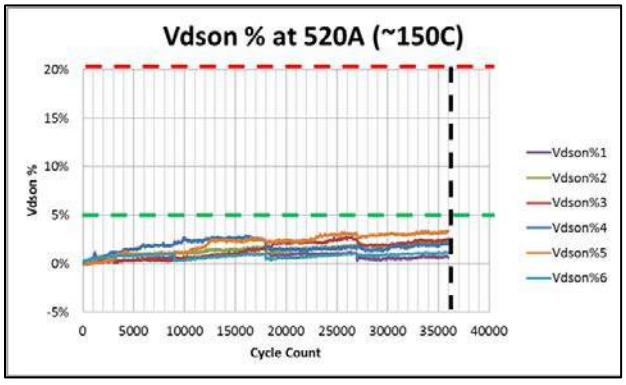


Figure II.6.4 - Shift percentage of on-state voltage drop of a power module with 5 x 650V/7mΩ SiC MOSFETs per switch position, in a wirebond-free assembly. After 36,000 power cycles with ΔT of 100˚C, the maximum shift in on-state was <5% (successful pass).
Delphi Technologies

## Conclusions

- Developed a $R_{DSON}$ 650V, 175°Junction Temperature SiC MOSFET device for Traction Drive Inverter Applications
    - 25° RDSON of 7.7mΩ, 175˚C to 10.7mΩ
    - Top side solderable and sinterable
    - $R_g$ optimized for Traction Drive Inverter applications
- Devices were assembled without wirebonds per switch in dual-side cooled power modules
- Characterized for performance (DC and dynamic) over temperature range, and found to be consistent up to 750A
- Module $R_{DSON}$ varied from 1.70mΩ at 25˚C to 2.35mΩ at 175˚C.
    - The electrical characteristics should allow up to 80% conduction loss reduction in the inverters during normal drive cycles.
- For reliability, initial measurements of power cycling ($\Delta_{TJ}$=100˚C, 36,000 cycles, no failures) and short-circuit (8μs) were both very encouraging.
- The developed device was tested in a inverter systems and the performance was compared to a state-of-the art silicon based semiconductor system. The resulting testing show loss reduction of up to 70% losses as compared to best in class silicon IGBT and Diode technologies.

## Key Publications


1. 650V, 7mOhm SiC MOSFET Development for Dual-Side Power Modules in Electric Drive Vehicles, Monty B. Hayes, John R. Fruth, Aditya Neelakantan, Robert J. Campbell, Erich W. Gerbsch, T.V. Sriram Delphi Automotive Systems, LLC, Kokomo, Indiana USA and Jeffrey Casady, Brett Hull, Jon Zhang, Scott Allen, John Palmour, Wolfspeed, a Cree Company, RTP, NC, USA. PCIM 2017, Nuremberg, Germany, June 5–7, 2017
2. Impact of Ultra-Low On-Resistance SiC MOSFETs On Electric Vehicle Drive-Train, Power Electronics Europe, Issue 4 2017, Pages 18-20, Jeff Casady, Business Development & Program Manager, Wolfspeed; Monty B. Hayes, Manager Advanced Hardware, Electronic Controls, Delphi.
3. http://www.power-mag.com/pdf/feature_pdf/1504017364_Wolfspeed_feature.pdf

## II.7 Wound Field and Hybrid Synchronous Machines for EV Traction with Brushless Capacitive Rotor Field Excitation

**Ian Brown, Principal Investigator**
Illinois Institute of Technology
3301 S Dearborn Street, #103
Chicago, IL 60616
Phone: (312) 567-5981
E-mail: ibrown1@iit.edu

**Steven Boyd, Program Manager**
U.S. Department of Energy
Phone: (202) 586-8967
E-mail: Steven.Boyd@ee.doe.gov

Start Date: October 1, 2017 End Date: September 30, 2019
Total Project Cost: $1,112,707 DOE share: $999,752 Non-DOE share: $112,955

### Project Introduction

For mass adoption of pure and hybrid electric vehicles (EVs) there is concern regarding the cost and materials supply chain for the vehicle main traction motor. While DOE programs have been successful at lowering the cost of traction inverters and wide bandgap power electronics, the cost of traction electric motors has been resistant to change. Today interior permanent magnet synchronous machines (IPMSMs) and induction machines (IMs) are the commercially dominant traction motors. The rare-earth permanent magnets (PMs) used in IPMSMs have been subject to market volatility and are largely single sourced from a foreign power. They are also a significant fraction of the cost of IPMSMs and impose temperature limits.

Additionally, the PMs provide a fixed flux level which is always, "on", leading to safety concerns during inverter faults and requiring additional current to be injected into the machine during field weakening to buck the magnetic flux. This additional current lowers the power factor of the machine, requiring that the traction inverter be oversized to supply the reactive current, leading to increased ohmic losses in the stator and inverter. Induction machines (IMs) must also draw reactive current from the traction inverter to magnetize the machine leading to lower power factor.

Would field synchronous machines (WFSMs) and hybrid excitation synchronous machines (HESMs) are potentially advantageous alternatives to the commercially dominant IPMSMs and IMs. WFSMs are PM free and because the DC field magnetization is from the rotor side the power factor of the machine is high if not unity over most of the operating space. The complete control of the field excitation also provides the potential for optimal field weakening and large constant power speed ranges with loss minimization. HESMs use a combination of PM and wound field excitation to combine the high efficiency of IPMSMs with the easy field weakening and high power factor of WFSMs while using considerably less PM. They also reduce the field power requirements.

EV traction applications require extremely high reliability and power density inhibiting the use of brushes and other classical field power transfer technologies such as brushless exciters. Brushless capacitive power transfer offers an attractive means of providing power transfer to the rotor field windings of WFSMs and HESMs.

### Objectives

The objective of this project is to design, develop, and demonstrate wound field and hybrid excitation (permanent magnet and wound field) synchronous machines with brushless power transfer to the rotor field capable of achieving the performance metrics in Table II.7-1. A focus of this project is the cost target of

4.7 $/kW. The brushless field power transfer will be accomplished using capacitive coupling or combined capacitive magnetic coupling.

Table II.7-1 - WFSM and HESM Performance and Cost Target Metrics

| Parameter | Budget Period 2 Prototype | Budget Period 3 Prototype |
|---|---|---|
| Peak Power (kW) | ≥55 | ≥55 |
| Continuous Power (kW) | ≥ 30 | ≥ 30 |
| Specific Power Density (kW/kg) | 1.5 | 1.6 |
| Volumetric Power Density (kW/l) | 5.0 | 5.7 |
| Cost ($/kW) | - | 4.7 |

## Approach

To meet the project cost and power conversion targets a number of approaches are being developed simultaneously in the context of wound field and hybrid excitation synchronous machines though many of the technologies will also apply to other electric machine types and applications.

- Hybrid excitation synchronous machines to lower the field power requirements
    - Bias the field flux for the most common operating point in a drive cycle with PMs.
    - Ideally utilize non-rare earth permanent magnets.
    - Extend the constant power speed range compared to pure permanent magnet machines.
- Lower the cost of the capacitive power coupler (CPC)
    - Increase the frequency (MHz) to shrink the required capacitance (A/Hz).
    - Lower the losses in the converter by operating in resonant soft switching.
    - Reduce the mechanical complexity of the rotating capacitors. Three simpler rotating capacitor designs are being investigated: journal bearings, integrated LC coupler, and printed circuit board (PCB) capacitive plates with a tank circuit.
- Reduce the punching scrap from the construction of the lamination stack. Typically 40% of the steel is scrapped when punching interior permanent magnet synchronous machine laminations.
    - Leverage cut core and roll-up stator and rotor designs.
    - Segmented lamination structures allow for higher fill factors with needle or bobbin winding both rotor and stator windings and even higher slot fills with die compressed windings with added benefit of reduced end turn length
    - Needle or die compressed windings require fractional slot concentrated windings with low space harmonic content to operate at high speeds

- Die compressed windings to allow the substitution of aluminum for copper and improved heat transfer
    - Use die compression to achieve a slot fill of ~75% to 80%.
    - Single thermal mass with no air voids and improved heat transfer at the spray/end turn interface.
    - Possible to utilize aluminum wire for significant cost and weight savings with similar performance to normal slot fill copper windings.

The overall concept model of the WFSMs and HESMs system incorporating some of the above approaches is shown in Figure II.7.1.

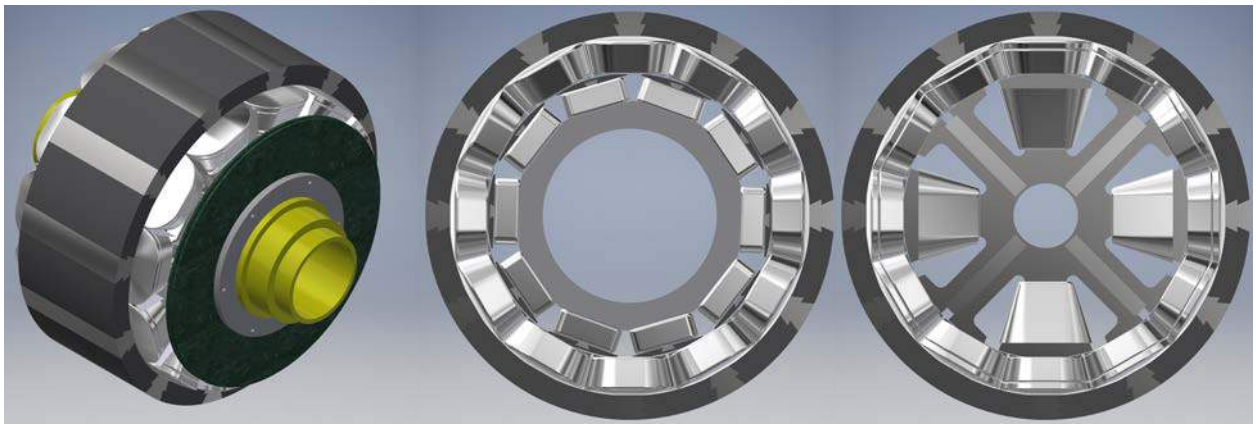


Figure II.7.1 - Conceptual model of (a) cost minimized WFSM or HESM with brushless CPC, (b) WFSM with die compressed aluminum stator and rotor windings, and (c) hybrid excitation rotor with parallel flux paths.

## Results

Major outcomes from this first budget period include the following items:

*1) Design and construction of a dual rotor parallel HESM*

A dual rotor HESM was developed to serve as a platform for exploring combined wound field and PM excitation, Figure II.7.2. Analytical sizing equations have been developed to determine the ideal hybridization ratio between the two field excitation sources. For this particular prototype field excitation sources were sized to allow for an infinite constant power speed ratio when the two field sources are aligned. The prototype was also designed to allow for different hybrid excitation concepts by mechanically shifting the excitation axes relative to each other, i.e., either enhancing/bucking the PM flux with the wound field excitation or canceling the armature reaction for improved power factor. The combination of the PM and wound field excitation combines the benefits of both excitation types. Figure II.7.2 shows the two rotor cross sections (a) and (c) and the predicted machine efficiency assuming that the two rotor types each comprise the entire rotor. The IPMSM rotor has a higher efficiency but much lower constant power speed ratio, (b), compared to an entirely wound field rotor (d). The efficiency maps under-estimate the constant power capabilities because of the number of sample points in the torque speed operating space. The prototyped combined rotor (e) has an improved efficiency compared to the pure wound field rotor with a greatly extended constant power speed ratio, theoretically infinite. Dynamometer testing and controls development for hybrid excitation machines is ongoing.

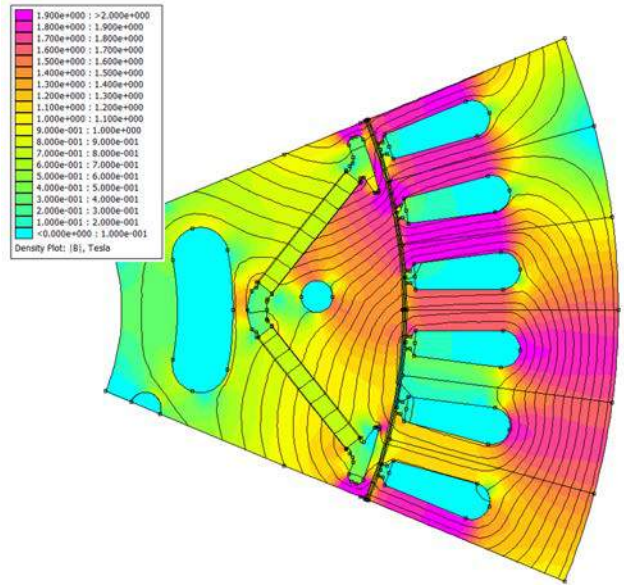
1.900e+000 : >2.000e+000
1.800e+000 : 1.900e+000
1.700e+000 : 1.800e+000
1.600e+000 : 1.700e+000
1.500e+000 : 1.600e+000
1.400e+000 : 1.500e+000
1.300e+000 : 1.400e+000
1.200e+000 : 1.300e+000
1.100e+000 : 1.200e+000
1.000e+000 : 1.100e+000
9.000e-001 : 1.000e+000
8.000e-001 : 9.000e-001
7.000e-001 : 8.000e-001
6.000e-001 : 7.000e-001
5.000e-001 : 6.000e-001
4.000e-001 : 5.000e-001
3.000e-001 : 4.000e-001
2.000e-001 : 3.000e-001
1.000e-001 : 2.000e-001
<0.000e+000 : 1.000e-001
Density Plot: |B|, Tesla

(a)

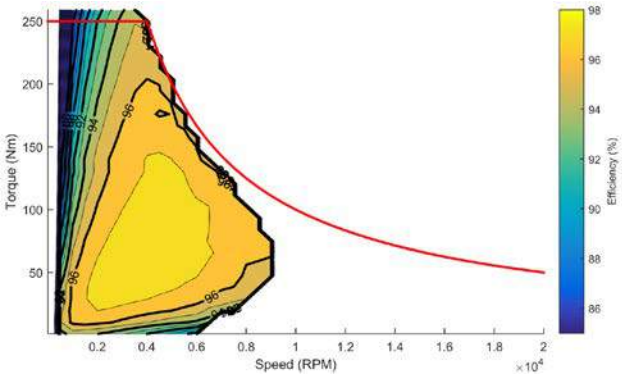
Torque (Nm)
Speed (RPM)
×10^4
Efficiency (%)

(b)

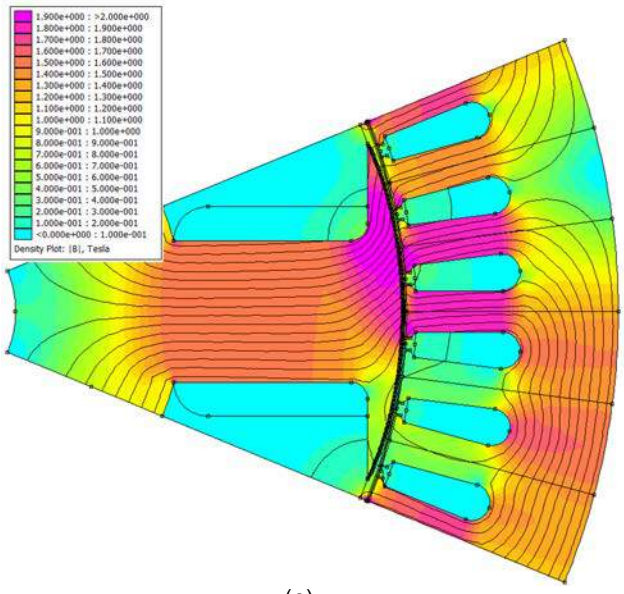
1.900e+000 : >2.000e+000
1.800e+000 : 1.900e+000
1.700e+000 : 1.800e+000
1.600e+000 : 1.700e+000
1.500e+000 : 1.600e+000
1.400e+000 : 1.500e+000
1.300e+000 : 1.400e+000
1.200e+000 : 1.300e+000
1.100e+000 : 1.200e+000
1.000e+000 : 1.100e+000
9.000e-001 : 1.000e+000
8.000e-001 : 9.000e-001
7.000e-001 : 8.000e-001
6.000e-001 : 7.000e-001
5.000e-001 : 6.000e-001
4.000e-001 : 5.000e-001
3.000e-001 : 4.000e-001
2.000e-001 : 3.000e-001
1.000e-001 : 2.000e-001
<0.000e+000 : 1.000e-001
Density Plot: |B|, Tesla

(c)

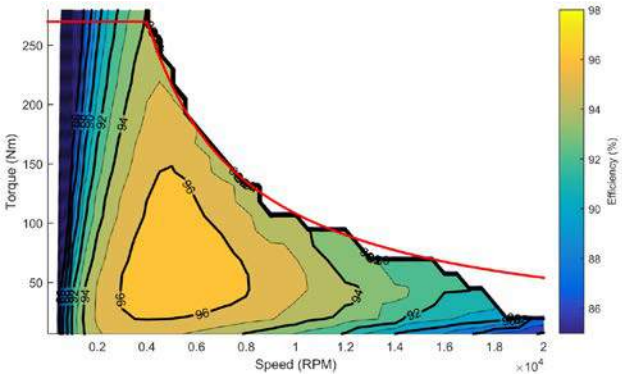
Torque (Nm)
Speed (RPM)
×10^4
Efficiency (%)

(d)

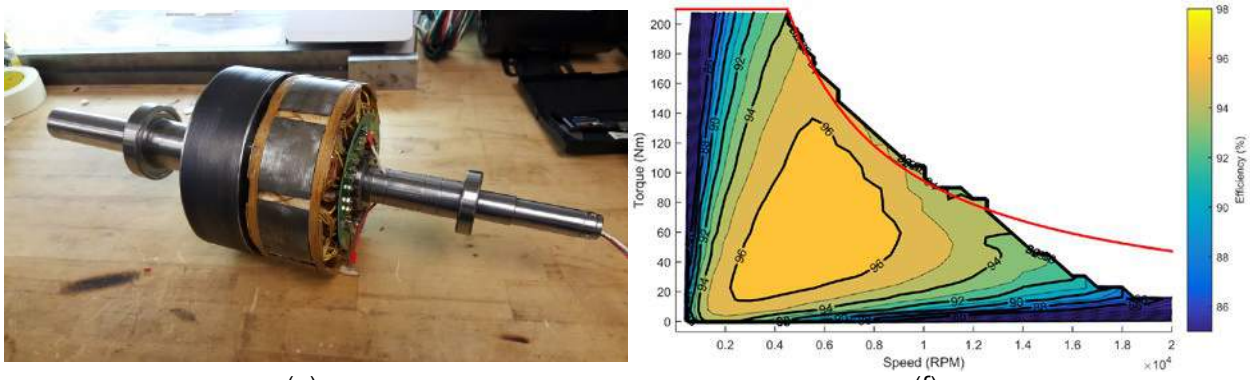


(e) (f)

Figure II.7.2 - Dual rotor HESM, (a) IPMSM rotor magnetic simulation, (b) simulated full IPMSM rotor efficiency map, (c) wound field rotor magnetic simulation, (d) simulated full wound field efficiency map, (e) prototyped dual rotor HESM, (f) simulated dual rotor HESM efficiency map.

*2) Mechanically Simple PCB Based Capacitive Power Coupler with High Switching Frequency GaN Inverter*

To provide brushless rotor field excitation power in a low cost, easy to manufacture, and mechanically robust solution a new capacitive power coupler based on printed circuit boards has been designed and prototypes. The CPC forms a three-phase rotating capacitor with ~500 nF of capacitive coupling per phase, Figure II.7.3. Three concentric ring traces are present on the boards forming the three phases. The pads for the rotating rectifier are shown in Figure II.7.3(a) but are not populated in the Figure. This assembly will be mounted on the shaft of the wound field or hybrid excitation machine. Due to the relatively small surface area and large gaps between boards a high frequency electric field is necessary to transfer the required rotor field excitation current. A new 3 to 5 MHz switching frequency 3 phase voltage source inverter (VSI) based on GaN systems devices has been designed and prototyped, Figure II.7.3(c). Currently, the main challenge of operating this inverter is the extreme dV/dt induced by the switching of the semiconductors, especially when the DC bus is above 150 V. During these conditions, shoot through can occur as the low side gate drive may be triggered by the switching of the high side device. Filters, damping resistors, Schmidt triggers and shielding are currently being implemented on the inverter to squelch spurious turn on events. Other CPC concepts including ceramic coated journal bearings and integrated electric/magnetic couplers are also being investigated.

(a) (b) (c)

Figure II.7.3 - Printed circuit board three phase rotating capacitor, (a) double sided rotor, (b) single sided stator, and (c) 3 to 5 Mhz 3 phase GaN inverter.

*3) Design of a WFSM with a Die Compressed Field Winding*

To increase the torque and power output from a WFSM with the same outer envelope as the proof of concept HESM and gain experience with winding die compression and magnetic joints a proof of concept WFSM rotor has been designed with die compressed windings to be used in the same HESM stator, Figure II.7.4. The design was selected from a Pareto front tradeoff of torque versus machine loss generated using a differential evolution optimization algorithm. The electromagnetic structure of the rotor consists of three parts the rotor pole body and yoke, die compressed field winding, and pole cap which retains the field winding radially using a dovetail joint, Figure II.7.4(a). Once the coil is compressed to an ~80% slot fill it becomes a solid body and individual turns cannot be wound around the pole body. The solid coil must be slipped over the pole body and retained requiring a joint between the pole body and the pole cap. The influence of likely tolerances and the airgap introduced by the joint, dovetail style in this case, on the machine power conversion capabilities has been studied, Figure II.7.4(a). The winding will be compressed to an approximate slot fill of 0.8 in the proposed die, Figure II.7.4(b). The dovetail has been designed to ensure the structural integrity of the rotor at the maximum design speed of 12,000 RPM, Figure II.7.4(c). The predicted torque production of the machine with the anticipated worst case airgap introduced by the dovetail joint is ~278 Nm. This predicted performance is substantially higher than previous WFSM prototypes. This proof of concept design is currently being finalized for construction and testing. The same die compressed winding technology is slated in budget period 2 to be applied to the stator with a low scrap cut core or roll up design.

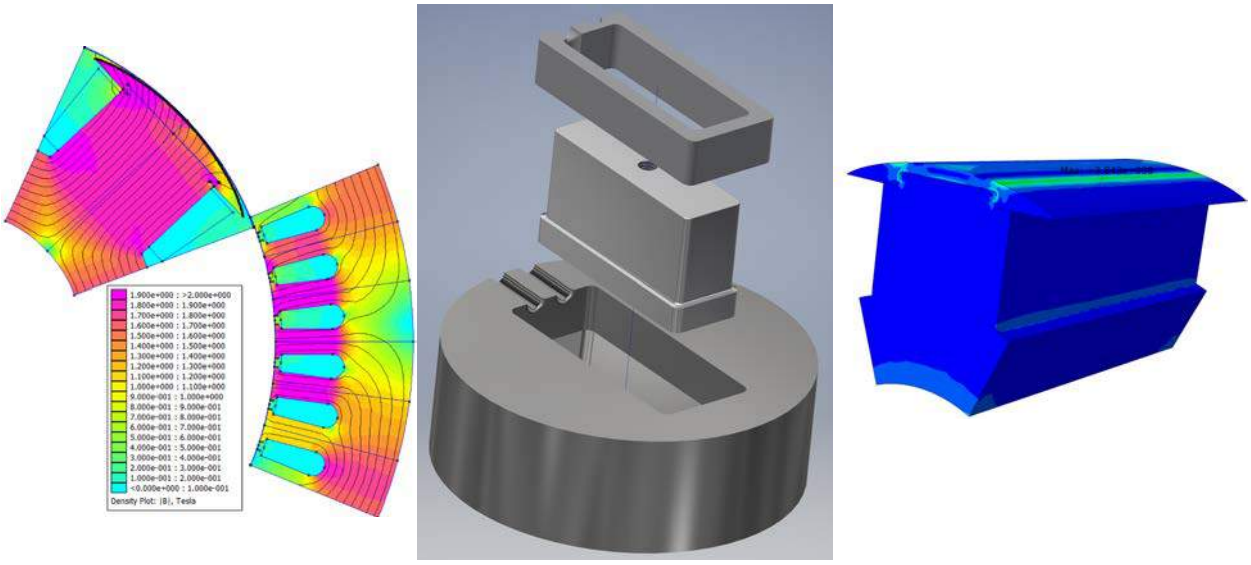

(a) (b) (c)

Figure II.7.4 - Proof of concept wound field synchronous machine rotor with die compressed field winding and magnetic joint including (a) magnetic simulation of down selected design, (b) die design, and (c) dovetail stress analysis at 12,000 RPM.

*4) Development of Deadbeat-Direct Torque and Flux Control Techniques for WFSMs*

Electric vehicle applications require high performance control of the traction motor. Very little literature exists about the control of WFSMs and HESMs. As part of this project a deadbeat-direct torque and flux controller has been developed for WFSMs. The state block diagram of the proposed controller is shown in Figure II.7.5. This state of the art control scheme decouples the torque, stator flux linkage, and field flux responses and allows for single PWM cycle step responses within the inverter voltage limits. The key step in the development of this controller was the derivation of the discrete time current and flux linkage observers. A field flux linkage command generator for unity power factor operation has also been developed. This control technique will

serve as a basis for the development of loss minimizing control schemes for wound field and hybrid excitation machines.

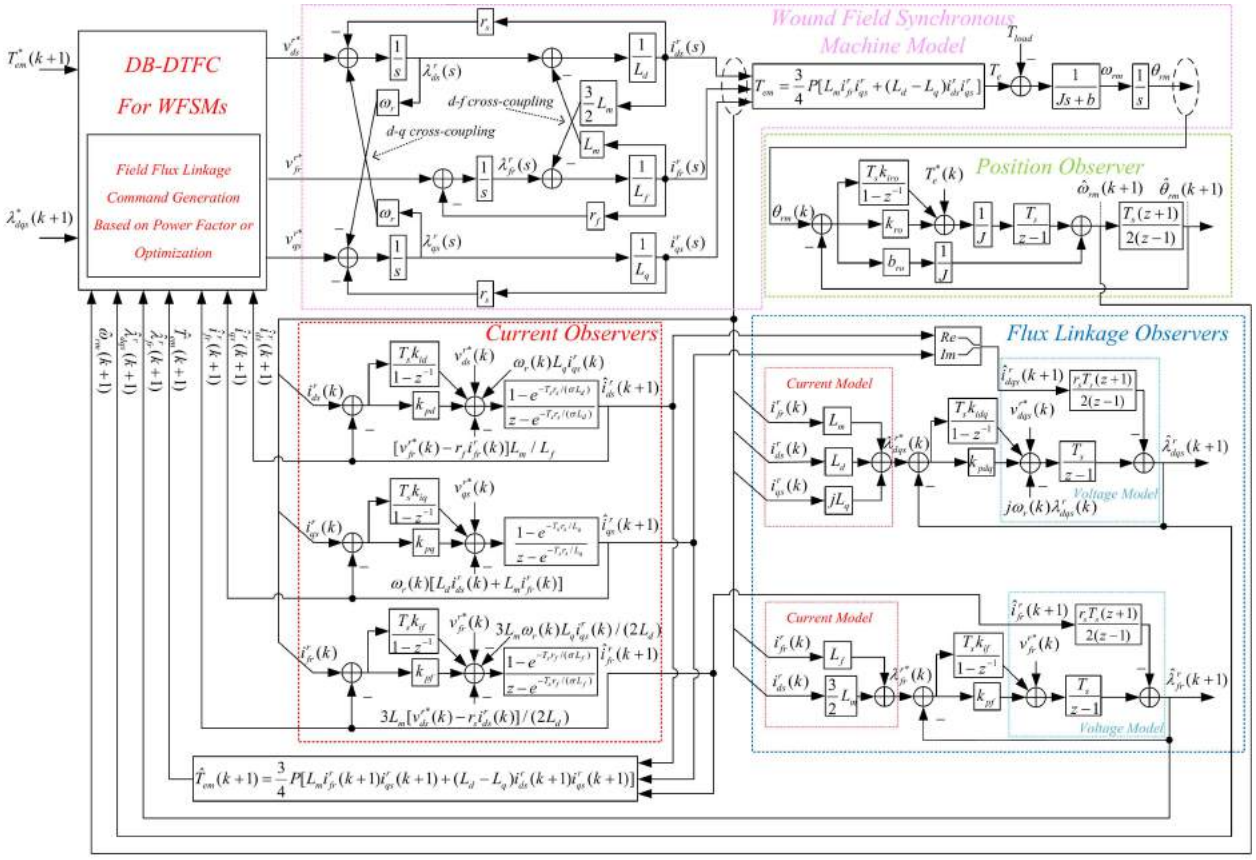


Figure II.7.5 - WFSM deadbeat-direct torque and flux control state block diagram.

## Conclusions

WFSMs and HESMs with brushless capacitive rotor field power transfer are being developed as a high performance low cost EV traction motor option. In the coming budget period prototype WFSMs and HESMs will be dynamometer tested at full power. Low scrap stator designs with die compressed windings will also be investigated. In the final budget year a through cost evaluation of the best in class WFSM or HESM will be carried out.

## Key Publications

1. Y. Nie, I.P. Brown, D.C. Ludois, “Deadbeat-Direct Torque and Flux Control for Wound Field Synchronous Machines,” IEEE Transactions on Industrial Electronics, DOI: 10.1109/TIE.2017.2739696.

## II.8 Development and Demonstration of Medium-Heavy Duty PHEV Work Trucks

**John R. Petras, Principal Investigator**
Odyne Systems LLC
W237 N2878 Woodgate Road, Suite 2
Pewaukee, WI 53072
Phone: (262) 544-8405
E-mail: John.Petras@Odyne.com

**Steven Boyd, Program Manager**
U.S. Department of Energy
Phone: (202) 586-8967
E-mail: Steven.Boyd@ee.doe.gov

Start Date: January 19, 2017 End Date: April 30, 2020
Total Project Cost: $6,172,732 DOE share: $2,149,644 Non-DOE share: $4,023,088

### Project Introduction

The heavy-duty vehicle market (Class 6-8) has been a difficult segment for the introduction of plug-in vehicles due to the large energy storage requirement (with corresponding cost), challenging duty cycles, and the diversity of vehicle configurations. The Work Truck market represents a significant opportunity for Heavy-Duty PHEV adoption. Odyne proposes development of a new class of PHEV Work Truck which will be modularized and customized to provide optimal ROI across multiple customers and applications. The proposed project will first demonstrate this technology as a Utility Work Truck variant:

- The usage cycle includes driving and stationary/worksite power requirements, ensuring full daily usage of the grid-charged battery (battery size: 25-40 kWhr). Though daily driving can often be short (an average of 26 miles per day), worksite power includes substantial demand (hydraulics, exportable 110/220V power, 12V support, HVAC).
- Worksite power demands for conventional vehicles require continuous loaded engine operation, resulting in significant emissions, fuel consumption and noise impacts.
- These trucks serve an industry that is strongly incentivized to promote vehicle electrification, and which has publically committed to spending a portion of their annual vehicle purchase budget on electrified vehicles (EEI press release of 11/18/14).

This project will develop and demonstrate a medium/heavy duty plug-in hybrid solution capable of meeting the needs of the work truck market while delivering fuel and emissions reductions of 50% when evaluated against the full-day work truck duty cycle.

### Objectives

The project goal is to design, develop, and demonstrate a new generation of medium/heavy-duty plug-in hybrid electric work truck that achieves a 50% reduction in fuel consumption versus a conventional vehicle baseline when evaluated across a full day work cycle representative of the vocational work truck. The primary objectives are:

- To simulate, design and develop unique and innovative integrated powertrain, software, and calibrations which will optimize the complete diesel/transmission/hybrid powertrain and yield driving fuel efficiency improvements greater than 50% with commensurate reductions in GHG emissions and no impact on NOx
- To develop and validate a modular Lithium Ion battery system based on high volume lower cost cells and modules that are utilized in the light-duty sector which will meet the power, energy, and duty cycle

requirements of the MD-HD vocational truck market at a cost approaching half that of currently available low volume solutions.

- To integrate fully electrified worksite functions and a daily duty cycle optimization function with the powertrain and battery solutions on an OEM class 7 chassis and demonstrate the capability of 50% improvement in driving efficiency and a 50% reduction in total fuel used when measured against a full day duty cycle's and real world performance.
- To demonstrate ten optimized PHEV work trucks and validate the vehicle's operating performance, emissions and full work cycle fuel reduction in excess of 50%

## Approach

The proposed solution incorporates a simple, parallel hybrid system that allows the torque of the electric motor to augment the torque output of the diesel engine, thus saving fuel. The motor speed is synchronized with the engine speed through the existing power take-off (PTO) unit. The traction motor drives the PTO, adding torque to the rear axle, or converts torque from the PTO into power to charge the PHEV batteries (see Figure II.8.1). Six patents have been granted, and other patents are pending.

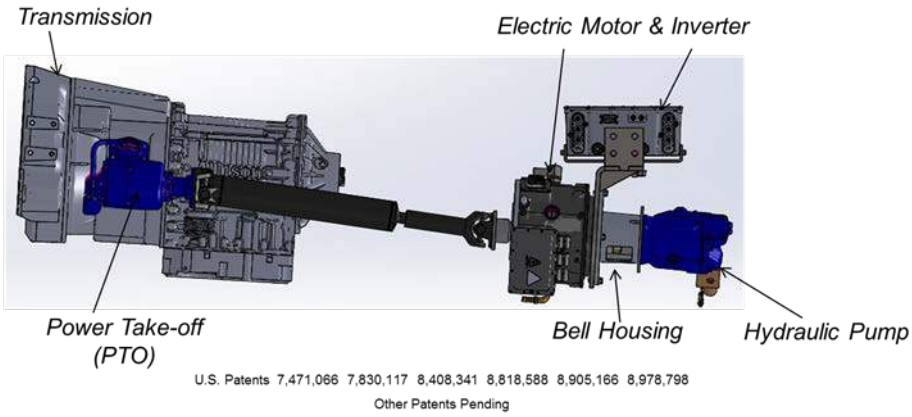


Figure II.8.1 - Odyne powertrain configuration

The system is also designed to provide full jobsite engine off electrification utilizing power from the lithium ion battery system to provide 120/240 V exportable power, 12V chassis systems support, high efficiency electric heating and air conditioning along with the power to drive the primary work equipment (Figure II.8.2).

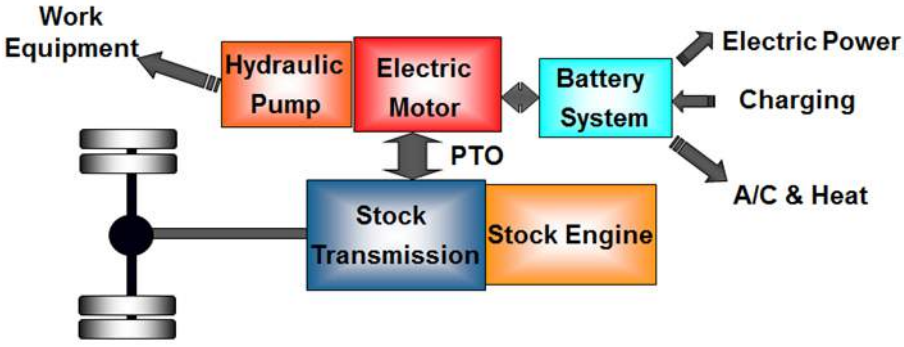


Figure II.8.2 - Odyne hybrid architecture

The project will be conducted in three periods:

***Period 1 (15 months): System Design and Analysis***: Analysis of existing fleet data will be performed and will be used for the establishment of baseline driving and full day usages cycles and current vehicle performance for system simulation, development and test. The project will create designs and systems which, when integrated, will produce a Medium-Heavy duty work truck capable of achieving requirements under real world conditions. The period will conclude with an analytical simulation verifying this performance improvement.

***Period 2 (12 Months): System and Vehicle Verification***: The subsystems will be verified and refined using prototype hardware and the full vehicle will undergo final development, functional and performance test. The prototype phase will conclude with test results confirming that the final design will provide a ≥50% reduction in fuel use under real world conditions. Approximately ten vehicles will be built to support field test and evaluation.

***Period 3 (13 Months): Prototype Vehicle Demonstration***: Ten vehicles will be put in regular service with telematics to measure performance. The Recipient will analyze the data along with customer feedback and will report the real-world reduction in fuel use and customer acceptance of the technology.

The three-year period of the project will integrate three development streams into a final Prototype vehicle solution and 10 vehicle field demonstrations:

*Powertrain Development and Optimization*

- Odyne - Lead, Hybrid Powertrain development and design, Hybrid optimization and control strategies
- NREL – Duty cycle analysis, Dynamometer test, Full-year fuel use simulation and analysis
- Oak Ridge National Lab – Powertrain simulation and optimization, HIL Test
- Allison Transmission – Transmission control and optimization strategies,

*Battery Development*

- Odyne – System Specifications and integration requirements, system integration test
- AVL – Battery System supply chain evaluation, development, and test
- Supplier TBD – Lithium Ion Module and BMS Supplier, Component System integration requirements

*Chassis Development & Integration*

- Odyne – System design, control, cost, and integration lead, Systems Efficiency & Sizing, System build
- Freightliner - OEM Chassis Integration improvements, Prototype and demonstration chassis supplier

## Results

In FY17 the project was kicked off and the three teams began developing initial information for period 1 development and design activities which will be concluded in FY18.

*Powertrain Development and Optimization*

Duty Cycle Development - Odyne provided telematics data to NREL from 119 vehicle ARRA fleet. NREL preprocessed the data into 26,539 vehicle days and completed duty cycle analysis. Driving data was divided into trips, with trips separated by at least 5 minutes when the vehicle was stopped. The trips were clustered using a k-medoids algorithm to identify groups of trips with similar driving average speed, kinetic intensity, stops/mile, speed standard deviation, aerodynamic speed, and characteristic acceleration. Four clusters were seeded, a decision stemming from testing which showed diminished returns from adding additional clusters. The 4-medoids algorithm found 4 trips that were median trips in n-dimensions. The remaining trips are

assigned to the cluster of the medoid point that they are nearest to. Interestingly, there are no clusters which represent vocations such as digger or aerial. Each make, model and vehicle vocation had trips in each cluster. Figure II.8.3 shows the data clusters relative to the principal components of Kinetic Intensity (aerodynamic speed and characteristic acceleration). Figure II.8.4 highlights the four clusters in comparison to several existing standard drive cycles.

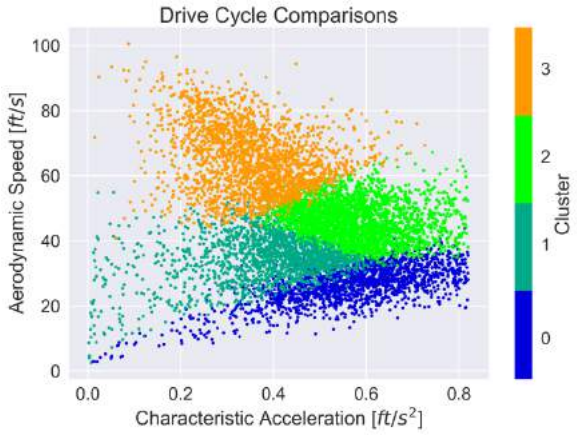


Figure II.8.3 - Odyne Data Clusters

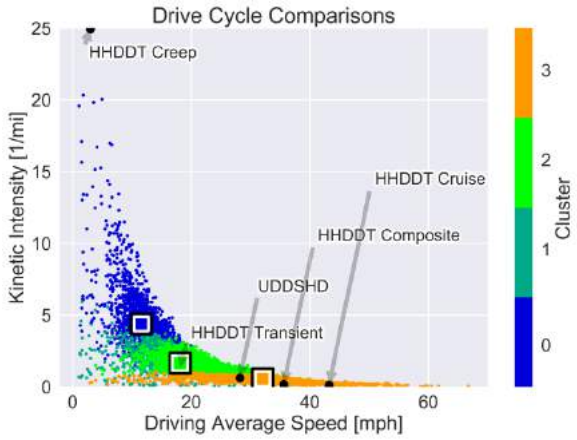


Figure II.8.4 - Odyne Custom and Standard Cycles

NREL researchers used the DRIVE tool, to generate representative drive cycles for each cluster. After close examination by the NREL and Odyne technical teams, cycles generated for clusters 1 and 2 were combined to form cycle 1.5. The combination saves testing time and lab resources, and was deemed appropriate because drive cycle 2 was comprised of one short drive cycle used twice. The custom cycles are referred to as Odyne Low, Mid, and Hi. UDDS and HHDDT drive cycles were also tested on the dynamometer. The Drive Cycles developed by NREL utilized in baseline testing are shown in Figure II.8.5–Figure II.8.7. A summary report from NREL is due in October, 2017

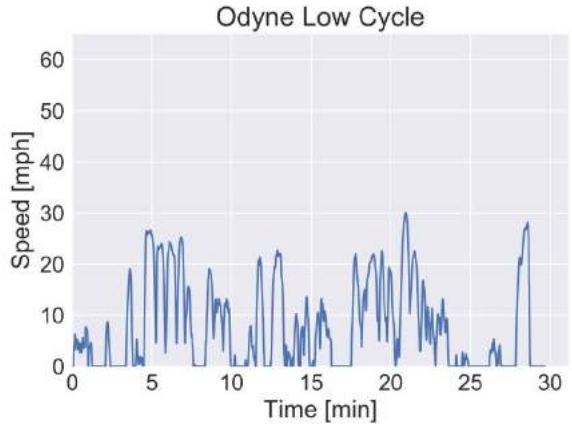


Figure II.8.5 - Odyne “Low” Cycle

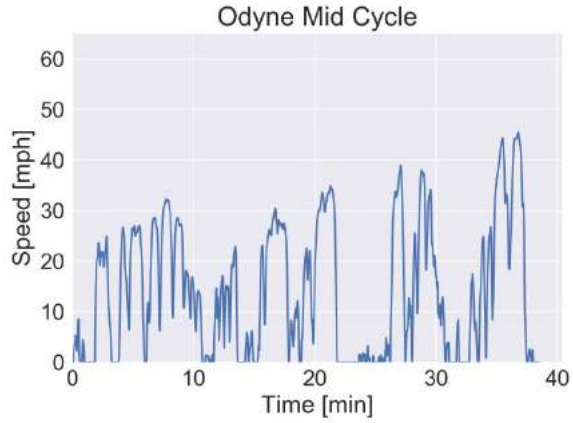


Figure II.8.6 - Odyne “Mid” Cycle

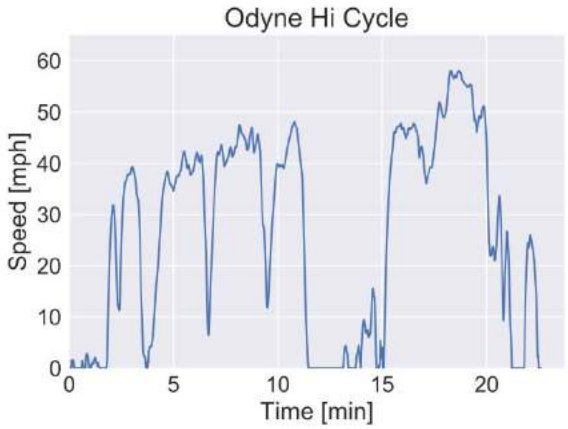


Figure II.8.7 - Odyne "Hi" Cycle

Baseline Dynamometer Testing - A 2017 Freightliner M2 vehicle which will be built into a production Hybrid Aerial Device for Duke Energies was selected as the test platform for baseline testing. Installation of the current Odyne hybrid system on the chassis was completed and delivered to NREL in July. The vehicle completed 2000 miles of "degreening" completed dynamometer testing in September. Analysis and reports are in process and scheduled for completion in November, 2017. Figure II.8.8 and Figure II.8.9 show the hybridized baseline test chassis.

Figure II.8.8 - Hybridized Freightliner M2

Figure II.8.9 - Close-up – Odyne PHEV system

Powertrain Simulation - Odyne provided a baseline Simulink model representing the current Hybrid system to Oak Ridge National Laboratory (ORNL) for evaluation and review. ORNL is currently updating the model to improve speed and accuracy. The first deliverable will be correlation to the NREL baseline dynamometer data scheduled for completion in November, 2017.

**Battery Development**

Odyne completed contract development with AVL in July and held a kick-off meeting on August 1st. Odyne worked with AVL to develop detailed commercial and performance specifications. AVL is in the process of assembling supply evaluation matrix to identify key supply alternatives with preliminary results planned for Mid-November.

**Chassis Development & Integration**

A kick-off meeting was held with Freightliner on July 11th. Discussion areas included detail planning for the project test chassis, means for improving integration of the chassis and hybrid systems, and the effects of

Phase 2 GHG legislation on the integration of the Odyne hybrid system with the Freightliner production and certification processes. The test chassis order was submitted to Freightliner on 7/28 with planned delivery to Odyne in Early December, 2017. Subsequent meetings were held with Freightliner Applications Engineering to discuss potential custom Odyne Chassis codes and design option features with the intent of aiding hybrid packaging and installation. Meetings held with Freightliner Powertrain Engineering to discuss potential methods for All-Electric Creep mode.

Odyne is currently working with power electronics suppliers to develop the next generation of low cost componentry which will be evaluated on the test truck in FY18 and on the demonstration trucks in FY19. Design decisions and evaluation parts are expected in the first quarter of CY18.

## Conclusions

In FY17, the project teams established baseline information which will be utilized in the conclusion of the system design and analysis period in FY18. The development of baseline duty cycles and dynamometer data was the critical first step in developing baseline performance and providing input into the simulation models which will be utilized to optimize the hybrid powertrain system. The investigations into new battery and power electronics systems in improvements in vehicle integration are progressing in parallel.

## Key Publications

There were no publications produced in FY17

## II.9 High Temperature DC Bus Capacitor Cost Reduction & Performance Improvements

**Angelo Yializis, Principal Investigator**
Sigma Technologies International Group
10960 N Stallard Place
Tucson, AZ 85737
Phone: (520) 575 8013
E-mail: ayializis@sigmalabs.com

**Steven Boyd, Program Manager**
U.S. Department of Energy
Phone: (202) 586-8967
E-mail: Steven.Boyd@ee.doe.gov

Start Date: October 1, 2013 End Date: March 31, 2017
Total Project Cost: $3,510,897 DOE share: $2,288,559 Non-DOE share: $1,222,338

### Project Introduction

The proposed project focuses on process development and scale-up to produce application-specific DC-link capacitors for automotive inverter applications. In Phase I of the program (2013 – 2015), the development work addresses optimization of the polymer dielectric formulation and thickness, to produce GEN 1 capacitors with a rating of 800 µF / 400 Vdc / 650 $V_{TRANSIENT}$. GEN 1 will demonstrate operation at -40°C to 140°C, a benign failure mode, direct cost < $15 and 3X reduction in the volume and weight, compared to today's baseline polypropylene (PP) capacitors. A significant part of the Phase I effort was to scale-up process steps to allow manufacture and assembly of an adequate number of parts for the various test protocols and to meet the Phase I deliverables. In the Phase II effort (2015 – 2017), GEN 2 capacitors were produced that further decreased capacitor volume by optimizing the polymer dielectric thickness and increasing the dielectric constant. GEN 2 capacitors were packaged, integrated into a Delphi inverter, and reliability tests were performed, to confirm that the target specifications are met.

### Objectives

- Reduce the cost, size and weight of the DC-link capacitor by >50%
- Increase durability in high temperature environments

*Technical Barriers*

- The performance and lifetime of capacitors available today degrade rapidly with increasing temperature (ripple current capability decreases with temperature increase from 85˚C to 105˚C). Therefore, today's capacitors are typically twice the size (up to 40% of the inverter's volume) and too costly (up to 30% of the inverter's cost).

*Technical Targets*

- A PML capacitor that will have a rating of 700-800 µF / 400 Vdc / 650Vtransient
- Designed for a 30-kW continuous, 55 kW peak (30 seconds) inverter
- Operating temperature: -40°C to +140°C
    - Projected volume: < 0.2L
    - Dissipation factor: < 0.01 up to 160°C

- Ripple current: 130Arms continuous
- Energy density: > 3X today's PP caps, or > 1 J/cc
- Cost: < $30 (with direct cost < $15)
- Benign failure mechanism

*Accomplishments*

Sigma and their partners Delphi Automotive and Oak Ridge National Laboratory have completed the project and have met and exceeded all of the above listed Technical Targets.

## Approach

Sigma has developed a solid-state Polymer-Multi-Layer (PML) capacitor comprising 1000s of radiation cured polymer dielectrics and Al electrodes to form a large area nanolaminate (Mother Capacitor) that is segmented into individual capacitors.

- Having a prismatic shape with low ESL and ESR
- Operating temperature range of -40°C to 140°C
- Dissipation Factor (DF) < 0.01
- Amorphous high breakdown strength dielectrics
- Dielectric constants in the range of $3.0 < k < 6.2$
- Benign failure mode
- Low-cost materials and process

This PML technology is a transformational and potentially disruptive technology in the following ways:

- Liquid monomer and Al wire are converted in a single step into Mother Capacitor material
- Eliminates film manufacturing and metallizing by outside suppliers

Capacitor manufacturer has opportunity to innovate and create application-specific products with different polymer dielectric properties

### Results

500 μF/600V GEN 2 capacitors were produced, packaged and integrated into a Delphi inverter. The capacitors were dyne tested in parallel to conventional metallized PP capacitors. The results show that the PML tested "proud" (without contacting the cooling rail) performed as well or better than the PP capacitors.

Sigma has spun-off a new company "PolyCharge" that will be focused in the production of DC-link capacitors for automotive applications. In addition to the high voltage PML capacitors developed in this project. Preliminary data suggests that PML capacitors for 48V inverters will have a significant size and performance advantage over aluminum electrolytic capacitors. Therefore, PolyCharge will also develop and manufacture lower voltage DC-link capacitors. Most of the major equipment for the first PML production line are on order and the production line is expected to be fully assembled and operational in a dedicated facility located in Tucson AZ, by the 1Q of 2019.


Figure II.9.1 - Comparison of Sigma PML 500µF/400V part to a PP 500µF/400V part

## Conclusions

In conclusion, Sigma and their partners, Delphi Automotive and Oak Ridge National Laboratory, have successfully produced capacitors which meet and exceed the DOE requirements. Work is continuing in transitioning the PML capacitor technology into production. Contacts with several US, European and Asian Tier-1 automotive suppliers have been made and samples have been provided for evaluation. PolyCharge is pursuing two different paths to commercialization. In one, PML capacitors will be used in a space allocated for metallized PP capacitors, without optimizing the inverter to take advantage of the smaller PML capacitor size. In the other path, inverter OEMs are designing an inverter specifically for the smaller PML parts, with the expectation to proceed in this direction once PolyCharge demonstrates a reliable supply of PML capacitors. In one case, a smaller inverter OEM is already producing a compact inverter for a Formula-e car that is using PML capacitors, which have a prismatic shape and size that cannot be met by any other capacitor product.

## Key Publications

1. 2017 DOE Annual Merit Review meeting presentation

2. A key patent on DC-link PML capacitors has been issued (US 9,711,286) and two other patent applications are pending.

# III. Grid and Infrastructure: Industry Awards

## III.1 Comprehensive Assessment of On-and Off-Board Vehicle-to-Grid Technology Performance and Impacts on Battery and the Grid

**Sunil Chhaya PhD, Principal Investigator**
Electric Power Research Institute (EPRI)
3420 Hillview Avenue
Palo Alto, CA 943041338
Phone: (650) 855-2148
E-mail: schhaya@epri.com

**Lee Slezak, Technology Manager**
U.S. Department of Energy
Phone: (202) 586-2335
E-mail: Lee.Slezak@ee.doe.gov

Start Date: October 1, 2016 End Date: December 30, 2019
Total Project Cost: $2,786,278 DOE share: $1,547,678 Non-DOE share: $1,238,600

### Project Introduction

There is heightened interest in the value for Vehicle-to-Grid (V2G) applications to provide energy management services to support grid reliability and resiliency. The research community is seeking to maximize the total value of a vehicle by exploring other services beyond transportation, but the automotive manufacturing and transportation battery communities remain reluctant to embrace V2G applications because of uncertainties associated with the exposure to grid applications and concerns about potential degradation of the transportation battery. Also, there are the challenges for enabling V2G technology development of bidirectional power electronics with the functionality, communications, and controls that are compliant with applicable regulatory and safety requirements, and standards. This proposal is to address the automotive industry concerns and the regulatory challenges to V2G technology.

The requirements for grid interconnected bidirectional inverters impose significant challenges to the automakers for on-vehicle inverter V2G functionality Automakers self-certify their vehicles to Society of Automotive Engineers (SAE) and Federal Motor Vehicle Safety Standards (FMVSS) requirements, and do not submit vehicles to National Recognized Test Laboratories (NRTL) such as UL. SAE is addressing this by developing SAE J3072 "Interconnection Requirements for On Board Utility Interactive Inverter Systems" providing communications and process requirements for validating the on-vehicle inverter certification. It incorporates the test certifications required by UL 1741 and requirements of IEEE1547. Acceptance by utilities of a J3072 compliant vehicle inverter certification is an open issue. As a part of a collaborative California Energy Commission program the team is to evaluate and verify these requirements for on-vehicle bidirectional inverters.

In contrast, off-vehicle inverter enabled V2G using DC charging avoids the issues and challenges relative to on-vehicle V2G inverters. DC chargers contain the charge control electronics and are a location fixed asset that is hard wire connected to the grid. Because DC chargers are a fixed standalone product they can easily be UL tested, certified, and site permitted. No vehicle UL certification would be required. The vehicle is only required to be DC charge capable with embedded J2847/2 communications software and J2931/1 power line communications (PLC) compliant connectivity with the DC charger which is standard with all DC charge capable Electric Vehicles.

The DC charger integrated off-vehicle bidirectional inverter is the most viable strategy and less challenging method for automakers to engage in commercialization of V2G as a distributed resource. However, there are still the automaker concerns with battery capacity degradation from V2G cycling and impacts on warranty services. This DOE project is to address the development, implementation, and verification of DC charging integrated off-vehicle bidirectional inverter enabled V2G; and to assess the impact of V2G cycling on battery durability. Also, will be working with the SAE J2847/2 task force in the development and testing of the control messaging requirements and protocol for V2G communications that is presently ongoing.

## Objectives

The objective of the program is to test and evaluate grid DER management / integration use cases using V2G bidirectional power flow (charging and discharging) integrated with solar and stationary energy distributed resources in the AC (on-vehicle) and DC (off-vehicle) domains. The outcome is data to be analyzed and evaluated for performance, durability, and usage characteristics of the V2G technology, and impacts on battery life and vehicle components. As such, the proposal involves evaluation of Vehicle to Grid (V2G) technologies for on-vehicle (AC) and off vehicle (DC) bi-directional inverters thereby providing the best research value for the DOE.

The project goals are:

- Provide experimental and analytical basis to V2G technology as a key enabler in improving the value of owning a Plug-in Electric Vehicle.
- Demonstrate the usefulness of off-vehicle Smart Power Integrated Node (SPIN) system to further enhance the value of V2G by enabling increased renewable generation on the grid and providing Vehicle to Home type services in conjunction with on-vehicle and off-vehicle storage.
- Provide experimental and analytical basis for assessing effect on EV batteries from their application to grid services
- Provide key metrics for evaluation of performance and value of an off-vehicle V2G system in comparison to an on-vehicle V2G system
- Assess the effect of transformer constraints on grid service implementation
- Provide analytical framework and research results on the valuation of V2G services for high-impact (high-stress) regions of the distribution grid

## Approach

The project is the comprehensive development, testing, and evaluation of Vehicle to Grid (V2G) and energy management technologies for on-vehicle bidirectional inverters, through a companion cost share project and for off-vehicle bidirectional inverters, through this DOE funding request. Figure III.1.1 provides a representative overview of the two V2G projects. The cost share funded project focuses on the effects of V2G energy management on the distribution system using on-vehicle inverter enabled bi-directional power flow to balance solar output for improved grid reliability and stability, including an economic evaluation of V2G services.

The focus of this DOE project is to develop, test, and demonstrate off-vehicle inverter enabled bidirectional power flow (V2G) utilizing a DC charging bi-directional converter integrated into a Smart Power Integrated Node (SPIN) system. The communications, control, and interface functionality for the SPIN system will be based on SAE standards (SAE J2847/2, J2931/1, and J2931/4). The intent is to demonstrate a fully functional, grid-compatible DC charging based V2G end-to-end system that provides secure, interoperable communications and information processing.

The uniqueness is the SPIN system capability to control and process power flow between PEVs (charging/discharging), the grid, local solar and backup energy storage with a single multifunctional modular unit. The SPIN system will synchronize these energy sources to act as dispatch able DER. Innovation lies within the development of V2G with DC bi-directional charging, and support of local Distributed Energy Resource (DER) integration use cases that will accelerate the deployment of V2G as a part of an integrated DER ecosystem.

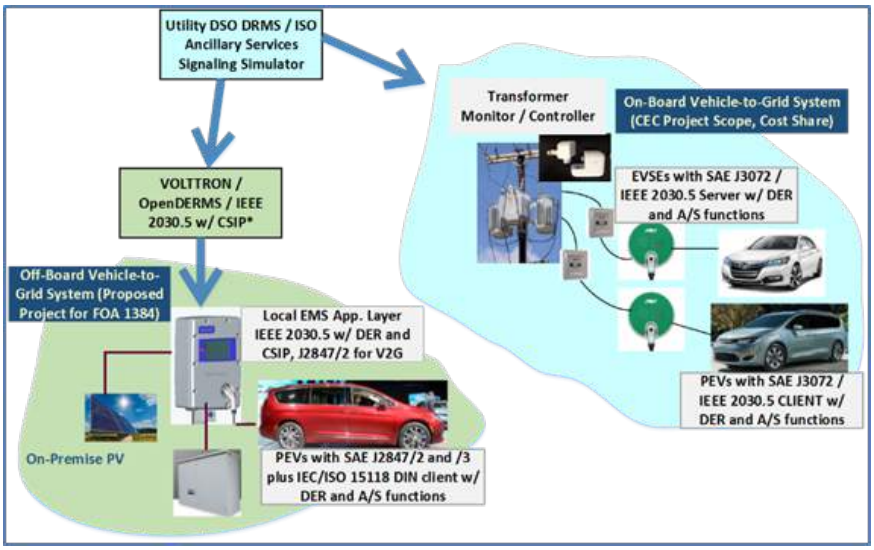


Figure III.1.1 - Project Structural Overview of On-Vehicle AC and Off- Vehicle DC V2G

The project is to achieve the objectives through accomplishment of the following activities:

- Development/fabrication of the Smart Power Integrated Node System hardware integrating a bidirectional dual active bridge converter using Wide Band Gap SiC power module technology with DC charging functionality (6.7 kW to 10 kW).
- Development/integration of the system control and communications software utilizing standards based protocols with interoperability between the SPIN system, utility or Energy Service Provider, and the PEV. This includes the development/integration of Energy Management System (EMS) control algorithms and functionality in the SPIN hardware for integrating V2G with solar and back up energy storage as coordinated distributed energy resources. Expectation is to extrapolate data on customer value and utility benefits for V2G DER integration.
- Develop/test determined cycle plan based on selected grid service use cases in both a lab environment and subsequently in a vehicle field demonstration. Evaluate battery life and conduct battery durability impact testing and analyses
- Conduct a 6-month field demonstration of the V2G grid service use cases utilizing 3 to 5 Fiat Chrysler Pacifica PHEVs and UL certified SPIN systems. The systems will be connected to a single transformer to allow evaluation of the grid impact from clustered EV charging and discharging.

The design, component technical specification, and simulation of the SPIN bidirectional converter has been completed by Flex Power Control (FPC) under a Technology Innovation contract from EPRI. ORNL has had specific experience in the development and integration of Wide Band Gap Silicon Carbide (SiC) power module devices in inverter systems for electric drive propulsion systems, and will provide engineering expertise to evaluate, test and verify the SPIN system design. Hardware fabricator Current Ways has established expertise and knowledge in power electronics manufacturing engineering and in UL certification processes. FPC, ORNL, and Current Ways have an established interaction on the design for the SPIN system and are collaborating on the design and fabrication of the FPC-designed SPIN technology.

The SAE J2847/2 and J2847/3 standards incorporating the required PEV/charger communications for PEV reverse power flow are in progress. EPRI is a working member of the SAE Task Force and is engaged in the

development of these standards. This project will correlate with the development of the standards and provide a basis for verification of the determined communications requirements.

Kitu Systems is presently developing the IEEE 2030.5 software into the AeroVironment EVSE for the CEC V2G project, which will be leveraged to successfully implement the software for the SPIN system. Additionally, EPRI will work with Fiat Chrysler to implement the required J2847/2 communications for V2G, which are based on the DIN 70121 protocol, into the Pacifica Mini Van PHEVs for the field demonstration.

EPRI has been working to develop and deploy DER management control algorithms in another project in Southern California around a community of Zero Net Energy homes, and these control algorithms will utilize the underlying stack developed by Kitu Systems that creates open standards-based communications. This experience integrating DER as well as the code-base will be leveraged to develop and implement the SPIN EMS control algorithms for coordinated DER management of V2G, solar, and back up energy storage, establishing the capability for micro grid operations at the local facility or residential level. EPRI's ongoing work with NREL on the INTEGRATE projects will inform the open DERMS and DRMS integration. In addition, EPRI will develop the grid models and provide the simulated utility DR and ISO regulation command/request signals for activating V2G during the lab testing and field demonstration phases.

LG Chem are the world leaders in electric mobility and grid-scale Lithium-ion batteries and will be an active participant in this project to lend both battery application, testing and data interpretation expertise, with battery hardware and test services to create data sets that can be analyzed.

Fiat Chrysler Group is making available Model Year 2017 Pacifica PHEVs for this pilot which will be modified to add V2G services related hardware and control algorithms. The on-vehicle V2G communications module utilizing J2847/3 standard application based on IEEE2030.5 protocol will be developed by EPRI and Kitu Systems. EPRI is developing the IEEE2030.5 translation to the vehicle CAN to ensure interoperability of the protocols for V2G functionality and control.

Special facilities access and planned utilization:

**ORNL:** Characterization and system integration testing of the Spin System will be accomplished at the ORNL *Power Electronics and Electric Machinery Laboratory* is in the National Transportation Research Center (NTRC), which has more than 9,000 square feet of space for developing, fabricating, and testing the next-generation power electronics and electric machine technologies. Lab testing of the complete V2G system with the SPIN system and LG battery packs will be accomplished at the *Distributed Energy Communications and Control (DECC) Laboratory* at ORNL which focuses on distribution system control and operation, grid interconnection and control of distributed energy resources including energy storage and electric vehicles, as well as smart grid, and communication applications.

**NREL*:*** The field demonstration consisting of 3 installations of the SPIN system with Fiat Chrysler Pacifica Mini Van PHEVs will be hosted and administered at NREL's Energy Systems Integration Facility (ESIF). The 182,500-square-foot (17,190-square-meter) facility is a first-of-its-kind design with a unique merging of three distinct and very specialized components: an ultra-green workplace, a high-performance computing data center, and a highly sophisticated high-bay laboratory. The vehicles are intended to be utilized within the NREL campus shuttle fleet on a scheduled basis to facilitate real world operation of the vehicles and utilization as a distributed energy resource for V2G services.

**Fiat Chrysler Group:** Fiat Chrysler group's Auburn Hills engineering center has world-class facilities and engineering staff that will be leveraged to do vehicle software and CAN bus integration of the grid communications hardware and software, as well as system commissioning and integration with SPIN module available for functional testing and performance assessment. One Pacifica PHEV will remain with Chrysler to validate any software or hardware changes in the lab before making them in the field.

## Results

The project kick -off meeting was conducted 9 Nov 2016. The primary results achieved within this first year of the project are:

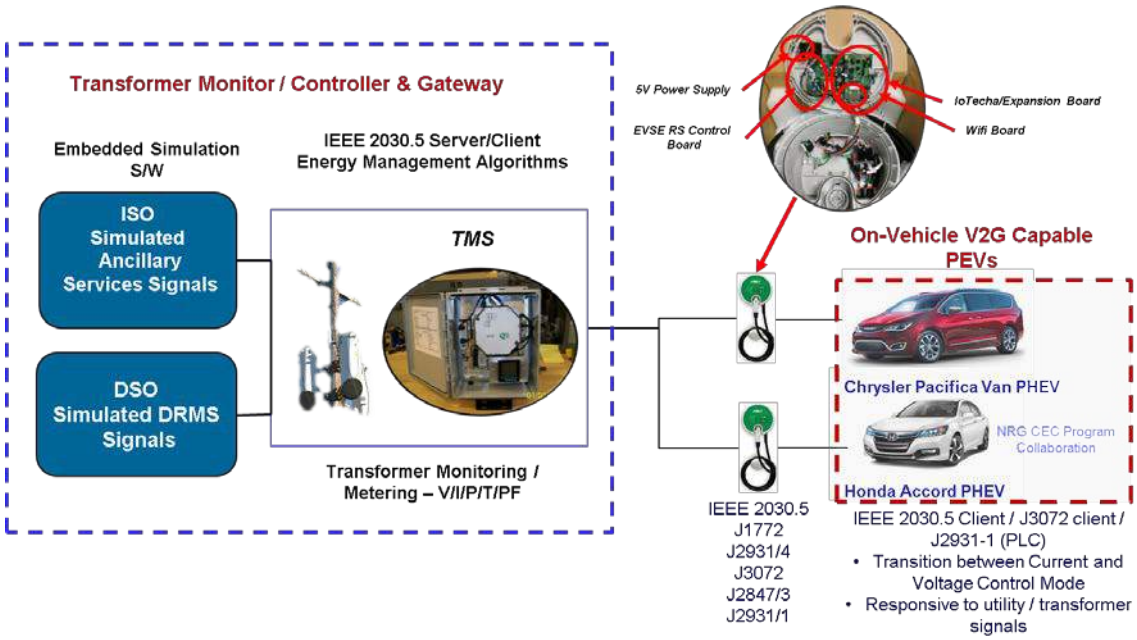


Figure III.1.2 - V2G Communications Architecture with On Vehicle Inverter

- Development of the V2G control algorithms and simulation test verification using an EV Emulator representing multiple V2G capable PEVs associated to a Transformer Management and Monitoring System within a residential application. Residential load and solar generation profile data used for the simulation testing is extrapolated from US Energy Information Administration data sources. The ISO and DSO signal simulators have been implemented into the simulation testing model for DR and DER functions and parameters.

- Development of the Smart Power Integrated Node (SPIN) system design architecture and Component Technical Specification

- Developing the SPIN master controller which integrates power electronics mode control functions for bi directional power flow management between DER assets (including PEV), the grid, and facility loads, Includes implementation of IEEE 2030.5 server /client software (DER and Demand Response Load Control (DRLC) function sets) for utility DSO /DRAMS interface and communications, meter telemetry for energy consumption and power flow data monitoring, and data analytics processing algorithms for energy utilization and cost optimization.

- Integrating the bidirectional on-board charge modules (OBCM) into the Chrysler Pacifica PHEV Vans. Four production vehicles provisioned for the project. The bidirectional OBCMs (Figure III.1.3) will provide reverse power flow functionality with both AC charging (on-vehicle inverter) and DC charging (off-vehicle inverter). On-vehicle V2G communications module is undergoing development and implementation, providing IEEE 2030.5 smart inverter functional communications with DER and DRLC functionality, IEEE 2030.5 translation/interoperability with

Figure III.1.3 - On Board Charge Module Providing Bidirectional Power Conversion

vehicle CAN protocol/communications., J2931/1 Power Line Communications implementation utilizing HomePlug GreenPhy chipset, and J3072 vehicle grid interconnected authentication and authorization standard.

- Assembled SPIN proof of concept rack system (Figure III.1.4) with 2 6 kW bidirectional converters (OBCMs), DC Switching, and battery simulator; and conducting integration with the master controller for multi-mode operational testing with power flow monitoring and configuration control, and implementation of data analytics algorithmic functionality for optimized DER/V2G energy management.

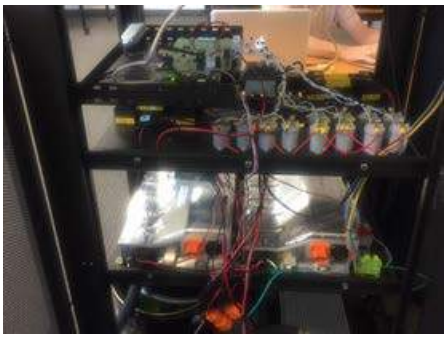

Figure III.1.4 - SPIN Rack Mounted Unit for Power Controls and Analytics Algorithmic S/W Integration and Testing

- Determined use case scenario for testing and data modeling: peak shaving for locational and wide area demand response, renewables or PV over generation mitigation in response to day ahead forecasts and response to observed grid conditions (volt/var); PV under generation ramping support in response to day ahead forecast and real-time response to latent grid conditions due to intermittent weather; ancillary services such as reg up/down; and cost optimization.

## Conclusions

The primary conclusions to date are derived from the PEV V2G simulation testing wherein the PEV charge/discharge control algorithms are executing as planned. The basis for the control algorithms is the capability to manage the V2G cycles within the constraints provided by the EV driver for minimum SOC, max SOC, and time charge in needed. Figure III.1.5 below is an example of graphic results of the V2G algorithms controlling charging and discharging of three vehicles in sync with solar generation profile. Additionally, with the application of real time data analytics, it is desired to verify the capability of the SPIN to configure the power flows of the DER assets with the grid to be able to comply with the requests by the utility and without inconvenience to the residential or facility owner. This coming year will provide the analysis and assessment of the cost benefit, distribution circuit impact, and deferred infrastructure upgrade costs.

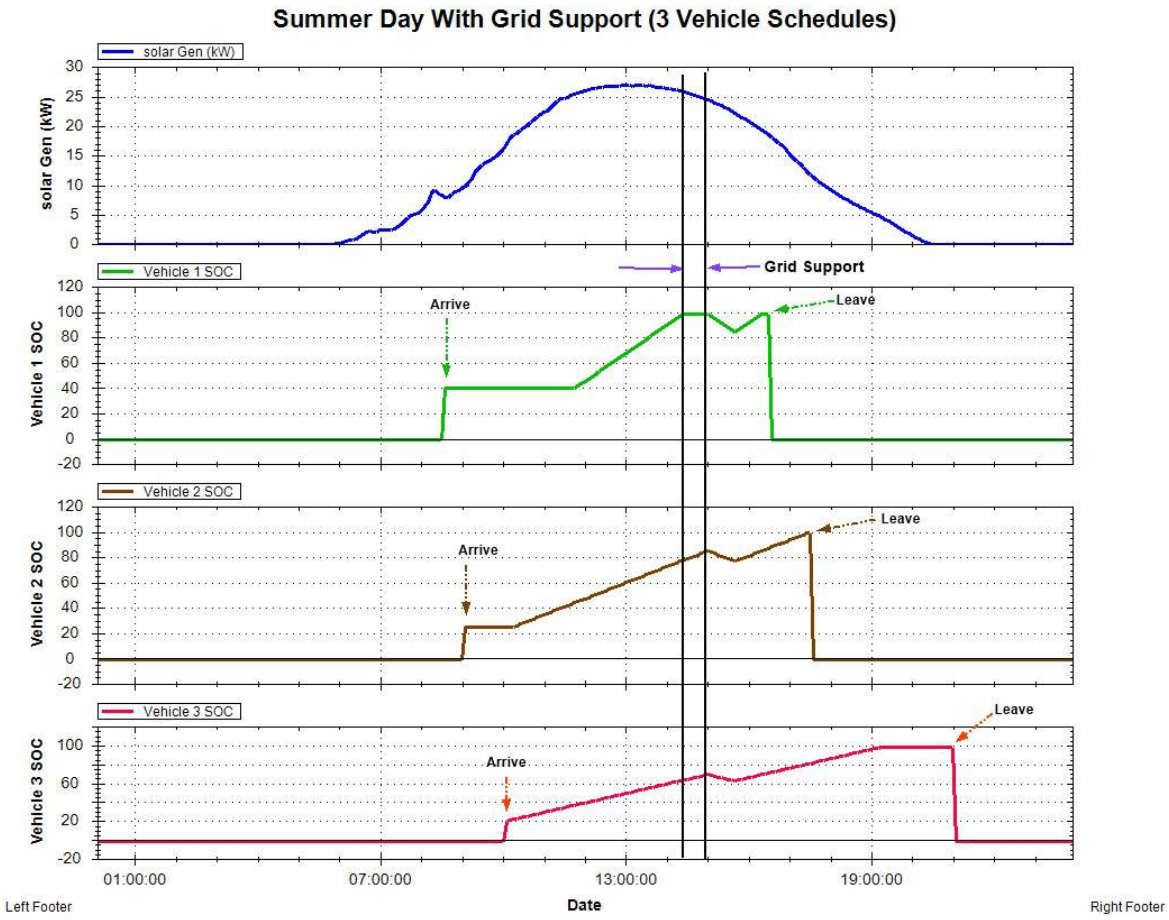


Figure III.1.5 - Simulation Results of V2G (Charging/Discharging) Control with Solar Generation

## Key Publications

The publications are in the form of reports and presentations. A list is provided and copies can be provided upon request.

1. DOE DE-EE0007792 Review 7-27-2017-final.ppt
2. DE-EE_0007792_Q2-2017_Report V1
3. V2G Cost Benefit Assessment Framework Document
4. V2G Vehicle Requirements and Algorithm Implementation Document V_1.0
5. System Requirements V3 Approved
6. Transformer Management System Algorithms – Graphs.ppt

## III.2 Medium-Duty Urban Range Extended Connected Powertrain

**Alexander Freitag, Principal Investigator**
Robert Bosch LLC
38000 Hills Tech Drive
Farmington Hills, MI 48331
Phone: (248) 876-7182
E-mail: Alexander.Freitag@us.bosch.com

**Lee Slezak, Technology Manager**
U.S. Department of Energy
Phone: (202) 586-2335
E-mail: Lee.Slezak@ee.doe.gov

Start Date: August 18, 2016 End Date: November 30, 2019
Total Project Cost: $6,716,791 DOE share: $4,731,884 Non-DOE share: $1,984,907

### Project Introduction

The purpose of this project is to develop and demonstrate a commercially-viable PHEV powertrain for MD vehicles that reduces fuel consumption by 50% on a real-world drive cycle by utilizing an advanced dual-planetary gear transmission with multiple clutches, coupled with cost-optimized electric machines. Such an improved powertrain efficiency will translate to a reduced fuel consumption of approximately 26 million diesel gallons per year, based on an average use of 22,000 miles per year at 8.3 mpg and a 30% market penetration for Class 4 delivery trucks.

The proposed design approach optimizes all powertrain components, particularly the internal combustion engine [ICE], the electric powertrain, and the battery pack to result in an incremental price and economic payback required for widespread commercial fleets' purchase without requiring financial incentives. Future developments are planned to explore the suitability of the MURECP powertrain for Class 2b – 8a delivery trucks.

### Objectives

The objective of this project is to develop and demonstrate a plug-in hybrid electric (PHEV) Class 4 delivery vehicle that reduces fuel consumption by at least 50% relative to an equivalent baseline vehicle by using an innovative, low-cost electric drive powertrain.

Key objectives:

- Dual Planetary Gear Transmission with multiple clutches, enabling the use of cost-optimized electric motors (PC/LD separated motor generators, high speed/ power dense design).
- Development of a multi-mode control strategy that ensures system optimal efficiency under a wide range of operating conditions, especially with the flexibility of powersplit operation.
- Efficient downsizing of the ICE for further reductions in fuel consumption.
- Electronic Horizon forward-looking input to HEV and EV driving modes, maximizing real-world fuel consumption reduction.
- Provide a ~35 mile all-electric range, achievable with existing battery packs on the CSHVC cycle.

## Approach

The project will be conducted in 3 budget periods:

Budget Period 1 (Aug ’16 – Nov ’17): **Powertrain Development**: Hybrid-electric vehicle topologies will be investigated through simulation and evaluation of each configuration on a real-world drive cycle to define the technical requirements and most promising architecture for the powertrain system.

Budget Period 2 (Dec ’17 – Nov ’18): **Powertrain Integration**: The supervisory control algorithms, battery management system, thermal energy management, and vehicle control strategy will be integrated with the conventional powertrain controller and further refined. The mechanical design and assembly of the hybrid drive system will also be completed along with the manufacturing of the prototype transmission. All PHEV solution components and a downsized diesel engine will be integrated onto the prototype vehicle.

Budget Period 3 (Dec ’18 – Nov ’19): **Powertrain Demonstration**: The prototype vehicle will be tested and deployed, including chassis dynamometer testing and demonstrations on closed courses or while shadowing an in-use delivery truck to quantify the achievable benefits and help finalize the control algorithms. In-use fleet operation with the prototype vehicle will be conducted.

## Results

*Task 1.1 – Develop a Class 4 Delivery Truck Simulation Model*

1D vehicle simulation models, both in Matlab and GT Suite, have been developed and validated. The baseline vehicle parameters are given in Table III.2-1.

**Table III.2-1 - Baseline Vehicle Input Parameters**

| Freightliner Custom Chassis Corp. MT45 + Morgan Olson Route Star Walk-In Delivery Cabin | Value/ Unit |
|---|---|
| Aerodynamic drag coefficient* Frontal Area (Cd*A) | 5.4 $m^2$ |
| Mass, loaded | 16,000 lbs. (tested at 15,410 lbs.) |
| Tire diameter, loaded | 0.48m |
| Tire rolling resistance: Overall/ Drive/ Steer | 7.38/ 7.5/ 7.1 kg/ton |
| Auxiliary consumed power | 1,300 watts |
| Center of Gravity Location, height/horizontal | 51 inches/ 108 inches |
| Wheelbase | 178 inches |
| Internal Combustion Engine | 2011 Cummins 6.7l ISB- 200hp @2,400 rpm/ 560 ft-lbs @ 1600 rpm |
| Transmission- type, ratios, and efficiency | Allison 1000 HS 5 speed automatic<br>3.1, 1.81, 1.41, 1, 0.71 & 98% |
| Final Drive Ratio & Efficiency | 4.3:1 & 95.5% (assumed) |

Utilizing data from NREL's Fleet DNA database, 81 class IV to class VI delivery trucks were selected as the most representative applications. After analyzing almost 75,000 miles over 1600 days of real-world data, the City Suburban Heavy Vehicle Cycle (CSHVC) was identified as the target drive cycle, when comparing kinetic intensity, stops per mile, etc. to the average of all the field data trips.

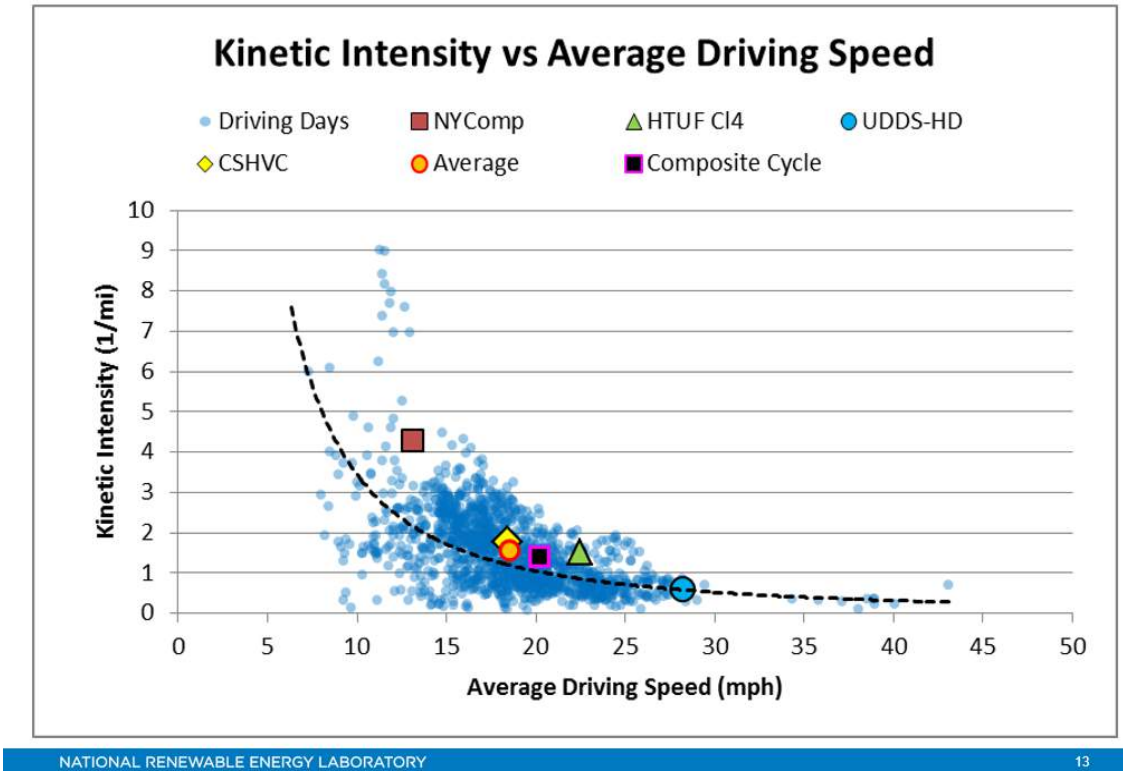


Figure III.2.1 - Target Drive Cycle Evaluation- Kinetic Intensity vs Average Driving Speed

For a previous study, NREL had performed chassis dyno fuel consumption measurements for a comparable chassis running the CSHVC. The baseline chassis had a measured fuel consumption of 0.765 gallons for the 6.68 mile cycle, resulting in a fuel economy of 8.7 MPG. The optimal Matlab model, which uses dynamic programing to determine the optimal gear selection, resulted in a simulated fuel economy of 10.3 MPG, which is ~17% better than the baseline measurement. Since the Matlab model will only be used to compare 2PG architectures amongst each other, this deviation was deemed to be acceptable. A more physical based vehicle model was also created in GT suite, which resulted in a much more accurate fuel economy of 8.3 MPG.

*Task 1.2 – Develop 2PG Hybrid Drive Simulation Models*

The top dual-planetary gear (2PG) architectures which meet or exceed the baseline vehicle performance while also reducing the fuel consumption by >50% were identified using the following methodology:

**Step 1:** Utilizing an automated modeling algorithm, all possible designs were modeled given the boundary conditions of two planetary gear sets, three speed/torque inputs (ICE & two electric motors), one output shaft to the rear axle, and three clutching elements to enable multi-mode operation.

**Step 2:** Conduct screening of all designs based on the desired attributes, such as no clutch on output shaft, ability to drive in reverse with engine on, powersplit mode, etc. Over 18 million designs were evaluated.

**Step 3:** Conduct screening of all designs based on the desired vehicle performance and acceleration parameters. The key parameters identified by the core team are given in table I-2 below.

Table III.2-2 - Basic Performance Parameters

| Performance Criteria | Performance Requirement | Baseline Vehicle Results |
|---|---|---|
| 0-60mph acceleration, level road | < 30.0 s | 22.4 s |
| 0-30mph acceleration, level road | < 12.0 s | 6.1 s |
| 40-60mph acceleration, level road | < 18.0 s | 13.0 s |
| Launch to 5m on 12% grade | < 60.0 s | 2.7 s |
| Minimum grade-ability @40mph | 7% grade | 15.1% grade |

**Step 4:** Conduct a fuel economy evaluation for all designs which meet the criteria defined in steps 1-3. The fuel economy evaluation is conducted in a two-step process; first utilizing Matlab dynamic programming to backwards calculate the optimum operating mode and torque split among the ICE, motor, and generator. With the optimum inputs, a forward looking simulation model is used to determine the cycle fuel consumption.

A total of 83 designs were identified which met the baseline vehicle performance results. A range of beta ratios (2:1 - 4:1) and final drive ratios (3.91:1 - 4.78:1) were evaluated. The results are shown in Figure III.2.2.

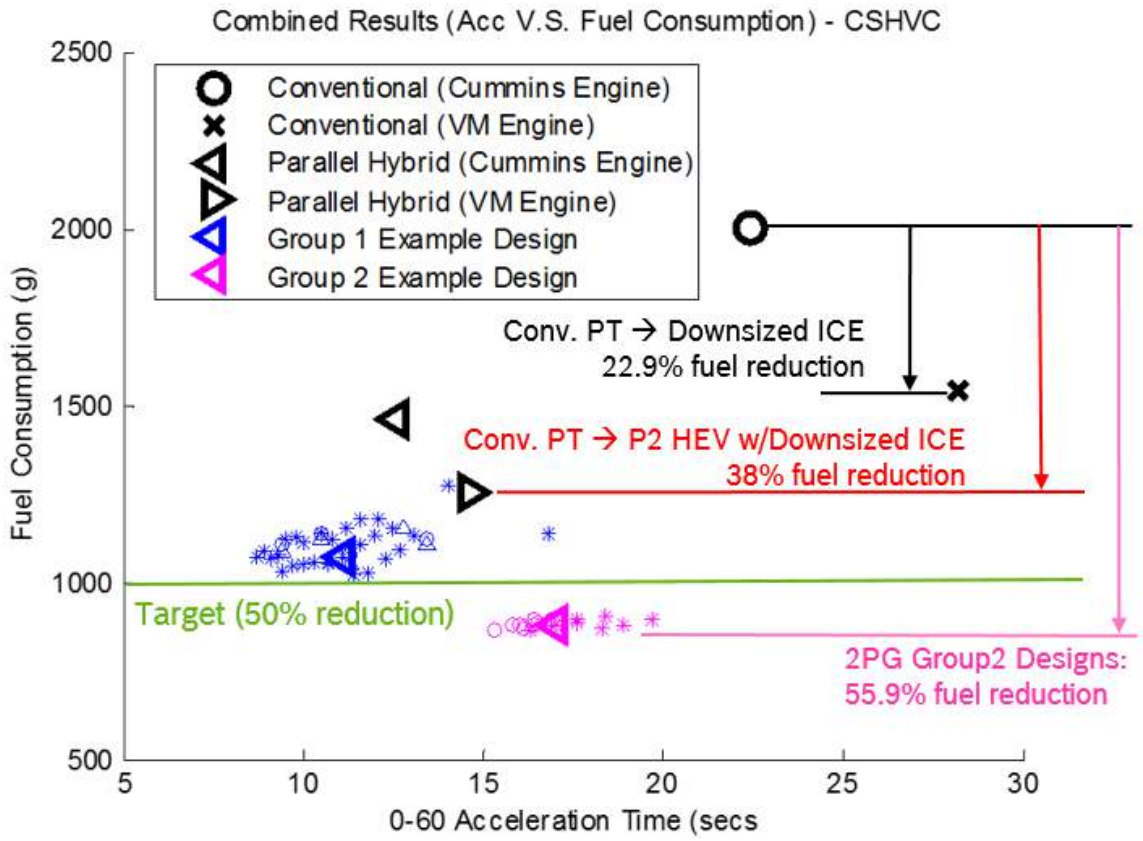


Figure III.2.2 - Fuel Economy Evaluation Results (Charge Sustaining Mode)

Group 1 example designs all share the following commonalities: ICE on carrier node, torque multiplication on output, and an ICE torque multiplication on the output node. Group 2 example designs, which achieved >50% fuel consumption reduction with 15-20s 0-60mph acceleration times, all shared the following commonalities: ICE on the ring node, a torque multiplication on output, and no engine torque multiplication on the output node. Based on expert discussions with the core team at BOSCH and Ricardo regarding control design, manufacturing, and performance, 6 designs were selected from the group 2 example designs. These are named design labels 23, 37, 94, 649, 698, and 789. These designs were subjected to in-depth analyses, including mode transition evaluations, component speed/torque load collective evaluations, and finally patent research. Only design 23 was found to be a potential for patent infringement and therefore excluded. The other five designs were unique enough to warrant a provisional patent application submission.

For the final design selection, detailed transmission modeling and control strategy development would be required, and therefore only a maximum of 3 designs could be selected, in order to meet the design freeze deadline of 6/30/2017. Designs 37, 94, and 698 were selected for the detailed modeling and controls development phase.

*Task 1.3 – Integrate 2PG hybrid drive into the target vehicle model*

Three transmission sub-system component models were created for designs 37, 94, and 698 in order develop control strategies and conduct a fuel economy study to support the final transmission architecture selection. An overview of the GT suite model for design 94 is shown in Figure III.2.3.

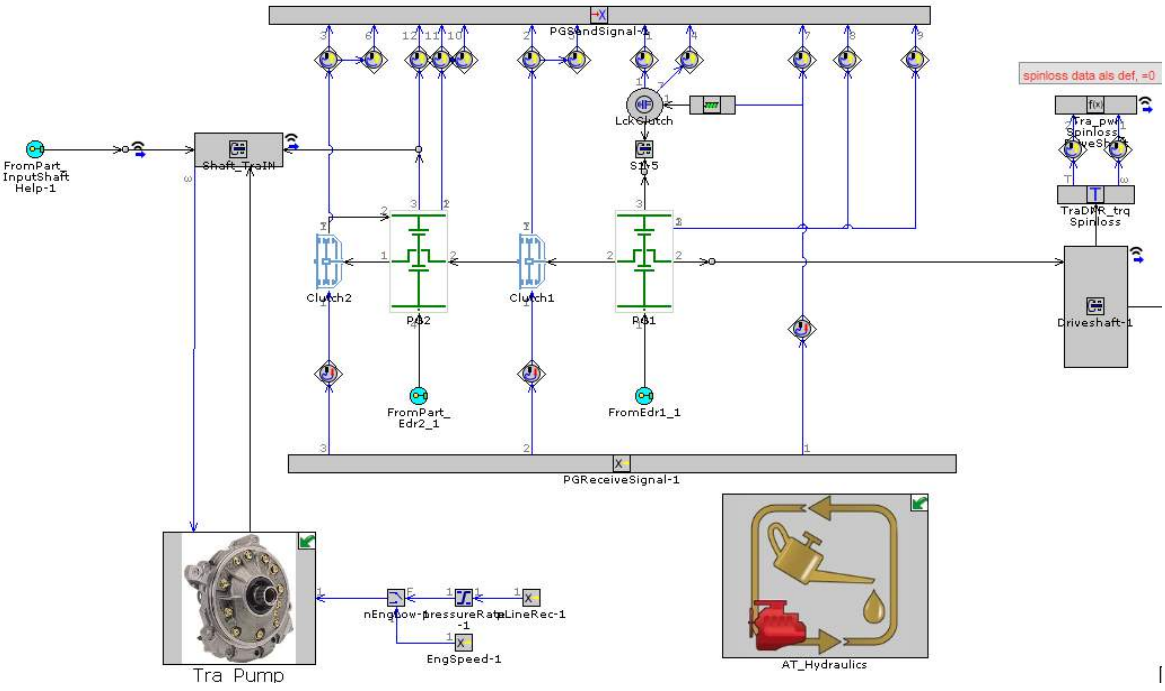


Figure III.2.3 - GT Suite Simulation Model- 1D Model of 2PG Transmission- Design Label 94

*Task 1.4 – 2PG Hybrid Drive Topology Evaluation*

To demonstrate the capability of the 2PG PHEV system, other more conventional PHEV architectures were benchmarked via Matlab DP simulations. To date, P2 parallel hybrid and P4 through-the-road hybrid powertrains have been studied. It is also planned to benchmark a series hybrid system. Results for the P2 parallel hybrid are shown in Figure III.2.3 above.

With a downsized ICE, a P2 hybrid can achieve a 38% reduction in fuel consumption on the CSHVC. For the P4 hybrid configuration a motor sizing study was also conducted. The lowest fuel consumption was achieved with the largest motor studied, namely a 250 kW/ 610 Nm (peak) variant. Even with a much more capable electric motor than used for the 2PG powersplit transmission (2x 80 kW/200 Nm) a fuel consumption reduction of only 34.1% was reached, significantly less than the 2PG benchmark of around 55%

*Task 2.1 – Develop rule based model for offline control of the PHEV powertrain system*

A model to determine the best transmission mode in the current driving situation (rule-based) has been developed. The operating modes are defined in three maps over transmission torque demand and vehicle speed. Maps are derived by analyzing dynamic programming simulation results of several drive cycles within representative SOC areas. The defined SOC areas/modes are: “charging”, “sustaining” and “discharging”.

*Task 2.2 – Develop PHEV operating strategy to maximize system efficiency on all drive cycles*

The initial rule-based controller was designed with the goal to minimize ICE fuel consumption, i.e., the speed/torque set point was selected based on the optimum BSFC curve. This strategy, however, was found to have its limitations in that the electric motor that counters the engine in powersplit mode was being driven at higher torques for longer periods of time, which caused thermal limitations to be reached within the motor. A key benefit of the powersplit transmission, however, is that the powersplit mode can be easily shifted to higher speed/lower torque (equal power) points. An optimal powersplit control strategy was developed to perform an online optimization, taking into account various thermal and mechanical limitations (which arise at different times based on the cooling system performance, ambient conditions, time at higher motor speed/torque, etc.). This strategy also aims to maximize the complete efficiency of the system.

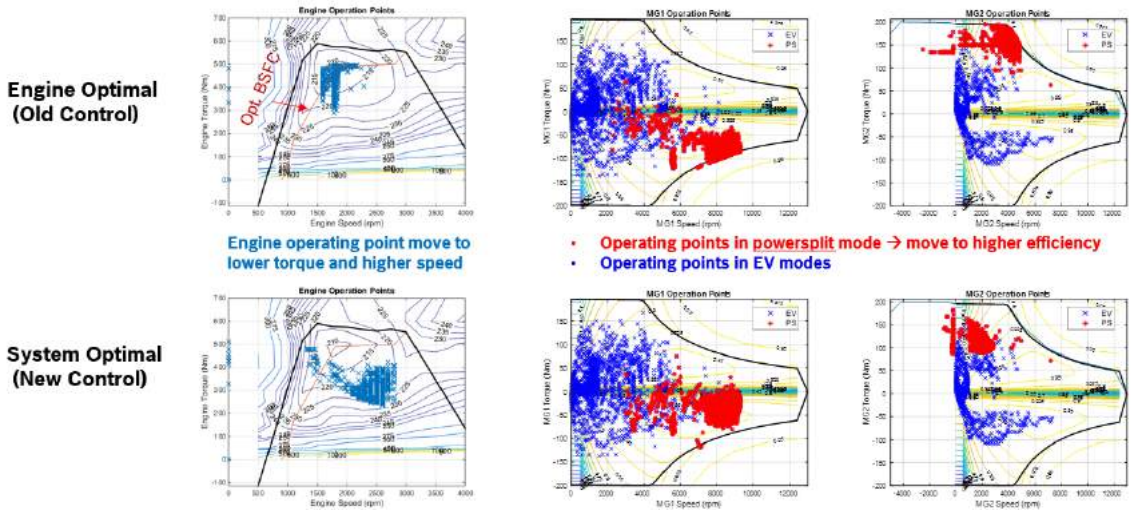


Figure III.2.4 - Optimal PHEV System Efficiency Controller Design

Table III.2-3 - Fuel Economy Performance, Design Label 698b, Charge Sustaining Mode

| Drive Cycle | Cycle Kinetic Intensity [1/mile] | Baseline Fuel Consumption [g diesel fuel] | Engine Optimal Controller, Fuel Consumption [g diesel fuel] | System Optimal Controller, Fuel Consumption [g diesel fuel] |
|---|---|---|---|---|
| **NYCC (Matlab)** | 4.2 | 1047.0 | 305.3 (70.8% reduction) | 302.6 (71.1% reduction) |
| **CSHVC (Matlab)** | 1.9 | 2049.0 | 928.0 (54.7% reduction) | 904.1 (55.9% reduction) |
| **UDDS_HD (Matlab)** | 0.61 | 1743.2 | 1204.9 (30.9% reduction) | 1135.2 (34.9% reduction) |
| **CARB_HHDDT (GT)** | 0.17 | 11025.4 | 7066.4 (35.9% reduction) | 6409.2 (41.9% reduction) |

*Task 4 – Hybrid Drive System Definition*

The target PHEV system architecture has been defined, as shown in Figure III.2.5. Two SMG180/120 electric motors (200 Nm/ 80 kW peak performance) with two AC/DC inverters were selected for integration with the 2PG transmission. These components were selected for two main reasons: they are readily available (Fiat 500e) and they demonstrate the flexibility of the transmission design.

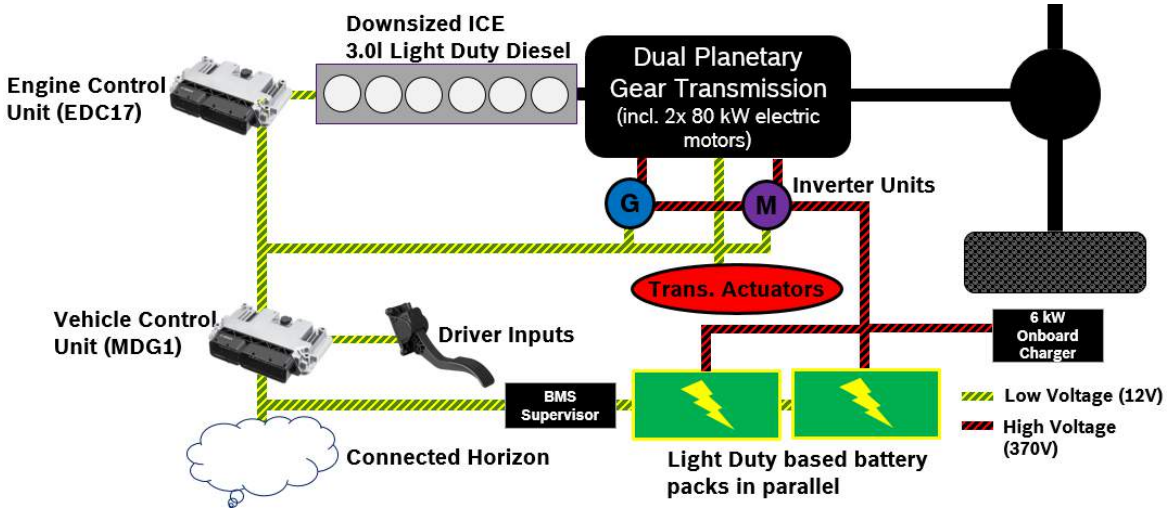


Figure III.2.5 - Optimal PHEV System Efficiency Controller Design

Ricardo has been engaged at each step of BP1's development activities, ensuring that the various transmission architectures which emerged from the concept selection were feasible to manufacture and control, based on their extensive transmission and electrical vehicle development experience. An in-depth design review was conducted, where each of the 3 final designs were evaluated amongst each other and against the baseline transmission. 3D Models of each design were also created, as shown in Figure III.2.6. Design 698b was selected due to its smaller packaging size, lower estimated cost, and higher efficiency.

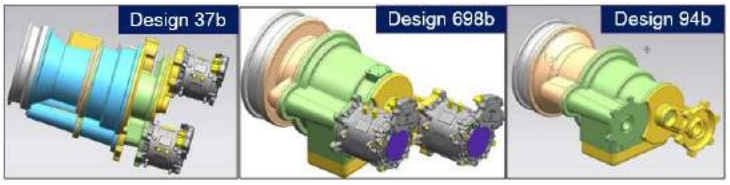


Figure III.2.6 - 2PG Transmission 3D Designs for Chassis Packaging Evaluation

## Conclusions

An innovative PHEV powertrain has been developed which can reduce fuel consumption reduction by over 50% in charge sustaining mode when utilizing a multi-mode powersplit transmission with integrated electric motors. Over 18 million designs were evaluated against given collocation, functional, and performance attributes, yielding 83 feasible designs. Of those 83 configurations, 14 were estimated to meet or exceed the program objective in charge sustaining mode. Design label 698b has been selected as the target architecture for the integration and demonstration phases of the project. Greater than 56% fuel consumption reduction has been achieved in simulation when operating in charge sustaining mode (~19 MPG). The flexible multi-mode/ powersplit transmission also enables an estimated all-electric range of greater than 60 miles, at an energy efficiency of 1.51 miles/kW-hr (56 MPGe) on the target drive cycle (CSHVC).

## Key Publications

1. Freitag, A., U.S. Department of Energy Vehicle Technologies Office 2017 Annual Merit Review and Peer Evaluation Meeting, June 7, 2017, Washington, D.C. Project ID-gi190, MURECP: Medium-duty Urban Range Extended Connected Powertrain

2. NACV 2017 Press Release: Bosch demonstrates future commercial vehicle technology- Automated, connected and electrified technologies empower the drive – today and tomorrow

3. U.S. Provisional Patent Application No.: 62/564,576; Filing Date: September 28, 2017 Title: MULTI-MODE POWER SPLIT HYBRID TRANSMISSION WITH TWO PLANETARY GEAR MECHANISMS Inventor: Ziheng PAN et al.

## III.3 Bidirectional Wireless Power Flow for Medium Duty Vehicle Grid Connectivity

**Omer C. Onar, Technical Principal Investigator**
Oak Ridge National Laboratory
Power Electronics and Electric Machinery Group
National Transportation Research Center
2360 Cherhala Boulevard
Knoxville, TN 37932
Phone: (865) 946-1351
E-mail: onaroc@ornl.gov

**Steven Sokolsky, Project Principal Investigator**
CALSTART
1509 Wendy Lane
Madison, WI 53716
Phone: (626) 744-5604
E-mail: ssokolsky@calstart.org

**Lee Slezak, Technology Manager**
U.S. Department of Energy
Phone: (202) 586-2335
E-mail: Lee.Slezak@ee.doe.gov

Start Date: October 1, 2016 End Date: December 31, 2019
Total Project Cost: $2,631,321 DOE share: $1,949,007 Non-DOE share: $682,314

### Project Introduction

Wireless power transfer (WPT) is a paradigm shift in electric-vehicle (EV) charging that offers the consumer an autonomous, safe, and convenient option to conductive charging and its attendant need for cables. With WPT, charging process can be fully automated due to the vehicle and grid side radio communication systems, and is non-contacting; therefore, issues with leakage currents, ground faults, and touch potentials do not exist. It also eliminates the need for touching the heavy, bulky, dirty cables and plugs. It eliminates the fear of forgetting to plug-in and running out of charge the following day and eliminates the tripping hazards in public parking lots and in highly populated areas such as shopping malls, warehouse loading areas, recreational areas, parking buildings, etc. Furthermore, the high-frequency magnetic fields employed in power transfer across a large air gap are focused and shielded, so that fringe fields (i.e., magnetic leakage/stray fields) attenuate rapidly over a transition region to levels well below limits set by international guidelines for the public zone. With the bidirectional wireless power transfer, not only vehicles can be wirelessly charged, but also the vehicles can wirelessly provide power back to the grid or the facility. With bidirectional power flow, vehicles can be enabled to provide micro grid or grid support or ancillary services. In the case of an outage, vehicle batteries can also serve as an emergency backup power for a period. In this project, CALSTART, ORNL, UPS, Workhorse Group, Cisco Systems, and the University of Tennessee, Knoxville proposed to model, research, analyze, design, develop, integrate, and demonstrate a bi-directional wireless power transfer system (BWPT) suitable for Class 5 and Class 6 medium-duty PHEV delivery trucks. The project team will design, develop, integrate, and test a bi-directional wireless charging system capable of meeting the 11-inch ground clearance needed for UPS delivery trucks. After integrating to a Workhorse manufactured plug-in hybrid electric vehicle (PHEV), the system performance will be demonstrated at the deployment site.

## Objectives

The overall project objectives can be summarized as follows:

1. Provide an automated, high power, interoperable, high-efficiency wireless charging of plug-in electric medium duty delivery trucks with a nominal ground clearance of approximately eleven (11) inches.

2. Optimize the add-on vehicle-side wireless charging components through integration and utilization of already existing vehicle-side components while implementing grid-side controls and regulations to reduce the vehicle-side cost, size, volume, and complexity.

3. Utilize bi-directional wireless charging systems when trucks are parked in the yard for staging to provide grid support applications or ancillary or grid support services such as frequency regulation, load leveling/peak shaving/load factor improvement/reactive power support/demand charge management, and spinning/non-spinning reserves.

4. Provide an integrated > 20 kW wireless charging system (grid to vehicle) with high efficiency (85%) while meeting the international guidelines on electromagnetic and electric field emissions during charging and include all other appropriate safety features.

5. In vehicle-to-grid mode, achieve 6.6 kW wireless power transfer to building or grid loads.

6. Provide modeling and analysis of the benefits of wireless charging technology with respect to operational efficiency improvements and overall vehicle and building energy efficiency.

## Approach

Wireless charging of plug-in electric vehicles (PEV) has received significant interest due to its inherent benefits such as safety, convenience, flexibility, and high efficiency. Wireless power transfer can displace today's plug-in chargers and promote the adoption of electric vehicles with its increased convenience since there are no cables to trip over, no heavy duty plugs or connectors to handle, no concerns about inadvertent disconnection, no fear of forgetting to plugin and the technology is unaffected by the weather conditions. Although the system principles sound very simple and rely on the well-known Ampere's and Faraday's Laws, the vehicular integration, control systems, and the communications systems are quite challenging to design, build, integrate, and control. Starting from the AC grid to the vehicle battery terminals, the system power converters must be well designed and operated in order to achieve high efficiency. In addition, power flow control to the pick-up system should be resolved where the control parameters (DC link voltage, frequency, duty cycle, phase-shift, etc.) are actively controlled to improve efficiency while meeting the vehicle-side target voltage, current, and/or power. Simultaneously, vehicle-side DC link or battery voltage, current, temperature, and the state-of-charge (SOC) should be carefully monitored and fed-back to the primary side for controls. Moreover, the battery management system (BMS) or other vehicle-side converters (onboard chargers or DC/DC converters) should be monitored for safety. The bidirectional wireless charging system that will be used in this project is shown in Figure III.3.1. This is the overall system architecture that is determined and agreed upon by the technical team. For this architecture, the baseline performance metrics have been defined and system specifications are currently being worked on as the proper sizing of the power electronic devices and passive components are important to meet the vehicle charging demands. Since the overall system architecture is now defined, the team is cascading down the system design to the subsystems, including both the grid and vehicle sides, and then to the components for hardware fabrication. As shown in Figure III.3.1, system utilizes a three-phase rectifier/inverter system that interfaces the system to the grid.

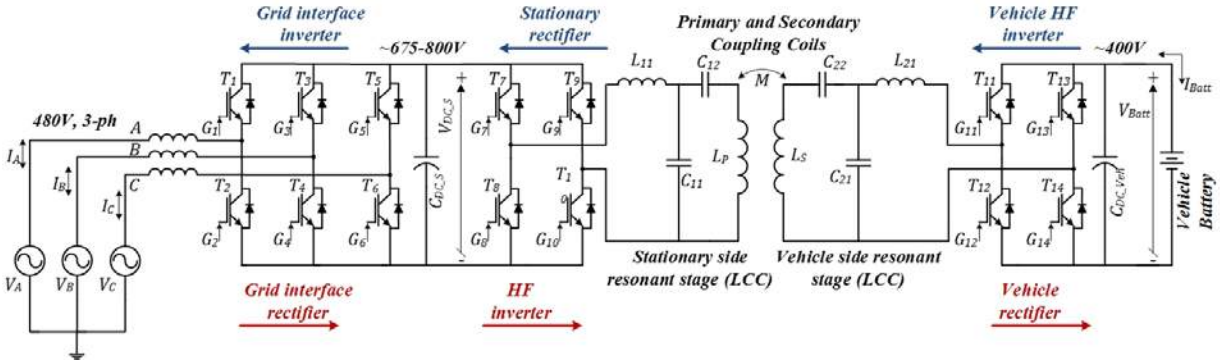


Figure III.3.1 - System level diagram of the proposed architecture for the bidirectional wireless charging system.

The proposed system is composed of a high-power wireless charging system that will be integrated into a commercially available and operational UPS PHEV delivery truck. The block diagram in Figure III.3.1 illustrates the proposed bi-directional wireless power system architecture. During charging, an active-front end rectifier with power factor correction (PFC), delivers power from the grid with high power factor to the high frequency power inverter's input. The input (grid) current is controlled in order to regulate the inverter input voltage, depending on the amount of power to be transferred to the battery. The high-frequency power inverter generates the high-frequency current for the primary coupling coil. The high-frequency transformer between the inverter and the primary coil provides galvanic isolation for safety and protection of the equipment. The transformer also provides voltage matching for the system and provides control flexibility for the voltage. On the vehicle side, there is a receive coil with a tuning capacitor, a rectifier/inverter, and a filter capacitor. During discharging or vehicle battery powering the AC grid/building loads, the vehicle-side converter is operated in an inverter mode and delivers high-frequency current to the vehicle coil. The vehicle-side coil generates a magnetic field that is linked to the ground coil. The ground coil induces a high frequency voltage that is rectified and inverted to 60Hz to power the building loads or to provide power to the AC grid.

## Results

The first step in the design process was to determine the architecture of the active front-end rectifier/inverter which is a bidirectional grid interface converter. Technical team performed a very comprehensive literature review on three-phase bidirectional grid-connected power electronics interfaces. Among other candidate interface topologies, team determined to use the two-level voltage source converter (VSC) due to the advantages among the other topologies as shown in Table III.3-1.

Table III.3-1 - Comparison of selected power electronics architectures.

| Converter topology | Two-level voltage-source converter | Four-leg two-level voltage-source converter | Two-level current-source converter |
|---|---|---|---|
| Number of devices | 6 IGBTs/MOSFETs, 6 diodes | 8 IGBTs/MOSFETs, 8 diodes | 6 IGBTs / MOSFETs, 6 diodes |
| Filtering requirements | 3 inductors at AC-side, 1 capacitor in DC-link | 4 inductors at AC-side, smaller capacitor in DC-link | 3 LC filters at AC-side, 1 inductor in DC-link, additional devices needed for 4-quadrant power flow |

The parameters for the grid-interface converter are also designed and analyzed. Accordingly, the input inductors have to be 750-780 µF and the DC-link capacitor has to be 1 mF in order to meet the maximum

allowed input current ripple and DC-link voltage ripple requirements. As the next step of the converter design, the switching-model (detailed model) and the average model of the grid-interface converter have been developed. The switching model is provided in Equation (1) whereas Equation (2) summarizes the average model that is developed.

$$\begin{cases} \dfrac{d\vec{i_{ph}}}{dt} = -\vec{i_{ph}}\dfrac{R}{L} + \dfrac{\vec{v_{grid}}}{L} - \dfrac{1}{3L}\begin{bmatrix} 2 & -1 & -1 \\ -1 & 2 & -1 \\ -1 & -1 & 2 \end{bmatrix}\vec{S_{ph}}\cdot v_{dc} \\ \dfrac{dv_{dc}}{dt} = \dfrac{1}{C}\left(\vec{s_{ph}}\right)^{T}\cdot\vec{i_{ph}} - \dfrac{v_{dc}}{CR_{dc}} \end{cases} \quad (1)$$

$$\begin{cases} \dfrac{d\vec{\bar{i}_{ph}}}{dt} = -\vec{\bar{i}_{ph}}\dfrac{R}{L} + \dfrac{\vec{\bar{v}_{grid}}}{L} - \dfrac{1}{L}\vec{d_{ph}}\cdot\overline{v_{dc}} + \dfrac{1}{3L}\begin{bmatrix} 1 & 1 & 1 \\ 1 & 1 & 1 \\ 1 & 1 & 1 \end{bmatrix}\cdot\vec{d_{ph}}\cdot\overline{v_{dc}} \\ \dfrac{d\overline{v_{dc}}}{dt} = \dfrac{1}{C}\left(\vec{d_{ph}}\right)^{T}\cdot\vec{\bar{i}_{ph}} - \dfrac{\overline{v_{dc}}}{CR_{dc}} \end{cases} \quad (2)$$

Based on the system parameters, a phase-locked loop (PLL) controller is designed in order to have a fast and precise synchronization with the grid. The performance of the PLL controller is presented in Figure III.3.2 with a damping factor of $\sqrt{2}/2$ and bandwidth of 120 (two times the grid frequency). According to Figure III.3.2, it is seen the PLL controller designed can lock into the grid phase-angle in less than quarter line period.

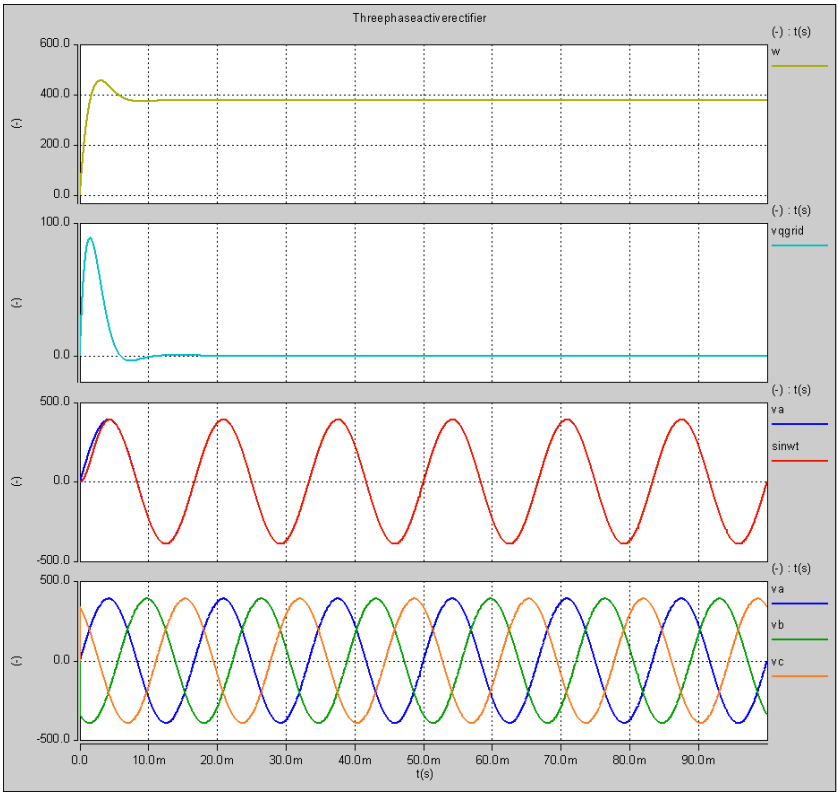


Figure III.3.2 - Phase-locked-loop (PLL) grid synchronization performance; red-line is the grid voltage and blue-line is the PLL output to the main controller.

Next, team simulated the grid-interface converter in stand-alone mode (feeding a DC voltage source) in order to evaluate the performance of the bidirectional operation with inductive, capacitive, and unity power factor operations. With 24 kW output power, system performance with a power factor of +0.6 is shown in Figure III.3.3. In Figure III.3.4, the system performance with a power factor of -0.6 is shown. According to Figure III.3.3 and Figure III.3.4, it is seen that the system can be operated in both inductive (reactive power absorption) and capacitive (reactive power injection) modes. Reactive power can be used in voltage control and regulation applications when supporting the grid with a grid connected vehicle or a stationary energy storage system.

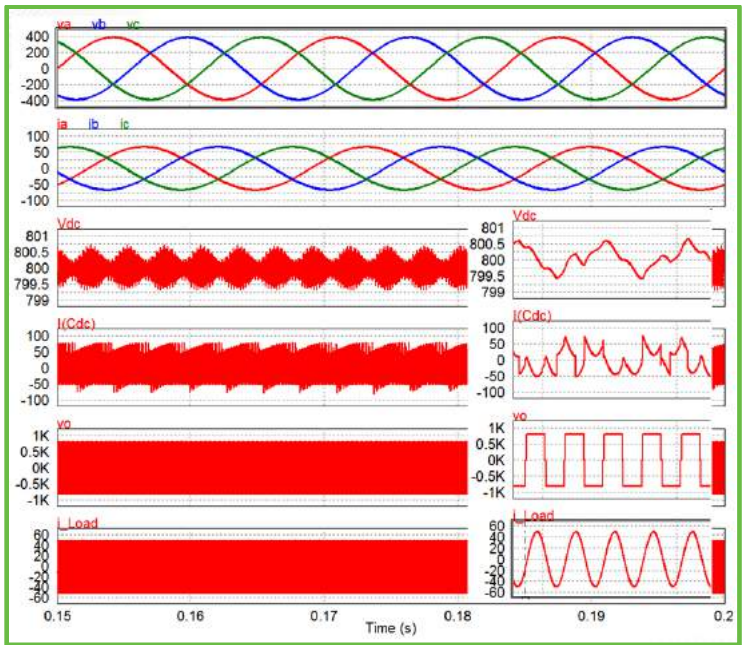


Figure III.3.3 - Simulation results of the grid-interface converter in stand-alone mode with 24 kW output power and inductive reactive power operation with a power factor of +0.6

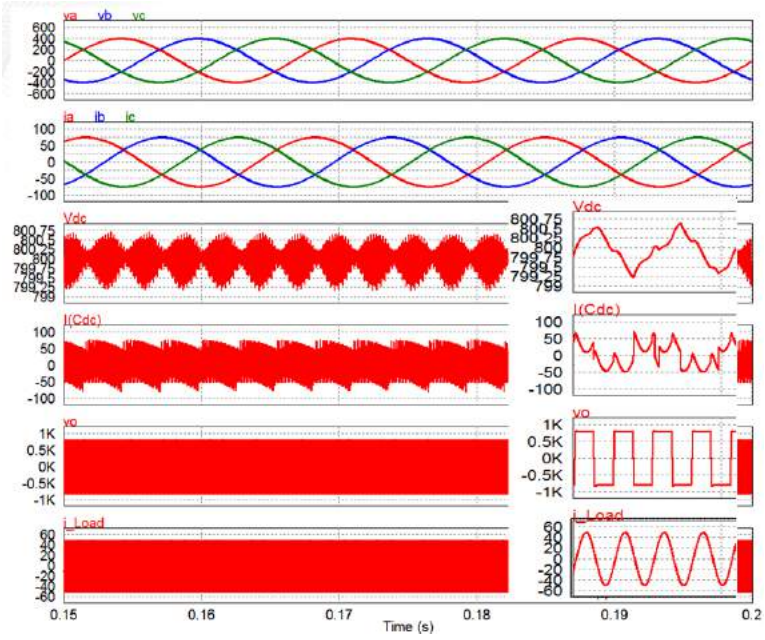


Figure III.3.4 - Simulation results of the grid-interface converter in stand-alone mode with 24 kW output power and capacitive reactive power operation with a power factor of -0.6.

Operational waveforms of the grid-interface converter with unity power factor (~0.99) are given in Figure III.3.5. In this case, apparent power is almost equal to the grid active power without absorbing or injecting reactive power from/to the power grid.

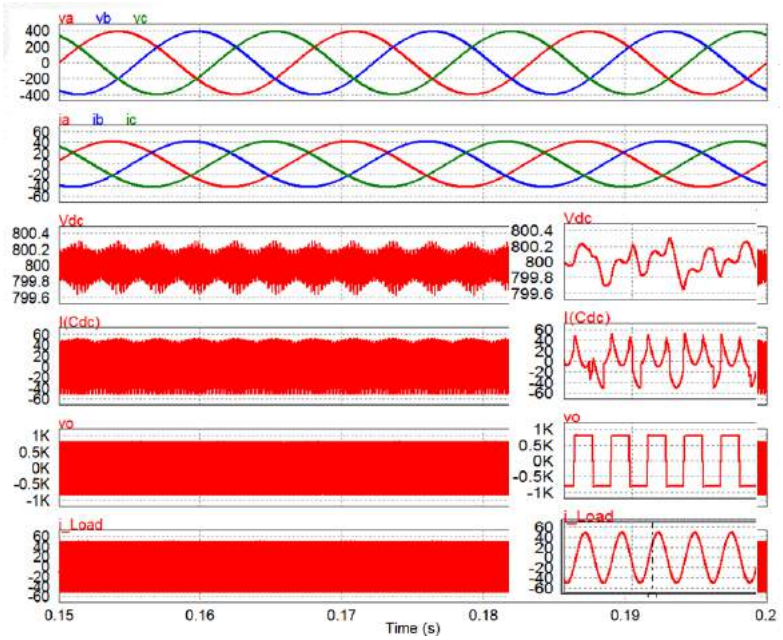


Figure III.3.5 - Simulation results of the grid-interface converter in stand-alone mode with 24 kW output power with a power factor of 0.99.

## Conclusions

From the start of this project in May 2017, the team has been working on modeling, simulations, analysis, and design of the system power conversion stages. This report mostly focuses on the progress made on the grid-interface power electronic converter which is a key subsystem for the bidirectional operation and power flow of the proposed technology. A grid-interface power electronic converter is determined based on the available converter architectures in the literature based on comprehensive evaluations and comparisons. A phase-locked-loop system is also designed and integrated with the three-phase rectifier/inverter model developed for this project. The simulation results demonstrate that the system can be operated in full active power, inductive reactive, and capacitive reactive modes of operation. During the rest of the budget period, all four-quadrant operation modes will be achieved including discharging inductive, discharging capacitive, charging inductive, and charging capacitive. The rest of the power conversion stages including the high-frequency power inverter, electromagnetic couplers and the resonant tuning configuration, and the vehicle side bidirectional rectifier/ inverter will be modeled, simulated, analyzed, and designed. Towards the end the first budget period, system parameters and power electronic devices will be determined before building the hardware required for the proposed system.

## Key Publications

No publications submitted yet since the project started in May 2017.

## III.4 Multi-Speed Transmission for Commercial Delivery Medium Duty PEDVs

**Bulent Chavdar, Principal Investigator**
Eaton Corporation
26201 Northwestern Highway
Southfield, MI 48076
Phone: (248) 226-6219
E-mail: BulentChavdar@Eaton.com

**Lee Slezak, Technology Manager**
U.S. Department of Energy
Phone: (202) 586-2335
E-mail: Lee.Slezak@ee.doe.gov

Start Date: October 1, 2014 End Date: October 31, 2017
Total Project Cost: $3,749,710 DOE share: $2,999,755 Non-DOE share: $749,955

### Project Introduction

The project addresses the following technical barriers:

- There are performance gaps between Electric Vehicles (EVs) and Internal Combustion Drive Vehicles (ICDVs) in terms of range, top speed, acceleration, and gradeability.
- There is no reliable, affordable, scalable, and low weight, multi speed transmissions available to the medium duty electric vehicle manufacturers on the market.
- The public acceptance of electric vehicles is low.

### Objectives

Overall objectives include increasing public acceptance and market penetration of EVs into the delivery truck market, which now relies heavily on gasoline and diesel. Multi speed transmission is a key sub-system to make medium duty electric vehicles (MD-EVs) more efficient and to provide a better overall payback. Hence, the main objective of this project is to develop a reliable, efficient, compact and low weight multi-speed transmission for MD-EVs to expand the vehicle's operating performance and range. The objectives of this budget period are completing the design, controls and the shift strategy of multi-speed transmission, prototyping the transmission and completing the vehicle integration and validation testing.

### Approach

We have recently completed the 3 year project successfully. Our approach started with the electric vehicle customer requirements and system analysis. The approach continued with the transmission concept development/selection, designing, prototyping, testing and validation. EV efficiency was improved by providing a multi-speed transmission and a shift controls strategy that operates the motor at its peak efficiency region and maximizes the capture of the regenerative brake energy. High gradeability and fast acceleration were provided by a low gear. Top speed and range were increased with a high gear in direct drive and high transmission efficiency. Advanced drive cycle data banks, modeling, testing and vehicle evaluation capabilities available at ORNL and NREL were leveraged. The opportunities for compact design, lightweighting (hollow shafts, aluminum housings), and additive manufacturing technologies were explored or implemented. A low cost and modular EV-Transmission was designed with flexibility to meet the needs of electric trucks from Class 2b to 7 (or 8500 lb. to 36K lb. GVW).

The project was conducted over three budget periods: Budget Period 1: Technology Development – The high-level vehicle powertrain models were used to optimize candidate transmission architectures and ratios along

with a variety of traction motor characteristics for concept selection. The detailed driveline designs and component dynamics were investigated to meet medium duty EV requirements.

Budget Period 2: Technology Development and Prototype Demonstration – The modeling and simulations with multi-speed transmissions were extended to other medium and heavy duty EV platforms. Clean sheet design of a compact, lightweight, flexible, and modular, 3 and 4-speed transmission was completed. Development of novel shifting and controls strategies started. The procurement of the prototype transmission and the controller hardware started.

Budget Period 3: Technology Integration, Testing, and Demonstration – The prototyping of 4-speed Automated Mechanical Transmission was completed. The transmission controls system and software development and preliminary gearbox dyno tests were done at Eaton. Integrated powertrain hardware in the loop (HIL) tests were conducted at ORNL. One of the prototype units was fully integrated into Proterra BE35 demonstration electric bus. Fine tuning of shift control strategy was conducted on the integrated vehicle at Eaton Marshall Proving Grounds. The vehicle was tested and the performance gains were validated at NREL.

## Results

### *Prototyping*

Totally 7 prototype transmissions were build: 6 of the units are fully functional and one unit is a display unit. Figure III.4.1 shows the prototyping of the 4-Speed Automated Mechanical Transmission in progress.

Figure III.4.1 - Left: Components of 4-Speed AMT are laid out before the assembly. Right: Eaton 4-Speed EV-AMT display unit integrated with a UQM Electric Motor.

### *Preliminary testing at Eaton*

Preliminary testing of the prototype transmissions at Eaton included the following tests: Initial shift calibration tests on bench, transmission break-in and efficiency tests on dyno, NVH testing in anechoic chamber, and steady-state speed and torque tests on dyno. Figure III.4.2 and Table III.4-1 show the transmission efficiency test results of three prototype units. The overall average efficiency of 4-speed EV-AMT is %97 +/- 1.5. Fourth gear is the most efficient gear since it is in direct drive. The transmission efficiency is higher at lower speeds, higher torques and higher gears. Steady state temperature tests involved continuous running of transmission at various operating conditions representing the electric transit bus duty cycle. The transmission oil sump temperature stays below 250 F during ten minute continuous runs. High speed operations at second and third gears cause the greatest temperature rise to 220 F that is still well below the allowable temperature limit of 250 F.

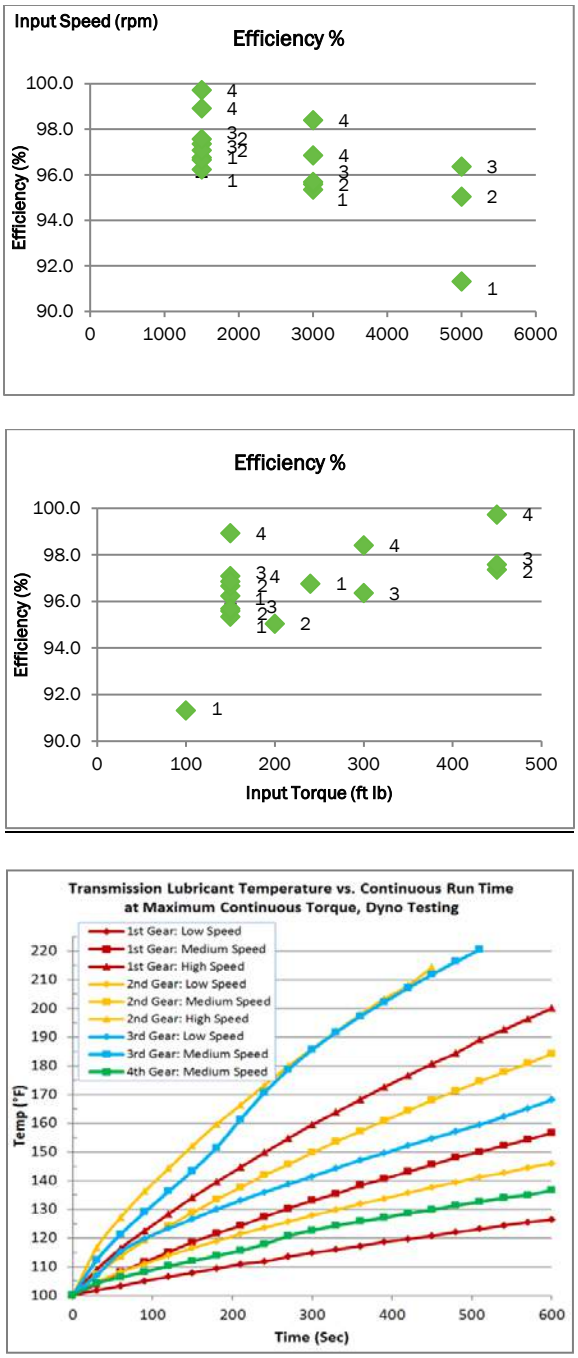


Figure III.4.2 - Top: Transmission efficiency vs input speed. Middle: Transmission efficiency vs input torque. The legends indicate gear positions. Bottom: Continuous run temperature rise tests. Oil sump temperature stayed below 250 F during the tests.

Table III.4-1 - Transmission efficiency test results

| | % Efficiency-Unit#2 | % Efficiency-Unit#3 | % Efficiency-Unit#4 | Average Efficiency (%) |
|---|---|---|---|---|
| **1st gear** | 95 | 96 | 94 | 95 |
| **2nd gear** | 96 | 97 | 96 | 96 |
| **3rd gear** | 97 | 98 | 95 | 96 |
| **4th gear** | 99 | 100 | 97 | 99 |
| **Overall** | 97 | 98 | 96 | 97 |

*Powertrain HIL tests at ORNL*

Figure III.4.3 shows the integration of powertrain consisting of Eaton 4-speed EV AMT and UQM Electric Motor on the HIL test setup at ORNL. Figure III.4.4 shows the efficiency gains as compared to the baseline 2-speed transmission. 4-speed transmission provides up to 15% efficiency improvement over 2-speed baseline with the same final drive ratio (FDR) of 6.2. FDR was the same since the 4-speed transmission is operated in 2-speed mode to make the comparisons. In the real life case of Proterra BE35 Electric Bus the FDR is 9.8 with 2-speed transmission. The small and efficient FDR of 6.2 was enabled by the new 4-speed transmission. Final drive with 6.2 ratio is 3% more efficient than the final drive with 9.8 ratio. Efficiency gain of 3% in FDR translates into additional 5 to 6% efficiency improvement in the drive cycles. 4-speed transmission can be launched either on 1$^{st}$ gear or 2$^{nd}$ gear in most grades. Launching on 1$^{st}$ gear provides slightly better efficiency gains than launching on 2$^{nd}$ gear as shown in Figure III.4.4. Zero to 50 mph acceleration is improved 30% with 4-speed transmission on HIL as compared to the published test data of baseline EV with 2-speed transmission on Altoona test track (Ref.1). Furthermore, gradeability is doubled from 13mph to 26 mph at 10% grade, with 4 speed transmission on HIL as compared to the baseline EV with 2-speed on Altoona test track.

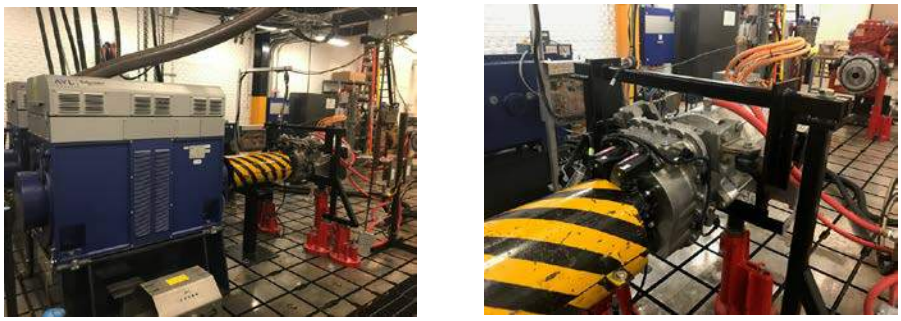

Figure III.4.3 - Eaton 4-speed EV AMT and UQM Electric Motor on the HIL test setup at ORNL

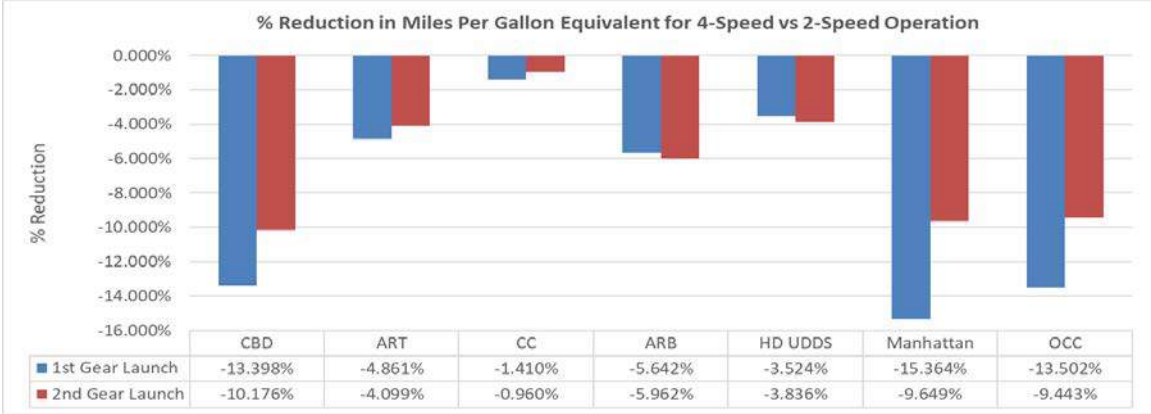


Figure III.4.4 - Energy consumption reduction in mpg-de between 4-speed and 2-speed configurations.

*Chassis dyno tests at NREL*

Proterra BE35 Electric Bus integrated with 4-speed transmission and FDR of 6.2 was tested on NREL's heavy-duty chassis dynamometer as shown in Figure III.4.5. Five different drive cycles were selected that vary in distance, acceleration rates, number of stops and driving speeds as listed in Table III.4-2. Acceleration rate and gradeability tests were also performed for two different payloads for the vehicle.

Figure III.4.5 - Vehicle mounted on NREL's heavy-duty chassis dyno with all data acquisition implemented and ready for testing

**Table III.4-2 - Chassis dynamometer selected drive cycle parameters**

| Cycle | Time (mins) | Distance (mile) | Max Sp. (mph) | Avg Sp. (mph) | Avg Driving Sp. (mph) | KI (1/mile) | Stops (#) |
|---|---|---|---|---|---|---|---|
| **Manhattan Bus Cycle** | 18 | 2.1 | 25 | 7 | 11 | 9.1 | 20 |
| **Orange County Bus** | 32 | 6.5 | 41 | 12 | 16 | 3.6 | 31 |
| **Urban Dynamometer Driving Schedule (UDDS)** | 18 | 5.6 | 58 | 19 | 28 | 0.6 | 14 |
| **Altoona - Modified Business-Arterial-Commuter (BAC)*** | 42 | 13.1 | 40 | 19 | 22 | 1.3 | 51 |
| **World Harmonized Drive Cycle (WHDC)** | 30 | 11.2 | 55 | 22 | 26 | 0.4 | 12 |

The efficiency improvements between 4-speed transmission and 1-speed and 2-speed baseline configurations at each drive cycle are shown in Figure III.4.6.The 4-speed transmission was run in 1-speed mode on 3rd gear and 2-speed mode on 1st and 3rd gears to emulate the baselines. Up to 17% and 13% efficiency gains were measured with 4-speed transmission as compared to 1-speed and 2-speed baselines depending on the drive cycles. As in the case of HIL testing the chassis dyno test results do not even include the 5-6% additional efficiency gains coming from the FDR change from 9.8 to 6.2. Chassis dyno tests verify the earlier predictions made in modeling simulations that the 4-speed transmission provides up to 20% improvement in energy efficiency as compared to the real baseline vehicle depending on the drive cycle (Table 6 of Ref. 2).

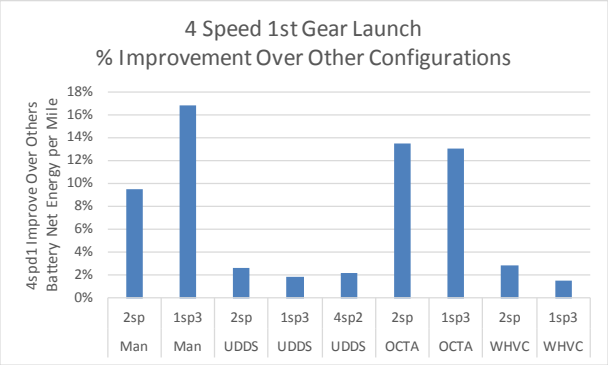


Figure III.4.6 - Efficiency improvement verification test results on NREL's heavy-duty chassis dyno.

## Conclusions

- All required project milestones have been achieved. Project is completed on time and on budget
- Transmission concepts were developed and a 4-speed AMT was selected as the winning concept
- Vehicle model was developed and validated with on-route data of Proterra BE35 electric transit bus
- Transmission and driveline gear ratios were optimized. Transmission system design was completed
- Simulations predicted up to 20% increase in system energy efficiency depending on drive cycles, a top speed of greater than70 mph on flat road, 40% faster acceleration and a doubled gradeability with 4-speed transmission as compared to the baseline EVs
- Prototyping of 6 fully functional and one display units of 4-speed transmission were completed
- Prototype units were integrated on dynos and tested at Eaton and ORNL
- Powertrain in the loop tests at ORNL validated all the performance gains predicted by the simulations
- One unit was integrated on Proterra BE35 Electric Bus and tested at Eaton and NREL
- Chassis Dyno Tests at NREL verified the simulation results and also the HIL test results at ORNL
- As the result of this project the performance gaps between MD-EVs and MD-ICDVs were either reduced (e.g., range), or eliminated (e.g., gradeability and top speed), or reversed in favor of EVs (e.g., acceleration performance)
- All performance targets have been met or exceeded. Feedback from the demonstrations to the stakeholders of this project showed high degree of excitement and acceptance on the 17 ton electric bus with 4-speed transmission.

- The new 4-speed EV transmission is efficient, reliable, modular, scalable, light weight, small size, and will be affordable. Furthermore, 4-speed transmission enables downsizing of motor, battery and final drive thereby reducing the total system cost.

## References

1. Partial STURAA Test, 12 year, 500,000 mile bus from Proterra Inc. Model BE35, PTI-BT-R1305-P, The Thomas D. Larson Pennsylvania Transportation Institute, May 2013.

2. DE-EE0006843 FY 2016 Vehicle Systems Annual Progress Report.

## Key Publications

1. Chavdar, B., 2015-DOE-AMR PowerPoint Presentation at Arlington, Washington, on June 11, 2015. Project ID-vss161, Multi-Speed Transmission for Commercial Delivery Medium Duty Plug-In Electric Drive Vehicles.

2. Chavdar, B., FY 2015 Vehicle Systems Annual Progress Report (FY 2015 VS APR), September, 2015.

3. Chavdar, B., 2016-DOE-AMR PowerPoint Presentation at Arlington, Washington, on June 9, 2016. Project ID-vss161, Multi-Speed Transmission for Commercial Delivery Medium Duty Plug-In Electric Drive Vehicles

4. Chavdar, B., Deng, Y., Naghshtabrizi, P., Genise, T., “Modular Multi-Speed Transmission for MD EV”, CTI Symposium China, Automotive Transmissions, HEV and EV Drives, 5th International Congress and Expo, 21-23 September, 2016, Shanghai, China.

5. Chavdar, B., FY 2016 Vehicle Systems Annual Progress Report (FY 2016 VS APR), September, 2016

6. One display unit of the new 4-speed EV Transmission was displayed at the IAA Commercial Vehicles Trade Fair in Hannover on September 22-29, 2016.

7. Chavdar, B., FY 2016 Vehicle Systems Annual Progress Report (FY 2016 VS APR), October, 2016.

8. Chavdar, B., Genise, T., Naghshtabrizi, P., Papp, G., “Development of Robust and Modular Drive System for MD-EV”, 11th International CTI Symposium, Automotive Transmission, HEV and EV Drives, 15-18 May, 2017, Novi, MI, USA

## III.5 Cummins Electric Truck with Range-Extending Engine

**John Kresse, Principal Investigator**
Cummins, Inc.
1900 McKinley Avenue
Columbus, IN 47201
Phone: (812) 377-3111
E-mail: john.kresse@cummins.com

**Lee Slezak, Technology Manager**
U.S. Department of Energy
Phone: (202) 586-2335
E-mail: Lee.Slezak@ee.doe.gov

Start Date: July 1, 2016 End Date: October 31, 2019
Total Project Cost: $6,295,281 DOE share: $4,126,570 Non-DOE share: $2,168,711

### Project Introduction

Many medium duty commercial vehicles (classes 5 - 7) have daily duty cycles with energy requirements that lend themselves to the use of a plug-in electrified powertrain. However, often the duty cycle energy requirements are near, or over, the limits that can be served by a pure battery electric vehicle (BEV). A range extending electric vehicle (REEV) architecture may enable the fleet operator's needs to be met using a substantial amount of grid energy, while also allowing the vehicle to fulfill a number of more challenging duty cycles typically realized by conventionally powered vehicles.

The Cummins Electric Truck with Range Extending Engine (ETREE) project makes use of grid energy to offset fuel consumption used by medium duty commercial vehicles and, specifically, those that are used for class 6 urban/suburban pickup and delivery applications.

The ETREE project aims to develop a class 6 (GVW 26k lb.) box truck, with equivalent performance to conventional diesel powered trucks, that reduces fuel consumption by at least 50% over a wide range of urban/suburban pickup and delivery applications.

### Objectives

In the target vehicle (a Kenworth K270 class 6 box truck which is usually equipped with a 6.7L diesel engine and automatic transmission), the electrified powertrain will achieve at least a 50% fuel consumption reduction for a wide range of pickup and delivery work day drive cycles.

The Kenworth K270 with the ETREE powertrain and complementary systems will be demonstrated in simulation, in a powertrain test cell, on a test track (SAE J1321 Type II testing), and in fleet operation.

### Approach

ETREE is a Cummins-led project with assistance from the following partners:

- PACCAR, Inc.,
- Argonne National Laboratory (ANL),
- National Renewable Energy Laboratory (NREL), and
- The Ohio State University (OSU)

The project will:

- Develop target **work day** duty cycles by employing NREL's Fleet DNA and DRIVE Analysis Tools.

- Use simulation (by ANL, Cummins and OSU) to determine component requirements for a plug-in series hybrid.
- Build two test vehicles, beginning in Q4 2017, which include:
  - The use of applicable electrified vehicle accessories,
  - Appropriate thermal management systems, and
  - An electric braking system (EBS) to promote kinetic energy recovery while maintaining conventional vehicle drivability.
- Employ a "test heavy" project schedule (simulation, powertrain test cell located at Cummins Technical Center, test tracks, and fleet operators) to confirm predicted results.
- Identify & deploy, beginning in Q4 2018, test vehicle(s) to fleet operators that will likely use these vehicles in production.

## Results

In FY 2017, the ETREE project developed target work day duty cycles which are used to measure the project against its objectives. These work day duty cycles, denoted NREL 80 and NREL 100 pickup and delivery (P & D), are 80 and 100-mile duty cycles and are applicable for class 6 pickup and delivery commercial vehicles. The required duty cycle energies are in the 80th and 95th percentile of all measured duty cycles available in NREL's Fleet DNA database for pickup and delivery applications. These cycles contain vehicle speed and road grade, versus time, and include highway, suburban, and urban segments. Also included are large amounts of stopped operation as is typically observed in these applications (as goods are loaded or unloaded during the work day). Discussion with many perspective fleet operators indicate these cycles are representative of the types of cycles encountered by this widely varied truck application.

Partial STURAA Test, 12 year, 500,000 mile bus from Proterra Inc. Model BE35, PTI-BT-R1305-P, The Thomas D. Larson Pennsylvania Transportation Institute, May 2013. Simulation was used by ANL, Cummins and OSU to identify the components to ensure the fuel consumption reduction targets are met for the target work day duty cycles. The results, which include a number of work day duty cycles beyond the NREL-developed cycles, are shown in Figure III.5.1.

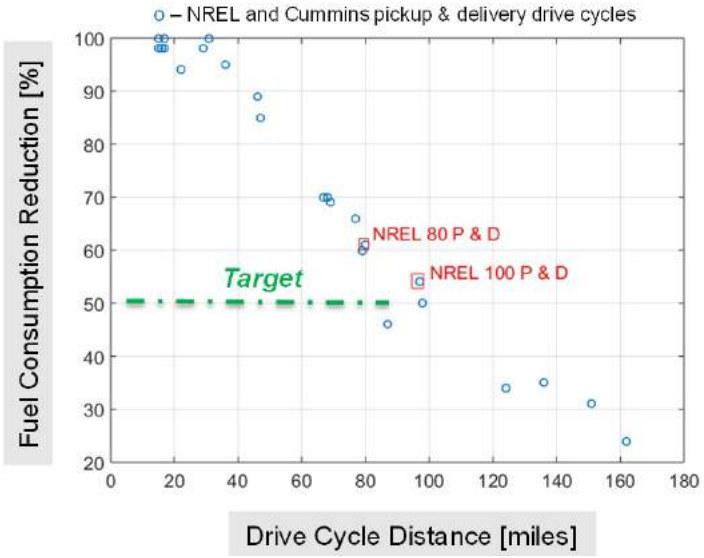


Figure III.5.1 - Predicted fuel consumption reduction, for the ETREE project, on a wide variety of work day duty cycles

The simulation process was used to select the powertrain components for the series hybrid architecture; these are described in Table III.5-1.

Table III.5-1 - Summary of ETREE Powertrain Components

| Component | Description |
|---|---|
| **Traction Motor** | 160 kW permanent magnet traction motor |
| **Transmission** | Allison 3000 ETREE transmission with input stop-start system |
| **Nominal DC bus voltage** | 700 VDC |
| **Energy Storage** | 112 kW-h NMC Li-ion battery |
| **Range Extender – Generator** | 130 kW permanent magnet generator |
| **Range Extender – Engine** | 155 kW ISB4.5 w/ full complement of aftertreatment components (diesel particular filter, selective catalytic reduction, diesel oxidation catalyst) |
| **Final Drive Ratio** | 5.29 |

The first three quarters of 2017 were focused on powertrain-in-the-loop test cell testing. The first step was establishing baseline fuel consumption for the conventional powertrain (a 6.7L diesel with an automatic transmission). This initial testing also allowed for the first-time use of the NREL 80 and NREL 100 duty cycles in a test cell.

The test cell setup included modeling of the vehicle, final drive, tires, vehicle operator and vehicle accessories; for the ETREE powertrain, a 250 kW battery emulator (modeled with the characteristics of the 112 kw-h NMC Li-ion battery and used to power the traction motor's inverter) was used to simulate the energy storage system.

After conventional testing, the next step was to install the ETREE powertrain components into the test cell (shown in Figure III.5.2). Like the conventional powertrain testing, the ETREE transmission is connected to the test cell dynamometer. ETREE's range extender (along with the traction motor's inverter when it is operating in kinetic energy recovery mode) simply provides electrical energy to the battery emulator.

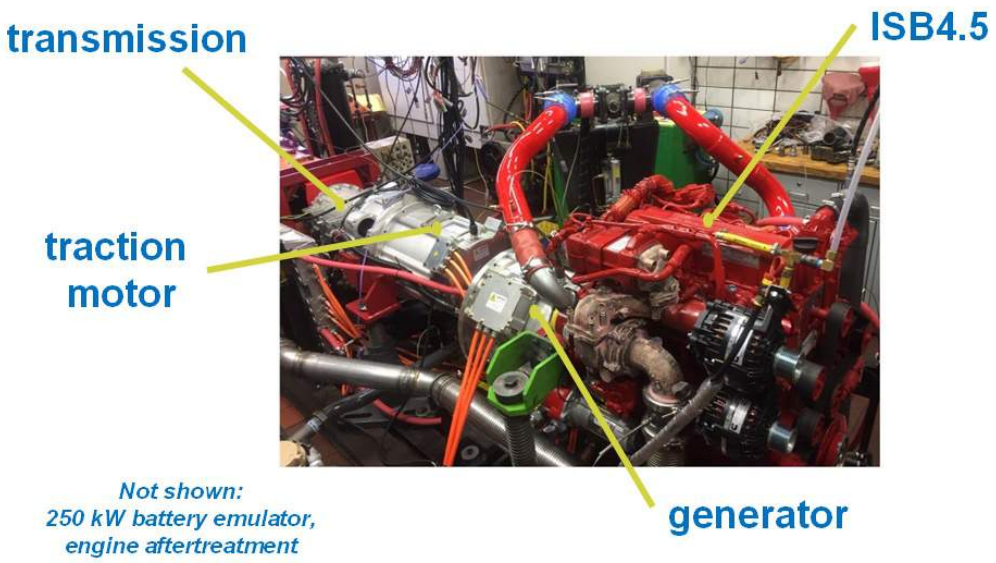


Figure III.5.2 - ETREE powertrain test cell located at Cummins Technical Center, Columbus, Indiana

Test cell testing demonstrated similar results, for the NREL 80 and NREL 100 duty cycles, as those predicted by simulation.

A summary of key technical results is shown in Table III.5-2.

**Table III.5-2 - Summary of Technical Results for FY 2017**

| Key Technical Result | Objective | Status |
|---|---|---|
| **Create target work day cycles** | Create two target work day duty cycles applicable to class 6 urban/suburban pickup and delivery | complete |
| **Identify & obtain powertrain components** | Via simulation, select components (incl. usable battery energy capacity) in order to achieve fuel consumption reduction objectives for target vehicle | complete |
| **Develop required system control functionality** | Develop system control functionality for:<br>- optimal operation of range extender<br>- acceptable drivability and performance<br>- transmission integration<br>- electronic braking system integration | complete (test cell);<br>in process (vehicle application) |
| **Demonstrate fuel consumption reduction target [NREL 80] in test cell** | Achieve ≥50% fuel consumption reduction in powertrain test cell | complete; achieved 60% fuel consumption reduction |
| **Measure fuel consumption reduction on NREL 100 in test cell** | Measure fuel consumption reduction in powertrain test cell | complete; achieved 50% fuel consumption reduction |

## Conclusions

It is important to consider the entire work day duty cycle of vehicles which use plug-in electrical energy. Simply extrapolating existing short-term duty cycles may not lead to the development of the correct battery requirements. The NREL 80-mile and 100-mile work day cycles will be valuable to other projects that aim to develop BEV or range extending electric commercial vehicle powertrains.

The ETREE project has selected and obtained the relevant powertrain components in order to meet the target objective of providing at least a 50% fuel consumption reduction across a wide range of class 6 pickup and delivery duty cycles. Test cell testing has increased the confidence in the simulation methods employed and, therefore, simulation can be used to continually optimize the system control algorithms.

## Key Publications

The following technical paper has been accepted for the 2018 SAE World Congress. It is the authors' intent that these duty cycles be used by the industry in the development of future electrified commercial vehicles.

1. Adam Duran, Ke Li, John Kresse, Kenneth Kelly, and Ram Vijayagopal, Development of 80 and 100 Mile Work Day Cycles Representative of Commercial Pickup and Delivery Operation, SAE International Paper #2018-01-1192, 2018, http://papers.sae.org/2018-01-1192/.

## III.6 Advanced Vehicle Testing & Evaluation

**D Jeremy Diez, Principal Investigator**
Intertek Testing Services NA, Inc.
430 S 2nd Avenue
Phoenix, AZ 85003
Phone: (480) 525-5873
E-mail: jeremy.diez@intertek.com

**Lee Slezak, Technology Manager**
U.S. Department of Energy
Phone: (202) 586-2335
E-mail: Lee.Slezak@ee.doe.gov

Start Date: October 1, 2011 End Date: September 30, 2018
Total Project Cost: $33,088,218 DOE share: $26,400,000 Non-DOE share: $6,688,218

### Project Introduction

The Advanced Vehicle Testing and Evaluation (AVTE) Project incorporates the conduct of advanced technology vehicle and infrastructure testing in the U.S. Department of Energy (DOE) Advanced Vehicle Testing Activity (AVTA). It is the only activity tasked by DOE to conduct independent field evaluations of vehicle technologies that use advanced technology systems and subsystems in vehicles to reduce petroleum consumption. The results are available through reports published on the AVTA website at http://avt.inl.gov/. The AVTE Project provides insight into advanced vehicle technology's long-term performance, durability, maintenance, and lifecycle costs that cannot be found through media outlets. The site is a resource for DOE stakeholders and the public to gain knowledge on advanced technology vehicle progress and innovation. Idaho National Laboratory (INL) has responsibility for technical direction of the overall project, along with data collection, analysis, and test reporting of light-duty vehicles in coordination with Intertek Testing Services NA, Inc. (Intertek). Medium and heavy-duty truck data collection, analysis, and test reporting is coordinated between Intertek and the National Renewable Energy Laboratory. The project is administered by the National Energy Technology Laboratory for DOE. All participating DOE laboratories coordinate with Intertek to determine project scope and direction within AVTA.

### Objectives

The objective of the AVTE Project is to conduct unbiased laboratory and field evaluations of advanced technology vehicles and their associated fueling infrastructure, as well as development of new test procedures and/or modifications of existing test procedures necessary to accomplish these performance evaluations. The scope of work includes baseline performance, accelerated reliability, and fleet testing of state-of-the-art light, medium, and heavy-duty advanced technology vehicles and the vehicle-to-infrastructure interface required for fueling/charging the vehicles throughout their life in the project.

### Approach

The AVTE Project is managed in separate tasks to accomplish testing of advanced technology vehicles and their respective infrastructure. The project tasks are as follows:

*Project Management*

This task includes activities necessary to provide management of AVTE activities, including budget and schedule control, fleet coordination, procurement, status reporting, presentations of activity results and status to DOE and industry, preparation of the project management plan, and quarterly updates of the project

management plan. Work under this task also includes management of test results reports and/or data sheets for each task.

*Vehicle Specification and Test Procedure Development*

Specifications for vehicles, components, and infrastructure are prepared to define specific design and performance requirements. Test procedures are developed that will evaluate requirements stated in the specification.

New testing procedures incorporate industry standard test procedures as applicable. Vehicle tests typically include limited access track testing of performance and operating characteristics and DOE laboratory chassis dynamometer testing.

*Baseline Performance Testing*

Baseline test procedures include, but are not limited to, testing of acceleration, speed within a set distance, gradeability, deceleration due to regenerative braking, braking distance, time to recharge and charging efficiency (for grid connected vehicles), energy storage capacity, and fuel efficiency on various dynamometer test cycles and in various operating modes. Additional baseline test procedures are developed, as required, for vehicles with unique operational characteristics.

Baseline vehicle performance testing is performed at a limited access test track. Chassis dynamometer testing is conducted at Argonne National Laboratory's Advanced Powertrain Research Facility. As part of baseline testing, beginning-of-test battery capacity and performance testing is conducted on all vehicles with battery energy storage. Vehicles will be purchased, leased, or rented unless provided by DOE or manufacturers and suppliers. All vehicles will be insured, operated, and maintained in accordance with manufacturer's recommendations.

*Accelerated Vehicle Testing*

During accelerated testing, at least one vehicle is tested under supervised and semi-controlled conditions in order to evaluate one or more characteristics of the vehicle's performance or operational characteristics and to obtain data in an accelerated timeframe, evaluating vehicle reliability, maintenance requirements, long-term performance, energy efficiency, and lifecycle costs. The assumption with accelerated testing is that the vehicle is unlikely or too expensive to operate in a long-term fleet application due to technical and manufacturing robustness.

The accelerated testing duration is based on the objectives of testing for the particular subject vehicle. Testing typically achieves a minimum of 6,000 miles on a subject vehicle, but may reach higher mileage as documented in the project management plan. Vehicles are purchased, leased, or rented unless provided by another program. All vehicles are insured, operated, and maintained in accordance with manufacturer's recommendations. Fueling infrastructure is provided, as required, to conduct testing and evaluation.

*Fleet Testing*

Fleet testing includes high-mileage testing of two or four production vehicles of the same make and model in an operating fleet to determine vehicle reliability, maintenance requirements, long-term performance, lifecycle costs, and user acceptance. Vehicles are driven on road to achieve a target mileage suitable for the advanced technology that is being studied during a 3-year minimum exposure to fleet operation. HEV and ICE vehicles are targeted to achieve 195,000 miles in fleet testing. PHEVs are targeted to achieve 160,000 miles in fleet testing due to the requirement to start the day in charge-depleting mode. BEVs are targeted to achieve 36,000 miles in fleet testing due to the limited range achievable per charge. Vehicles are purchased, leased, or rented unless provided by another organization. All vehicles are insured and maintained in accordance with the

manufacturer's recommendations. Fueling infrastructure is provided, as required, to conduct testing and evaluation.

Data collection systems necessary for collecting operating data as required per test procedures are installed on all fleet vehicles. Repair and maintenance costs are collected manually from the fleet. The fleet operator provides data on fuel dispensed, including electricity on plug-in electric vehicles, and odometer readings. Operating data and repair and maintenance costs are maintained current on a monthly basis. Quality checks and trend analysis are performed to ensure data are accurate and vehicles are performing properly.

*Interim Component Testing*

This task includes testing of vehicle components during accelerated or fleet testing. Interim component durability (ICD) tests for traction-battery-equipped vehicles are to determine capacity and performance between baseline and end-of-testing. For vehicles using CNG as a fuel, compression testing is conducted for engine performance over the life of the vehicle. Raw data from the testing are provided to AVTA at INL for analysis and verification.

*End-of-Test Vehicle and Component Testing*

This task consists of vehicle and component testing at completion of fleet or accelerated testing and includes, but is not limited to, vehicle performance, mechanical components, batteries, and other energy storage devices. Tests are performed as required by the project management plan and are conducted in accordance with procedures developed under test procedure development. Raw data from the testing is provided to AVTA at INL for analysis and verification.

*Infrastructure Test and Evaluation*

This task consists of testing vehicle and infrastructure interface, operations, and reliability. For grid-connected electric-drive vehicles, the testing includes DC fast charging at various temperatures and DC fast charging via a unit that utilizes onboard energy storage. The evaluation will collect data on installation, operation, energy, and maintenance costs of the infrastructure and track user feedback related to overall interface and operation of the infrastructure. Deliverables include test result data sheets and a report on the cost, safety, operation, maintenance, and reliability of the infrastructure.

*Additional Procedure Development, Testing, or Test Support*

This task consists of various additional procedure development, testing, and test support activities that may be determined necessary by DOE and Intertek. The activities will be detailed in the project management plan and the planned work will be reviewed and approved by DOE.

*Vehicle Testing Intervals*

All fleet test vehicles must meet a minimum of 3 years in fleet use for each vehicle and a minimum mileage target. The fleet and interim component durability testing results of these vehicles have historical AVTA test results for comparison.

The mileage target for ICE vehicles and HEVs is a minimum of 3 years and 195,000 miles of fleet testing. For PHEVs, the minimum is 3 years and 160,000 miles of fleet testing. For BEVs, the minimum is 3 years and 36,000 miles of fleet testing.

Component testing for each vehicle is adjusted based on the new mileage targets. For ICE vehicles and HEVs, baseline testing occurs at approximately 4,000 miles and ICD testing occurs at approximately 50,000, 105,000, and 160,000 miles, with a final test at approximately 195,000 miles. For BEVs, initial baseline component testing occurs at approximately 400 miles and ICD testing occurs at approximately 4,000, 12,000, and 24,000

miles, with a final test at approximately 36,000 miles. For PHEVs, due to their capability to drive in charge sustaining mode after the energy storage device is depleted in charge-depleting mode from an overnight charge, their testing is based on time intervals in the fleet after the initial baseline testing at 4,000 miles. ICD testing occurs at approximately 6 months, 1 year and 6 months, and 2 years and 6 months of fleet testing, with a final test at approximately 3 years of fleet testing with a minimum of 160,000 miles obtained during this period.

*Collaboration between Intertek and DOE National Laboratories*

Deliverables for the AVTE Project consist of vehicle baseline reports, interim component durability reports, and end-of life component and vehicle reports that are posted to the INL AVTA website. INL provides technical direction for the project and direction on data required from the vehicles, infrastructure projects, and analysis of the data collected. When putting together the initial vehicle baseline report, data are compiled from literature review, closed track testing at a proving ground, vehicle inspection, and fuel economy results from chassis dynamometer testing at the Argonne National Laboratory's Advanced Powertrain Research Facility. Highway, city, and air-conditioning cycle results at multiple ambient temperatures are included in the baseline report. The multiple ambient temperatures provide background on functioning of the propulsion systems, the secondary heating and cooling systems, and their effects on fuel economy, which are not evident in the Environmental Protection Agency fuel economy ratings for the vehicle. Argonne National Laboratory also conducts additional testing that is requested for Autonomie simulations with the AVTE vehicles and provides public access to all obtained data through their Downloadable Dynamometer Database website at http://www.anl.gov/d3.

*Partners*

There are two industry partners that have helped to make AVTE vehicle testing successful. Our first partner is EZ Messenger, which is a courier and legal document delivery service, pictured in Figure III.6.1. They operate AVTE fleet vehicles in multiple fleet locations, including Phoenix, Tucson, Houston, Dallas, Austin, and Oklahoma City. Location of vehicles is based on the best possibility to obtain fleet mileage objectives while still meeting their business needs. For example, the 2012 Honda Civic CNG vehicles and 2015 Chevrolet Impala Bi-Fuel vehicles were based out of Oklahoma City and Texas due to the large network of CNG filling stations in the area. The Phoenix, Arizona CNG filling stations were limited, which led to limited utilization of these vehicles until they were redeployed. Our second partner is AutoEnginuity, a company that provides vehicle diagnostic equipment from Mesa, Arizona. Their equipment and insight has been crucial in obtaining vehicle information throughout fleet testing.


Figure III.6.1 - AVTE fleet vehicles charging at the EZ Messenger fleet partner location in Phoenix, Arizona/Intertek

*Direct Current Fast Charging at Various Temperatures*

All direct current fast charge (DCFC)-capable BEVs perform testing at 0, 25, and 50°C while DCFC to provide analysis about the effects of ambient temperature on charge times and energy delivered. Figure III.6.2

is a picture of a vehicle inside the temperature chamber with the adjacent DCFC unit charging the vehicle. DCFC baseline testing is conducted at 4,000 miles, 24,000 miles, and 36,000 miles, which coincides with baseline and component testing intervals for BEVs. Progress reports are posted on the AVTA website and summarize testing completed for the 2013 Nissan Leaf, 2012 Mitsubishi i-MiEV, 2014 BMW i3 BEV, 2015 Chevrolet Spark EV, 2015 Kia Soul EV, and the 2015 Volkswagen e-Golf EV.

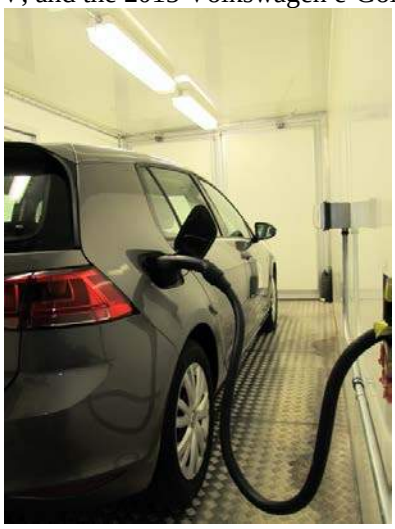

Figure III.6.2 - A 2015 Volkswagen e-Golf DC fast charging in the temperature chamber at Intertek in Phoenix, Arizona/Intertek

*Storage Assisted Vehicle Recharging*

A Storage Assisted Vehicle Recharging (StAR) unit pictured in Figure III.6.3 is housed in a temperature-controlled chamber at Intertek in Phoenix, Arizona due to a maximum operating ambient of 40°C, which can easily be exceeded by the Phoenix ambient temperature during the summer. The unit is under evaluation utilizing DCFC-capable AVTE fleet vehicles. The StAR unit, sourced from VLI-EV, is the only one that met all project requirements, which included having both the CHAdeMO and the Combined Charging System (CCS) connectors and an onboard energy storage system. A 12-kWh onboard ESS is designed into the unit and is being evaluated for its overall capability to avoid electric utility demand charges that would have been present with a standard DCFC that does not have an ESS onboard.

Figure III.6.3 - A 2014 BMW i3 BEV DC fast charging using the StAR unit (enclosed in red chamber) at Intertek in Phoenix, Arizona/Intertek

## Results

A total of 83 vehicles were under test during FY 2017, accumulating 829,594 miles of fleet testing and multiple reports updated on the AVTA website. Vehicles under test during the fiscal year are summarized in Table III.6-1.

Table III.6-1 - AVTE Vehicles Tested During FY 2017

| # of Vehicles at start of FY 2017 | Year | Make | Model | Type | Component Test Focus | FY 2017 Test Miles | # of Vehicles at end of FY 2017 |
|---|---|---|---|---|---|---|---|
| 2 | 2011 | Chevrolet | Volt | PHEV | Energy Storage System (ESS) | 50,663 | 0 |
| 4 | 2013 | Chevrolet | Malibu | HEV | ESS | 9,713 | 0 |
| 4 | 2012 | Honda | Civic CNG | ICE | Compression Testing/12V Accessory Loads | 71,993 | 0 |
| 4 | 2013 | Chevrolet | Volt | PHEV | ESS | 2,480 | 0 |
| 2 | 2013 | Toyota | Prius Plug-In | PHEV | ESS | 12,624 | 0 |
| 4 | 2013 | Volkswagen | Jetta Hybrid | HEV | ESS | 39,945 | 0 |
| 2 | 2012 | Mitsubishi | i-MiEV | BEV | ESS | 3,365 | 0 |
| 4 | 2013 | Nissan | Leaf | BEV | ESS | 21,223 | 2 |
| 2 | 2013 | Ford | C-Max Hybrid | HEV | ESS | 22,960 | 0 |
| 3 | 2013 | Ford | C-Max Energi | PHEV | ESS | 15,400 | 0 |
| 4 | 2013 | Ford | Focus EV | BEV | ESS | 20,683 | 0 |
| 3 | 2013 | Ford | Fusion Energi | PHEV | ESS | 35,135 | 0 |
| 3 | 2014 | Smart | ED | BEV | ESS | 3,242 | 0 |
| 4 | 2014 | Chevrolet | Cruze Turbo Diesel | ICE | 12V Accessory Loads | 80,462 | 0 |
| 3 | 2014 | Mazda | Mazda3 i-ELOOP | ICE | Capacitor | 84,738 | 0 |
| 3 | 2014 | BMW | I3 Range Extender | PHEV | ESS | 16,430 | 0 |
| 3 | 2014 | BMW | I3 | BEV | ESS | 27,657 | 2 |
| 4 | 2015 | Kia | Soul EV | BEV | ESS | 16,480 | 0 |

| # of Vehicles at start of FY 2017 | Year | Make | Model | Type | Component Test Focus | FY 2017 Test Miles | # of Vehicles at end of FY 2017 |
|---|---|---|---|---|---|---|---|
| 4 | 2015 | Chevrolet | Spark EV | BEV | ESS | 18,964 | 2 |
| 4 | 2015 | Honda | Accord Hybrid | HEV | ESS | 51,197 | 0 |
| 4 | 2015 | Volkswagen | e-Golf | BEV | ESS | 31,755 | 2 |
| 4 | 2015 | Mercedes | B-Class EV | BEV | ESS | 16,898 | 0 |
| 4 | 2015 | Chevrolet | Impala Bi-Fuel CNG | ICE | Compression Testing/12V Accessory Loads | 26,389 | 0 |
| 4 | 2016 | Chevrolet | Volt | PHEV | ESS | 149,198 | 2 |
| 83 | Total | Vehicles | Under | Test | FY 2017 Total Miles: | 829,594 | 10 |

Prior to the start of FY 2017, there were 83 vehicles that were underway with mileage accumulation and advanced component testing. Due to a FY17 change in project direction to focus on vehicles with DCFC capability and the 2016 Chevrolet Volts, only 10 vehicles were under test at the end of the fiscal year. During FY 2017, the vehicles completed a total of 42 vehicle component durability tests, some of which were part of the end-of-test for those vehicles. A 2013 Chevrolet Volt and a 2013 Toyota Prius Plug-In both completed full end-of-life testing during the fiscal year. Throughout all testing, there was strong collaboration amongst Intertek and the participating DOE national laboratories for coordination of testing and reports.

## Conclusions

The AVTE Project provides data, reports, and lessons-learned from vehicle testing that are available for further study by DOE national laboratories and dissemination to the public. This valuable unbiased information provides performance data that cannot be found in media outlets, such as capacity and performance of the ESS over the life of the vehicle, maintenance cost/mile, fuel economy over the life of the vehicle, and charging economy, which are all available through the AVTA website. Data and summary information obtained from vehicles and infrastructure tested in AVTE can be utilized as lessons-learned to benefit future advancement in advanced technology vehicles.

## Key Publications

All listed reports can be found on the Idaho National Laboratory AVTA website. Vehicle-specific reports are organized by vehicle make and model. Access http:avt.inl.gov/ for more information on vehicle testing.

1. “Vehicle Specifications and Testing Results, Series of Reports," Idaho National Laboratory, Intertek Testing Services NA, 2016-2017.

2. “Battery Pack Laboratory Testing Results, Series of Reports," Idaho National Laboratory, 2016-2017.

3. “DC Fast Charging at Different Temperatures, Series of Reports," Idaho National Laboratory, Intertek Testing Services NA, 2016-2017.

## III.7 Houston Zero Emission Delivery Vehicle Development

**Andrew J. DeCandis, Principal Investigator**
Houston-Galveston Area Council
3555 Timmons Lane, Suite 120
Houston, TX 77027
Phone: (832) 681-2589
E-mail: Andrew.DeCandis@h-gac.com

**Lee Slezak, Technology Manager**
U.S. Department of Energy
Phone: (202) 586-2335
E-mail: Lee.Slezak@ee.doe.gov

Start Date: October 1, 2012 End Date: January 30, 2019
Total Project Cost: $3,990,177 DOE share: $1,230,177 Non-DOE share: $2,760,000

### Project Introduction

The Houston-Galveston Area Council (H-GAC) and the Center for Transportation & the Environment (CTE) have partnered to establish the Houston Zero Emission Delivery Vehicle Demonstration Project. The primary objective of the project is to demonstrate the effectiveness of all-electric delivery vehicles in the Houston-region and to show that these vehicles can perform at the same level of operation as similarly sized diesel delivery vehicles, while reducing vehicle emissions and petroleum consumption. To meet this objective, this project has supported the deployment of 18 all-electric delivery trucks that have been deployed in the Houston-Galveston-Brazoria NAAQS 8-hour ozone nonattainment area.

Vehicles and the demonstration fleet were selected through a Call for Projects process. This Call was open to national, regional, and/or local fleets with the stipulation that the vehicle deployment and operation would occur within the Houston-Galveston region. In addition to funding the deployment of delivery vehicles and charging infrastructure for the winning fleet, the project demonstrates vehicle operations, collects data, and reports on project results for a period of two years after deployment.

### Objectives

The primary objective of this project is to deploy eighteen (18) zero-emission all electric trucks and demonstrate the effectiveness of the all-electric delivery vehicles to at the same level of operation as similarly sized diesel delivery vehicles while reducing vehicle emission and petroleum consumption.

The project vehicles are deployed and selected through a Call for Projects process and deployed on delivery routes in the Houston-Galveston area. Large national fleets and progressive regional fleets that operate diesel and gasoline delivery vehicles in the region were initial targets for fleet deployment and testing. The process for integration of all-electric vehicles into fleets will result in both emission and noise reductions over diesel and gasoline counterparts. Fleets will also be able to reduce their reliance on petroleum-based fuels and realize significant cost savings over conventional counterparts.

As a result of the Call for Projects process, United Parcel Service (UPS) and Workhorse were selected as the fleet/vehicle team for this project. UPS has accepted and deployed 18 project that were manufactured by project OEM Workhorse. Additionally, CTE has worked with Workhorse to plan, select, and model the routes on which the project vehicles have been deployed. The project team procured, installed, and tested vehicle charging stations in preparation for vehicle deployment. With the demonstration period in progress, the project is now conducting a series of tests to validate vehicle performance against the model and is currently collecting operational data for all 18 project vehicles.

## Approach

*System Description*

Workhorse has developed a new chassis for this project and for the commercial market. The W88 chassis is designed to meet the needs of a wide range of customers. At the same time, it is a universal chassis from an operations perspective and closely matches the existing UPS package truck specifications.

The Workhorse E-100 electric vehicle is 100% electric powered by a 120 kWh battery pack giving it a useful range of 80 miles in a typical 120-150 stop per 8-hour package delivery shift. The range of the Workhorse truck should be more than adequate to cover the average 50 to 65 mile per day routes in Houston. The vehicle has no transmission — it is a direct drive to the differential making it very efficient. The electric motive drive is a 2200NM regenerative drive capable of powering a 23,000-pound vehicle from a dead stop up a 23% incline.

Top speed of the vehicle is limited to 65 mph. Typical differential ratios are 4.78 to 1 and 5.1 to 1 for the direct drive. The vehicle has a supervisory controller that interfaces with the Battery Management System, the Body Control Module, and the Brake Module, and the charging system to control the vehicle. There is an onboard level two J1772 charger, either 7KW or 18KW depending on the customer preference. The vehicle can also be fitted with inductive charging if needed, however this configuration is not used in the current project.

*Testing*

UPS, in partnership with CTE and Workhorse, is reporting vehicle and charger specifications as well as operational and maintenance data for all project vehicles. Data collected also includes powertrain and battery operational data. Additionally, average data from the UPS non-electric fleet vehicles is taken into consideration as may be required for comparative analysis. All information collected by Workhorse and UPS shall be provided to CTE. CTE will analyze the data and, with H-GAC, will summarize for submittal to DOE.
Testing Variables

- Vehicle Operations
    - Daily Mileage
    - Operating Time
    - Payloads
    - Speed
    - State of Charge
    - Auxiliary Loading
    - Maintenance Logs
- Charging Operations
    - Daily Charge Times
    - State of Charge
    - Energy Consumption
    - Utility Costs
    - Maintenance Logs

- Data Collected will be used to calculate a number of analytical factors, including, but not limited to:
    - Fuel Efficiency (i.e., $/mile, kWh/mile, etc.)
    - Cargo Ton-Miles/Vehicle
    - Cargo Ton-Miles/Fleet
    - Reduction in Petroleum Consumption
    - Reduction of Green House Gas Emissions (Million Metric Tons of Carbon Equivalent (MMTCE)/year)
    - Reduction of Criteria Pollutant and Toxic Emissions
    - Expected Life Cycle Benefit Analysis

*Demonstration Period*

The project includes a two-year demonstration of each project-procured all-electric truck under real world conditions.

*Data Collection Strategy*

The 18 Workhorse vehicles were tested for durability and are equipped with data collection and monitoring systems to tract variables from the battery management, drive system, cooling systems, etc. Coast-down testing was used to determine projected energy usage per mile; use case testing was accomplished to verify that vehicle energy usage is consistent with projected usage. Limits of charge and discharge were set as to ensure that the main battery will operate to its projected life without overstressing it.

Real time data is sent to a server for storage and analysis and parameters are modified as necessary to insure the vehicle performs to its design parameters.

Vehicles prototypes are tested on steep hills and anticipated normal driving conditions locally to get baseline data before TRC testing. Data is collected to determine energy usage per mile under various driving conditions and compared to predicted models to determine battery life, range, acceleration etc. Major vehicle maintenance for production vehicles can be performed at Workhorse dealers across the country.

*Infrastructure Requirements*

Each vehicle comes with a water-cooled J1772 level 2 charger on-board. The charger is typically 12 kWh, 220 Vac. Vehicles may be optionally equipped with 25KW induction charging.

*Commercialization*

It is believed that the vehicles used in this project will result in a positive business case on a total cost of ownership basis for UPS and other selected fleets. This is due to the lower cost of electricity and lower maintenance costs as compared to fuel and maintenance of diesel medium- and heavy-duty vehicles.

**Results**

The project team has contracted with United Parcel Service (UPS) to for the purchase of eighteen (18) all-electric delivery vehicles. These vehicles were purchase from Workhorse (formerly known as AMP Electric). The resultant vehicle is the Workhorse E-100 Electric Delivery Van. All 18 of these vehicles have been fully manufactured. These vehicles have been fully manufactured and delivered by Workhorse and subsequently deployed by UPS to deliver packages within the Houston region.

Basic information about the project vehicles:

**Table III.7-1 - Project Vehicle Information**

| | |
|---|---|
| **Vehicle Range** | 80 to 90 miles |
| **Top Speed** | 65 mph |
| **Battery Capacity** | 120 kWh |
| **Motor** | 180 kW |
| **Motor Torque** | 1,106 ft-lbs |


Figure III.7.1 - The Workhorse E-100 Electric Delivery Van
(Courtesy Workhorse/UPS)

From the beginning of the demonstration period until September 30, 2017, the 18 project vehicles have traveled a total of 85,815 miles within the Houston region for an average of 4,768 miles per vehicle. On a per trip basis, these vehicles travel approximately 49 miles per trip with an average of 1.95 stops per mile or over 95 stops per trip. This is well within the stated maximum range for this model of 80 to 90 miles per trip. For these 18 vehicles, trip lengths range from 35 miles per trip to 66 miles per trip.

Project vehicles have resulted in significant fuel savings at UPS over the course of the project to date. Project vehicles have used approximately 85,632 kWh of electricity through normal operation. The same number of diesel powered package trucks would have used 9,247 gallons of fuel to accomplish the same distance of travel. Additionally, the average cost of operation of these electric vehicles in the Houston-based UPS fleet is approximately $0.07 per mile. Based on an average diesel cost per mile, the project vehicles have resulted in

an estimated cost saving of $16,259 to date. Finally, as a result of this project, UPS has reduced feet NOx emissions (an ozone precursor by 0.0351 tons and reduced CO2 emissions by 206,954 pounds.

*Significant Issues*

The Workhorse E-100 Electric Vehicles have been in service since May/June of 2016. Throughout this time, the vehicles have been tracked by the Workhorse monitoring system, Metron. Since the beginning of the demonstration period in November 2017, project vehicles have seen various amounts of downtime. Over a possible 4,194 service days, project vehicles have operated for 1,714 of those days. This has resulted in a project-wide 41% utilization rate. The issues that have resulted in these utilization rates can be separated into a couple of different areas: software issues with the Battery Management System, third-party hardware issues, and manpower issues.

The Battery Management System (BMS) has multiple functions including helping to load balance the cells while charging and to also monitor the electrical system. When a cell appears to be out of balance then the BMS unit throws a fault. Workhorse found the software algorithm in the unit to be more sensitive than necessary for the application. Workhorse has potentially fixed this issue by working with the vendor to decrease the voltage monitoring sensitivity and adjusting the mounting of the BMS.

There have also been additional issues with third-party vehicle components that have reduced utilization rates among project vehicles. Major components with issues include: DC/DC converters that showed significant failure rates; vehicle chargers from small manufacturers with slow project turnaround; and a small number of trucks that could experience “Limited Power” conditions due to multiple potential issues. Additionally, long lead times from many of these component suppliers has resulted in longer vehicle downtimes that would otherwise have been expected.

Finally, other downtimes that have resulted in a decrease in utilization rates resulted from a combination of Workhorse’s lack of personnel to service the vehicles in a timely fashion as well as a multitude of both significant and minor issues with parts in the vehicles. At this time, Workhorse believes that the issues detailed here have been mostly resolved and that utilization rates will increase through the remainder of the demonstration period. See Figure III.7.2 for monthly utilization rates.

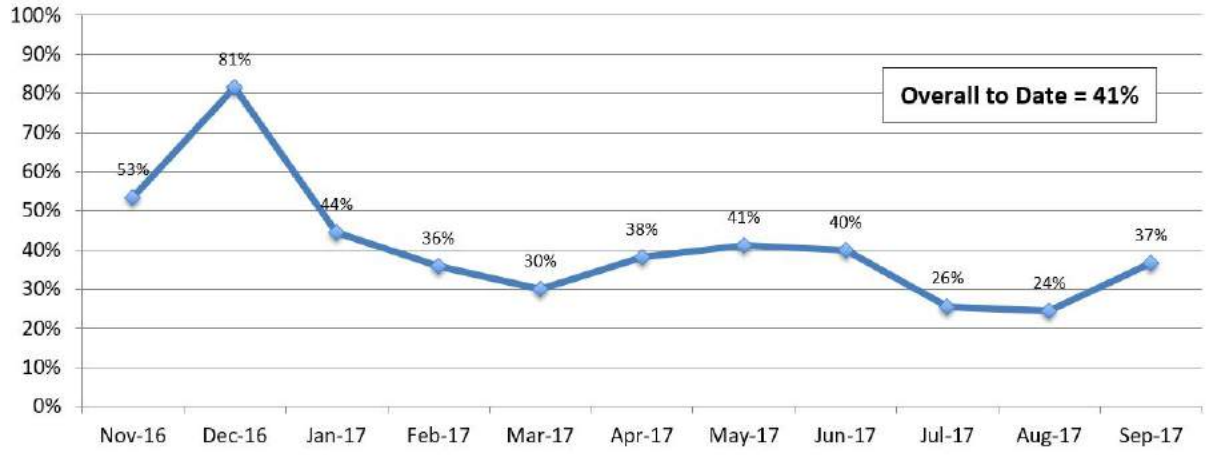


Figure III.7.2 - Project Vehicle Utilization by Month

## Conclusions

This project is producing a record of on-road experience and operational data which will serve to accelerate the introduction and penetration of electric transportation technologies. To accomplish these goals, 18 zero-emission all-electric trucks manufactured by Workhorse have been deployed at UPS distribution facilities across the Houston region and are currently delivering packages as part of an ongoing a two-year demonstration period. The project has experienced delays due to financial challenges faced by the originally intended OEM and in identifying appropriate routes and carriers within the Houston area as a result of large are of the Houston region area and resultant longer than typical travel routes.

Through the ongoing demonstration period, the project vehicles have been able to adequately meet the needs of UPS for delivery of packages within the region. Utilization of the project vehicles has been lower than expected. This has largely been due to issues regarding vehicle software, faulty vehicle components sourced by Workhorse from external suppliers, and personnel shortages to enact the necessary repairs. At this time, these issues appear to be resolved and vehicle utilization is increasing. H-GAC will continue to monitor, analyze and report the demonstration data for 18 existing all-electric vehicles for the remainder of the demonstration period.

## Key Publications

No publications to date.

## III.8 Zero Emission Drayage Trucks Demonstration

**Matt Miyasato, Principal Investigator**
South Coast Air Quality Management District
21865 Copley Drive
Diamond Bar, CA 91765
Phone: (909) 396-3249
E-mail: mmiyasato@aqmd.gov

**Brian Choe, Co-Principal Investigator**
South Coast Air Quality Management District
Phone: (909) 396-2617
E-mail: bchoe@aqmd.gov

**Lee Slezak, Technology Manager**
U.S. Department of Energy
Phone: (202) 586-2335
E-mail: Lee.Slezak@ee.doe.gov

Start Date: October 1, 2012 End Date: September 30, 2018
Total Project Cost: $9,374,641 DOE share: $4,169,000 Non-DOE share: $5,205,641

### Project Introduction

On-road heavy-duty diesel trucks are one of the largest sources of diesel particulate matter and NOx emissions in the South Coast Air Basin. The impact on air quality and public health is more pronounced in the surrounding communities along the goods movement corridors near the San Pedro Bay Ports - Ports of Los Angeles and Long Beach, and next to major freeways in Southern California. As a measure to reduce the impact and to meet federal ambient air quality standards, South Coast Air Quality Management District (SCAQMD) has been working with regional stakeholders, including the Ports of Los Angeles and Long Beach, to promote and support the development and deployment of advanced zero emission cargo transport technologies. In 2012, SCAQMD applied for and received a $4.17 million grant from the DOE under the Zero Emission Cargo Transport Demonstration Program to develop and demonstrate Class 8 electric drayage trucks with zero emission operation capability in real world drayage service.

### Objectives

This project is to develop and demonstrate zero emission capable electric truck technologies in real world drayage operations to assess its technical feasibility to support demanding drayage duty cycles. The project is also to promote and accelerate market adoption of electric truck technologies in cargo transport operations, by engaging trucking fleets, the end users, in demonstrations to experience the technologies first hand.

### Approach

SCAQMD, as the award recipient, will provide overall project management in this project. TransPower and US Hybrid, locally based EV system developers and vehicle integrators in Southern California, are to develop a total of eleven Class 8 zero emission capable drayage trucks for demonstration, based on four different architectures, consisting of two types of battery electric vehicles (BEVs) and two types of plug-in hybrid electric vehicles (PHEVs) with all-electric range capability as summarized in Table III.8-1. Initial portfolio of demonstration technologies included a fuel cell truck by Vision Motors and another battery electric truck from Balqon. However, with these two technology providers dropping out due to financial hardship, the portfolio was amended to the current mix by adding two PHEV technologies in 2015.

Upon completion, demonstration vehicles are deployed in real world drayage service for up to two years of demonstration with fleet partners at the San Pedro Bay Ports. During the demonstration, vehicle performance and O&M data will be collected and analyzed by National Renewable Energy Laboratory (NREL) to assess technical feasibility and market viability of the technologies in drayage truck applications. In addition, at least one truck from each technology is tested on chassis dynamometer at the University of California, Riverside (UCR) for performance validation and optimization.

Table III.8-1 - 2012 Zero Emission Cargo Transport Demonstration Portfolio

| | Battery Electric Trucks | | Plug-In Hybrid Electric Trucks | |
|---|---|---|---|---|
| **Developer** | TransPower | US Hybrid | TransPower | US Hybrid |
| **No. of Trucks** | 4 | 2 | 2 | 3 |
| **Hybrid Architecture** | N/A | N/A | Series | Parallel |
| **Chassis** | International Prostar | International Prostar | International Prostar | Peterbilt 384 |
| **Traction Motor** | Dual PM Motor 300 kW | Induction Motor 320 KW | Dual PM Motor 300 kW | 223 kW PM Motor (403 kW combined) |
| **Transmission** | Automated Manual | Direct Drive | Automated Manual | Automatic |
| **Auxiliary Power Unit** | N/A | N/A | 3.7L CNG | 8.9L LNG |
| **Battery/Storage Capacity** | 215 kWh-311 kWh | 240 kWh | 138 kWh/60 DGE | 80 kWh/72 DGE |
| **Charger** | On-Board ICU 70 kW | On-Board 60 kW | On-Board ICU 70 kW | On-Board 20 kW |
| **Refuel Time** | 2.5–4 hrs | 3-4 hrs | 2 hrs/15 min | 3-4 hrs/15 min |
| **Drayage Range** | 75-150 miles | 70-100 miles | 200 miles/ 30-40 AER miles | 250+ miles/ 30 AER miles |

## Results

*Battery Electric Trucks (BETs)*

### a) TransPower

TransPower has completed all four BETs funded under this project. Three of the four BETs, EDD2 - EDD4, have continued operation in drayage service throughout 2017, with EDD3 and EDD4 having been deployed in service for almost two years, and EDD2 in service for nearly three years since January 2015. As of this report, the four EDD trucks, including EDD1 which has been out of service due to a series of problems relating to its batteries, have accumulated approximately 38,000 miles of testing and drayage operations. Table III.8-2 summarizes daily average use and performance characteristics for EDD trucks, in comparison to baseline diesel trucks in comparable duty cycles running short-haul drayage operations. As shown in the table, EDD trucks averaged 5.14 hours and 44.2 miles of operation per day, similar to the baseline diesel trucks that operated 6 hours per day, averaging 52.26 miles in drayage service. What is notable is that both EDD trucks

and diesel trucks spent well over 50% of their operating hours idling, mostly while waiting in queues to load and unload cargo containers at the port terminals. This is typical for short-haul drayage trucks operating at the ports and such duty cycles are an ideal match for electric trucks which, unlike conventional diesel trucks that keep its engine running for A/C and other amenities during such operations, can use battery power for hoteling loads with zero tailpipe emissions, thus providing significant fuel savings as well as considerable benefits in air quality and public health. Also noted is that the EDD trucks demonstrated much higher fuel efficiency, averaging 2.16 kWh/mi or 17.43 $MPG_{de}$, which is three times better than the 5.67 MPG for the baseline diesel trucks, providing significant savings in fuel costs.

Table III.8-2 - Average Daily Use – TransPower BETs

| | EDDs (EDD1 – EDD3) | Baseline Diesel Filtered[1] |
|---|---|---|
| **Operational Time (hr)** | 5.14 | 6.02 |
| **Idle/Stationary Time (hr)** | 2.89 | 3.67 |
| **Daily Distance (mile)** | 44.20 | 52.26 |
| **Average Driving Speed (mph)** | 19.68 | 22.45 |
| **Regen Energy (%)** | 17.21 | N/A |
| **A/C Energy Use (kWh)** | 3.11 | N/A |
| **Remaining SOC (%)** | 54.41 | N/A |
| **Energy Efficiecy (kWh/mi)** | 2.16 | 6.64[2] |
| **Fuel Economy ($MPG_{de}$)** | 17.43[2] | 5.67 |

1. Filtered out days with distance >100 mi and Ave. driving speed >40 mph
2. kWh/mi and MPGde calculated using 37.656 kWh/gallon of diesel fuel

EDD trucks continue to generate interest within the local and national trucking industry. After starting out with only two fleets for demonstration, namely TTSI and SA Recycling in January 2015, many more fleet operators have since participated in demonstration of these electric trucks, including Cal Cartage, National Retail Transportation, Knight Transportation, PASHA, and 3 Rivers Trucking. Feedback from fleet operators and drivers was generally positive, describing the trucks as quiet, clean and easy to drive, especially in the stop and go traffic at the ports. However, the range limitation was cited as the main challenge to overcome for the fleets to readily adopt and deploy the trucks in drayage service without any limitations. In order to address this challenge, TransPower has been looking into several high density battery chemistries, including new Nissan Leaf batteries that have twice the energy capacity of the batteries currently used in EDD trucks. Also, as Nissan projects further improvements in energy density over the next few years, TransPower expects the operating range of EDD trucks could increase from the current fully-loaded range of 70 miles to 200 miles, considered by many fleets as the minimum range for drayage trucks.

Figure III.8.1 - TransPower EDD trucks on display

**b) US Hybrid**

US Hybrid completed and delivered first of their two BETs to TTSI in late 2016, however, due to unexpected delays in permitting and installation of EVSEs at the TTSI's new location in San Pedro, the truck was not deployed in drayage service until July 2017. Since its deployment, this truck has completed 11 days of service, having logged 368 drayage miles. There are several factors for the truck's limited use during the initial deployment period, including driver training, dispatcher scheduling as well as troubleshooting of some glitches and maintenance issues that are expected during initial deployment of any prototype technologies. Once initial deployment issues are ironed out and fleet drivers and dispatchers gain more confidence in the truck's capability, US Hybrid expects to see more use for the truck by fleet operators. Preliminary data, as reported by NREL, shows that the truck averaged 8.9 hours and 33.4 miles of daily operations, and consumed, on average, 2.35 kWh/mi in energy. US Hybrid has also conducted additional testing for validation and optimization. The testing included medium and long distance excursions on surface streets and highways, as well as pulling a fully loaded trailer over the Vincent Thomas Bridge, a suspension bridge located in the San Pedro Bay Port complex with a steep 7% grade. The truck demonstrated sufficient power to manage the bridge with a full load while maintaining posted speed limits.

US Hybrid has all but completed its second BET except for battery modules. After having experienced more than usual share of glitches and reliability issues with the batteries in the first BET, US Hybrid switched its battery supplier and also opted to use NMC batteries for the second truck, which has 30% higher energy density than the lithium iron phosphate batteries used in the first truck. With A123, the new battery supplier, to deliver these batteries by January 2018, US Hybrid expects to complete the second BET by the end of Q1 2018.

Figure III.8.2 - US Hybrid Battery Electric Truck

*Plug-In Hybrid Electric Trucks (PHETs)*

**a) TransPower**

TransPower has made good progress, having completed first of the two contracted PHETs in 2017. The truck is currently undergoing a series of testing for validation and optimization, including local and highway driving, in-field operation of the auxiliary power unit (APU) for extended range, and initial load pulling exercises. TransPower also continues to perform additional research to characterize variable valve control signals for higher RPM and power on its test dyno cell, which has been constructed using all of the parts and features of the production article generator sets to run calibration testing of custom engine control software. Furthermore, custom kits have been created to convert the stationary-trim APUs used in the demo trucks to automotive-trim. These kits consist of a custom controller, harness, software, fuel injectors and incidentals, so that field technicians will be able to easily upgrade the demonstration vehicles to higher power with reduced or minimal impact on emissions. TransPower has also completed most of the subsystems for the second PHET, including the CNG APU, Motive Drive Subsystem with traction motors and transmission, and Power Control and Accessory Subsystem. Also, the battery modules are under assembly after additional testing of the Yinhe batteries used in the first PHET has provided renewed confidence in the quality and reliability of the product.

Figure III.8.3 - US Hybrid PHET pulling a container for TTSI

**b) US Hybrid**

In this project, US Hybrid is demonstrating a hybrid system to convert existing LNG trucks equipped with the 8.9L ISLG engine, which is considered underpowered for heavy-duty drayage operations, to plug-in hybrid trucks that are capable of providing sufficient power and torque, even comparable to those equipped with larger Cummins ISX12 engines, to support a full range of demanding drayage duty cycles. Although this PHEV technology was added in midstream in late 2015, US Hybrid has made considerable progress, having completed and delivered two of the three contracted PHETs to TTSI in 2017. After completing necessary paperwork and vehicle inspections, the trucks were deployed in drayage service in July 2017. Based on preliminary data, as provided by NREL, the two trucks collectively operated 79 days and logged over 3,000 miles in drayage service as of September 2017. Daily use averaged 4.06 hours and 32 miles, with the first of the two trucks seeing heavier use over the other. However, given that these trucks are identical in both technologies and capabilities, such disparities in vehicle usage is not expected to continue. The third PHET has been delivered to UCR for chassis dyno testing. US Hybrid will work with UCR on improving engine control and SOC control strategies to further reduce NOx emissions and enhance fuel economy.


Figure III.8.4 - TransPower PHET pulling its first trailer

## Conclusions

Despite many challenges, including withdrawal of two technology providers in 2015, this project has been largely successful. As of September 2017, seven of the eleven electric trucks funded under this project have been completed with the remaining four scheduled for completion in coming months. Collectively, these electric trucks have logged over 41,000 miles in real world drayage service, providing valuable data on performance and operational characteristics to help evaluate its technical feasibility and viability in drayage applications. These trucks have also generated significant interest from trucking companies, which will certainly help to promote and accelerate market adoption of electric truck technologies in cargo transport operations.

Based on available data collected from demonstration vehicles and feedback from fleet operators and drivers, these electric trucks have demonstrated sufficient power and torque to support real world drayage operations, while providing superior fuel economy over conventional diesel trucks in short-haul drayage duty cycles. The feedback from drivers was generally positive, with comments on its quiet and easy operations as well as smooth accelerations during take offs. These trucks also demonstrated sufficient capability to manage steep grades, even with a full load, including the Vincent Thomas Bridge, a suspension bridge located in the San Pedro Bay Port complex with a steep 7% grade. As expected, fleets expressed concerns over limited operating range for battery electric trucks. Fleets cited the range limitation as a significant barrier for them to fully adopt and deploy these trucks in regular drayage service. In order to address this barrier, TransPower has been looking into several high density battery chemistries, including Nissan Leaf batteries, which has twice the energy capacity of the batteries currently used in the EDD trucks. Furthermore, as the next generation of

batteries is introduced with even higher energy density in the next few years, TransPower expects to increase the operating range of EDD trucks from the current 70 miles to over 200 miles, even with a full load, supporting a wider range of drayage operations.

As one of the four technologies funded under this project, US Hybrid is demonstrating a hybrid system to convert existing LNG trucks with Cummins 8.9L ISLG engine, which is considered underpowered for heavy-duty drayage applications, to plug-in hybrid trucks. These PHETs will be capable of sufficient power and torque, even comparable to those equipped with larger Cummins ISX12 engines, to support a full range of drayage duty cycles without penalties in fuel economy and emissions that are typically associated with larger engines. Two of the three PHETs have been deployed in drayage service since July 2017 and received positive feedback from drivers and operators alike, especially on its exceptional power and torque. Upon successful demonstration in this project, US Hybrid aims to market the system to drayage fleets as a viable technology to convert LNG trucks with the 8.9L ISLG engine for augmented power and torque with lower emissions.

## Key Publications

None

## III.9 San Pedro Bay Ports Hybrid & Fuel Cell Electric Vehicle Project

**Joseph Impullitti, Principle Investigator**
South Coast Air Quality Management District
21865 Copley Drive
Diamond Bar, CA 91765
Phone: (909) 396-2025
E-mail: jimpullitti@aqmd.gov

**Lee Slezak, Technology Manager**
U.S. Department of Energy
Phone: (202) 586-2335
E-mail: Lee.Slezak@ee.doe.gov

Start Date: October 1, 2014 End Date: September 30, 2019
Total Project Cost: $20,410,075 DOE share: $9,725,000 Non-DOE share: $10,685,075

### Project Introduction

The proposed project area is known as the Los Angeles Goods Movement and Industrial Corridor. This area is adjacent to the Ports of Long Beach and Los Angeles, the busiest port complex in North America. The area is in an industrial setting with diesel truck activity mingled with a variety of uses including residences, schools, daycares and senior centers. The area is also a known Environmental Justice Community made up of predominantly low-income and minority populations.

The proposed technologies, fuel cell range extenders and hybrid electric trucks, face many challenges in the process of commercialization: proper sizing of the fuel cell stack, battery and fueling system; system integration and packaging of power train components and systems for safe, efficient and economical deployment of the technologies are just a few of the challenges. Many options exist in sizing the energy systems for these type of vehicle architectures – making the battery, engine or fuel cell dominate in size; plug in charging versus operation in charge sustaining mode and sizing of the energy storage system. Considerations for the power requirements of vehicle under load and providing enough onboard energy to attain the range requirements for the drayage operation and duty cycles all come into play in the design of the energy storage and power systems. Another challenge is to design the energy and power train systems described above and then integrate them into a vehicle for safe and efficient operation that can be made economical in volume and series production.

### Objectives

- Reduce criteria pollutants and GHG's in South Coast Air Basin by reducing diesel emissions from transportation and movement of goods
- Accelerate introduction and penetration of zero and near-zero emission fuel cell and hybrid technologies in cargo transport sector
- Execute a joint project with the Port of Los Angeles and Long Beach consisting of demonstration, data collection and analysis of seven fuel cell and hybrid trucks on five different vehicle architectures.

## Approach

Our approach to implementing the proposed technology is to address some of the challenges of developing the fuel cell range extended and hybrid truck platforms with the cost and time constraints of this FOA. By bringing together small to medium sized vehicle integrator contractors along with global manufactures and developers our strategy is to obtain the best partners with innovation and experience for this project. Vehicle integrators Transportation Power, Hydrogenics and U.S. Hybrid, are extremely cost effective in demonstrating proof of concept and exploring design variants in a timely fashion; OEM's BAE Systems a global defense and security company, Kenworth Trucks a major truck OEM and Ballard Power Systems an international fuel cell manufacturer have engineering and manufacturing capabilities and experience; both BAE and Ballard have experience in developing fuel cell transit buses. Together our project contractors offer the opportunity to explore design variations concurrently and address many of the challenges developing new technologies in a timely and cost effective manner. Some of the metrics that will be used to evaluate the design variants of the five fuel cell range extended and hybrid architectures are: operational capabilities, energy usage and efficiency, fueling/charging requirements and costs compared to diesel powered trucks.

*ZECT 2 Projects:*

**CTE/BAE Systems and Kenworth** are developing a battery electric truck with a hydrogen fuel cell range extender. The vehicle will operate in electric mode at all times and all speeds until the battery energy system reaches a lower operating state of charge level, at which point the hydrogen range extender would be activated to supplement power.

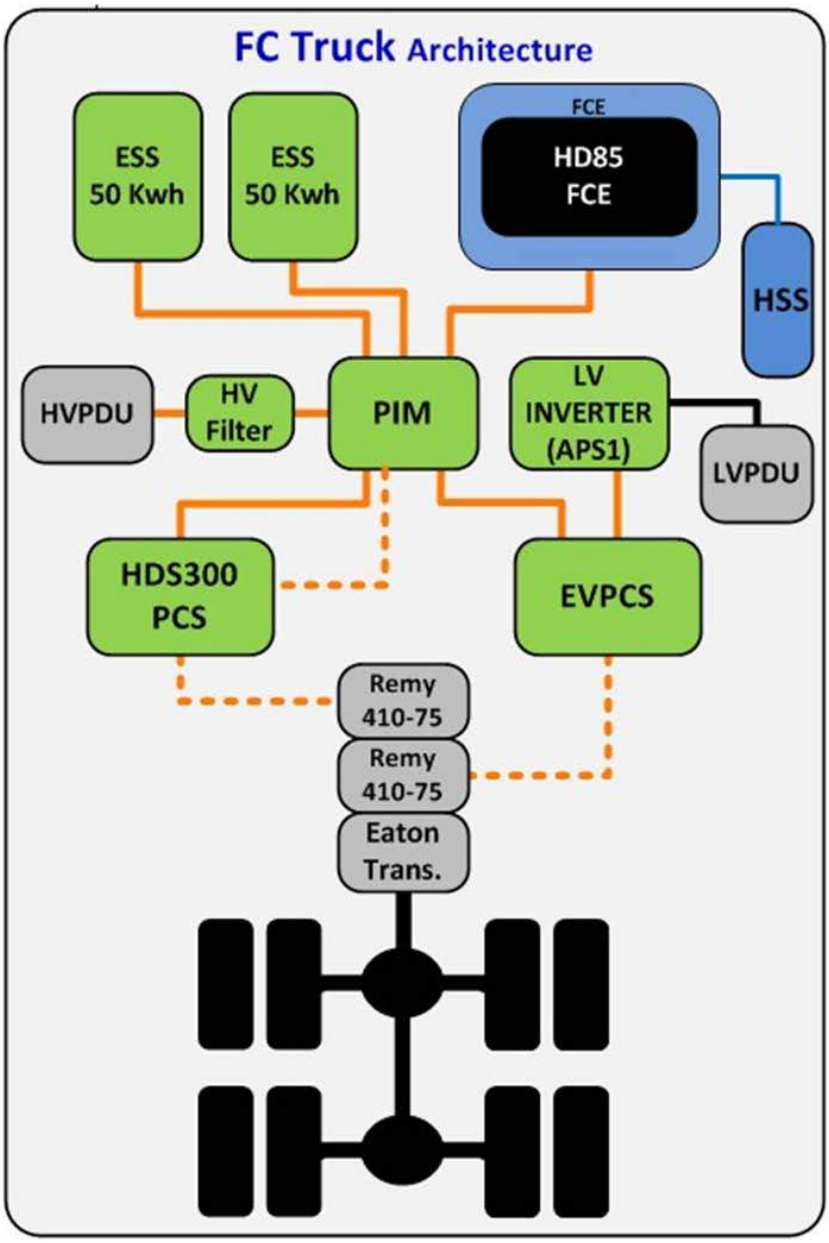


Figure III.9.1 - BAE/Kenworth vehicle system

**TransPower** is developing two battery electric trucks with hydrogen fuel cell range extenders. These trucks will employ a small fuel cell and stored hydrogen. One truck will be equipped with a 30 kW fuel cell and one with a 60 kW fuel cell, enabling a direct comparison of both variants.

Figure III.9.2 - Transpower Fuel Cell Truck (foreground) and CNG Truck (background)

**U.S. Hybrid** is developing two equivalent battery electric trucks with an on-board hydrogen fuel cell generator. Each truck is estimated to have 20 kg of hydrogen storage at 350 BAR with an estimated fueling time under 10 minutes.

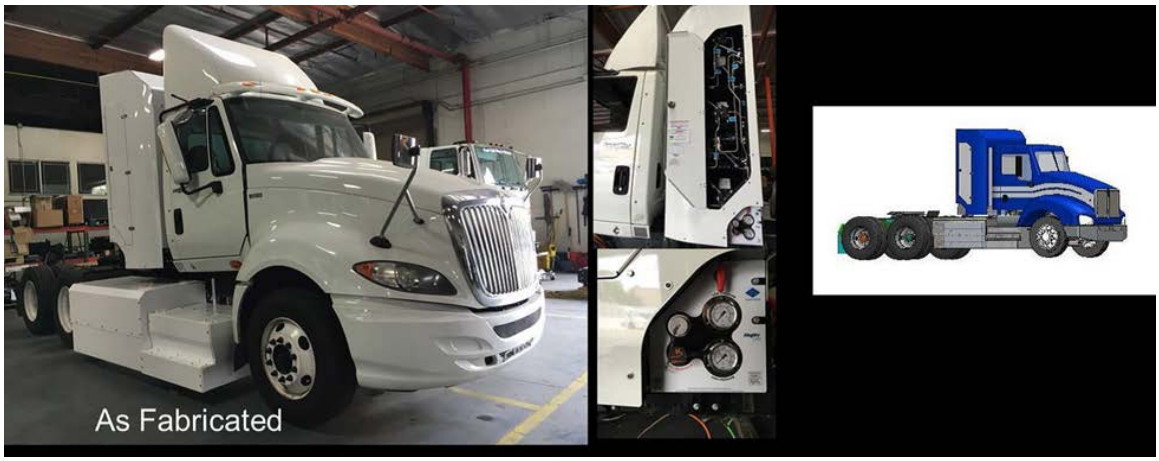


Figure III.9.3 - U.S. Hybrid Truck: Design to Fabrication

**GTI/BAE Systems and Kenworth** are developing one hybrid battery electric truck with CNG range extender. The proposed technical concept provides an all-electric mode, and in a conventional hybrid mode using CNG. The truck will have an on-board battery charger to fully charge the batteries in daily use

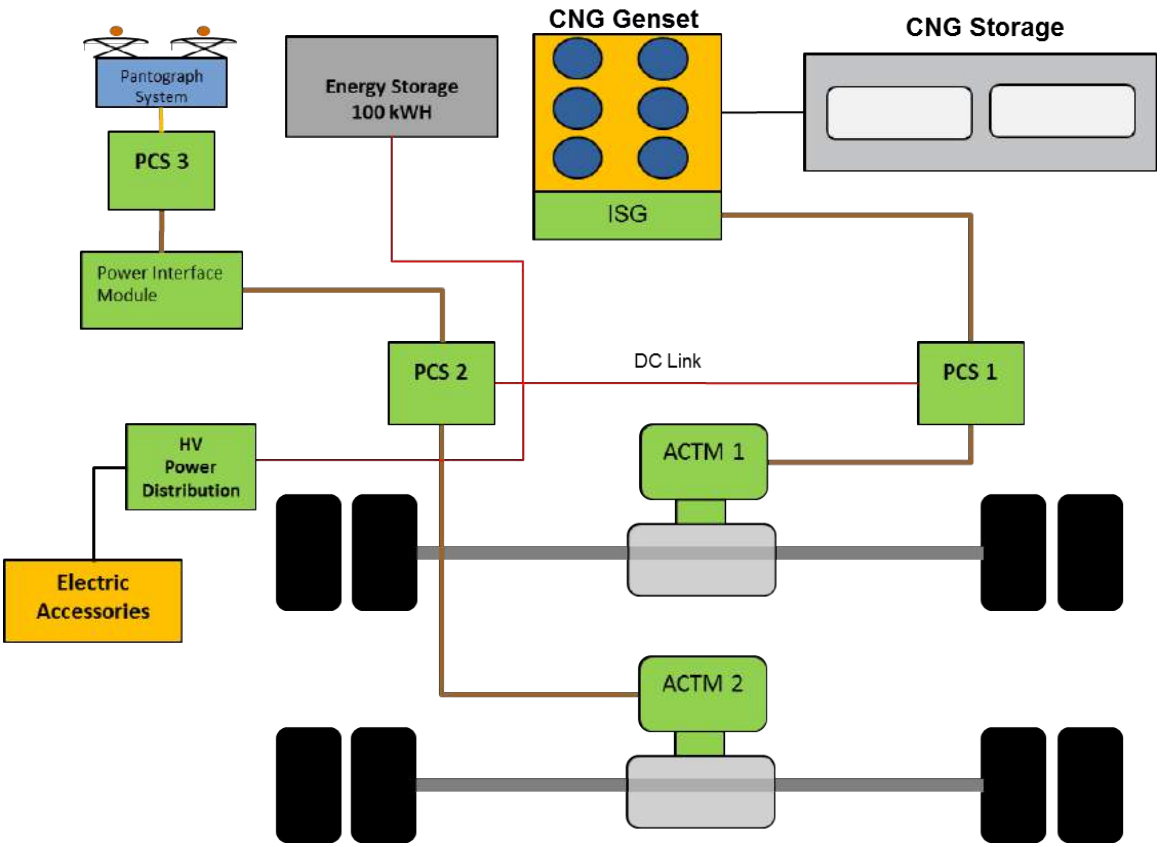


Figure III.9.4 - BAE CNG Hybrid System Architecture

**Hydrogenics** is replacing International Rectifier in the ZECT 2 San Pedro Bay project and they will be developing and demonstrating a fuel cell range extended Class 8 truck. Hydrogenics working with Daimler's VVG dealership group developing a fuel cell range extended truck under a California Energy Commission (CEC) project.

Table III.9-1 - Hydrogenics Vehicle Systems Specifications

| Item | Target Specification |
|---|---|
| Chassis | Daimler Freightliner Cascadia Day Cab |
| GVWR | 80,000 lbs |
| Fuel Cell Power System | Hydrogenics CelerityPlus |
| Electric Drive | Siemens ELFA PM Motor |
| Battery | ACTIA100 kWh |
| System Voltage | 650 V |

| | |
|---|---|
| Hydrogen Storage | 30 kg @ 350 bar |
| Refuel Time | 10-15 minutes |
| Expected Range | 150-200 mi |

## Results: FY 2017

*TransPower*

*Fourth Quarter 2016:* Battery design progressed with development of CAD models for a 360Ah, 4P120S KAM cell configuration. The cells are more compact than the cells TransPower has used on earlier vehicles, and have higher energy density. The net result should be a slight increase in performance as compared to the 300Ah cells used on earlier vehicles. The cells are in route, with arrival expected in January. A full BoM has been developed for this battery, with detail drawings completed. Critical items have been bid, ordered, and first items received inspected and approved. There are ongoing design and bid discussions, it is planned these will be concluded in January such that battery assembly can proceed in mid first quarter.

*First Quarter 2017:* Several fuel storage options were considered, with the end result of selection of A1 Alternative Fuel Systems as the hydrogen tank integrator. The system has been built around four Type 3 tanks which were supplied by Worthington/SCI (formerly Structural Components Incorporated) and offer approximately 19kg of fuel on board. The valves for these tanks includes manual and automatic shutoff on each tank, temperature actuated pressure relief capability on both ends of the tanks, and an excess flow shutoff valve which will cut off fuel flow in case of plumbing damage. These fuel storage systems are complete and in house, and the first system has been installed onto the first fuel cell truck.

*Second Quarter 2017:* A Navistar chassis has been used with the Elec-Truck drive train components mated to the battery system and the fuel cells, DC-DC converters and fuel system. With the four tanks and 19 kg hydrogen it is expected range will be extended to approximately 145 miles with performance similar to that of the battery electric truck, except that sustained freeway travel in excess of battery range will be subject to some speed limitations, which will be very dependent on prior use of the truck.

*Third Quarter 2017:* The first prototype truck is complete and has been test driven on public roads on and off throughout the third quarter of 2017. Use of the truck to carry containers has been delayed by discovery of a design flaw in the mounting of the fuel cells and fuel tanks behind the cab – insufficient space was left for containers to swing freely while the truck is turning. To resolve this issue, the two trucks will be sent to a local truck body shop to have their frames extended. This work will be performed on the first truck in October, enabling it to be used for container movement by the end of October if no new problems are encountered.

*US Hybrid*

*Fourth Quarter 2016:* The US Hybrid team in Torrance, CA completed the Cell Stack placement location in the Stack Enclosure (SE) and the SE placement location in the vehicle. The load study report was generated for the SE, in collaboration with stress analysis personnel, as well as completion of the design, fabrication and integration of the frame mount brackets. Also, the unit cross beams design was revised, fabricated, and welded to the SE. The redesign of the external brackets and air inlet/outlet ducts for the SE was completed, fabricated, and welded, followed by a fit-check performance with the components received from the Connecticut office. The design for two stainless DI water tanks was finalized, as well as the sheets fabrication (no welds) with additional attached fittings.

*First Quarter 2017:* The engineering department completing the Fuel Cell enclosure components design, specifically the Fuel Processing System (FPS) flow path mounts blocks. The fabrication of the mentioned blocks was completed, as well as the final fit-check of assembled fabricated parts. All components related to

FC enclosure were then packaged and shipped to the Connecticut office to be reassembled for system test process.

*Second Quarter 2017:* The FCe™80 fuel cell underwent some performance and duty cycle testing. The performance data is provided in engine efficiency and Kwh/kg of hydrogen. At such performance one kg of hydrogen is equivalent energy of 180kg (396 lbs.) of battery weight. The stack performance and at the end of life, we see this value reduce by 15%. The data shows that the FCe™80, fuel cell engine running on ambient pressure and using the high efficiency isolated dc-dc converter, is the best in its class. We are still expecting further optimization of the fuel cell engine.

*Third Quarter 2017:* U.S. Hybrid successfully unveiled the first H2 Truck at the 2017 Advanced Clean Transportation (ACT) Expo in Long Beach, California. This display represented the beginning of the path ahead toward commercialization. FCe™80 fuel cell engine was integrated along with the air and fuel system. The engineering team also fit checked and installed the traction motor, customized drive shaft fuel cell cooling system, Electric driven air compressor unit and the electro-hydraulic steering. Additionally, the battery, auxiliary system housing, mounting, and high voltage and low voltage wiring harness were integrated.

### *CTE/BAE and Kenworth Trucks*

*Fourth Quarter 2016:* A mockup of the truck cab and hood has been started. This permits test fitting the subsystems on a representative truck frame. Metal brackets designed to position and mount the fuel cell to the truck chassis were fabricated and used to install the fuel cell mockup to the truck mockup. Fuel cell accessories are currently being mounted to the fuel cell mockup to control clearances and routing of hoses and wiring.

*First Quarter 2017:* During the critical design review, the truck layout, subsystem FMEA, truck weight analysis, propulsion system architecture, simulation results, and truck integration plan were all reviewed and found acceptable with only a few exceptions. The exceptions were minor problems and easily fixable. An example is a missing backflow prevention device in one of the cooling loops. These exceptions were noted and will be corrected in the design. In one case, Ballard suggested a simplification to the fuel cell water system that will reduce cost and complexity without sacrificing performance. Based on the design review, Ballard, BAE, Kenworth, and CTE all agreed that the design was acceptable. The pre-production meeting did not find or identify any obstacles to production of the vehicle and so production was approved.

*Second Quarter 2017:* BAE finalized their requirements documents, control laws, and interface documents with Kenworth. The design is still subject to minor revisions as needed because of any problems found during integration, but these will be reported under the integration tasks. Kenworth successfully implemented a change in motor design addressing the high voltage interlock which resolved a safety concern. Successful updates of the design of the high voltage routing and the cooling routing are complete. Continued software development for the truck controller (VECU) represents the closing of the design phase. Design for all parts of the ESS is complete. Fuel cell air intake and exhaust plenums are fabricated and preparation for incorporation into the truck is underway. Software was developed for the four independent cooling systems on the truck. Software development for the master controller continues.

*Third Quarter 2017:* BAE performed a full range of tests on the AM Racing traction motor system (ACTM). The firmware was updated to optimize the performance and control. The test results were documented, and they showed successful test across a range of speeds and torque settings. The software control of the ACTM was implemented; the tests validate the expected performance and control. For the battery energy storage system, the updated XPAND software was installed and tested. BAE worked with XALT to resolve several remaining issues. The XPAND software will be used in the initial testing on the truck.

*GTI/BAE and Kenworth Trucks*

*Fourth Quarter 2016:* The Project Team sent a list of critical information to Siemens for the pantograph integration with the hope of getting "non-proprietary" information that could support the continued development of the major truck components. Siemens replied that they are not able to share any information until the Agreement is in place. This will slow, or halt, progress on the final design as several interfaces with the pantograph are unknown. The administrative efforts with Siemens have caused significant delays that may lead to changes in schedule and budget for the program.

*First Quarter 2017:* Besides the Siemens pantograph, the truck design and fabrication is on schedule for a field test in early 2018. The major issues around the design and fabrication of an electric drive train capable of hauling an 80,000 lb. GVW tractor combination up a 6.5% grade at 35 mph have been addressed and hardware is in fabrication or in-house. Any issues around using the Cummins Westport L9N near-zero emissions engine are being resolved. At this point, the project remains on target to complete the vehicle (without the pantograph) and turn it over for extended testing early in 2018.

*Second Quarter 2017:* Technicians have stripped the host chassis of non-essential components required to ensure safe delivery from the production plant. Frame modifications are complete and technicians have begun preliminary assembly of hybrid specific components. First priority was to the energy storage system and testing manual access between battery packs to complete power and coolant routings. Parts were modified to simplify access then powder coat painted to protect from rusting. Pre-assembly began as the parts were returned from paint. The team built and tested some of the chassis specific cooling loops, calibrated and logged all pumps to be used on the different systems and have fed this information back to the simulation teams to update models and recheck or confirm results.

*Third Quarter 2017:* Technically, there has been excellent progress on all portions of the mechanical and electrical sub-system and vehicle integration tasks (as shown in the photos below). Harness designs are nearly complete and ongoing modifications depict the as built condition. As the vehicle assembly progresses additional modifications will be tracked and logged as required. Test fitting the components have ensured all subassemblies can be completed quickly and efficiently. Open issues remain and are related to the high voltage wire routings and the potential interference and clearance with coolant lines running through the same passages, air lines and low voltage wire interference. The handshake and initial integration between the vehicle and hybrid drive control was successfully completed but was not entirely without incident. Both teams jointly developed a resolution task list and are working to solve the discrepancies before installing the VECU and PCS on the chassis.

*Hydrogenics*

*Third Quarter 2017:* The design and procurement phase of the project with CEC to design and develop the first of two trucks is 90% complete. Completed tasks include but not limited to the following:

- Truck Chassis: Received Daimler chassis at Hydrogenics Mississauga facility. Took detailed chassis and component placement measurements to ensure fit of components on the truck including fuel cell cradle
- Fuel Cell System & Cradle: Commenced build of Celerity Plus fuel cell power system; received fuel cell cradle and passed QC inspection
- Battery System: Finalized form factor with ACTIA after numerous discussions, ACTIA confirmed and concluded that NMC solution will not be ready for the CEC project and will use LTO form factor.
- Electric Drive: Conference calls held with Siemens to revise and finalize the high voltage architecture. Siemens components finalized and compatibility with accessories motors confirmed.

## III.10 Medium Duty Vehicle Powertrain Electrification and Demonstration

**Mr. Wiley McCoy, Principal Investigator**
McLaren Engineering Division of Linamar
32233 W Eight Mile Road
Livonia, MI 48152
Phone: (248) 473-3213 x41213
E-mail: Wiley.Mccoy@Linamar.com

**Lee Slezak, Technology Manager**
U.S. Department of Energy
Phone: (202) 586-2335
E-mail: Lee.Slezak@ee.doe.gov

Start Date: June 1, 2016 End Date: March 31, 2020
Total Project Cost: $3,650,000 DOE share: $2,640,000 Non-DOE share: $1,010,000

### Project Introduction

This project is intended to address a number of technical barriers regarding use of electric / hybrid drive systems in the medium duty marketplace as described in the Vehicle Technologies Multi-Year Program Plan. Specifically, the technical barriers are:

- Acceptance of electric drive as Medium Duty vehicle choice
- Reduce the carbon footprint of transportation (FE Improvement)
- Cost of hybridization (medium duty TCO).

A team consisting of industry leading engineering, production and user companies was formed to specify, design, build and test a commercially viable medium duty drive system that would reduce fossil fuel use by a minimum of 50% in real world drive cycles. McLaren Linamar, AVL, & UPS are partnered to achieve the program objectives.

### Objectives

Project Objective / Expected Outcome - to attain a 100% improvement in Fuel Economy over real world drive cycles for medium duty package delivery vehicles & achieve a system at project conclusion that can be commercialized at a reasonable Total Cost of Ownership.

### Approach

•Project Approach - Team has developed the hybrid system specifications in simulation and completed the first milestone by showing a 100% fuel economy improvement over real world drive cycles measured over UPS delivery routes. This completed the first phase of the program. The second phase, which is still in progress is to design and develop a plug-in hybrid powertrain, incorporating a novel medium duty electric drive axle. The team is in the process of building 4 demonstration vehicles and will conduct a demonstration of performance, cost and reliability for a period of up to 12 months.

Future work will include a third phase of system demonstration. This demonstration will commence in Q1 of the 2018 CY. At present, the team is in the process of final design and release of the components for build of the demonstration vehicles. McLaren / Linamar is responsible for design and build of the eAxle; AVL will simulate the system & design, build and install the energy storage and range extender systems and integrate all systems to complete the build of 4 vehicles; UPS will conduct the demonstration of real world package delivery routes and transmit data back to the design team for ongoing analysis of performance, durability and

reliability. This project is intended to support commercialization of the system. An analysis of the system cost and complexity, as well as a calculation of total cost of ownership will also be completed with the support of UPS and their partner in vehicle up-fitting. At the end of or during the demonstration phase a decision will be made regarding commercialization of the systems on a broader group of package delivery vehicles.

## Results

In simulation on a real world drive cycle, the fuel economy objectives are met across the vehicle weight range experienced during normal package delivery usage. Points shown are Curb + 1500# and Curb + 10000#

**Table III.10-1 - Real World Drive Cycle Simulation Results**

| All Electric Range Curb + 1500lbs | | | |
|---|---|---|---|
| | Energy Economy | All Electric Range | Usable Energy |
| Cycle | [kWHr/mi] | [mi] | [kWHr] |
| VBS008 Day1 | 0.758 | 39.9 | 30 |
| VBS010 Day2 | 0.801 | 37.7 | |
| VBS001 Day4 | 0.670 | 45.2 | |
| Average | 0.780 | 38.8 | 30 |

| Diesel Curb + 1500lbs | | | |
|---|---|---|---|
| | Conventional | Hybrid | Improvement |
| Cycle | [mpg]* | [mpg]* | [%] |
| VBS001 Day4 | 9.4 | 20.6 | 119% |

| All Electric Range Curb + 10000lbs | | | |
|---|---|---|---|
| | Energy Economy | All Electric Range | Usable Energy |
| Cycle | [kWHr/mi] | [mi] | [kWHr] |
| VBS008 Day1 | 1.040 | 29.1 | 29 |
| VBS010 Day2 | 1.121 | 27.0 | |
| VBS001 Day4 | 0.998 | 30.3 | |
| Average | 1.081 | 28.0 | 29 |

| Diesel Curb + 10000lbs |
|---|

| | Conventional | Hybrid | Improvement |
|---|---|---|---|
| Cycle | [mpg]* | [mpg]* | [%] |
| VBS001 Day4 | 6.0 | 17.8 | 196% |

The vehicle drive system can meet all performance requirements specified by the end user partner.

Table III.10-2 - Vehicle drive system requirements, design specifications, and simulated performance parameters

| | Requirement | HDEAXLE HVH250-90 mm-DOM | | Unit |
|---|---|---|---|---|
| **Mass**<br>**All Hybrid values at Test weight unless otherwise stated.** | **Curb:4408**<br>**Test:5089**<br>**GVW:13154** | **Test:5089** | | **[kg]** |
| **Gear1** | | 18.15 | | [-] |
| **Gear2** | | 8.8 | | [-] |
| **Final Drive** | | 1 | | [-] |
| **Total Gear1** | | 18.15 | | [-] |
| **Total Gear2** | | 8.80 | | [-] |
| **Peak Power Mechanical** | | 344 | | [kW] |
| **Continuous Power Mechanical** | | 246 | | [kW] |
| **Motor Peak Power Time Const.** | | 1 | | Min |
| **Acceleration 0-100kph** | 23 | 10.12 | | [sec] |
| **Acceleration 60-100kph** | 15 | 6.29 | | [sec] |
| **Acceleration 0-60kph** | 8 | 3.83 | | [sec] |
| **Peak Traction Effort Stall** | 27 | 32 | | [KN] |
| **Continuos Traction Effort Stall** | | 22 | | [KN] |
| **Top Speed** | 113 | 155 | | [kph] |
| **Maximum Launch Grade @GVW** | 20 | 20 | | [%] |
| | | **Pk**<br>**[30 sec.]** | **Cnt** | |
| **Grade Speed 20%** | 38 | 102 | 50 | [kph] |
| **Grade Speed 17%** | 40 | 109 | 88 | [kph] |
| **Grade Speed 10%** | 70 | 130 | 120 | [kph] |
| **Grade Speed 5%** | 90 | 149 | 135 | [kph] |

| | Requirement | HDEAXLE HVH250-90 mm-DOM | | Unit |
|---|---|---|---|---|
| **Grade Speed 2%** | 110 | 155 | 150 | [kph] |
| **Grade Speed 0%** | 115 | 155 | 155 | [kph] |
| **Fuel Economy HDUDDS:(Diesel)** | 11.4 | 23 | | [mpg] |
| **Fuel Economy HDUDDS:(Propane)** | 7.4 | 15 | | [mpg] |
| **All Electric Range** | 35 | 38 | | [mi] |
| **Fuel Capacity (Propane)** | 45 | 45 | | [gal] |
| **Total Range** | 369 | 500-600 | | [mi] |

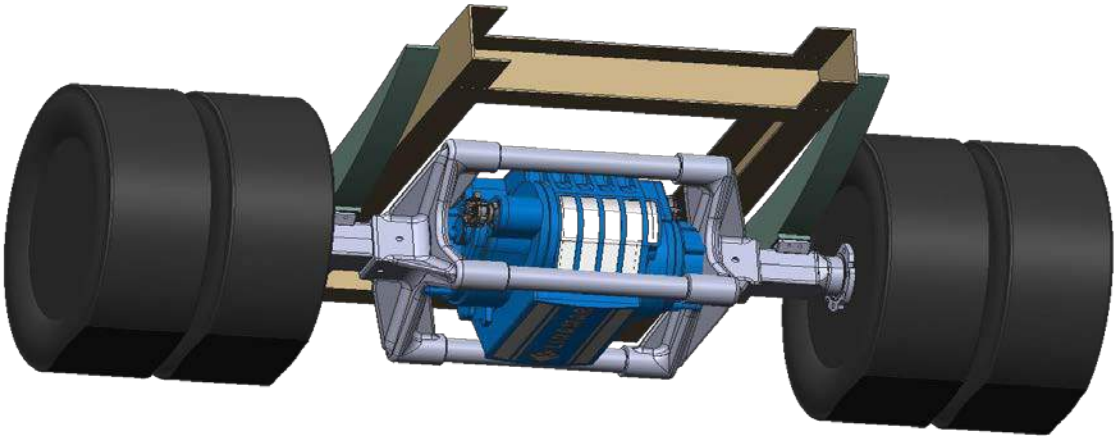

Figure III.10.1 - eAxle Drive System Design (In process of prototype build)

## Conclusions

As of the end of FY17, the conclusions of this program to date are:

- A system can be specified using advanced modeling and simulation tools that will show the design parameters for an electrified vehicle powertrain system that will achieve the overall program objectives
- A novel eAxle system, energy storage & range extender systems can be designed and is being built for installation in 4 Demonstration vehicles
- A 4 vehicle demonstration on real world package delivery routes can commence in Q1 of CY 2018
- Commercial interest is increasing. This full team is capable of full volume production of a successfully demonstrated system.

## Key Publications

The project did not produce any publications.

# IV. Grid Modernization

The Grid Modernization project performers were members of the Grid Modernization Laboratory Consortium (GMLC). The original GMLC team was composed of ten national laboratories. The original GMLC members include Argonne National Laboratory (ANL), Brookhaven National Laboratory (BNL), Idaho National Laboratory (INL), Lawrence Berkeley National Laboratory (LBNL), Lawrence Livermore National Laboratory (LLNL), National Renewable Energy Laboratory (NREL), Oak Ridge National Laboratory (ORNL), Pacific Northwest National Laboratory (PNNL), Sandia National Laboratory (SNL), and Savannah River National Laboratory (SRNL).

Grid Modernization projects during FY 2017 were categorized as either general or vehicle specific projects. The vehicle specific project in this APR include GM0062, GM0085, GM0086, and GM0163. The general project numbers include GMLC 1.2.3, GMLC 1.4.2, and GMLC 1.4.10.

## IV.1 Vehicle to Grid Integration Pathway

**Rick Pratt, Principal Investigator**
PNNL
P.O. Box 999, K5-17
Richland, WA 99354
Phone: (509) 375-3820
E-mail: rmpratt@pnl.gov

**Lee Slezak, Technology Manager**
U.S. Department of Energy
Phone: (202) 586-2335
E-mail: Lee.Slezak@ee.doe.gov

Start Date: April 1, 2016 End Date: September 30, 2018
Total Project Cost: $3,400,000 DOE share: $3,400,000 Non-DOE share: $0

### Project Introduction

The Vehicle to Building Integration Pathway project (GM0062) will develop and demonstrate pre-normative methods needed to develop a standardized and interoperable communication pathway and control system architecture between Plug-in Electric Vehicles (PEVs), Electric Vehicle Support Equipment (EVSE) and Building/Campus Energy Management Systems (BEMSs) to enable the integration of clean variable renewable sources with workplace PEV charging infrastructure to promote greater PEV adoption. This communications and control platform will provide access to real-time system monitoring information, establish an infrastructure to coordinate intelligent assets, manage energy consumption behind the meter, reduce peak demand charges resulting from vehicle charging, and potentially participate in energy and/or ancillary services markets.

### Objectives

A successful project includes developing use cases for scalable systems and demonstrating at multiple laboratories affordable, communications and control platforms controlling multiple PEVs charging. The demonstrations will use transactive control constructs showing demand charge reductions, providing value to PEV owner and grid, and integrating rooftop solar and building controls. Use cases and testing plans that leverage ongoing work will be developed in FY16. Annual demonstrations will show increasing capability, control algorithm advancement, and leverage existing test beds at ANL, NREL, and PNNL. An FY18 task includes integrating an INL-developed cyber communications monitoring capability.

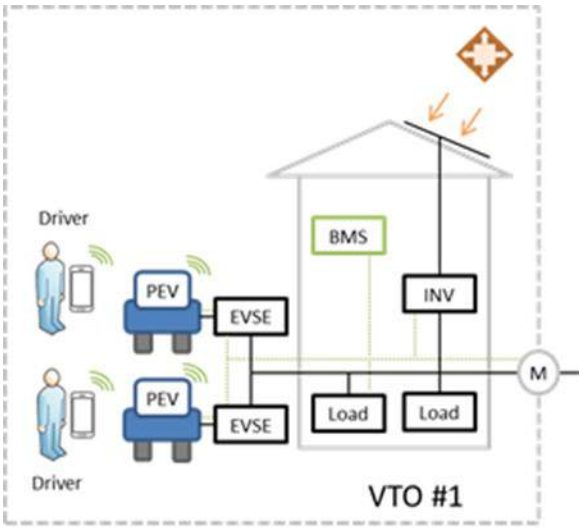


Figure IV.1.1 - GM0062 Workplace Charging Project Scope

## Approach

ANL, INL, LBNL, NREL and PNNL jointly developed the workplace vehicle charging demonstration use cases, communication requirements and control requirements needed to demonstrate coordinated PEV charging under time varying commercial building load conditions that minimize demand charges. These use cases have been reviewed by an Industry Advisory Board (IAB) and integrated with the communication and control requirements to form the basis for performing four electric vehicle charging demonstrations.

1. The demand response demonstration will show that the integration platform design will enable the aggregated PEVs to each provide their maximum power variation (e.g., 3.3 kW or 6.6 kW) in response to the DR signal within the developed communication and control requirements and be completed by 4/1/2017.

2. The second demonstrate will include aggregated building loads, multi-vehicle charging loads, and the dynamic workplace PEV charging use cases to show that the integration platform design mitigates peak demand charges from vehicle charging, maximizes available charging power delivered to the PEVs, and prioritizes energy delivery to PEVs with highest energy needs (e.g., low state of charge / short charging time available) and be completed by 10/1/2017.

3. The third demonstration will integrate variable renewable resources and market signals (energy price, carbon emissions intensity of fuel source, etc.) into the workplace charging demonstration with aggregated building loads, multi-vehicle charging loads, and dynamic workplace PEV charging use cases developed. A successful demonstration will verify that the integration platform design mitigates peak demand charges from vehicle charging and prioritizes renewable energy delivery using state of charge, charging time available, and the customer's desire for "greenest", "cheapest", or "fastest" charge. With these inputs the platform's control algorithms will optimize charging based on the building's priorities and the PEV driver's preferences.

4. Demonstrate the control system's capability to use Transactive Control methods with aggregated building loads, multi-vehicle charging loads, variable renewable resources, and dynamic PEV charging use cases. A successful demonstration will verify the control system's capability to use Transactive Control methods; maximize available charging power delivered to the PEVs; and prioritize energy delivery to PEVs with highest energy needs (e.g., low state of charge / short charging time available).

## Results

NREL led the multi-lab GM0062 Use Case development task and the process was guided through feedback from the Industry Advisory Board. Feedback was received from seventeen of fifty vehicle manufacturers (OEMs), utility, and regulatory entities. Follow-up was provided via conference calls, a February Grid Integration Tech Team meeting, and at the Grid Modernization Lab Consortium (GMLC) annual review poster session in April. Several entities were very excited about the work and eager to receive updates.

Figure IV.1.2 provides a graphical representation of the feedback received with a stronger emphasis wanted by the Advisory Board in load control areas (e.g., demand response, capacity deferral, and price-based controls) as well as demand charge mitigation. This industry feedback has provided valuable guidance toward maximizing the value of demonstrations performed.

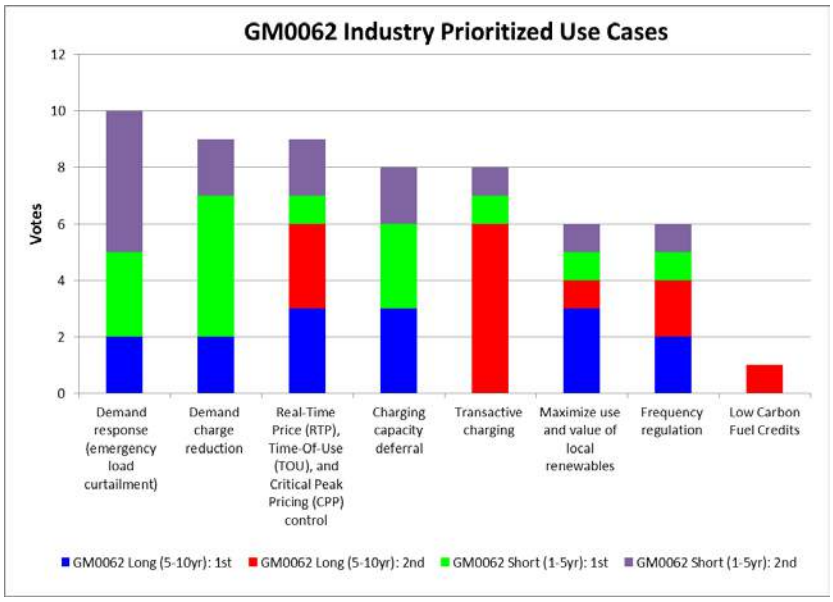


Figure IV.1.2 - GM0062 Industry Advisory Board Prioritized Use Cases

A standards-compliant (OpenADR), multi-vehicle, workplace charging demand response (DR) use case was demonstrated at ANL, NREL and PNNL using ANL's CIP.io platform to coordinate scheduled charge control variations (charge power, load shedding, timing, etc.). The demonstrations showed that each platform design enabled the aggregated PEVs at each location to provide their maximum power variation in response to the DR signal generated by an OpenADR VTN hosted by ANL. The ANL Demand Response demonstration results are shown in Figure IV.1.3 below with the Demand Response event within the red ellipse.

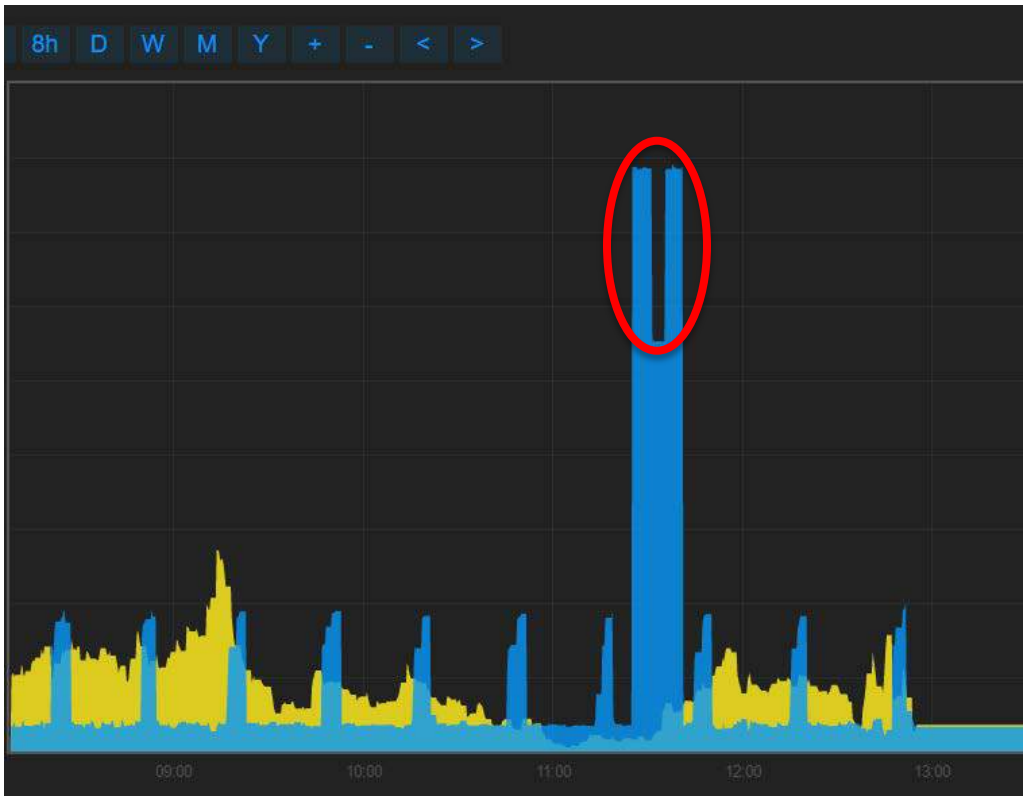


Figure IV.1.3 - ANL Demand Response

Demand Charge mitigation control was also demonstrated at ANL, NREL and PNNL with an objective of limiting the aggregated PEV charging load as the total building load increases toward the monthly peak power. Additional charges must be paid (~$7-10/kW) if the 15-min average building load exceeds the monthly peak power. Implementing PEV charging controls to prevent PEV charging from causing payment of demand charges was the focus of this demonstration. Figure IV.1.3 shows that if building and PEV loads were allowed to increase above the 16 kW Demand Charge mitigation threshold to the projected peak load could cause up to a $40/month additional utility charge for the building owner in this demonstration.

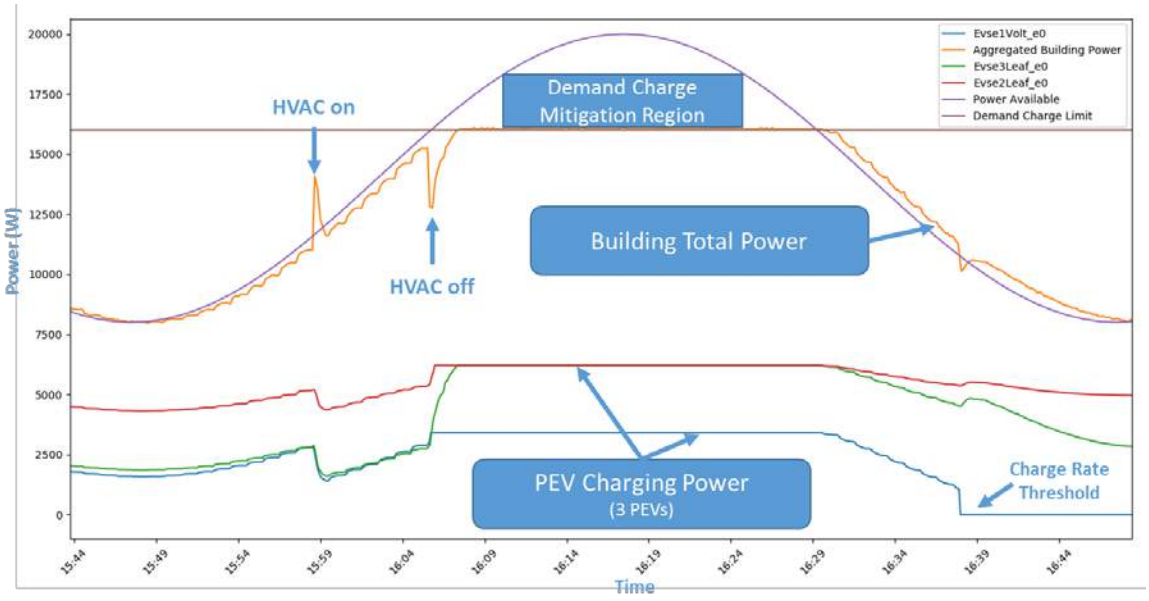


Figure IV.1.4 - PNNL Demand Charge Mitigation EVSE / PEV Control Response

Figure IV.1.4 shows two Nissan LEAFs and one Chevy VOLT charging using the PNNL charging control. Each PEV's charging power differs based on the state of charge, maximum charging rate, charging time and the current Available Power.

Workplace charging demand control with aggregated campus building load was demonstrated at NREL on September 11, 2017. The monthly peak demand for September, up until the morning of September 11, 2017, was 4.2 MW. As a result, charge management is active when the real-time campus net load is above a 4.0 MW threshold that includes a 200 kW buffer. Figure IV.1.5 shows the test results of charge management. The load of the charging stations was 127 kW before the event started and was 55 kW after the event started. This control achieved about 72 kW of load reduction. During the event 22 of the 36 charging stations participated based on the energy requirement using method 3, the departure time provided by the user, and the adjusted charging power calculated by the algorithm.

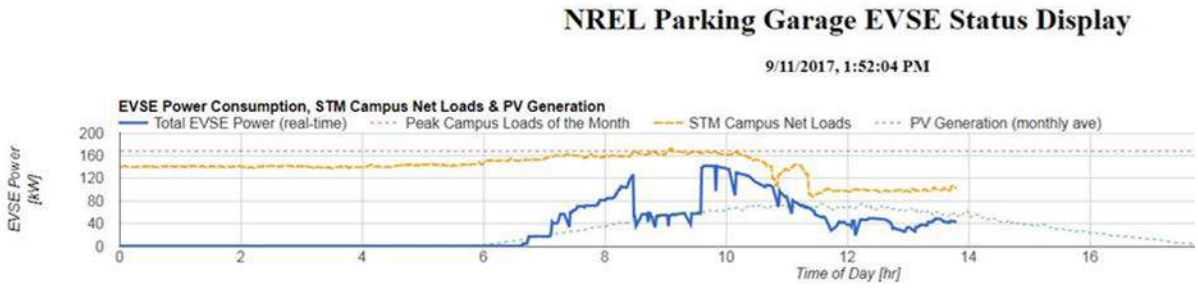


Figure IV.1.5 - NREL Control System Shifting PEV Charging from Demand Charge Mitigation to Renewables Only

*Control system capabilities*

**Table IV.1-1 - Test Bed / Control System Capabilities**

| Test Bed / Control System Capabilities | ANL System | NREL System | PNNL System |
|---|---|---|---|
| **Control Approach** | Central Control | Central Control | Distributed Control |
| **EVSEs** | 6 | 36 | 4 |
| **Components** | Smart Energy Plaza, CIP.io & Smart Charge Adapters | NREL Parking Garage & Raspberry Pi controllers | PNNL Lab Homes, Bldg. 3820 & Raspberry Pi controllers |
| **Control Goal** | Maintain total load below configurable peak | | |
| **Functional Approach** | Building EMS controls each charging PEV to meet buildings goal (demand charge mitigation, frequency reg., etc). Control based on PEV's needs. | System controller optimizes each PEV charge schedule to not exceed Demand Charge Limit | Each PEV controller optimizes its PEV charge schedule to not exceed system goal |
| **Operation** | • PEV's ranked by Instantaneous missing DC Ah; control adjustments based upon available power and PEV's use of available power<br>• Minimum charge rate maintained | • PEV amp-hours needed updated each second<br>• Minimum charge rate maintained<br>PEV's ranked by energy required, highest deficit increased to limit; then next PEV | • Available power = Bldg Goal – Current Power<br>• PEV priority = kWh needed / (time remain * charge rate) updated each second<br>• PEV power change = Available Power * priority / total priority |

**Table IV.1-2 - Standards and Equipment Gaps Identified**

| Gaps Identified | Standards |
|---|---|
| **Standards** | • The SAE J1772 requirement for a charging PEV to respond within 5 seconds of a change in charge limit could restrict there use in grid services that require faster response times, such as frequency regulation. |
| **Current EVSEs** | • OCPP 1.6 (Building to EVSE Communication) is the first standardized attempt at smart charging control for EVSE. Limited implementation.<br>• EVSE OEM specific API access into EVSE controls / data is limited with varying degrees of latency. |

| Gaps Identified | Standards |
|---|---|
| Current PEVs | • Current SOC, final SOC and Time Charge is Needed (TCIN) is only available through 3rd party solutions or vehicle owner input into control system. The ISO-15118 standard could provide this information. |
| Current EVSE/PEV | • Currently, only one EVSE and one PEV vendor have implemented the communications (ISO-15118) between the EVSE and PEV that would enable digital communication to be shared between the PEV and EVSE. |

## Conclusions

Each lab (ANL, NREL and PNNL) has successfully implemented Demand Response and Demand Charge mitigation methods into commercially available PEVs and EVSEs using the existing Society of Automotive Engineering (SAE) standards. The following conclusions have been developed:

- No PEV or PEV control modifications are needed to adjust the PEV charging rate. All charging rate control can be implemented by adjusting the EVSE / PEV signal that sets the maximum charging rate the EVSE can support (EVSE Control Pilot Duty Cycle).
- The charging rate control was implemented by implementing external control of the EVSE Control Pilot signal to overcome the limited API and external charging rate control capabilities of commercially available EVSEs.
- The existing standards (SAE-J1772 and ISO-15118) need to be updated to enable PEV charging rate control that will support all developed use cases.

## Key Publications

1. GM0062 poster presentation on 4/18/2017 at the GMLC Peer Review in Washington, DC.
2. GM0062 prioritized use cases were presented on 2/22/2017 to the GITT Meeting in Denver, CO.

## IV.2 Systems Research for Standards and Interoperability

**Don Scoffield, Principal Investigator**
Idaho National Laboratory
755 University Boulevard
Idaho Falls, ID 83415
Phone: (208) 526-5958
E-mail: don.scoffield@inl.gov

**Lee Slezak, Technology Manager**
U.S. Department of Energy
Phone: (202) 586-2335
E-mail: Lee.Slezak@ee.doe.gov

Start Date: May 1, 2016 End Date: April 30, 2019
Total Project Cost: $3,480,000 DOE share: $3,480,000 Non-DOE share: $0

### Project Introduction

As plug-in electric vehicles (PEVs) increasingly penetrate the marketplace, the integration of electric vehicles into the grid is essential to ensure the continued reliability and security of the grid. To accomplish this, the project has developed a hardware-in-the-loop platform to study integration of numerous electric vehicles on a residential distribution feeder. Using this platform uncontrolled electric vehicle charging will be analyzed for many different electric vehicle penetration scenarios. These scenarios will begin to answer the following questions regarding uncontrolled electric vehicle charging:

1. Will widespread uncontrolled electric vehicle charging cause grid problems?
2. At what electric vehicle penetration does uncontrolled electric vehicle charging begin to cause grid problems?
3. What are the grid problems caused by uncontrolled electric vehicle charging?

Another key deliverable of this project is to develop a charging control strategy that can be used to help mitigate grid problems associated with uncontrolled electric vehicle charging, to enable electric vehicles to provide grid services, and to ensure electric vehicle owners charging needs are met. The benefits of this control strategy is described in the Results section below.

### Objectives

- Quantify impact of widespread uncontrolled charging
- Develop a control strategy to manage PEV charging.
- Understand the cybersecurity risks associated with controlled PEV charging.
- Determine the feasibility of PEVs providing grid services at the electric utility distribution level.

### Approach

The objective of the proposed project is to address the considerable uncertainty regarding the degree to which uncontrolled PEV charging will impact the grid and if PEVs can provide grid services and mutually benefit the electric utilities, PEV owners, and auto manufacturers.

This project will answer this question by leveraging capabilities of multiple national laboratories with vehicle/grid integration (VGI) to perform HIL studies that integrate communication and control system hardware with simulation and analysis activities. These studies will do the following:

- Quantify the impact of widespread uncontrolled charging.
- Study how to effectively incorporate PEVs into the grid as controllable loads.
- Perform controller development to verify the viability of controlling PEV charging to provide grid services.
- Understand the cybersecurity risks associated with controlled PEV charging
- Provide an understanding of the impact of using PEVs as distributed energy resources (DERs) on the PEV owner, on distribution network system dynamics, power quality, and stability.

The work will focus on the integration of PEVs at the electric utility distribution to provide grid services. This will be done in the HIL environment to allow the following:

- Develop strategies for controlling PEV charging with respect to system dynamics at the distribution feeder level.
- Perform experiments that emulate distribution-level vehicle grid integration in a variety of scenarios and use cases.
- Verification of open communication standards.

All this will be done using open-source control architectures and communication protocols that adhere to current standards, so that methodologies may be shared and standards can be improved. This project will develop distribution-level hardware-in-the-loop (HIL) scenarios to emulate a large number of vehicles and other DERs at numerous facilities. The project will be based on dynamic real-time simulation (DRTS), which performs low-level physics modeling of the electrical system.

The platform will develop controls approaches to understand how to prioritize the needs of the PEV customer and the grid in multiple use cases, by the means of a Distribution Management Systems (DMS) and/or 3rd party aggregator. To accomplish this, this project will develop a front-end controller (FEC) to enable coordination of PEV charging with the utility and other entities. The FEC will be built into controller cards that each interface with a single electric vehicle supply equipment (EVSE) unit to control the charging of an individual vehicle. The FEC will determine when to start and end charging and establish the charge power level, based on information received from the vehicle, EVSE, and a coordinating entity behind the meter, such as a DMS or 3rd party aggregator.

The project will emulate a DMS/3rd party aggregator to generate control signals that communicate with the FECs. To do this, the project will partner with Siemens to leverage its open-architecture Smart Energy Box (SEB) to implement the FEC and interface with DMS and aggregator models. The SEB is an open-source, vendor-neutral controller development platform and a scalable automation middleware. SEB will enable emulation of distribution management system software and create a bridge between the distribution-level power system simulation running in the DRTS and the FEC cards.

Initially, the FEC will be developed and tested using up to four actual vehicle/EVSE pairs connected to the HIL platform. Then, to simulate a large number of vehicles connected across an entire distribution network (i.e., 1,000 or more), high-fidelity dynamic vehicle charging models will be used. These models will be created by characterizing the actual charging behavior of a variety of production plug-in electric vehicles and EVSE. Dynamic models based on these characterizations will be embedded in the HIL system.

## Results

Dynamic PEV charging models have been created for the HIL test platform for the following production PEVs: 2015 Nissan Leaf, 2016 Chevy Volt, and the 2013 Ford Fusion. The behavior of these charging models very accurately represents the actual charging behavior of the production PEVs. The following steps were used to create the PEV charging models.

- Performed many tests that captured the PEVs charging behavior in a variety of grid conditions.
- Created the equations describing the PEV charge from the test data.
- Created models in software using these equations.
- Integrated these software models to run on raspberry pi cards and communicate in real time with the RTDS.

A strategy to control the charging of PEVs at the distribution feeder level has been developed and is currently being tested and refined. The charging control strategy has the following desirable characteristics:

- The strategy ensures that the PEVs are charged in such a way to maximize charging efficiency and power quality.
- The strategy is scalable. It can be used to control the charging of hundreds, thousands or even millions of vehicles.
- The strategy is computationally efficient. A single PC can perform the calculations controlling the charging of hundreds, thousands or even millions of vehicles.
- The strategy helps ensure that the PEVs charging needs are met. PEVs that require a lot of energy in a short amount of time are allowed to charge before PEVs that require less energy or have more time to charge.
- The strategy is not sensitive to internet latency. It does not require low latency communication between the PEVs and the aggregator.

The real-time platform to demonstrate the ability of 4,000 PEVs to provide voltage support and frequency regulations on a PG&E sub-transmission grid. This work was published in a paper cited in the Key Publications section below [2].

## Conclusions

The HIL platform is in the final stages of integration and testing. When this platform is complete the impact of uncontrolled PEV charging on a residential distribution feeder will be studied for several different PEV penetrations. In order to accurately model PEV charging in these scenarios, dynamic PEV charging models have been created for three production PEVs: 2015 Nissan Leaf, 2016 Chevy Volt, and the 2013 Ford Fusion.

A charging control strategy has been developed that can be used to help mitigate grid problems associated with uncontrolled PEV charging, to enable PEVs to provide grid services, and to ensure that PEV owners charging needs are met.

## Key Publications


1. Markel, T., A. Meintz, K. Hardy, B. Chen, T. Bohn, J. Smart, D. Scoffield, R. Hovsapian, S. Saxena, J. MacDonald, S Kiliccote, K. Kahl, and R. Pratt, "Multi-Lab EV Smart Grid Integration Requirements Study," National Renewable Energy Laboratory, NREL/TP-5400-63963, May 2015.
2. Dias, F. G., Luo, Y., Mohanpurkar, M., Hovsapian, R., & Scoffield, D. (2017, June). Potential for Plug-In Electric Vehicles to provide grid support services. In Transportation Electrification Conference and Expo (ITEC), 2017 IEEE (pp. 294-299). IEEE.

# IV.3 Modeling and Control Software Tools to Support Vehicle to Grid Integration

**Samveg Saxena, Principal Investigator**
Lawrence Berkeley National Laboratory
1 Cyclotron Road
Berkeley, CA 94720
Phone: (510) 269-7260
E-mail: ssaxena@lbl.gov

**Andrew Meintz, Principal Investigator**
National Renewable Energy Laboratory
15013 Denver W Parkway
Golden, CO 80401
Phone: (303) 275-3179
E-mail: Andrew.meintz@nrel.gov

**Lee Slezak, Technology Manager**
U.S. Department of Energy
Phone: (202) 586-2335
E-mail: Lee.Slezak@ee.doe.gov

Start Date: June 1, 2016 End Date: May 30, 2019
Total Project Cost: $2,810,000 DOE share: $2,810,000 Non-DOE share: $0

## Project Introduction

A substantial opportunity exists in vehicle-grid integration (VGI) – if 25% of US light-duty vehicles were PHEVs there would be nearly 1,000 GWh of energy storage – an unprecedented scale. This storage is deployed for clean mobility objectives, yet vehicles are parked a majority of the time allowing vehicle batteries to support grid objectives such as renewables integration. From the grid perspective, there is a low capital cost of grid storage using vehicles (capital cost is absorbed for mobility objectives), yet the grid services from vehicles can be used to lower the operating costs for PEV owners. In this manner, a synergy exists where storage from clean transportation becomes an enabler for a clean grid, while the value captured by vehicles to support the clean grid further accelerates the deployment of clean vehicles. Furthermore, flexibility in vehicle charging can provide valuable grid support on various temporal and spatial scales of aggregation, from behind-the-meter load management, to distribution systems support, to wholesale market support with ancillary services. Despite this opportunity, it remains unclear whether VGI is feasible in terms of its values, costs, complexity, and risks, and whether it is competitive with other technologies that can offer similar grid services.

This project aims to determine the feasibility of VGI by quantifying the potential value, cost, complexity, and risks in different implementations of VGI. Another important goal is to allocate available value among stakeholders and determine pathways for electrification of transportation to enable beneficial grid services such as mitigating renewables intermittency. These project outcomes will occur over a 3-year timeline. The core VGISoft framework will be completed in Years 1 and 2, and applied towards renewables integration and VGI feasibility case studies in Years 2 and 3. Optimal VGI implementation approaches will be explored in Year 3.

The project will be conducted in close coordination with the multi-lab team within VTO's EV Smart Grid Working Group, including LBNL (prime), ANL, INL, NREL, ORNL, and PNNL. The methodologies, case studies, and timeline for this project will be closely coordinated with four other proposals submitted by the EV Smart Grid Working Group (GM0085, GM0150, GM0062, and GM0163).

The multi-lab EV Smart Grid Working Group has established working relationships with several stakeholders for VGI, including OEM automakers, utilities, regulatory agencies, and EV charging station manufacturers. Through these partnerships and working relationships, the tools and results from this project will directly advance VGI. Furthermore, the case studies of this project will be developed in coordination with California's Interagency VGI Working Group. This interagency group oversees the rollout of VGI in a rapidly growing market for PEV deployment and grid integration. It is convened under the California Governor's Office and is comprised of four major State agencies: the California Energy Commission, the California Public Utilities Commission, the California Air Resources Board, and the California Independent System Operator.

## Objectives

The overall objective defining success for this project is:

Determine the feasibility of VGI by quantifying the potential value, cost, complexity, and risks in different implementations of VGI. Allocate available value among stakeholders and determine pathways for electrification of transportation to enable beneficial grid services such as renewables intermittency mitigation. In support of this objective, there will be two key outcomes that further define success for the project:

1. Developing and releasing the VGISoft co-simulation framework for examining vehicle-grid interactions in any implementation of VGI. VGISoft will enhance GMLC activities by coupling with GMLC foundational models in valuation, design and planning tools, and SETO models to address solar variability.

2. Application of VGISoft to address critical knowledge gaps for VGI through targeted case studies that quantify the feasibility of VGI, quantify potential for VGI to provide grid services such as supporting renewables integration, and determine the optimal implementation approaches for VGI.

## Approach

The VGISoft framework that will be created and applied across several case studies is comprised by a collection of toolkits. Several toolkits (especially the PEV estimation toolkit) will leverage prior methodologies and tools created by the DOE national laboratories. A schematic flowchart is provided in Figure IV.3.1 to show the main structure and approach of this project.

Figure IV.3.1 is articulated as text below:

- **PEV Estimation Toolkit:**
    - Initializes individual vehicle profiles
    - Model temporally resolved individual vehicle state information (e.g., SOC, battery health, etc.)
    - Determine individual vehicle constraints
    - **Prior DOE and other models planned to be leveraged:**
        - (LBNL) V2G-Sim for its methodology for tracking the state of N vehicles and resolving grid loads under uncontrolled and controlled charging/discharging scenarios, and built-in battery life models.
        - (LBNL/ANL) Autonomie powertrain models, where necessary, for energy consumption of vehicles while they are driving (can be initialized and run within V2G-Sim)
        - (LBNL/ANL) If necessary, travel demand models, such as MatSim/SmartBay (or Polaris/TUMs), for spatially resolved vehicle travel itineraries. Alternatively, can use data sources such as the National Household Travel Survey for vehicle travel itineraries.
        - (NREL) BlastV for battery life models that are calibrated against measurement data.
        - (INL) Data insights from vehicle charging datasets

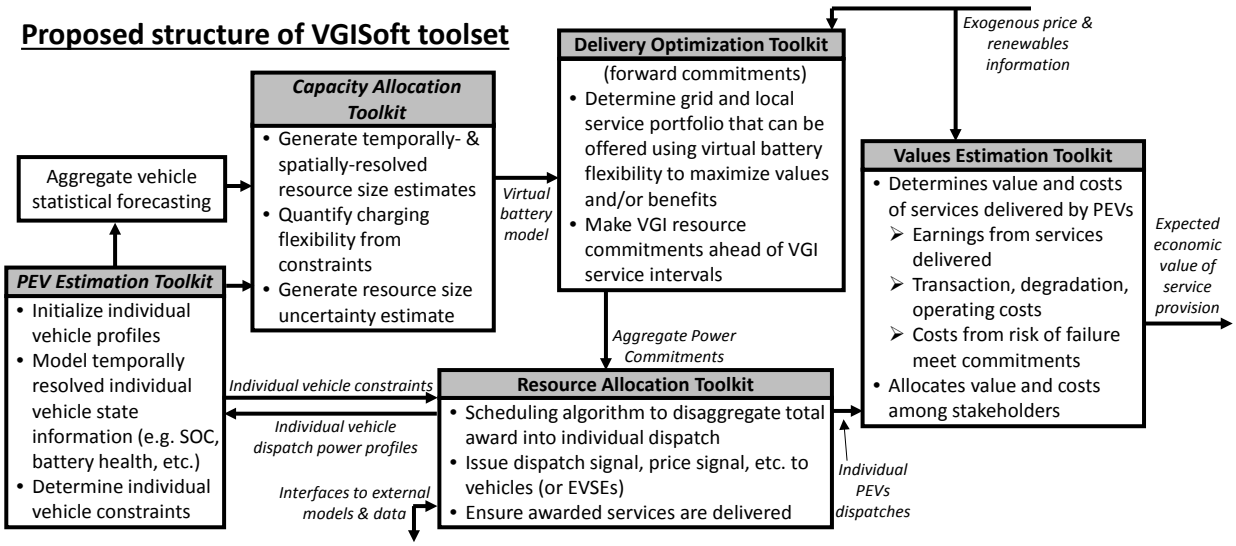


Figure IV.3.1 - Schematic overview of intended functionality and information flow within VGISoft toolkits

- Capacity Allocation Toolkit:
  - Generate temporally- and spatially-resolved resource size estimates
  - Quantify charging flexibility constraints
  - Generate resource size uncertainty estimates
  - **Prior DOE and other models planned to be leveraged (not exhaustive):**
    - (LBNL) V2G-Sim module for quantifying available flexible capacity for collections of vehicles.
    - (ANL) Models for capacity (electricity and ancillary services) assessment from individual and aggregated PEVs.

  In order to define the flexible capacity of a fleet of EVs, we use a virtual batter model [1]. All EVs, which are connected to the grid in a specific area, form an aggregate virtual battery. The virtual battery is defined by four parameters: 1) upper bound of the aggregate energy; 1) lower bound of the aggregate energy; 1) upper bound of the aggregate power; 1) lower bound of the aggregate power. The virtual battery model will work as important constraints in the following optimization toolkit.

- Delivery Optimization Toolkit (forward commitments):
  - Determine grid and local service portfolio that can be offered using virtual battery (e.g., aggregated vehicles) flexibility to maximize values and/or benefits
  - Make VGI resource commitments ahead of VGI service intervals
  - **Prior DOE and other models planned to be leveraged:**
    - Will require application of forward commitments algorithms available in the academic literature, or the creation of new algorithms for forward commitment of vehicles.

In this toolkit, we consider the aggregator's portfolio optimization problem in day-ahead market. The bidding strategy will be optimized for multiple grid services including the bulk energy, frequency regulation, spinning reserve, flexible ramping product and demand response. Through optimization, the aggregator is able to make forward commitments for multiple grid services to maximize its own profits. A risk-averse model can be adapted if the aggregate is exposed to high non-compliance penalties.

- **Resource Allocation Toolkit:**
    - Scheduling algorithm to disaggregate total award into individual dispatch
    - Issue dispatch signal, price signal, etc., to vehicles (or EVSEs)
    - Ensure awarded services are delivered
    - **Prior DOE and other models planned to be leveraged:**
        - (LBNL) V2G-Sim-integrated control algorithms that optimally control vehicle charging/discharging for several grid objectives (e.g., demand response, wholesale-level renewables integration, frequency regulation, etc.)

  The forward commitments will be exercised in real time. We need to allocate the aggregate charging/discharging power which is obtained from the optimization toolkit into individual EVs, considering the uncertainties in the real-time market. To be specific, the problem is to decide in real-time: 1) which EVs are to be charged/discharged; 2) the charge/discharge power of each EV. Some classic real-time scheduling methods like EDF, LLF and MPC can be employed to solve this problem.

- **Values Estimation Toolkit:**
    - Determine value and costs of services delivered by PEVs
        - Earnings from services delivered
        - Transactions, degradation, and operating costs
        - Costs from risks of failure to meet forward commitments
    - Allocates value and costs among stakeholders
    - **Prior DOE and other models planned to be leveraged:**
        - (NREL) Plexos, and customized NREL static marginal energy cost model (to be developed).
        - (ANL) Grid economic and reliability models
        - (PNNL) GridLabD distribution systems models, and values quantification sub-models
        - Additionally, new frameworks will need to be developed that allow for quantifying values and costs simultaneously captured across multiple temporal and spatial scales

## Results

Our efforts for FY 2017 focus on developing and integrating all components of VGISoft. We have finished the development and integration of all sub-modules of VGISoft. A demonstration on the functionalities of

VGISoft has been given to our industrial advisory board. A demonstration on the functionalities of VGISoft for 100,000 PEVs is also given.

Figure IV.3.2 is the output from capacity availability toolkit. Any cumulative trajectories between the upper bound and low bound are valid charging path, which can guarantee all vehicles have enough energy for traveling and avoid exceed their maximum capacities. The power boundaries are decided by charging facilities. In this paper, we assume two levels of charging power: L1 (1.44 kW) at home and L2 (6.6 kW) at workplaces. As shown in Figure IV.3.2, the power range between 8:00-17:00 are wide, because most of PEVs park at workplaces which have L2 chargers. The energy and power boundaries will work together as important constraints in the following optimization.

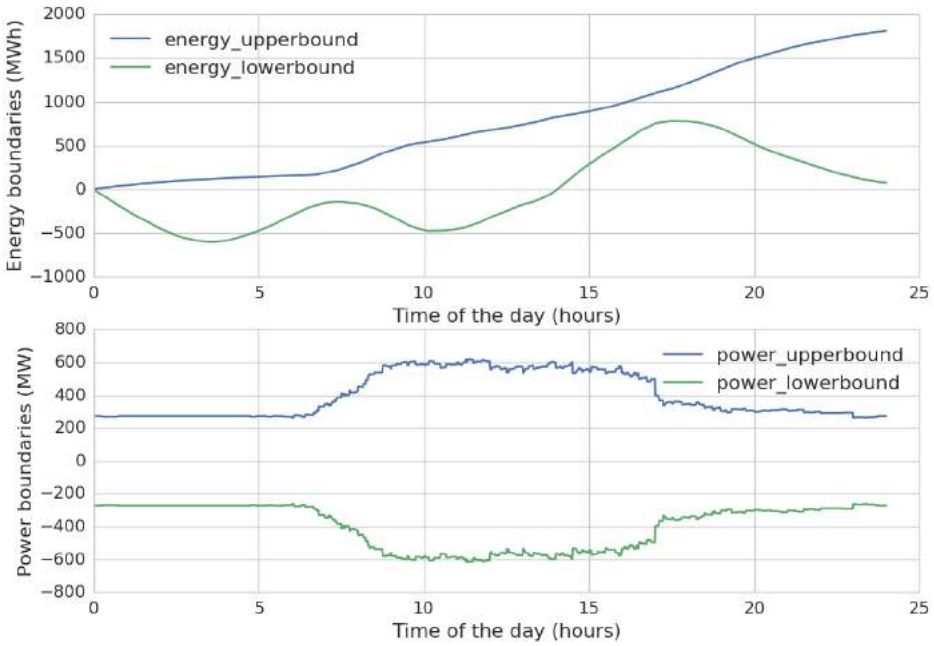


Figure IV.3.2 - Capacity allocation toolkit output for 100,000 PEVs

Delivery optimization toolkit has been developed to quantify the benefits of PEVs for participating in the electricity market. With the energy and power boundaries obtained from “capacity availability toolkit”, this toolkit optimizes day-ahead bidding strategy to decide how much capacity should go to which grid service, in order to maximize the total profits. Sample outputs from this toolkit are given in the Figure IV.3.3. Here we show two scenarios: (1) no battery degradation cost; (2) 0.16$/kWh battery degradation cost.

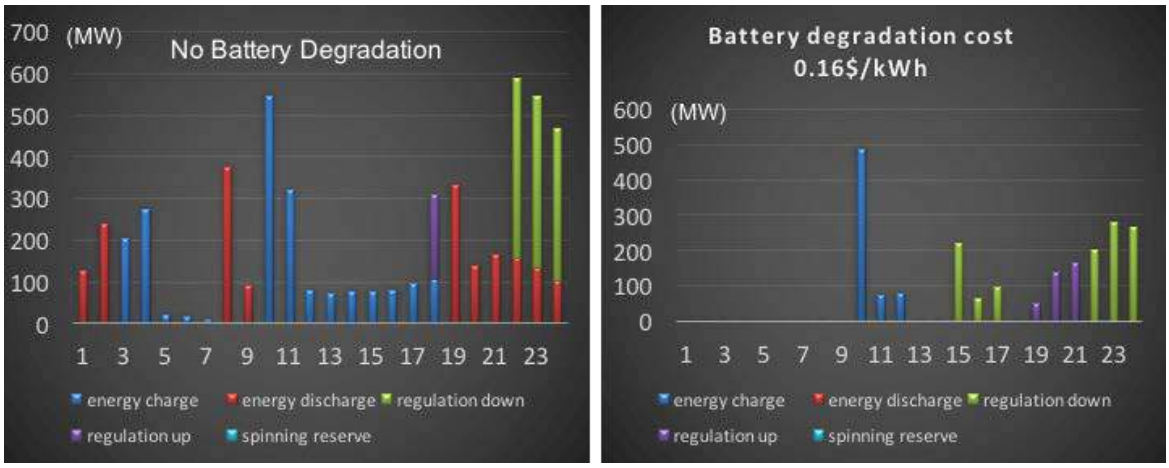


Figure IV.3.3 - Delivery optimization toolkit output for 100,000 PEVs

In real time, the system operator will decide how much awarded commitments should be called, according to the status of the grid. Resource allocation toolkit has been developed to allocate the aggregate dispatched power into individual PEVs in the real time. A sample of the resource allocation toolkit output is given in Figure IV.3.4.

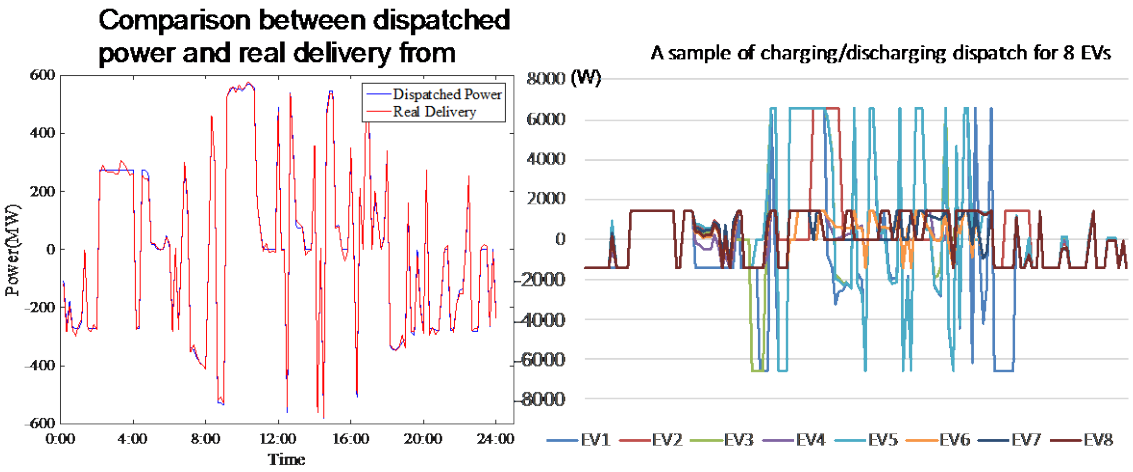


Figure IV.3.4 - Resource allocation toolkit output for 100,000 PEVs

Finally, the value estimation toolkit outputs the benefits and costs. The total uncontrolled charging cost is $17,782. This is the baseline. After the optimization of VGISoft, the total charging cost can be reduced to $12,054. If we do not consider the battery cost, the aggregator can earn $290,150.

## Conclusions

- The aggregate flexibility of a collection of PEVs can be described by energy and power boundaries. The aggregate model changes the large-scale, discrete, randomly distributed individual charging demands into a single, smooth and comparatively steady storage-like aggregate model. As the aggregate model is in a large scale and hence stable, the model reduces uncertainty in individual PEV plug-in schedules and enhances reliability in the scheduling problem.
- Based on our cost-benefit analysis, the battery degradation is still an obstacle which hinders the large-scale deployment of V2G.

- The proposed bidding strategy can reduce the cost in wholesale market by 18.3%. However, the monetary benefits from providing wholesale market services during normal days are not lucrative due to the relatively low prices in the wholesale market. Thus, we suggest that PEV should be regarded as a "sometime resource" rather than a "regular resource" in the wholesale market.
- Compared with classical centralized control methods, the proposed predictive method in the resource allocation toolkit can greatly enhance the real-time allocation performance, reduce the computational burden and alleviate the communication delay.

## Key Publications

1. Two conference papers entitled "Optimal Bidding Strategy for Regulation Services from Plug-in Electric Vehicle" and "Dynamic Distribution Network Reconfiguration Considering Travel Behaviors and Battery Degradation of Electric Vehicles" have been published on IEEE PES General Meeting, Chicago, 2017.
2. Two journal papers entitled "Clean Vehicles as an Enabler for a Clean Electricity Grid" and "VGISoft – An Integrated Solution to Bring Flexible Capacity of Electric Vehicles into Electricity Market" will be submitted to Science Advances and Applied Energy, respectively.

## IV.4 Diagnostic Security Modules for Electric Vehicle to Building Integration

**Kenneth Rohde, Principal Investigator**
Idaho National Laboratory
2525 N Fremont Avenue
Idaho Falls, ID 83415
Phone: (208) 526-0672
E-mail: kenneth.rohde@inl.gov

**John Smart, Co-Principal Investigator**
Idaho National Laboratory
2525 N Fremont Avenue
Idaho Falls, ID 83415
Phone: (208) 526-5922
E-mail: john.smart@inl.gov

**Lee Slezak, Technology Manager**
U.S. Department of Energy
Phone: (202) 586-2335
E-mail: Lee.Slezak@ee.doe.gov

Start Date: May 1, 2016 End Date: September 30, 2018
Total Project Cost: $1,650,000 DOE share: $1,650,000 Non-DOE share: $0

### Project Introduction

America faces several important challenges in the next 10 to 15 years in terms of modernizing the electric grid to ensure it is safe, secure, resilient and efficient, so that the grid is able to withstand and recover from unexpected outages, maintain high quality of service, and conserve energy. Vehicle-to-Grid (V2G) technologies have been receiving increased attention as a network service that would be integrated into the Building Energy Management Systems (BEMS) to more efficiently operate their resources. However, the lack of established communication standards between devices, vehicles, and supervisory systems makes the BEMS extremely vulnerable to cyber-attacks.

### Objectives

The overall goal of this project is to develop a Diagnostic Security Module (DSM) Framework for creating an end-to-end security architecture for the integration of modern Plug-in Electric Vehicles (PEV) with Electric Vehicle Supply Equipment (EVSE) and a Building Energy Management System (BEMS). The DSM Framework will create a secure communications channel to coordinate PEV charging activities with a BEMS operator while notifying the BEMS operator of any cyber security problems associated with the PEV or EVSE. The DSMs will integrate with a wide range of device types (EVSE, PEVs, etc.) and vendors, and provide enhanced awareness of the security state when implementing an integrated building and PEV environment.

Major activities in this project includes (1) the investigation of potential security vulnerabilities, (2) development of the DSMs modules, (3) development of the prototype environment, and (4) implementation of a security protocol that can be used to further design and implement future standards and protocols. The later years include the integration of the DSM prototype into the building-level PEV charging environment created by the Multi-lab EV Smart Grid Working Group partners as proposed by *GM0062 Vehicle to Building Integration Pathways*.

## Approach

The Idaho National Laboratory and the University of Louisiana at Lafayette are performing the following research and development activities to create a Diagnostic Security Module Framework.

**Assessment of security vulnerabilities**: The integration of smart grid enabled devices, such as EVSE units and PEVs with enhanced communication capabilities poses new risks to the electric grid. The vulnerabilities of the devices and implications of these risks are still not well understood. Given that these new electric vehicles and their chargers are now available to the general public, these devices can be exploited by the cyber security community at large (i.e., hackers) to find potential vulnerabilities. A theory currently posed by the cyber security community is that a compromised PEV can be used as a mechanism to infect the smart charging stations available to the public. Thus the infected PEV becomes a transport mechanism for malware that specifically targets EVSE stations.

**DSM Modules for end-to-end monitoring and integrated security monitoring**: The DSMs will be designed to provide an additional layer of security by monitoring the devices to which they are connected and reporting any suspicious behavior or abnormal conditions. A safety and security framework will be developed to address the need for a distributed and collaborative intelligent system to monitor and protect a modern automated building. This framework will be distributed as a component of the DSMs located throughout the connected building environment. This will allow for the monitoring and detection of physical and cyber problems that might affect the overall health of the integrated building environment. The development of the DSM modules and communications framework addresses the need of the Vehicle Technologies Office to provide a security framework for the integration of Electric Vehicles and charging equipment into a central monitoring and management station (e.g., BEMS).

**Prototype implementation & demonstration**: The work performed during this project will integrate DSMs with multiple PEVs, a variety of EVSEs (Level 1, Level 2, and DC Fast), and a single BEMS. A new ChargePoint EVSE will be added to the existing equipment located at INL. This additional EVSE, along with other Smart Grid enabled EVSEs located at INL, will provide a variety of equipment for which to test and develop the DSM Framework. The ChargePoint EVSE is a new system yet to be evaluated for cyber security issues, so a portion of the first year of development will include an assessment of this device. The other EVSEs at INL have already been assessed as part of a previous DOE project. This prototype environment will allow research and testing of a subset of an integrated building environment with a deep understanding of the potential cyber security issues present in the systems.

**Security protocols and standards for seamless and secure integration of PEV's charging equipment and BEMS**: The DSM Framework will implement a security based protocol for sharing physical and cyber security information of the components to which they are connected. This protocol will be used to further develop standards that are currently being implemented throughout the electric vehicle industry, such as Smart Energy Profile (SEP) 2.0 and SAE J2931/7.

## Results

The following list summarizes the project milestones completed to date:

1. Procured two (2) commercial AC Level 2 Electric Vehicle Supply Equipment (EVSE) charging stations. One unit is a dual-head system from ChargePoint and the second is a single-head unit from SemaConnect.
2. Completed low-level cyber security assessments and risk analysis of both commercial EVSE units. All of the findings were documented and submitted to ChargePoint and SemaConnect for their review.
3. Selected suitable hardware (Figure IV.4.1) for the implementation of DSM units to integrate with PEVs and EVSE. The initial communications framework is complete and provides interconnectivity between DSMs and the BEMS.

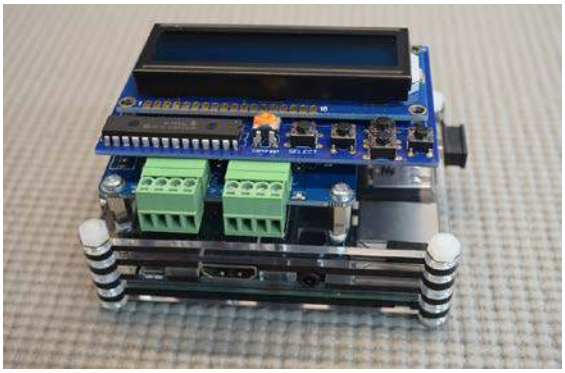

Figure IV.4.1 - Prototype DSM Hardware - RaspberryPI, CAN Interface, LCD

4. Selected two (2) PEVs for use in the development laboratory space (Figure IV.4.2); one 2012 Nissan Leaf and one 2012 Chevrolet Volt.

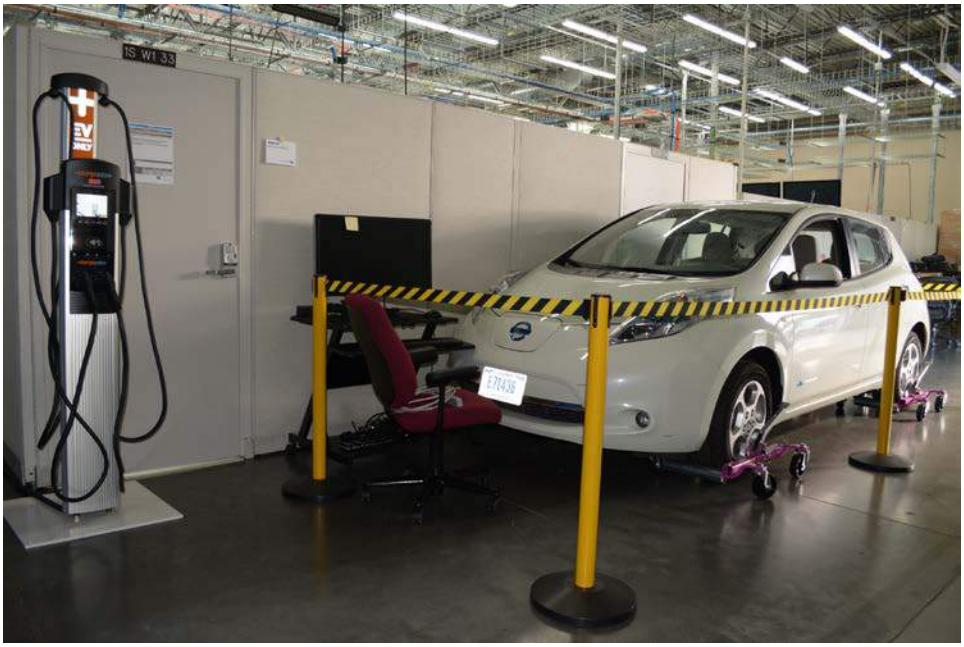

Figure IV.4.2 - Vehicle Development Lab - PEV, EVSE, and BEMS Station

5. Customized DSM hardware (Figure IV.4.3) for use in each of the research PEVs. The initial development of the PEV monitoring algorithms is complete, but specific algorithms for the different PEVs are still in development.

Figure IV.4.3 - DSM Installed in Nissan Leaf – Showing Status

6. An initial DSM for integration with the ChargePoint EVSE is complete. Development of the monitoring algorithms will take place during year three.

## Conclusions

At the conclusion of this project, a functional DSM Framework will be demonstrated by connecting two different DOE labs that host a variety of PEV and EVSE. This demonstration is in collaboration between INL, NREL, and the University of Louisiana at Lafayette. The demonstration will provide an opportunity for all interested parties from industry to observe the capabilities of the research performed by this project (GM 0163) and GM 0085.

During the third and final year of this project, the following activities are planned:

1. Testing and tuning the monitoring algorithms for the Volt and Leaf PEVs. Development of a "generic" DSM for use in the Toyota iQ vehicles at NREL.
2. Completion of the algorithms to monitor the ChargePoint and SemaConnect EVSE using DSM. The ABB DC Fast Charger located at INL will also be used if sufficient development time is available.
3. A dedicated internet connection between INL and NREL will be established. This will provide the required connectivity for both GM 0163 and GM 0085.
4. Setup and testing of DSM equipment in the NREL vehicle lab.

## Key Publications

1. Diagnostic Security Modules for Electric Vehicle to Building Integration, GMI Peer Review Meeting, April 2017
2. Electric Vehicle Cyber Security Research, SANS Automotive Cybersecurity Summit, Detroit, MI, May 2017
3. Diagnostic Security Modules for Securing Electric Vehicles, Energy Exchange 2017, Tampa, FL, August 2017

## IV.5 Testing Network and Open Library

**Matthew Lave, Principal Investigator**
Sandia National Laboratories
P.O. Box 969
Livermore, CA 94551-0969
Phone: (925) 294-4676
E-mail: mlave@sandia.gov

**Rob Hovsapian, Co-Principal Investigator**
Idaho National Laboratory
1955 N. Fremont Avenue
Idaho Falls, ID 83415
Phone: (208) 526-8217
E-mail: rob.hovsapian@inl.gov

**Lee Slezak, Technology Manager**
U.S. Department of Energy
Phone: (202) 586-2335
E-mail: Lee.Slezak@ee.doe.gov

Start Date: April 15, 2016 End Date: April 15, 2019
Total Project Cost: $2,600,000 DOE share: $2,600,000 Non-DOE share: $0

### Project Introduction

This project works to accelerate grid modernization by (a) providing comprehensive information about testing infrastructure available at DOE national labs and beyond, and (b) creating a repository of models and testing resources such as testing protocols. These goals are critical to accelerate development, validation, standardization, adoption and deployment of new grid technologies. A related goal is to enable national laboratories to drive innovation more effectively and synergistically.

The electric power grid is a complex system comprised of devices connected electrically and through controls, communications, and markets. The grid involves a wide variety of rapidly evolving technologies and performance characteristics that are increasing system complexity and demanding new requirements. In order to achieve a truly modernized electric power grid, industry and other organizations need access to testing resources across a wide range of technology readiness levels to accelerate commercialization of new technologies and improve grid planning.

Vast testing capabilities are available within national laboratories, universities, and industry. However, these capabilities are difficult to identify because there is no consistency regarding how and when information on these testing capabilities is communicated to the public. The level of detail available and the location of such information even varies greatly across the different laboratories, programs, etc. within a single organization. For example, a national laboratory may have detailed information regarding its PV systems testing capabilities available online, but no available information regarding its energy storage testing capabilities. Further, there is no overarching coordination framework, making it difficult to integrate capabilities into more effective multi-institutional test beds that can handle systems-level testing and validation with live data—as opposed to isolated device testing. This lack of coordination results in inefficient utilization and the potential for ongoing duplication.

In addition to testing capabilities and resources, there is also a gap in the availability of information and accessibility to validated models for grid devices and simulation tools. Easy and open access to these models and corresponding documentation could accelerate modernization activities. A central repository for models and test-related resources for interconnection and interoperability (procedures, scripts, and equipment specifications) will drive standardization and adoption of best practices related to device characterization, model validation, and simulation capabilities.

## Objectives

This project will pursue two major objectives by PY3 (FY18-19):

- Objective 1 – Establish a Grid Modernization Laboratory Consortium Testing Network (GMLC-TN) that will function as an agreement-based association to maintain and disseminate information related to testing capabilities, information about models and testing-related resources.

- Objective 2 – Develop and establish a Grid Modernization Laboratory Consortium – Open Library (GMLC-OL) that serves as a public repository for component models tools and testing resources. The GMLC-OL will be designed in a manner such that it is self-maintained through user inputs and feedback.

As depicted in Figure IV.5.1 below, these two objectives are inter-dependent. While the GMLC-OL and testing capabilities database will be the main products and the focus of this project's efforts, it is envisioned that the GMLC-TN framework and mission will allow for the incorporation of other related initiatives such as information relevant to grid device and systems standards, simulation tools, etc.

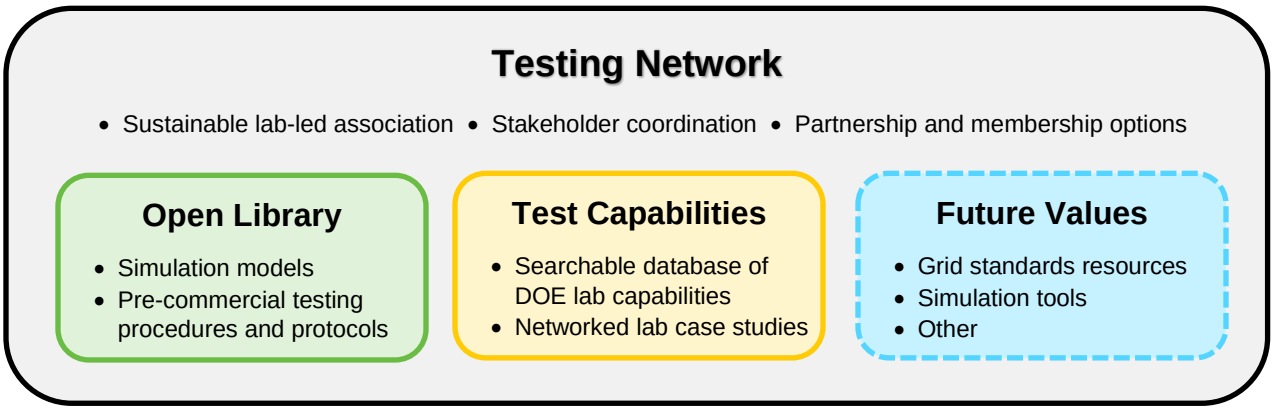


Figure IV.5.1 - Relationship between the Testing Network and Open Library

## Approach

The work is organized into two major tasks: Task 1 focuses on the establishment of the Testing Network, including collecting and disseminating information on grid-related testing capabilities. Task 2 focuses on the establishment of the Open Library an open database for validated models, simulation tools, and testing resources.

### *Task 1 – Establishment of the GMLC Testing Network (GMLC-TN)*

The overall goal of this task is to identify a collaboration mechanism that enhances the ability of the national laboratories to more effectively federate testing capabilities, and to collaborate with universities, utilities and other industry entities on standards-based testing activities at the device and systems level.

*Task 1.1 – Identification and initial formation of a viable GMLC-TN framework*

This task involves consultation with national labs and major industry stakeholders to determine new or revised mechanisms that need to be put in place to accomplish the stated objectives. Based on the industry consultation and the drivers, a viable GMLC-TN framework, including a charter and governance structure will be established. We will formally constitute GMLC-TN as an entity by adoption of the framework. After adoption of the framework, this task will focus on creating a public website through which users can interact with members of the GMLC-TN to understand and utilities testing capabilities, and on sustainability of the GMLC-TN.

*Task 1.2 – GMLC-TN Testing Capability Catalog and Gap Analysis*

Under this subtask, we will pursue two objectives: (a) Catalog the grid-related testing capabilities across the GMLC FFRDC complex, and (b) conduct a gap analysis to identify opportunities for enhanced device and systems testing capabilities that can be pursued in the short, medium and longer term. The catalog will be updated periodically to reflect new capabilities and to increase the detail of the information. The catalog information will be posted to the GMLC-TN public website to best disseminate the information, allow for quick updates, and allow for customized sorting and searching of the testing capabilities.

*Task 2 – Establishment of Model, simulation tools and testing resources*

The task is to develop the Open Library (GMLC-OL), an open, validated, and accessible component model library encompassing the full range of grid devices. The GMLC-OL will host the results from on-going and future device characterization activities across the national laboratories, academic partners and industries.

*Task 2.1 – Create and release the GMLC-OL*

The GMLC-OL will include open-source models and data. Specifications of the model, assumptions, theoretical background, validation procedure and data, and use-cases will be listed along with each model. An accreditation procedure by model users for evaluation of all models in the library for credibility and usefulness will be introduced. Special emphasis related to the validated models will be created for each entry under accreditation. A utilization score for each model will also be created which will collect basic information from the user about the purpose of the model use. Three factors will primarily determine the merit of the models in GMLC-OL: (i) validation of model via experimentation (ii) count of downloads, and (iii) citations in peer-reviewed publications. The accuracy of models will also continue to improve through constant feedback from peers and users in the community, as newer versions of model keep being added to system. In addition, the GMLC-OL will be capable to store proprietary models and data, whereby only the model name will be indexed with information on the point of contact for accessing or using the model. Providing further information of a proprietary model will be possible and fully controlled by the owner.

Each model in the GMLC-OL needs to have a common approach towards development and documentation. Since the goal is to avoid duplication of efforts and save time, individual models should be easy to discover, understand, manipulate, use and re-use in testing and development of new algorithms, practices or protocols for the modern power grid. All models will be stored in a common database and indexed using a broad range of categories for easy (and intuitive) access and retrieval. A standard naming convention for all the models will be adopted such that the type (steady- state / transient) and usability (electrical / mechanical / mathematical / thermal) of a model is immediate from the nomenclature. Index terms describing a model will be broadly categorized into: (i) Assumptions, (ii) Attributes, (iii) Applications, and (iv) Accreditation.

*Task 2.2 – Add a testing library to the GMLC-OL*

A model library needs to be complemented by a testing resource library. The testing resource library is intended to serve as a guideline to create functional test cases to validate the model. The testing resource library will be a compilation of scripts, standards used for validating models and experimental setup, protocols

and procedures for validation and information on developing testbeds for further experimentation using the model. The library will comprise tools and models built using a wide variety of software, each of which is built with certain core specializations and objectives. An important component of the testing resource is guidance on the proper interoperability of the model with other models. This will also address any interface issues along with interfaces necessary for integrated system testing. The test resource library will contain bridging scripts to federate the assortment of tools and models for maximizing the utility of each available resource.

## Results

### *Stakeholder Workshop*

A GMLC TN/OL Stakeholder Workshop was held on September 14, 2016 at NREL in Golden, CO. The workshop brought together a group of stakeholders with a variety of interests in order to solicit feedback regarding how the GMLC 1.2.3 project team can provide a framework, and ultimately a publicly-available instrument, that will achieve the activity's goals and serve as a leading national resource on grid-device and -systems testing.

Workshop participants heard presentations from members of the project team and were then asked to participate in breakout sessions. The most salient conclusions and recommendations based on the breakout sessions were focused on:

- *Branding and Awareness* – critical to clearly communicate value, intentions, and user scenarios
- *Industry Participation* – sustainability strategy that can provide industry with confidence in the effort
- *Efficient Access* – provide information that is categorized and detailed for quick, informed decisions

### *Catalog of Testing Capabilities*

The Catalog of National Laboratory Testing Resources contains information about testing facilities and capabilities at the 10 national laboratories that made up the original project team (ANL, BNL, INL, LBNL, LLNL, NREL, ORNL, PNNL, SNL, and SRNL). Information in the Catalog was collected through self-assessment by laboratory facility owners, and facilitated by the project team members at each National Lab. The Catalog contains information on 39 distinct laboratory facilities and covers 168 capabilities / application technology pairs. The information is presented both in a summary matrix (example shown in Figure IV.5.2), and in full detail paragraphs which describe each facility and capability.

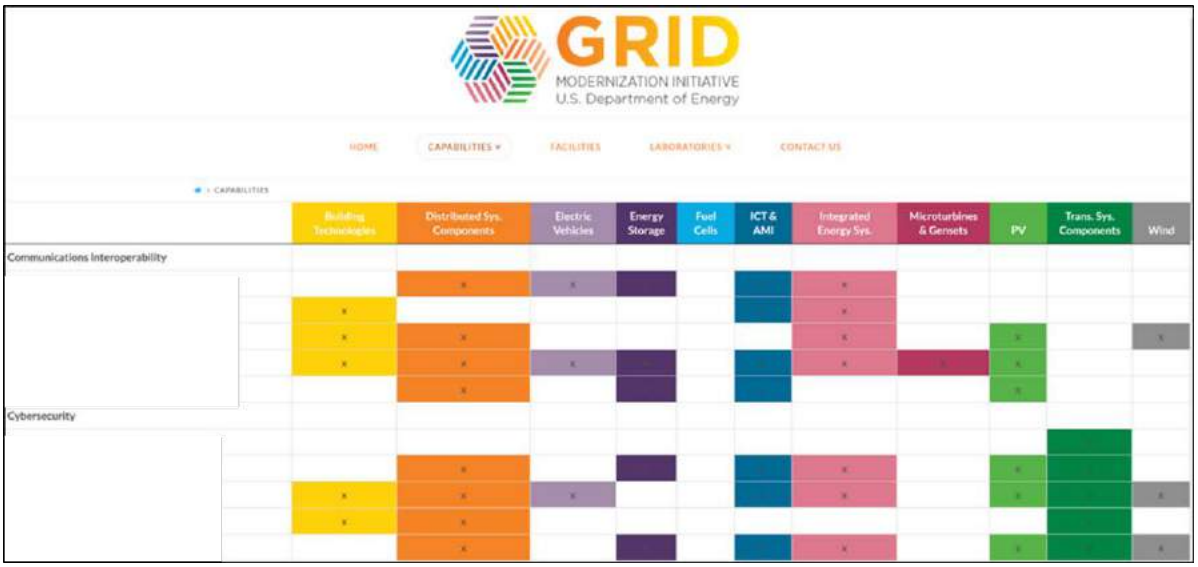


Figure IV.5.2 - Catalog of Testing Network resources showing capabilities (rows) and techonlogy areas (columns).

The information contained in this catalog focuses on testing and characterization of devices and systems that are connected to, or interface with, the electric grid. Isolated generation systems were considered beyond the scope of this project, but information regarding how generation assets interact with the grid was accepted. The catalog only includes resources where a national laboratory has established capabilities and infrastructure that are actively being used to conduct testing, or that have previously been used to conduct significant testing for a particular technology area and continue to be maintained for such work. The information only reflects capabilities and facilities that are hosted at national laboratories. Some laboratories participate in partner facilities, but these were not included in this version of the catalog.

Although the information is robust, additional efforts are ongoing to keep the information in the Catalog updated through integration into a publicly accessible website, which will allow for quick updating as well as search and sort capabilities.

*Testing Network Charter, Governance Structure, Adoption*

A charter detailing the gridCONNECT consortium functions as the membership vehicle for both the testing network and open library was developed and circulated among the team for comments. gridCONNECT is the Testing Network described in Figure IV.5.1. The charter defines members, users, operation, goals, and more for gridCONNECT. The charter was modeled closely after charters from other successful DOE consortia with similar goals, such as the LightMAT consortium. Based on these previous consortia, we expect to be able to setup a joint CRADA and NDA among the gridCONNECT members which will make partnership with members much easier: if a user accepts the specified terms, the CRADA and NDA, which will have already been approved by the members, can be accepted very quickly.

A General Assembly Meeting was held on October 3rd, 2017, where the project team discussed and adopted the charter, and laid out next steps in building the gridCONNECT consortium.

*Beta version of the Open Library as a web interface*

A beta version of the open library interface has been newly developed and has been peer-reviewed by the GMLC 1.2.3 team members. OL development environment was established and the data management organized, including a graphical user interface as shown in Figure IV.5.3. A bank of new functions has been implemented, such as advantageous search bar, new dynamic model template, automated ownership control. Significant feedback was received and updates to the interface are being implemented according to the defined priority list developed based on user feedback. The continuously improved beta version will be used and extensively tested by the GMLC 1.2.3 team in the first production.

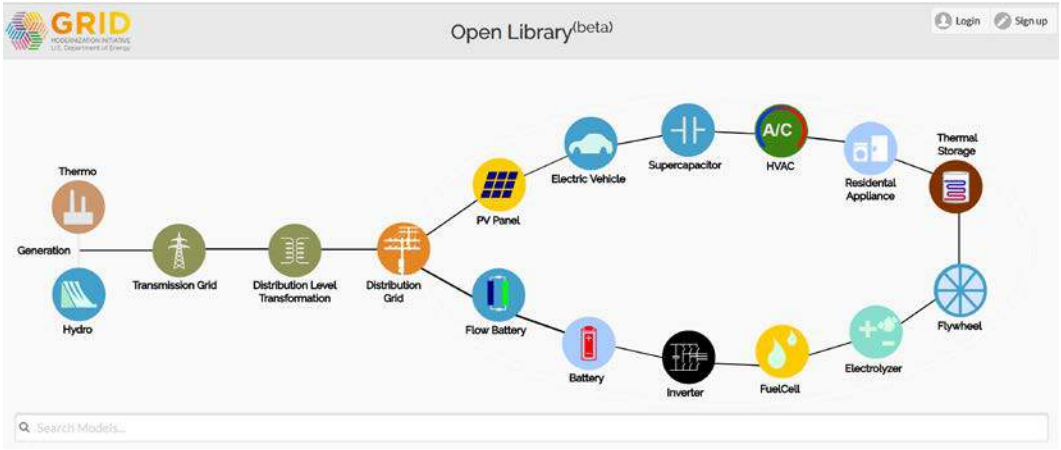


Figure IV.5.3 - Open Library interface showing model categories and search feature

An advanced search option of the OL database has been implemented. Instead of using predefined static categories that are curtailing the search options, a user friendly and intuitive dynamic "search bar" approach has been implemented. The search bar follows the design paradigm that has been successfully used on popular websites, such as google.com, amazon.com, etc. The user enters in the search bar the key-word(s) or any information contained in the model description, which in turns engages the search operation and narrows the OL database to the list of models relevant to the search action. Apart from search, an alphabetical index of all GMLC-OL models is also available. Clicking on each model will open a readable portable document.

*Populate the Open Library*

With implementation of the beta version of the open library and after responding to the feedback, the open library is now ready in the next quarter to collect models. The targeted simulation models and tools are those developed within projects funded by the DOE, in the first line within GMLC projects series, whereby initial activities have started. INL will also further incorporate the already existing models and tools provided by non-DOE related entities that will support the project effort, such as RTDS, OPAL-RT and Typhoon HIL as real-time simulator manufacturers, as well as MIT Lincoln Laboratory and Electric Ship Research and Development Consortium (ESRDC).

Initial model collection was undertaken to understand the basic format of the models which will be collected and to optimize design of the open library. Project team members were asked to provide several simulation models and tools as inputs for the OL, which resulted in populating the database with 15 sample models and tools described using a standardized template.

## Conclusions

Through our outreach and information collection activities, we validated the need for the Testing Network and Open Library. Through a stakeholder workshop we heard that industry was looking to the National Labs for leadership in the fields of grid modernization testing and modeling. Through a pre-survey of publicly available National Laboratory testing facility and capability information, we observed the lack of information and lack of consistency available on National Laboratory test facilities and capabilities. In collecting models, we noted the lack of organization and public availability of models created through GMLC projects and by the National Labs in general.

Key outcomes so far in the project have established a foundation to address these needs. We conducted a self-assessment of laboratory facilities and capabilities at the National Labs, collecting and curating this information into an organized catalog for quick reference. We drafted and adopted a charter to establish a consortium to allow for quicker and more straightforward access by industry and other groups to test facilities and models available at the National Labs. And, we developed and populated a beta version of the Open Library which collects and organizes models created in GMLC projects and beyond. As these efforts continue to grow and mature, the result of this project will be accelerated development and deployment of new grid technologies through a greater value and utilization of National Laboratory resources.

## Key Publications

1. D. Grubbs, "Report on the GMLC TN/OL Stakeholder Workshop held September 14, 2016 at NREL in Golden, Colorado"
2. M. Lave, "GMLC Project 1.2.3: Testing Network and Open Library," presented at the U.K. / U.S. Grid Modernization Collaboration Workshop in Golden, CO on March 1, 2017.
3. A. Ellis, "GMLC Testing Network and Open Library," presented at 2017 IEEE ISGT Conference in Washington, D.C., on April 25th, 2017.
4. M. Lave, "Overview of DOE Grid Modernization Lab Consortium (GMLC) and Details on GMLC 1.2.3 (Testing Network and Open Library)," presented at UVIG 2017 Fall Meeting in Nashville, TN on October 12, 2017.

## IV.6 Definitions, Standards and Test Procedures for Grid Services from Devices

**Robert Pratt, Principal Investigator**
Pacific Northwest National Laboratory
P.O. Box 999
Richland, WA 99354
Phone: (509)375-3648
E-mail: robert.pratt@pnnl.gov

**Teja Kuruganti, Principal Investigator**
Oak Ridge National Laboratory
P.O. Box 2008
Oak Ridge, TN 37831
Phone: (865) 241-2874
E-mail: kurugantipv@ornl.gov

**Lee Slezak, Technology Manager**
U.S. Department of Energy
Phone: (202) 586-2335
E-mail: Lee.Slezak@ee.doe.gov

Start Date: April 15, 2016 End Date: April 1, 2019
Total Project Cost: $5,209,000 DOE share: $5,209,000 Non-DOE share: $0

### Project Introduction

This project's (GMLC Foundational Topic 1.4.2's) overarching goal is to enable and spur the deployment of a broad range of distributed energy resource (DER) devices with the ability to provide much of the flexibility required for operating a clean and reliable power grid at reasonable cost. The required flexibility, expressed in the form of a growing number of increasingly valuable services at the bulk system and local distribution levels, is largely embodied in grid services that are provided by power plants and substations today. However, it is also increasingly reflected in wholesale market products or utility programs in which DERs participate. The project's objectives address the primary barriers that limit the ability of grid operational and planning tools to assess the ability of such devices to provide these services, at scale, in the future power grid.

The project addresses the most important device classes expected to play critical roles in a modernized grid: responsive equipment and appliances in buildings, batteries, electric vehicle chargers, hydrogen infrastructure (fuel cells and electrolyzers), and smart inverters for PV solar and batteries.

Existing grid services include ancillary services (regulation, reserves, ramping) that keep the grid in supply-demand balance, managing peak loads to reduce infrastructure capacity requirements, and managing wholesale purchase and production costs. Industry has also envisioned new reliability services from DERs such as artificial inertia and participation in remedial action schemes that enhance the reliability and stability of the bulk grid, and new distribution-level services such as mitigating rapid voltage changes and reverse power flows from high solar PV penetrations.

As its primary technical goal, ***the project will provide a general, standard device model with a battery equivalent interface applicable to each device class.*** This will be in the form of an equivalent battery model, useful for comparing and aggregating the capabilities of devices from different classes and extrapolating their ability to perform grid services. This model is designed to be modular and readily incorporated in grid planning and operational tools. It will be simple and generic to use, representing all device types together with

only a single, simple dispatch algorithm for each grid service, rather than a custom algorithm for each device class. Such a model is required for the tools used to plan and design new and modernized grid infrastructure, and to operate transmission- and distribution-level grid management/control systems and markets, to properly take into account the roles and functions of DER devices in the future grid.

Developing a unified modeling approach for evaluating the performance of grid services from DER devices is the basis for achieving the project's **overall strategic outcomes:**

- Enable utilities and grid operating entities to accurately assess the contribution of DER devices at the planning and operational time scales by using models of their performance that can be incorporated into the tools used to plan and operate the grid.
- Encourage device manufacturers to add the capabilities needed to supply existing and new grid services by clearly articulating the performance characteristics required and a means for evaluating their engineering and economic potential in various regions of the nation.

The project will help improve the capability of devices to provide an increasingly valuable and broader range of grid services by completely articulating the device performance needed to supply grid services, many of which are not well understood by device manufacturers. It will also identify and quantify the effects of performing grid services on devices' efficiency, and tabulate impacts that may affect equipment lifetimes or that reduce their ability to provide other services to the user, so that any such negative impacts can be mitigated by improved device designs or grid operational strategies.

Finally, the project encourages manufacturers to build the required capabilities into their devices at the factory, where it is far less expensive than adding them later in field retrofits by utilities or customers. This ultimately lowers the costs for devices that must ultimately be borne by the power grid, whether through purchase or incentives, and hence increases their penetration at scale.

### Objectives

The project's objectives address the need to construct the capability for planning and operational tools to estimate how well the devices can provide a wide range of services, at scale, in the future power grid. Building upon the accomplishments of the first year of the project, which was oriented toward an overlapping but *somewhat different set of objectives, the project will:*

1. **Define prototypical "drive cycles" representing the time-series injection or withdrawal of real and reactive power that each of a wide variety of grid services require from device fleets,** including a method for summarizing the performance of devices against those drive cycles in engineering and economic terms.
2. **Develop and publish a standard set of device models describing the operational and engineering constraints (including human factors) for each of a wide variety of device classes** so that fleet performance in providing grid services can be readily estimated with high-fidelity.
3. **Develop and publish a battery equivalent model interface for each of the device classes** to provide a simple, standard, and common (across device classes) "virtual battery" interface so that high-level grid planning and operation tools can readily evaluate grid services from device fleets.
4. **In collaboration with industry, develop characterization test protocols for three device classes (water heaters, commercial refrigeration systems, and electric vehicles**), and conduct actual tests on a typical such devices and validate that the protocols, and the device and battery equivalent models produce valid results.

5. **Conduct a study of existing DOE appliance and equipment efficiency testing protocols to identify existing results and suggest additional test elements or analyses of data already being collected** that could characterize important parameters describing the response capabilities of relevant device classes.

## Approach

Before DER devices can penetrate the marketplace for grid services at scale, grid planners and operators need to be able to accurately and conveniently assess and value services that DERs can provide, in order to design appropriate markets and incentives for them and to properly account for their capabilities in the planning process. Similarly, manufacturers need a means of evaluating the degree to which their equipment could potentially provide various services, and how much potential value would be derived by the grid from doing so. The presumption is that a large share of that value would accrue to the purchaser of the device, but that must exceed the marginal cost of providing those capabilities in the equipment.

So, ***the project will develop and validate a model-based procedure to asses a device fleet's ability to provide any grid service*.** This will consist of a device model encapsulating the physical and human factors constraints pertinent to each class of DER device. The device models account for limitations on input and output power, the duration that the device can sustain (i.e., the energy it has available), and the energy efficiency of operating the device in the pattern required to supply a service. The device model is used to update these parameters, which interact in complex, non-linear ways, on a time-series basis as the device is dispatched to provide a grid service. One model will be developed to represent each device class in the project. Others may be added at a future date.

Further, the analyses conducted in the course of operations and planning must be able to readily access the information in these device models. Embedded in operational and planning tools are algorithms that dispatch DER device fleets to accomplish grid services. The complexity of doing this for each of a wide variety of device classes is a key barrier that must be overcome. So, ***the project will develop a single, common, battery interface from the device models to these high level models, so they can use a single algorithm to dispatch DER fleets of any type.*** This will greatly facilitate the incorporation of the latest device models into them, and allow new device classes to be readily added as device models with battery-equivalent interfaces are developed for them.

It is important to be able to link the device models to actual, measured physical performance characteristics of devices. So, **in collaboration with industry, the project will develop short, low cost device characterization test protocols for three device classes (water heaters, commercial refrigeration systems, and electric vehicles)** for use by manufacturers, utilities, and other organizations to measure the relevant performance parameters. **The project will conduct validation tests for these devices, comparing modeled to actual performance,** using segments of the prototypical annual drive cycles for each grid service.

Finally, an important opportunity for DOE is the potential to leverage existing appliance and equipment efficacy standards tests to obtain measured values for device characteristics that define device's ability to perform grid services. So, ***the project will review the efficiency testing procedures to determine a) characteristics and parameters that are already measured, b) characteristics and parameters that can be derived from data collected during the tests with further analysis, and c) marginal additions to the tests that could obtain additional parameters at low additional cost.***

PNNL is the prime national laboratory leading the project. Table IV.6-1 lists the roles and responsibilities of all the national laboratories in the project. The work will be divided among various device classes, with a track for each of them managed by a national laboratory with the expertise to develop and test the device models. A second track, several laboratories lead also lead a task on grid services, as indicated in Table IV.6-1.

Table IV.6-1 - Device Class and Grid Services Responsibilities by Laboratory

| Laboratory | Device Class Lead | Grid Services Lead |
|---|---|---|
| PNNL | | (1) Peak load management, and<br>(2) Artificial inertia/frequency response |
| NREL | (1) Water heaters, and<br>(2) PV/inverters | Distribution voltage management/PV impact mitigation |
| SNL | Batteries/inverters | |
| ANL | Electric vehicles | Capacity market dispatch |
| ORNL | (1) Heating/cooling equipment, and<br>(2) Commercial refrigeration systems | |
| LBNL | | (1) Regulation,<br>(2) Spinning reserve, and<br>(3) Ramping |
| INL | (1) Fuel cells, and<br>(2) Electrolyzers | |
| LLNL | (Liaison to other modeling projects) | Wholesale energy market/production cost dispatch |

PNNL and ORNL will share responsibility for producing the deliverable associated with Objective 5: a report on opportunities to leverage and extend existing DOE appliance and equipment efficiency testing protocols to characterize devices subject to such testing. This will include residential air conditioners, water heaters, refrigerators; commercial rooftop units and refrigeration. PNNL will lead this task.

## Results

*Changes in Project Scope*

Under the direction of Mr. Lee Slezak of DOE-EERE-Vehicle Technologies Office, during July and August Rob Pratt (Principal Investigator) extensively revised the project's scope, budget, and milestones. The primary objective of the project was changed, from the development of a *Recommended Practice* for testing the ability of devices to provide grid services, to instead focus on the development of a standardized means of representing devices in high-level simulation tools – the Battery Equivalent Model – that was the technical cornerstone of developments in FY17 under the original scope. In addition, the project will now deliver operational software embodiments of the grid services dispatch algorithms and detailed device models with battery equivalent interfaces.

The scope of testing devices was reduced and moved to Project Year 3. Only water heaters, commercial refrigeration, and electric vehicles will now have device characterization protocols developed and tested. The development of device models for commercial lighting and thermal energy storage were dropped from the project scope. An additional effort was added to the project in the form of an analysis (and report) on how the testing protocols for DOE energy efficiency standards could be leveraged or extended to obtain the characteristics needed for the project's device models.

The project halted in May as Project Year 1 funds were exhausted and Project Year 2 funds had not been released, pending the revision of scope. Milestones scheduled for Q4 FY16 were obviated by the lack of

funding and change in scope. Funding for the revised scope for Project Year 2 was received by the participating laboratories in mid- to late September and technical work re-commenced on October 1, 2017.

*The following sections on Key Technical Results and Industry Outreach document progress made in FY17 toward the original scope, highlighting the accomplishments that remain relevant to the revised scope of work.*

### *Key Technical Results*

The project's key technical accomplishments in FY17 were the development of:

1. Draft specifications of detailed engineering and behavioral models for nearly all device classes
2. Definitions of a broad range of grid services that can be supplied by DER (distributed energy resource) devices
3. Draft specifications of drive cycles that represent a number of the grid services
4. Generic performance metrics for how well devices perform grid services, in engineering and economic terms, and for impacts on their energy efficiency, user efficacy, or that may affect equipment lifetime
5. Derivation of the energy balance equations for a generic device
6. Definitions for the power supplied for a grid service by a generic device fleet
7. Definitions of the device nameplate parameters and other variables in a battery equivalent model suitable for describing the performance of any device class.

All these accomplishments will directly contribute to the Project Year 2 (FY18) scope, albeit with some differences in role or method that remains to be determined. Some technical results associated with Accomplishments 2, 5, 6, and 7 (in the list above) are highlighted in some detail below.

**Definitions of Grid Services.** The project defined a set of grid services that could be supplied by DER devices, and the associated operational objectives from which their value is derived, as follows:

- ***Peak capacity management*** – Reduce net load as needed so that it never exceeds the capacity of the grid infrastructure to deliver power. Typically this occurs over a span of several hours on 10 to 15 of the hottest summer days of the year (or, for some regions, coldest winter days).
    - Objective – Reduce the need for capital expenditure for expansion and/or upgrades to generation, transmission, and distribution capacity.
- ***Energy market price response*** – Reduce net load when prices are high, with any associated increases in *net load* taking place when prices are low. This tends to occur in predictable, seasonal, daily patterns over periods of a few hours when power plants with expensive fuel and/or low efficiency are required to supply power. Random disruptions to daily price patterns occur due to weather conditions, plant outages, shortages in expected output from renewable generation, or unusual wholesale market conditions.
    - Objective – Reduce wholesale energy production costs or wholesale market purchase costs.
- ***Meet obligation to supply capacity in a wholesale energy market*** – Reduce net load when called upon by an independent (transmission) system operator to meet a contractual obligation to do so, for which they have received a capacity payment (often through a market intermediary known as an aggregator). When provided by DERs, this grid service is typically utilized as reserve capacity for extreme events lasting a few hours, and may be called upon at any time as a performance test.

  - Objective – Ensure sufficient regional generation capacity exists and obtain it from the lowest-cost resources using a wholesale capacity market.

- ***Frequency regulation*** – Increase or decrease net load to restore balance between supply and demand in response to a ~4-second-interval signal from the grid operator. This service is traditionally supplied by power plants, which take many seconds up to a few minutes to respond.

  - Objective 1 (fast regulation) – Maintain grid frequency within acceptable range in the face of continual, momentary imbalances between supply and demand; imbalances typically vary from oversupply to undersupply within ~1 minute or less.

  - Objective 2 (slow regulation) – Maintain contractual balance of imports and exports for a regional balancing authority's balancing area; imbalance varies from oversupply to undersupply within 10–15 minutes (slow regulation may or may not be combined with fast regulation into a single service, depending on the region involved).

- ***Spinning reserve*** – Remain on standby, ready and able to rapidly reduce net load and sustain the reduction until replaced by generators that are available but off line (typically 15–30 minutes).

  - Objective – Rapidly restore balance between supply and demand when a large grid asset (power plant or transmission line) suddenly and unexpectedly trips off line. Spinning reserve is required to prevent blackouts.

- ***Ramping*** – Remain on standby, ready and able to rapidly increase or decrease net load when the available generation cannot change its output rapidly enough to follow changes in total net demand (i.e., regional load less total renewable output). This is a new type of service, whose need is being driven by rapid penetration of renewables. It is typically used in either of two situations. In regions with high levels of solar generation, the service is engaged over a couple of hours in the morning and evening when insolation levels are in rapid transition. In regions with large amounts of wind power, it may be called upon to assist with the rapid increase or reduction in output when a wind front moves through.

  - Objective – Meet the requirement to rapidly change the output of total generation to maintain balance between supply and demand in response to rapid changes in power production by renewables.

- ***Artificial inertia*** – Remain on standby, ready and able to detect when grid frequency drops rapidly or increases, and act to complement the grid's angular momentum and generator governor controls by instantly and autonomously decreasing or increasing net load (within ~1 second; less is preferred). Inertia is traditionally supplied by a combination of the angular momentum of turbines in steam- or hydro-based power plants and autonomous governor controls on large generators; there is emerging need to supplement these sources with a new type of service as renewable generation displaces steam-based plants.

  - Objective – Slow and stop the otherwise precipitous change in frequency that begins instantly when a large grid asset (power plant or transmission line) or a similar amount of load suddenly and unexpectedly trips off line and creates a large imbalance between supply and demand.

- ***Distribution voltage management*** – Remain on standby, ready and able to detect when the distribution voltage drops rapidly, and act instantly and autonomously by rapidly adjusting net load in the form of its reactive and/or real power components (within ~1 second; less is preferred). This is a new type of service, the need for which is driven by rapid penetration of distribution-connected solar generation. Rapid changes in the combined power output from such systems can occur due to crossings of cloud fronts, which can result in unacceptable voltage fluctuations.

- Objective 1 (fast response) – Maintain distribution system voltage within the normal range in response to rapid changes in net demand for power.
- Objective 2 (slow response; not described above) – Assist in maintenance of distribution system voltage within the normal range by coordinating reactive power output with distribution-voltage management systems (transformer tap changers, voltage regulators and capacitor banks), either on command or autonomously, based on self-sensed voltage fluctuations.

**Energy Balance for a Generic Device.** The project developed a conceptual model for a generic device supplying a grid service, and a corresponding energy balance, are illustrated in Figure IV.6.1.

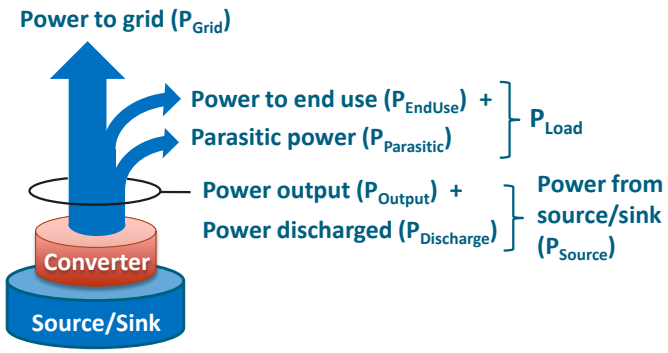


Figure IV.6.1 - Energy Balance and Power Flows in a Generic Device Fleet

Referring to Figure IV.6.1, the following variables are defined for the battery-equivalent model:

1. ***Power Output*** – the term *power from source* (or sink) refers to the AC power delivered from the device fleet's generators, after any conversion losses from the form of energy generated by the devices, and is denoted by $P_{Output}(t)$.
2. ***Power Discharged***– the term *power discharged* refers to the AC power delivered from the device fleet's storage, after any conversion losses from the form of energy stored by the devices, and is denoted by $P_{Source}(t)$.
3. ***Power from Source*** – the term *power from source* refers to the AC power delivered from the device fleet's storage or generator, after any conversion losses from the form of energy stored or generated by the device, and is denoted by $P_{Source}(t)$:

$$P_{Source}(t) = P_{Output}(t) + P_{Discharge}(t) \quad (1)$$

4. ***Power to End Use*** – the term *power to end use* refers to the AC power consumed by the device fleet itself to serve any load the device fleet is obligated to meet in order to maintain the device's current state of charge, and is denoted by $P_{Enduse}(t)$.
5. ***Parasitic Power*** – the term *parasitic power* refers to any AC power consumed by the device fleet that is required to maintain the device fleet's current state of charge—for example, to provide power to keep the device fleet within proper operating temperature range—and is denoted by $P_{Parasitic}(t)$.
6. ***Power to Load*** – the term *power to load* is denoted by $P_{Load}(t)$, and refers to the power required to keep the device fleet at its current state of charge, which is the sum of the *power to end use* and *parasitic power* for the device fleet:

$$P_{Load}(t) = P_{Enduse}(t) + P_{Parasitic}(t) \quad (2)$$

7. ***Power Injected into Grid*** – the term *power injected into grid* by the device fleet, denoted by $P_{Grid}(t)$, refers to the difference between the device fleet's *power from source* and its *power to load*:

$$P_{Grid}(t) = P_{Source}(t) - P_{Load}(t) \quad (3)$$

Or, by substitution of Equation (1) for $P_{Source}(t)$ and Equation (2) for $P_{Load}(t)$ in Equation (3),

$$P_{Grid}(t) = P_{Output}(t) + P_{Discharge}(t) - P_{Enduse}(t) - P_{Parastic}(t) \quad (4)$$

**Power Delivered for a Grid Service**. The project developed a generic definition for the *power delivered for a grid service* from a device fleet. It is denoted by $P_{Service}(t)$ and refers to the difference between the electric power injected into the grid by the fleet when providing the grid service ($P_{Grid}(t)$) and the power injected into the grid when no service is being provided, i.e., the base case, denoted by $P_{GridBase}(t)$:

$$P_{Service}(t) = P_{Grid}(t) - P_{GridBase}(t) \quad (5)$$

for all times (t) when a grid service is being provided. When a grid service is not being provided, $P_{Service}(t)$ is defined as zero and Equation (2) does not hold, because the device class may be recharging, in which case $P_{Grid}(t) \neq P_{GridBase}(t)$.

Substituting Equation (3) in both terms but retaining the subscript (*Base*) indicating base-case conditions,

$$P_{Service}(t) = [P_{Source}(t) - P_{Load}(t)] - [P_{SourceBase}(t) - P_{LoadBase}(t)] \quad (6)$$

at all times (*t*) when a grid service is being provided; otherwise $P_{Service}(t)$ is zero.

Substituting Equation (1) for $P_{Source}(t)$ and Equation (2) for $P_{Load}(t)$ in Equation (6),

$$P_{Service}(t) = \left[P_{Discharge}(t) - P_{DischargeBase}(t)\right] + \left[P_{Output}(t) - P_{OutputBase}(t)\right] - [P_{Enduse}(t) - P_{EnduseBase}(t)] - [P_{Parastic}(t) - P_{ParasiticBase}(t)] \quad (7)$$

at all times (*t*) when a grid service is being provided; otherwise $P_{Service}(t)$ is zero.

Using the operator Δ to represent the difference between the actual power and the base-case power, Equation (7) is reduced to

$$P_{Service}(t) = \Delta P_{Discharge}(t) + \Delta P_{Output}(t) - \Delta P_{Enduse}(t) - \Delta P_{Parasitic}(t) \quad (8)$$

at all times (t) when a grid service is being provided; otherwise $P_{Service}(t)$ is zero.

Noting that the last two terms (including the minus signs) represent the *power conserved* by the device fleet in the course of providing the grid service, denoted by $\Delta P_{Conserved}(t)$, and reflect any change in the *end use* or *parasitic load*s due to changed operational conditions as the *device* fleet responds, we can write

$$P_{Service}(t) = \Delta P_{Discharge}(t) + \Delta P_{Output}(t) + \Delta P_{Conserved}(t) \quad (9)$$

at all times(t) when a grid service is being provided; otherwise $P_{Service}(t)$ is zero.

The *power conserved* represents, for example, reduced need to heat a battery under cold conditions if it is actively being charged, or reduced air conditioning load when the indoor air temperature is higher than in the base case. Note that the *power conserved* can be either positive or negative, depending on the situation.

Thus, the *power delivered for a grid service* is the sum of the increase in the power discharged from storage plus the increase in power output from distributed generation plus the power conserved in the course of providing the service, compared to the base case. Note that the *power delivered for a grid service* can be positive or negative, since some grid services require that it be negative at times.

**Battery Equivalent Model.** The project developed a generic *battery equivalent model* as a standard interface between a high-level grid model (such as a production cost model or an expansion planning model) and the detailed engineering and behavioral models constructed by the project for each device. It is described in Table IV.6-2, Table IV.6-3, and Table IV.6-4 below. These definitions are still being refined and tested for sufficiency and completeness in FY17.

Table IV.6-2 - Definitions of Device Nameplate Parameters with Associated Variables in the Battery-Equivalent Model

| Parameter | Definition | Units | Name-plate | Variable |
|---|---|---|---|---|
| **Energy storage capacity** | Potential energy capacity of storage (prior to conversion to AC) when the state of charge (SoC) changes from 100% to 0% | kWh | $C^*$ | $C(t)$ |
| **Maximum real power for services** | Maximum real power deliverable for grid services | kW | $P_{max}^*$ | $P_{max}(t)$ |
| **Minimum real power for services** | Minimum real power deliverable for grid services (may be <0) | kW | $P_{min}^*$ | $P_{min}(t)$ |
| **Maximum reactive power for services** | Maximum reactive power deliverable for grid services | kvar | $Q_{max}^*$ | $Q_{max}(t)$ |
| **Minimum reactive power for services** | Minimum reactive power deliverable for grid services | kvar | $Q_{min}^*$ | $Q_{min}(t)$ |
| **Ramp rate real power up** | Maximum rate of increase of real power output to the grid | kW/s | $dP_{up}/dt^*$ | $dP_{up}/dt(t)$ |
| **Ramp rate real power down** | Maximum rate of decrease of real power output to the grid | kW/s | $dP_{down}/dt^*$ | $dP_{down}/dt(t)$ |
| **Ramp rate reactive power up** | Maximum rate of increase of reactive power output to the grid | kvar/s | $dQ_{up}/dt^*$ | $dQ_{up}/dt(t)$ |
| **Ramp rate reactive power down** | Maximum rate of decrease of reactive power output to the grid | kvar/s | $dQ_{down}/dt^*$ | $dQ_{down}/dt(t)$ |
| **Charging efficiency** | Fraction of energy supplied by the grid that is stored | % | $e_{in}^*$ | $e_{in}(t)$ |
| **Discharging efficiency** | Fraction of energy drawn from storage that is delivered to the grid | % | $e_{out}^*$ | $e_{out}(t)$ |

Table IV.6-3 - Definitions of Other Variables in the Battery-Equivalent Model

| Parameter | Definition | Units | Variable |
|---|---|---|---|
| **Energy stored** | Available energy stored in the storage media | kWh | $E(t)$ |
| **Power discharged from storage, real** | Real power withdrawn from storage and converted to AC | kW | $P_{Discharge}(t)$ |
| **Power discharged from storage, reactive** | Reactive power withdrawn from storage and converted to AC | kvar | $Q_{Discharge}(t)$ |
| **Power output from generator, real** | Real power withdrawn from storage and converted to AC | kW | $P_{Output}(t)$ |
| **Power output from generator, reactive** | Reactive power withdrawn from storage and converted to AC | kvar | $Q_{Output}(t)$ |
| **Power injected into grid, real** | Real power being output to the grid while providing a grid service (for loads PGrid(t) will always be negative) | kW | $P_{Grid}(t)$ |
| **Power injected into grid, reactive** | Reactive power being output to the grid while providing a grid service | kvar | $Q_{Grid}(t)$ |
| **Power injected into grid, real, (base case)** | Real power being output to the grid while not providing a grid service (for loads, PGrid(t) will always be negative) | kW | $P_{GridBase}(t)$ |
| **Power injected into grid, reactive, (base case)** | Reactive power being output to the grid while not providing a grid service | kvar | $Q_{GridBase}(t)$ |
| **Power delivered for service, real** | Real power being delivered for a service | kW | $P_{Service}(t)$ |
| **Power delivered for service, reactive** | Reactive power delivered for a service | kvar | $Q_{Service}(t)$ |
| **Load** | Power that must be supplied by the grid to maintain current SoC under actual conditions, i.e., the sum of any end-use load served and any parasitic load for the device class while providing a service | kW | $P_{LoadBase}(t)$ |
| **Base load** | Power that would have been supplied by the grid to maintain initial SoC under “no response” conditions, i.e., the sum of any end-use load served and any parasitic load for the device class in the base case (not providing a service) | kW | $P_{Load}(t)$ |

Table IV.6-4 - Definitions of Behavioral Parameters and Constraints in the Battery-Equivalent Model

| Parameter | Definition | Units | Variable |
|---|---|---|---|
| **Time limit, hold** | Maximum duration of "hold state" for SoC at other than initial condition | hours | $\Delta t_{hold}$ |
| **Time, restoration** | Time of day at which the initial SoC condition must be restored | hour of day | $t_{restore}$ |
| **Strike price** | Price/incentive threshold at which a *device* initiates response to price | $/kWh | $SP(t)$ |
| **Price elasticity** | Response rate to prices/incentives (i.e., ~ percent change in output / $/kWh) | – | TBD |

**Draft Characterization and Modeling Framework.** The project prepared and published a draft of the characterization and modeling framework for industry review in the form of Chapters 1 and 2 of the *Recommended Practice*. The document was cleared for publication for industry review and feedback by DOE's Office of Energy Efficiency and Renewable Energy (EERE) and the Office of Electricity (OE). It was delivered to the project's technology managers Lee Slezak (DOE-EERE) and Dan Ton (DOE-OE) and posted on the GMLC web site for download March 9th. Chapter 1 is an informative (not normative) description of the goals, scope, and desired features of the *Recommended Practice*. Chapter 2 contains the normative, general definitions that provide the foundational framework for the *Recommended Practice* in terms of the characterization tests, the device models, the grid services drive cycles, dispatch algorithms, the battery-equivalent model used to dispatch the device models, and the metrics used to quantify the performance of a device under test.

The project's lab teams spent most of their effort in FY17 on developing their respective device model and grid services (see Table 1) that were intended to be documented in Chapters 3 and 4 of the *Recommended Practice*. Chapter 3 describes the details of the characterization test sequence and test apparatus, and the device-specific details of the device model for each class of device addressed by the project. Chapter 4 describes the details pertinent to each of the various grid services in the project, in terms of its purpose and eligibility requirements, the drive cycle(s) used to represent it's time series nature, the data source for the drive cycle, the battery equivalent dispatch algorithm used to drive the device models, and any service-specific changes to the general performance metrics described in Chapter 2.

*Industry Outreach*

In preparation for the 2nd industry workshop in late March, the project team organized a series of webinars and made presentations at industry meetings to raise awareness and involvement in the project. Most of these were organized around a device class or a couple of related device classes. Device-class specific presentation materials were prepared for each event. This effort was undertaken to address the need for more industry awareness and engagement, and to build attendance for the industry workshop. These webinars and their participation are summarized below. The attendance counts indicate below exclude DOE and national laboratory participants:

- GridWise Alliance pre-workshop webinar (project team; n = 35)
- Commercial lighting webinar (LBNL; n = 27)
- PV/batteries/inverters webinar (NREL & SNL; n= 321)
- HVAC and appliances webinar (ORNL & NREL; n=21)

- Thermal energy storage briefings to key manufacturers (PNNL; n = 2)
- Electric vehicle industry meeting presentation (PNNL; n = 13)
- Electrolyzers webinar (INL; n=84).

The project partnered with the GridWise™ Alliance for its second industry meeting, which was co-sponsored by GE and Intel at GE's GridIQ conference center in Atlanta March 21-22 (two half-days). The project team prepared the announcement and meeting agenda in collaboration with the Alliance. The project prepared and delivered presentations and posters at the workshop describing the general scope, objectives, and technical framework for the project (Rob Pratt, PNNL), with deep dives on two device classes:

- Battery/inverters (David Rosewater, SNL)
- Heating, cooling, and refrigeration equipment (Teja Kuruganti, ORNL)

And two grid services:

- Frequency regulation (Peter Schwartz, LBNL)
- Wholesale price response (Tom Edmunds, LLNL).

The materials prepared for this workshop completed the project's Q2 FY17 Progress Measure: Extrapolating Characterized Device Parameters to Metrics of Grid Services Performance (draft specification of standard procedure for extrapolating device characteristics to performance of grid services, in presentation form, ready for Industry Meeting 2).

## Conclusions

The project produced number of key methods and specifications in the course of its FY17 activities, which were directed toward the original project scope of developing of a *Recommended Practice* for testing the ability of devices to provide grid services. At the direction of DOE, at the end of May the project was halted, re-scoped, and the project's scope, budget, and milestones were extensively revised during July and August.

The primary objective of the project was changed to instead focus on the development of a standardized means of representing devices in high-level simulation tools. This leverages one of the primary technical accomplishments of the project in FY17 – specification of a generic Battery-Equivalent Model capable of representing the engineering and behavioral characteristics of any of the device classes in the project in a common form. The project will now deliver the grid services dispatch algorithms as an example of a high-level tool, and detailed device models with a battery equivalent interface, in the form of operational software. An additional deliverable was added in the form of an analysis on how the testing protocols used by DOE energy efficiency standards could be leveraged or extended to obtain the characteristics used in the project's device models.

Most of the other key technical developments of the project in FY17 will be used in FY18 to meet the objectives of the revised project scope. These include detailed engineering and behavioral model specifications for device classes, definitions of grid services, and derivations of the energy balance for a generic device and the power supplied for a grid service by a device fleet. These will be reviewed and in some cases require modifications in FY18 to adjust them to the new project scope. The prototypical grid service drive cycles and performance metrics for 1) how well devices perform grid services, and 2) impacts on equipment and users, will be re-purposed to allow testing of the device models and battery-equivalent interface. This testing will simultaneously produce meaningful results that provide some general guidance to the utility industry and device manufacturers as to which kinds of services are appropriately served by which device classes, which will be embodied in a report.

## Key Publications

1. Recommended Practice for Characterizing Devices' Ability to Provide Grid Services – Working Draft for Comment Only. Pratt, R.G. and Z.T. Taylor. March, 2017. Pacific Northwest National Laboratory, Richland, Washington. PNNL-26253. On line at: https://gridmod.labworks.org/resources/recommended-practice-characterizing-devices%E2%80%99-ability-provide-grid-services.

## IV.7 Control Theory

**Scott Backhaus, Principal Investigator**
Los Alamos National Laboratory (LANL)
P.O. Box 1663, MS C921
Los Alamos, NM 87545
Phone: (505) 667-7545
E-mail: Backhaus@lanl.gov

**Karan Kalsi, Principal Investigator**
Pacific Northwest National Laboratory (PNNL)
P.O. Box 999
Richland, WA 99352
Phone: (509) 375-5904

**Lee Slezak, Technology Manager**
U.S. Department of Energy
Phone: (202) 586-2335
E-mail: Lee.Slezak@ee.doe.gov

Start Date: April 1, 2016 End Date: May 30, 2019

| Total Project Cost: | DOE EERE share: | DOE OE share: | Non-DOE share: |
|---|---|---|---|
| $2,150,000 | $290,223 | $1,859,777 | $0 |

### Project Introduction

In this three-year project, we will develop new control solutions including control topologies, control algorithms and control deployment strategies for the US power grid. The major focus will be on distribution systems to support the GMLC MYPP vision for transitioning the power grid to a state where a huge number of distributed energy resources (DER) are participating in grid control to enable the grid to operate with lean reserve margins and to enable resilient distribution feeders with high percentage of low carbon DER. The theory effort will recognize the need to engage legacy control concepts and systems as we transition to more distributed control.

Although our emphasis is on distribution, we do not ignore transmission. We will address the integration of a huge number of DERs into transmission and market operations (e.g., automatic generation control (AGC), security constrained economic dispatch, etc.) using hierarchical control theory and solutions, including the coordination between bulk system controls and the new controls and optimization developed in this work. Rather than duplicate, our research will leverage the large amount of research and development already performed on these transmission-level applications.

### Objectives

Achieving the GMLC MYPP goals requires significant advancements beyond the current state of the technology and innovations in several interrelated areas: 1) Co-Development of Control Theory and System Architecture to create concrete directions of theoretical development, which will be measured against metrics also developed in this project; 2) Theory for Hierarchical, Decentralized, Distributed and Risk-Aware Control that develops the theory to enable the design and analysis of control algorithms for at least 10,000 DER embedded in distribution and transmission networks; and 3) At-Scale Testing By Simulation to validate the performance of the developed control solutions and foster the development of transition plans for industry demonstrations.

*Co-Development of Control Theory and System Architecture*

In order to achieve transferable, resilient, and deployable control solutions, we will leverage the expertise and experience of our industry partners (Oncor, PJM) co-develop control approaches and theory along with control, communications, and information system architectures. Although informed by industry, co-development will ensure these architectures are also informed by control theory and not simply predefined by what exists today. These architectures will be economically deployable, representative of industry approaches, demonstrate a continuous evolution from today's legacy systems to the MYPP future vision. The architectures will be designed to be resilient to impacts of natural or malicious events. We will collaborate with the Architecture Team (1.2.1), but will push those efforts much farther by instantiating several of the architectures to develop controls and by performing early testing and evaluation of these architectures against a set of control system metrics also developed within this task.

By directly incorporating grid systems, information and communications systems, and markets and industry structure into a single architectural representation; the spatiotemporal availability and resolution of sensor data and actuation signals and their respective aggregation and disaggregation are known and clearly defined. This upfront architectural integration enables us to develop control theory and associated algorithms that provide high performance on each of the proposed architectures. It also enables the evaluation of the performance of architecture as the information and actuation availability is compromised by a natural event or cyber-attack. At the same time, the control theories will inform architecture in GMLC Task 1.2.1 so that useful structural changes that support advanced control can be suggested to other parts of the industry, thus easing the adoption of new controls.

*Theory for Hierarchical, Decentralized, Distributed and Risk-Aware Control*

*In order to accommodate the massive numbers of DERs in the MYPP vision, the architectural options that emerge are expected to be hierarchical in nature. We will develop the theoretical underpinnings at each level of these hierarchical architectures. These candidate architectures will be developed early in the first year of the project, but are anticipated to include three distinct but related levels—Device-Level Control, Distribution Reliability Coordinator (DRC), Wholesale/Bulk Markets—which we use here as examples to ground the discussion.*

The proposed control framework is expected to be open, flexible and interoperable, exhibiting "plug-and-play" features, supporting dynamic system configuration, and respecting the existing mechanisms and engineering realities within each subsystem. DRC-level objectives include estimating the bounds of DER flexibility and controlling within those bounds to meet "external" demands (e.g., a reference signal provided by the ISO Bulk Market) while respecting "internal" constraints (e.g., voltage magnitude and power flow limits on the host distribution circuits and substations). The DRCs may coordinate with neighboring DRCs to ensure that the overall system reliability is being maintained. The device-level control objectives drill deeper into the device physics to develop theory for aggregating large numbers of diverse DER (generation, storage and loads) into ensemble models that ensure computational tractability while systematically incorporating end-use dynamics and physical constraints. The ensemble models should provide predictions of the average response, the fluctuations and uncertainty about that average response, and predictions of the impacts of both effects on the power system via the physics of power flow. Both the device-level and DRC control systems should integrate seamlessly with the ISO Bulk/Wholesale Market control systems as defined in the candidate architectures.

*At-Scale Testing By Simulation*

Key to the adoption of these new approaches by industry and development of transition plans for industry-led demonstrations in FY19/20 are testing and validation of the control systems that result from the developed architectures and control theory. We will develop test methods, scenarios, and protocols in collaboration with our industry partners (Oncor, PJM) to ensure relevance to their operating conditions and requirements. Via an industry workshop, the testing results will be shared and vetted with our industry partners and wider set of industry stakeholders (utilities, regional reliability organizations, control system developers, and software

vendors) to ensure they understand the test protocols and results and the availability of control solutions for future demonstration and transition to practice.

The control systems developed in this project will be tested for stability and performance in unique numerical simulation environments. The development of the simulation environments, and the testing itself, will be an iterative process in close coordination with the control theory developments and with GMLC project 1.4.15, Co-Simulation of Transmission, Distribution, and Communications (TDC). Modeling and analysis of advanced grid control applications requires a fundamental understanding of the behavior of the physical systems and an integrated modeling approach that portrays the control system performance in the setting of the surrounding bulk generation, transmission infrastructure, market systems, reliability coordination, and other aspects of utility operations.

The complexity and nature of the required testing is determined by many factors such as the size of the control network, location and type of constraints, time scale and time step, resource and load characteristics, aggregation of the loads and DERs, temporal and spatial diversity of the resources, markets and regulations. Initial testing will include simplifications of these factors to prototype and improve the control implementations. These simplifications will be replaced with more realistic assumptions as the control designs reach a desired level of performance and move toward a more integrated, at-scale testing. Through simulation and modeling, the performance of the control designs will be assessed and iteratively improved to guarantee stability and reliability under a wide variety of test scenarios including those identified by our industry partners.

## Approach

Achieving the ADMS and GMLC goals requires significant advancements beyond the current state of the technology and innovations in several interrelated areas: 1) Co-Development of Control Theory and System Architecture to create concrete directions of theoretical development, which will be measured against metrics also developed in this project. 2) Integrated optimization and control to enable the design and analysis of control algorithms for at least 10,000 DER embedded in distribution networks. The specific tasks will be to:

- Develop individual and aggregate DER flexibility models and associated constraints
- Design real-time control strategies for aggregated DERs with uncertainty quantification
- Develop power flow relaxation and approximation methods for distribution systems
- Develop optimization methods that integrate uncertain real-time control into risk-aware power flow optimization
- At-scale simulation testing to validate the performance of the developed control solutions and foster the development of transition plans for industry demonstrations. In particular, the control strategies for aggregated DERs, including power flow models will be tested on ~10 distribution feeders including~10,000 DERs.

The focus of FY17 was to develop a specific decomposition of the integrated optimization and control problem (as shown in the figure below) and begin development of the modeling, theory and algorithms to support the individual optimization and control components. This decomposition is intended to frame the technical approaches by providing well defined interfaces between the different levels of optimization and control.

At the lowest level, the aggregated device controllers (ADC) are envisioned as “capacity controllers" that are not required to account for the physics of power flow within their control domain. The ADC locations must be chosen to ensure that power flow congestion does not occur in their control domain but that a sufficient number of loads and DERs are downstream of the ADC to achieve the benefits of statistical aggregation with regard to a reduction in the fluctuations of the power injection at the ADC's connection to the rest of the

network. It is expected that there will be many ADCs in each distribution circuit, but far fewer than the total number of total controllable DERs. It is anticipated that the ADCs are located physically close the DER they control to promote low-cost, low-latency two way communication between the ADC and the DER.

The PFO is envisioned as a "network optimizer" that optimally dispatches the setpoints and control response of each of the ADCs while respecting all power system constraints in the network between the substation and the ADCs, including managing the uncertainty in the controlled and uncontrolled injections into this network. The PFO may reside within a substation and be physically close to the head of many distribution circuits, however, this is not a requirement and other locations are possible depending on the type of commutations between the PFO and ADC. The network optimization solved by the PFO interacts with the ADC on a relatively slow time scale by generating both power dispatch points (e.g., from an energy market clearing) and parametrized control functions (e.g., from an ancillary services market clearing) for the ADC to track in real-time in between iterations of the PFO solutions.

The ADCs' objective is to track the dispatch points and control functions between iterations of the PFO solutions. The figure displays an example of a simple parameterized control function that relates desired deviations in the ADC's power from its power dispatch point based on local observation of frequency. In this example, the uncertainty in the ADC response is statistically characterized by two parallel lines representing the confidence interval of the response around the desired mean response.

## Results

The major accomplishments for FY17 were

1. The completion of the integrated optimization and control theory roadmap consisting of:
    - Reference control system architectures
    - Cataloged existing and alternative power flow approximations and relaxations
    - Method for determining aggregate DER real and reactive power controllable domains
    - Design of real-time control strategies for aggregated DERs with uncertainty quantification.
2. Initial development of the modeling, theory and algorithms to support the individual optimization and control components. The roadmap was reviewed and approved by the Industry Advisory Board and DOE. Individual progress on modeling, theory and algorithms was published or submitted as peer-reviewed journal articles or conference proceedings.

A more detailed discussion on the technical progress is given below.

**Task 2.1**—Developed two methods for determining aggregate DER real and reactive power controllable domains by approximating Minkowski sums of the individual DER controllable domains. The first approach is a geometric method using homothets for approximating the flexibility region of individual DERs and a computationally efficient algorithms for computing the Minkowski sum of the individual approximate homothets. We look at the choice of the parameters of the homothets, such that the outer (and inner, when applicable) approximations of the flexibility domains are as tight as possible. Also metrics of goodness are developed of the approximation (such as the maximal Euclidean norm between points on the outer approximation and their projection on actual domain) to inform the selection of prototypes. The second approach utilizes a discrete convex hull of the individual DER controllable domains and an optimization formulation to compute the maximum available aggregate reactive power at any given aggregate real power. Under the conditions stated, the optimization problem can be solved analytically and transformed into an algorithm that efficiently and accurately solves for the Minkowski sum of the individual real and reactive power controllable domains.

**Task 2.2**—More than 50 existing and alternative power flow approximations and relaxations were cataloged and characterized in a hierarchy of accurately versus computational efficiency. Several power flow formulations were implemented in Matlab and early stage code in Julia. An algorithm for computing worst-case errors in linear power flow approximations was developed to assist in comparing the performance of different power flow representations. The results were summarized in a monograph titled "A Survey of Relaxations and Approximations of the Power Flow Equations," In preparation for invited submission to Foundation and Trends in Electric Power Systems, 2017.

**Task 2.4**—Designed real-time control strategies for aggregated DERs. ADC real-time control algorithms were developed for tracking of power set point and ancillary service control functions. The team developed time-varying social-welfare maximization problem formulations for ADCs with distributed energy resources (DERs) and developed online distributed algorithms to identify (and track) its solutions. In the considered setting, ADC operator and DER-owners pursue given operational and economic objectives, while concurrently ensuring that voltages are within prescribed limits. The proposed algorithm affords an online implementation to enable tracking of the solutions in the presence of time-varying operational conditions and changing optimization objectives. It involves a strategy where the ADC operator collects voltage measurements throughout the feeder to build incentive signals for the DER-owners in real time; DERs then adjust the generated/consumed powers in order to avoid the violation of the voltage constraints while maximizing given objectives. The stability of the proposed schemes is analytically established and numerically corroborated.

**Task 2.3**—Implemented risk aware power flow optimization including network nodes representing ADCs. This implementation was used to compute the optimal response of the ADCs for both linear and nonlinear representations of power flow. These results were used to build intuition regarding the ADC response and subsequently rigorously prove that piecewise linear ADC control functions provide the optimal response to fluctuations in nodal injections. Empirical exploration show that, under reasonable levels of power flow fluctuations, only a single segment of the piecewise linear ADC control function was active and that simple linear ADC control functions are close to optimal. Empirical results on full nonlinear power flow representation demonstrated that, again under reasonable levels of nodal injection fluctuations, simple linear control functions are very close to optimal compared to second-order (quadratic) ADC control functions.

## Conclusions

The increasing penetration of stochastic and variable renewable generation (both centralized and distributed) in many electrical transmission and distribution grids is decreasing the availability of traditional forms of generation used to control real power for balancing load and reactive power for regulating voltage magnitude. These changes are driving an emerging transition to leverage a large latent capability in the grid by controlling distributed energy resources (DER, including distributed generation, battery storage, and loads) to supplement and replace the control of traditional generation. These expected and ongoing changes in the nature of the electrical power system are being limited by the lack of effective controls to manage these new DER. Where control solutions do exist, they are stressed or limited because they operate too slowly, do not provide the required control accuracy, do not enable the actuation and control of diverse sets of large numbers of new intelligent DER, do not effectively manage the uncertainty of DER response on multiple time and grid scales, do not integrate these new DER with existing system controls, and are not easily transferrable to multiple control settings. To address these concerns, solutions must be developed and deployed that allow a vast number of DERs to participate in “grid control,” enabling the grid to operate with leaner power reserve margins, and thus more reliably and cost effectively for stakeholders such as utilities and consumers.

The main impact of this project is the development of novel control solutions that create a system that is more flexible than the legacy system to enable:

- Integrated optimization and control systems that are more effective at keeping operating conditions within safety margins.
- A 33% decrease in the cost of power reserve margins, while still maintaining reliability.

Interconnection of intermittent power generation with less need for electrical storage and lower integration costs.

## Key Publications


1. K. Dvijotham, P. Van Hentenryck, M. Chertkov, M. Vuffray, S. Misra, Graphical Models for Optimal Power Flow.

2. Proceedings of 22nd International Conference on Principles and Practice of Constraint Programming (CP 2016) [best paper award], extended version is published in Constraints, p. 1-26 (2016), arxiv:1606.06512.

3. D.K. Molzahn, C. Josz, and I.A. Hiskens, "Moment Relaxations of Optimal Power Flow Problems: Beyond the Convex Hull," IEEE Global Conference on Signal and Information Processing (GlobalSIP), December 2016.

4. K. Dvijotham and D.K. Molzahn, "Error Bounds on the DC Power Flow Approximation: A Convex Relaxation Approach," IEEE 55th Annual Conference on Decision and Control (CDC), December 2016.

5. D.K. Molzahn, "Incorporating Squirrel-Cage Induction Machine Models in Convex Relaxations of OPF Problems," IEEE Transactions on Power Systems (Letters), 2017.

6. X. Zhou, E. Dall'Anese, L. Chen, and K. Baker, "Incentive-based Voltage Regulation in distribution Systems," American Control Conference, Seattle, WA, May 2017.

7. M. Chertkov and V. Chernyak, "Ensemble of Thermostatically Controlled Loads: Statistical Physics Approach" arxiv:1701.04939, to appear (accepted) in Scientific Reports (Nature Group).

8. M. Chertkov and V. Chernyak, Ensemble Control of Cycling Energy Loads: Markov Decision Approach, arxiv:1701.04941, to appear (accepted) by Springer, Series: Institute of Mathematics and Applications, Title of book: Energy Markets and Responsive Grids: Modeling, Control and Optimization, editors: S. Meyn, T. Samad, S. Glavaski, I. Hiskens, J. Stoustrup

9. J. Lian, D. Wu, K. Kalsi and H. Chen, "Theoretical framework for integrating distributed energy resources into distribution systems," accepted by 2017 IEEE PES General Meeting, Chicago, IL, July 2017.

10. Stavros Karagiannapoulous, Line Roald, Petros Aristidou, Gabriela Hug, "Operational Planning of Active Distribution Grids under Uncertainty", IREP Conference, August 2017

11. L.A. Roald, D.K. Molzahn, and A.F. Tobler, "Power System Optimization with Uncertainty and AC Power Flow: Analysis of an Iterative Algorithm," to appear in IREP Symposium on Bulk Power System Dynamics and Control-X. The Power System of the Future: Global Dynamics arising from Distributed Actions, August 27 - September 1, 2017.

12. "Identifying Critical Resiliency of Modern Distribution Systems with Open Source Modeling," Resilience Week 2017 (IEEE xPlore).

13. "Electricity Distribution System Resilient Control System Metrics," Resilience Week 2017 (IEEE xPlore).

14. S. Kundu, J. Hansen, J. Lian, and K. Kalsi, "Assessment of optimal flexibility in ensemble of frequency responsive loads," submitted to IEEE International Conference on Smart Grid Communications, October, 2017

15. H. Chen, W. Zhang, J. Lian and A. Conejo, “Robust distributed Volt/VAR control of power distribution systems,” accepted by 56th IEEE Conference on Decision and Control, Melbourne, Australia, December, 2017

16. A. Bernstein, N. J. Bouman, and J.-Y. Le Boudec. "Real-Time Control of an Ensemble of Heterogeneous Resources," submitted to CDC 2017.

17. X. Zhou, E. Dall'Anese, L. Chen, and A. Simonetto, "An Incentive-based Online Optimization Framework for Distribution Grids," IEEE Trans. on Automatic Control, submitted Mar. 2017; under review.

# V. Vehicle Systems

## V.1 PEV-Grid Connectivity

**Keith Hardy, Principal Investigator**
Argonne National Laboratory
9700 S. Cass Avenue
Lemont, IL 60439
Phone: (630) 826-7383
E-mail: khardy@anl.gov

**Lee Slezak, Technology Manager**
U.S. Department of Energy
Phone: (202) 586-2335
E-mail: Lee.Slezak@ee.doe.gov

Start Date: July 1, 2016 End Date: September 30, 2021
Total Project Cost: $1,560,812 DOE share: $1,560,812 Non-DOE share: $0

### Project Introduction

Plug-in electric vehicles are a growing part of global automotive industry sales, necessitating expansion of the charging infrastructure. Workplace charging is growing (e.g., medium/large companies, campuses, government facilities and national labs) and a national network of public charging stations will be rolled out starting in 2018. The growth in demand for electricity is being anticipated by electric service providers and considered in mid- and long-term strategies to meet the needs of their customers ... while increasing clean power generation, distributed energy resources and grid storage. And on the customer side of the meter, smart building systems and connected campuses are being implemented (with DERs and storage in many cases) to reduce energy use and avoid demand charges. The driver is that intelligent use of energy, combined with local generation and storage, can minimize overloads or disruptions and contribute to grid stabilization and resiliency. However, achieving this level of integration requires networked communication and control of grid-connected devices, including EV charging equipment, in coordination with electric service providers.

Argonne's EV-Smart Grid Interoperability Center (IOC) primarily focuses on grid integration and smart energy management, i.e., research and development of enabling technologies for sensing, communication and control. Most activities include industry partners and provide data/knowledge for standards development or verification. The IOC also participates in several multi-lab foundational and program-specific tasks of the Grid Modernization Laboratory Consortium (GMLC), i.e., those that are directly related to interoperability and vehicle-grid integration R&D.

Since the IOC was initially established to facilitate harmonization of EV interoperability requirements and test procedures in the US and Europe, Argonne participates in Global InterOP with multi-national automotive manufacturers and its partner lab, the EC's Joint Research Center (JRC). The second 5-year DOE-JRC agreement to cooperate was signed in July 2016; areas of interest have expanded from EV interoperability to common test equipment/procedures for high power DC charging and grid integration/resiliency. The IOC also supports efforts by the Departments of Energy and Commerce to harmonize with Asia through the APEC Automotive Dialog. And more recently (Q4 FY 2017) VTO initiated a Network Interoperability Study, conducted by NREL and ANL, to understand supply and demand side expectations, as well as the technical implications, for a national electric vehicle charging infrastructure.

## Objectives

Grid Integration - Develop enabling technologies and a grid integration testbed (aka Smart Energy Plaza or SEPØ2) to support R&D for PEV-grid integration and GMLC VTO-specific projects.

- Common Integration Platform (CIP.io) - Enable standard connectivity and communication with PEVs, EVSE (AC, DC and wireless) and grid-connected systems (PV inverter, building systems and batteries); to enable grid integration studies with non-proprietary communication protocols.
- Smart Charge Adaptor (SCA) - Enable universal PEV metering, charge load control and charge network integration for smart energy management; to support load management studies in the Smart Energy Plaza Ø2 (SEPØ2) and demonstration of the GMLC use cases with legacy and 'smart' EVSE.
- Compact submeters applied to EV charging – Apply latest submeter developments to meter multiple EV charging circuits in a standard power panel.
- Grid integration testbed (aka SEPØ2) - Develop a research/test environment to study the integration of grid-connected devices and communication, including PEV, networked charging stations, controllable building systems, energy storage, renewable distributed energy resources, and grid service signals; to support GMLC use cases, PEV-grid integration studies, microgrid operation.
- Hardware-in-the-loop (HIL) capability - Begin setup and integration of grid simulator and Opal RT into CIP.io; to support scaling of grid-connected device loads and for aggregated grid services.
- Prepare for testing high power DC charging systems (>150 kW, aka 'XFC') – Identify infrastructure modifications for up to 350 kW charging systems; specify and source test equipment

International Cooperation/Harmonization

- Europe - Complete comparison of PEV test procedures, coordinate DC interoperability test procedures and equipment to be used for XFC testing in FY18
- Asia - Support USG/USTR efforts to establish cooperative interoperability center(s).

National Network Interoperability Study

- Determine supplier (i.e., charging network) and customer expectations, as well as the technical implications, to implement a national electric vehicle charging infrastructure.

## Approach

*Enabling Technologies*

- Common Integration Platform (CIP.io) - Further develop CIP.io to enable standard connectivity and communication with PEVs, EVSE (AC, DC and wireless) and grid-connected systems (PV inverter, building systems and batteries); utilizing open-source software and further developing Node-Red nodes for vehicle grid integration research. (partner - CSS)
- Smart Charge Adaptor (SCA) - Based on the proof of concept SCA developed in FY16, develop alpha prototype and backend integrated in CIP.io; produce 30 alpha prototypes for field testing. (partner – CAD)
- Compact submeters for PEV-grid integration - Leverage developments for BTO Efficient Buildings program that enables 16 charge stations to be metered in one load center with a 2x2" submeter. (partners – 2G Engineering, Amzur Technologies)

*Grid Integration Testbed*

- Smart Energy Plaza (SEPØ2) - Converted former gas station to a laboratory environment to integrate PEV charging, DERs, building systems and enabling technologies for grid integration; installed a flexible infrastructure (multiple AC busways with voltage levels up to 480 VAC-3Ø plus a DC bus), building components and L2/DCFC EVSE with industry-adopted protocols plus local monitoring and control, solar array, static switch for microgrid operation. (partner – ANL Sustainability Program)

- HIL capability – Create MQTT publish and subscribe Simulink blocks to facilitate communication between real and emulated hardware in the Opal RT environment. Acquire hardware and necessary software to setup the Power HIL lab. (partner – Michigan Technological University)

*International Cooperation/Harmonization*

- Europe - Complete comparative vehicle testing and analysis at JRC; Coordinate high power DC charging infrastructure requirements, interoperability test procedures and equipment
  (partners – CCS Fast Charging Consortium, JRC-Ispra)

- Asia – Represent DOE IOC in technical workshops to support APEC Automotive Dialog
  (partner – U.S. Department of Commerce)

*National Network Interoperability Study*

- Stakeholder interviews to determine the expectations for the charging experience – for both the customer and supplier/charging network; translate to technical requirements and necessary level of interoperability between charging networks. (partner – NREL)

**Results**

Common Integration Platform (CIP.io) – All hardware connected to the electric infrastructure in SEPØ2 has been integrated into CIP.io; enabling a variety of energy management scenarios to be explored, e.g., demand response, V2B and microgrid operation. Node development in FY17 included custom nodes for the ABB static transfer switch, Ideal Power SunDial inverters, Starline meters, Open Charge Point Protocol (OCPP), and BACnet.

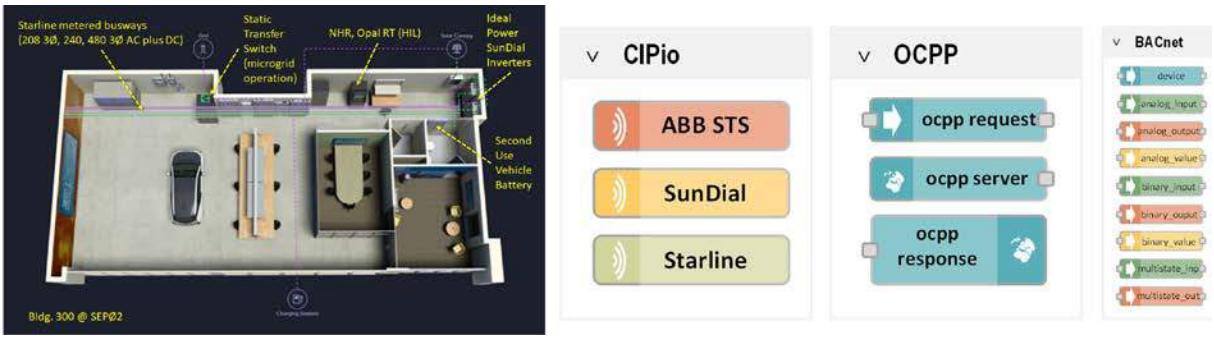


Figure V.1.1 - Additional hardware installed/integrated and CIP.io Node-Red nodes developed in FY 2017 (Source: ANL)

Smart Charge Adaptor (SCA) - Alpha prototype has been developed and tested; alpha backend has been developed and integrated in CIP.io. Assembly of 30 alpha units will be completed in Q1 FY 2018 and deployed for field testing. The smart charging module was granted a US patent in Q4 FY 2017.

Figure V.1.2 - ANL SCA locked to a public EVSE and connected to a GM Volt while charging
(Source: ANL)

Compact submeters for PEV-grid integration - Completed AC EVSE load center, with mains measurement on a single self-contained submeter, connected to a work-in-progress meter data dashboard application software. The hardware will be installed in parallel with conventional metering to assess the benefits of individual circuit metering.

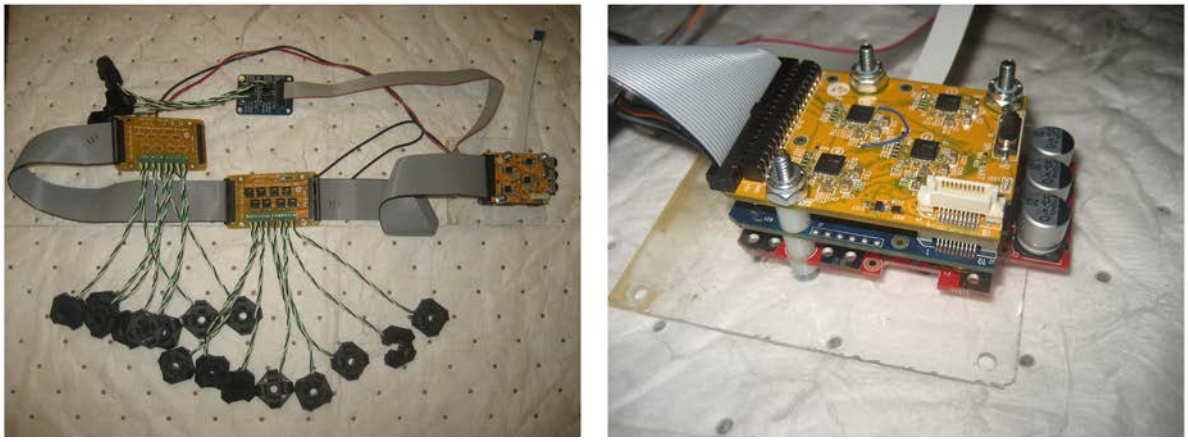

Figure V.1.3 - Submeter package with multiple current sensors for power panel; 1.5" x 2" input meter detail on right
(Source: ANL)

Smart Energy Plaza (SEP Ø2) – All building systems, the solar canopy and EVSE are functioning and integrated with CIP.io with the exception of the second use vehicle battery; it has been mounted and will be electrically connected in Q1 FY 2018 for use as energy storage for the building. The 160 kW DC EVSE is expected to arrive by Q2 FY 2018 and will be installed on the charging island with the existing 50 kW DC EVSE. Necessary infrastructure modifications to install the XFC system (350 kW) will be initiated in Q1 FY 2018. An additional 40 kW solar canopy and six Level 2 AC EVSE will be installed in partnership with the Argonne Sustainability Program.

To address questions pertaining to vehicle-grid integration (VGI) such as grid services provided by aggregated EVs, an NHR 9410 grid simulator and Opal RT real-time simulator have been integrated into CIP.io; HIL scaled simulations can now utilize actual SEP Ø2 data/hardware with emulated systems to answer questions pertaining to VGI.

A visual model was constructed that utilizes the device data from CIP.io, enabling real-time monitoring of energy flows and visualization of the impact of energy management strategies.


Figure V.1.4 - Smart Energy Plaza Ø2
(Source: ANL)

International Cooperation – The comparison of reference vehicle testing at ANL and JRC was published. APEC meetings have resulted in requests from several countries in Asia for cooperation on PEV-grid integration activities and interoperability assessment.

National Network Interoperability Study – Stakeholder interviews were reported and summarized in a draft report by NREL to DOE; customers expect a charging experience to be seamless, with clear pricing and no more complicated than a gas station. Initial technical implications focused on the transaction method and interoperability required between charging networks, e.g., cash requires no interoperability and credit cards or exclusive network cards necessitate substantial interoperability for 'roaming'.

## Conclusions

*Enabling Technologies*

- Common integration platform (CIP.io) – Development and integration at SEPØ2 has proceeded according to plan. Integrated monitoring and communication/control of the building systems, solar array and various EVSE has been demonstrated; including EVSE control based on a demand response, vehicle-to-building power and basic microgrid operation. The portfolio of open source developed to date will be expanded in FY 2018 to include most common communication protocols used in EVSE, building systems or DERs.

- Smart Charge Adaptor (SCA) – Alpha development and testing of the SCA is near completion; these devices will be used with non-networked EVSE for PEV-grid integration and GMLC studies. The SCA has been integrated in CIP.io and has demonstrated the ability to control the charge rate in networked and non-networked EVSE.

- Compact submeters for PEV-grid integration – Vehicle-grid applications have benefited from the BTO-sponsored commercialization project (which was initiated based VTO-sponsored development at ANL). The submeters for building applications have been successfully tested on the bench, the prototype EVSE 'load center' has been fabricated and will be tested with multiple EVSE in FY 2018.

*Grid Integration Testbed*

- Completion of the Smart Energy Plaza Ø2 facility and integration of the devices into the common integration platform has enhanced the ability of the interoperability center to support VTO's PEV-grid integration tasks and evaluate GMLC use cases in FY 2018/19. Integrating high power charging in FY 2018 will allow for grid integration studies/testing with EVSE ranging from 6.6 kW to 320 kW.

- Integration of the power HIL capabilities will allow scaling to characterize the potential benefits of services provided by aggregated grid-connected devices such as electric vehicles.

## Key Publications

*Publications*

1. Chong Cao, Luting Wang, Bo Chen, Jason D. Harper, Theodore P. Bohn, Daniel S. Dobrzynski, and Keith S. Hardy, "Real-Time Modeling to Enable Hardware-in-the-Loop Simulation of Plug-in Electric Vehicle-Grid Interaction," Best Student Paper Award at 2017 ASME/IEEE International Conference on Mechatronic and Embedded Systems and Applications (MESA2017), Cleveland, Ohio, August 6-9, 2017.

2. Piyush Aggarwal, Bo Chen, and Jason D. Harper, "Integration of OpenADR with Node-RED for Demand Response Load Control Using Internet of Things Approach," SAE 2017 World Congress, Detroit, MI, April 4-6, 2017.

*Patents/Copyrights*

1. J. D. Harper, D. Dobrzynski "Plug-in electric vehicle (PEV) smart charging module", September 12, 2017, Argonne National Laboratory, United States Patent, 9,758,046.

2. J. D. Harper, B. Nystrom, "node-red-contrib-ocpp", Copyright 2017, Argonne National Laboratory, Submitted.

3. J. D. Harper, A. Kurup, "node-red-contrib-bacnet", Copyright 2017, Argonne National Laboratory, Submitted.

4. J. D. Harper, C. Cao, "Opal-RT MQTT Blocks", Copyright 2017, Argonne National Laboratory, Submitted.

5. J. D. Harper, "node-red-contrib-abb-sts", Copyright 2017, Argonne National Laboratory, Submitted.

6. J. D. Harper, "node-red-contrib-ipc", Copyright 2017, Argonne National Laboratory, Submitted.

7. J. D. Harper, "node-red-contrib-starline", Copyright 2017, Argonne National Laboratory, Submitted.

8. J. D. Harper, "Node-Red PEV Smart Charging Algorithm Flow", Copyright 2017, Argonne National Laboratory, Submitted.

## V.2 Technology Harmonization and Technical Team Activities

**Richard "Barney" Carlson, Principal Investigator**
Idaho National Laboratory
P.O. Box 1625
Idaho Falls, ID 83415-2209
Phone: (208) 526-0378
E-mail: richard.carlson@inl.gov

**Lee Slezak, Technology Manager**
U.S. Department of Energy
Phone: (202) 586-2335
E-mail: Lee.Slezak@ee.doe.gov

Start Date: October 1, 2016 End Date: September 30, 2016
Total Project Cost: $380,000 DOE share: $380,000 Non-DOE share: $0

### Project Introduction

INL's Advanced Vehicle team evaluates grid-connected plug-in electric vehicle (PEV) technology in order to understand and identify the technology gaps towards high power, clean, efficient and even hands-free charging operation. Knowledge gained from 20 years of testing electric drive vehicles and charging infrastructure is used by INL staff to contribute to various industry and government groups that are primarily interested in developing policies, standards, codes, and regulations that ensure safety and interoperability within technology sectors.

### Objectives

The objective of this project was to contribute vehicle, component, and charging infrastructure testing results and knowledge gained by Idaho National Laboratory (INL) staff from laboratory evaluations and characterization to industry and government groups developing and modifying standards, codes, best practices, and regulations.

### Approach

The Electric Vehicle Infrastructure (EVI) lab at Idaho National Lab is utilized to conduct testing and evaluation of advanced PEV charging systems. The EVI lab has unique testing capabilities for the evaluation of wireless power transfer (WPT) system both as install on a vehicle as well as stand-alone off-board a vehicle. Additional EVI lab capabilities include conductive charging system characterization for AC Level1 / Level2 and DC Fast Charging. The specialized capabilities include measurement of performance characteristics, efficiency, power quality, harmonics, and transient grid response evaluation. The combination of these capabilities enables a complete understanding of the charging system operation and performance under the wide range of operating conditions.

INL developed collaborative research agreements with Witricity, Nissan, Toyota, Daimler, Jaguar Land Rover, and Qualcomm to enable a testing project by INL that encompassed the evaluation of eight wireless charging systems. The test results from the collaborative efforts enabled the SAE J2954 codes and standards committee to develop and refine WPT system requirements for interoperable efficiency, safety, and power quality.
As a member of a technical committee or industry group, participation is intended to contribute to the common body of knowledge being applied to develop standards and other industry practices.

## Results

*SAE J2954 Task Force (Wireless Charging):*

INL supports the SAE J2954 committee by providing detailed test results from wireless charging systems and providing detailed test setup information. In FY16 and FY17, INL supported the SAE J2954 committee by conducting a two-phase testing program to support the knowledge and understanding of wireless charging interoperability requirements. Interoperability is when the ground-side and the vehicle-side of a wireless charging are not produced by the same manufacturer or are not of the same design topology. When the two halves of the wireless charging system (ground-side and vehicle-side) are of the same design, from the same manufacturer, it is referred to as a matched set.

In FY17 INL completed the testing of the fourteen interoperable combinations of the wireless charging systems. Additionally analysis was completed to quantify the performance, efficiency, power quality, and radiated electro-magnetic (EM) field from the wireless charging system. These efforts are in continuation to the FY16 work INL completed to prepare and test eight wireless charging systems in matched configuration (ground side and vehicle side both from the same manufacturer). Together the results from the matched and interoperable configurations enable data-driven decisions in developing and refining the codes and standards for automotive wireless power transfer systems.

The bench test setup utilized at INL is shown in Figure V.1.1. It comprises a servo-motor driven, coil positioning system that accurately positions the ground coil assembly (GA) with respect to the vehicle coil assembly (VA) to with accuracy better than 1 mm. A fiberglass channel strut frame is utilized to support all the vehicle components. A DC load bank is utilized to absorb the output power from the WPT system and it is controlled to emulate a vehicle's high voltage battery including internal resistance.

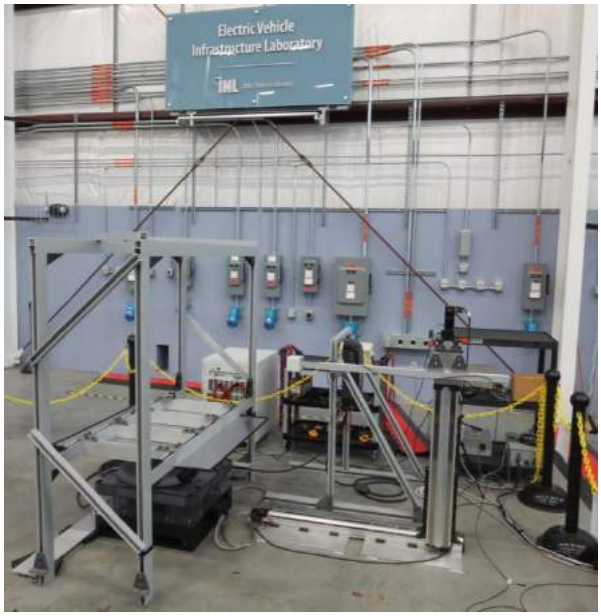


Figure V.2.1 - Bench Testing of Wireless Charging Interoperability to Support SAE J2954
(Source: INL)

For measuring the EM-field safety, power quality, and efficiency of each WPT combination, a data acquisition system is utilized with a high accuracy power meter and an EM-field measurement probe. The power meter with current and voltage measurement capabilities is utilized to measure the input and output power of the WPT system to determine the overall system efficiency (AC to DC efficiency). The power meter is also utilized to quantify the power quality of the WPT system, specifically the power factor at the input grid supply

during operation. The EM-field measurement probe is utilized to measure the magnetic field and electric field near the WPT system during operation as well as measure the operating fundamental frequency of the WPT system. All the measured data during testing is recorded and time aligned via the data acquisition system for subsequent, in-depth analysis and visualization of the performance and safety metric across the wide range of operating conditions during testing.

A primary scope of the testing is to quantify the system efficiency of the matched and interoperable WPT system combinations. The system efficiency is calculated from the concurrent, steady state measurements of DC output power from the VA and input power from the 60 Hz AC grid power source. The test results from matched and interoperable operation across a range of aligned and misaligned conditions are detailed below. The test results have been separated into three alignment ranges to detail the impact of coil-to-coil misalignment. The three alignment categories are *Aligned* (0, 0), *Maximum Misalignment* (+/-75, +/-100), and *Moderate Misalignment* (values between the aligned and maximum misalignment cases). The test results from each of the three alignment categories include the full range of evaluated ground clearances and output voltages.

Figure V.1.2 shows a histogram of all full power system efficiency measurements for interoperable WPT results across the range of ground clearance, coil to coil misalignment, and output battery voltage. A majority of the interoperable WPT system efficiency results are greater than 87% with a few test results showing efficiency exceeding 93%. Some test conditions resulted in system efficiency between 79% and 87%.

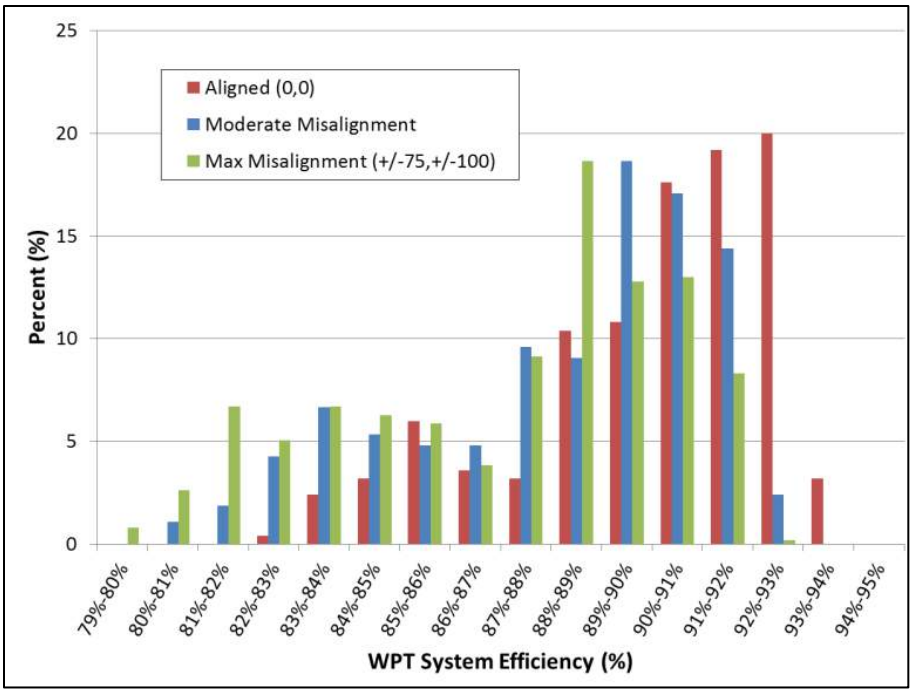


Figure V.2.2 - Efficiency Results from Interoperable Bench Testing of Wireless Charging Systems
(Source: INL)

EM-field results from the interoperable WPT operation, shown in Figure V.2.2 shows a histogram of the measured magnetic field strength. The magnetic field results have a large number of results below 14 A/m. However, a significant number of results are greater than 21 A/m (the industry safety guideline) and some results range up to 120 A/m for interoperable operation at maximum misalignment when the GA is nearest to the measurement probe. Additionally, the highest aligned operating conditioned resulted in a measurement of more than 80 A/m.

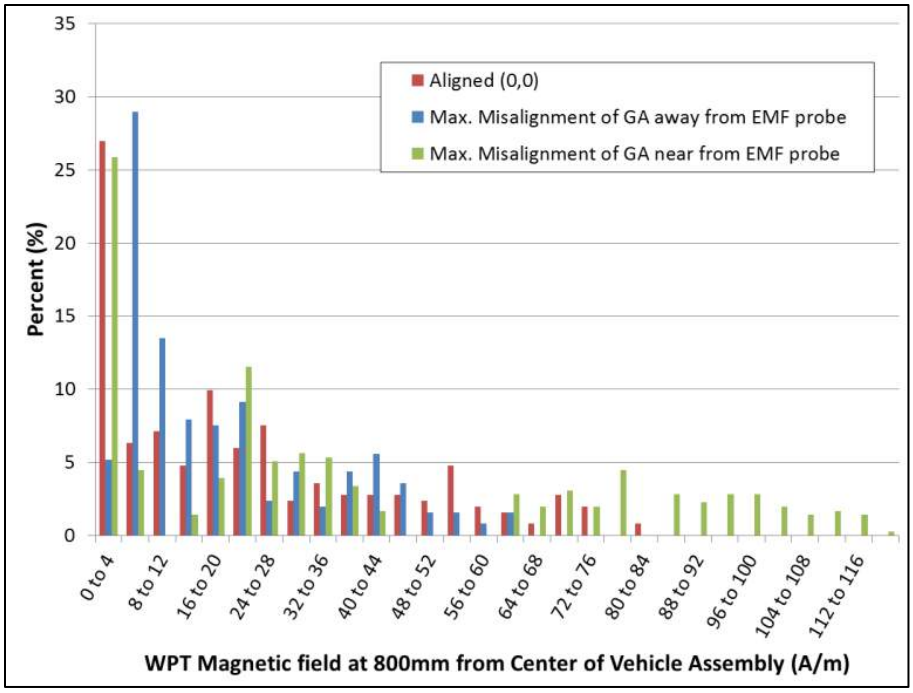


Figure V.2.3 - Magnetic Field Results from Interoperable Testing of Wireless Charging Systems
(Source: INL)

Test results show the EM- field strength is within the ICNIRP 2010 public exposure limit for many operating conditions across the various interoperable WPT configurations tested. However, several measurements show that there are many operating conditions (alignment, ground clearance, and output voltage) in which the EM-field strength is above the industry safety guidelines. These results show that there are still technical revisions and new solutions needed to reduce the EM-field emissions at all the interoperable operating conditions in order to meet the industry EM-field safety guidelines.

*Vehicle Systems Analysis Tech Team:*

INL is a long-time member of the Vehicle Systems Analysis Tech Team due to INL's history of testing performed for DOE. INL staff contributes, via presentations and papers, the results of benchmarking the advanced automotive powertrain components and subsystems from INL's whole vehicle system and component testing. This testing includes fuel use, efficiencies, auxiliary loads, and energy storage results that are subsequently used by other team members as modeling inputs.

*Grid Integration Tech Team:*

Because of the nature of the infrastructure testing INL performs for DOE, INL is a founding member of the Grid Integration Tech Team. This includes wireless power transfer and conductive charging, which includes direct current fast charging, and INL's data collection, analysis, and reporting on how 8,000 PEV drivers utilize 17,000 Level 2 EVSE and direct current fast chargers.

*Infrastructure Working Council:*

INL is a 20-year member of the Infrastructure Working Council, which is sponsored by the Electric Power Research Institute and is a group of individuals whose organizations have a vested interest in the emergence and growth of the electric vehicle, plug-in, and hybrid electric vehicle industries, as well as electrification of truck stops, ports, and other transportation and logistics systems. Infrastructure Working Council members include representatives from electric utilities, vehicle manufacturing industries, component manufacturers,

government agencies, related industry associations, and standards organizations. The various committees meet several times a year to address electric vehicles, plug-in hybrid electric vehicles, truck stop and port electrification, and infrastructure research and development. INL supports the Plug-in Hybrid and Electric Vehicle Working Group, the Transportation Electrification Committee, and serving on the Infrastructure Steering Committee. Results from INL's testing of vehicles and charging infrastructure supports the Infrastructure Working Council's decision processes.

*SAE J2894 Task Force (Power Quality Requirements for Plug-In Electric Vehicle Chargers):*

The SAE J2894 committee is developing requirements and test procedures to ensure PEV chargers do not cause power quality issues and PEVs can continue to function properly in the presence of power quality issues caused by adjacent loads. INL testing of PEV charging systems provides detailed results to this task force to support results-based decisions for development of the procedures, requirements, and recommendations.

INL characterized eight, level 2 on-board charge systems from a range of PEVs. The testing investigated the performance of the systems across a wide range of operating conditions such as power transfer level, input voltage, battery state of charge, and more. Figure V.2.4 shows the AC to DC efficiency of the on-board charge systems. The efficiencies range from >95% to <80%. Overall the efficiency is high when the charge system is operating above half power.

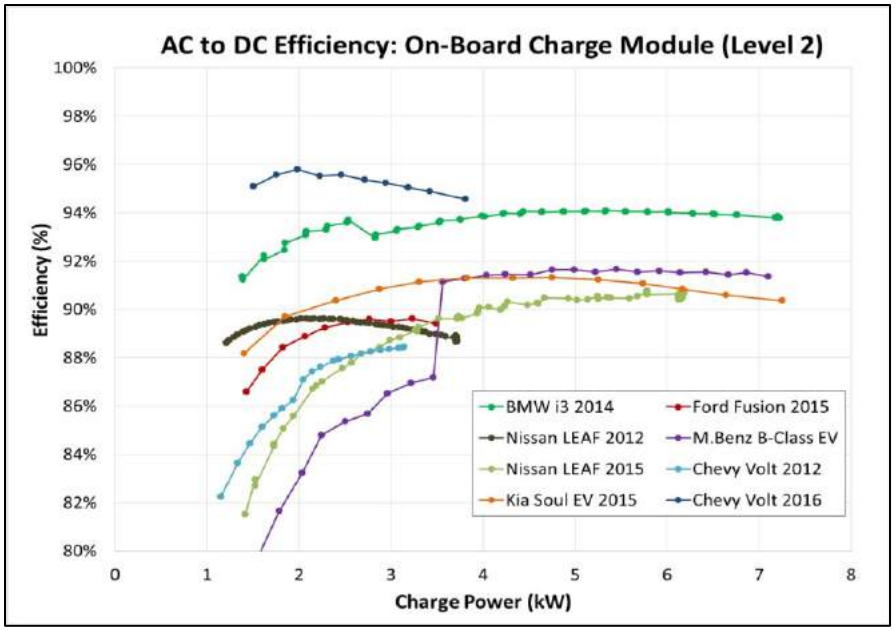


Figure V.2.4 - Efficiency results from eight vehicle on-board charging systems

(Source: INL)

Testing also investigated the power quality and harmonics performance of the on-board charging systems. This is important in regards to possible impact to other electronic systems near the charging system connected to the same circuit. The higher the harmonics produced on the input current, the higher the potential to impact other devices operating on the same circuit. Figure V.2.5 shows the total harmonic distortion on the input current from the on-board charging systems. Again note that the harmonics are lowest when the charger is operating near full power.

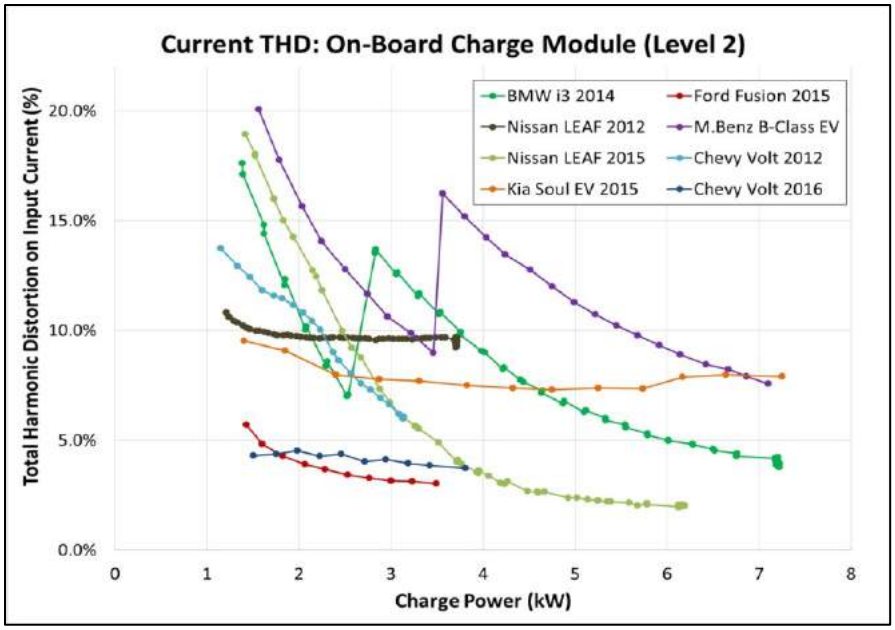


Figure V.2.5 - Total Harmonic Distortion from eight vehicle on-board charging systems
(Source: INL)

INL's testing and evaluation of on-board charging systems provides the SAE J2894 task force with results to enable results-based decisions on recommended practices and standards for the performance, power quality, and harmonics of charging systems for PEVs.

## Conclusions

The intent of the work performed is to leverage laboratory testing results and staff knowledge gained as a resource for various industry groups that are putting into place industry-led or government-led codes, standards, requirements, or best practices.

## Key Publications

1. Schneider, J., Carlson, R., et al.; Bench Testing Validation of Wireless Power Transfer up to 7.7 kW Based on SAE J2954, SAE 2017-01-2448; 2017.

## V.3 Wireless and Conductive Charger Evaluation

**Richard "Barney" Carlson, Principal Investigator**
Idaho National Laboratory
P.O. Box 1625
Idaho Falls, ID 83415-2209
Phone: (208) 526-0378
E-mail: richard.carlson@inl.gov

**Lee Slezak, Technology Manager**
U.S. Department of Energy
Phone: (202) 586-2335
E-mail: Lee.Slezak@ee.doe.gov

Start Date: October 1, 2016 End Date: September 30, 2017
Total Project Cost: $300,000 DOE share: $300,000 Non-DOE share: $0

### Project Introduction

INL's Advanced Vehicle team evaluates grid-connected plug-in electric vehicle (PEV) technology in order to understand and identify the technology gaps towards high power, clean, efficient and even hands-free charging operation. Knowledge gained from 20 years of testing electric drive vehicles and charging infrastructure is used by INL staff to contribute to various industry and government groups within advanced transportation technology sectors.

### Objectives

- Provide the U.S. Department of Energy (DOE) with independent and unbiased benchmark testing results by evaluating emerging technologies developed via DOE and industry investments
- Benchmark the efficiencies and safety of wireless power transfer (WPT) systems, conductive electric vehicle supply equipment (EVSE), and direct current fast chargers (DCFC)
- Benchmark the cyber security of charging systems
- Benchmark DCFC and Level 2 EVSE compatibility with new generations of plug-in electric vehicles (PEVs)

### Approach

The Electric Vehicle Infrastructure (EVI) lab at Idaho National Lab is utilized to conduct testing and evaluation of advanced PEV charging systems. The EVI lab has unique testing capabilities for the evaluation of wireless power transfer (WPT) system both as install on a vehicle as well as stand-alone off-board a vehicle. Additional EVI lab capabilities include conductive charging system characterization for AC Level1 / Level2 and DC Fast Charging. The specialized capabilities include measurement of performance characteristics, efficiency, power quality, harmonics, and transient grid response evaluation. The combination of these capabilities enables a complete understanding of the charging system operation and performance under the wide range of operating conditions.

### Results

*Wireless Charging: Hyundai / Mojo Mobility WPT System*

The Hyundai / Mojo Mobility WPT system, as installed on a Kia Soul EV, is tested in the EVI lab at INL using a specific test setup specifically intended to test and evaluate the performance and safety of WPT systems including efficiency, power quality, and EM-field emissions. The EVI lab test setup includes specific laboratory equipment

for accurate positioning of the WPT coil assemblies. The EVI lab testing capabilities also include high accuracy data acquisition system to measure and record the electrical power flow, power quality, and EM-field emissions during testing. Figure V.3.1 shows the Hyundai / Mojo Mobility WPT system during testing in the EVI lab.

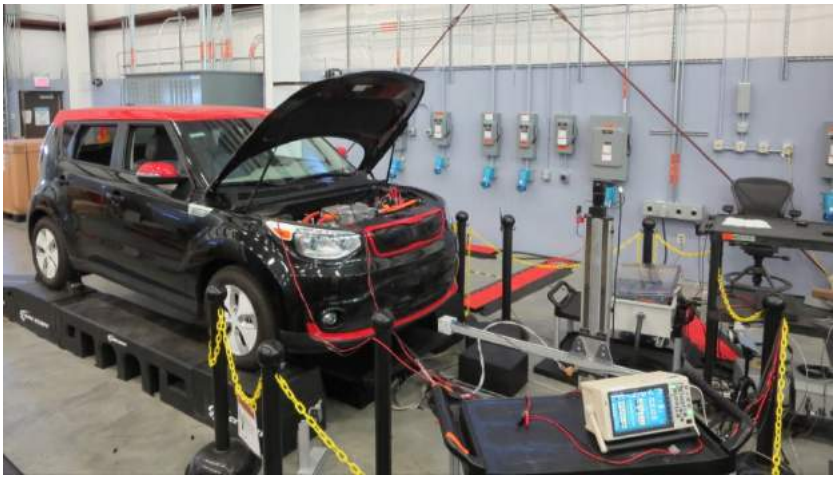

Figure V.3.1 - Testing and Evaluation of the Hyundai / Mojo Mobility WPT system on a Kia Soul EV at INL's EVI lab (Source: INL)

The WPT system is tested across a wide range of operating conditions including coil misalignment, coil to coil gap, and power transfer level. Nominal operating conditions are defined as 7.0 kW DC output with the coils in alignment and a coil to coil gap of 200 mm. Table V.3-1 details the performance and safety results as measured during nominal operation. The measured 88.4% total system efficiency is defined as the total DC output power provided to the vehicle's high voltage DC bus (in which the vehicle's battery system is connected) divided by the total grid AC input power drawn by the WPT system. The measured magnetic field is 18.3 A/m and the measured electric field is 278 V/m. These measurements are recorded at nominal WPT operating conditions measured with the center of the EM-field probe at a distance of 200 mm from the front surface of the vehicle's front bumper, along the center line of the vehicle, and vertically centered within the coil gap. The measured power quality of the WPT is 9.5% input current THD and a power factor of 0.995. Additionally, it is notable that the operating fundamental frequency of the WPT system is 88.3 kHz.

Table V.3-1 - Measured Safety and Performance Metrics at 7.0 kW DC output power

| Measured Parameter | Value |
|---|---|
| Ground Clearance (coil gap) | 200 mm |
| Total System Efficiency (AC to DC) | 88.4% |
| Magnetic field at front of vehicle | 18.3 A/m |
| Electric field at front of vehicle | 278 V/m |
| Input Current THD | 9.5% |
| Power Factor | 0.995 |
| Operating Frequency | 88.3 kHz |

Coil to coil misalignment and coil to coil gap are primary factors influencing the efficiency of WPT systems. To quantify the impact of coil to coil misalignment along the X-axis (fore to aft of the vehicle) and Y-axis (side to side) on the total system efficiency of the Hyundai / Mojo Mobility WPT, a full range of tests are conducted to detail the total system efficiency. Figure V.3.2 shows the total system efficiency (AC to DC) when operating at 7.0 kW output power and a coil to coil gap of 200 mm across a range of X and Y coil to coil misalignment. As expected, the peak efficiency of 88.4% occurs where the coils are in magnetic alignment. With misalignment in either the X or Y direction, a decrease in total system efficiency is measured. Note the mostly symmetrical system efficiency results with respect to coil misalignment as well as the difference in magnitude of misalignment impact on system efficiency along the X-axis and Y-axis. The reduction in system efficiency is greater in the Y-axis for a given coil to coil misalignment. This is primarily due to the non-square coil assembly design of the WPT system. Recall the dimensions along the Y-axis of the ground assembly and the vehicle assembly are 920 mm and 800 mm respectively whereas the dimensions along the X-axis are 1,180 mm and 740 mm respectively. This results in a ground coil assembly to vehicle coil assembly overlap of +/-60 mm along the Y-axis and +/-220 mm along X-axis.

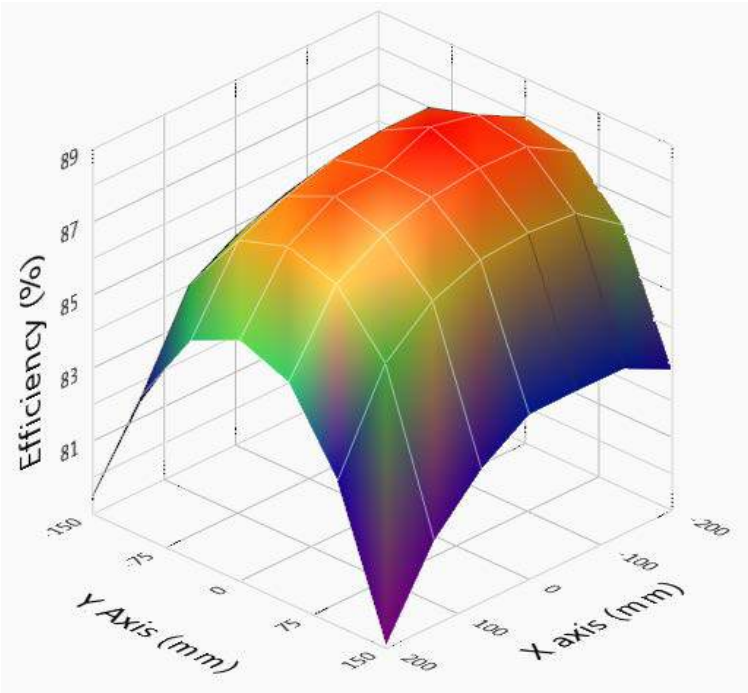


Figure V.3.2 - WPT Total System Efficiency variation due to coil misalignment at 7.0 kW and 200 mm coil gap (Source: INL)

Electromagnetic field (EM-field) measurements are conducted at the front of the vehicle in a precise grid pattern to characterize and visualize the magnitude of the EM-field adjacent to the front bumper of the vehicle. This was accomplished by using an EM-field measurement probe to measure the magnetic and electric field during steady state operation of the WPT system during full power transfer. For all of the measurements, the center of the EM-field probe is positioned as a distance of 200 mm from the forward most surface of the vehicle front bumper.

Figure V.3.3 shows a photo of the front of the vehicle with the Y and Z axis overlaid for reference. The vertical center line of the vehicle, which is the Z-axis, is indicated by the dashed yellow line. For reference the lower surface of the vehicle coil assembly is at Z-axis = 0.0 mm. The ground surface is Z-axis = -200 mm since testing is conducted at the nominal condition of 200 mm ground clearance.

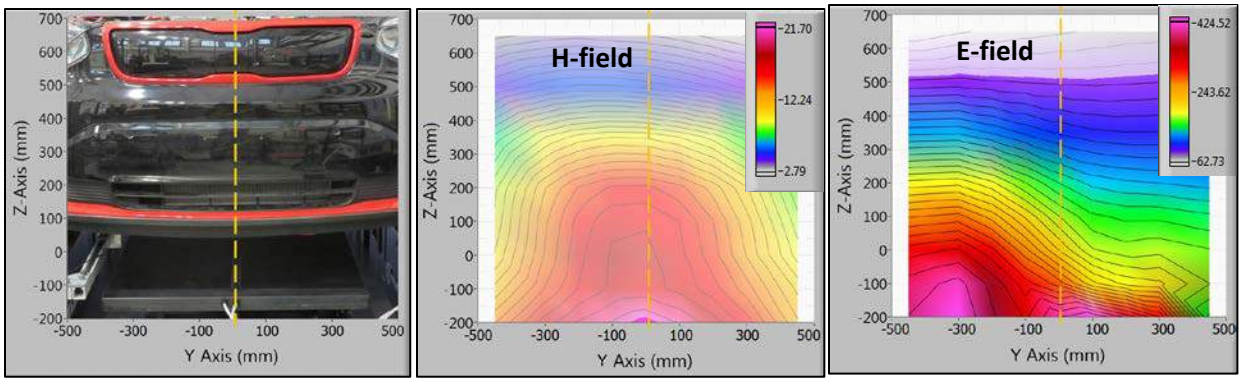


Figure V.3.3 - Photo of front of vehicle, and the WPT measurements of H-field (A/m) and E-field (V/m) 200 mm from the front of the vehicle
(Source: INL)

The EM-field measurements are conducted during 7.0 kW steady state operation, at a coil to coil gap of 200 mm, with the coils in alignment. Figure V.3.3 shows the magnetic field measurements in A/m at the front of the vehicle. The muted color regions are below the ICNIRP 2010 general public exposure limit of 21 A/m, whereas the brightly colored region (lower center) is greater than the ICNIRP 2010 limit. Note the H-field symmetrical characteristic across the Y-axis. The maximum measured H-field strength is 21.7 A/m. This measurement is closest to the ground coil assemble and along the vehicle's center axis. Overall the H-field measurement results at the front of the vehicle, verify that nearly the entire region next to the vehicle is within the industry public exposure limit during 7.0 kW power transfer.

Electric field measurements are concurrently conducted with the magnetic field measurements discussed previously at the pre-described measurement locations at front of the vehicle. Figure V.3.3 shows the electric field measurements in V/m. The muted color section is below the ICNIRP 2010 general public exposure limit of 83 V/m, whereas the brightly colored region (below Z=500 mm) is greater than the ICNIRP 2010 limit. Note the non-symmetrical E-field characteristic in the Y direction which shows a larger E-field on the passenger side of the vehicle (negative Y direction). The maximum measured E-field strength is 425 V/m which occurs at two locations. One maximum location is closest to the passenger side of the ground coil assemble and the second maximum location is near the Litz wires connection to the ground coil assembly from the inverter power electronics. Overall the E-field measurement results indicate a majority of the area 200 mm in front of the vehicle, exceeds the general public exposure limit, by up to five times, during 7.0 kW output WPT operation.

The EM-field emissions measurements around the WPT system at the front of the vehicle exceeded the ICNIRP 2010 public exposure limit. The highest magnetic field measured is 21.7 A/m which is only slightly higher than the public exposure limit of 21.0 A/m. However the highest electric field measured is 425 V/m is more than five times above the public exposure limit of 83 V/m.

The testing and evaluation of the Hyundai / Mojo Mobility WPT system at INL measured the total system efficiency, sub-system efficiencies, electrical power quality, and EM-field emissions of the WPT system during 7.0 kW power transfer. These measurements are accomplished through utilizing laboratory testing equipment and fixtures specific for the evaluation of WPT systems.

*Charge System Response to Dynamic Grid Events:*

INL has completed testing and evaluation of nine PEV charging systems that include Level 2 and DC Fast Charging. The evaluation includes characterizing the operation and response of the charging system during variation of input power grid conditions such as varying input voltage and frequency. The testing includes

evaluation of slow moving, quasi-static changes in voltage and frequency, as well as fast transients such as voltage sag or momentary outages. Understanding the response of the charging system is important to know if the charging system will 'ride through' the event or is user intervention required to reset and restart the charge session. Additionally it is important to quantify the interaction and impact of the charge system response on the electric grid. If the response is bad, then the impact to the local distribution grid may also cause issues for other loads on the grid.

INL completed testing of three PEVs response to a voltage sag event. Prior to the voltage sag, the three PEVs are charging at steady state. A voltage sag event from 240 V RMS to 100 V RMS (L-N) is introduced for 12 cycles (0.2 seconds) to the input power to the three PEVs charge systems. The response is shown in Figure V.3.4. During the voltage sag event, PEV-A and PEV-B increase current draw in an attempt to maintain full charge power. Note PEV-C ceases charging shortly after the voltage sag, but it did resume charging approximately 10 seconds after the end of the voltage sag event. The total current draw by the three PEVs is 57 A RMS prior to the voltage sag event, yet during the voltage sag event, the combined current draw of PEV-A and PEV-B is 90 A RMS. This increase in current draw during the voltage sag event is not beneficial to the grid supply and could likely cause additional or greater magnitude of issues.

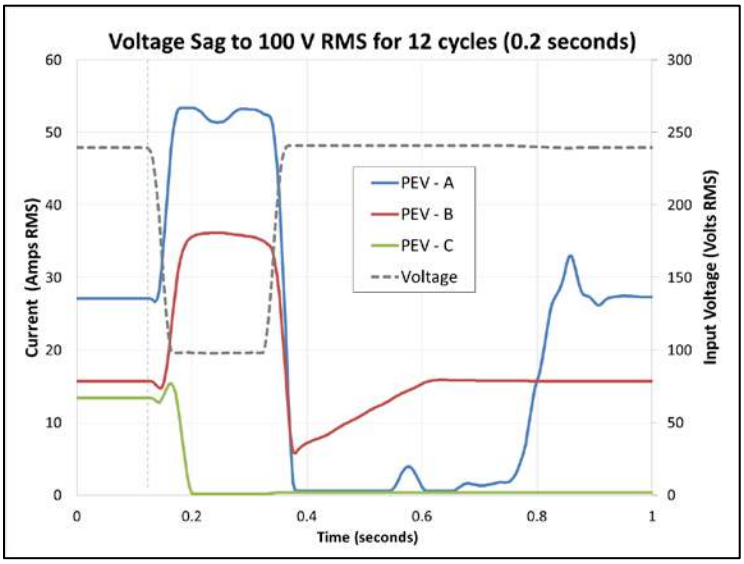


Figure V.3.4 - Response of three PEVs to an input voltage sage event for 12 cycles
(Source: INL)

To investigate the magnitude of the potential interaction and impact of PEV charging systems with the electric grid, INL completed hardware-in-the-loop emulation of 4,000 PEVs charging during a voltage sag event. The 4,000 PEVs are comprised of a mix of PEV-A, B, and C and these vehicles are subjected to a voltage sag event from 240 V RMS to 100 V RMS (L-N) for 12 cycles (0.2 seconds). The emulation incorporated a detailed model of the distribution node in the San Francisco bay area. The results showed the same response from the PEVs as shown in Figure V.3.4 which resulted in impacts to the electric grid that caused oscillations in the voltage and frequency for up to 15 seconds after the voltage age event. Figure V.3.5 show the magnitude of the voltage oscillation as well as the impact to the frequency. Note the oscillation dampens over 15 seconds and does not exceed industry limits for voltage or frequency deviation once the voltage sag event is cleared. But as more PEVs enter the market place and penetration level increase, the number of PEVs concurrently charging will increase. Additionally, it is expected that charge rates will also increase. This interaction between PEV charging and the electric grid is important and controls solutions are needed to mitigate the interaction impacts between PEVs and the electric grid.

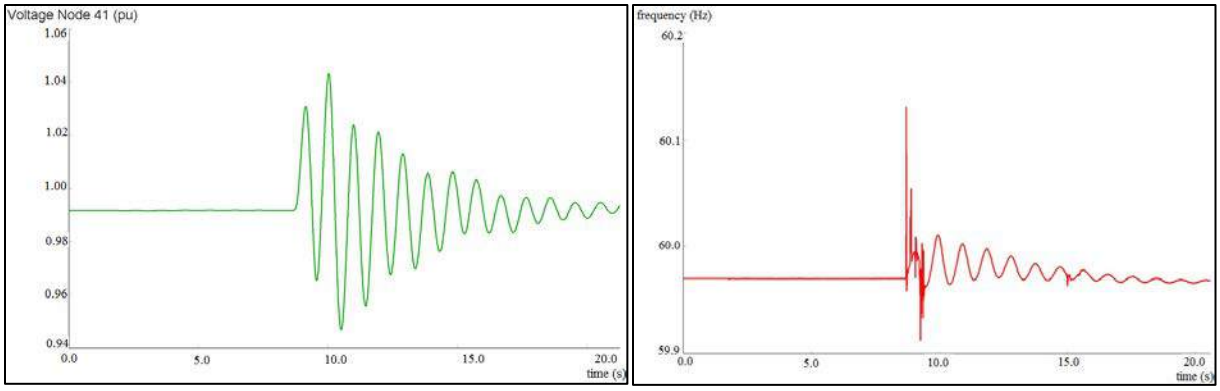


Figure V.3.5 - Oscillation in supply voltage and frequency due to voltage sag event when 4,000 PEVs are charging (Source: INL)

INL's testing and evaluation of charging systems has shown the interaction and impact between PEVs and the electric grid. This effort is important to provide concrete results for the basis of revising and creating industry-lead I for PEV charging systems.

## Conclusions

Charging infrastructure is important to the successful adoption of grid-connected vehicles; therefore, multiple key factors to the successful integration of vehicles and charging infrastructure are critical to the success of PEVs. This includes interoperability, safety, test methodology, and efficiency. Therefore, INL is working with industry to develop robust testing methodologies for evaluation of wireless and conductive charging systems.

## Key Publications

1. Carlson, R., Chabaan, R., et al.; Laboratory Performance and Safety Test Results of the Hyundai / Mojo Mobility 7.0 kW WPT System, EVS30 Symposium, 2017.

## V.4 Design and Implementation of a Thermal Load Reduction System for a Hyundai Sonata PHEV for Improved Range

**Cory Kreutzer, Principal Investigator**
National Renewable Energy Laboratory (NREL)
Transportation and Hydrogen Systems Center
15013 Denver West Parkway, MS 1633
Golden, CO 80401
Phone: (303) 275-3772; (303) 275-4413
E-mail: Cory.Kreutzer@nrel.gov; John.Rugh@nrel.gov

Lee Slezak, Technology Manager
U.S. Department of Energy
Phone: (202) 586-2335
E-mail: Lee.Slezak@ee.doe.gov

Start Date: October 1, 2014 End Date: September 30, 2017
Total Project Cost: $3,055,000 DOE share: $2,444,000 Non-DOE share: $611,000

### Project Introduction

NREL, in partnership with Hyundai America Technical Center, Inc. (HATCI), Pittsburgh Glass Works (PGW), PPG Industries, Hanon Systems, Sekisui S-LEC America, Gentherm, and 3M, developed and integrated a complete thermal load reduction system for a light-duty electric vehicle (EV). The project scope was planned in response to the FY14 Vehicle Technologies Office-wide funding opportunity announcement solicitation for the Advanced Climate Control Auxiliary Load Reduction area of interest. The overall goal of the project was to provide technology solutions that improve customer acceptance of electric-drive vehicles (EDVs) and increase the penetration of these vehicles into the national fleet. To achieve the project goals, the project objective was to increase grid-connected EDV range by 20% at peak heating and cooling conditions over the combined city/highway drive cycle. The project duration was three years, divided into an individual technology development and assessment phase (Phase I) followed by a technology integration and performance evaluation phase (Phase II). At the completion of the project, information generated will include vehicle performance results of the thermal load reduction system obtained through standardized experimental testing performed at HATCI's test facilities as well as estimation of national-level range improvements based on validated models.

### Objectives

- Increase grid-connected EDV range by 20% during operation of the climate control system by reducing thermal loads
- Implement a thermal load reduction system on a production vehicle and quantify performance of the system over the combined city/highway drive cycle at peak heating and cooling conditions
- Maintain occupant thermal comfort, verified through experimental evaluations.

### Approach

To evaluate thermal load reduction technologies both independently and as an entire system, the project was divided into two phases. During Phase I, the project team focused on identification of candidate thermal load reduction technologies, determination of the design specifications for the technologies, implementation on a pre-production vehicle, and individual evaluation of the technologies. In addition, analysis tools were constructed during Phase I, including a vehicle cabin thermal model; heating, ventilating and air conditioning (HVAC) system model; overall vehicle model; and national-level analysis process tools. Analysis tools were

validated with Phase I experimental results and will be leveraged in Phase II to provide an estimate of the impact of the thermal load reduction system on vehicle range on the national scale. Phase I concluded with a Go/No-Go decision point for the integration of the candidate thermal load reduction technologies into the Phase II vehicle. FY17 focused on completion of Phase II, integrating the thermal load reduction system into the vehicle and evaluating its performance experimentally through outdoor cold and hot weather testing in addition to environmental chamber evaluation.

The project leveraged collaboration between NREL and its project partners to complete all components of the project work plan. HATCI provided the vehicle platform, modeling data, and technology interfacing I for Phase I evaluation of technologies. HATCI led Phase II of the project, including integration of technologies into the Hyundai vehicle platform and evaluation at HATCI facilities to characterize the performance of the vehicle. In addition to HATCI's contributions, the project relied on select tier one and tier two supplier research teams to develop, manufacture, aid in testing and analysis tasks, and provide general direction for the project. PGW provided automotive glass manufacturing capabilities for the project in addition to advanced glass technologies for evaluation. Sekisui provided advanced materials and integration expertise for candidate thermal load reducing glass technologies, collaborating with PGW for manufacturing. PPG Industries developed and provided baseline and solar reflective paint formulations for the Phase I and Phase II vehicles in addition to their thermal property characterization. Gentherm interfaced directly with both NREL and HATCI to develop and provide active seating, door glass defogging, and individual heated surface technologies. Finally, Hanon Systems performed experimental characterization of the vehicle HVAC system and model inputs for the construction and validation of the HVAC system model in addition to expertise in HVAC system control.

*Phase II Cold and Hot Weather Field Evaluation*

Cold weather field-testing was completed for two 2016 Hyundai Sonata plug-in hybrid electric vehicles (PHEVs), one that represented the baseline vehicle, and a second that contained the thermal load reduction system. The evaluations were performed in Fairbanks, Alaska, and consisted of transient and steady-state warmup tests in addition to defrost tests. Ambient temperatures ranged from -14°C to -1°C during the testing, and the vehicles were operated at moderate speeds during the drive events due to adverse weather conditions. Transient drive segments were approximately 30 minutes in duration, followed by a 30-minute steady-state segment. For the stationary defrost test, approximately 500 mL of distilled water was uniformly applied to the windshield and driver/passenger door glass prior to the start of the test. The baseline vehicle for the defrost test was operated in "Auto" mode with a display setpoint of 73ºF, while the modified vehicle used only the heated windshield and door demisters. Hot-weather field testing was completed for the two vehicles in HATCI's California Proving Grounds and in Death Valley, California. Evaluations consisted of transient and steady-state driving cooldown tests and a 1-hour stationary idle cooldown test. Ambient temperatures ranged from 38°C to 50°C during the test sequence. Transient drive segments were approximately 10 minutes in duration, followed by a 30-minute steady-state segment. For the 1-hour stationary idle cooldown test, both vehicles were set at "maximum cooling" mode and 100% recirculation. Prior to the drive in both the cold and hot weather field evaluations, the vehicles were soaked in ambient conditions for a minimum of 4 hours and charged to 100% state of charge. During the drive events, the baseline vehicle HVAC was set in "Auto" mode with a display setpoint of 73°F, while the modified vehicle was set in "Auto" mode with setpoint adjusted to attain occupant comfort.

*Phase II Chamber Evaluations*

Cold and hot weather chamber evaluations were performed in HATCI's environmental test chamber located at HATCI Headquarters in Superior Township, Michigan. The chamber evaluations used both the baseline vehicle and the vehicle equipped with the thermal load reduction system. The cold-weather evaluation was performed using the U.S. Environmental Protection Agency's FTP-75 driving schedule with the chamber set at -7°C for the overnight soak and drive. The first part of the test procedure (referred to as Section 1 and

equivalent to the FTP-72, or Urban Dynamometer Driving Schedule [UDDS]) consisted of a cold-start transient phase combined with a stabilized phase while Section 2 consisted of a hot-start transient phase. The baseline vehicle HVAC was set in "Auto" mode with a display setpoint of 73°F at the beginning of the drive, while the modified vehicle HVAC setpoint was reduced below 73°F and adjusted during the test to attain occupant comfort equivalent to the baseline vehicle.

The hot-weather evaluations of the two vehicles were performed using a modified AC17 test procedure. The test conditions were modified to represent more severe conditions seen in the United States than what the standard AC17 conditions specify. Prior to the test, the vehicles were soaked indoors at room temperature. Thereafter, the vehicles were placed in the chamber and the chamber temperature was held at 35°C with a humidity of 100 g/lb. In addition, 850 W/m$^2$ of solar was applied to the vehicle using lamps during the hot solar soak, SC03 and Highway Fuel Economy (HWFET) test phases. The baseline vehicle HVAC was set in "Auto" mode with a setpoint of 72 at the beginning of the drive, while the modified vehicle HVAC setpoint was increased above 72 and adjusted during the test to attain occupant comfort equivalent to the baseline vehicle.

## Results

### *Cold Weather Field Evaluation*

Cold-weather Phase II performance evaluation of the thermal load reduction system included the heated seats, heated windshield, door demisters, and heated surfaces. The percent of time the engine was off for both vehicles during three drive events is shown in Figure V.4.1. The system provided an average of 31.1% and 24.2% improvement in the engine-off time for the transient and steady-state segments, in addition to an average 40% reduction in the time for the occupants to achieve thermal comfort. In addition, the thermal load reduction system provided large improvements for the stationary defrost time and energy consumption. The results of the stationary defrost evaluation are shown in Figure V.4.2. The thermal load reduction system completely cleared the iced windshield in 6 minutes, while the baseline system required 19 minutes. During this time, the thermal load reduction system used 0.1 kWh of energy while the baseline system required 2.6 kWh of energy. Finally, the cold weather field evaluations provided valuable control strategy information for system operation during the cold-chamber evaluation.

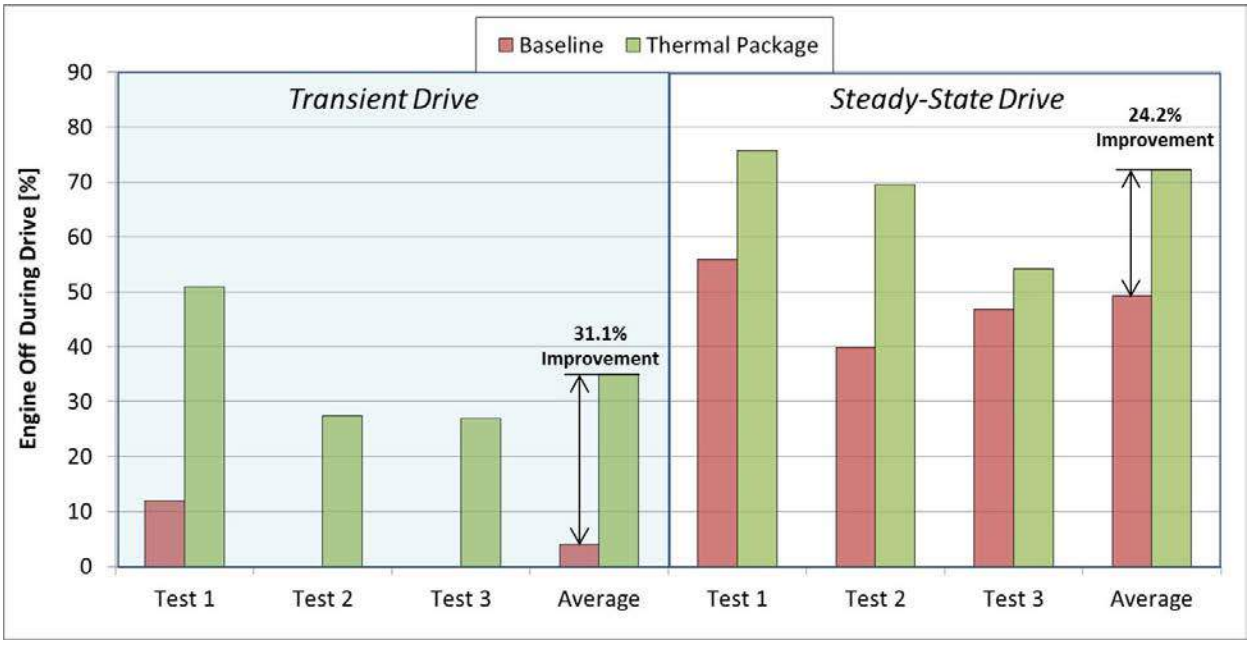


Figure V.4.1 - Percent of time engine was off during cold-weather field transient and steady-state drives for both the baseline and thermal load reduction system vehicles

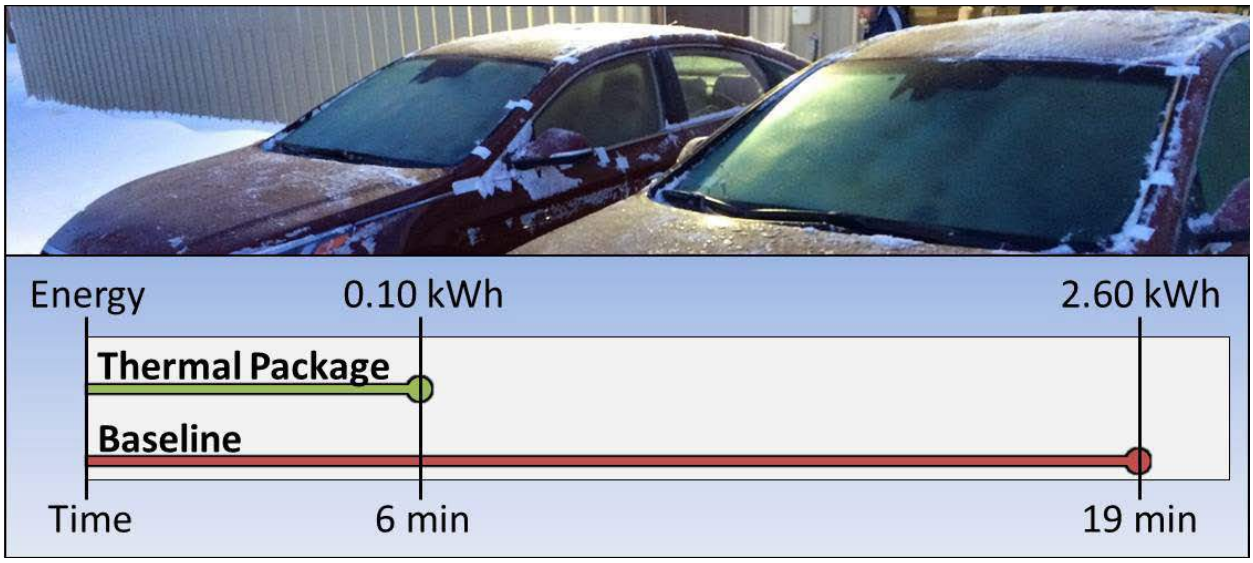


Figure V.4.2 - Results of stationary defrost cold-weather field evaluation for both the baseline and thermal load reduction system

*Hot-Weather Field Evaluation*

Hot-weather Phase II performance evaluation of the thermal load reduction system assessed the impact of ventilated/cooled seats, solar control glass, and solar reflective paint. These technologies reduced the soak temperatures of the modified vehicle and air-conditioning (A/C) energy as well as improved the time-to-comfort for the occupants. For the drive events, an average reduction in climate control energy of 14.2% and 19.4% was obtained for the transient and steady-state segments, respectively. In addition, a drive evaluation was completed at moderate steady speeds with the vehicles locked in EV mode. For the EV drive, A/C energy was reduced by 23.7% compared to the baseline, equating to an 11.4% improvement in EV range. Throughout the evaluations, the vehicle containing the thermal load reduction package was able to maintain the cabin breath level temperatures approximately +3°C higher than the baseline vehicle. During the stationary 1-hour idle max cooling test, the thermal load reduction system vehicle attained the following improvements compared to the baseline vehicle:

- 10°C reduction in exterior roof surface temperature due to solar reflective paint
- Inside glass surface temperature reduction of 17°C due to solar control glass
- 3.3°C lower cabin breath air temperature compared to the baseline
- 4.5% A/C compressor energy usage reduction due to reduced thermal loads from the solar control glass and reflective paint.

*Cold-Chamber Evaluation*

Cabin heating energy consumption for the cold-chamber evaluation for both the baseline and thermal load reduction system vehicles is provided in Figure V.4.3. In Section 1, a large reduction in HVAC and positive temperature coefficient (PTC) energy consumption was observed, but the total energy consumption was only 2.9% due to the energy to operate the technologies. Although energy reductions were modest in this section, occupants benefited by attaining thermal comfort 13 minutes sooner with the thermal package compared to the baseline. In Section 2, a 34.9% reduction in energy was attained due to significant reductions in HVAC and PTC heating energy with only a small technology energy cost. Significant energy reduction for Section 2 of the test likely took place due to a combination of elevated coolant temperatures due to reduced HVAC demand, thermal storage of the advanced technologies, fast response time of the technologies, and associated

elevated breath-level temperatures. The heating energy reduction for the thermal package compared to baseline was 12.9%, equating to an 8.9% improvement in fuel economy for the PHEV for the FTP-75 cycle (Sections 1 and 2).

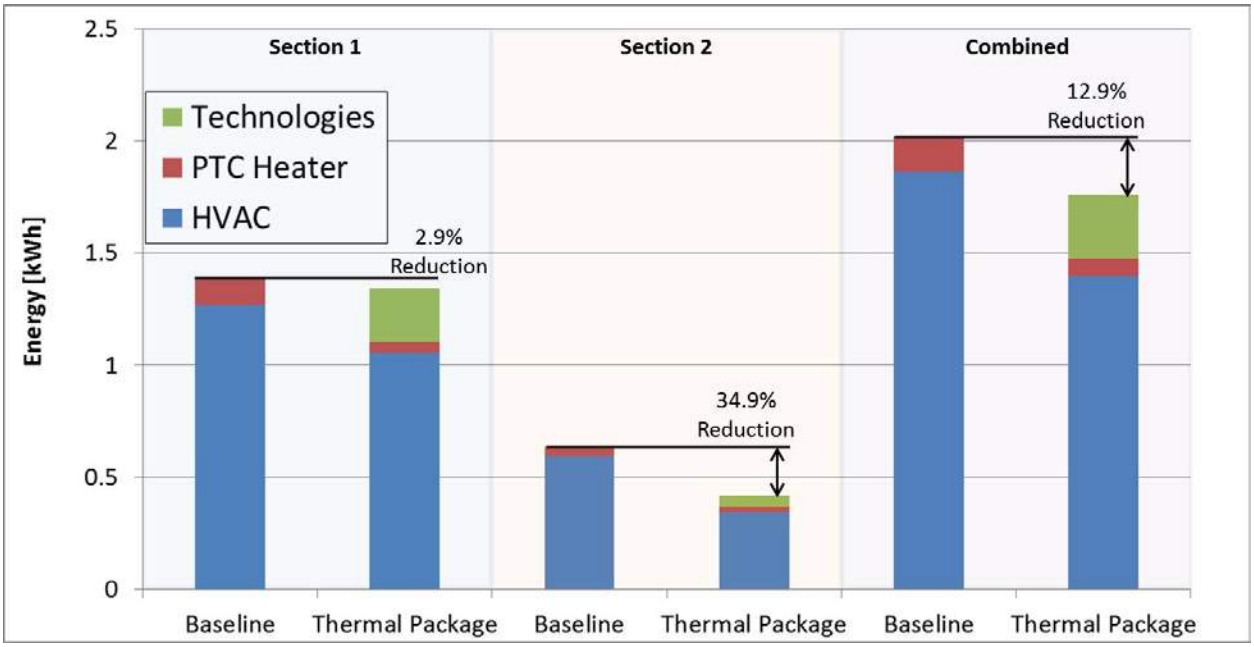


Figure V.4.3 - Heating energy use results for the cold-chamber evaluation of the baseline and thermal load reduction vehicles

*Hot-Chamber Evaluation*

The energy needed to cool the passenger compartment for each section of the hot chamber evaluation for both the baseline and thermal load reduction system vehicles is shown in Figure V.4.4. In Section 1, a 22.9% reduction in energy was measured with the thermal package due to a reduction in thermal loads during the vehicle soak and drive events and accounting for the energy used by the ventilated/cooled seat. In Section 2, a 27.8% reduction in energy was attained using the technologies. Significant energy reduction for both sections of the test resulted from a reduction in the vehicle cabin air and component temperatures during the solar soak and reduced thermal loads during the drive due to the solar control glass and solar reflective paint. Another significant contributing factor to reducing energy consumption was that thermal comfort was attained with a higher cabin air temperature setpoint due to the operation of the ventilated /cooled seats. The cooling energy reduction for the thermal package compared to baseline was 25.5%, equating to a 21.8% improvement in fuel economy for the PHEV over the modified AC17 drive cycle.

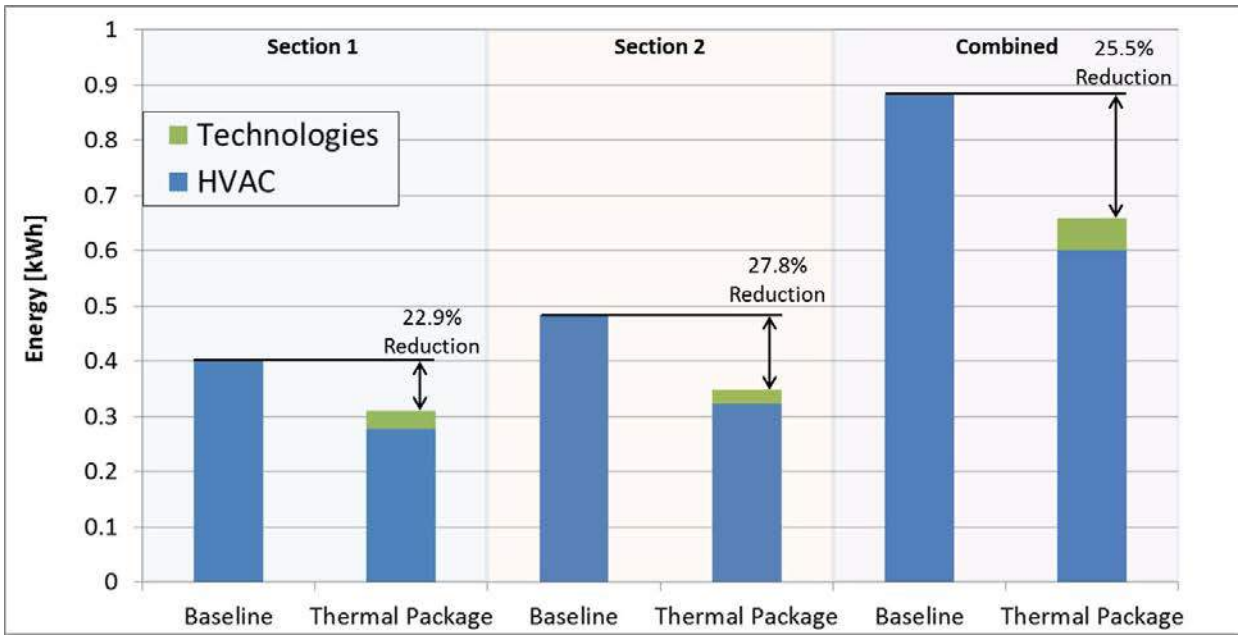


Figure V.4.4 - Cooling energy use results for the hot-chamber evaluation of the baseline and thermal load reduction vehicles

## Conclusions

Environmental chamber and field evaluations were completed for the thermal load reduction system in Phase II of the project. Hyundai Sonata PHEVs equipped with baseline and thermal load reduction systems were evaluated at HATCI's chamber test facility in Ann Arbor, Michigan. Cold-weather field evaluations were completed in Fairbanks, Alaska, while warm-weather field evaluations were completed in Death Valley, California. Cold-chamber and field evaluation of the modified Sonata PHEV included heated seats, heated windshield, door demisters, and heated surfaces. Cold-weather field testing provided an opportunity to develop a control strategy and demonstrate performance of the thermal load reduction system in real-world driving conditions. The cold-chamber evaluation demonstrated a 12.9% heating energy reduction with the thermal load reduction system from the baseline Sonata PHEV, equating to an 8.9% improvement in fuel economy. Hot-chamber and field evaluation of the modified Sonata PHEV included solar control glass, solar reflective paint, and cooled seats. Hot-weather field testing provided an opportunity to demonstrate the system performance using HATCI field test protocols in extreme heat conditions. The hot-chamber evaluation demonstrated a 25.5% cooling energy reduction with the thermal load reduction system from the baseline vehicle. This energy reduction corresponded to a 21.8% improvement in fuel economy during the test cycle. Overall, the project provided technical data and multi-disciplinary evaluation methods/analysis tools that can be used by the automobile industry to assess the system-level thermal impacts of vehicle design to minimize the impact of climate control on EDV range.

## Key Publications

1. Kreutzer, C., Rugh, J., Titov, G., Gallagher, J., and Scott, M. "Performance Evaluation of a Thermal Load Reduction System in a Hyundai Sonata PHEV." Presentation at 2017 SAE TMSS, Plymouth, MI, October 10-12, 2017.

2. Kreutzer, C., Rugh, J., and Tomerlin, J. "Thermal Load Reduction System Development in a Hyundai Sonata PHEV." SAE Technical Paper 2017-01-0186, 2017, doi:10.4271/2017-01-0186.

3. Kreutzer, C., Rugh, J., and Tomerlin, J. "Test Method for Quantifying Climate Control Technologies that Target the Vehicle Occupant," Presentation at the 2016 SAE TMSS, Mesa, AZ, October 18-20, 2016.

## V.5 Advanced Vehicle Testing Activity

**Shawn Salisbury, Principal Investigator**
Idaho National Laboratory
P.O. Box 1625
Idaho Falls, ID 83415
Phone: (208) 526-3430
E-mail: shawn.salisbury@inl.gov

**Lee Slezak, Technology Manager**
U.S. Department of Energy
Phone: (202) 586-2335
E-mail: Lee.Slezak@ee.doe.gov

Start Date:October 1, 2016 End Date: September 30, 2017
Total Project Cost: $1,350,000 DOE share: $1,350,000 Non-DOE share: $0

### Project Introduction

In 2016, Idaho National Laboratory was tasked by Vehicle Technologies Office to perform vehicle technology evaluation as a continuation of the Advanced Vehicle Testing Activity (AVTA). The purpose of this activity is to conduct field evaluations of light-duty vehicles that use advanced technology systems and subsystems to reduce petroleum consumption. Most of the advanced technology vehicles tested by AVTA have some degree of electrified propulsion, including electric motors and advanced energy storage systems. However, other vehicle technologies that employ advanced designs, control systems, or other technologies with production potential and significant petroleum reduction potential are also considered viable candidates for testing by ATVA.

A main focus of AVTA is evaluating grid-connected plug-in electric vehicle (PEV) technologies in order to understand their capabilities to significantly reduce petroleum consumption when compared to traditional internal combustion technology. PEVs are becoming more common throughout the United States, including many companies and groups that are proposing, planning, or have already started the introduction of PEVs into their fleets.

The concept of advanced onboard energy storage and grid-connected charging raises a number of questions that require detailed data sets, such as those collected in the AVTA program, to answer sufficiently. These unknowns include the life and performance of these larger batteries as they are used over the life of a vehicle, the amount and location of charging infrastructure required to sustain PEV penetration, consumer driving and charging behavior patterns, and the actual petroleum displacement achieved.

### Objectives

The field evaluations of light-duty vehicles through AVTA are performed in order to:

- Provide efficiency, maintenance, and life-cycle cost data for advanced hybrid electric vehicles (HEVs), plug-in hybrid electric vehicles (PHEVs), battery electric vehicles (BEVs), and advanced internal combustion engine vehicles.
- Provide real-world usage data from advanced technology vehicles for use in research, modeling, and planning.
- Benchmark battery performance and life in HEVs, PHEVs, and BEVs to support progress in battery development and aid understanding of vehicle battery degradation.

## Approach

The accelerated testing of HEVs, PHEVs, BEVs, and internal combustion engine vehicles is performed by Intertek Testing Services North America in Phoenix, Arizona. Intertek is working with INL on data collection, analysis, reporting, and procedure development. INL has responsibility for technical direction and management of work performed under AVTA, as well as publication of results. The sections of this task jointly cover the testing work performed by INL in addition to work over which INL maintains technical oversight.

Under the Advanced Vehicle Testing and Evaluation project in 2017, there are several test methods used to evaluate vehicles and their subsystems, each of which is discussed in detail as follows.

### *Baseline Performance Testing*

To understand the capabilities of a vehicle when it is new and to independently verify performance ratings, vehicles are tested on a closed track and a chassis dynamometer. These tests are completed following published procedures and are highly controlled for comparability across vehicles and powertrain types. Track testing characterizes performance metrics such as acceleration, constant-speed range, braking, and fuel consumption (which can include electricity, gasoline, or any other fuel used) throughout the operating range of the vehicle. The vehicles are also coast-down tested to determine dynamometer coefficients, which are used during the various urban and highway dynamometer test cycles. Note that the AVTA dynamometer testing is conducted by Argonne National Laboratory at their Advanced Powertrain Research Facility. AVTA shares vehicles with other testing entities, leveraging capability and testing expertise to reduce costs to DOE. Reports are published to document how the vehicles performed during each test, with a focus on fuel consumption.

### *Fleet Testing*

For most production advanced vehicles, AVTA partners with various fleets that utilize light-duty vehicles in high-mileage missions (e.g., document couriers or taxis). This allows testing to be performed at the lowest possible cost to DOE, and ensures that the vehicles will be tested with a wide variation in drive cycles. AVTA partners with government, private, and public fleets for fleet testing because these fleets are often the earliest adopters of advanced technology vehicles. Note that AVTA fleet testing normally does not include operation by the general public due to the level of management needed to ensure strict reporting for data quality assurance.

Electronically logged data are continuously sent from the vehicles to INL servers and are processed daily. For all vehicles, data are recorded on a second-by-second basis during driving and charging, such that energy can be precisely tracked. These data are used for specific subsystem studies at INL, and they have been provided to other national laboratories to support their modeling and simulation efforts. The conditions under which the vehicle was operated are documented and presented with the fuel and energy consumption data.

Throughout the mileage accumulation process for each vehicle, subsystems of interest, particularly traction batteries, are tested for performance. Intertek Testing Services has several battery testing laboratories in the Phoenix area for the performance of these tests. Reports are generated to document battery capability and degradation over the life of the vehicle.

## Results

87 vehicles were operated as a part of the AVTA test fleet in 2017. As no new models were added to the fleet in the past year, all of the vehicles were continuing testing from previous years.

Vehicles with high voltage tractions batteries continued their battery performance tests, which are completed five times throughout the life of each vehicle. Figure V.5.1 shows results from the battery capacity testing of a 2013 Ford C-Max Energi throughout the vehicle life. The full results of battery testing are compiled into battery testing results reports.

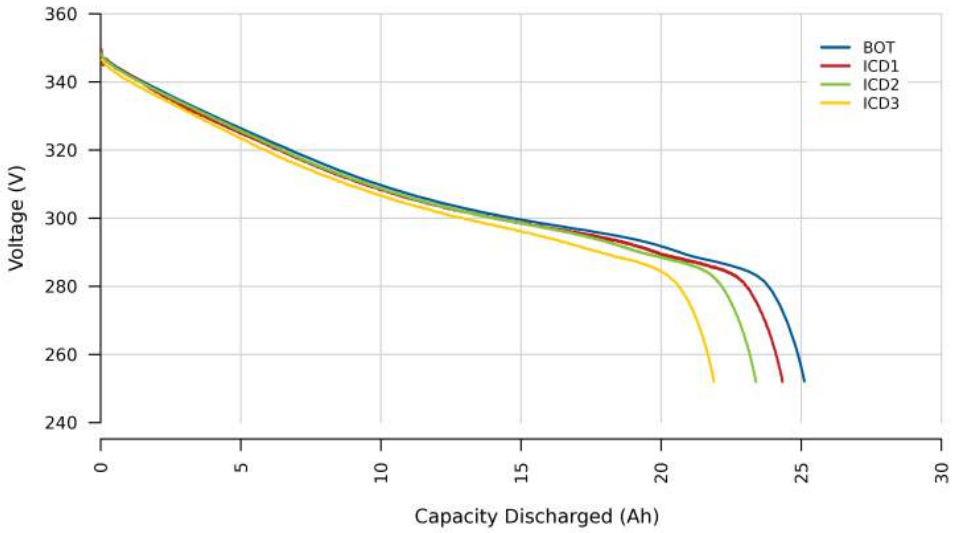


Figure V.5.1 - Static capacity test results for the battery from a 2013 Ford C-Max Energi. The tests were performed at approximately 5,000, 26,000, 71, 000, 130,000 miles

In 2017, several vehicles reached the end of their test life. To compare vehicle energy use and performance at the beginning and end of life, some of the vehicles repeated components of the baseline testing that were also performed when the cars were new. At this time, end-of-life testing has been completed and reports have been published for two vehicles, the 2013 Honda Civic Hybrid and the 2013 Chevrolet Malibu ECO.

As direct current fast charging (DCFC) becomes a larger issue in the electric vehicle space, some additional tests were developed to understand the fast charging capabilities of different vehicles, especially at extreme temperatures. At its testing facility, Intertek has a DC fast charger compatible with all battery electric vehicles in the AVTA fleet, as well as a vehicle-sized temperature chamber. Each vehicle undergoes a full fast charge while the vehicle is held at either 0°C, 25°C, or 50°C. The charging is monitored in order to capture differences in charging behavior seen at different temperatures and by different vehicles. Figure V.5.2 shows a portion of the testing results from the four 2015 Chevrolet Spark EVs in the AVTE fleet. The full results of testing on each of the fast charge capable vehicles are compiled into reports and published to the INL website.

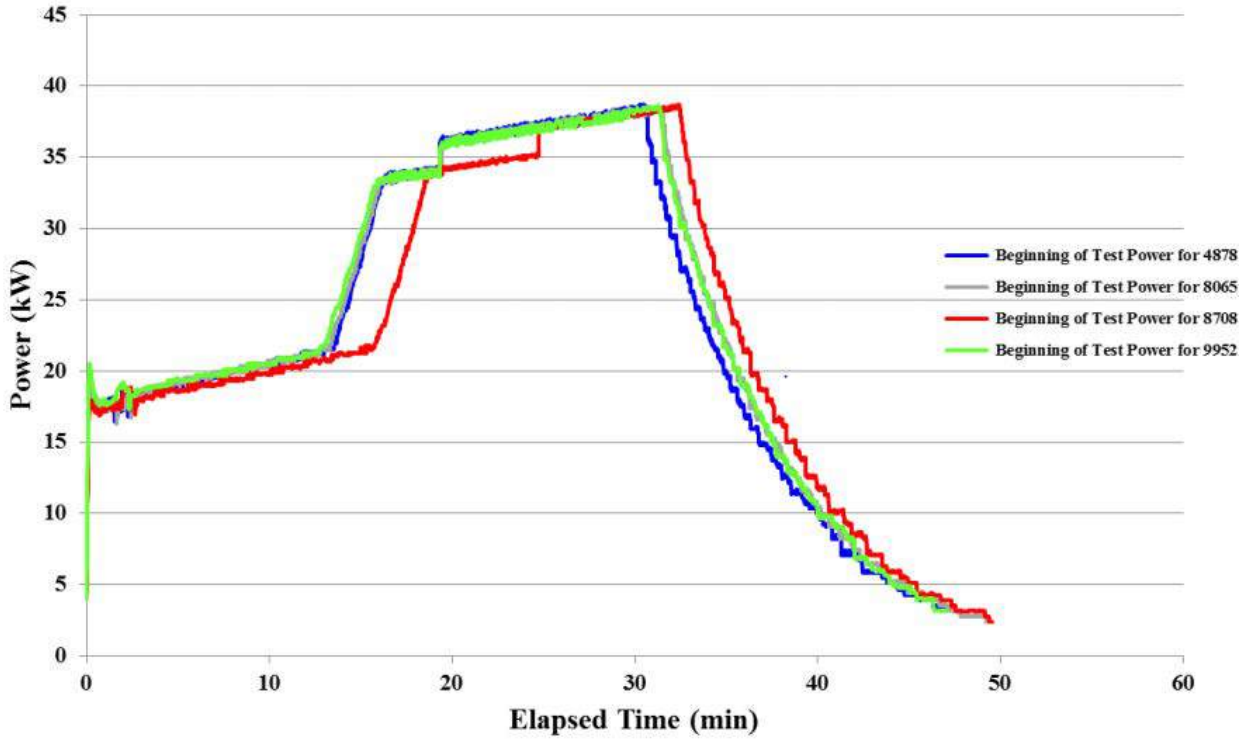


Figure V.5.2 - Power of DC fast charging tests for 2015 Chevrolet Sparks at 0°C.

## Conclusions

AVTA has continued to provide the real-world testing needed to benchmark DOE technology investments, including the critical tasks of determining suitability for deployment, lifetime performance, and life-cycle costs of new technology components and vehicle systems. This testing provided information used to help understand the infrastructure requirements, operating costs, and petroleum displacement of plug-in electric vehicles, other alternative fuels, and hybrid electric vehicles, as well as proper placement of supporting infrastructure. The quality of the vehicles and the batteries (i.e., expected operational life) has improved significantly and fleets have been found that can significantly accumulate high per-vehicle mileage. Though the durability of these vehicles has improved significantly, the need for on-road testing is still very relevant to understand off-cycle performance and how on-road usage compares to standardized test procedures.

## Key Publications

1. "Battery Pack Laboratory Testing Results, Series of Reports," Idaho National Laboratory, 2017.
2. "Vehicle Specifications and Testing Results, Series of Reports," Idaho National Laboratory, Intertek Testing Services North America, 2017.
3. “End of Life Vehicle Specifications and Testing Results, Series of Reports,” Idaho National Laboratory, Intertek Testing Services North America, 2017.
4. “DC Fast Charging at Different Temperatures, Series of Reports,” Idaho National Laboratory, Intertek Testing Services, 2016.

(This page intentionally left blank)

U.S. DEPARTMENT OF
ENERGY

Office of
ENERGY EFFICIENCY &
RENEWABLE ENERGY

**For more information, visit:**
energy.gov/eere/vehicles

DOE/EE-1710 • May 2018